NASA-TM-103599

Research and Technology 1992

Annual Report of the Marshall Space Flight Center

NASA TM-103599

National Aeronautics and
Space Administration

George C. Marshall Space Flight Center
Marshall Space Flight Center, Alabama 35812

Introduction

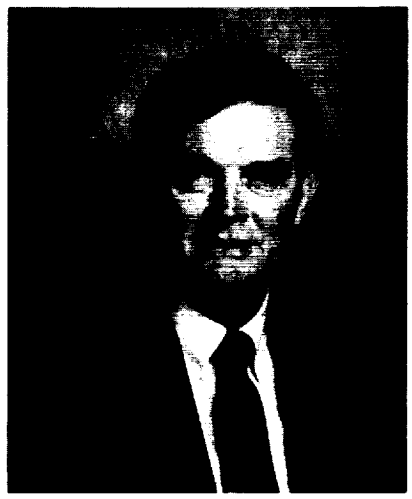

Innovation: Key to the Future

As the Marshall Space Flight Center team continuously strives for improvement in all endeavors, we especially encourage innovation and creative solutions to problems facing us. In our dynamic world of engineering, scientific, and technology changes, we recognize that innovation is a significant key to our Nation's future in space, as well as its economic strength. We are proud of our past accomplishments and of the activities under way. Join with us in developing the "keys" to unlock the space challenges of the future.

T. J. Lee

T.J. Lee
Director

Acknowledgements

The point of contact and coordinator at MSFC for this report is H.C. Stinson (ER41/205–544–7239). She was assisted by an editorial committee consisting of G.F. McDonough, C.R. Chappell, S.H. Morgan, W.C. Snoddy, and G.R. Wallace. Detailed editorial support and production assistance was provided by MSI, a Division of The Bionetics Corporation. The research and technology work at MSFC is a cooperative effort, but, because of space restrictions, it is impossible to list all those involved in the projects described in this report.

To assist the reader, the MSFC contact, office code, telephone number, and sponsoring organization are included at the end of each article. Please note that some sponsoring organizations have implemented organizational name changes. An alphabetical index of all contacts is presented at the end of this report.

Cover

The cover, designed by the MSFC Graphics Branch/CN32, illustrates past, present, and future NASA programs managed by MSFC including:

- Mercury-Redstone vehicles, which boosted America's first astronaut, Alan Shepard, on a suborbital flight in 1961
- The Saturn rocket family, the largest of which boosted astronauts to the Moon in 1969
- The lunar roving vehicle for transporting astronauts on the Moon's surface from the lunar module
- Skylab, America's first manned orbiting space station
- Space shuttle elements, i.e., the space shuttle main engine, solid rocket boosters, and the external tank, which provide nearly 6M lb of thrust
- The Hubble Space Telescope, an optical observatory providing an unprecedented view of the universe
- Space Station *Freedom* elements including pressurized modules provided by the United States
- The heavy lift launch vehicle concept, an augmentation to the U.S. space launch fleet.

Also shown on the cover is the MSFC Building 4200 Complex. MSFC occupies approximately 1,800 acres within the U.S. Army's Redstone Arsenal reservation and has other locations outside of Huntsville, AL.

Contents

Earth Science and Applications

Solar Terrestrial Physics

Ionosphere-Thermosphere-Mesosphere Physics

Magnetosphere Physics

Technology Programs

Information, Electronic, and Optical Systems

Materials and Manufacturing Processes

Propulsion

Structures and Dynamics

List of Key Words

Advanced Stu...

Innovation is the key to the future of the American space program. In advanced studies, we continuously search for innovative approaches to conducting business and in developing concepts for space transportation systems, infrastructures, and space experiments. Advanced transportation system studies are directed at meeting the requirements of industry and future NASA missions. Also, we are investigating new ways to design, develop, manufacture, and operate transportation systems that are safe and cost-efficient.

Advanced studies are defining requirements and refining concepts for the eventual return of humans to the Moon and for a human mission to Mars. Recommendations from the Stafford Synthesis Committee are incorporated in the present efforts. Innovative ideas for low-cost space physics and astrophysics missions, such as the Lunar Ultraviolet Transit Experiment (LUTE), are also under consideration.

Other advanced studies include electromagnetic actuators (EMA's) and laser power beaming. Recent advances in high-power semiconductor switching technology enable the development of EMA's that are capable of gimbaling large rocket engines. The ability to transmit power from the ground to space platforms can benefit a variety of users like astronomers and communications companies. The projects described in this section are examples of how innovation begins in advanced studies.

Charles Darwin
Director, Program Development


UNITED STATES

Space Science

Astrophysics

An integral first step in the Space Exploration Initiative (SEI) is the development and placement of early-return science missions on the lunar surface. Several such payloads have been identified by NASA's Office of Space Science and Applications (OSSA) as candidates for lunar deployment. The lunar surface provides a stable base and suitable environment for these science projects that cannot be otherwise accomplished on Earth or in space with free-flying spacecraft. Among the chief advantages of the lunar surface for science missions are the low gravity, slow rotation (allowing for long observation times), reduced terrestrial radio emissions (a source of noise), a dark sky (no airglow), and the ultrahigh vacuum (UHV) of space.

The **Lunar Ultraviolet (UV) Transit Experiment (LUTE)** is a 1-m (3.3-ft) **UV telescope** that can be emplaced on the lunar surface by the Artemis lunar lander or can be transported to a lunar site by astronauts during a mission to the lunar outpost. **LUTE** achieves a wide field-of-view (FOV) with a compact optical system using lightweight mirrors. The focal plane instrument is a two-dimensional (2–D) mosaic of charge coupled devices (CCD's) arranged to give a 1.4-degree FOV. **LUTE** will not track specific targets but will be pointed continuously at a chosen declination, thereby relying on the very stable motion of the **Moon** to sweep out a swath of the sky.

LUTE has been proposed by Dr. John McGraw of the Steward Observatory of the University of Arizona as an early precursor experiment to a lunar **transit telescope** of a 2-m (6.6-ft) aperture. **LUTE** is a scientifically important **UV telescope** that makes use of the unique opportunity to observe a fraction of the sky in the 0.1- to 0.3-μm wavelength regime, specifically at Lyman α, which is unobscured by the geocorona at the orbit on the **Moon**. **LUTE** is a simple, self-sufficient, meridian-pointing telescope that requires no adjustment after the initial alignment.

The **LUTE** technical concept is being analyzed and engineered by MSFC together with Dr. McGraw as a potential early payload for the **Artemis lander**. Because the **Artemis lander** is estimated to be able to land a maximum 200-kg (440-lb) science payload on the lunar surface, it becomes important that **LUTE** is designed as a super-lightweight flight experiment. This requires that weights for such subsystems as the optics, communications and data handling, and power reflect stringent control. For this reason, it may not be possible to operate the telescope during the lunar night since energy storage for 14 d would result in an excessive weight. Utilizing radio isotope thermal generators (RTG's) for power generation during the lunar night would be ideally suited because components and subsystem temperatures can be maintained at a tolerable level, while keeping systems weight at a lower level than can be attained with a photovoltaic system. Trade studies in these areas are now being conducted to optimize the systems that support **LUTE** on the Artemis and to assess the Artemis interfaces.

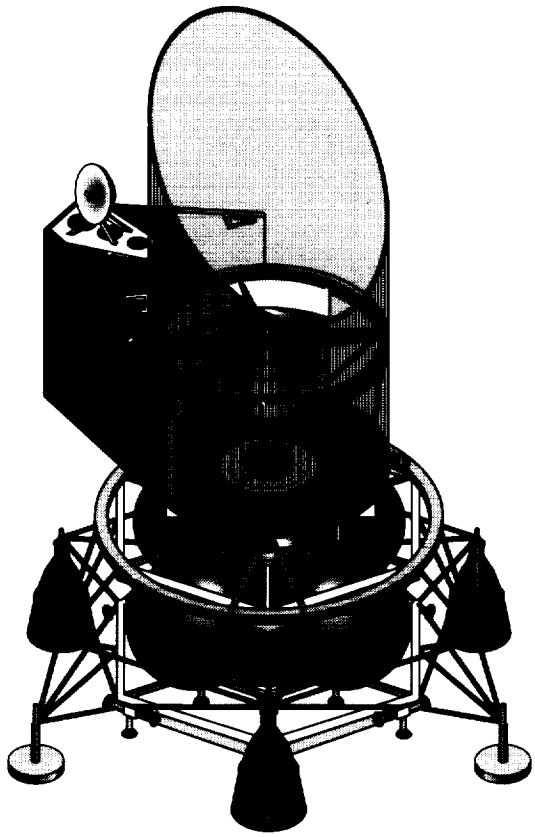

LUTE on the Artemis lander.

Deployment of **LUTE** on the **Moon** during the third Artemis flight is projected for early 1998. Although this constitutes a tight schedule, plans are being made to reduce the historically lengthy review phases occurring in the development of flight systems through introduction of "new way of doing business" approaches for this program. Typically in this approach is concurrency engineering and maximum use of computer-assisted design.

M.E. Nein/PS02
205–544–0619
Sponsor: Office of Space Science and Applications

Inner Magnetosphere Imager

Imaging the Earth's **magnetosphere** from space will enable scientists to better understand the global shape of the **magnetosphere**, its components, and processes. The proposed inner **magnetosphere** imager (IMI) mission will obtain the first simultaneous images of the component regions of the inner **magnetosphere** and will enable scientists to relate these global images to internal and external influences as well as local observations. MSFC is performing a concept definition study of the proposed mission. As currently envisioned, the baseline mission calls for an instrument complement of seven imagers to be flown on a spacecraft in an elliptical Earth orbit with an apogee of seven Earth radii, perigee between 1,000 km (621 mi) and one Earth radius, and a 90-degree inclination.

The IMI science working group (SWG) defined the requirements for the mission. The specific measurement objective of the mission is to obtain the first simultaneous images of component regions of the inner **magnetosphere**, including:

- The ring current and inner plasma sheet using energetic neutral atoms (ENA's)
- The plasmasphere using extreme ultraviolet (EUV)
- The electron and proton auroras using far ultraviolet (FUV) and x-rays
- The geocorona using FUV.

In order to meet this objective, a list of strawman instruments was developed and parameterized by the IMI SWG. The strawman instruments and their measurement capabilities include the following:

- Hot plasma imager—20 to 1,000 keV ENA's
- **Plasmasphere** imager (helium (He^+) 304)—304 Å
- **Plasmasphere** imager (oxygen (O^+) 834)—834Å
- Geocoronal imager—1,216 Å

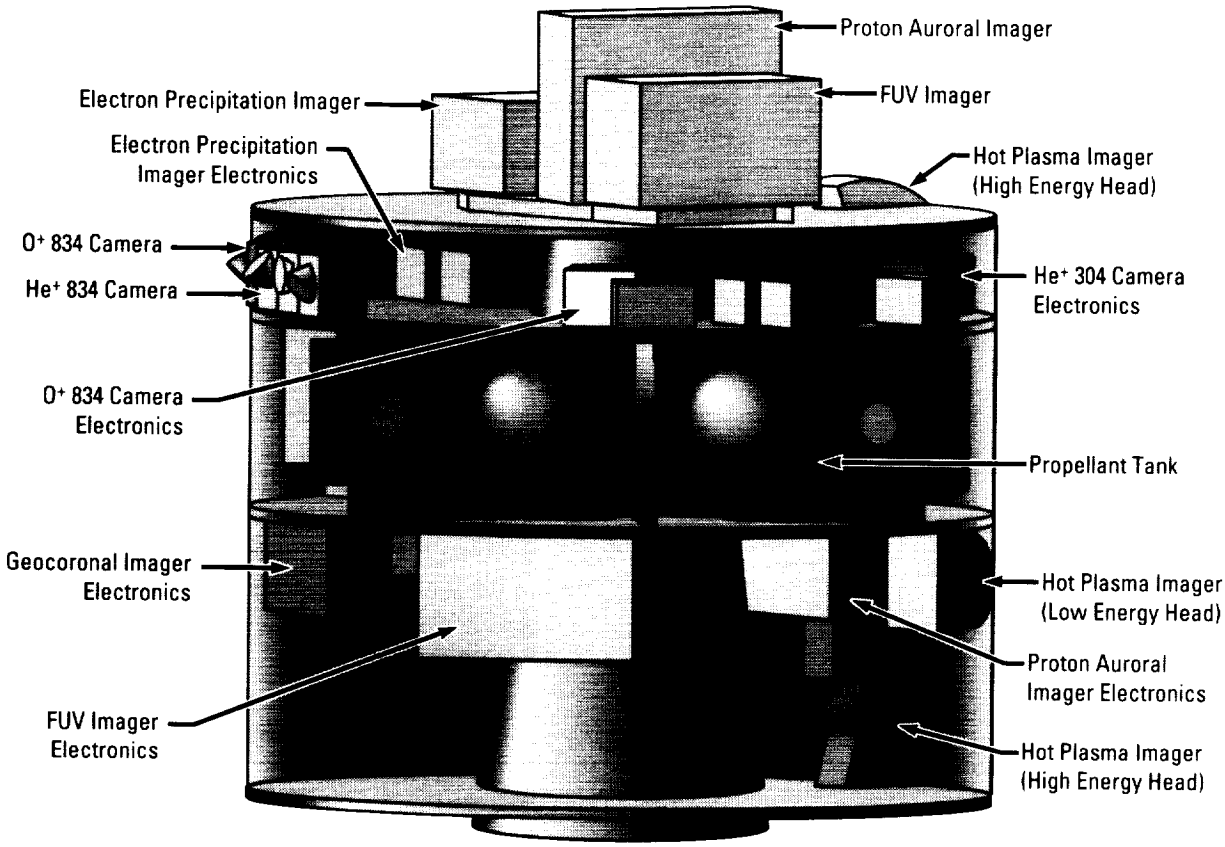

Conceptual design for the IMI spacecraft.

- Auroral imager—1,304 to 1,356 Å
- Proton auroral imager—1,216 Å
- Electron precipitation imager—0.3 to 10 keV x-rays.

The mission is currently scheduled to begin phase development in 1996, and it is to be launched in the year 2000. The baseline mission spacecraft is envisioned to be spin-stabilized with a counter-rotating or "despun" platform allowing some instruments to always be pointed in the same direction. Two optional configurations are being considered. The first option being examined is the inverse of the baseline: a three-axis stabilized spacecraft would accommodate the pointed instruments with the rest of the complement located on a rotating platform. The second option splits the instruments onto two distinct spacecraft: the pointed instruments would be flown on a three-axis stabilized spacecraft and the spinning instruments on an equivalent spinning spacecraft bus. The two spacecraft would be co-orbital and, hence, share essentially the same viewing aspect as the baseline or single-spacecraft option. The baseline spacecraft is configured to launch on a Delta launch vehicle.

"Inner Magnetosphere Imager Scientific Rationale and Mission Concept, Volume I: Executive Summary," NASA/MSFC, Huntsville, AL, 1991.

Herrmann, M.C., and Johnson, C.L., "Spacecraft Design Considerations for an Inner Magnetosphere Imager Mission," Proceedings of the International Conference on Optical Applied Science and Engineering, Society of Photo-Optical Instrumentation Engineers (SPIE) Proceedings, vol. 1744, San Diego, CA, July 19–24, 1992.

C.L. Johnson/PS02
205–544–0614
Sponsor: Office of Space Science and Applications

Solar Ultraviolet Radiation and Correlative Emissions

The goal of the solar **ultraviolet** (**UV**) radiation and correlative emissions (SOURCE) mission is to significantly advance the ability to specify the spectral irradiance of the Sun in the **extreme UV** (**EUV**) wavelength range from 1 to 125 nm (10 to 1,250 Å). To achieve this goal, space-based and correlative ground-based observations of the Sun will be used in combination with empirical modeling to develop and validate a more accurate system of proxy measurements.

Currently, neither the magnitude nor the temporal variability of the solar **EUV** radiative output can be specified with sufficient accuracy for space physics applications. This radiation is especially important because it creates the ionosphere and is primarily responsible for the structure and dynamics of the terrestrial upper atmosphere. The upper atmosphere is very responsive to variations in the Sun's output, contributing to a "space weather" system that affects low Earth orbit (LEO) satellites through atmospheric drag and reentry dynamics so that both military and civilian operational systems need improved models of the upper atmosphere with reliable solar **EUV** irradiance inputs for specification and forecasting.

The primary, space-based segment of the SOURCE measurements could be achieved with an explorer-class payload of approximately 55 kg (120 lb), launched by a Pegasus vehicle, into a low-inclination orbit with perigee in excess of 600-km (325-nmi) altitude. The power required for the payload is estimated at 100 W or less. Peak telemetry rate is largely dependent on how the data from the imagers are downloaded and varies from 10 to 400 kb/s. The mission is planned to exceed a 2-yr duration.

The satellite would carry a payload consisting of a suite of well-calibrated spectroradiometric instruments and imagers to provide absolute measurements of the solar **EUV** spectrum and near-monochromatic images of the full solar disk. Images will be obtained at three wavelengths corresponding to emitting source regions in the solar chromosphere, solar transition region, and corona. The desired spatial resolution for the imagers is 5 arc sec. The associated spacecraft pointing requirements are ±3 arc min pointing with ±2 arc sec knowledge. Observations are required approximately once per orbit.

MSFC is supporting the Space Physics Division of the Office of Space Science and Applications (OSSA) in the definition of this mission with a planning goal of flight in 1998. In-house and contractor pre-phase A efforts have been completed.

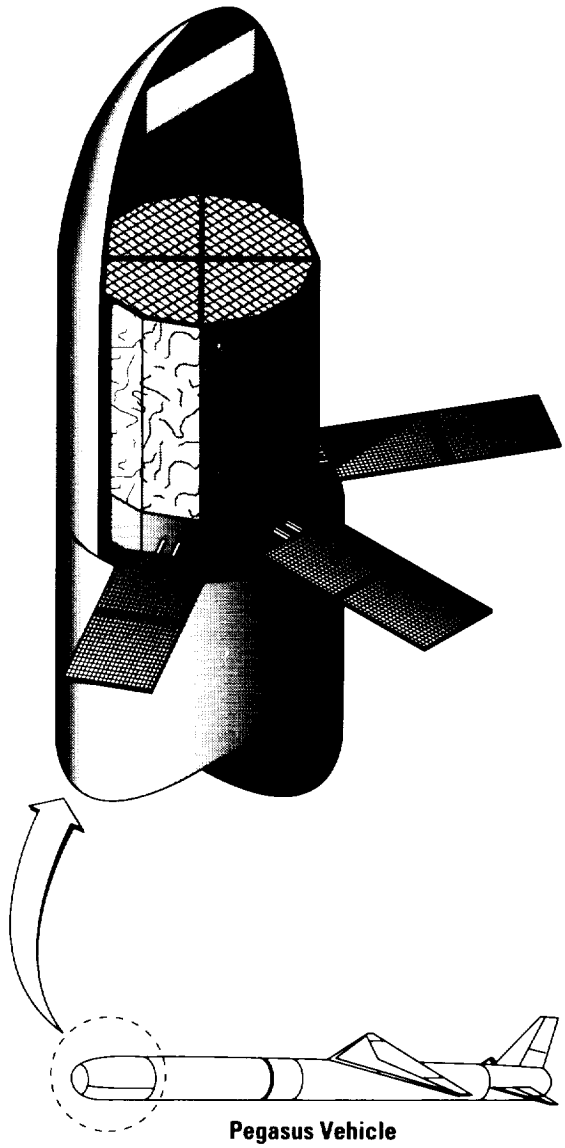

SOURCE launch configuration.

J. Dabbs/PS02
205-544-0623
Sponsor: Office of Space Science and Applications

Space Physics

An evolutionary approach to performing science from the Moon is being formulated in support of the Astrophysics and Space Physics Division of NASA's Office of Space Science and Applications (OSSA). A **lunar environment monitoring system** is being investigated for potential deployment on the Artemis lunar lander or by humans at the First Lunar Outpost (FLO). The system would monitor the lunar surface environment before, during, and after the initiation of manned activities. The solar wind, lunar surface charging, energetic ion environment, near-surface propagation of electric and magnetic fields, instrument and outpost outgassing, and disturbed dust distributions would be measured. Each segment of the system will comprise many different science instruments, many of which have a strong space flight heritage, including:

- Direct current (dc) electric field monitor
- Energetic ion detector
- Fast plasma analyzer
- Ion/neutral mass spectrometer
- Ultraviolet (UV) spectrometer
- Dust measurement package
- Cosmic ray experiment package.

A **lunar solar observatory** would include a variety of instrumentation to investigate the basic plasma physics processes responsible for the metastable and impulsive energy releases in **solar flares**. More fundamental research might also be conducted into the cause of the solar activity cycle. Such an observatory would consist of several instruments beginning with an early high-resolution extreme UV (EUV)/x-ray telescope deployed either by an Artemis lander or by the astronauts at the FLO and culminating with a very large pinhole occulter facility (POF). The POF, which will require the resources of a mature lunar base for assembly, would consist of a pinhole occulter mask positioned perpendicular to a detector array separated by a distance of 100 m (328 ft). When this system is aimed at the Sun, the solar x-ray photons pass through the mask and are counted by the detectors. The occulting mask moves along an overhead arch, which, in turn, rotates around the vertical by moving along the circular tracks at the base of the assembly. The instrument complement is located at the center of the arch and track. In addition to fundamental science, in all phases, such an observatory could provide the functional capability of flare alert and warning for the proposed lunar base.

A lunar-based **energetic neutral atom (ENA) imager** would provide the first global images of energetic neutral hydrogen (H_2) atoms emitted from the Earth's magnetospheric plasmas and would further an understanding of the processes involved in their creation and dynamics within the **magnetosphere**. A box containing a segmented neutral atom imager would be partially buried in the lunar regolith with only the front Earth-pointing face exposed. The instrument would have a 2-m (6.6-ft) aperture and would be composed of several thin-film time-of-flight detectors. An image of the impinging neutral atoms could be made with velocity and directional information extracted from the data. The imager would be deployed at a permanently manned lunar base.

A lunar-based **cosmic ray calorimeter** would explore the composition of cosmic ray nuclei with energies in excess of 10^{15} eV and aid in the determination of the sources and acceleration mechanisms of the highest-energy **cosmic rays**. The calorimeter would consist of layers of plastic scintillator counters viewed by photomultiplier tubes. Each layer should be separated by lunar regolith. The detector is to be position-sensitive for trajectory and time-of-flight measurements. The calorimeter would be assembled at the permanently manned lunar base.

The goals of a lunar-based **magnetopause sounder** would include active sounding of the magnetopause boundary using dipole transceiver arrays with pulse/coded outputs located kilometers (miles) apart on the lunar surface. The sounder would operate in frequency regimes from 5 to 100 kHz in 5-kHz steps. The receiving antenna would be large: nine dipole arrays, each 2,500 m (8,200 ft) long and mounted on a short mast to yield an effective aperture of 20,000 m (12.4 mi).

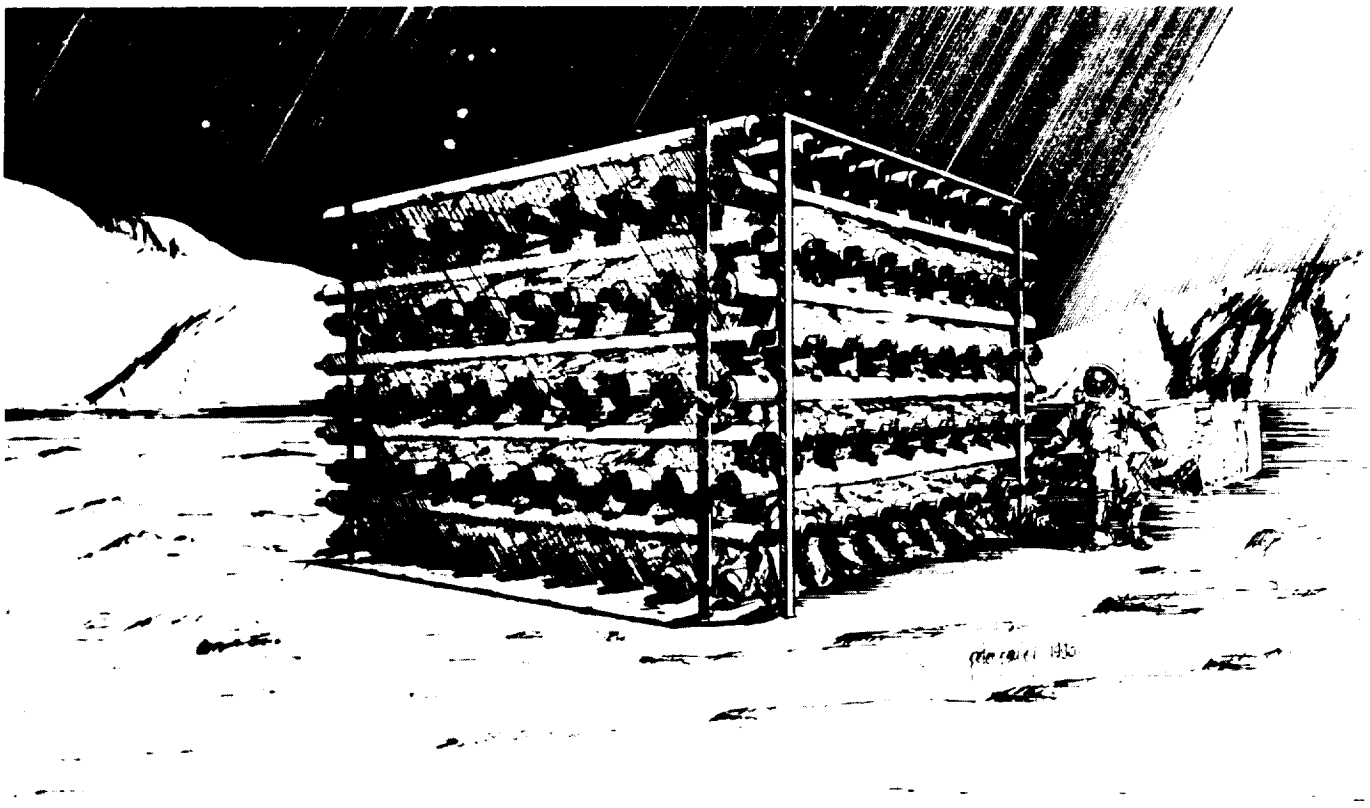

Lunar-based cosmic ray calorimeter concept.

Johnson, C.L., and Brown, N.S., "Near-Term SEI Science Missions Utilizing an Evolutionary Lunar Transportation System," 43rd Congress of the International Astronautical Federation, Washington, DC, August 28–September 5, 1992.

Nein, M.E., Davis, B., and Hilchey, J.D., "Systems Concept for a Series of Lunar Optical Telescopes," Proceedings of the Third International Conference on Engineering, Construction, and Operations in Space, Space 92, Denver, CO, June 1–4, 1992.

Wallace, R.A. et al., "SEI Science Payloads: Descriptions and Delivery Requirements," JPL D–7955, Jet Propulsion Laboratory (JPL), Pasadena, CA, 1990.

C.L. Johnson/PS02
205–544–0614
Sponsor: Office of Space Science and Applications

Space Systems

Geostationary Earth Observatory Program

The **Geostationary Earth** Observatories (GEO's) are the space-based elements of NASA's Mission to Planet **Earth** Program that provide the excellent temporal resolution data required for a thorough understanding of **Earth** processes and their role in global climate change. **Geostationary** observations complement polar and other low-orbit observations by providing nearly continuous hemispheric coverage. Excellent temporal resolution is available from **geostationary** orbit. In a point-and-stare mode, coverage provided by **geostationary** sensors over a specified region is essentially continuous, limited only by sensor engineering constraints and cloud blockage.

The baseline mission concept (and the one endorsed by the GEO Science Steering Committee) calls for multiple **geostationary** satellites to be deployed concurrently around the **Earth** to provide complete global coverage of **Earth/atmosphere** system processes. But whether several GEO's are simultaneously situated about the **Earth** or just one or two fully instrumented GEO's are deployed over specific regions to obtain high temporal resolution measurements and a better understanding of specific transient phenomena, GEO's are critical to a full understanding of **Earth's** dynamic behavior. GEO's will help answer diurnal variability questions and eliminate data aliasing concerns. Because each GEO is always stationed over a specific region of the **Earth**, repeated scans over that area minimize cloud blockage problems and provide the time-frequent data required to adequately address **global change**.

Three types of instruments are being studied: (1) facility instruments that are multidisciplinary in nature; (2) principal investigator instruments for specific **Earth**-system processes measurements; and (3) operational or precursor operational instruments that could fulfill the next-generation National Oceanic and Atmospheric Administration (NOAA) operational **geostationary** sensor requirements. Due to the R^{-2} dependence of signal strength on distance, the **geostationary** orbit is better suited to passive instruments (i.e., imagers, sounders, etc.) rather than active instruments (i.e., lasers, radars, etc.), which depend on a reflected signal.

The GEO three-axis stabilized **spacecraft** must accommodate the relatively large (approximately 4-m (13-ft) diameter) mechanical scanning antenna of the passive microwave instrument; meet the stringent pointing and stability requirements of the imaging instruments; provide the capability for cooling numerous infrared (IR) detectors to very cold temperatures (90 K); and provide an unobstructed simultaneous view of **Earth** for several instruments over an anticipated 5- to 10-yr lifetime. Early GEO conceptual configurations utilized a single **spacecraft** to accommodate the entire instrument complement. Configuration options that distribute the candidate instruments onto multiple smaller **spacecraft** are currently being studied. Single-**spacecraft** configurations require a Titan IV/Centaur-class launch vehicle, while utilization of multiple **spacecraft** permits use of a smaller class launch vehicle such as the Atlas IIAS and an apogee kick motor. Multiple **spacecraft** also allows the grouping of instruments that induce large disturbances onto one **spacecraft** and those that require the most stringent pointing requirements onto another **spacecraft**. This is an important consideration since meeting the imaging instrument pointing stability requirements is a major design driver on the GEO pointing, navigation, and control subsystem.

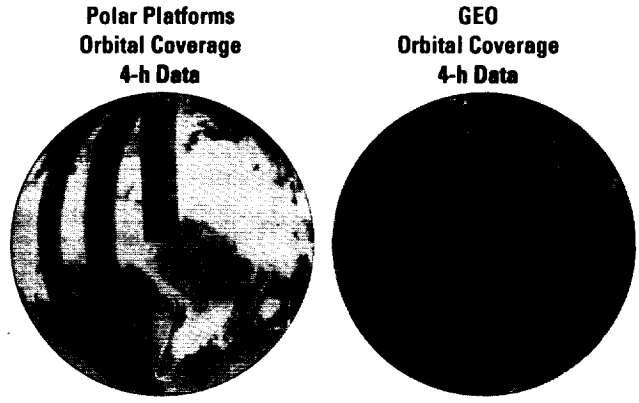

GEO Provides Continuous Coverage

Frequency of observations.

V.W. Keller/PS02
205–544–2470
Sponsor: Office of Space Science and Applications

Laser Power Beaming

Over the past several years, the Department of Defense (DOD) and the Department of Energy (DOE) have done development work on **laser power** beaming, which has now been declassified. This provides a body of knowledge and some developed technologies that should be useful to NASA and others. The ability to beam **power** from the ground to elements in space could benefit a variety of users. Basic disciplines, such as astronomy, communications, and others, could also benefit from the technology development.

During fiscal year 1992 (FY92), MSFC led an inter-Center activity, in cooperation with segments of DOD and DOE, to build on these foundations and to continue work on development of technologies critical to **laser power** beaming. The major thrust has been toward development of items that would support accomplishment of a **laser power** beaming demonstration in 1998, with output **power** levels of approximately 1 to 3 MW (1,340 to 4,021 hp), using a beam expander of approximately 10- to 12-m (33- to 39-ft) diameter. Potential applications of an operational system could be to provide **power** to geostationary Earth orbit (GEO) satellites, **power** to electric orbit-transfer vehicles, **power** to the lunar surface, etc.

Technology work in progress in FY92 included development of free-electron **laser** accelerator modules, **adaptive optics** segments, control algorithms, beam expander elements, and others. The dimensions of atmosphere turbulence drive the optical segment sizes to be on the order of 2 to 3 cm (0.8 to 1.2 in) in diameter. Consequently, many thousands of such segments must be used to cover an entire primary mirror of 10 to12 m (33 to 39 ft) in diameter. For economic reasons, segments must be able to be easily and cheaply mass-produced.

Each segment must be controllable, and the large number of segments drives the control system toward a hierarchical, decentralized system that uses a large degree of parallel processing. Several segments were produced and tested at MSFC in FY92, leading toward a cluster of segments to be built and tested in a cluster test-bed in FY93.

E. Montgomery/PS04
205–544–1767
Sponsor: Office of Aeronautics and Space Technology

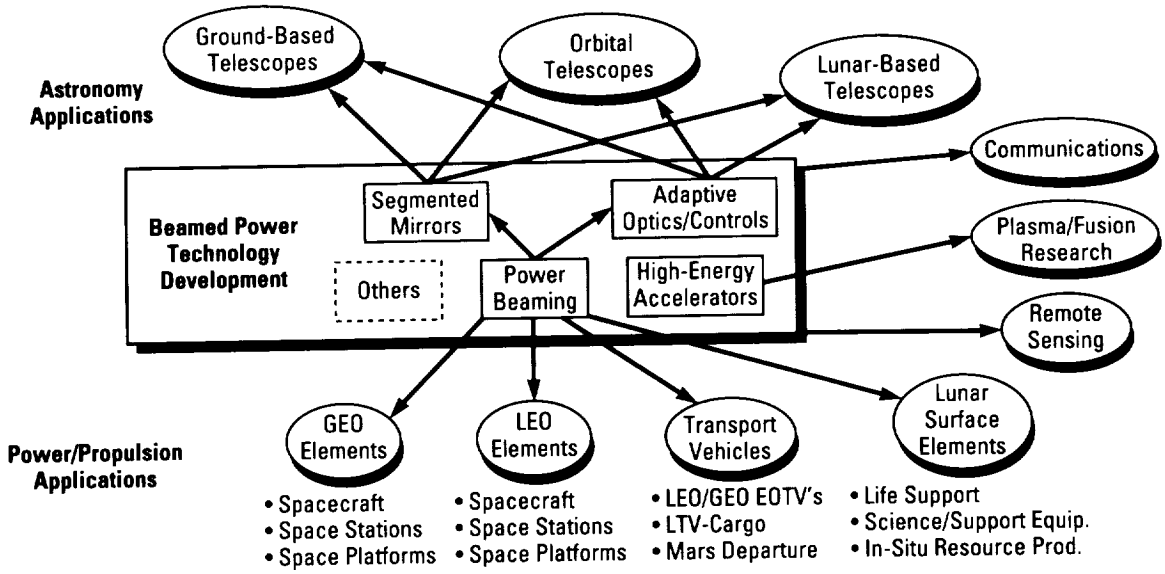

EOTV — Earth Orbit Transport Vehicle
LEO — Low Earth Orbit
LTV — Lunar Transfer Vehicle

Laser power beaming technologies, which are applicable to many missions.

Space Station Advanced Programs

During 1992, MSFC continued its **advanced programs** activities related to the evolutionary **space station**. Examinations of the latest user requirements and mission models have indicated that the need for growth of internal systems within a given module appears to be minimal. The principal approach for increasing the size of the crew and/or for adding major internal systems capabilities is through the addition of modules. It is anticipated that improved technologies for various internal systems can be accommodated within the basic power, thermal, and volume constraints now levied on the permanently manned capability (PMC) systems. The eight crew capability (ECC) growth configuration would follow the PMC configuration, and "**evolution**" configurations would follow after that.

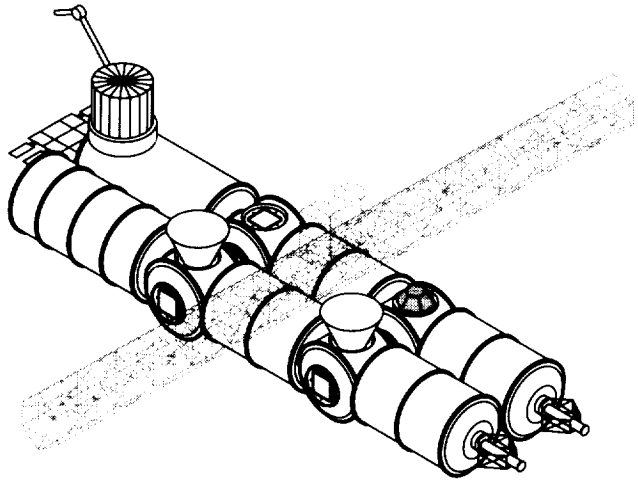

S.S. *Freedom* ECC ("growth" configuration).

Assessment was begun, and is continuing, of level III **evolution** requirements to determine impacts on level III elements. The main thrust here is to minimize impacts on **Space Station** *Freedom* (S.S. *Freedom*), yet ensure that S.S. *Freedom's* main features will not preclude reasonable **evolution**. Studies of evolutionary logistics requirements and systems concepts were also done in 1992. Attention was given to options utilizing the cargo transfer vehicle (CTV), as well as the space shuttle, as an expendable logistics vehicle.

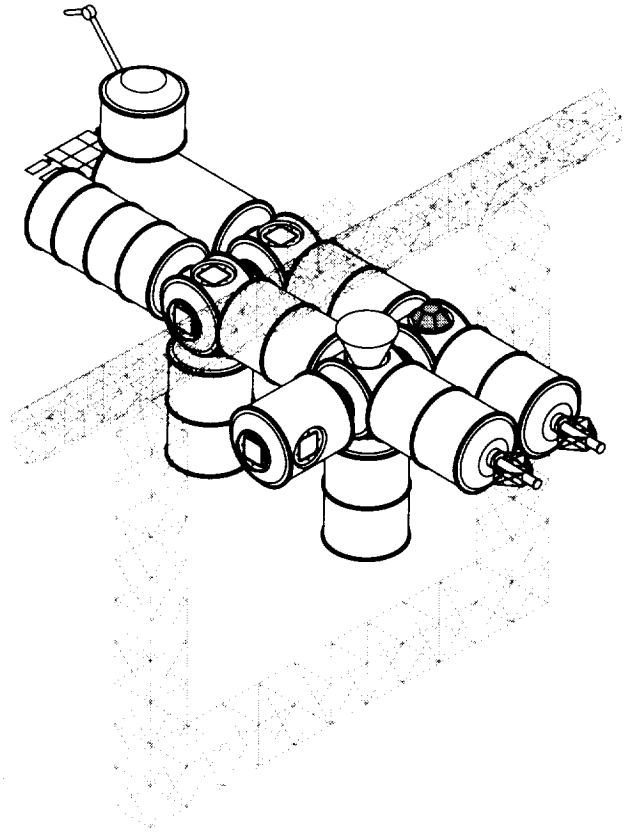

S.S. *Freedom* "evolution" option.

Advanced development work continued in **automation** of (1) the carbon dioxide (CO_2) removal assembly (CDRA) and (2) the power management and distribution (PMAD) subsystem. Automated CDRA fault detection and diagnosis technology was integrated into the predevelopment operational systems test (POST), leading to potential incorporation of such capabilities in the S.S. *Freedom* baseline system. Automated PMAD monitoring and control software was developed and demonstrated in the PMAD test-bed, and work began on modification of portions of the software for potential use in the S.S. *Freedom* baseline system.

J.M. Butler/PS04
205-544-4833
Sponsors: Office of Space Systems Development and Space Station Engineering

Tether Applications in Space

The objective of research into **tether** applications in space (TAS) is to develop the use of **tethers** in a broad range of space activities. During 1992, NASA's first **tether** system, the tethered satellite system (TSS), had a successful initial flight on the shuttle, demonstrating electrodynamic effects using a **tether**, deployment/retrieval of a **tether**, stationkeeping, and other attributes. NASA's second type of **tether** deployer, the small expendable deployer system (SEDS), is being readied for flight. SEDS will fly as a secondary payload on a Delta expendable launch vehicle in 1993 and will demonstrate a low-cost method of deploying **tether** systems where retrieval is not required.

Planning and engineering support continued for follow-on SEDS missions, such as the closed-loop control mission, Johnson Space Center's (JSC's) plasma motor generator (PMG) mission to study electrodynamic effects, and a student-developed satellite (called SEDSAT), which is a mission to study upward deployment and release of a tethered payload. A very limited amount of work was also done on a low-frequency communication system utilizing a **tether** as an antenna and on a tethered payload for atmospheric research. Planning is also continuing for a small artificial gravity facility (SAGF) as a follow-on SEDS mission and for reflight of the electrodynamic mission with additional instrumentation.

Definition continued of the "**tether** tracker," which will provide a television (TV) instrumentation system capable of viewing a **tether** as it deploys. Improvements were made in **tether** control laws and models/simulations, incorporating data from ground tests of the SEDS deployer and command/data assembly.

A small amount of effort was given to reexamination (updating work previously performed) of the potential use of a **tether** for momentum exchange between **Space Station** *Freedom* (S.S. *Freedom*) and deorbiting elements. Many thousands of pounds of vehicles, **trash**, payload carriers, and other equipment must be deorbited from the vicinity of S.S. *Freedom* each year. Under present planning, propulsion systems and propellant for deorbit of all such **trash** must be provided and carried to orbit. If a safe, efficient **tether** system between S.S. *Freedom* and the **trash** could be implemented, the resulting momentum exchange would provide a needed reboost to S.S. *Freedom*, simultaneously eliminating the need for deorbit systems and/or propellant and the cost to transport them to orbit. Work on **tether** systems for deorbiting S.S. *Freedom* **trash** and recoverable items is planned to continue.

C.C. Rupp/PS04
205–544–0627
Sponsor: Office of Space Systems Development, Advanced Programs

Transportation Systems

Advanced Transportation System Study

NASA is currently analyzing alternatives to establish the desired path for future **unmanned** and **manned** launch vehicles. MSFC recently initiated four major **advanced transportation system study** (**ATSS**) contracts to investigate future **manned** and **unmanned** launch vehicle needs, their propulsion systems, and the overall space transportation architecture. These efforts are with Rockwell International Corporation (RIC), Lockheed Missiles and Space Company (LMSC), Rocketdyne (RKD), and General Dynamics Corporation (GDC). These activities are directed at satisfying the civil needs requirements, including those that the **Space Exploration Initiative** (**SEI**) will place on the **Earth-to-orbit** (**ETO**) transportation systems early in the next century.

The **SEI** requirements will dictate the need for new **heavy lift launch vehicle** (**HLLV**) capabilities. The studies will determine the best path to follow, both technically and programmatically, to develop the capability to meet these requirements. They will examine the entire **ETO** infrastructure, including ground-processing and supporting facilities, as well as the launch vehicles themselves. Specific areas to be addressed are resiliency/assured access, safety, operability, and affordability. The results of these studies will be used to formulate credible **ETO** infrastructures needed to satisfy both the **manned** and **unmanned** space transportation requirements.

A multi-Center activity to investigate all aspects of returning to the Moon by 1999 for the First Lunar Outpost (FLO) mission began in January 1992 and is continuing. Among the areas of concentration is the conceptual design of candidate space transportation systems (STS's) that meet the FLO requirement of placing 34 t (75,000 lb) on the lunar surface. This equates to a post translunar injection (TLI) requirement of 93 t (205,000 lb). A single **HLLV** will be utilized for each flight to the Moon to minimize complex space operations. The first mission will place the habitat module on the surface followed by a second mission containing the crew, lander, and ascent system.

A number of vehicle concepts has been investigated, but two concepts have been baselined that meet mission requirements while maximizing use of existing equipment and designs. One concept is derived primarily from the **National Launch System** (**NLS**) and uses a stretched external tank (ET) core with four **space transportation main engines** (**STME's**). Four strap-on boosters with two F–1A engines each provide the necessary additional thrust at liftoff. The TLI stage uses a single **space shuttle main engine** (**SSME**). The total vehicle height is approximately 107 m (350 ft). Another concept is derived from the **Saturn** V. The vehicle uses five F–1A engines as the core stage, two strap-on boosters with two F–1A engines each, a second stage with six J–2S engines, and a TLI stage with a single J–2S engine. This vehicle height is approximately 125 m (410 ft), which is more than 40 ft taller than the **Saturn** V. MSFC has contracted with LMSC to further investigate the baselined vehicles as well as additional derived and "clean-sheet" concepts.

Manned launch systems studies generally fall into one or more of the following three paths: space shuttle evolution, the **personnel launch system** (**PLS**), and the **advanced manned launch system** (**AMLS**). Shuttle evolution deals with major block changes to the space shuttle, as opposed to the current shuttle improvements under way. A near-term block change is the planned incorporation of the advanced solid rocket motors (ASRM's). Future changes under study include advanced avionics, use of electromechanical actuators (EMA's), and use of aluminum-lithium (Al-Li). The **PLS** study is assessing the feasibility of separating man from cargo. The potential of launching a **manned** capsule or cargo return vehicle (CRV) on existing and/or new launch vehicles is being studied. The launch vehicle options include the **NLS** 1.5-stage vehicle. The **AMLS** will be the next-generation reusable **manned** transportation system to replace the existing space shuttle. The vehicle may be capable of transporting both crew and cargo to low Earth orbit (LEO). However, its cargo-carrying capability may be less than the shuttle since alternate **unmanned** vehicles will be available for heavier payloads.

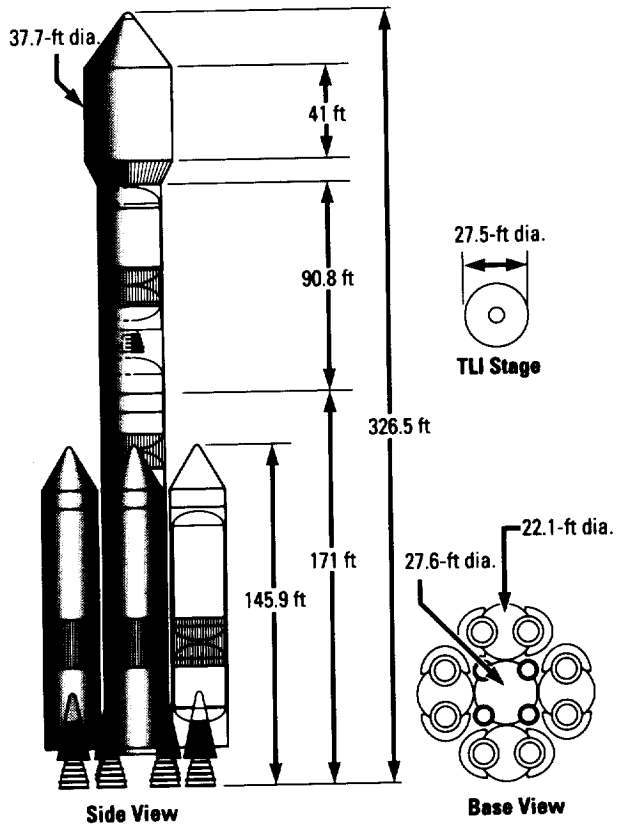

NLS-derived HLLV for lunar mission.

Activities toward development, remanufacture, or modification of the engines for these vehicles are under way. The **STME**—a new gas generator, 650,000 lbf (2,900 N) thrust, low-cost engine (estimated cost per engine of approximately $10M per unit)—is being actively developed by the Department of Defense (DOD)/ NASA Joint Program Office utilizing an engine consortium consisting of RKD, Pratt and Whitney (P&W), and Aerojet. A key feature of this development is the ability to manufacture for minimum cost.

Remanufacture of the F–1A and J–2S engines from the **Saturn** program is being actively investigated to determine the specific configurations to remanufacture. The necessary approach, development, testing, cost, and schedules are also under study. Consideration is being given to the use of new materials for selected components, since improved materials are available today for the pumps and turbine blades and other parts. Also, new features, such as health monitoring and throttling, are being considered for modernizing these engines.

Modification of the **SSME** for use as a TLI engine is being studied to determine which new systems are needed, modifications to existing systems, required development and testing, cost, and schedules. For this application, the engine must start at an altitude prior to orbital injection and must restart at least once in orbit. At altitude, due to the lower atmospheric pressure, the normal bootstrap startup of the **SSME** is done with reduced inlet pressures, lower flowrates, and changed valve settings and orifices to accommodate correct startup fuel/oxidizer ratios.

Overall, the **ATSS** contracts, which consider **manned** and **unmanned** launch vehicles, new and improved propulsion systems, and a coordinated architecture approach, should provide a balanced space transportation program for the future.

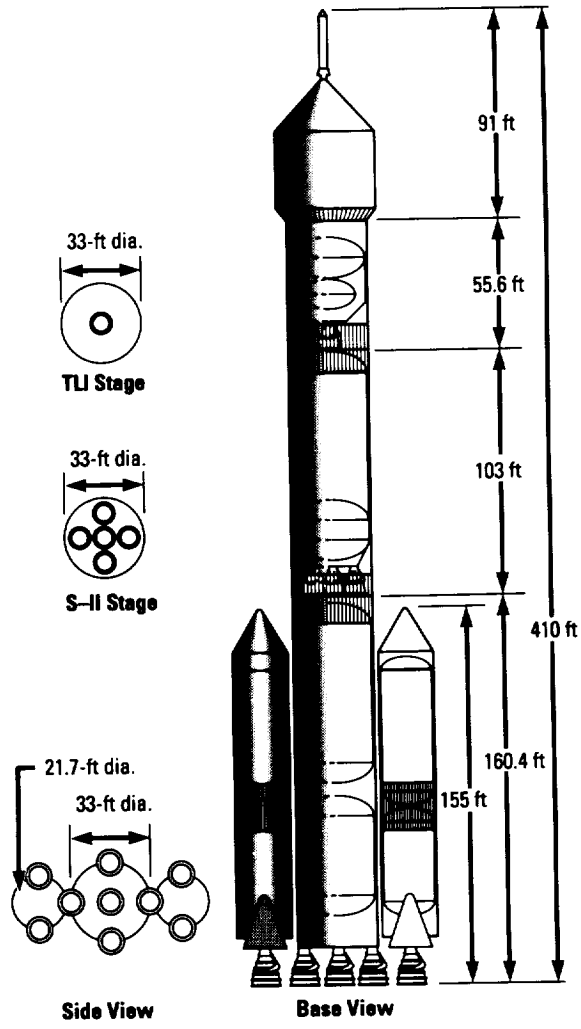

Saturn V-derived HLLV for lunar mission.

G. Johnson/PT21
205–544–0636
Sponsor: Office of Space Systems Development

Electromechanical Actuation for Launch Vehicles

Electromechanical actuators (**EMA's**) have undergone a rebirth of design and development at MSFC in the area of launch vehicle ascent control. In the very early days of rocketry, control vanes that deflected the thrust of a rocket engine were driven by small electrical motors. However, as the size of launch vehicles increased, entire rocket engines had to be gimbaled in order to achieve the required degree of **thrust vector control** (**TVC**). Until recently, the tremendous power requirements of these **TVC** systems were far beyond the capabilities of available electrical switching technology. Hydraulic **TVC** systems have traditionally been called upon to perform this task, with an impeccable record of successful launch and ascent control spanning three decades. However, the success of these complex, distributed hydraulic **TVC** systems has come at the expense of significant integration, operational, and maintenance costs. Recent advances in high-power semiconductor switching technology have thus warranted the development of a new generation of **EMA's** as part of NASA's pursuit of better and more cost-effective launch vehicles.

This past year, a multidiscipline team of MSFC engineers from the Component Development Division of the Propulsion Laboratory and the Guidance, Control, and Optical Systems Division of the Information and Electronic Systems Laboratory successfully fabricated, assembled, and tested a 35-kW (50-hp) electromechanical-**TVC** (EM–**TVC**) system to establish the feasibility of developing even higher power, protoflight units. The generic design of this EM–**TVC** system encapsulates the basic performance requirements of the hydraulic **TVC** systems on the space transportation system (STS). This dual-channel actuator employs two 17.5-kW (25-hp) brushless, direct current (dc) permanent magnet (PM) motors attached through a common gear train (8.75:1 reduction ratio) to a linear roller screw to control the position of a large inertial pendulum, simulating a **space shuttle main engine** (**SSME**), at rates of 14 cm/s (5.5 in/s) at a rated load of 178 kN (40,000 lb). Already, this EM–**TVC** system has successfully demonstrated the capability of following both **SSME** and solid rocket booster (SRB) command profiles, as recorded in the STS flight data base, with a linearity and accuracy that exceeds the current flight systems.

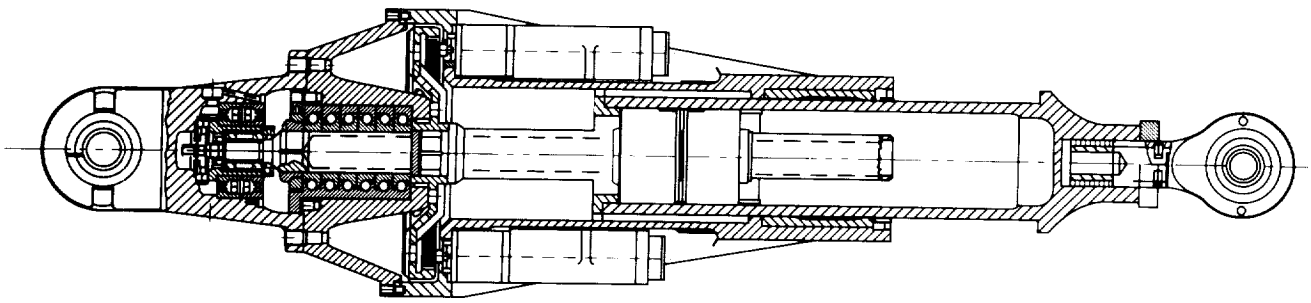

- Four-Channel, 15-hp PM dc Motors
- 9.6:1 Single Pass Gear Reduction w/0.4-in Roller Screw Lead
- Rated Load of 60,000 lbf
- Rated Velocity of 5 in/s
- Maximum Stroke of ±5.25 in
- 4.2-Hz Control Bandwidth

MSFC 45-kW (60-hp) EMA with four PM motors.

The **EMA** team at MSFC has also completed the design and is currently engaged in the fabrication of a four-channel EM–**TVC** system that will meet the redundancy requirements of the existing **SSME TVC** system. This advanced development EM–**TVC** employs four 11.2-kW (15-hp) dc PM motors acting in unison, any three of which are capable of meeting the **SSME TVC** power requirements. An aggressive EM–**TVC** test plan will subject this unit to a series of simulated **SSME** flight profiles, comprised of position commands and external loads derived from flight telemetry, followed by vibration, shock, thermal, and electromagnetic interference (EMI) verification tests. The pinnacle of this quad-channel 45-kW (60-hp) EM–**TVC** development plan will be an **SSME** hot-fire demonstration on MSFC's technology test-bed (TTB) in late 1994.

The above **EMA** technology development at MSFC has been paralleled by the development of EM engine control valves (ECV's), such as the main oxidizer valve (MOV) on the **SSME** and the main propellant valve (MPV) on the **space transportation main engine** (**STME**). A prototype EM–MOV, which had been previously designed, fabricated, and assembled by the MSFC **EMA** team, is completing a series of characterization tests this year. This single-channel unit, featuring a single 10-kW (13.4-hp) dc PM motor, is the precursor to a set of flight-quality EM–ECV's that are being developed under contracts managed by MSFC. This year, an EM–MOV actuator will be delivered that has been designed as a line replaceable unit (LRU) for the existing, hydraulically actuated **SSME** MOV. This unit will undergo a rigorous set of qualification tests, analogous to the quad-channel EM–**TVC** test series, in preparation for an **SSME** hot-fire demonstration in late 1994 on the TTB. An EM–MPV, being developed under another contract managed by MSFC, for the **STME** has completed a critical design review this year and will be fabricated, assembled, and tested over the next 2 yr in preparation for an **STME** hot-fire test in 1996.

The combined development of **EMA's** for **TVC** and ECV's will provide the capability to replace all of the distributed hydraulic systems on current launch vehicles with self-contained, line-replaceable **EMA's** with built-in test (BIT), health-monitoring, and redundancy management capabilities. As **EMA** design issues are resolved by the development and test programs outlined above, the last critical item to be resolved in maturing this technology application will be the integration of **EMA's** with the electrical power source systems. Studies are under way to demonstrate integrated **EMA** tests with both advanced battery and turbo-alternator technologies over the next 2 yr. These combined efforts offer such promising rewards that **EMA** systems have been baselined for the **new launch system** (**NLS**).

J.P. Sharkey/EP64
205–544–1437
Sponsors: Office of Space Systems Development and Office of Aeronautics, Exploration, and Technology

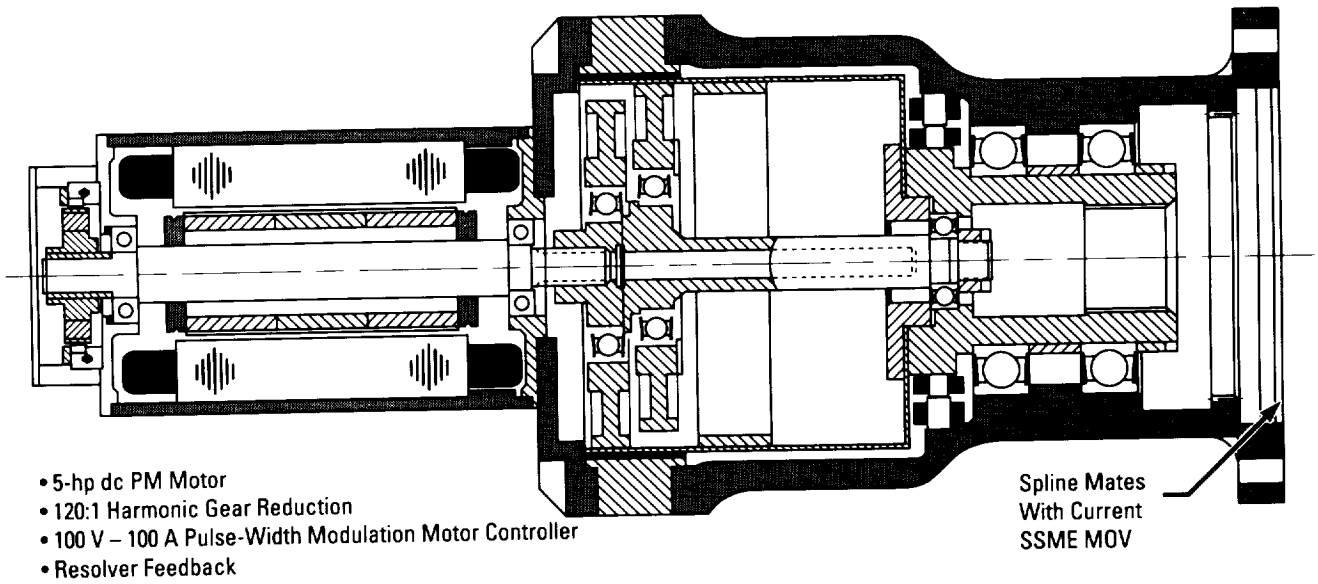

MSFC simplex SSME propellant valve actuator.

Space Exploration Initiative

The **Synthesis Group**, under the leadership of Lt. General Tom Stafford (U.S. Air Force (USAF), retired), was formed to assess the innovative ideas about the **Space Exploration Initiative (SEI)** received through the Outreach Program. Over the 10-mo period, the group sifted through the many submissions and listened to a variety of presentations, and, as a result, developed four architectures, or paths, for pursuing exploration. These architectures provide the framework for defining the scope and scale of the **SEI**. The methodology used by the group characterizes the architectures in terms of operational capabilities, such that decisions are assumed at key milestones to formulate the architecture path. This original concept of decision flexibility, based on knowledge gained, has been adopted by NASA for **SEI** mission planning.

Several recommendations were made by the **Synthesis Group** in order to best advance the **SEI** efforts. These recommendations included:

- Initially, do not overemphasize any single architectural theme
- Focus on the near-term missions (within the overall architectural context)
- Advocate robotic, precursor missions to the Moon and Mars in support of human missions
- Follow a campsite approach for the first human lunar missions
- Fly minimum crew size on initial lunar missions
- Determine the most effective heavy lift launch vehicle (HLLV) capability for the approach chosen by **SEI**.

NASA's Exploration Programs Office has already accepted these recommendations and is currently involved with planning for lunar precursors, martian precursors, and lunar campsite missions. Definition studies are being conducted for a lunar campsite option called the **First Lunar Outpost (FLO)**, which is the initial manned component of **SEI**. The **FLO** design activity is an on-going mission definition and requirements development process that will progress through numerous iterations before the final selection of a technical approach. These studies have already begun to provide new details and new decisions. For example, the human return missions to the Moon will be designed to stay for 45 d in a campsite mode. This will require a **lunar habitat** that will be reusable and will provide the option to return to the campsite. Hence, evolution options to the initial campsite include establishing alternative campsites or enhancing the campsite for longer duration missions.

MSFC continues its assigned role to analyze the space transportation concepts and options in support of the definition studies for the **FLO** project. The scope of this effort includes designing the HLLV, the translunar injection (TLI) stage, and the surface habitat in support of the mission requirements. Additionally, MSFC supports the design activities for other **FLO** elements such as the lunar cargo/piloted lander and crew module, as well as science surface activities.

The HLLV concepts under consideration to support the **FLO** project include an evolutionary version of the **National Launch System (NLS)**, a derived version from the **Saturn V** vehicle, and new "clean-sheet" versions. All options utilize liquid oxygen (lox)/rocket propellant (RP) boosters. Both the cargo and piloted flights utilize a "lunar-direct" mission mode to the Moon with no rendezvous and docking, thereby greatly simplifying the operations on the ground and on-orbit required in a multiple launch scenario. A direct mission mode also allows global lunar access combined with the capability to return to Earth at any time.

The lunar transportation systems concepts include both expendable and partially reusable vehicles. The TLI stage is a cryogenic propellant stage that is designed to perform a suborbital burn to Earth orbit as well as to perform the translunar burn for both the cargo and piloted vehicles. Because the required delivery masses to the lunar surface are similar for both the habitat and the piloted vehicle, a common cryogenic lander descent stage design is being pursued.

The present design for the return stage of the piloted vehicle utilizes a storable propellant concept for a direct return to Earth of an Apollo-type crew module. However, cryogenic propellant options are also being studied.

First Lunar Outpost.

The habitat requires minimal activation operations by the crew prior to occupation. Since the habitats are predeployed to the surface and verified before the crew begins their part of the mission, the crew will have a high confidence that only a nominal set of extravehicular activity (EVA) operations will need to be conducted before they can occupy the habitat. The present concept utilizes a Space Station *Freedom* (S.S. *Freedom*)-derived module on a similar cryogenic lunar lander as the piloted vehicle. The habitat must be capable of a 45-d mission and, with resupply of consumables, it can sustain multiple revisits evolving to longer crew missions. Other configurations are being studied to reduce mission costs and hardware development.

In order to reduce the transit time between Earth and Mars, the **nuclear thermal propulsion** capability must be developed for both the human and cargo transportation to Mars. With its higher specific impulse, nuclear systems promise high performance with significant savings in propellant mass as compared to chemical systems. Since launch rates are heavily dependent on the initial mass to low Earth orbit (LEO), the nuclear systems with their commensurate smaller propellant needs involve lower overall launch demands. However, **nuclear thermal propulsion** is not being considered as an option for lunar transportation.

In the area of nuclear surface power systems, the recommendation to use nuclear power is principally based on the reliability and mass savings over photovoltaics with energy storage. The initial nuclear unit development is for the lunar outpost where deployment and safe, reliable operations are validated.

Concept studies will continue leading to phase studies.

W.J. Pattison, Jr./PT31
205–544–0465
Sponsor: Office of Space Exploration

Research Programs

Innovative approaches and techniques in Marshall's ground-based, suborbital (balloons, aircraft, and rockets), and orbit-based research programs have produced many notable advances in space science during the past year. Included are exciting advances in understanding the structure of protein molecules through microgravity science experiments aboard the shuttle and ground-based experimentation. Among these, crystals suitable for the structure determination of an antibody to the human immunodeficiency virus (HIV–I) type were grown and the three-dimensional structure determination of the antibody was solved.

Center astrophysicists and their colleagues, using an MSFC-designed and -built instrument, the Burst and Transient Source Experiment (BATSE) aboard the Compton Observatory, have made important discoveries concerning gamma-ray bursts. To date, over 400 bursts have been observed and, contrary to what was expected, BATSE investigators have found that these bursts are not confined to the plane of the Milky Way galaxy, but appear to be isotropic. In addition, a gamma-ray pulsar source and the strongest x-ray nova yet observed were discovered.

In Earth science research, microwave radiometers have been flown on satellites since 1978 to measure the thermal emission of radiation by oxygen in the atmosphere. The analysis of the entire microwave sounding unit data archives had never before been attempted. Using these data, Marshall scientists were able to determine the global temperature variations over the 10-year period from 1979 to 1988.

The analysis of solar data from the Marshall/ Stanford rocket-borne solar telescope has yielded several exciting results, including confirmation that coronal loops have a constant cross section resulting in a "rope-like" structure.

A Marshall-developed infrared imaging camera has, for the past 5 years, been the most sensitive infrared camera in the world, operating at long infrared wavelengths from ground-based observatories. Among the many exciting observations made with this instrument is the investigation of particles in other "planetary systems." The star Beta Pictoris is thought to have a planetary system now forming around it. The Marshall array camera was used to detect particles in the planetary disk of that star and made the first measurement of the composition of those particles.

E.A. Tandberg-Hanssen
Acting Director,
Space Science Laboratory

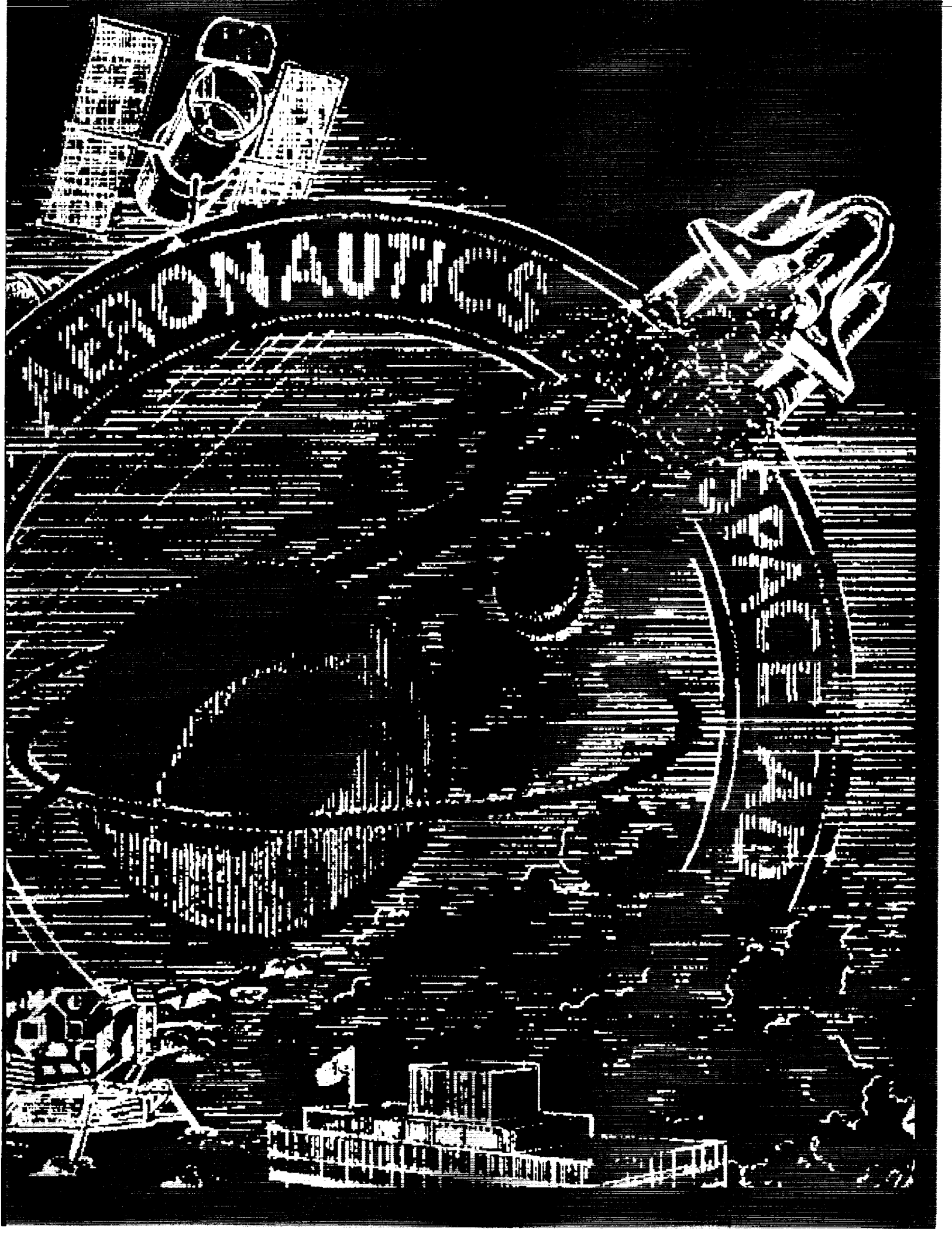

Astronomy and Astrophysics

Exploration of the universe, which involves astronomy and astrophysics, is one of NASA's major missions. Information about the state and evolution of the universe comes to researchers in the form of radiation, which covers the whole spectrum of electromagnetic radiation from radiowaves through infrared (IR), visible, and ultraviolet (UV) to the high-energy radiation of x rays and gamma rays and the particle radiation of cosmic rays. The Earth's atmosphere blocks incoming radiation in large regions of the spectrum; this requires observations to be made from space outside the Earth's atmosphere.

MSFC has a long history of developing scientific experiments and managing scientific projects and missions in astronomy and astrophysics starting with Skylab and including the three high-energy astronomy observatories, the Hubble Space Telescope (HST), and several Spacelab missions with a variety of experiments including the Astro-1 payload. Astro-2 and the Advanced X-Ray Astrophysics Facility (AXAF) are future missions presently under development.

The Astrophysics Division of the Space Science Laboratory has ongoing research programs in x-ray and gamma-ray astronomy, cosmic ray research, and IR astronomy. Research activities cover experimental and theoretical research, development of scientific instruments and space flight experiments, and related advanced technology including superconducting instrumentation. A balloon flight program is being conducted for high-energy astrophysics research and to test new detector systems and instruments for x-ray and gamma-ray astronomy and cosmic ray research. Presently, one of the major science operations is the data acquisition and analysis from the Burst and Transient Source Experiment (BATSE) on the orbiting Compton Observatory.

Burst and Transient Source Experiment Discovery of a Gamma-Ray Pulsar

The **Burst and Transient Source Experiment** (**BATSE**) on the **Compton Observatory** has as its principal objective the observation and mapping of the enigmatic **gamma-ray** bursts; however, it can also observe pulsed sources over the entire sky. For sources with periods greater than a few seconds, searches can be performed on the data after receipt. To permit detection of shorter period objects, special hardware exists in the **BATSE** data system to fold the data onboard at the approximate period of a candidate object.

During orbits when playback of burst data is not in progress, which is approximately 75 percent of the time, pulsar data collected from four to six objects fill the telemetry space. An example of the new discoveries that **BATSE** has made is the detection of the pulsar PSR1509–58 at **gamma-ray** energies, which is summarized in this report.

Prior to the launch of the **Compton Observatory** in April 1991, only two of the approximately 450 known radio **pulsars** had been detected at **gamma-ray** energies: the Crab and Vela **pulsars**. While the pulse profiles of these two objects are very similar at energies above 35 MeV, the spectra of the objects in the hard x-ray region (50 to 500 keV) must be very different, since only the Crab pulsar is observed there.

Both these objects are among the youngest of the known **pulsars**, as estimated by the period spindown rate. At x-ray energies (5 to 40 keV), another radio pulsar had been observed by the Japanese "Ginga" experiment. The hard spectrum they measured suggested a **BATSE** observation might be successful.

In results obtained by **BATSE** from a 723,000-s (8.4-d) observation of the source, the pulse profile is similar, but somewhat more narrow than that found at x-ray energies, and it is much different than that obtained for the Crab pulsar, as shown in the **BATSE** profile for that source.

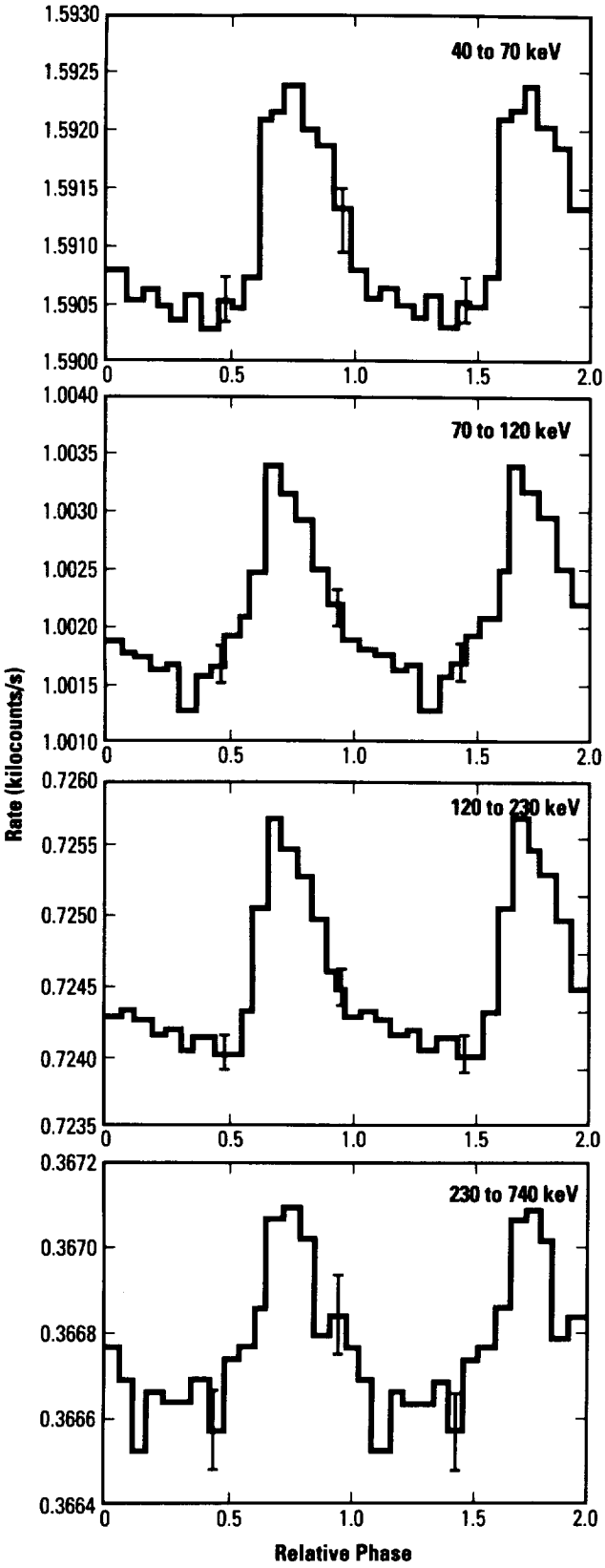

Pulse profiles for PSR 1509–58 obtained by BATSE for a 723,000-s exposure.

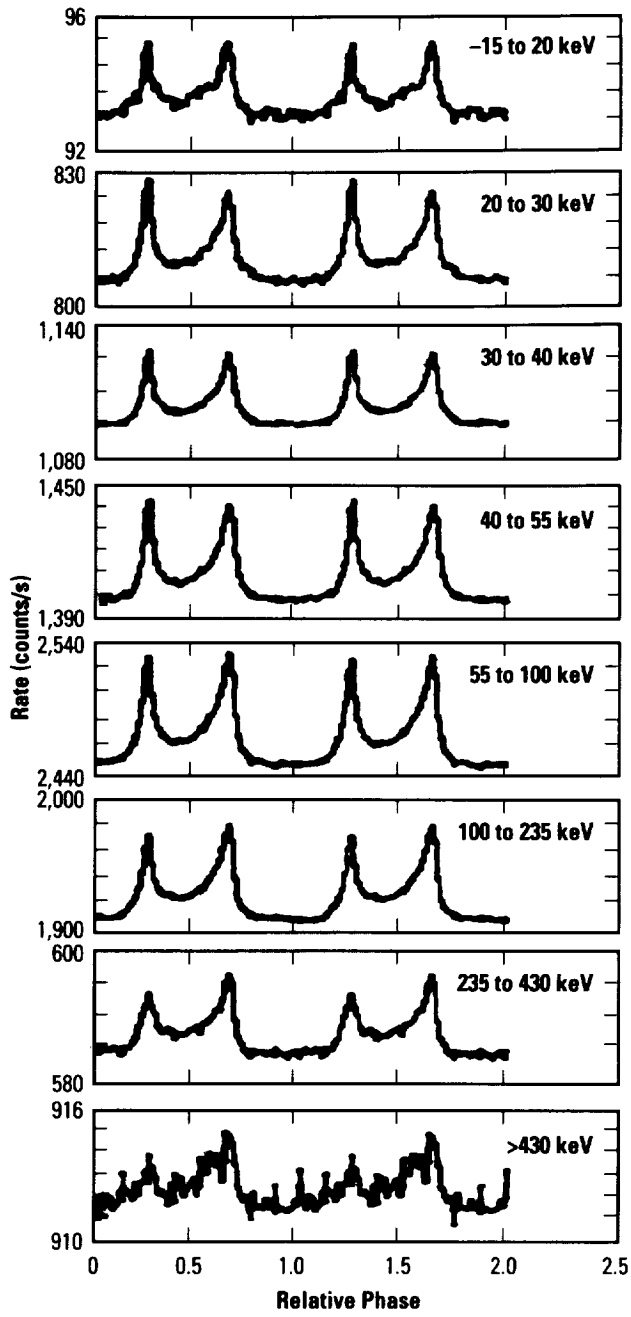

Pulse profile of the Crab pulsar obtained for a 2-wk Compton Observatory pointing.

Evidence exists in the **BATSE** data for continuance of the hard spectrum to even higher energies: in the integral energy channel recorded by the experiment, greater than 1.8 MeV, a weak source emission feature appears at the same phase as the peak measured at lower energies. Efforts to explain the observed spectrum of **gamma-ray pulsars** have yet to be fully successful. The data from the third such object, PSR 1509–58, should supply useful discriminants among the currently favored models.

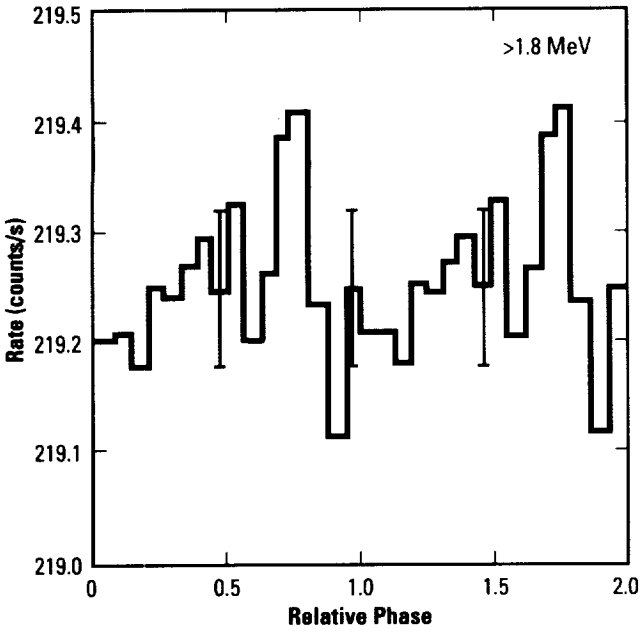

Pulse profile for PSR 1509–58 at energies above 1.8 MeV.

Data are being collected at the periods of other young radio **pulsars**, with the goal of detecting other **gamma-ray pulsars**.

Fishman, G.J., Meegan, C.A., Wilson, R.B., Paciesas, W.S., Parnell, T.A., Matteson, J.L., Teegarden, B.J., Cline, T.L., Pendleton, G.N., and Schaefer, B.E., "The Burst and Transient Source Experiment (BATSE): Scientific Objectives and Capabilities," Proceedings of the Gamma-Ray Observatory Science Workshop, April 1989, Greenbelt, MD, W.N. Johnson, ed., p. 3–47.

Wilson, R.B., Harmon, B.A., Finger, M.H., Fishman, G.J., Meegan, C.A., and Paciesas, W.S., "Long-Term Source Monitoring With BATSE," Proceedings of the Compton Observatory Science Workshop, September 1991, Annapolis, MD, C.R., Shrader, N. Gehrels, and B. Dennis, eds., p. 35.

Wilson, R.B., Finger, M.H., Pendleton, G.N., Fishman, G.J., Meegan, C.A., and Paciesas, W.S., "BATSE/CGRO Observations of Isolated Pulsars," Proceedings of the Taos Workshop on Isolated Pulsars, February 1992, N.M. Taos, K.A. Van Riper, R. Epstein, and C. Ho, eds., in press.

R.B. Wilson/ES62
205–544–7695
Sponsor: Office of Space Science and Applications

Burst and Transient Source Experiment Observations of the Distribution of Gamma-Ray Bursts

Gamma-ray bursts remain one of the most puzzling phenomena in astrophysics. They last from a fraction of a second to hundreds of seconds and have never been detected with certainty at any other wavelengths. In spite of two decades of research, the source objects and emission mechanisms are still unknown. Most theories of **gamma-ray bursts** assume they are caused by some cataclysmic event on a neutron star, such as a thermonuclear explosion of accreted matter or a collision with a comet or asteroid.

One of the main goals of the Burst and Transient Source Experiment (BATSE), one of four instruments on the **Compton Observatory**, is to determine the spatial distribution of the sources of **gamma-ray bursts**. By comparing the count rates on the eight BATSE detectors, the direction to a burst can be computed with an accuracy of a few degrees. It was expected that BATSE would find the **bursts**, particularly the weaker ones, clustered in the plane of the galaxy. Previous experiments were able to obtain locations only for the brightest **bursts**, which were believed to be too nearby to reveal the galactic plane.

Contrary to expectations, BATSE observations[1] revealed that the **bursts** were distributed isotropically in the sky. There is no concentration in the galactic plane or toward the galactic center. Statistical tests confirm that the distribution is truly random. By itself, this observation would indicate a uniform distribution of sources in space, out to the maximum distance from which **bursts** can be seen by BATSE. However, the number of weak **bursts** detected by BATSE is much smaller than expected for such a model. Statistical tests that properly account for instrument sensitivity indicate that the density of burst sources must decrease with distance.

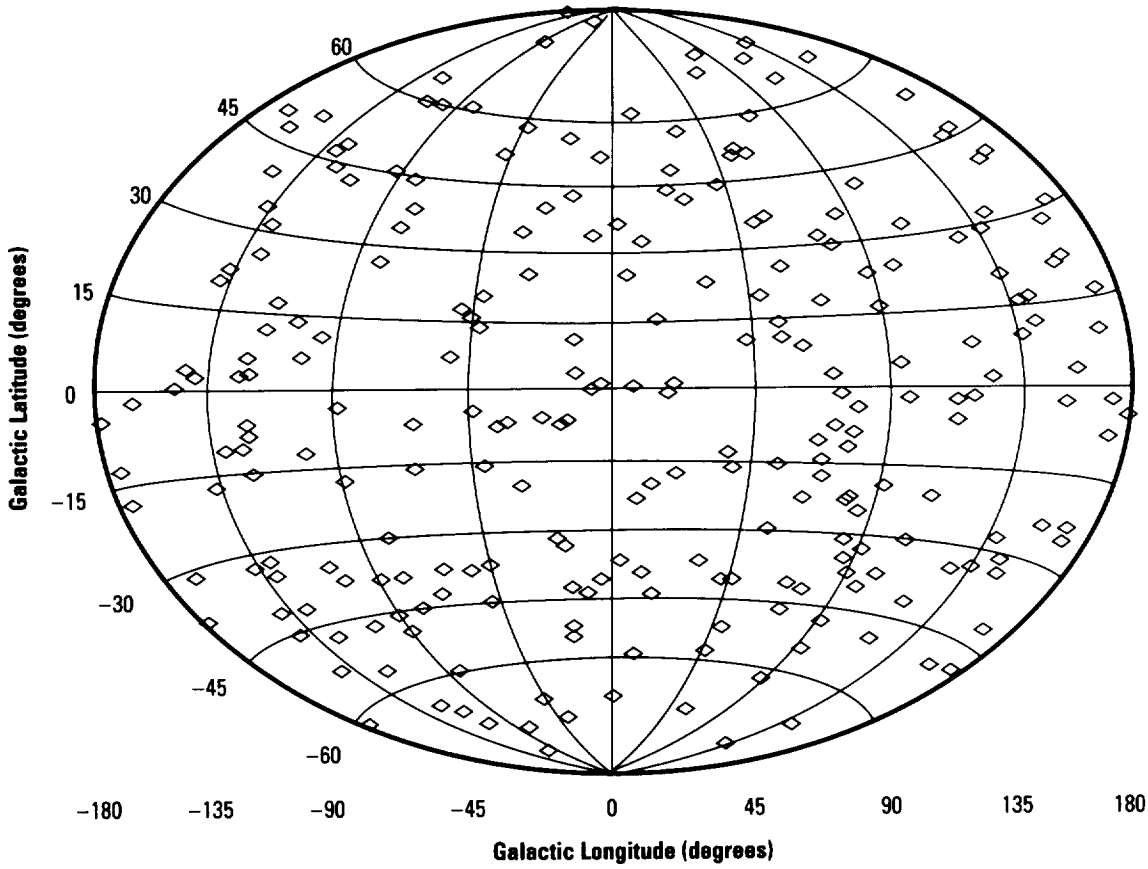

The angular distribution of 261 gamma-ray bursts observed by BATSE.

These observations imply a roughly spherical distribution of burst sources centered approximately on the Earth, with the density decreasing with distance. No known objects in the Milky Way galaxy have such a distribution. Nearby objects are isotropic, but have uniform spatial density. More distant objects show concentrations in the galactic plane or toward the galactic center.

Several possible solutions have been suggested. The **bursts** may be some outer solar system phenomenon, perhaps in the cloud of comets around the Sun. But there appears to be no satisfactory way of generating **gamma-ray bursts** from comets. Another possibility is that there is a very extended halo around the galaxy containing the burst sources. However, this halo would have to be much larger than the distance from the Sun to the galactic center, and there is no evidence for such a halo, nor any satisfactory way to populate it with neutron stars. The last possibility is that the **bursts** are occurring in very distant galaxies. The isotropy is naturally explained by this suggestion and redshift effects would account for the deficit in the number of weak **bursts**. This model would suggest that **bursts** are much more energetic than previously believed. Future BATSE observations may resolve the question of the origin of **gamma-ray bursts**. Whichever explanation turns out to be correct, the BATSE observations have revolutionized researchers' ideas about these enigmatic events.

[1]Meegan, C.A. et al., "Spatial Distribution of Gamma-Ray Bursts Observed by BATSE," *Nature*, vol. 355 (1992), p. 143.

C.A. Meegan/ES62
205-544-7694
Sponsor: Office of Space Science and Applications

Gravity Probe-B

Gravity Probe-B (GP–B) is an experiment in fundamental physics that requires flight in Earth orbit for its execution. Its primary goal is to perform two very precise tests of **Einstein's** general theory of relativity, which is the basis for an understanding of the large-scale structure of the universe. Today, despite important progress in the last 25 yr, **general relativity** remains a very imperfectly tested theory. Through observations of the behavior of **gyroscopes** in a "**drag-free**" satellite in polar orbit around the Earth, GP–B will provide (1) a measurement for the first time, and with high precision (approximately 0.3 percent), of one of the most challenging predictions of **Einstein's** theory—the dragging of the inertial frame of space by rotating matter, and, (2) a measurement to approximately one part in 10^5 of the geodetic precession of a gyroscope due to its motion through the curved space-time around the Earth. The latter furnishes, by far, the most precise test of any of the positive predictions of **general relativity** yet performed. In a polar orbit, the two effects are at right angles and amount respectively to 0.042 and 6.6 arc sec/yr.

In order to meet these extremely demanding performance requirements, the GP–B program has progressed through an extended program definition phase and developed the following significant new technologies for application in its payload design:

- Long-life superfluid helium (He) **dewars** for space flight
  - The use of porous plugs as a gaseous/liquid phase separator
  - Launch supports for the He tank with extremely low thermal conductivity on orbit
  - A low-weight, high-strength composite **dewar** neck tube with extremely low heat transfer characteristics
  - **Dewar** designs using vapor-cooled shields
- A satellite system that has active drag compensation
- Low flow proportional thrusters that use the boil-off of He for attitude and translational control
- Ultra-precision gyroscope (quartz rotor) manufacture and metrology
- Establishment of an ultra-low and stable magnetic field region for the **gyroscopes**
- Precision gyro spin axis readout system employing **superconducting quantum interference device** (**SQUID**) magnetometers.

In March 1984, the NASA Administrator approved a partial start of GP–B known as the shuttle test of the relativity experiment (STORE). The STORE program consists of the ground demonstration of an entire prototypical GP–B system and the flight demonstration of the highly sensitive gyroscope package on a space shuttle mission. The initial goals of STORE were achieved in June 1990 with the successful conduct of the first integrated systems test (FIST), a full-scale early configuration science instrument mounted in an engineering development **dewar** (EDD). This test will be followed by additional testing using prototypical hardware and more sophisticated test configurations. The shuttle test unit (STU) to be launched in calendar year 1995 (CY95) has completed the design phase and is proceeding to flight hardware fabrication.

Status of the GP–B experiment

- STORE engineering development program initiated FY85
- Initial ground systems demonstration (FIST) conducted in CY90
- Additional ground systems testing scheduled for CY92/93
- STU critical design review completed in CY92
- Spacecraft systems studies completed in CY92
- Science mission launch planned for CY99

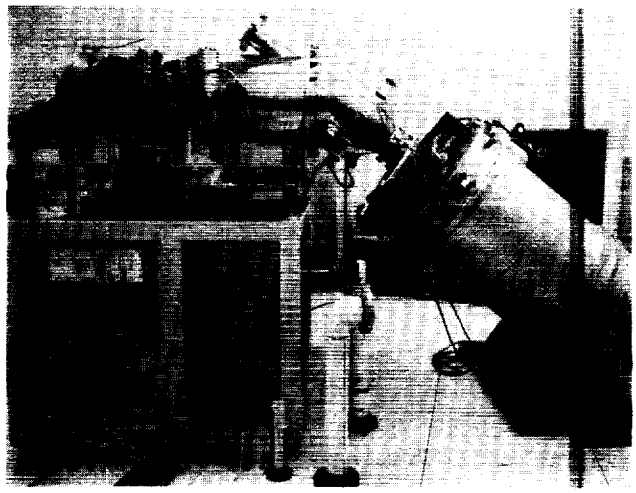

The GP–B experiment.

R. Ise/JA91
205–544–1962
Sponsor: Office of Space Science and Applications, Astrophysics Division

Induced Activation Study of the Long Duration Exposure Facility

Analysis of the induced radioactivity of the **Long Duration Exposure Facility (LDEF)** is continuing with the extraction of specific activities for various spacecraft materials. Data and results of activation measurements from eight national facilities are being collected for interpretation at NASA/MSFC and Eastern Kentucky University. The induced activation measurements will eventually become part of a national data base that will include all radiation measurements of **LDEF**, as well as studies of systems, meteoroids and debris, and materials on the spacecraft.

The major activation mechanism in the **LDEF** components is the **proton flux** in the South Atlantic anomaly (SAA) inner radiation belt. This flux is highly anisotropic and exposes the west side of the spacecraft to higher radiation doses. The directionally dependent activation due to these protons has clearly been observed in the data from aluminum (Al) experiment tray clamps (isotope ^{22}Na) and steel trunnions (isotope ^{54}Mn and others),[1] and is also indicated by the presence of a variety of radioisotopes in other materials. The results of these measurements are now being used as a benchmark for radiation environmental calculations of **LDEF**.

A secondary production mechanism, **thermal neutron capture**, has been observed in three materials having large capture cross sections: cobalt (Co), tantalum (Ta), and indium (In). Unlike the direct activation of materials by protons incident from the Van Allen radiation belts, most neutrons are produced in secondary reactions. These neutrons are then thermalized in low-Z (atomic number) material. A number of samples composed of the neutron-sensitive metals were placed aboard **LDEF** before launch and have been analyzed in low-level background laboratories for gamma-ray counting. Preliminary data were gathered for three **nuclides** (^{60}Co, ^{182}Ta, and ^{114m}In) formed by neutron capture from samples in four **LDEF** experiments. Two of these (experiments M0001 and P0006) were known to have substantial amounts of hydrogenous materials, and have significantly elevated activities for the In and Co isotopes. ^{182}Ta in experiment M0001 appears to be the exception to the trends indicated by either the ^{114m}In and ^{60}Co, and may be related to the geometry, half-life, and relative cross sections for these isotopes. Detailed radiation modeling of these experiments is in progress.[2]

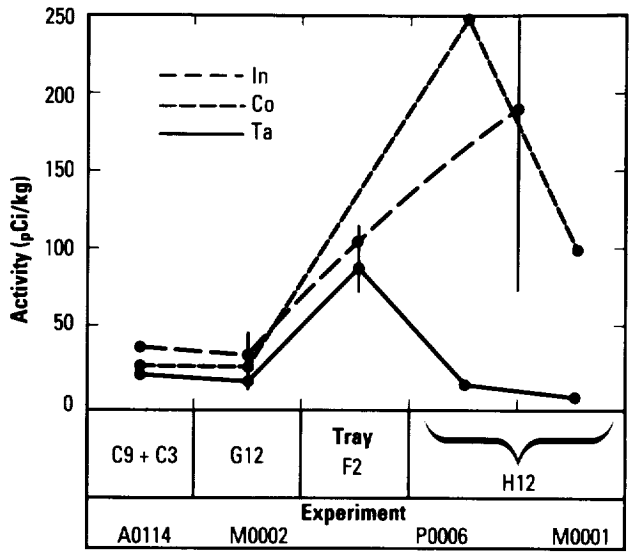

Neutron activation of In, Co, and Ta samples taken from four experiments on LDEF–1.

Other mechanisms that activate spacecraft material and are not as easily separable from SAA proton activation, such as galactic proton bombardment and secondarily produced fast neutrons, are being investigated by comparison to radiation environmental calculations.[2] Deviations from one-dimensional (1–D) activation models indicate that these mechanisms are more important at greater shielding depths and are being investigated for their impact on future spacecraft design.

[1]Harmon, B.A. et al., "LDEF Radiation Measurements: Preliminary Results," *Nucl. Tracks Radiat. Meas.*, vol. 20, No. 1, 1992, pp. 131–136.

[2]Armstrong, T.W., and Colborn, B.L., "Predictions of Induced Radioactivity for Spacecraft in Low Earth Orbit," *Nucl. Tracks Radiat. Meas.*, vol. 20, No. 1, 1992, pp. 101–130.

B.A. Harmon/ES62
205–544–4924
Sponsors: Office of Aeronautics, Exploration, and Technology and Office of Space Science

Infrared Space Astronomy and Space Research

In 1992, **infrared** (**IR**) astronomy at MSFC has focused on three research areas: (1) the extensive observation of star-forming regions in other **galaxies**, protoplanetary disks around other stars, and the nucleus of Earth's own galaxy, the Milky Way, using the previously developed MSFC mid-**IR** camera; (2) the development of a new advanced **IR** camera for astronomical and shuttle-related observations; and (3) scientific and technical participation in the European Space Agency's (ESA's) **IR Space Observatory** (ISO) program.

The mid-**IR** camera, with 20 extremely sensitive bolometer detectors, has been operational for 7 yr. This camera has permitted a broad range of astronomical observations at major observatories, including the only extensive program to map regions of star formation in other **galaxies**. Analysis of these unique **IR** images has led to a recognition of the causes of extremely intense episodes of star formation in the cores of many **galaxies**. During the last year, the dusty disk surrounding the probable black hole in the core of the Milky Way galaxy was imaged at the NASA **IR** Telescope Facility (IRTF) on Mauna Kea, HI. These long-wavelength images show previously undetected detail in the dusty disk, and they will permit a determination of the true mass and luminosity of the black hole as well as insight into how the black hole interacts with its environment.

In late 1991, the MSFC mid-**IR** camera confirmed and substantially extended the discovery, also made with the MSFC mid-**IR** camera at the IRTF, of the "silicate feature" from a protoplanetary disk. This broad spectral feature in the mid-**IR** is a signature of silicate dust grains and is an important diagnostic of particle sizes and evolutionary histories. The discovery of this feature around the star Beta Pictoris opens the way to a better understanding of the evolution of a disk that may be in the process of forming **planets**.

The development of an advanced, high-speed, mid-**IR** camera was begun at MSFC in the summer of 1991. This camera, which will use an extremely sensitive array containing nearly 10,000 detectors, will permit rapid imaging with very high spatial resolution. In addition to its use for astronomical observations, this new camera will provide ground-based imaging of the orbiting shuttle in order to better understand the environment of the shuttle during its missions.

In parallel with the **IR** observational and instrumental programs, the MSFC **IR** astronomy program has continued to contribute to the development of the ISO spectrophotometer (ISOPHOT), an **IR** spectrophotometer that will be one of the four **IR** instruments to be flown aboard ESA's ISO scheduled for launch in 1994. ISO will be the next major **IR** space experiment and will be available to all American astronomers for guest observations.

Telesco, C.M., and Gezari, D.Y., "High-Resolution 12.4-μm Images of the Starburst Region in M82," *Astrophys. J.*, vol. 395 (1992), in press.

C.M. Telesco/ES63
205–544–7723
Sponsor: Office of Space Science and Applications

Measurement of the Cosmic-Ray Composition and Spectra Above 10^{13} eV

The **cosmic-ray** group at MSFC performs balloon-borne experiments to study the "chemical" composition, energy spectra, and interactions of **cosmic-ray** nuclei above 10^{13} eV (10 TeV). This research is performed with colleagues in the United States, Japan, and Poland who form the Japanese-American cooperative emulsion experiments (JACEE) collaboration. The collaboration has flown instruments almost every year since 1979. These instruments consist of large passive detector assemblies (**emulsion chambers**) combined with electronic instruments on a few flights. Because of the steep energy spectra of **cosmic rays** (approximately proportional to $E^{-2.7}$), the investigation of **cosmic rays** above 10 TeV requires large exposure factors (area×solid angle×time). The JACEE balloon-borne experiments have achieved nearly 1,000 m^2/sr/h (1,197 yd^2/sr/h) above 38 km in 11 balloon flights from the United States, Japan, Australia, and the Antarctic. The typical passive **emulsion chamber**[1] is 0.8 m^2 (8.6 ft^2) in area, approximately 20 cm (8 in) thick, and contains 600 kg

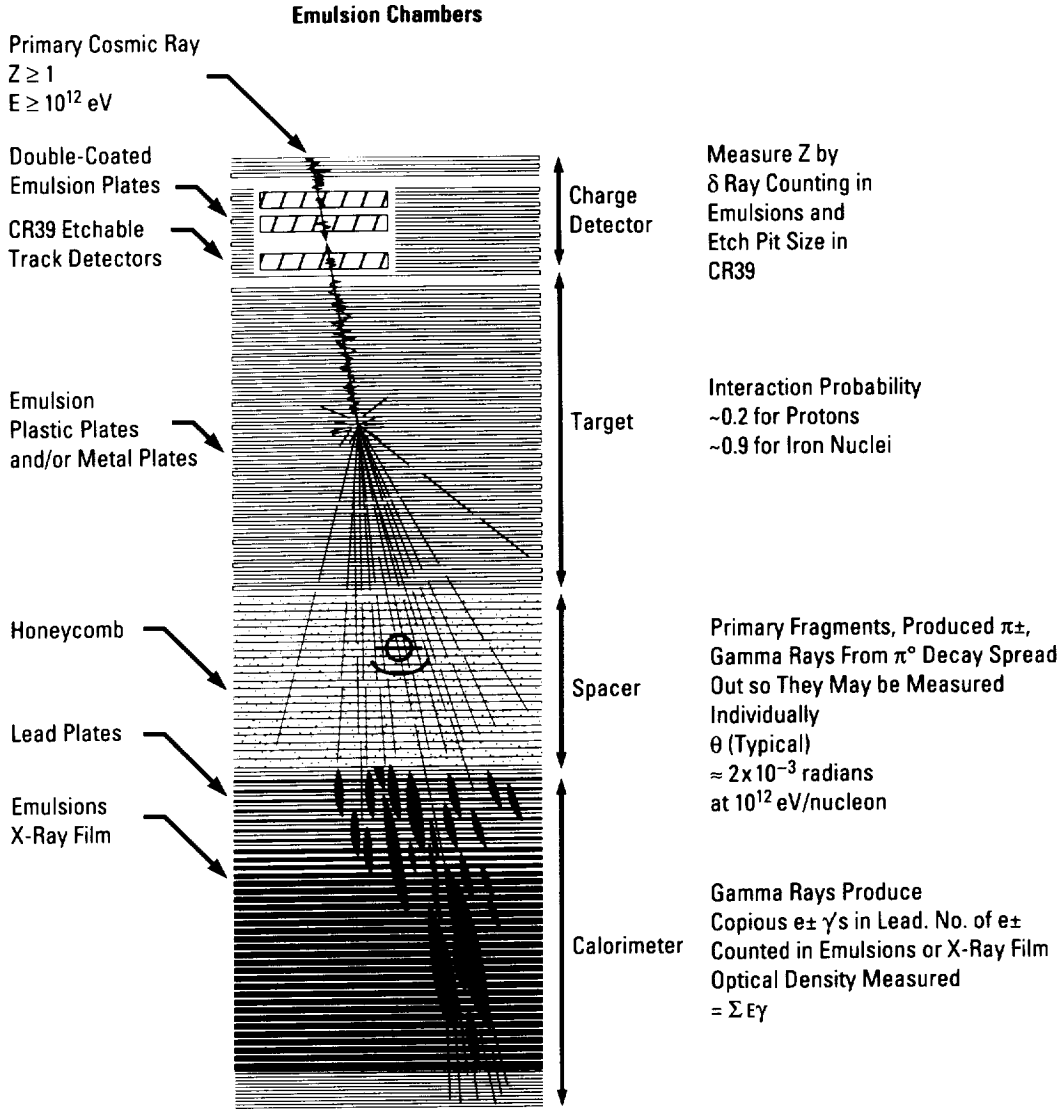

A schematic diagram of an emulsion chamber of the type flown by the JACEE collaboration. The typical chamber is 100×80×12 cm^3 (3.3×2.6×0.4 ft^3) and weighs 600 kgm (1,320 lb).

(1,320 lb) of material. It includes multiple layers of photographic emulsion, acrylic plates, x-ray film, passive nuclear track detectors (CR39), and lead plates.

Following the flights, the photographic materials and other passive track detectors are developed, and, after initial analysis of the x-ray film with microdensitometers at MSFC, are divided among the collaborators for microscope measurements of particle tracks in the emulsions and other passive detectors. The analysis[1] determines the atomic number of each incident nucleus (above a threshold of approximately 10^{13} eV), the energy it deposits in the chamber following a nuclear interaction, and the characteristics of the mesons and other particles produced in the interaction. Approximately 1,500 nuclei from hydrogen (H) through iron (Fe) have been analyzed. Although data from **cosmic-ray** air shower experiments (with detectors on the ground) show that **cosmic rays** extend to 10^{20} eV, no direct information on the primary particle can be obtained from the air shower technique. The JACEE group has produced the highest energy direct data on the composition and spectra, extending a factor of 10 in energy above other experiments. The air shower experiments show a sharp steepening in the **cosmic-ray** spectrum at 3×10^{15} eV, from $E^{-2.7}$ to $E^{-3.1}$. This has been speculated to be due to the nonuniformity of **cosmic rays** in space, with the majority contained in the **galaxies** by magnetic fields. The spectral steepening would be due to the **cosmic rays** "leaking out" of the **galaxy** at higher energies. The most recent JACEE data are consistent with this scenario. The spectra of protons (H nuclei) and Fe nuclei, recently published by JACEE,[2] show the proton spectra steepening above 10^{14} eV, whereas the Fe nuclei show no change in the energy range and are becoming relatively more abundant. According to the "standard" scenario, the protons "leak out" of the **galaxy** at the lowest energy per particle, followed by Fe nuclei, a factor of approximately 56 times higher in energy. This scenario requires acceleration of **cosmic rays** in the **galaxy** by shock waves around **supernovae remnants**, and possibly by electromagnetic phenomena near pulsars. The present model of **shock acceleration** does not appear powerful enough to boost the cosmic ray energy beyond 10^{15} eV, so direct acceleration by pulsars or acceleration in "active" **galaxies** would be required to explain the full energy spectrum. The JACEE collaboration plans further experiments with larger chambers and longer duration balloon flights. Further measurement with exposures approximately 30 times that already achieved would extend the composition and spectra data above 10^{15} eV and would confirm the acceleration processes and the galactic containment model.

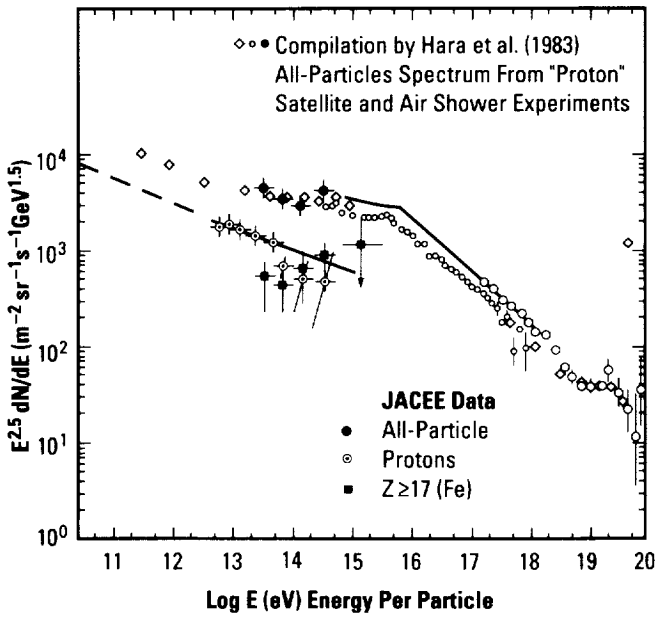

The differential energy spectra of cosmic rays in total energy per particle.

[1]Parnell et al., *Advance in Space Research*, vol. 9, No. 12, 1989, pp. 45–54.

[2]Asakimori, K. et al., Papers of the 22nd International Cosmic Ray Conference, Dublin, Ireland, vol. 2, 1991, pp. 57–60, 97–99.

T.A. Parnell/ES62
205–544–7690
Sponsor: Office of Space Science and Applications

Observation of Hard X-Ray Transients With the BATSE/ Compton Observatory

The Burst and Transient Source Experiment (BATSE) on the **Compton Observatory** has been functioning in orbit for over a year and has produced data on a variety of phenomena such as **gamma-ray** bursts, pulsars, and other high-energy **x-ray/gamma-ray** sources. One of the primary uses of BATSE, because of its near full-sky coverage, is to monitor transient behavior from high-energy galactic and extragalactic objects. The large-area detectors (LAD's) on BATSE are able to detect hard **x-ray** sources by Earth occultation. The flux from these sources is measured by the step-like features observed in the detector counting rate as the **Compton Observatory** orbits the Earth. Measurements of the difference in count rate before and after an occultation in each energy channel of the detector thus provides a spectrum of bright sources twice per orbit. Approximately 30 sources are now being monitored on a daily basis for transient behavior and for studies of their long-term variability. Searches for occultation steps of unknown or unmonitored sources are also carried out daily.

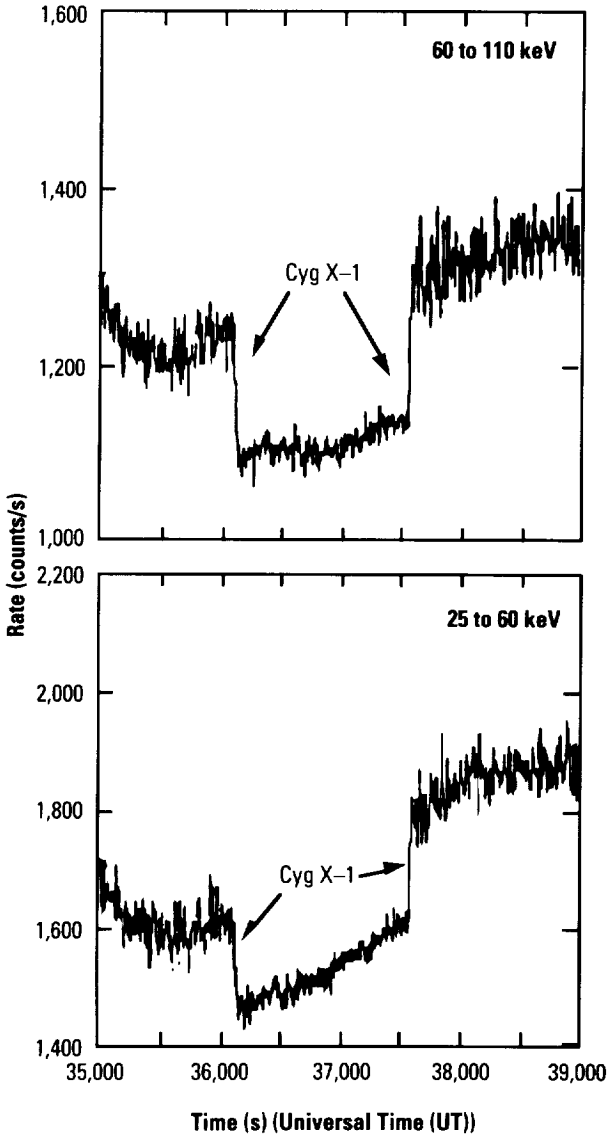

Count rate in BATSE LAD's showing occultation edges for the x-ray source Cyg X-1.

Researchers have observed 1-d averaged count rate histories for two transient sources, GX339–4 and 4U1543–47, during outburst periods for each source. GX339–4 is a black hole candidate, although its nature is disputed,[1] and was being monitored routinely when the increase in hard **x-ray** flux in late June 1991 was observed. The source is known to undergo relatively extreme changes in spectral shape,[1] making a transition from a low-energy (less than 20 keV), high-intensity soft state to a hard, lower-intensity state with flux extending to several hundred kiloelectronvolts. Only the latter state is observable with the LAD's. This observation, lasting from late June to October 1991, is the first to cover a complete hard state episode of GX339–4. Also observed was the source 4U1543–47, which is classified as a recurrent **x-ray** nova or **x-ray** transient.[2] 4U1543–47 was not being monitored on a daily basis and was detected using the searching routine on April 19, 1992. Its position (and therefore its identification) was deduced from the timing of the occultation step features. Previous outbursts were observed by the Uhuru[2] satellite in 1971 and Tenma[3] in 1983. Researchers have observed a rise time in the flux of approximately 2 d in agreement with these observations, but with a faster fall time (12 to 14 d) in the high-energy flux. This indicates a spectral evolution that may be related to changes in the configuration of the accretion disk surrounding the compact object. Attempts have been made to classify these sources as either black hole or neutron star binary systems, but their nature is not completely understood.

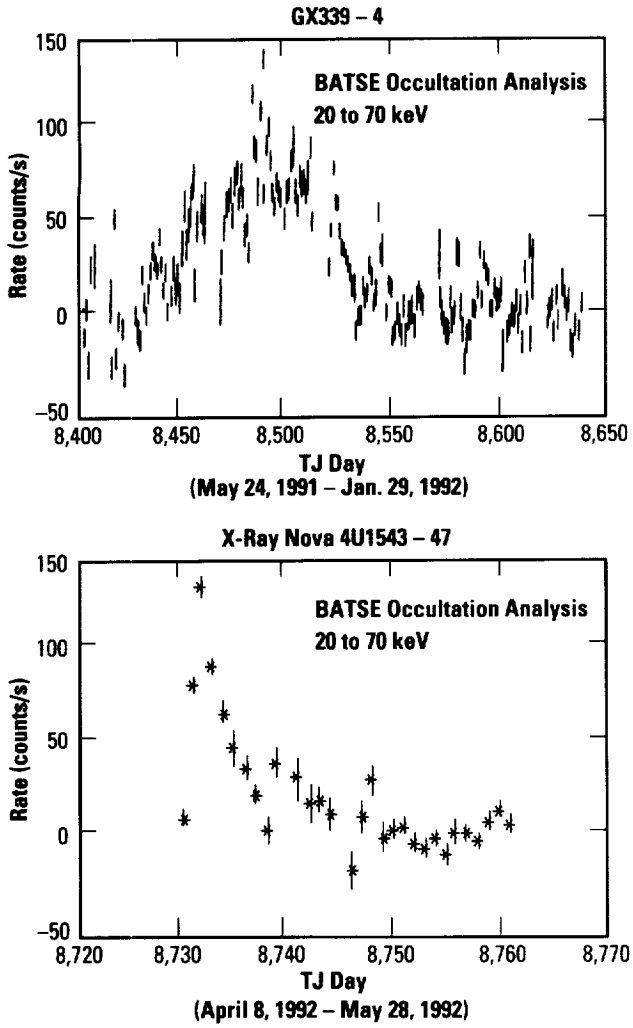

TJ – Truncated Julian

Daily flux averages for two transient x rays detected by BATSE.

[1]Grebenev, S.A. et al.,"Detection of 0.8 Hz Quasi-Periodic Oscillations From the Black Hole Candidate GX339–4," *Sov. Astron. Lett.*, vol. 17 (1991), p. 985.

[2]Matilsky, T. et al., "The Transient X-Ray Source 4U1543–47 Observed From Tenma," *Ap. J. Lett.*, vol. 174 (1972), p. L53.

[3]Kitamoto, S. et al., "A New Transient Source Observed by Uhuru," *Publ. Astron. Soc.*, Japan, vol. 36 (1984), pp. 799–806.

B.A. Harmon/ES62
205–544–4924
Sponsor: Office of Space Science and Applications

Superconducting Magnetic Suspension

Superconducting **magnetic bearings** offer several advantages compared to common rolling element **bearings**. Because there is no mechanical contact between the rotating shaft and its support, such a bearing has no mechanical friction or wear, which results in a very long life. Other features include self-centering and reduced vibrations. One application under investigation is the use of such a bearing in a rocket engine hydrogen (H_2) turbopump in conjunction with a hydrostatic bearing. The purpose of the superconducting bearing is to suspend the pump rotor during startup and shutdown to reduce wear when the hydrostatic bearing is not operational. **Magnetic bearings** using present state-of-the-art materials cannot provide the full load and stiffness capability required during the main operating cycle of the turbopump.

Yttrium-barium-copper-oxide (YBCO) high-temperature **superconductor** (HTS) material, together with permanent magnets, will be used in the bearing. Bearing capability and performance depends on the properties of the **superconductor** including magnetization characteristics and **magnetic** flux trapping. In the turbopump, the bearing will operate at a temperature of approximately 30 K. Little information about HTS material is available for this temperature region. (Most measurements have been made around 77 K, the temperature of liquid nitrogen (LN_2)). Research and technology work at MSFC includes the investigation of **superconductor** properties over the temperature range from 25 to 77 K and above. A measuring system using helium (He) exchange gas was developed and first measurements were performed. HTS material made in-house and procured from different sources is used in the measurement program. A system to measure the total magnetization of samples up to 3 cm (1.18 in) in diameter and 2 cm (0.79 in) thick as a function of the applied **magnetic** field and temperature has been assembled along with devices to measure axial and radial force capacities. The **magnetic** field for magnetization (up to 0.5 T) is provided by a laboratory electromagnet; rare-Earth permanent magnets used in bearing designs and force

measurements rarely exceed this field strength. **Magnetic** properties of large HTS samples have been mapped at 77 K by measuring the force on small diameter nickel (Ni) spheres and by using small-area Hall probes. These measurements, which showed a rather nonuniform distribution of trapped flux in the HTS samples (resulting from physical defects such as cavities and nonuniform structure), are now being extended to lower temperatures.

P.N. Peters/ES63
205–544–7728
Sponsor: Office of Aeronautics, Exploration, and Technology

X-Ray Astronomy Research

This work has centered on the development of new detectors for hard **x-ray** astronomy. These detectors are based on a gas-filled **proportional counter** with the addition of several new techniques to improve their performance. Among these are Penning gas mixtures and multistep operation to enhance energy and spatial resolution, and fluorescent gating and advanced detector body materials that combine to reduce the instrument **background** and thus increase sensitivity. All of these techniques are well established and are incorporated in a flight unit to be flown on a high-altitude balloon in the fall of 1992.

New areas of development are the microstrip **proportional counter** and a novel **x-ray polarimeter**. The microstrip counter makes use of photolithographic technology, developed for the integrated circuit industry, to etch a series of fine conducting lines on a semi-insulating substrate.[1] These then replace the usual discrete anode and cathode wires in multiwire **proportional counters**. The benefits include much higher mechanical accuracy and uniformity than can be achieved with wire planes and the ability to place very fine anodes (down to 1 μm (39 μin)) on closely spaced centers. All of this translates into far superior energy resolution and much lower operating voltages than is possible with conventional wire-wound detectors. To date, many such devices have been fabricated in-house, and an out-of-house contract has been placed to develop a large-area flight version.

The **polarimeter**, a continuation of work funded through the Center Director's Discretionary Fund, utilizes an intensified charge coupled device (CCD) camera to image the tracks produced by photoelectrons in detector gases.[2] The initial emission direction of these electrons is a measure of the **polarization** of the incident photon. Initial results with a prototype system have demonstrated good spatial resolution and **background** rejection in addition to **polarization** sensitivity. Plans are being made to develop a large-scale flight version.

The MSFC **X-Ray** Astronomy Branch also continues its active participation in the development of the stellar **x-ray polarimeter** (SXRP) experiment scheduled for flight aboard the SPECTRUM-X-Gamma mission in 1995. Sensitivity calculations for various cosmic **x-ray** sources were completed as part of the international consortium's effort to draft a preliminary observing plan.

Work in theoretical **x-ray** astronomy has focused on the study of clusters of galaxies, many of which are strong **x-ray** sources. Elemental abundances, as determined by **x-ray** emission lines, provide information on the distribution and origin of the cluster gas and on star formation within the constituent galaxies. Work is now in progress to provide simulated, spatially resolved, **x-ray** spectroscopy for such clusters, surveying the effects of elemental abundance and their gradients and atomic physics uncertainties.

The hydrodynamics of the cluster gas can alter the **x-ray** emission, which may be studied for correlations with observations in other bands. For example, the cluster gas will follow the distribution of cluster mass and will peak in density toward the center of the cluster. There, radiative cooling can remove the thermal pressure of the gas in a short time, forming a "cooling flow" of gas into the center of the cluster. The possibility has been considered that these large-scale inflows may suppress the formation of a cluster-wide magnetic field, and thus explain the apparent anticorrelation of clusters that possess cluster-wide synchrotron radio halos with those containing **x-ray cooling flows**.[3] In addition, the mass cooling rates of cooling flow clusters suggest that long-lived ones will deposit approximately 10^{11} solar masses near the cluster center. Evidence for this cool matter has been conspicuously absent. A popular theory is that the cool gas is made into faint low-mass stars, forming a halo associated with large galaxies in clusters. K-band imaging of the giant galaxy NGC1275 in the Perseus cluster has been performed by the **X-Ray** Astronomy Branch. Analysis of these data suggests that an extremely large amount of mass is cooling the cluster. However, the work found no evidence for a population of low-mass stars associated with NGC1275. Work is now in progress to provide improved models of the stellar populations that may be formed by **cooling flows**.

[1]Fulton, M.A., Kolodziejczak, J., and Ramsey, B.D., "Microstrip Proportional Counter Development at MSFC," Society of Photo-Optical Instrumentation Engineers (SPIE), vol. 1743, 1992.

[2]Austin, R.A., and Ramsey, B.D., "Detecting X-Rays With An Optical Imaging Chamber," SPIE, vol. 1743, 1992.

[3]Burns, J.O., Sulkanen, M.E., Gisler, G.R., and Perley, R.A., "Where Have All the Cluster Halos Gone?" *Ap. J. Letters*, vol. 388 (1992), pp. L49–52.

M. Weisskopf/ES65
205–544–7740
Sponsors: Office of Space Science and Applications
and Center Director's Discretionary Fund

Earth Science and Applications

The Earth Science and Applications Division conducts theoretical and experimental research in hydrologic and atmospheric dynamic processes and associated Earth system science. It develops measurement systems and missions to advance scientific and technical knowledge in this field. The Division establishes and interprets the Earth natural environment parameters and design criteria used in NASA development programs, in addition to providing scientific and technological assistance to NASA programs.

The focus of the Earth Science and Applications Division is the support of NASA's Mission to Planet Earth with selected scientific research, laboratory and flight experiments, and advanced information systems development. Implementation of the Hydrologic Cycle Distributed Active Archive Center is under way at MSFC as part of the Earth-observing system data and information system.

Hydrologic cycle and atmospheric dynamics research includes ground and space-based measurements of Earth parameters. This research uses these measurements to develop and verify analytical and theoretical models of global and mesoscale processes. Field experiments produce data required to verify the operation of airborne and spaceborne sensors. Data derived from observations are used as input to model computer codes. Extensive use is also made of interactive data display and access systems to study time-dependent development of Earth system processes on all scales.

Advanced Optical Technologies for Geostationary Orbit Remote Sensing

The Geostationary Earth Observatory (GEO) is planned to be an important component of NASA's **Mission to Planet Earth**. It will include several optical instruments to monitor the Earth's environment from the perspective of geostationary orbit and will serve as a complement to NASA's Earth-observing system (EOS) in low, polar orbit.

The geostationary orbit imposes a severe thermal environment on any optical instrument that is on a three-axis-stabilized spacecraft. At the same time, optical resolution requirements are higher in geostationary orbit than in low Earth orbits (for comparable ground resolution) because of the orbit's farther distance from Earth. The Earth's rotation (and the rotation of the spacecraft over the Earth) allows direct solar flux onto the optical ports of Earth-viewing remote sensors. The higher thermal and optical performance required of instruments in this orbit can take advantage of research presently under way in several new technology areas, including **silicon carbide** (**SiC**) optics and structures, tunable liquid crystal spectral filters, and diffractive optics.

SiC is emerging as a serious alternative to beryllium for spaceborne, lightweight telescope and mirror applications. It has excellent thermal properties, significantly lower cost, and simpler, nontoxic fabrication processes. Surface thermal stability of better than 0.25 wave of visible light has been demonstrated over temperature ranges from room temperature to below 90 K.

Recent advances in liquid crystal technology have enabled the construction of tunable birefringent filters with bandwidths between 1 and 25 nm. The center wavelength of these filters can be selected electronically in a few milliseconds with no moving parts. These liquid crystal filters, together with existing charge coupled device (CCD) detectors, make possible a new generation of lightweight, rugged, high-resolution imaging instruments. Important advantages exist in the aperture, image stability, power consumption, size, and weight compared to current instrument design approaches for multispectral scene analysis.

Diffractive optics have a variety of potential applications within spaceborne remote-sensing instruments. While not suited to be used in the front-end reflective telescopes that are typically used to collect energy in multispectral remote sensors, diffractive optics can be used to create hybrid diffractive/refractive lens elements (resulting in potentially simpler imaging systems), polarization control elements, and antireflection structured surfaces for windows, spectral filters, and detectors. Complex optical elements (having aspheric and high-speed surfaces) can be made physically simpler and with better performance.

Research is under way to develop these advanced optical technologies to the point where they can be used for the GEO remote-sensing instrument complement to provide unprecedented performance under the severe environment of the GEO.

Koczor, R.J., "NASA's Geostationary Earth Observatory and Its Optical Instruments," Proceedings, Society of Photo-Optical Instrumentation Engineers (SPIE) Conference on Current Developments in Optical Design and Optical Engineering, vol. 1527, July 21, 1991, pp. 98–110.

R.J. Koczor/ES41
205–544–3078
Sponsor: Office of Commercial Programs,
Small Business Innovative Research
Program

Detection of Trace Organic Compounds in Water

Qualification and quantification of many trace **organic** compounds require time-consuming laboratory analysis. However, there may be times when a much faster measurement of trace **organics** is needed. For example, NASA's Space Station *Freedom* (S.S. *Freedom*) project could benefit from prompt identification of trace **organic** contaminants in the environmental control and life support system (ECLSS) water process streams. Prompt and reliable measurement of trace **organics** would help engineers and scientists make important decisions about water usage.

One method for quickly measuring trace **organics** in water has been advanced through a Small Business Innovative Research (SBIR) contract with Boston Advanced Technologies, Inc. This method involves the use of laser Raman spectroscopy and **surface enhanced Raman scattering (SERS)**. Raman spectroscopy avoids the problem of water absorbance blocking out certain spectral regions, which occurs in infrared (IR) spectroscopy. **SERS** increases the intensity of the Raman signal by placing the sample to be measured in contact with signal-enhancing microspheres that are coated with an appropriate metal. The intensity increase in the scattered signal is thought to arise from the interaction between adsorbed molecules from the sample and the electrostatic field of the metal surface electrons. Adsorbed molecules display an increased polarizability change relative to unadsorbed molecules resulting in an increase in scattered signal intensity.[1] The **SERS** system is not simply a trace **organics** detector. It will be able to both sense trace levels of **organic** contaminants and to identify their molecular base.[2]

The approach used in phase I of the SBIR contract consisted of a diode **laser** interfaced to an optical fiber bundle that terminated in a porous sample chamber

filled with silver-coated microspheres. This setup both transmitted the **laser** light to the sample chamber and collected the scattered light from the sample chamber. The collected light was then directed through a transmission grating and onto a solid-state diode detection array. Using various mixtures of **organic** liquids, phase I testing confirmed that this approach had sufficient sensitivity for monitoring certain trace **organic** contaminants. There were also indications that this approach may be useful for detecting bacteria in water.

Under phase II of the SBIR contract, the microsphere coating has been changed from silver to gold to reduce the potential of water contamination. Enhancement of the Raman spectra with gold is expected to be equal to or better than that observed with silver. A new method of gold enhancement is also being studied. In this method, gold is deposited directly onto the end of an optical fiber bundle. This method could potentially simplify the sample chamber with a resultant increase in **sensor** performance. Measurement of organic molecules using **SERS** continues with particular attention being given to the **organics** that NASA considers potential contaminants on S.S. *Freedom*.

The phase II SBIR contract requires delivery to NASA of a completely functional prototype **SERS laser** diode **fiber-optic** sensor system. This system will include a computer containing a library of spectra for various **organic** compounds. This system will be capable of taking sample measurements, comparing these measurements to the library, and matching the spectra to identify trace **organics**.

[1]"Chemical Sensor System for the Identification of Organic Compounds in Water," Phase I Proposal, Chemical Testing and Consulting Company, June 1989.

[2]Sinofsky, E., "Chemical Sensor System for the Identification of Organic Compounds in Water," SBIR Phase I Final Report, NASA Contract NAS8-389446, August 1990.

A. Jones/EL64
205-544-8586
Sponsor: Office of Commercial Programs,
Small Business Innovative Research
Program

Diagnostics of the Global Hydrologic Cycle

The Earth's **hydrologic cycle** is intimately connected to both the physical climate and the biogeochemical components of the **Earth system**. The thrust of this research program is to understand how the cycling of water, particularly within the Earth's atmosphere, helps determine the character of climate on different time and space scales. Near-term research tasks include documentation of the global **hydrologic cycle** and its variability, with an emphasis on merging **remotely sensed** data from space with conventional gridded analyses of atmospheric state variables (e.g., wind, temperature, and humidity).

An analysis has recently been conducted of synoptic to intraseasonal variability of column-integrated water vapor and liquid water as measured from the polar orbiting special sensor microwave/imager (SSM/I). Bandpass analyses, one-point lag correlation maps, and power spectra have been produced that document atmospheric moisture variability. Mid-latitude oceanic storm tracks are defined by high 2- to 8-d bandpass variance maxima in the water vapor and liquid water fields. Moisture variability has proven an especially useful tool in documenting Southern Hemisphere oceanic storm systems because of the paucity of data there. In the tropics, it has been noted that the largest variance in water vapor on all time scales is found on the periphery of the Western Pacific warm sea surface temperatures (SST's). Along the SST maxima, water vapor variability is at a minimum and liquid water variability is at a maximum.

At present, global data sets of moisture have rather poor determinations of vertical structure. Researchers are continuing an investigation of combining SSM/I integrated water vapor with kinematic constraints (u, v, and omega) from global gridded analyses (e.g., those produced by the European Centre for Medium Range Weather Forecasts (ECMWF)) as a means of reconstituting vapor, cloud, and precipitation in three

dimensions and in time. The basic formalism for this four-dimensional (4–D) multiphase water (4–DMPW) analysis is what is termed a diagnostic assimilation procedure. Wind fields from ECMWF gridded analyses have been used to drive conservation equations for vapor, liquid, and ice. These equations, which also use bulk parameterizations of microphysics (e.g., condensation, autoconversion, collection, precipitation, evaporation, and fallout), are updated or constrained in such a way that, where SSM/I observations are available, the evolving model vapor is nudged to those values.

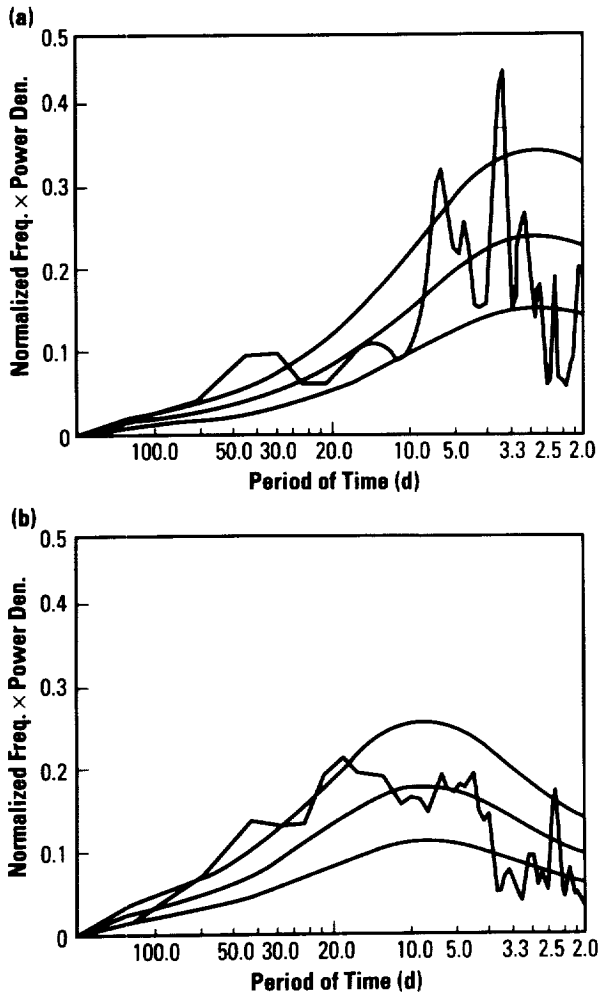

Normalized power spectra of column-integrated water vapor as sensed by SSM/I: (a) east of Japan (30° N. 150° E.); (b) north of Australia (15° S. 110° E.). Top and bottom curves are 5- and 95-percent confidence intervals about red noise (curve center).

A parameterization of convection has been formulated that now allows researchers to explore the role of vertical moisture transport by subgrid processes. At present, researchers are examining the production of cirrus originating from convective detrainment. These diagnostic results will be compared to available climatology such as cloud statistics from the International Satellite Cloud Climatology Project (ISCCP).

Because the three-dimensional (3–D) structure of moisture is strongly constrained by vertical transport processes, researchers have spent some effort this year evaluating the consistency between ECMWF omega fields and SSM/I vapor, liquid water, and ice. For features of scales greater than 1,500 km (approximately 1,000 mi), substantial agreement is found in patterns of large-scale ascent and positive anomalies of water vapor and condensate, even on a daily basis.

This effort at MSFC is part of a larger interdisciplinary investigation whose long-term objective is to determine the scope and interactions of the global water cycle with all components of the Earth system and to understand how it stimulates and regulates change on both global and regional scales.

Robertson, F.R., and Cohen, C., "Global Analyses of Water Vapor, Cloud, and Precipitation Derived From a Diagnostic Assimilation of SSM/I Geophysical Retrievals," Preprints, Fifth Conference on Satellite Meteorology and Oceanography, London, England, September 3–7, 1990.

F.R. Robertson/ES42
205–544–1655
Sponsor: Office of Space Science and Applications

Earth-Observing System Data and Information System

The **Earth-observing system** (**EOS**) program is a comprehensive Earth-observing program scheduled for initial space flight in late 1998. NASA plans to launch a series of polar-orbiting platforms furnished with a full complement of instruments that will remotely sense the Earth's surface, atmosphere, oceans, and cryosphere. The primary goal of **EOS** is to create an integrated space-based observing system that will enable multidisciplinary study of the Earth's critical, life-enabling, interrelated processes involving the atmosphere, the oceans, the land, and the solid Earth. To accomplish this goal, an extensive **data and information system**, including a data processing and retrieval system, must be developed. Although the space platforms will not be in operation until the end of the decade, the development of the MSFC component of the **EOS data and information system** (**EOSDIS**) has already begun.

The **EOSDIS** is a continually improving system. Throughout the lifetime of the **EOS** program there will be several major **EOSDIS** versions (software and hardware improvements). These major versions will coincide with milestones in the **EOS** program as a whole. The initial **EOSDIS** (version 0) is a prototype currently under development and will be based on existing data processing, archive, and distribution facilities at each of the proposed **EOSDIS** centers. The version 0 **distributed active archive center** (**DAAC**) will contain some of the basic elements and services of the latter versions, but it is not considered to be a full-service **DAAC** for support of the EOS platform data streams. The version 0 **EOSDIS** is scheduled to be operational in July 1994. The next major version change (i.e., version 1 scheduled for operation in 1996) will be a system employing all the **EOSDIS** functionality. Subsequent major versions will coincide with implementation milestones of the EOS instrument platforms.

The **EOSDIS** overall system is based on an open and distributed architecture. There are eight **EOSDIS** data centers (**DAAC's**). Each **DAAC** specializes in some aspect of Earth science data processing. The eight **DAAC's** and their Earth science emphases are:

- Alaska Synthetic Aperture Radar (SAR) Facility (ASF)—Cryosphere studies using SAR imagery
- Earth Resources Observation Systems (EROS) Data Center (EDC)/U.S. Geological Survey—Land processes
- NASA/Goddard Space Flight Center (GSFC)—Upper atmosphere, ocean biology, and meteorology
- NASA/Jet Propulsion Laboratory (JPL)—Oceanography and air-sea interaction
- NASA/Langley Research Center (LaRC)—Radiation budget and upper atmosphere
- National Snow and Ice Data Center (NSIDC)—Snow and ice studies
- NASA/MSFC—Hydrologic cycle and the dynamics of water and energy in the climate system
- Department of Energy (DOE)/Oak Ridge National Laboratory—Trace gases in the atmosphere.

A **DAAC** is composed of three subsystems that perform separate but integrated tasks. A **DAAC** consists of a data archive and distribution system (DADS), a product generation system (PGS), and an information management system (IMS). In addition to archiving and distributing data, DADS is the system component responsible for data ingest. In the version 0 timeframe, the MSFC

DAAC will ingest real-time data from several passive microwave instruments onboard polar orbiting satellites. In addition to the real-time data stream, the **DAAC** will archive historical surface climatological data sets, weather radar, lightning data, and other pertinent data sets. The data will be permanently archived at the site and made available for distribution to the EOS science teams and the user public.

The PGS component is responsible for processing the input data streams into geophysical data products. In the MSFC version 0 **DAAC**, passive microwave data from several satellite-based platforms will be processed to produce global images of water vapor, cloud cover, precipitation, marine wind speed, vegetation coverage, tropospheric temperature variations, and other geophysical data products.

The IMS provides the science user access to the data stored in the **DAAC** archive. Through the IMS, the scientist can search and browse through data sets; obtain project, instrument and data descriptions; obtain data processing histories; determine data set availability; and place data orders. The MSFC **DAAC** is leading the development of the image browse component for the overall version 0 **EOSDIS**. The browse system software is being designed to display coverage maps for archived data sets, to display reduced resolution browse images, to pan and zoom on the images, and to manage the search and retrieval of the browse images.

As the development of the DADS, PGS, and IMS components progresses in 1993, the MSFC **DAAC** will test and integrate the various prototype subcomponents of the version 0 **EOSDIS**. The goal is to become an operational data ingest, processing, archiving, and distribution center by July 1994.

H.M. Goodman/ES44
205–544–8006
Sponsor: Office of Space Science and Applications

ER–2 Investigations of Lightning and Thunderstorms

In recent years, observations of **lightning** and **thunderstorms** from high-altitude U–2/ER–2 aircraft have furnished data essential for the design and development of satellite-based **lightning** detectors and have supported investigations of **lightning** relationships. This research is motivated by the desire to develop an understanding needed for the effective utilization and interpretation of data from the **lightning** imaging sensor (LIS), the **lightning** mapper sensor (LMS), and other satellite-based **lightning** detectors planned for the late 1990's and early 2000's. LIS is being developed by NASA for the tropical rainfall measuring mission (TRMM) satellite.

The emphasis, now, is to "quantify" the **lightning** relationships that have been determined. It is hoped that, as a result of these kinds of investigations, **lightning** data alone and/or in conjunction with other **remote sensing** techniques will provide quantitative information about such storm characteristics as the occurrence and location of embedded convection, the strengths of updrafts and downdrafts, thermodynamic and electrical energy budgets, precipitation amounts and distributions, and atmospheric chemistry processes. **Lightning** rates, distribution, and characteristics (i.e., number of strokes per flash, ratio of intracloud to cloud-to-ground **lightning**, discharge energy, etc.) are all factors that may prove useful in devising quantitative algorithms, and these factors can be studied appropriately with the ER–2 aircraft.

During May 1991, **lightning** instruments were integrated onto the ER–2 aircraft. This **lightning** instrumentation detects total storm **lightning** and differentiates between intracloud and cloud-to-ground discharges. The ER–2 **lightning** instruments are also flown with other sensor systems (e.g., infrared (IR), passive microwave, Doppler radar, etc.) to provide new understanding of **thunderstorms** and precipitation and support detailed satellite simulations of storm measurements through the acquisition and analysis of multiparameter data sets. By developing and maintaining the capability to monitor **lightning** and **thunderstorms** with the ER–2 aircraft, NASA will also be able to provide important ground truth verifications and calibrations when the LIS and other **lightning** detectors begin operations in the late 1990's.

During July and August 1991, ER–2 science flights were conducted as part of the convective and precipitation/electrification (CaPE) experiment. The CaPE experiment will provide extensive multiparameter data sets referred to above. More importantly, two of the major scientific goals of this experiment coincide with primary objectives of the ER–2 investigations and NASA's overall **lightning** program. These goals are: (1) the identification and investigation of the relationships among the co-evolving wind, water, and electrification within the convective cloud and (2) rainfall estimation. A large number of storm overflights were obtained during CaPE, including a number of cases of multiple storm passes. In February and March 1992, the ER–2 aircraft participated in the storm scale operations and research meteorology (STORM) fronts experiment systems test (FEST) (STORM–FEST) experiment. STORM–FEST provided an opportunity to study wintertime **thunderstorms**.

R. J. Blakeslee/ES43
205–544–1652
Sponsor: Office of Space Science and Applications

Global Aerosol Backscatter Experiments

The feasibility of satellite-borne **Doppler** laser-radar (lidar) wind sensing systems depends on the **backscatter** distribution in the troposphere and lower stratosphere at the lidar's operating wavelength. The accuracy of wind estimates depends on the signal-to-noise ratio (SNR) of the **Doppler** shifted return signal, which, in turn, depends on the atmospheric **backscatter**. At the present time, efforts are under way to assess global patterns of **backscatter** to assist in the design and development of NASA's space-based infrared (IR) laser atmospheric wind sounder (LAWS), which will measure global tropospheric wind fields. Key to LAWS development is the lidar **backscatter** sensitivity study and establishment of an optimum operating wavelength to ensure scientifically meaningful data. To address these needs, the global **backscatter** experiment (GLOBE) program has been designed and is led by MSFC; this program includes scientific contributions from several Federal agencies, universities, and international organizations.

As part of the GLOBE research program, MSFC designed two major airborne survey missions in the remote Pacific during fall 1989 and spring 1990 to measure aerosol **backscatter** and microphysical properties. Two MSFC carbon dioxide (CO_2) **Doppler** lidars, operating at 9.1 and 10.6 μm, were deployed in these missions along with other instruments from various institutions. Additionally, two Mauna Loa **backscatter** intercomparison experiments (MABIE's) involving an MSFC **Doppler** lidar have been conducted. Analysis of the MSFC lidar data involving detailed calibration of the lidars is currently being conducted. An outstanding scientific result from the GLOBE survey missions data suggests the occurrence of a well-defined background mode that is fairly consistent over the Northern and Southern Hemispheres in the upper troposphere. This background mode consists primarily of submicrometer sulfuric acid **aerosols** with **backscatter** coefficient ranging between 10^{-11} t 10^{-10} $m^{-1}sr^{-1}$ at 9.1 μm, which is currently the prospective wavelength for LAWS.

A GLOBE data base has been established at MSFC. Detailed intercomparison and quality control of the data sets submitted to the data base are being performed. State-of-the-art data visualization techniques are employed to examine the extensive data obtained during GLOBE. Intercomparisons are also made with meteorological data from the European Centre for Medium-Range Weather Forecasts (ECMWF) global gridded analyses and geostationary satellite data in an effort to establish the extent of correlation between **backscatter** and meteorological variables. Aerosol extinction climatologies from stratospheric aerosol and gas experiment (SAGE) satellite data are being compared with GLOBE data to convert global extinction measurements to global **backscatter** estimates at wavelengths considered for LAWS. Modeling of aerosol optical properties using measured microphysical data and Mie theory is incorporated in the GLOBE data analysis. **Backscatter** of atmospheric-type **aerosols** similar to that encountered in the GLOBE mission is also being experimentally measured in the laboratory at MSFC using the two CO_2 **Doppler** lidars. This is compared with theoretical analysis to validate the use of Mie theory for aerosol modeling. Preliminary intercomparisons between calculated **backscatter** using in-situ measurements of aerosol microphysical data and direct measurements of **backscatter** from the two MSFC **CO_2 lidars** show good agreement. The **backscatter** ratios obtained between measurements from Goddard Space Flight Center's (GSFC's) 1.06-μm and Jet Propulsion Laboratory's (JPL's) 9.25-μm pulsed lidars flown on the GLOBE missions agree with theoretical predictions using both modeled and measured aerosol microphysics data.

It is planned to continue scientific research and data management work under the GLOBE program to establish a global scale tropospheric aerosol **backscatter** model and provide inputs of measured and modeled aerosol **backscatter** to observing systems simulation experiments (OSSE's) in support of LAWS.

Srivastava, V., Jarzembski, M.A., and Bowdle, D.A., "Comparison of Calculated Aerosol Backscatter at 9.1- and 2.1-μm Wavelengths," *Appl. Opt.*, vol. 31, 1992, pp. 1904–1906.

Bowdle, D.A., Rothermel, J., Vaughan, J.M., Brown, D.W., and Post, M.J., "Aerosol Backscatter Measurements at 10.6 μm With Airborne and Ground-Based CO_2 Lidars Over the Colorado High Plains—1. Lidar Intercomparison," *J. Geophys. Res.*, vol. 96, 1991, pp. 5327–5335.

Bowdle, D.A., Rothermel, J., Vaughan, J.M., and Post, M.J., "Aerosol Backscatter Measurements at 10.6 μm With Airborne and Ground-Based CO_2 Lidars Over the Colorado High Plains—2. Backscatter Structure," *J. Geophys. Res.*, vol. 96, 1991, pp. 5337–5344.

M. Jarzembski/ES43
205–544–0240
Sponsor: Office of Space Science and Applications

Global Atmospheric Modeling

The response of the atmosphere to changes at the Earth's surface is a crucial aspect of the Earth's climate. In particular, understanding the response of the climate in mid-latitudes to changes in tropical **sea surface temperature** (**SST**) is key to making short-term climate forecasts and in the development of true coupled models of the ocean-atmosphere system. For example, as the tropical Pacific **SST** anomaly events known as "El Niño" become better known, it is possible to make surface temperature forecasts a few months ahead with some skill. Translating these forecasts into predictions of the rainfall or temperature in North America, for example, is much more difficult.

Computer models of the atmosphere can be used for climate analysis and prediction, much as the daily weather forecasts are made in the meteorological centers. The models used for climate are derivatives of the forecasting models, generally simplified, and at lower resolution for the longer runs that are necessary. The development, testing, and verification of these models is at the forefront of research in climate analysis and understanding **climate change**.

The atmospheric response to surface processes is being investigated using the National Center for Atmospheric Research (NCAR) community climate model (CCM). Experiments have dealt with the formulation of the land surface parameterization, particularly the soil moisture, and its effect on the response to **SST** perturbations. The verification of simulation results using recent climate is an important part of this work. The most effective way to document global **climate change** is from space using satellite observations.

Work is under way comparing simulations with satellite observations from the **microwave sounding unit** (**MSU**), the outgoing longwave radiation (OLR), and the special sensor microwave/imager (SSM/I). Temperature, radiation, and rainfall variations observed by these instruments during the recent past provide a means to verify computational results over the entire globe, and thus to contribute toward improvement of models of global **climate change**.

D. Fitzjarrald/ES42
205–544–1651
Sponsor: Office of Space Science and Applications

Global Climate Monitoring From Satellites

Temperature and oceanic rainfall monitoring from satellites for both climate research and global warming monitoring is being performed with the microwave sounding units (MSU's) flying since 1979 on the TIROS–N series of National Oceanographic and Atmospheric Administration (NOAA) satellites. The MSU's measure the thermal emission of radiation by oxygen (O_2) in the atmosphere at four frequencies near 60 GHz, a region of strong interaction between radiation and the O_2 molecules. Out of a total of seven MSU's flying on seven separate spacecraft to date, typically, two are operating at any one time, with newer ones replacing older ones as they are launched. Intercalibration of overlapping satellites to high precision is necessary to construct the long-term climate record, and these intercomparison periods serve to document stability of the instruments.

The eruption of the Mount Pinatubo **volcano** in the Philippines during June 1991 has had a significant impact on tropospheric and stratospheric temperatures. Within 1 mo of the eruption, lower tropospheric temperature began to fall, with globally averaged cooling of 0.6 °C (1.1 °F) through May 1992. This is probably due to reduced levels of sunlight passing through the volcanic veil of sulfuric acid aerosols in the stratosphere. Concurrently, stratospheric temperatures rose by up to 1.4 °C (2.5 °F) due to trapping of some of this energy by the aerosol layer.

A moderate **El Niño** also occurred during late 1991 and early 1992. (An **El Niño** is a temporary warming of tropical eastern Pacific sea surface temperatures (SST's) associated with weakened trade winds.) The changes in SST can disrupt the usual weather patterns over much of the globe. While **El Niño's** usually cause significant warming of globally averaged tropospheric temperatures, it is believed that the cooling effects of Pinatubo's eruption resulted in the warmth being isolated to the eastern Pacific Ocean region.

A new oceanic **rainfall** algorithm has been developed from the MSU data and has been calibrated with global rain gauge data. Because rainfall is such an important element in determining the general circulation of the atmosphere, this satellite data set is expected to be a valuable resource for climate modelers in their attempts to understand the operation of the climate system, at least since the satellite record began in 1979. Preliminary analyses suggest that tropical warm events are closely associated with markedly increased **rainfall**, while cool events have decreased **rainfall**.

R.W. Spencer/ES43
205–544–1686
Sponsor: Office of Space Science and Applications

Infrared Measurements of Atmospheric Moisture Variability

Recent research has been done to apply the physical split window (PSW) technique for deriving precipitable water to visible-**infrared** (**IR**) spin scan radiometer (VISSR) atmospheric sounder (VAS) data. VAS provides 8-km (5 mi) nadir resolution data in the 11- and 12-μm split window channels. The 11-μm channel is positioned in a spectral region where moisture absorption is a minimum. The 12-μm channel is located in a region that is subject to water vapor absorption. This differential absorption allows for computations of the column-integrated water vapor in the atmosphere, commonly known as precipitable water.

The 8-km (5 mi) resolution data are spatially averaged to 32-km (20-mi) resolution to increase the signal-to-noise ratio (SNR). The PSW algorithm is then applied to the averaged data. The resulting precipitable water retrievals have been found to be comparable to those of similar **remote-sensing** techniques, to exhibit good temporal and spatial continuity, and to depict significant mesoscale moisture variability. Radiosondes from the cooperative Huntsville meteorological experiment (COHMEX) served as "ground truth" for verifying the results. A mean absolute retrieval error of 2.4 mm (0.09 in) (or 8.1 percent) and a root-mean-square (RMS) error of ±2.9 mm (±0.11 in) were obtained in the June 19, 1986, case study. Unlike many other techniques, the PSW procedure was implemented using a minimum of a priori data and uses routinely available half-hourly data. The retrievals have been shown to identify preferred regions for cloud and thunderstorm development.

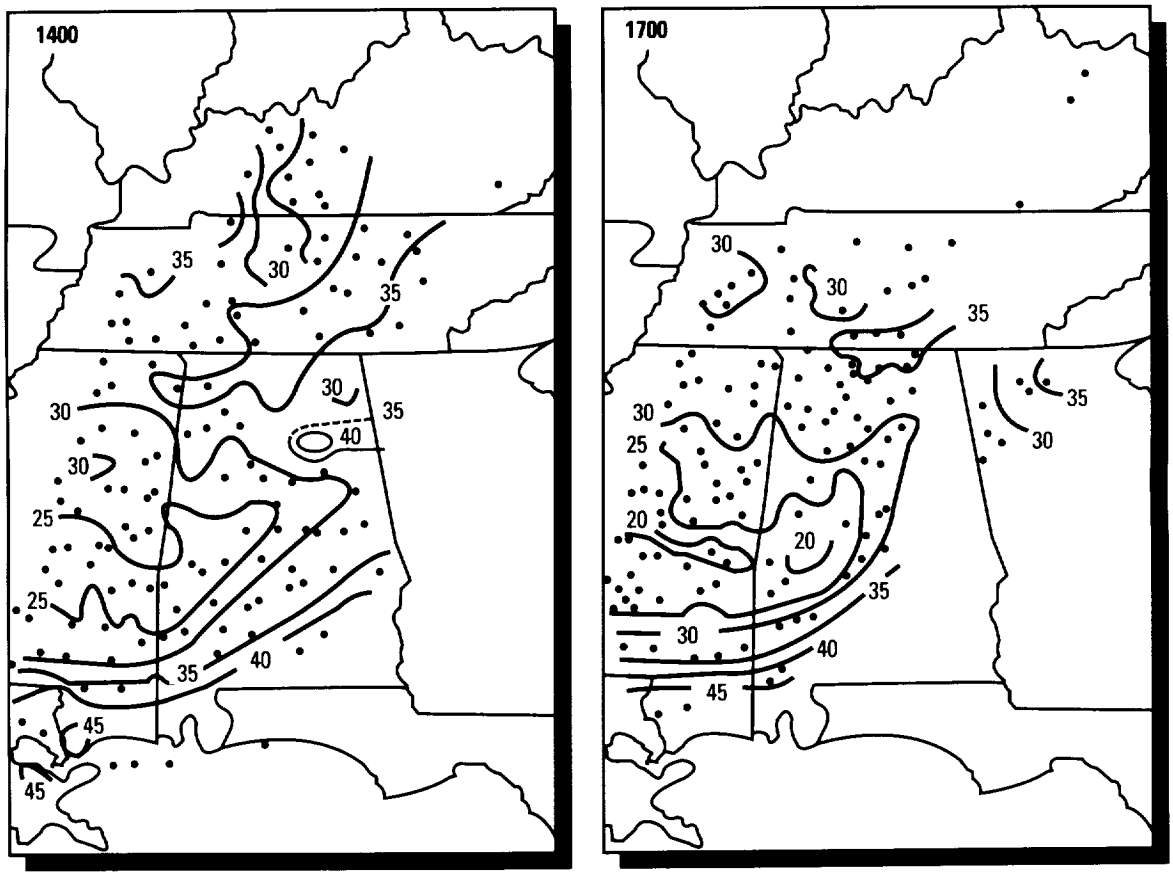

PSW technique precipitable water (mm) analyses for 1400 and 1700 universal time coordinated (UTC), June 19, 1986. (Retrieval locations are indicated by dots.)

Preliminary work has been done to apply the PSW procedure to simulated advanced very high-resolution radiometer (AVHRR) data and **geosynchronous operational environment satellites (GOES's)** I–M series imager and sounder data. This work shows promise for each of these instruments, with each providing a unique perspective of the **atmospheric moisture** variability. For example, AVHRR provides 1-km (0.62-mi) nadir resolution data with better SNR's than VAS, while the **GOES** I–M imager will provide data with similar noise characteristics to AVHRR, but at a much higher temporal resolution (every 30 min). Because of its polar orbit, AVHRR also provides the opportunity to apply the technique on a worldwide scale for global moisture studies.

Finally, the differential absorption basis of the PSW makes it applicable to retrieving other atmospheric constituents. Investigations are under way to retrieve total ozone content using the algorithm.

Carlson, G.S., and Jedlovec, G.J., "Remote Sensing of Ozone Variability Using an Airborne Scanning Infrared Spectrometer," Digest of *the Fifth Topical Meeting on Optical Remote Sensing of the Atmosphere*, Optical Society of America, Williamsburg, VA, 1991, pp. 109–111.

Guillory, A.R., Jedlovec, G.J., and Fuelberg, H.E., "A Physical Split Window Technique for the Retrieval of Precipitable Water From Satellite Measurements," Preprints, Sixth Conference on Satellite Meteorology and Oceanography, American Meteorological Society, Atlanta, GA, 1992, pp. 297–300.

Guillory, A.R., Jedlovec, G.J., and Fuelberg, H.E., "A Technique for Deriving Column-Integrated Water Content Using VAS Split-Window Data," submitted to *J. Applied Meteorology*, 1992.

A.R. Guillory/ES43
205–544–6462
Sponsor: Office of Space Science and Applications

Lightning Radiative Transfer Modeling

For several years, researchers at NASA/MSFC have been analyzing **lightning** cloud-top optical and electric field data derived from high-altitude U–2 aircraft missions over thunderstorms. The general aim of these missions is to better understand the electrification of thunderstorms, **lightning** phenomenology, and the relationship between the development of **lightning** and the evolution of thunderstorms, storm microphysics, and precipitation. The possibility of using satellite-based observations of **lightning** as a tool for remotely inferring storm structure, dynamics, and evolution has motivated current efforts at NASA to build and deploy a geostationary-Earth-orbiting **lightning** mapper system (LMS) and a low-Earth-orbiting **lightning** imaging sensor (LIS). These instruments, designed primarily to detect the total number and location of both intracloud and cloud-to-ground **lightning** during the day and night, will provide valuable information about total rain volume and **thundercloud** currents.

However, in order to fully comprehend the information content of cloud-top illuminations due to **lightning**, efforts are now being made to more precisely model the **radiative transfer** properties of **lightning**. Ultimately, it is hoped that cloud-top optical measurements can be formally inverted to provide direct information about cloud microphysics and/or the **lightning** source.

Because **thunderclouds** are finite, three-dimensional, multiple-scattering media, and because the **lightning** sources embedded within **thunderclouds** are often spatially tortuous and highly transient phenomena, modeling efforts at NASA/MSFC currently employ sophisticated **radiative transfer** techniques. Using the general equations of Boltzmann transport, a similarity between neutron transport in nuclear reactors, and **lightning radiative transfer** in **thunderclouds** has been made. In particular, standard procedures of neutron diffusion theory have been useful.

Model results of cloud-top **lightning** optical waveforms have been found for two cuboidal cloud geometries, each with a dimension equal to 10 km (6.21 mi), but with photon mean free paths of 16 and 32 m (52.48 and 104.96 ft), respectively. When a transient point source (or delta function source) is placed at the center of the cloud, the effect of the cloud is to time-delay and pulse-width-broaden the signals received at cloud top.

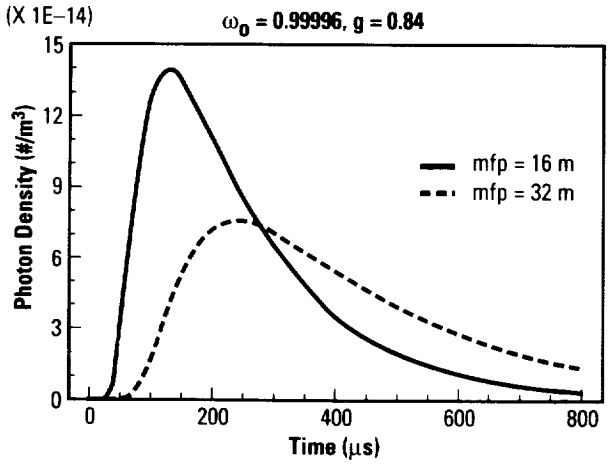

mfp — Photon Mean Free Path
ω_0 — Single Scattering Albedo
g — Asymmetry Factor

Cloud-top lighting optical pulse.

W.J. Koshak/ES43
205–544–8749
Sponsor: Office of Space Science and Applications

Mars-Global Reference Atmosphere Model

The advent of such NASA projects as the **Mars** Observer, the **Mars** Environmental Survey (MESUR), and proposed manned **Mars** missions, in support of the lunar/**Mars** Space Exploration Initiative (SEI), has necessitated the construction of a more detailed global, climatological **model** for **Mars**—the **Mars** Global Reference **Atmosphere Model** (**Mars**-GRAM).

This personal **computer** (PC)-based **model** operates with run characteristics similar to MSFC's highly successful Earth-global reference **atmosphere model** (Earth-GRAM). Both models provide total density, temperature, pressure, and wind conditions for any location, any date, and any time of day from the surface to 600 km (373 mi). Small-scale density perturbations and long-term average density values are also calculated. **Mars**-GRAM also provides realistic modeling of dust storms and their effect on the thermodynamics and wind structure of the martian **atmosphere**.

Mars-GRAM couples the Culp-Stewart upper **atmosphere model** with a lower **atmosphere** parameterization scheme based on data received from previous **Mars** missions. To enhance areas where data were sparse, theoretical calculations were added. More than 40 different data sets were utilized throughout the empirical modeling process.

Mars-GRAM/release #2 is currently in its final phases of development. This new version incorporates many upgrades that have been added to the code since its original release in 1989. One of the most significant is the **model's** new ability to handle dust storm effects on the structure of the **atmosphere**. The **model** now has the capability of simulating small-scale, local dust storm effects, rather than just global-scale storms in the original version. Also, a wave perturbation **model** has been added to more realistically simulate the martian **atmosphere's** response to middle **atmosphere** waves and tides.

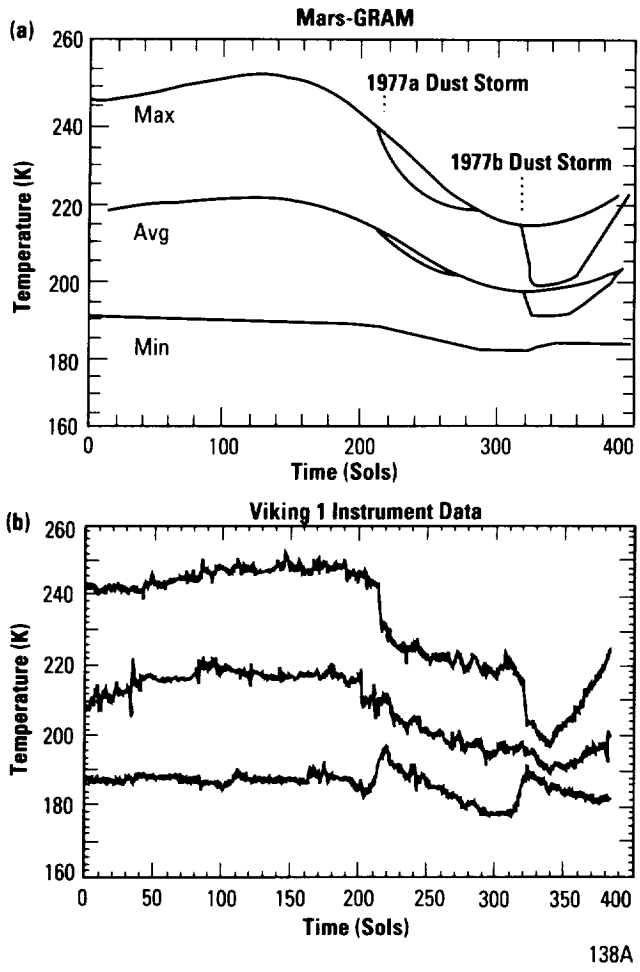

Seasonal variation of the temperature at the Viking Lander 1 site (a) computed by Mars-GRAM and (b) from Viking 1 instrument data.

Release #2 will be distributed to the entire user community in October 1992. Since the **model's** first release, the number of users has grown tremendously, both in the United States and internationally. Currently, **Mars**-GRAM is being used in NASA's **Mars** Observer Program, MESUR, and the joint U.S./Soviet **Mars** 1994 balloon mission. **Mars**-GRAM is also being used by **researchers** in Finland, France, Germany, Great Britain, Hungary, Spain, Cuba, and the Netherlands.

Continued analysis of additional observational data from the Mariner and Viking programs, provided by newly forming, on-line **computer** networks, analysis of new results from **Mars** global circulation **models**, and analysis of new data expected from **Mars** Observer and **Mars** '94 will provide a basis for continued enhancements in the **Mars**-GRAM.

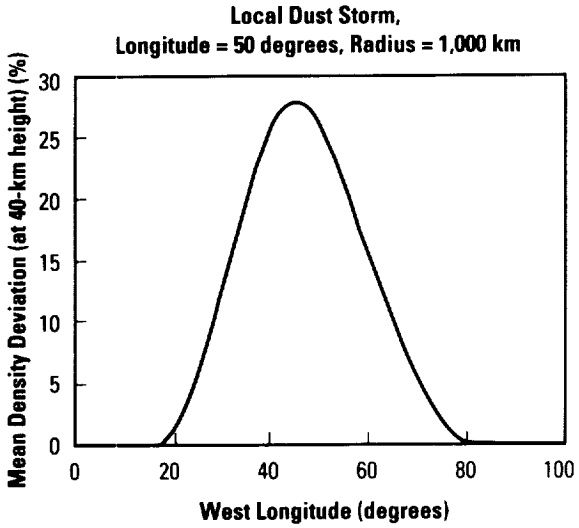

The effect on mean atmospheric density due to a local dust storm of radius 1,000 km (621 mi), centered at 0° N., 50° W.

B.F. James/ES44
205–544–6985
Sponsor: Office of Space Flight

Multi-Center Airborne Coherent Atmospheric Wind Sensor

In April 1992, funding began for development of the multi-Center airborne coherent atmospheric wind sensor (MACAWS). The 4-yr project will culminate in an airborne scanning pulsed carbon dioxide (CO_2) Doppler **laser-radar** (**lidar**) for multidimensional wind and calibrated backscatter measurement from the NASA DC–8 research aircraft. MACAWS is under joint development by the **lidar** remote sensing groups of MSFC, the National Oceanic and Atmospheric Administration (NOAA) Wave Propagation Laboratory (WPL), and the Jet Propulsion Laboratory (JPL). MSFC has the lead responsibility for overall coordination, science definition, and mission planning. To minimize costs, each organization is sharing major hardware components and subsystems, which, in nearly all instances, have been used previously in ground-based or airborne applications. The principle of operation is similar to that successfully employed by MSFC during previous airborne **lidar** experiments. During operation, a pulsed **lidar** beam is generated and directed anywhere within a 64° cone using a scanning device mounted on the left side of the aircraft. The backscattered, Doppler-shifted radiation is measured to infer the line-of-sight (LOS) wind velocity, assuming the scattering particles act as passive wind tracers. By scanning the **lidar** beam slightly forward and aft during flight, fields of two-dimensional (2–D) wind estimates can be obtained within the scan plane. Multiple scan planes, revealing a three-dimensional (3–D) view of the velocity and backscatter structure, can be obtained by appropriately directing the scanner during flight. Aircraft attitude and speed contributions to the radial velocity measurements are eliminated from the wind estimates using a dedicated inertial navigation system.

Following integration and successful checkout, MACAWS will be devoted to a series of specialized field measurements designed to improve understanding of atmospheric dynamic processes over critical scales within the boundary layer and free troposphere. Specifically, MACAWS wind measurements will contribute to improving parameterization schemes for subgrid scale processes related to the hydrological cycle, which is necessary for climate and general circulation models.

Additionally, measurements with MACAWS will also contribute to an improved understanding of **mesoscale** features including: orographic windstorms; generation of instability along dry lines; evolution of **mesoscale** circulations in differentially heated boundary layers; interaction of thunderstorms with the environment including generation of new convection by thunderstorm outflows; regional air quality degradation; and land surface processes. In short, the unique measurement capability of MACAWS has the potential to improve predictive capabilities for weather and climate.

In addition, MACAWS is applicable to a reduction of uncertainties in performance studies of the **laser atmospheric wind sounder (LAWS)**. **LAWS**, a spaceborne Doppler **lidar** used to measure global tropospheric wind fields, is currently under development by MSFC. Ground-based **lidar** studies can provide only limited insights, thus influencing **LAWS** performance simulations. MACAWS can be used to duplicate the **LAWS** measurement perspective, thereby providing unique information not present in ground-based observations. For example, **LAWS** data will contain a surface return signal that can be used for calibration, atmospheric extinction estimation, and "ground-truth" velocity estimates. This information can be used to minimize biases in **LAWS** measurements, and airborne studies with MACAWS can provide insight into developing the necessary **LAWS** algorithms. Other **LAWS** performance issues that can be addressed are the impact of spatial variability in velocity and backscatter, detailed cloud properties, Doppler estimation (particularly near aerosol gradients), and long-term monitoring of natural surfaces that are potential **LAWS** calibration targets for backscatter estimation as well as for monitoring instrument health. Of course, an airborne **lidar** system with simulated **LAWS** perspective could be applied to postlaunch performance validation studies as well.

J. Rothermel/ES43
205–544–1685
Sponsor: Office of Space Science and Applications

Multispectral Atmospheric Mapping Sensor

NASA's **multispectral atmospheric mapping sensor (MAMS)** is a line scanner with eight visible and three infrared (IR) channels. (There are actually four IR channels; however, only three are available at any one time on the scanner.) The visible channels range from 0.42 to 1.05 μm with the IR channels varying from 2.47 to 12.71 μm.

MAMS IR channels

Channel	Central Wavelength	Bandwidth (μm) (@ 50% response)
9	3.73	3.47–3.86
10	6.54	6.28–6.98
11	11.12	10.55–12.24
12	12.56	12.32–12.71

Only three of the IR bands are available during any configuration and the 6.54- and 3.73-μm bands cannot be used together. **MAMS** data are being used to determine atmospheric moisture variability and its importance for cloud formation and storm development at scales not available from satellites. The **MAMS** instrument is flown aboard NASA's ER–2 high-altitude aircraft where data are recorded on a 14-track high-density instrument tape recorder.

The baseline system flown in 1985 consisted of a 5-mrad aperture that produced a ground instantaneous field-of-view (IFOV) of 50 m (164 ft). With the scan mirror rotation of 12.5 r/s, the noise equivalent change in temperature (**NEΔT**) ranged from 0.5 to 0.9 K. In 1986, the configuration was changed to improve the **NEΔT's** down to the 0.3- to 0.5-K range. This resulted from having a larger aperture of 5 mrad that produced a 100-m (328-ft) IFOV at a scan rate of 6.25 r/s. The slower scan speed and larger aperture allowed more radiant energy to fall on the detectors and increased the integration period, improving the **NEΔT's** of the thermal channels. The scan head or primary optics used by the **MAMS** spectrometer is also used by other spectrometers such as the thematic mapping sensor (TMS) and the **advanced ocean color imager (AOCI)**. Several changes that directly affect data quality have been made to the scanner system to accommodate the **AOCI** spectrometer. These changes have improved data quality in all scanner applications. The axe-blade scan mirror was upgraded to a full face mirror. This change increased the amount of energy falling on the detectors

and increased the signal-to-noise ratios (SNR's) in all channels. With the improved dynamic range, the digitization resolution was upgraded from 8 to 10 b for the IR channels. The averaging electronics for the blackbodies were also changed to average over more samples of the blackbodies to reduce the sensitivity of the detectors to noise. With these improvements, sensitivity became less than 0.1 K, with **NEΔT** less than 0.2 K. Based on current instrument performance, minimal changes are necessary for collection of high-quality data in the future.

The early deployments demonstrated a deficiency in on-site data analysis capabilities for scientific evaluation of the **MAMS** data. The MSFC **quick view system (QVS)** is being developed to provide a near real-time analysis capability by reading data directly from the data tape after a deployment. The **QVS** consists of a single personal computer (PC) form factor card that performs the bit and frame synchronization of the incoming single serial Bi-phase-L encoded data. Once the start-of-frame code is detected, five scan lines are stored in a local buffer before transfer to the PC hard disk drive is performed. Data are recorded in frames of 750 bytes with start-of-frame code, housekeeping data, scene data, and end-of-frame code comprising a single frame. Software drivers developed for the PC will read five line blocks through a direct memory access (DMA) transfer to a man/computer interactive data access system (McIDAS) area file that is then read by McIDAS/operating system-2 (OS2) for calibration, presentation, and navigation. In addition, the ingesting software allows for contrast stretching of the imagery as it is being read off the tape. Additional software provides the ability to do three-channel color composites.

Jedlovec, G.J., Batson, K.B., Atkinson, R.J., Moeller, C.C., Menzel, W.P., and James, M.W., "Improved Capabilities of the Multispectral Atmospheric Mapping Sensor (MAMS)," NASA Technical Memorandum 100352, MSFC, Huntsville, AL, 1989. (Available National Technical Information Society (NTIS) N89–20430)

Jedlovec, G.J., James, M.W., Smith, M.R., and Atkinson, R.J., "The MAMS Quick View System–2 (QVS2): A Workstation for NASA Aircraft Scanner Data Evaluation," Preprints, Seventh International Conference on Interactive Information and Processing Systems for Meteorology, Hydrology, and Oceanography, American Meteorological Society (AMS), Boston, MA, pp. 198–203.

M.W. James/ES43
205–544–5020
Sponsor: Office of Space Science and Applications

Numerical Modeling of Air-Sea Interaction Processes

A recent interest in **cyclogenesis** is generally based on studying oceanic cyclones that undergo a rapid period of development. The occurrence of these types of storms is often associated with changes in the planetary wave pattern. Therefore, atmospheric processes acting on the mesoscale and synoptic scales within a rapidly developing cyclone can have a significant impact on the planetary scale flow regime. Numerical models provide a powerful tool that can be used to study the scale interaction processes involved in rapid **cyclogenesis**. Several years ago, MSFC initiated a cooperative effort with Drexel University through which the Drexel **limited-area mesoscale prediction system (LAMPS)** dynamical model, along with pre- and postprocessing software, would be implemented on MSFC supercomputing facilities for use in studies of atmospheric processes. The model predicts atmospheric potential temperature, winds, and moisture subject to physical laws governing hydrodynamic flow; also created are radiative processes, cloud cover, subgrid-scale deep convection, and exchanges of energy with the underlying land or ocean.

Currently, MSFC is investigating the sensitivity of oceanic **cyclogenesis** to lower boundary conditions. In particular, the goal of this work is to quantify the extent to which a **sea-surface temperature (SST)** front associated with the north wall of the Gulf Stream can influence the development and mesoscale structure of rapidly deepening oceanic cyclones off the east coast of the United States and Canada. Data collected during the experiment on rapidly intensifying cyclones over the Atlantic (ERICA), held during the winter of 1988–89, afford the opportunity to investigate the effect of the Gulf Stream on well-documented, rapidly developing systems. Five cases have been selected from the ERICA intensive observing periods (IOP's). The approach is to use **LAMPS** to perform a series of sensitivity experiments on each case in which the observed position (CTRL experiment) of the Gulf Stream's north wall is shifted 354 km (220 mi) southward (SOUTH experiment) and 354 km (220 mi) northward (NORTH experiment).

Each experiment is divided into two phases. The first phase consists of a preforecast period in which a **four-dimensional data assimilation (FDDA)** technique known as Newtonian nudging is employed. Model

variables of wind and potential temperature are nudged toward a gridded analysis derived from observations that are valid at the end of the preforecast period (0 h). A unique aspect of this work is the specification of a spatial weighting function. The function excludes nudging within the marine planetary boundary layer (PBL) so the lower atmospheric thermodynamic variables are allowed to respond to the imposed **SST** field. The second phase of each experiment consists of a 24-h forecast period in which no nudging is performed.

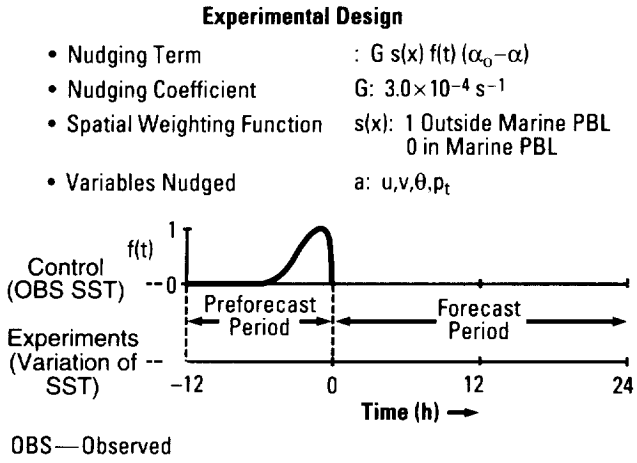

Schematic of experimental design.

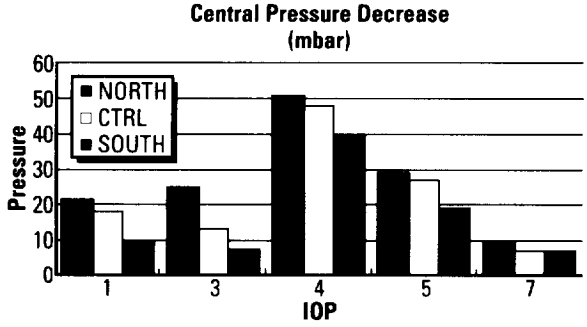

Change in cyclone central pressure (millibars) in experiments NORTH, CTRL, and SOUTH for all cases studied.

Results to date suggest that rapidly deepening oceanic cyclones are sensitive to the position of the Gulf Stream's north wall. In all cases studied, the most intense cyclone developed when the **SST** front is shifted northward (NORTH) and the least intense when the **SST** front is shifted southward (SOUTH). This result contradicts the generally accepted hypothesis that the period of most rapid deepening is in some way physically connected to the strong **SST** gradient. In fact, results show that rapid development occurred well removed (241 to 321 km (150 to 200 mi)) from the **SST** gradient. Therefore, it appears that these storm systems may be more sensitive to the underlying **SST** itself as opposed to the **SST** gradient.

The next phase of research involves diagnostic evaluation of the model atmospheres generated in the sensitivity experiments. In particular, the energy and moisture exchanges between the ocean and atmosphere will be examined, along with the moisture transport through the cyclone's environment. It is hypothesized that these processes are related to the underlying **SST** and that their effect on the cyclone environment needs to be evaluated. Other work will include comparison of model simulations and **special sensor microwave/imager (SSM/I)** observations to aircraft radar returns and in-situ measurements of atmospheric temperature, moisture, wind, and microphysics data.

Lapenta, W.M., Perkey, D.J., Kreitzberg, C.W., and Robertson, F.R., "The Role of the Sea-Surface Temperature Distribution on Explosive Cyclogenesis During ERICA," *Preprints*, Ninth Conference on Numerical Weather Prediction, Denver, CO, October 10–15, 1991.

Lapenta, W.M., Perkey, D.J., Kreitzberg, C.W., and Robertson, F.R., "The Effect of the SST Distribution on Explosive Cyclogenesis: Numerical Results," *Preprints*, Fifth Conference on Mesoscale Processes, Atlanta, GA, January 5–10, 1992.

W.M. Lapenta/ES42
205-544-1667
Sponsor: Office of Space Science and Applications

Numerical Modeling of Nonlinear Baroclinic Fluid Systems

In developing an understanding of the processes that affect global change of the planet Earth, a component that offers one of the greatest challenges is the fluid system comprised of the atmosphere and oceans. Clearly, the objective of understanding this system is an important one, since the atmosphere is the fluid system in which humans live, which supplies the land with fresh water, and which shields life from harmful solar radiation. Due to the complex nature of this system and the difficulty in obtaining sufficient observational data on it, accurately predicting or even understanding its behavior for all but very short time periods remains an elusive goal. The goal of the research efforts described here is to develop a better understanding of the Earth system through the use of computer models that allow the study of the complicated behavior of a rather simple fluid system which is driven by horizontal temperature gradients and influenced by rotation of the planet.

One of the means for studying the behavior of the Earth's atmosphere and oceans is to conduct laboratory experiments in cylindrical and spherical containers where a fluid such as water is differentially heated and rotated. Depending on the strength of the differential heating and the rate of rotation, the flow may be very simple—steady in time and axisymmetric in structure (with no variations in longitude). For other values of the heating and rotation, the flow may be made of steady, regular waves, or it may be quite irregular and chaotic. Such experiments have been conducted in the laboratory, both at MSFC and elsewhere, and a numerical model developed at MSFC is being used to test the ability to predict the type of flow and to assist in the development of an understanding of such processes as heat and momentum transport. Studies are being performed additionally to help design future spaceflight experiments using the **geophysical fluid flow cell (GFFC)** apparatus.

The model that has been developed for the study of these flows, called the **geophysical fluid flow simulator (GEOSIM)**, is able to study either spherical or cylindrical flows. Analysis of the flows may proceed in several steps: (1) calculation of the axisymmetric flow (that which would be seen if no variations in longitude are allowed); (2) calculation of the linear stability of that flow to three-dimensional (3–D) wave perturbations; (3) calculation of the wave amplitude where interaction between the wave and the longitudinal mean flow is allowed; and, finally, (4) the calculation of the fully nonlinear flow with full interaction between all components of the flow. The extent to which each of these steps can be directly applied to the actual flows depends on the nonlinearity of the flow, which, in turn, depends on the experimental parameters. For highly nonlinear flows, time series of images of the predicted flow are produced, and these are shown in computer animations to illustrate the interactions between various types of structures in the flow.

Recent work has placed emphasis on vacillatory flow in the **baroclinic annulus** experiments. The flow occurring in the gap between two concentric, corotating cylinders that are differentially heated is computed with high resolution and for (typically) several tens of rotational periods. For certain combinations of rotation rates and temperature differences, the resulting flow is 3–D and undergoes a periodic oscillation in the amplitude of the "wave" part of the structure. Agreement between the computer simulations and previous laboratory experiments is very good. The computer calculations allow more detailed analysis of the flow to determine the mechanics of the **vacillation**. It is seen that the **vacillation** is due to a first-order interaction between the wave and the mean flow, although the details are sensitive to processes in the lower boundary layer.

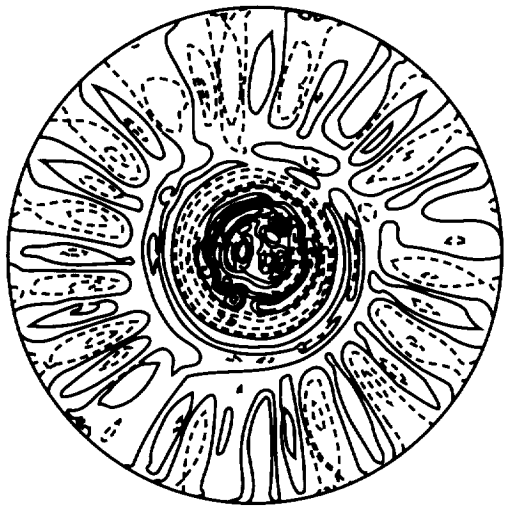

Vertical Velocity at 0.450
Contour Interval = 1.00000E-02
Maximum = 3.59665E-02
Minimum = -3.65326E-02

Vertical motion field produced by motions in the GFFC, as predicted by the computer model GEOSIM. Units used are cm-s^{-1}.

Miller, T.L., and Butler, K.A., "Hysteresis and the Transition Between Axisymmetric Flow and Wave Flow in the Baroclinic Annulus," *J. Atmos. Sci.*, 48 (1991), pp. 811–823.

Miller, T.L., and Reynolds, N.D., "A Study of Baroclinic Instability in a Cylindrical Annulus With the Temperature Gradient Imposed on the Lower Surface," *J. Fluid Mech.*, 233 (1991), pp. 495–518.

Miller, T.L., Lu, H.I., and Butler, K.A., "A Fully Nonlinear, Mixed Spectral and Finite Difference Model for Thermally Driven, Rotating Flows," *J. Comput. Phys.*, vol. 101,1992, pp. 265–275.

T.L. Miller/ES42
205–544–1641
Sponsor: Office of Space Science and Applications

Optical Linescan System Data System/Global Survey of Lightning

A global **lightning climatology** is being assembled from the nighttime imagery of the Defense Meteorological Satellite Program (DMSP) optical linescan system (OLS). **Lightning** saturates the visible channel of the OLS at nighttime and can be identified as a horizontal streak on the order of 50 to 100 km (30 to 50 nm) in horizontal extent. **Lightning** streaks apparent in the film strips located at the National Snow and Ice Data Center (NSIDC) prior to 1991 are being digitized.

An initial survey was completed for the F7 **satellite** observation period January 1986 to October 1987 and for the Q **satellite** for the period June to July 1973. Comparisons between the OLS **lightning climatology** with the Arkin Global Precipitation Index (GPI) data set during the 1986–87 El Niño event shows similar regional variations in convective activity. The digital archive of global DMSP data began at the end of February. Software is being developed at both MSFC and NSIDC to extract, navigate, and view the OLS fine and smooth imagery.

With the demise of the OLS instrument on satellites F8 and F9, digital **lightning** extraction will concentrate on satellites F10 and F11. Digital F8, F9, and F10 data collected over Florida during July through August 1991 will be processed. Limited ground truthing of the OLS **lightning** signatures will be performed with the 1991 data. During the period June to August 1992 in central Florida and November 1992 to February 1993 in the Solomon Islands (during the tropical ocean global atmosphere/coupled atmosphere response experiment (TOGA/COARE), partial ground truth data will be collected from ground-based sensors and from the global positioning **satellite** (GPS) nuclear detection sensor (NDS) instrument. OLS **lightning** data from F7, F8, and F9 are being processed for comparison with WETNET precipitation algorithms. The first routinely available global OLS Exabyte tapes in a standard format will not be available from NSIDC until summer 1992 due to the need for extensive software development to ramp-up the operational processing software. For this reason, **lightning** signatures will be extracted from Exabyte tape copies at MSFC.

Additional research activities with the nighttime OLS data are being evaluated and include the following: (1) evaluation of the urban warming bias of the surface thermometer temperature record using the visible channel to delineate urban areas and the thermal channel to measure the skin temperature of the Earth's surface; (2) assessment of global biomass burning by using the nighttime visible channel to estimate the area of anthropomorphic fires mapped to different biomes; and (3) assessment of the navigation accuracy for interrelating different data sets (e.g., special sensor microwave/imager (SSM/I) and OLS images of clouds) and the use of a geographic information system.

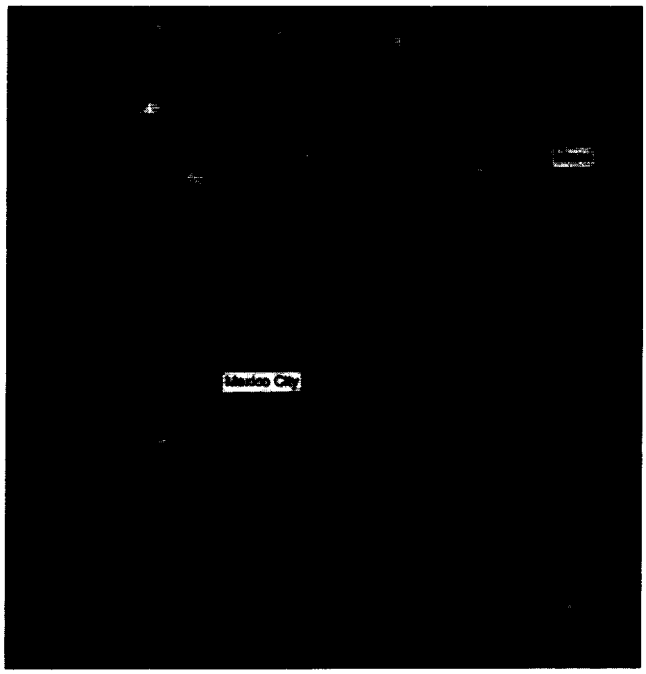

Nighttime DMSP F7 satellite OLS visible channel image of North and Central America.

Goodman, S.J., and Christian, H.J., "Lightning," Chapter to appear in *Global Change Atlas*, to be published in 1992 by Cambridge University Press.

Christian, H.J., and Goodman, S.J., "Global Observations of Lighning From Space," *Preprints*, Ninth International Conference on Atmospheric Electricity, St. Petersburg, Russia, June 13–17, 1992.

S. Goodman/ES44
205–544–1683
Sponsor: Office of Space Science and Applications

Sensor Development: Lightning Imaging Sensor Calibration

The Remote Sensing Branch of the Earth Science and Applications Division is supporting the development of electro-optical instrumentation for space applications. Under the **Earth-observing system** (**EOS**) program, an optical facility is being developed to calibrate the **lightning imaging sensor** (**LIS**) and to measure its performance through the use of realistic simulations. The **LIS** will image the large-scale distribution of lightning from low Earth orbit (LEO) in a 1-nm wide, near-infrared (NIR) wavelength band using a 128×128 pixel silicon (Si) charge coupled device (CCD) focal plane array. The sensor is being designed to detect lightning during both low-background (nighttime) and difficult, high-background (daytime) conditions, when the background flux exceeds the signal by many orders of magnitude. The instrument specifications also include a 2-ms frametime and a field-of-view (FOV) of approximately 80×80°.

The **calibration** facility will consist of three distinct systems that can be defined functionally as: focal plane **calibration**, radiometric **calibration**, and lightning scene simulation. The first item, currently being assembled, will directly measure the following parameters of individual focal plane arrays: responsivity versus wavelength, dark current and noise, linearity, crosstalk, pixel uniformity, and readout speed. This characterization will enable the determination of **calibration** coefficients and performance parameters such as dynamic range.

The focal plane **calibration** system will utilize three sources of NIR radiation: a monochromator for responsivity measurements, a laser diode for temporal response and crosstalk measurements, and an incandescent quartz tungsten (W) halogen lamp for background flux generation. To maintain traceable radiometric accuracy, a calibrated Si detector reference will be utilized.

Radiometric **calibration** will be performed on each completed sensor to verify FOV, alignment, linearity, responsivity, polarization sensitivity, and the wavelength accuracy of the **LIS** narrowband filter. A 0.5-m (1.64-ft) monochromator is being procured to achieve the required subnanometer wavelength resolution. The sensor will be rotated about its entrance pupil by a computer-controlled, motorized positioner. Detailed optomechanical design of this system is under way, and several components have already been purchased.

The **lightning simulator (LSIM)** will use a 3-mW NIR diode laser as the source of simulated lightning. Through an acousto-optic (AO) modulator and an AO deflector, the laser beam will be pulsed and scanned across a rear projection screen to simulate a dynamic lightning scene. A static background image can also be projected onto the screen and its intensity varied by the use of neutral density filters. A simple combination of plastic field lenses and a collimating lens is used to place the lightning scene at the infinite conjugate plane and to obtain wide FOV coverage. The anticipated FOV coverage of the present design is greater than 60×60°. The original **LSIM** design is currently being modified to account for manufacturing limitations discovered in the projection screen and lenses already purchased and tested.

The system design of the data acquisition electronics for the **calibration** facility has been completed. A 486-based compatible computer will be the central processor. High-speed, commercially available data acquisition modules have been ordered wherever possible. To meet the speed requirements of driving the **LSIM** AO components, a custom-designed digital-to-analog (D/A) module will be developed.

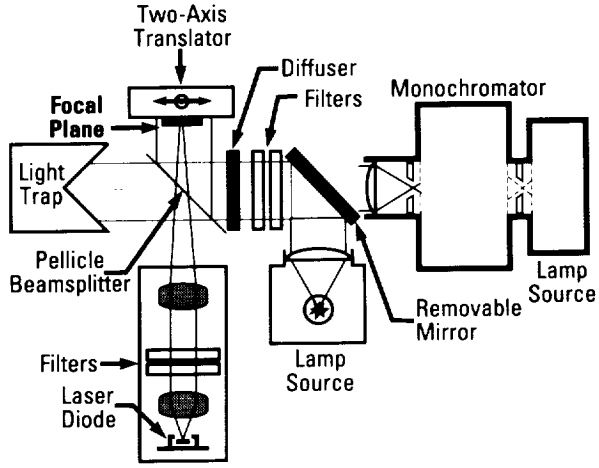

LIS focal plane characterization system.

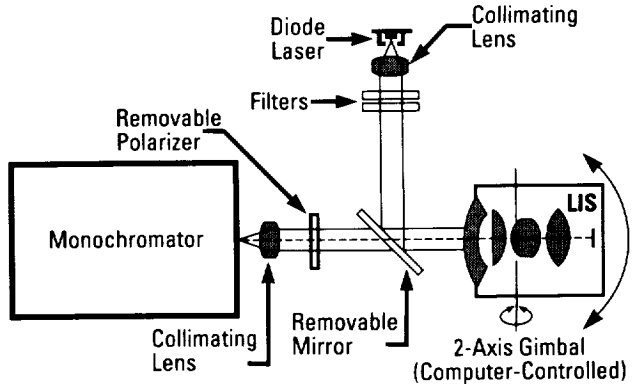

LIS radiometric calibration system.

M.W. James/ES43
205–544–5020
Sponsor: Earth-Observing System Program Office

Simulating Lightning Imaging Sensor Observations From the Tropical Rainfall Measuring Mission Orbit

Satellite observations of **lightning** hold the promise of providing information on convective **precipitation**, the global electric circuit, trace gas processes, magnetospheric/ionospheric coupling, and planetary scale circulation and convection. The **lightning imaging sensor** (**LIS**) instrument will detect **lightning** flashes (both intracloud and cloud-to-ground) from low Earth orbit (LEO) with a detection efficiency near 90 percent. The **LIS** has been selected to fly on the **tropical rainfall measuring mission** (**TRMM**) satellite, which will orbit about the Earth at an inclination of 35° and a height of 350 km. From this orbit, **LIS** will observe an area beneath the spacecraft of approximately 360,000 km^2 for approximately 80 s as it passes overhead.

A data base of 6 yr of cloud-to-ground **lightning** observations for a 3°×3° study area is being used to examine how well 1- to 3-min **LIS** observations would describe the observed monthly, seasonal, and yearly **lightning** totals and variations. Although **LIS** will observe total **lightning**, the cloud-to-ground data provide a natural population data base for simulation purposes. At lat. 34.3° N., the satellite overflies the study area three to four times a day at approximately 90-min intervals. The remaining part of the day is not sampled. The visit times change throughout the month, completing a cycle in approximately 30 d.

Observed and **LIS** simulated monthly variations of **lightning** over the 6-yr period are very similar. For the **LIS** simulation, satellite visit times were computed for the 6-yr period and the amount of **lightning** occurring in a 1-min interval at each visit was recorded. The **lightning** seen by **LIS** during each month is time-proportionately scaled for comparison with the actual observations. The correlation coefficient between monthly observed and **LIS**-simulated **lightning** for individual years ranged from 0.76 to 0.97, while the correlation for the entire 6-yr period is 0.87.

These results suggest that monthly **lightning** occurring over a 3°×3° study area can be estimated from 1-min sampling intervals for simulated **LIS** visit times. Simulations for other latitudes and for yearly and seasonal periods are also being investigated. A sensitivity test is being run by varying the starting satellite position to determine the variance in the resulting **LIS** estimates.

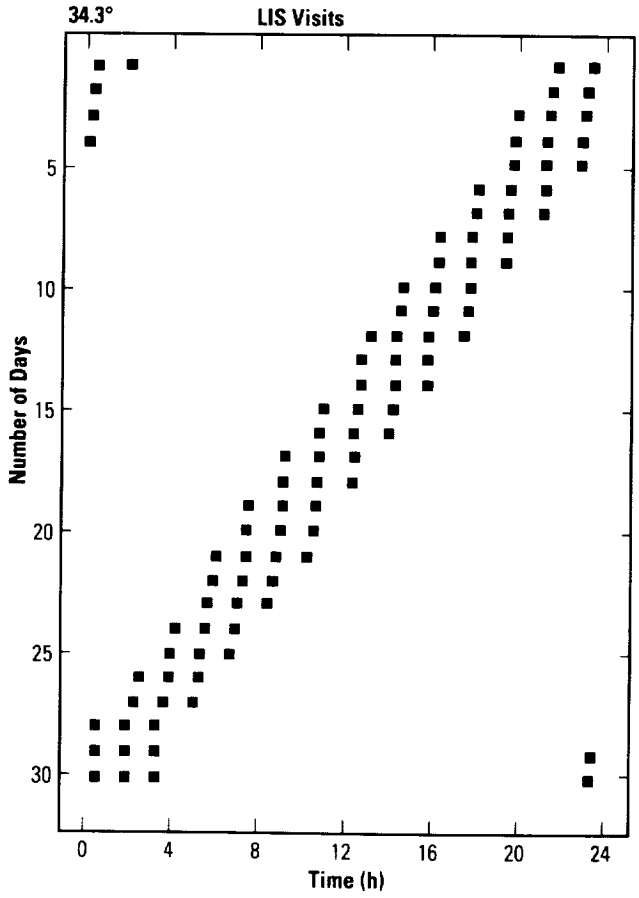

The variation and frequency of LIS visits for a 1-mo period for a 3×3° study area centered at lat. 34.3° N.

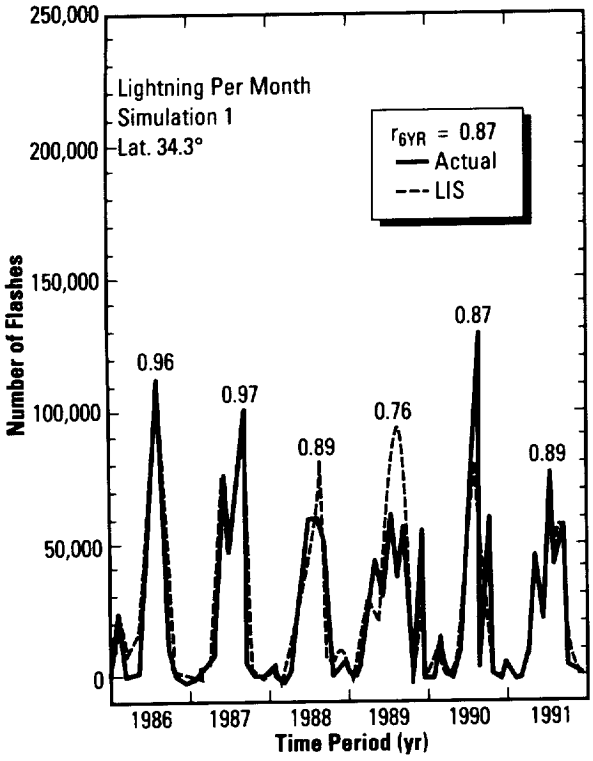

Monthly observed versus LIS-simulated lightning over a 6-yr period.

Buechler, D.E., and Blakeslee, R.J., "Cloud-to-Ground Lightning Observations Used to Simulate Observations From a Low Earth Orbiting Satellite," *Preprints*, Ninth International Conference on Atmospheric Electricity, American Geophysical Union (AGU), St. Petersburg, Russia.

R.J. Blakeslee/ES43
205-544-1652
Sponsor: Office of Space Science and Applications

Space Shuttle Lightning Research

The **shuttle mesoscale lightning** experiment (MLE), flown on earlier **shuttle** flights, and most recently flown on various space transportation systems (STS's) flights (i.e., STS-31, -32, -35, -37, -38, -40, -41, and -48), has continued to focus on obtaining additional quantitative measurements of **lightning** characteristics and to create a data base for use in demonstrating observation simulations for future spaceborne **lightning** mapping systems. These flights are also providing design criteria data for the design of a proposed **shuttle** MLE-type **lightning** research instrument called **mesoscale lightning** observational sensors (MELOS's), which are currently under development here at MSFC.

The MELOS instrument package, consisting of a video camera, an optical pulse detector, and spectrometer, will record video images and optical and electronic signatures from the observed **lightning** events. This instrument will be designed to be operated in day- and nighttime periods, when crew time is available, during an assigned mission, or a modified instrument could be installed on a pallet in the **shuttle's** payload bay and operated from the ground.

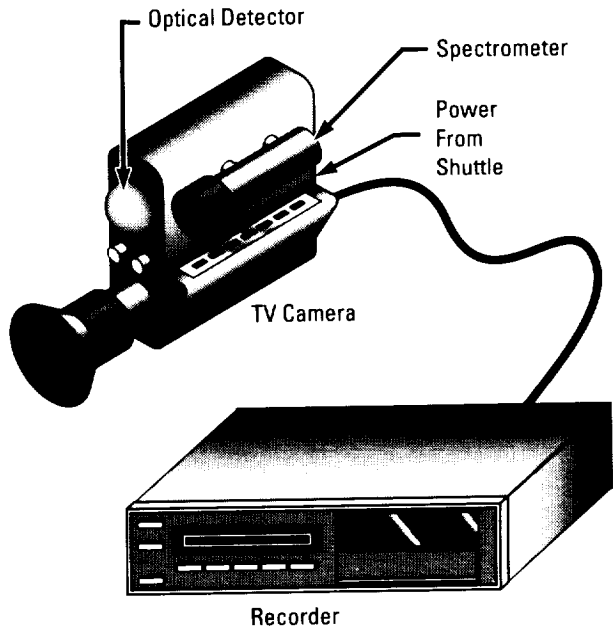

Artist concept for a prototype of MELOS.

A number of selected video frames from different **shuttle** flights shows a special type of **lightning** that is called **vertical lightning**, which has been observed from the **shuttle** payload bay television (TV) cameras while conducting the MLE. This type of **lightning** occurs when the discharge moves vertically out the top of a thunderstorm. It has been observed to occur over Africa, Australia, South America, and the United States during the nighttime passes over active thunderstorms. At the present time, it is not known what causes this type of **lightning** discharge to occur. NASA/MSFC personnel have been working with researchers at NASA/Goddard Space Flight Center (GSFC) in the development of a computer model to determine the amount of radio frequency (RF) energy that could be radiated from this type of event. GSFC researchers are developing a radio spectrum analyzer, a wide-band waveform receiver, and a microprocesssor to be flown on a future **shuttle** mission. This instrument could be flown as part of the MLE to provide RF data on the vertical-type events.

A video sequence of a transient luminosity was seen to occur in the airglow in coincidence with a **lightning** flash in a tropical oceanic thunderstorm directly below this area of the airglow. This event is believed to provide evidence of direct coupling between **lightning** and the ionospheric events. This is a new phenomena that researchers have been fortunate to observe and hopefully will see more of these effects in future **shuttle** flights. A recent paper by Boeck et al. discusses, in more detail, the analysis of this type of event.

Data from analysis of the MLE video has provided information on the frequency of **lightning** flashes, the length of **lightning** discharge within a storm complex, and estimates of **lightning** activity in storm systems that are oblique to the **shuttle's** orbital track.

These **shuttle**-type video observations will continue to provide information for use in the development of observation techniques and simulations for future satellite missions. The tropical rainfall measurement mission (TRMM) is now scheduled to carry the **lightning** imaging sensor (LIS) being developed here at MSFC; the video data from the MLE has helped in the development of operational procedures for this experiment and in developing data analysis techniques.

In April 1992, NASA Headquarters, Code SE, approved 10 additional **shuttle** flights for continuing the MLE-type **lightning** research program, and Mr. O.H. Vaughan, Jr., of MSFC, who has in the past worked with the **shuttle** payload integration managers at NASA/Johnson Space Center (JSC) and the astronaut training personnel, will continue to be the principal investigator for this research program, which uses the **shuttle** as an Earth observational platform to conduct **lightning** research. This type of research can provide other researchers with a data base for their use in understanding terrestrial **lightning** processes as well as it should help in the understanding of **lightning** processes on other planets. The cloud-to-stratospheric **lightning** discharges, or what is known as **vertical lightning**, may be more representative of the type of **lightning** discharges that could be occurring in other planetary atmospheres, such as on Jupiter and/or Neptune.

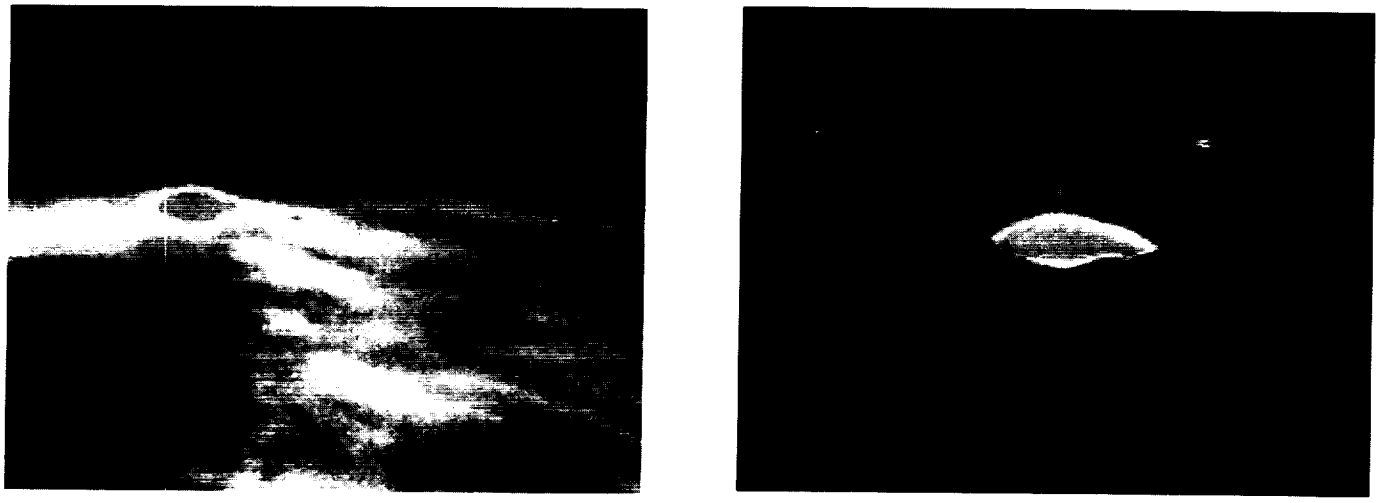

Vertical lightning events.

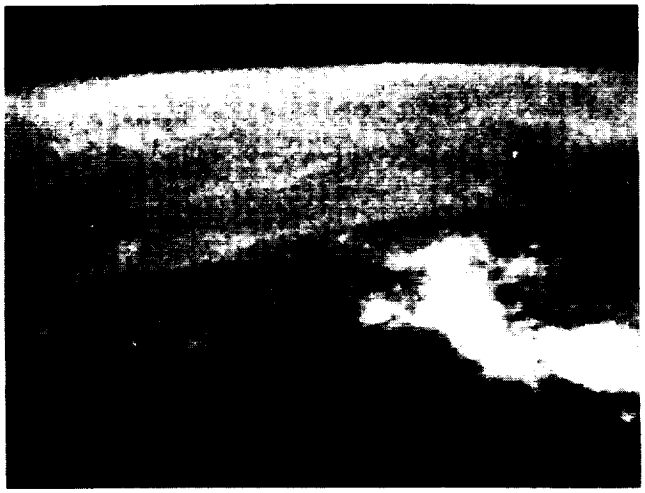

(a) The darker area in the lower part of the picture is French Guiana. The Atlantic Ocean is the gray area in the middle part of the picture. The bright areas on the shore and over the ocean are moonlit clouds. The airglow layer is visible in the sky at the upper part of the image.

(b) The airglow layer at the top of the image has an area of enhanced luminosity that appeared in 1/60-s interval between figure (a) (left) and this figure. There is a small increase in luminosity produced by a lightning flash directly under the airglow enhancement.

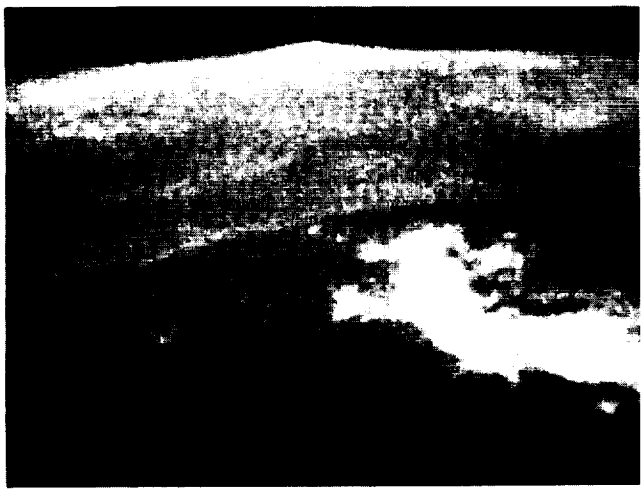

(c) A lightning flash near the horizon produces an elongated gray "bloom" in the image. The luminosity enhancement in the airglow layer decreases from figure (b) above.

(d) The lightning flash near the horizon decreases in intensity, producing a smaller gray "bloom" than in the previous figure (c). The luminosity enhancement in the airglow layer decreases from figure (c) left.

Airglow video frames.

Vaughan, O.H., Jr., Blakeslee, R., Boeck, W.L., Vonnegut, B., Brook, M., and McKune, J., "Picture of the Month: A Cloud-to-Space Lightning Discharge as Recorded by the Space Shuttle Payload Bay TV Cameras," *Monthly Weather Review*, vol. 120, No. 7, July 1992, pp. 1459–1461.

Boeck, W.L., Vaughan, O.H., Jr., Blakeslee, R., Vonnegut, B., and Brook, M., "Lightning-Induced Brightening in the Airglow Layer," , *Geophysical Review Letters*, vol. 19, No. 2, January 1992, pp. 99–102.

Ferrell, W.M., and Desch, M.D., "Cloud-to-Stratospheric Lightning Discharges: A Radio Emission Model," *Geophysical Research Letters*, 1992.

O.H. Vaughan, Jr./ES43
205–544–1648
Sponsor: Office of Space Science and Applications

The Advanced Microwave Precipitation Radiometer

The **advanced microwave precipitation radiometer** (**AMPR**) is an aircraft instrument originally designed to meet three primary scientific goals. The first of these goals is to investigate the vertical structure of oceanic rain systems. The second goal is to support the development and validation of current satellite **precipitation** retrieval algorithms, and the third is to provide information about the instrument design of future spaceborne sensors. The **AMPR** passively detects a unique combination of microwave frequencies, and, when mounted on a **high-altitude aircraft** platform, it also offers unparalleled surface resolution capabilities at these frequencies.

The **AMPR** and its accompanying data acquisition systems are designed to fly aboard the NASA ER–2 **high-altitude aircraft**. The instrument is a cross-track scanning, total-power microwave radiometer with four channels centered at 10.7, 19.35, 37.1, and 85.5 GHz. It has a dual-lens antenna to accommodate two separate feedhorns. One horn is a copy of the special sensor microwave/imager (SSM/I) spaceborne multifrequency feedhorn, which is currently flying aboard the defense meteorological satellite program (DMSP) F8 and F10 satellites. This horn feeds the 19.35-, 37.1-, and 85.5-GHz channels, while the other **AMPR** feedhorn was designed for the 10.7-GHz frequency. The instrument is currently configured with a rotating polarization for all four channels during scanning. This polarization varies from horizontal at 45° to the right of nadir to vertical at 45° to the left of nadir. At the nadir position, the polarizations are equally mixed. The surface resolutions of the nadir-viewing footprints range in size from 2.8 km (1.7 mi) for the 10.7- and 19.35-GHz channels down to 0.64 km (0.4 mi) at 85.5 GHz when collected at a **high-altitude aircraft** height of 20 km (12 mi).

Thus far, the **AMPR** has collected **precipitation** data in two major field experiments. The first was the convection and **precipitation**/electrification (CaPE) experiment, which was a multi-Agency effort conducted in the vicinity of Cape Canaveral, FL, during the summer of 1991. This life histories of several tropical thunderstorms are included in this data set. The second deployment was part of the storm-scale operation and research meteorology (STORM)-fronts experimental systems tests (FEST) (STORM–FEST), which was another multi-Agency effort designed to study winter weather in the Midwestern United States during 1992. Information collected during both experiments will provide useful insight into the seasonal variations of the microwave signatures of **precipitation**.

R.E. Hood/ES43
205–544–5407
Sponsors: Office of Space Science and Applications
and Center Director's Discretionary Fund

The Geophysical Fluid Flow Cell

Large-scale motions of the **atmospheres** of planets and in the convection zones of rotating stars are strongly constrained by rotation, under the action of Coriolis forces, and gravity, which is manifest in the buoyancy forces that drive thermal circulations. The resulting atmospheric structures are often surprising and continue to baffle scientists seeking fundamental understanding of such phenomena as the zonal bands of Jupiter; the numerous spots and other isolated cloud patterns on Jupiter, Saturn, and Neptune; the origin of extremely high winds in the tropics and subtropics of these bodies; and the persistent differential rotation of the Sun where the equatorial **atmosphere** rotates faster than that near the poles.

The **geophysical fluid flow** cell (GFFC) provides a means of examining thermal convection on a rotating sphere. The GFFC experiment simulates a wide variety of thermal convection phenomena on a spherical surface with a radially directed body force. By applying an electric field across a spherical capacitor filled with a dielectric liquid (low-viscosity silicon (Si) oil), a body force analogous to gravity is generated around the fluid. The force acts as buoyancy in that its magnitude is proportional to the local temperature of the fluid and is in the radial direction perpendicular to the spherical surface. In this manner, cooler fluid sinks toward the surface of the inner sphere while warmer fluid rises toward the outer sphere. The value of this artificial gravity is proportional to the square of the voltage applied across the sphere and can thus be imposed electronically as desired. With practical voltages, its magnitude is only a fraction of Earth's gravity and so requires a microgravity environment to be significant. A unique feature of these experiments is the latitudinal dependence of the Coriolis effect resulting in flows more relevant to geophysical applications. The experiment was flown on **Spacelab** 3 (SL3) and is scheduled for reflight on a future **Spacelab** mission. The reflight of the GFFC on **Spacelab** will provide opportunities for significant fundamental scientific research in dynamic processes.

The focus of this research has been on constructing multiple solutions of atmospheric **baroclinic waves** and of Jovian convection (for the same external parameters) using a high-resolution numerical model. Cattaneo and Hart proved that there are, in general, an infinite number of multiple states possible for problems of giant planet and stellar circulations. Numerical computations have shown that typically more than one of these is stable in both of these settings. The transition to turbulence and the nature of allowed vacillations and index cycle fluctuations are different for each type of solution. The results have a bearing on the question of multiple climate regimes and on the breakdown of banana cells in the GFFC experiments. Research is also focused on interpreting the results of these complex simulations by obtaining low-order descriptions based on the nonlinear orthogonal functions appropriate to the coherent structures in the original partial differential equation calculations. Some of the 10^4 degree-of-freedom (DOF) spectral numerical simulations can be replicated by as few as six nonlinear ordinary differential equations for the amplitudes of the coherent structures. This method of reduction of a set of partial differential equations to a small number of ordinary differential equations provides a useful interpretive tool as well as an efficient predictive method.

Researchers wish to further investigate nonlinear baroclinic flows, which are important in internal **climate variability**. The emphasis will be on the following questions. Under what circumstances can high-resolution model results or laboratory data be represented by a robust low-order description? What are the errors involved, data requirements, etc? Once a low-order description is found, how can the low-order structures be interpreted physically and perhaps arrived at beforehand from first principles?

These ideas shall be applied to the columnar (banana cell) convection models of circulation in the giant planets as well. In both this and the Earth's **atmosphere** baroclinic instability problem, researchers shall pursue

further the numerical simulations of transition to chaos, fractal behavior, and the effects of additional realistic physical processes like small-scale boundary layer turbulence on the same.

Brummel, N., and Hart, J.E., "Numerical Models of Columnar Convection," in preparation, 1991.

Cattaneo, F., and Hart, J.E., "Multiple States for Quasi-Geostrophic Baroclinic Channel Flows," *Geophysical and Astrophysical Fluid Dynamics*, 54 (1990), pp. 1–34.

Cattaneo, F., Brummel, N.H., Toomre, J., Malagoli, A., and Hurlburt, N.E., "Turbulent Compressible Convection," *Astrophysical J.*, 370 (1991), pp. 282–294.

F.W. Leslie/ES42
205–544–1633
Sponsor: Office of Space Science and Applications

Validation of NASA's 50-MHz Radar Wind Profiler

The primary objective of this project is to report on the research and technology in identifying wind and **turbulent** regions from the surface to 16 km (9.94 mi) by the FPS–16 radar/**jimsphere** system and to use these wind and **turbulent** assessments to validate NASA's 50-MHz **radar wind profiler**. Eleven wind profiles obtained from two space shuttle launches, STS–37 and STS–43, during the day of launch were compared. Wind profile statistics from the two wind sensors were compared at a 150-m (492-ft) wavelength. This important calculation of 150-m (492-ft) wavelength was obtained by computing autospectra, cross-spectra, and coherence squared spectra from 20 **jimsphere** balloons tracked simultaneously by FPQ–14 and FPS–16 radars.[1,2] It is further demonstrated that the NASA prototype wind profiler is an excellent monitoring device illustrating the measurements of the winds within 0.5 h of launch zero (L–0). This fills in the time gap of wind profiles closer to L–0 since the space shuttle ascent wind loads are computed 2.0 h before launch, based on winds aloft obtained by the **jimsphere** thereby increasing the probability of a successful mission. Thus, the emerging technology of electromagnetic probing of the atmosphere by clear-air radar is clearly a valuable asset in today's wind persistence monitoring for launches of the space shuttle.

For the end of the 1990's and the upcoming 21st century, NASA's 50-MHz **radar wind profiler** could play an important role in monitoring winds for substantial profile changes for the National Aerospace Plane (NASP) and the National Launch System (NLS) being developed by NASA and the U.S. Air Force (USAF). In addition, the rapid turnaround wind measurements by NASA's 50-MHz **radar wind profiler** will be a tremendous boost for the speed-up schedule for NASA's Space Station *Freedom* (S.S. *Freedom*) program and for human space exploration of the Moon and Mars in the next century.

The spacial difference between the two launch sites at Kennedy Space Center (KSC) is approximately 20 km (12.4 mi). The wind profiler beams are stationary and the balloon is not. Depending on the speed and direction of the upper-level winds, the **jimsphere** can be transported up to 100 km (62.1 mi) from the Cape Canaveral balloon facility.[3] The temporal differences result from different measurement techniques. The **radar wind profiler** will obtain a new wind profile on the order of every 30 min based on a consensus average of 10 wind profiles measured every 3 min at a height interval of 150 m (492 ft) to 20 km (12.4 mi). The **jimsphere** measurement is an instantaneous measurement. The **jimsphere** rise rate of 5 m/s (19.4 ft/s) takes 50 min to reach 16 km (9.9 mi).

To account for the spatial and temporal differences, the profiler winds were reconstructed to conform to the path of the **jimsphere**. For example, the **jimsphere** is downstream 50 km (31 mi) from the launch pad with an elapsed time of 30 min at an altitude of 10 km (6.2 mi). The time and altitude of the **radar wind profilers** data translate to the same time and altitude of the **jimsphere**, which is 30 min at 10 km (6.2 mi).

A statistical comparison of the u and v wind components for the FPS–16 radar/**jimsphere** system and NASA's 50-MHz **radar wind profiler** was made for two space shuttle launches, STS–37 (Atlantis) on April 5, 1991, and STS–43 (Atlantis) on August 2, 1991. The **radar wind profiler** wind data are computed for a length scale every 150 m (492 ft) and averaged over 30 m (98.4 ft), while the **jimsphere** is computed every 30 m (98.4 ft).

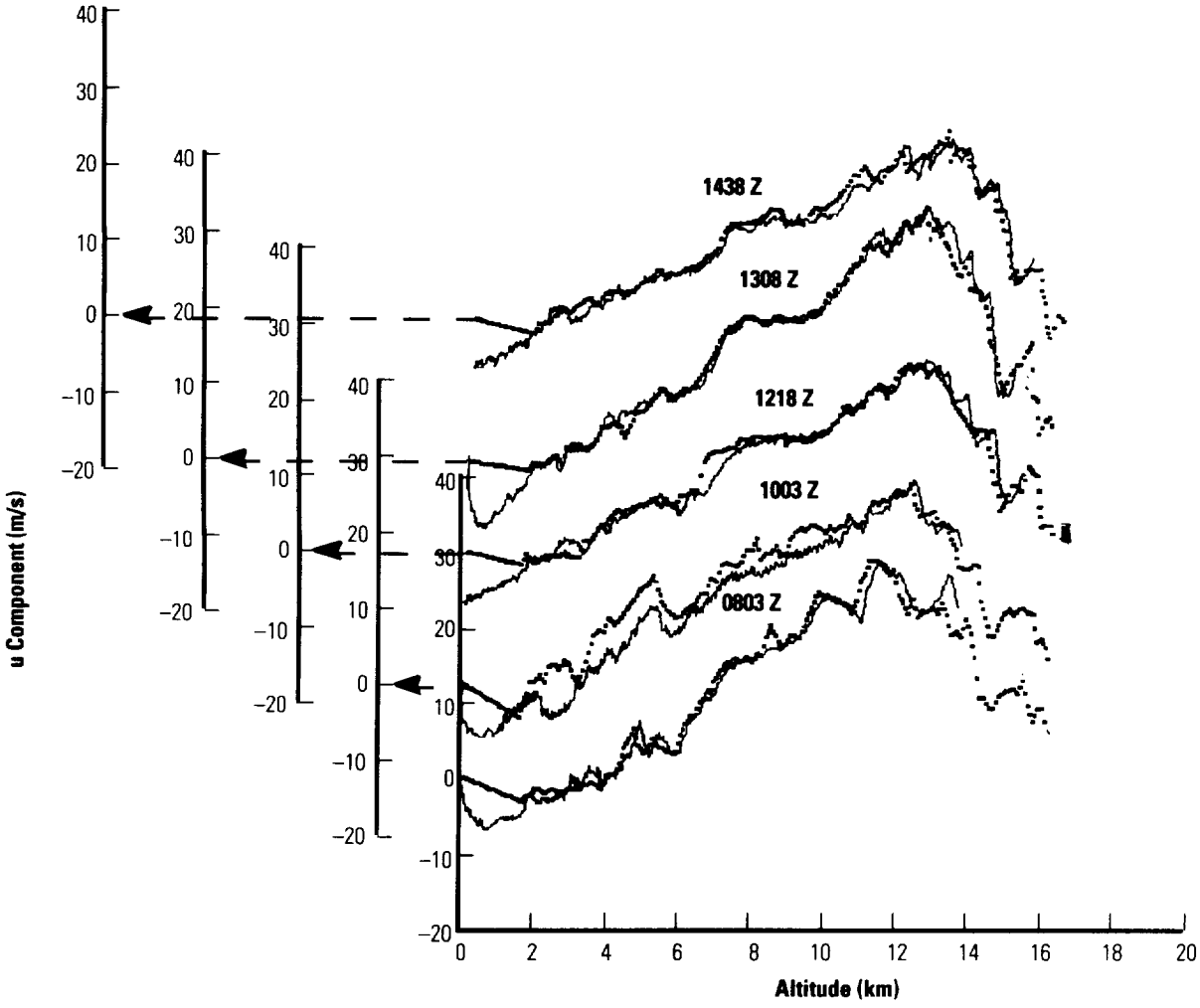

Five u wind components of the NASA 50-MHz radar wind profiler overlayed on the wind profile of FPS–16 radar/jimsphere measured during the STS–37 launch, April 5, 1991, at KSC, FL.

The standard deviation of the u and v wind components for STS–37 (five **jimsphere**/profiler data sets) was 1.94 and 1.67 m/s (6.36 and 5.48 ft/s), while for the STS–43 launch (comparison of six profiles) it was 1.39 and 1.44 m/s (4.46 and 4.72 ft/s), respectively. The overall standard deviation for the 11 profiles was 1.66 m/s (5.44 ft/s) for the u component and 1.55 m/s (5.08 ft/s) for the v component.

The launch scenario of the **jimsphere**/profiler winds aloft during launch of STS–37 on April 5, 1991, at KSC, FL, illustrates the comparison. The pairs of **jimsphere** and wind profiler wind data were compared at 0803 Z (L–6 h before launch), 1033 Z (L–4 h before launch), 1308 Z (L–70 min before launch), 1423 Z (L–0, profiler data only), and 1438 Z (L+15 min after launch). This

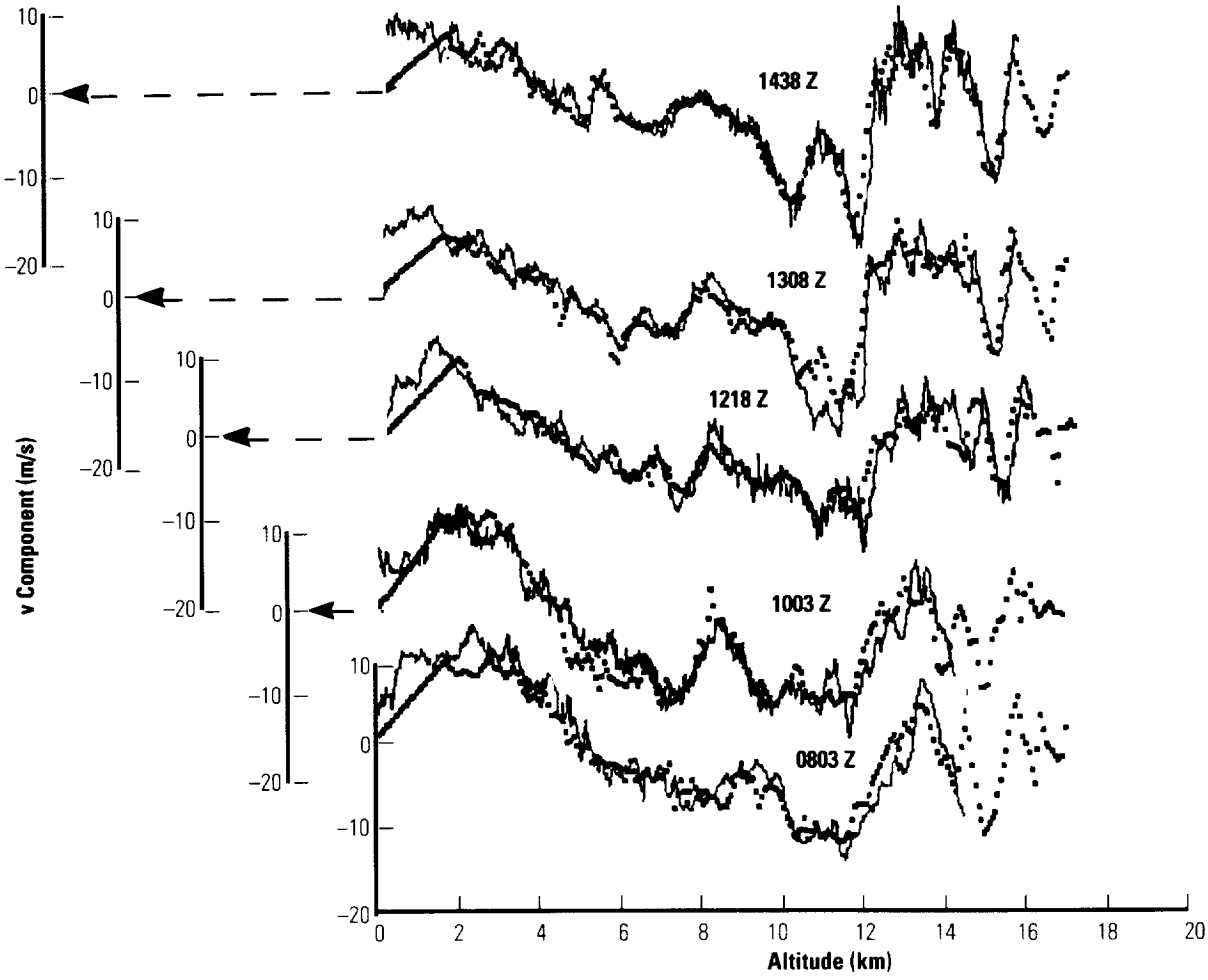

Five v wind components of the NASA 50-MHz radar wind profiler overlayed on the wind profile of FPS–16 radar/jimsphere measured during the STS–37 launch, April 5, 1991, at KSC, FL.

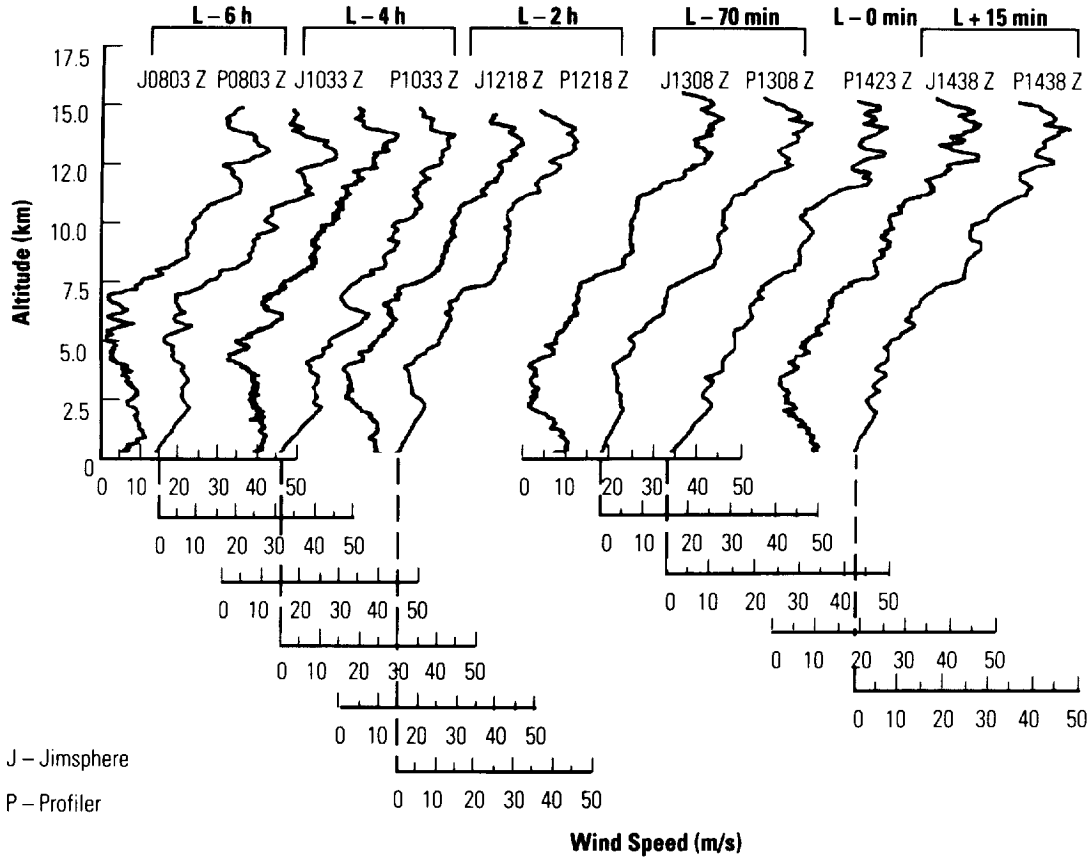

Comparison of the scalar wind speed from the jimsphere and the wind profiler, April 5, 1991, during launch of STS–37 at KSC, FL.

comparison shows very well the buildup and backoff wind fluctuations occurring simultaneously in both wind sensors.

The profiler wind data at L–0 demonstrates that NASA's 50-MHz **radar wind profiler** plays an important role in monitoring winds to determine substantial wind profile changes during shuttle launch operations by illustrating the persistence of the wind speed changes. It would be an asset in the 21st century during launch procedures for the NASP and the NLS being developed by NASA and the USAF. In addition, the rapid turnaround wind measurements by NASA's 50-MHz **radar wind profiler** will be a tremendous boost for the speed-up schedule for NASA's S.S. *Freedom* program and for human space exploration of the Moon and Mars in the next century.

[1]Susko, M., "Wind Measurements by Electromagnetic Probes," NASA TM 4066, September 1988, pp. 1–23.

[2]Smith, S.A., "Cross Spectral Analysis to Determine the Resolution and Precision of Jimsphere and Windsonde Wind Measurements," Third International Conference on the Aviation Weather System, Anaheim, CA, American Meteorological Society, Boston, MA, January 30 to February 3, 1989, pp. 385–386.

[3]Wilfong, T.L., Smith, S.A., and Creasy, R.L., "High Temporal Resolution Velocity Estimates From the 50-MHz Wind Profiler," American Institute of Aeronautics and Astronautics (AIAA) paper 92–0719, January 1992.

M. Susko/ES44
205–544–1660
Sponsor: Office of Space Flight

Solar Terrestrial Physics

Ionosphere-Thermosphere-Mesosphere Physics

Ionosphere-thermosphere-mesosphere refers to the regions of neutral and ionized gases that make up the atmosphere from approximately 60 km (40 mi) to the lower fringes of the magnetosphere (approximately 800 km (500 mi)). This is a region that responds very directly to the large variations in ultraviolet (UV) solar irradiance that take place in the course of a solar cycle. It is also a region that is directly coupled to a highly variable influx of energy in the form of energetic charged particles that originate in the solar wind and are accelerated into the atmosphere by the Earth's magnetic field. Massive magnetospheric current systems close in the ionosphere and their effects play a fundamental role in establishing the nature of these regions. From below, atmospheric tides break against the lower boundaries and turbulence dissipates its energy in eddies. Chemical species, such as water vapor products, penetrate the region from below, and other species, such as nitric oxide, pass through to the upper stratosphere. This region of the atmosphere plays a key role in the coupled solar-terrestrial system. One of the most important parts of this region, the mesosphere-lower thermosphere region, is rather poorly understood at the present time, and it is this region on which the Ionosphere-Thermosphere-Mesosphere Branch of MSFC is concentrating its attention.

Far-Infrared Spectroscopy of the Upper Atmosphere

Infrared (IR) thermal emission **spectroscopy** provides a powerful tool for studies of stratospheric thermal structure and constituent distributions. Many trace constituents exhibit pure rotational transitions in this spectral region along with the magnetic dipole lines of molecular oxygen (O_2). Stratospheric limb observations carried out with high spectral resolution and high-sensitivity spaceborne instruments provide thermal emission spectra that may be analyzed for retrieval of vertical temperature and constituent distributions. Some recent results retrieved from far-**IR** spectra obtained with high-altitude, balloon-borne instruments include the following stratospheric trace constituents: H_2O, $H_2{}^{17}O$, $H_2{}^{18}O$, HDO, $^{16}O^{16}O^{18}O$, $^{16}O^{18}O^{16}O$, CO, HCN, HF, HCl, OH, $O(^3P)$, HOCl, and H_2O_2 (e.g., Abbas et al., 1987, Traub et al., 1990).

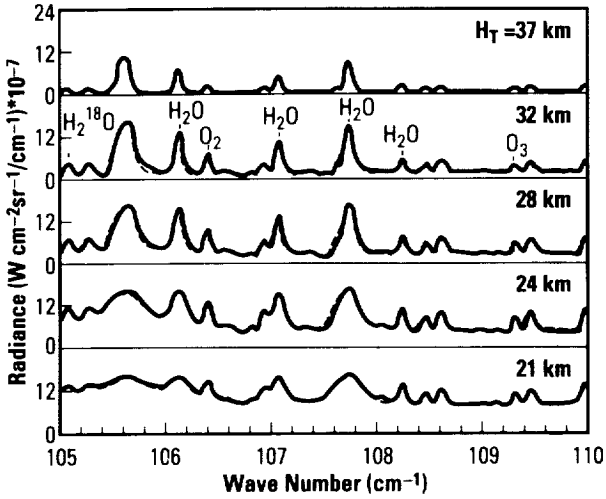

A limb sequence of the observed (solid line) thermal emission spectra in the 105- to 110-cm^{-1} region with tangent heights from 21 to 37 km, along with the calculated spectra (dashed line) using retrieved mixing ratio profiles. Some isolated $H_2{}^{16}O$, $H_2{}^{18}O$, and O_2 lines are identified.

Far-**IR** stratospheric limb thermal emission spectra in the 80- to 220-cm^{-1} region were obtained by the Harvard/Smithsonian group with a double-beam Fourier transform spectrometer launched on a balloon flight from Palestine, TX, on June 23, 1983, in conjunction with the Balloon Intercomparison Campaign (BIC–2). The results for the vertical profiles of H_2O, HF, HCℓ, and $O(^3P)$ obtained from an analysis of the observed spectra by the Harvard/Smithsonian group have been presented in previous publications (World Meteorological Organization (WMO), 1985).

After the surprising measurements indicating an enhancement in the stratospheric heavy ozone concentrations, there has been a considerable amount of interest in observing the isotopic distribution of other constituents, in particular of **water vapor**. Theoretical considerations indicate a small depletion in the stratospheric $H_2{}^{18}O$ and $H_2{}^{17}O$ distributions relative to normal **water vapor**.

An analysis of the BIC–2 observed data was performed at MSFC for retrieval of the vertical distribution of some stratospheric constituents with a focus on the isotopic **water vapor**. The retrieved vertical profiles of O_3, H_2O, $H_2{}^{17}O$, $H_2{}^{18}O$, HF, and HCℓ were obtained and compared with the results obtained simultaneously by other experiments on BIC–2.

In an overview of the observed spectra in the 105- to 202-cm^{-1} range for a complete limb sequence of five angles with tangent heights varying from 20 to 37 km, the spectral features due to the rotational lines of $H_2{}^{16}O$, $H_2{}^{17}O$, $H_2{}^{18}O$, and O_2 are identified. The vertical profiles of the stratospheric constituents are determined from the observed features employing analytical inversion techniques.

In a comparison of the vertical profiles of $H_2{}^{16}O$, $H_2{}^{18}O$, and $H_2{}^{17}O$ retrieved from the observed spectra, the profiles indicate the concentrations of the two heavier **isotopes** of **water vapor** to be essentially the same, within the uncertainties. This result is consistent with those obtained in previous investigations, indicating no evidence for stratospheric isotopic enhancement or depletion of the water **isotopes** $H_2{}^{18}O$ and $H_2{}^{17}O$ with respect to the main **isotope**.

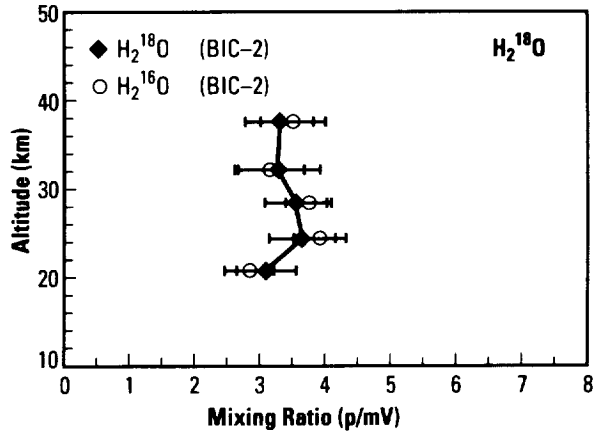

The $H_2{}^{18}O$ mixing ratio profile retrieved from the BIC–2 far-IR data analyzed in this work. The mixing ratios are normalized to their natural abundance in accordance with the HITRAN data base. Also shown for comparison is the normal $H_2{}^{16}O$ profile retrieved in this work.

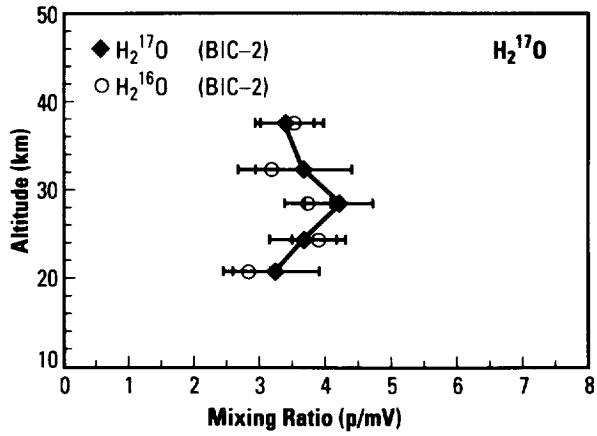

The $H_2{}^{17}O$ mixing ratio profile retrieved from the BIC–2 far-IR data analyzed in this work. The mixing ratios are normalized to their natural abundance in accordance with the HITRAN data base. Also shown for comparison is the normal $H_2{}^{16}O$ profile retrieved in this work.

Abbas, M.M., Guo, J., Carli, B., Mencaraglia, F., Bonetti, A., Carlotti, M., and Nolt, I.G., "Stratospheric O_3, H_2O, and HDO Distributions From Balloon-Based Far-Infrared Observations," *J. Geophys. Res.*, 92 (1987), pp. 8354–8364.

Traub, W.A., Johnson, D.G., and Chance, K.V., "Stratospheric Hydroperoxyl Measurements," *Science*, 247 (1990), pp. 446–449.

WMO, Atmospheric Ozone, Report 16, WMO, Geneva, 1985.

M.M. Abbas/ES55
205–544–7680
Sponsors: Office of Space Science and Applications
and Center Director's Discretionary Fund

Imaging Spectroscopy of the Thermosphere and Mesosphere From the ATLAS–1 Shuttle Mission

Spectroscopy provides a means for **remote sensing** the composition and temperature of the atmosphere as well as processes occurring within the atmosphere. The **mesosphere** (60 to 100 km (37 to 62 mi)) and the thermosphere (100 km (62 mi) to approximately 500 km (312 mi)) are regions that have extensive emission spectra in the vacuum ultraviolet (UV), visible, and near-infrared (NIR). Much of the **spectroscopy** of this region has been carried out from the ground, where it is limited to nighttime and visible wavelengths, or by relatively small instruments flown on rockets or scientific satellites, which have covered limited portions of the wavelength range at any one time. In addition, very little work has been done on the region between approximately 60 to 150 km (37 to 74 mi). This region, which has sometimes been referred to as the "ignorosphere," is too low to be studied by conventional satellites, and so its exploration has had to await the development of appropriate remote-sensing instrumentation to probe down into it.

The imaging spectroscopic observatory that flew on the Atmospheric Laboratory for Applications and Science-1 (ATLAS–1) shuttle mission (March 24 to April 2, 1992) was designed to take advantage of the shuttle's payload capacity to carry a very comprehensive instrumentation into orbit and to measure, for the first time, the emission spectrum of the **mesosphere**, thermosphere, and ionosphere under both sunlit and dark conditions, over a broad wavelength range (300 to 8,300 Å).

The imaging spectrometric observatory is an array of five state-of-the-art spectrometers, each with an intensified charge coupled device (CCD) focal plane detector, allowing each spectrometer to image hundreds of angstroms simultaneously. As a result, this instrument had the potential to measure emissions from almost all the species of interest in this broad altitude region.

During the 9-d ATLAS–1 mission, a most successful series of observations was made of a variety of atmospheric regions of interest, using operating modes optimized for different targets. The instrument's flight computer was used to run certain sequences automatically, while others were commanded by the science team on the ground. In addition, a lap-top computer interface was provided to the payload crew with which they were able to interact with the investigation, a mode that was particularly useful during those times when the orbiter was not in direct communication with the ground. In particular, the instrument was most successful in fulfilling the primary objective of spectrally mapping the dayglow and the nightglow. Due to activity during the mission, it was also possible to spectrally map the aurora. By taking advantage of vehicle maneuvers in some cases, and by using a scanning mirror in other cases, it was possible to scan the field-of-view of the instrument down through the atmosphere and thus to obtain altitude profiles of the many emission features, some of which have not been observed in the dayglow previously. An exceptionally high-quality data base has been obtained, some examples of which are given below.

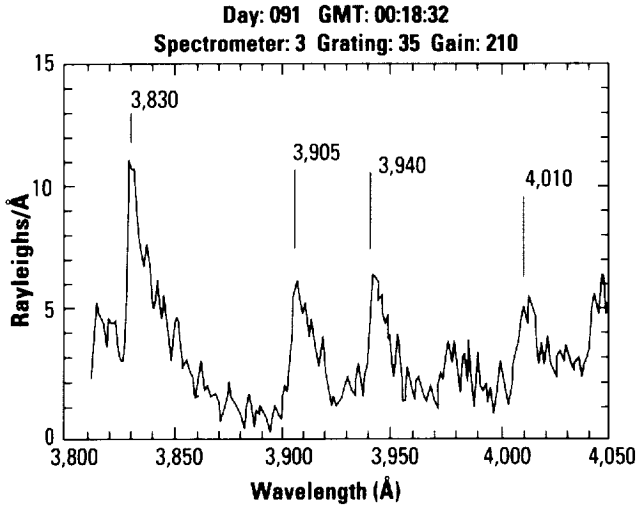

GMT—Greenwich Mean Time

An example of a portion of the near-UV dayglow taken looking at 120 km (75 mi).

In an example of a portion of the near-UV dayglow, taken looking at 120 km (75 mi), the spectrum shows the emission features of various bands of molecular oxygen (O_2) known as the Chamberlain and Herzberg bands. These are important in that they allow researchers to infer the concentrations of atomic O_2, a species which is extremely difficult to measure at these altitudes. A surprising aspect, however, is that researchers had not expected to be able to measure these bands so clearly at such high altitudes.

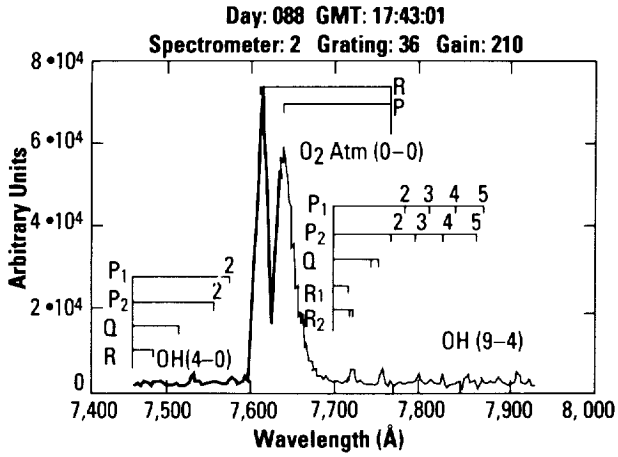

An example of the 1–0 band of the O_2 atmospheric system. This feature is useful in determining the temperature of the mesosphere.

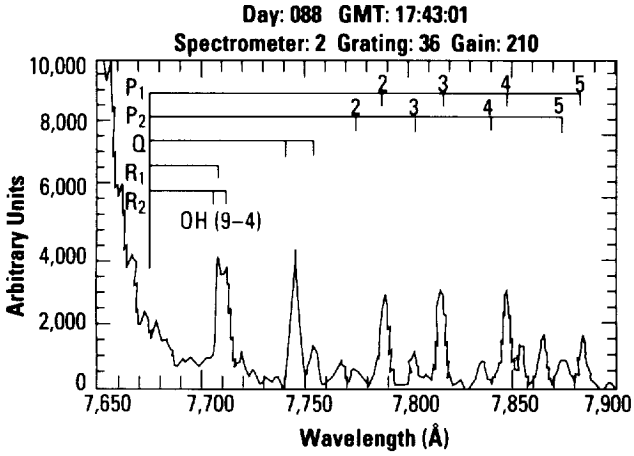

An enlargement of the tiny features in the wings of the large O_2 feature in the 1–0 band of the O_2 atmospheric system, showing the bands of an excited form of the hydroxyl radical, known as the OH Meinel system.

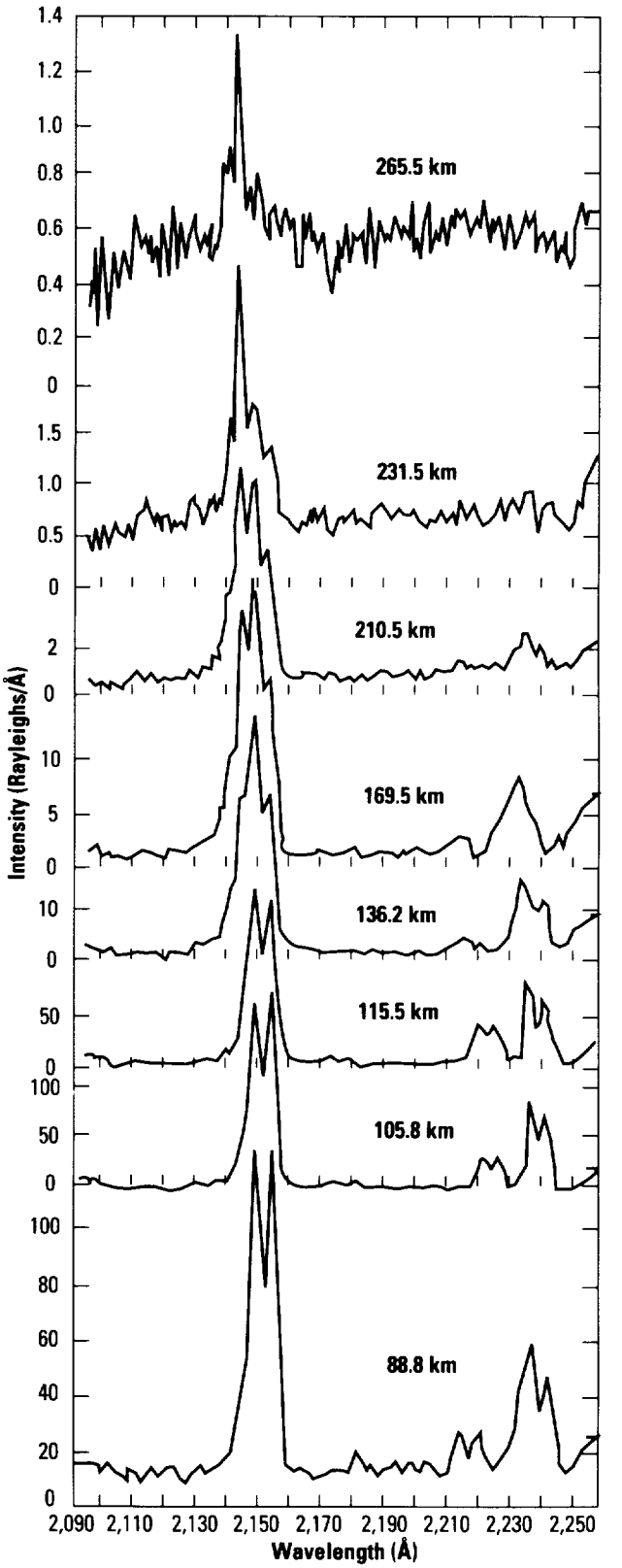

An example of an altitude profile in which a line of state of atomic N_2 can be seen at the higher altitudes, changing into nitric oxide bands as the altitude decreases. The profile was obtained by making a special roll maneuver with the orbiter.

Torr, M.R., Torr, D.G., Chang, T., Richards, P.G., Baldridge, T.W., Owens, J.K., Dougani, H., Fellows, C., Swift, W., and Hladky, J., "The First Negative Bands of N_2^+ in the Dayglow From the ATLAS–1 Shuttle Mission," *J. Geophys. Res.*, in press, 1992.

Torr, M.R., and Sullivan, K.D., "The ATLAS–1 Shuttle Mission," *Eos*, vol. 73, No. 105, 1992.

Torr, D.G., Torr, M.R., Baldridge, T.W., Chang, T., Dougani, H., Fellows, C., Fennelly, J., Owens, J.K., and Tejada, A., "Early Results of the Imaging Spectrometric Observatory on ATLAS–1," *Geophys. Res. Lett.*, in press, 1992.

M.R. Torr/ES51
205–544–7591
Sponsor: Office of Space Science and Applications/
Space Physics Division

Magnetosphere Physics

What happens to a planet immersed in a supersonic blast of magnetized plasma emanating from the star around which it dutifully orbits? The answer depends on the relative importance of many physical effects, which form the subject matter of magnetospheric physics. In neighboring unmagnetized planets, researchers can see wide-ranging, long-term outcomes from the dense atmosphere of Venus to the nearly missing atmosphere of Mars. Mercury is magnetized and has no atmosphere, whereas Earth is magnetized and, luckily, has retained a very significant atmosphere. On shorter time scales, variations are found in the wind from the Sun that produce storms which are manifested as bright displays of auroral light, electrical currents capable of tripping circuit breakers and disrupting power transmission, and electromagnetic noise capable of disrupting communications and radar surveillance. MSFC research has made the science community increasingly aware of the transport of energy from the solar wind toward the Earth, dissipating energy in the ionosphere and atmosphere resulting in the escape of atmospheric gases into space in conjunction with these other effects.

Spacecraft orbiting at high velocity in the plasmas of space interact with these plasmas in ways that influence the design of space systems, particularly electrical and electronic systems. Two particularly notable examples are the tethered satellite system (TSS) and Space Station Freedom *(S.S.* Freedom*). The long conducting tether forms an electrical dynamo, driving current through the tether and the conducting plasma through which it flies, inducing electrodynamic drag far in excess of that due to collisions with the rarefied atmospheric gases. The solar cell array for the space station will tend to charge the entire station relative to the plasma around it and other objects within that plasma, such as the orbiter. Operational understanding of these effects is dependent on basic knowledge of electrodynamic plasma interactions with bodies in space, a discipline closely allied with magnetospheric physics, particularly within the Magnetospheric Physics Branch at MSFC.*

During 1991–92, research and technology activities in the areas of magnetospheric and space plasma physics at MSFC led to the following notable highlights:

- *Extensive phase A study of the Office of Space Science and Applications (OSSA) inner magnetosphere imager (IMI) mission by the Science Study Team and the MSFC Program Development Team*

- *The successful flight of the thermal electron capped hemisphere spectrometer (TECHS) aboard the combined release and radiation effects satellite (CRRES) AA–4 sounding rocket from Puerto Rico*

- *Analysis of data from the third sounding rocket flight of the superthermal ion composition spectrometer (STICS) aboard the Cornell University Topside Probe of the Auroral Zone-3 (TOPAZ–3) payload*

- *Initial development of instrumentation and flight plans for a rocket flight known as sounding of the cleft ion fountain energization region (SCIFER)*

- *Discovery of complex motions of solar particles entering the magnetosphere in the region of the polar cusp, leading to a new definition of the entry boundary or inner edge of the magnetosphere's plasma mantle*

- *Discovery of gyrophase effects in the substorm precipitation of energetic ions*

- *Determination that dayside ionospheric upwelling is unaffected by the direction of the interplanetary magnetic field, but increases strongly with the dynamic ram pressure of the solar wind*

- *Development of plasma wave raytracing tools applicable to more realistic "warm" plasma conditions in the magnetosphere*

- *Analysis of the plasma wave populations associated with the strong plasma density gradients in the outer plasmasphere*

- *Near completion of the archival of dynamics explorer/retarding ion mass spectrometer data to optical disk*

- *Development toward delivery of the thermal ion dynamics experiment/plasma source instrument (TIDE/PSI) for the international solar terrestrial physics (ISTP) program (POLAR) spacecraft*

- *Completion of mission preparedness for the TSS, including the research in orbital plasma electrodynamics (ROPE) investigation.*

Failure of Solar Plasma to Enter the Magnetosphere

The solar wind has long been thought to enter the Earth's magnetosphere mainly in the two regions, known as "**cusps**," located high over the magnetic poles of the Earth and somewhat shifted toward the sunward direction (Ashour-Abdalla et al., 1991). The **cusps** mark the location where the Earth's magnetic field tends to puncture through the magnetosphere into interplanetary space. Delcourt et al. (1990, 1992) have investigated the entry of **solar wind plasma** by this route using three-dimensional (3–D) single particle trajectory tracing in models of the geomagnetic and geoelectric fields. Solar wind-like protons were started at numerous points distributed just inside the dayside magnetopause and tracked until they escaped from the model system, which extended to 70 Earth radii (R_E) downstream. Complex motions developed in the cusp regions. Some protons travel to very low altitudes and are lost in the atmosphere at the "footprint" of the cusp magnetic field lines. Other particles underwent bouncing trajectories, trapped in a local minimum of the magnetic field strength in the outer cusp region. These particles penetrated the farthest into the magnetosphere, defining an entry boundary. Solar wind particles were unable to gain access to the magnetospheric plasma sheet within the 70 Earth radii limit of the model space.

The magnetospheric fields were described by the empirical models of the magnetic field with an empirical model of the convection electric field mapped throughout. **Ion trajectories** were initiated along the noon meridian at the dayside magnetopause and tracked using the full equations of motion in regions where criteria for guiding center motion were violated, or the guiding center equations of motion elsewhere.

The following two categories of nonadiabatic behavior were produced.

- Energy decreases with significantly enhanced penetration of the particles to low altitudes in the cusp as contrasted with cases in which the motion was assumed to remain adiabatic.

- Energy increases with bouncing motions in the high-altitude **cusps**, owing to trapping in the magnetic field minimum there. Nevertheless, these nonadiabatic motions ceased as the particles convected antisunward to field lines that contain no magnetic field minimum along their lengths between the ionosphere and the system boundary. The result was injection to adiabatic convecting trajectories along a surface defined as the first field line to exhibit a monotonic decrease of field magnitude with position along the field line. The significance of this surface is that it implies a closely related inner limit of solar plasma penetration into the **magnetotail**, which is referred to as the entry boundary.

The following features are included in the noon-midnight meridian cross section of the magnetosphere:

- The magnetopause

- The entry boundary, i.e., the most tailward cusp field line exhibiting a minimum along its length (just inside the magnetopause for negative x)

- The convective motions for protons released at intervals along this boundary with initial pitch angles of 90°, and selected energies.

The entry boundary is shown for ion energies of 1 keV, 0.1 keV, 0.01 keV, and 0.001 keV for a cross polar cap potential of 40 kV, corresponding to slow magnetospheric convection characteristic of magnetically quiet periods. The 1-keV trajectories are indistinguishable from the entry boundary. Convection of solar plasma to the inner plasma sheet requires much stronger magnetospheric convection, or perhaps a magnetic field with a more widespread field minimum than the one used. This result is compatible with direct observations of the mantle, lobes, and plasma sheet, as embodied in numerous schematic diagrams of the magnetosphere that have been developed empirically.

Based on these results, the plasma that does have access to the plasma sheet along the route usually associated with solar wind entry would be the ionospheric outflows, 100 eV or less in flow energy with similar thermal energies and containing helium and oxygen ions as well as protons. Delcourt et al. (1989, 1990) suggest that plasma sheet acceleration effects are adequate to energize these ionospheric outflows to plasma sheet energies, especially in conjunction with **magnetotail** substorm dynamics.

There are a few obvious qualifications of these results. First, stronger magnetospheric convection would carry the solar wind flow to the plasma sheet closer to Earth than in the case of a 40-kV cross-tail potential drop. However, results suggest that the quiet H^+-dominated plasma sheet cannot be formed directly from mantle plasma.

It is possible that solar wind flows arriving at the plasma sheet at great distances could be convected back to the inner plasma sheet to supply it. Such trajectories have been neglected in view of the large computing task of following them and the lack of empirical basis for model fields beyond 70 R_E. The model used contains a neutral line near 100 R_E, and ions that arrive at the plasma sheet beyond it will be lost. Therefore, it is unlikely that the solar wind flow will be convected back to the inner plasma sheet.

A more feasible entry route may exist in the low-latitude boundary layer along the "flanks" of the magnetosphere. In view of the present results, this would appear to be the best hope for solar plasma access to the inner magnetosphere.

The present understanding of global magnetospheric plasma circulation is thus inconsistent with the direct entry of **solar wind plasma** into the plasma sheet under quiet conditions inside of 70 R_E. It is possible to make a strong case for the production of the plasma sheet from the convective recycling and acceleration of ionospheric plasma, but these results do not support the concept of a solar plasma origin for the plasma sheet inside 70 R_E in the **magnetotail**. While ionospheric outflows would appear to dominate this particular entry route to the plasma sheet, it is clear that similar processes will produce a plasma sheet from solar plasma at greater distances in the **magnetotail**.

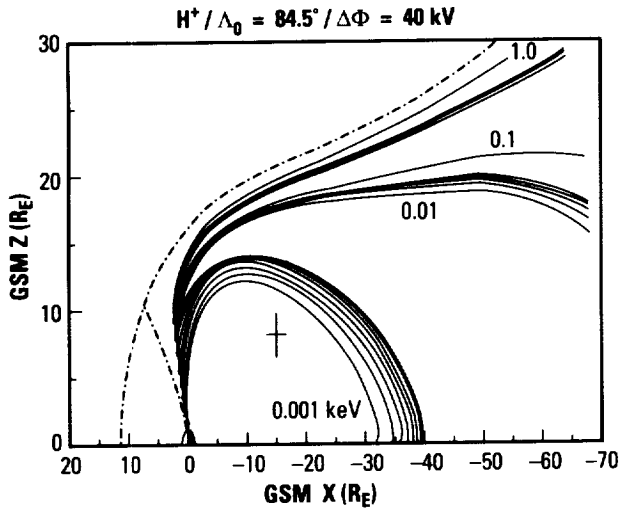

Trajectories of protons projected into the noon-midnight meridian cross section of the magnetosphere. Geocentric solar magnetosphere (GSM) trajectories are plotted in the coordinate system (positive x toward the Sun).

Ashour-Abdalla, M., Berchem, J., Buchner, J., and Zelenyi, L.M., "Large- and Small-Scale Structures in the Plasma Sheet: A Signature of Chaotic Motion and Resonance Effects," *Geophys. Res. Lett.*, vol. 18, No. 1603, 1991.

Delcourt, D.C., Sauvaud, J.A., and Moore, T.E., "Cleft O^+ Contribution to the Ring Current," *J. Geophys. Res.*, vol. 95, No. 20937, 1990.

Delcourt, D.C., Moore, T.E., and Sauvaud, J.A., "Nonadiabatic Transport Features in the Upper Cleft Region," *J. Geophys. Res.*, vol. 96, in press, 1992.

T.E. Moore/ES53
205-544-7633
Sponsor: Office of Space Science and Applications

The Plasmasphere Bulge Region

The thermal plasma of the **magnetosphere** is a system that has a memory: the distribution of plasmas at any time are dependent on convection activity, instabilities, and the **magnetosphere**-ionosphere interchange fluxes to which individual plasma packets have previously been exposed. This perspective is of particular importance in studies of the duskside **bulge region** of the **plasmasphere**, a region that today remains poorly known and understood. The bulge plasma exhibits the effects of strong interactions between convection and corotation electric fields, such that there is often a type of reversal with latitude values (or L values) from predominantly eastward flow (in a stationary frame) to predominantly westward flow. By analogy to the mid-latitude trough, the bulge may contain adjacent plasma regions whose preceding flow histories differ widely. The fact that the **bulge region** is poorly known and understood is not surprising when one considers its immense size, extending from the main **plasmasphere** to essentially the magnetopause or tail region within the local time interval from approximately 12 to 24 magnetic local time (MLT).

The **bulge region** is considered to be geophysically important because of its apparent involvement in the erosion of the **plasmasphere** by the action of enhanced convection electric fields and because of interactions between substorm-associated hot plasmas and the cool **plasmasphere**. The region is important for the flow into **magnetosphere** boundary layers of plasma entrained by convection electric fields, as well as the flow and distribution of dense plasmas that are effectively removed from the main **plasmasphere** but do not escape from the outer **magnetosphere**.

The purpose of this research has been to provide an updated view of the properties of the **bulge region**, with emphasis on its structural complexity and the main features of its dynamic behavior. Emphasis is also placed on the distribution of dense plasma in the aftermath of erosion events and the interplay between convection and **magnetosphere**-ionosphere interchange fluxes during recovery periods. This broad approach is made possible by the availability of measurements from several multiday periods in 1982 on satellites Dynamics Explorer-1 (DE-1), International Sun-Earth Explorer-1 (ISSE-1), and Geodetic Earth-Orbiting Satellite-2

(GEOS–2), each in a unique orbit, and from the longitudinally spaced ground whistler stations Siple, Halley, and Kerguelen. In a rendezvous situation involving ISEE–1, DE–1, and the Siple ground whistler station, good mutual agreement, within an order of 30 percent between ground and satellite data acquired in rendezvous situations, is demonstrated by comparing equatorial density profiles. A plasmapause decrease is clearly shown in both the ISEE–1 and DE–1 data, although at slightly different L values. The whistler data show the beginning of a plasmapause effect where the steep falloff begins on the ISEE–1 profile. The straight line is a reference for the quiet or "saturated" **plasmasphere** from recent empirical modeling work.

By analyzing many such rendezvous within the **bulge region**, the following evidence has been found.

- The **bulge region** and main **plasmasphere** are really two separate but related entities, with the bulge being plasma that has been or is being eroded from the main **plasmasphere.**

- From a statistical point of view, the main **plasmasphere** is roughly circular in equatorial cross sections, with only a slight bulge at dusk.

- The abrupt westward edge of the bulge observed from whistlers represents a state in the evolution of sunward-extending streamers.

- In the aftermath of a weak magnetic storm, 10 to 30 percent of the plasma "removed" from the outer **plasmasphere** appears to remain in the afternoon-dusk sector beyond the main **plasmasphere.**

- Outlying dense plasma structures may circulate in the outer duskside **magnetosphere** for many days following an increase in convection, unless there is extremely deep quieting.

- A day-night plasmatrough boundary may be readily identified in equatorial satellite data.

- A factor of 2-to-10 density irregularities appears near the plasmapause in the postdusk sector in the aftermath of weak magnetic storms.

- During the refilling of the plasmatrough from the ionosphere at L=4.6, predominantly bidirectional field-aligned and equatorially trapped light ion pitch angle distributions give way to predominantly isotropic distributions when the plasma density reaches a level factor of approximately 3 below the saturated **plasmasphere** level.

- Some outlying dense plasma structures are effectively detached from the main **plasmasphere**, while others appear to be connected to the main **plasmasphere**.

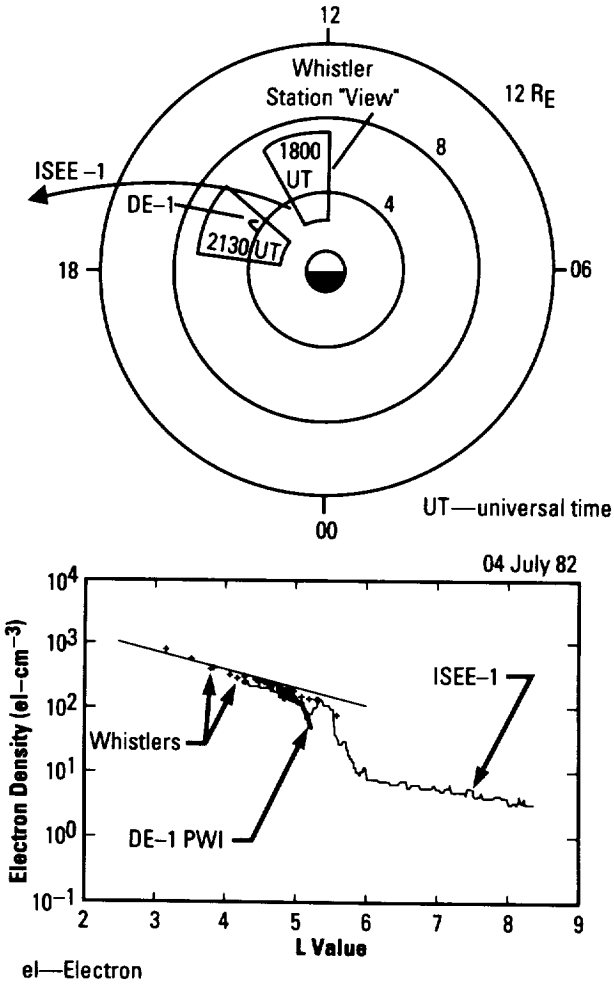

Data comparison involving DE–1, ISEE–1, and the Siple, Antartica, ground whistler station.

Carpenter, D.L., Giles, B.L., Chappell, C.R., Decreau, P.M.E., Anderson, R.R., Persoon, A.M., Smith, A.J., Corcuff, Y., and Canu, P., "The Plasmasphere Bulge Region Revisited," submitted to *J. Geophys. Res.*, 1992.

Carpenter, D.L., Smith, A.J., Giles, B.L., Chappell, C.R., and Decreau, P.M.E., "A Case Study of Plasma Structure in the Dusk Sector Associated With Enhanced Magnetospheric Convection," *J. Geophys. Res.*, 97 (1992), pp. 1157–1166.

B.L. Giles/ES53
205–544–7637
Sponsor: Office of Space Science and Applications

Use of N^+ to Study the Ionosphere/Plasmasphere

In order to understand any region of the Earth's **magnetosphere**, it is important to know and understand the behavior of all the constituents of that region. The ion of atomic nitrogen, N^+, is being used in this sense to extend knowledge that has been gained of the ionospheric and plasmaspheric regions from previous and ongoing investigations of the major ionic species, **ions** of atomic oxygen (O^+), hydrogen (H^+), and helium (He^+), respectively. A comprehensive investigation is in progress that will use both measured data and a theoretical model for case studies and for statistical studies of the ionospheric and plasmaspheric interactions. The minor ion N^+ is being used extensively in the study because it has been found to be almost as ubiquitous as O^+ in the rather extensive data base formed from the retarding ion mass spectrometer (RIMS) on Dynamics Explorer-1 (DE–1). It has been found from the RIMS data set that N^+ generally follows the same patterns as O^+ but at a lower level, and one that varies relative to O^+. Since the ion chemistry, energetics, and dynamics of each of the minor **ions** are not completely independent of influence from the major **ions**, although the effect of the minor **ions** on the major **ions** is negligible, all measurable aspects of the **ions** should be matched in a model, i.e., the model should predict the temperature, density, and velocity of the ion being studied. Solutions for N^+ have to use the solutions for the other three important **ions** (O^+, H^+, and He^+) because N^+ has a source related to He^+ and also depends on O^+ and H^+ through diffusive interactions.

The field line interhemispheric plasma (FLIP) is the computer-programmed theoretical model used in this study. It is a self-consistent model of the **plasmasphere** that includes ion chemistry, photoelectron energetics, and ion dynamics. The numerics of the FLIP model are described by Young et al. (1980). Torr et al. (1990) give a brief overview and some description of the underlying physics. In the present study, predictions of this model have been compared to ion data from the Atmospheric Explorer (AE) program. In order to do this, densities from the AE ion spectrometers (magnetic ion spectrometer and Bennet ion mass spectrometer), ion temperatures from the retarding potential analyzers, and electron temperatures from the Langmuir probes have been averaged over 6 h in local time, across hemispheres, geomagnetic activity, and over the years of low solar activity (the solar minimum) during which AE was operating.

In order to match the conditions prevailing during the time of the AE measurements, the FLIP model was run with an F10.7 (a measure of solar activity) representative of low solar activity and an Ap (an indicator of the level of geomagnetic activity) representative of quiet geomagnetic conditions. One of the free parameters used in the FLIP model is a trapping factor that gives the percentage of the photoelectrons trapped in the **plasmasphere** that lose their energy in the **plasmasphere**. The trapping factor was chosen so that temperatures from the model and the measured AE data would match as closely as possible.

When the ion temperatures of the model and the measured data are closely matched, the model values for density and velocity are generally also in good agreement with the measured values. However, the AE data are low-altitude, generally below 1,200 km. Measurements of low-energy **ions** taken with the RIMS on DE–1 are being combined with the AE data to obtain statistically averaged altitude profiles of the temperature and density of the four major **ions** that can be used to compare both high- and low-altitude measured data with the predictions of the FLIP model. Such comparisons will help to understand ionospheric and plasmaspheric interactions and the influences of solar and geomagnetic activity on such interactions.

Torr, M.R., Torr, D.G., Richards, P.G., and Yung, S.P., "Mid- and Low-Latitude Model of Thermospheric Emissions, 1, $O^+(^2P)$ 7,320 Å and $N_2(^2P)$ 3,371 Å," *J. Geophys. Res.*, vol. 95, No. 21147, 1990.

Young, E.R., Torr, D.G., Richards, P.G., and Nagy, A.F., "A Computer Simulation of the Mid-Latitude Plasmasphere and Ionosphere," *Planet Space Sci.*, vol. 28, No. 881, 1980.

P.D. Craven/ES53
205–544–7639
Sponsor: Office of Space Science and Applications

Wave Propagation in Hot Plasmas

The **magnetosphere** is filled, to varying degrees, with **plasma** that originates in the Earth's atmosphere and to a lesser extent in the Sun. This **plasma** is constantly changing in its speed, temperature, and composition in response to the influence of the solar wind and the Earth's rotation. In concert with these changes, **waves** are produced in the **plasma** that contribute to the transport of energy from one **plasma** population to another and to the loss of **plasma** back into the Earth's ionosphere.

A majority of the studies of propagating **plasma waves** has been conducted with the assumption that the **plasma** has a zero temperature. Under this condition, **wave** properties and propagation can be described by relatively simple mathematical equations. Cold **plasma wave** propagation also includes many of the same physical effects that are characteristic of **wave** propagation in a warm or hot **plasma**. As a result, cold **plasma wave** propagation physics can be used to establish the general features of the transport of energy between **plasma** populations in the **magnetosphere**.

Magnetospheric **plasma** populations, however, do not exist at zero temperature and important physical effects are missed when a zero temperature is assumed. **Wave** dispersion surfaces are significantly altered by the presence of temperate **plasma**: unique hot **plasma wave** modes can appear, cold **plasma** phase and group velocities can be significantly modified, new forms of **wave** growth and damping can occur, new resonances and cutoffs can appear, and there is a greater variety of **plasma wave** mode conversion processes.

An example of the potentially important effects, due to hot **plasma**, on **wave** propagation compares and contrasts the propagation of an ultra-low-frequency (ULF) **wave** in a cold **plasma** with a nearly identical **wave** mode propagating in a **plasma** in which the oxygen (O_2) temperature has been set to 100 eV. The hot **plasma** code RATRACE (Ronnmark and Andre, 1991) has been used in the computations. Both ray paths are nearly identical until the **wave** in a hot **plasma** encounters a cutoff of a resonance-cutoff pair near twice the O_2 cyclotron frequency. The **wave** in the cold **plasma** penetrates deeper into the **magnetosphere** before it encounters the cold **plasma** cutoff of the O_2-helium (O_2-He) resonance-cutoff pair and is reflected. In general, further analysis is required to determine what actually happens to a **wave** when it encounters a cutoff or a resonance, i.e., reflection, tunneling, damping, or mode conversion.

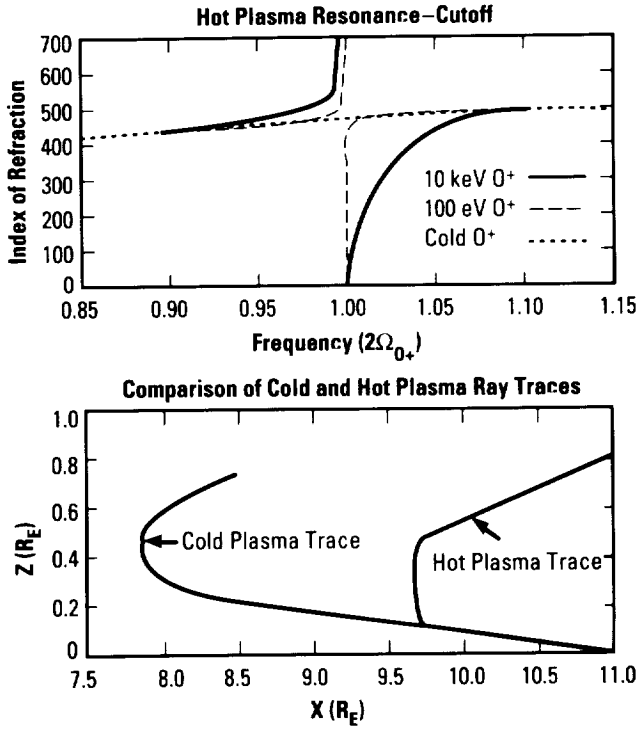

The top panel highlights the effect of finite O_2 temperature on the cold plasma ULF wave index of refraction. For inward propagating waves, the bottom panel shows that ULF waves will be refracted away from low altitudes much sooner in a hot plasma than in a cold plasma.

The technique of incorporating hot **plasma** effects in **plasma wave** propagation studies is currently being used in two areas. In the vicinity of the Earth's equatorial plasmapause, magnetosonic **waves** are produced as a consequence of free energy in the ring current. These **waves** are thought to participate in the perpendicular heating of low-energy, field-aligned ion flows. Cold **plasma** physics have revealed the general consistency of features observed for these **waves**, providing circumstantial evidence for this cascade of energy from the ring current to outflowing ionospheric **plasmas**. Hot **plasma** physics will now be used to further establish a consistency in the detailed spacial distribution of **wave** energy, **wave** amplitudes, and heating levels. Hot **plasma** effects are also needed to complete an understanding of the propagation of ULF **wave** energy from the equatorial magnetopause on the dayside of the Earth into the near-Earth environment. Detailed analysis will be required before the relative importance of reflection, transmission, **wave** mode coupling, and absorption can be determined.

Boardsen, S.A., Gallagher, D.L., Gurnett, D.A., Peterson, W.K., and Green, J.L., "Funnel-Shaped Low-Frequency Equatorial Waves," *J. Geophys. Res.*, in press, 1992.

Ronnmark, K., and Andre, M., "Convection of Ion Cyclotron Waves to Ion-Heating Regions," *J. Geophys. Res.*, vol. 96, No. 17573, 1991.

D.L. Gallagher/ES53
205–544–7587
Sponsor: Office of Space Science and Applications

Solar Physics

In everyday life, the constancy of the Sun is taken for granted. However, it is now known that the Sun is, in fact, a variable star. Over the past 15 yr, observations from space have shown that the total solar output varies slowly in a periodic manner that may be in phase with the familiar sunspot cycle. Although the amplitude of the variation is small, observations of stars that are similar in size and evolutionary development to the Sun, often referred to as solar analogs, show considerably larger variations. If the Sun's variations were of similar amplitude, they would have significant climatic consequences for the Earth. The cause of these variations is unknown, but, if, as appears to be the case for the Sun, it is related to the sunspot cycle, then its source is almost certainly controlled by the interplay between the rotational and convective forces within the solar interior that gives rise to the solar magnetic field.

Although still in their infancy, techniques are being developed that will allow scientists to probe the solar interior by observing the Sun's global oscillations. These oscillations carry information about the medium through which they pass in much the same way that the transmission of shock waves generated by earthquakes tell researchers about the Earth's interior. This discipline is called helioseismology. Two programs currently under development to provide the first extensive observations are: (1) a ground-based global oscillations network and (2) a space-based solar oscillations imager that will fly on a joint European space agency (ESA)/NASA spacecraft called the solar heliospheric observatory (SOHO) in the mid-1990's.

On shorter time scales, variability is even more closely linked to the solar magnetic field. At the base of the atmosphere, the magnetic fields are continually being pushed and jostled by the convective motions present in the Sun's outer layers. These motions can create instabilities in the structures of the outer atmosphere. The resulting disruptions give rise to phenomena called solar flares and coronal mass ejections that release energy in the form of high-energy radiation and particles. The latter propagate outward, reaching the orbit of Earth in times of tens of minutes to several hours. The particles are prevented from penetrating to the Earth's surface, except at the poles, by the Earth's magnetic field. Outside this protection, for instance between the Earth and the Moon or Mars, or on the lunar surface, the flux of these particles can present a serious threat to the health and safety of astronauts.

Understanding solar variability of all forms is inexorably linked to the physics of the solar magnetic field, which forms the basis of solar research at MSFC. Through direct observation of the vector field, a capability developed at MSFC that is still quite unique, there has been considerable success in understanding how the energy stored in the magnetic field by the convective motions of the Sun's atmosphere is released. Currently, MSFC personnel are testing a data-based algorithm to locate, in real time, those magnetic regions that will give rise to large flares. The output of these studies is transmitted to the National Oceanic and Atmospheric Administration's (NOAA's) Space Environment Laboratory where it is used in the preparation of solar activity forecasts. In a second collaboration with NOAA, researchers are developing a solar x-ray imager that will fly on the next series of geostationary operational environment satellites (GOE's) and will also be used to characterize solar activity and its influence on the space environment. Also under development is an experimental vector magnetograph that will be used as a test-bed for advanced technologies, including improved polarimeters and large focal plane arrays with high-speed readouts. Based on these ideas, plans include development of a balloon-borne magnetograph that will be a candidate for flight under NASA's program to study the mechanisms of solar variability, which is a new initiative focused on obtaining high-resolution solar observations.

Solar Flares and Coronal Mass Ejections

Solar **flares** and coronal mass ejections are explosions of large internally stressed bipolar magnetic bubbles in the solar atmosphere. The largest of these events are the greatest explosions in the solar system: the power of the energy burst, approximately 10**32 erg in approximately 10**3 s, or approximately 10**29 erg/s, far exceeds the steady power of the solar wind (approximately 3×10**27 erg/s).

An erupting chromospheric filament typically rides in the core of the exploding magnetic bubble that becomes the coronal mass ejection that blasts out into the solar wind. For hours to days before the explosion, the filament is present and traces out greatly sheared **magnetic field** in the core of the magnetic bubble. Hence, in the explosion, the erupting filament is a tracer of the erupting sheared field in the core of the explosion. If the core field is strong enough (100 to 1,000 G), the field eruption and launching of the coronal mass ejections produce intense particle acceleration and plasma heating. If the core field is weaker (approximately 10 G), the particle acceleration and heating are much weaker, but a large coronal mass ejection can still be produced. Apparently, regardless of the field strength, all of these events are the same kind of magnetic explosion, and so all are appropriately called eruptive **flares**.

Basic unresolved questions about eruptive **flares** include: why do these magnetic bubbles explode and what triggers the explosion? Progress in answering these questions was achieved by solar scientists at MSFC during the past year in a study that built on previous related **flare** research at MSFC.

The study took the three-dimensional (3–D) configuration of the **magnetic field** in and before eruptive **flares** as the main guide to how the field comes to lose its stability and erupt. The typical erupting field configuration for eruptive **flares** was constructed from observed characteristics of: (1) the preflare **magnetic field** configuration, (2) the onset and development of the eruption of this configuration, and (3) the onset and development of the heating and particle acceleration within the erupting field. The observational centerpiece for this construction is the evidence from the MSFC vector **magnetograph**: strong magnetic shear along the main magnetic inversion line (i.e., along the boundary between the two opposite polarity domains of the photospheric roots of the bipolar bubble) is critical for large eruptive **flares**. From the empirical field configuration and the observation that the initial **flare** heating typically stems from points where opposite-polarity flux is gradually merging and cancelling at or near the main inversion line, the MSFC scientists inferred the following: (1) that eruptive **flares** are driven by the eruptive expansion of the strongly sheared core of the preflare **magnetic field**; (2) that this eruption is triggered by preflare slow **reconnection** accompanying flux cancellation in the sheared core; and, (3) in some **flares**, the triggering **reconnection** and flux cancellation is between opposite-polarity strands of the extant preflare sheared core field, while, in other **flares**, it is between the sheared core field and the newly emerging **magnetic field**.

The new idea in this work is that eruptive **flares** are not triggered by the **reconnection** that happens with the initial **flare** heating, but by slower **reconnection** that precedes the initial **flare reconnection** at the same sites. The **flare reconnection** is fast **reconnection** that is driven by and sustains the core eruption; the preflare triggering **reconnection** is a much slower **reconnection** in flux cancellation driven by photospheric flows. The preflare cancellation **reconnection** continues until the core field becomes so weakly tethered that it can begin to erupt and drive fast **reconnection** under it over the main inversion line. The trigger is that last bit of slow **reconnection** that renders the core field globally unstable to eruption and fast **reconnection**.

Solar Magnetic Fields

Eruptive solar flare seated near the limb of the Sun.

Moore, R.L., Hagyard, M.J., and Davis, J.M., "Flare Research With the NASA/MSFC Vector Magnetograph: Observed Characteristics of Sheared Magnetic Fields That Produce Flares," *Solar Phys.*, vol. 113 (1987), p. 347.

Moore, R.L., "Hallmarks of the Magnetic Field in the Solar Atmosphere: Structure, Evolution, Heating, and Flaring," *Solar Magnetic Fields*, G. Poletto, ed., *Memorie della Societa Astronomica Italiana (Journal of the Italian Astronomical Society)*, vol. 61, No. 2, 1990, p. 317.

Moore, R.L., and Roumeliotis, G., "Triggering of Eruptive Flares: Destabilization of the Preflare Magnetic Field Configuration," *Eruptive Solar Flares*, Z. Svestka, B.V. Jackson, M.E. Machado, eds., Springer-Verlag, Berlin, 1992, p. 69.

R.L. Moore/ES52
205-544-7613
Sponsor: Office of Space Science and Applications

The interaction of **magnetic fields** and plasmas is the root cause of the dynamic, high-energy phenomena of flares, mass ejections, and eruptive filaments observed on the **Sun**. Thus, in current solar research, extensive observational studies are carried out to develop an understanding of just how the solar magnetic field plays this key role in solar activity.

MSFC has a unique instrument for observing the **Sun's** magnetic field—the MSFC solar **vector magnetograph**—and the information derived from observations with it has made significant contributions to an understanding of solar activity. In particular, this instrument permits observations of the transverse component of **magnetic fields** from which calculations of important solar parameters, such as electric currents and magnetic shear, can be made; these parameters cannot be obtained from conventional solar magnetographs. Research at MSFC has shown significant correlations of these parameters with the occurrence of major **solar flares**. Thus, the MSFC research shows promise in developing techniques to predict major flares. Such predictions will be necessary as the Agency enters the era of space station, lunar bases, and planetary exploration when people in space will be susceptible to the harmful effects of energetic particles and radiation produced by **solar flares**.

Over the past year, research in this program has been concentrated in three main areas, which are: (1) observational programs, (2) data analysis and modeling, and (3) the experimental vector magnetograph (EXVM). Significant accomplishments in these areas are summarized below.

Solar observing programs were carried out in coordination with the Compton Observatory, the United States/Japanese Yohkoh solar satellite, and the MAX'91 program. During June 1991, a high level of solar activity prompted a world-wide solar observing program; results of MSFC observations during this period were presented at the Compton Observatory Science Workshop in September 1991.

MSFC was selected as part of the Compton Observatory guest investigator program and has initiated analyses of solar **magnetic fields** associated with gamma-ray flares; initial results were presented at the Compton Observatory Science Workshop in September 1991.

Researchers continued to study nonpotential fields associated with flares with daily analyses of vector magnetograms of active regions. Several new computational techniques were developed to analyze the data for relevant nonpotential parameters. A summary of results through 1991 was presented in a seminar at the National Oceanic and Atmospheric Administration's (NOAA's) Space Environment Laboratory in March 1992.

A study was completed on the magnetic field associated with a small flare that produced surging material. A paper describing these results has been accepted for publication.

Collaborations with French scientists at the Meudon Observatory have led to two papers. Also, a paper was published describing coordinated observations of an active region with the MSFC **vector magnetograph** and the Mees Solar Observatory's Stokes polarimeter. Researchers also completed a collaboration with G. Poletto to model extended magnetic structures between active regions. The topology of large interconnecting loop systems seen by Solar Maximum Mission x-ray observations was studied with this model to determine processes that form these loops.

The EXVM, now under development, represents a state-of-the-art **vector magnetograph** that will permit measurements of the solar magnetic field with the highest accuracy that modern technology allows. Recent accomplishments include the completion of the optical design, testing the 65-mm (2.56-in) Fabry-Perot etalon, testing the unique polarimeter, design of an optical image dissector to interface the optics with the large-array charge coupled device (CCD) camera, testing the CCD camera, and developing software for the special data system designed to accommodate the fast data rates from the CCD camera.

Gary, G.A., and Musielak, Z.E., "A Regularization Method for the Extrapolation of the Solar Potential Magnetic Fields," *Astrophys. J.*, 392 (1992), p. 722.

Hagyard, M.J., West, E.A., Smith, J.E., Treussart, F.M., and Kenney, E.G., "Magnetic Field Configuration Associated With Solar Gamma-Ray Flares in June 1991," *The Compton Observatory Science Workshop*, 1992, NASA CP-3137, p. 490.

Hagyard, M.J., "Optical Synthesizer for a Large Quadrant-Array CCD Camera," NASA TM-103571 (1991).

M.J. Hagyard/ES52
205-544-7612
Sponsor: Office of Space Science and Applications

Microgravity Science

As a center of excellence for microgravity science with emphasis on materials science and protein crystal growth, combined with the regional universities (i.e., The University of Alabama in Huntsville; Alabama A&M University, The University of Alabama, Birmingham; Fisk University; Vanderbilt University; and Clark Atlanta University), MSFC has become a focus for microgravity research. In an effort to study the influence of weightlessness on basic materials science and biotechnology, a number of ground-based microgravity research and science programs in support of flight programs is continuing at a high level of activity. MSFC scientists and engineers and the regional universities are utilizing microgravity opportunities on the KC–135 aircraft, the MSFC drop tube, and the space transportation system (STS) to conduct research and checkout of potential flight hardware and experiments. More than 20 principal investigators have had proposals selected as a result of peer reviews in MSFC-managed microgravity ground-based disciplines. MSFC scientists and engineers have prepared and flown several state-of-the-art experiments on recent International Microgravity Laboratory (IML–1) and U.S. Microgravity Laboratory (USML–1) flights, and they are preparing state-of-the-art experiments aimed at the U.S. Materials Payload (USMP), future IML's and USML's, Space Station Freedom *(S.S.* Freedom*), and other shuttle flight opportunities. The results of these efforts have been the selection and participation of 14 MSFC scientists as experiment principal investigators and 8 MSFC scientists as flight hardware development project scientists or assistant mission scientists for flights occurring during 1992.*

Several MSFC scientists are expected to be chosen as experiment principal investigators upon the completion of the NASA Research Announcements (NRA's) selections expected during the summer of 1992. These experiments, as well as the data from recently flown USML–1 and IML–1, will clarify how the absence of gravity-driven convection and sedimentation can beneficially influence solidification and crystallization processes for inorganic and organic materials.

High-Temperature Solidification Research During Aircraft Parabolic Maneuvers

The NASA KC–135 **aircraft** provides materials science researchers routine access to 30-s low-gravity periods (0.01 g) punctuated by 90-s periods of high gravity (1.8 g). The **aircraft's** capabilities to provide **lunar** and martian gravity levels are increasingly being utilized. Often concepts have been proven and refined that were later successfully flown in space. MSFC continues to support a broad range of solidification experiments utilizing the KC–135 unique gravity environment in the fields of **metal alloys**, semiconductors, glasses, and **composite materials**.

This year, under a Center Director's Discretionary Fund (CDDF)-sponsored collaboration between the Space Science and the Materials and Processes Laboratories, one of the first productions was achieved of **glass fibers** from **lunar**-like materials under controlled 1/6-g conditions. Producing technically useful materials from **lunar** or martian ore is of interest to the Space Exploration Initiative (SEI), since the Stafford Report Architecture IV relies heavily on the processing of extraterrestrial materials to greatly reduce costs for Earth-to-orbit launches. These results show that fiber jet diameter compared to that in 1 g is approximately 50 percent smaller in **lunar** gravity. This could have important implications for the materials processes and mechanical properties of **glass fibers** produced on the Moon.

Some **aircraft** solidification experiments (i.e., metal matrix composites) require bulk sample to be both melted and solidified in a single low-gravity period. For this purpose, under funding from NASA Headquarters, researchers have upgraded and flown the rapid melt/rapid quench furnace system. The furnace is designed to hold a 0.5-cm (0.2-in) diameter sample at just below its melting point until **low gravity**. The furnace then moves a super heat (rapid melt) zone over the sample. Before the end of **low gravity**, a water spray nozzle is moved over the sample (rapid quench) and the sample is solidified before entering high gravity. Utilizing the upgraded system, samples of aluminum (Al) matrix silicon carbide (SiC) particle composite samples have been melted and solidified in a single low-gravity parabola for the first time. This enables a new class of high-temperature solidification experiments to be performed on the **aircraft**.

Research in immiscible alloy solidification during **aircraft low gravity** was continued under the MSFC-sponsored graduate student research fellowship program with The University of Alabama in Birmingham (UAB). Experiments this year show a correlation between aligned fiber production and gravity level. New studies are beginning to determine the effect of gravity on the solid/liquid interface and to correlate these data with the Mullins and Sekerka morphological stability criterion.

Recently, there has been interest in the data accumulated during solidification in KC–135 high gravity. This resulted in MSFC contributing an invited paper to the first conference on solidification in centrifuges in Dubna, Russia. Analysis of MSFC high-gravity solidification results has shown no evidence of convective flow dampening counter to that found in some centrifuge studies. It has been hypothesized that diffusion-controlled solidification conditions can occur in centrifuges by counterbalancing buoyancy-driven flows with those due to gravity gradients and the Coriolis force. MSFC's sample microstructural and numerical analysis shows that KC–135 high-gravity arcs, compared to centrifuges at the same gravity, have less of these counterbalancing forces by a factor of 100. Thus, the KC–135 **aircraft** is shown to provide a unique high-gravity environment, allowing the separation of high-gravity from gravity-gradient and Coriolis forces.

Much excitement has been generated by the new oxide high-transition temperature superconducting materials. The first material superconducting above liquid nitrogen (LN_2) temperature was discovered, in part, under

C-2

MSFC CDDF funding. Commercial utilization of these materials is still hampered by poor materials properties, such as low critical current. MSFC researchers have investigated the hypothesis that **low gravity** could increase crystal alignment during solidification (higher alignment tends to increase critical current). In conclusion of a CDDF-sponsored effort, researchers have solidified Y-Ba-Cu superconducting materials during **aircraft low gravity**. Results show that **low gravity** increases the grain alignment. The experiments found that optimum starting composition for ytterbium-barium-copper (Y-Ba-Cu) is different in **low gravity** than that in 1 g. This information is critical to MSFC's proposed plans to solidify these materials in space.

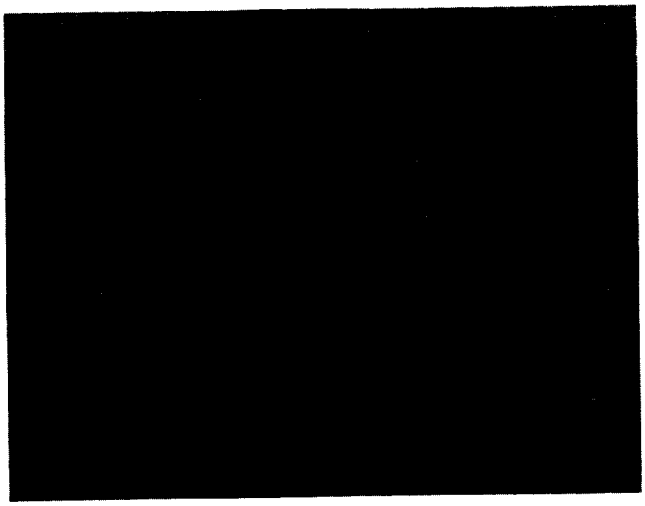

Glass fiber pulled from simulated lunar material.

Curreri, P.A., "The Effectiveness of Coriolis Dampening of Convection During Aircraft High-Gravity Arcs," *Journal of Crystal Growth*, 119 (1992), pp. 141–151.

Vijayakumar, M., Tewari, S.N., Lee, J.E., and Curreri, P.A., "Dendrite Spacings in Directionally Solidified Superalloy," Materials Science and Engineering, A132 (1991) pp. 195–201.

Tucker, D.S., Ethridge, E.C., and Curreri, P.A., "Production of Continuous Glass Fiber Using Lunar Simulant," *SAMPE Journal*, Proceedings of the 23rd International Society for Advancement of Material and Process Engineering (SAMPE) Technical Conference, October 1991, Space Science Laboratory Preprint No. 91–123.

P.A. Curreri/ES75
205–544–7763
Sponsor: Center Director's Discretionary Fund

MSFC 105-m Drop Tube Undercooling and Nucleation Studies

In order to improve present metals and alloys through space processing, it is necessary to first understand the effect of low-gravity processing on the structure and properties of the material. The effect of low gravity coupled with **containerless** processing is being studied using the MSFC 105-m (344-ft) Drop Tube Facility. This environment, achieved in both the drop tube and during a **containerless** space flight, is conducive to large degrees of **undercooling** before solidification of the metal occurs. Therefore, the MSFC 105-m (344-ft) Drop Tube Facility provides an ideal environment for **undercooling** and nucleation studies of undercooled metals.

In the past year, efforts have been directed into two areas of research. The measurement of the histogram of nucleation temperatures for pure metals has continued with emphasis being shifted from pure niobium (Nb) to both pure zirconium (Zr) and nickel (Ni). The results of these investigations will have a direct effect on the Electromagnetic **Containerless** Processing Facility (TEMPUS) electromagnetic positioner, and related experiments, to be flown aboard the International Microgravity Laboratory–2 (IML–2) Spacelab mission.

Additional studies have begun in the area of deep **undercooling** followed by rapid solidification. A recent patent was granted for this concept and current research will determine the value of this technique in materials processing.

Hofmeister, W.H., Bayuzick, R.J., and Robinson, M.B., "Noncontact Temperature Measurement of a Falling Drop," *International Journal of Thermophysics*, vol. 10, No. 1, January 1989.

Robinson, M.B., Bayuzick, R.J., and Hofmeister, W.H., "A Review of Drop Tube and Drop Tower Facilities and Research," *Space Commercialization: Platforms and Processing*, edited by F. Shahrokhi, G. Hazelrigg, and R. Bayuzick, *Progress in Astronautics and Aeronautics*, American Institute of Aeronautics and Astronautics (AIAA), vol. 127, Washington, DC ISBN 0–930403–76–2.

Rathz, T.J., Robinson, M.B., Hofmeister, W.H., and Bayuzick, R.J., "The Marshall Space Flight Center Drop Tube Facility," *Review of Scientific Instruments*, vol. 61, No. 12, December 1990.

M.B. Robinson/ES75
205–544–7774
Sponsors: Office of Space Science and Applications, Microgravity Science and Applications Division

Organic Separation by Partitioning in Immiscible Polymer Systems

Increased understanding of the utility of natural body **biologicals** in the treatment of **disease** and rapid advances in techniques to produce new biological materials pose the need for improved and higher resolution techniques[1] to separate these medically important **biologicals**.

Biological and **macromolecular** particles, mixed with certain aqueous polymers, readily separate into two phases with the **biologicals** tending to separate at an interface according to their differential affinities for either phase.[2] Purification obtained in one separation step can be optimized via multistep (**countercurrent distribution (CCD)**) extractions[3] in which solutes in the top and bottom wells of a divided chamber are progressively indexed to give higher resolution separations.

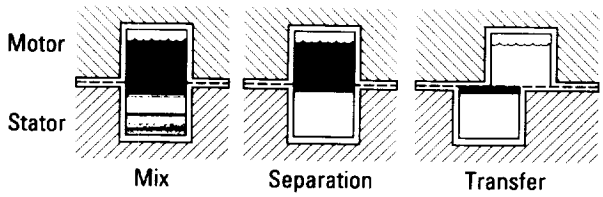

Countercurrent distribution (CCD) showing progressive separation steps.

Innovative flight hardware is currently being developed that is expected to help bioscientists refine this process on Earth and to investigate the role gravity plays in this process. MSFC is sponsoring the development of this unique tool under a Small Business Innovative Research (SBIR) contract that is being developed by Space Hardware Optimization Technology (SHOT), Inc.

[1]Todd, P., "Space Bioprocessing," *Bio/Technology*, 1985, vol. 3, pp. 786–789.

[2]Walter, J., Brooks, D.E., and Fisher, D., "Partitioning in Aqueous Two-Phase Systems: Theory, Methods, Uses, and Applications to Biotechnology," Academic Press, New York, 1985.

[3]Van Alstine, J.M., Snyder, R.S., Karr, L.J., and Harris, J.M., "Cell Separation With Countercurrent Chromatography and Tin-Layer Countercurrent Distribution in Aqueous Two-Phase System," *J. Liq. Chrom.*, 1985, vol. 8, pp. 2293–2313.

K. Taylor/PS01
205–544–0640
Sponsor: Office of Commercial Programs, Small Business Innovative Research Program

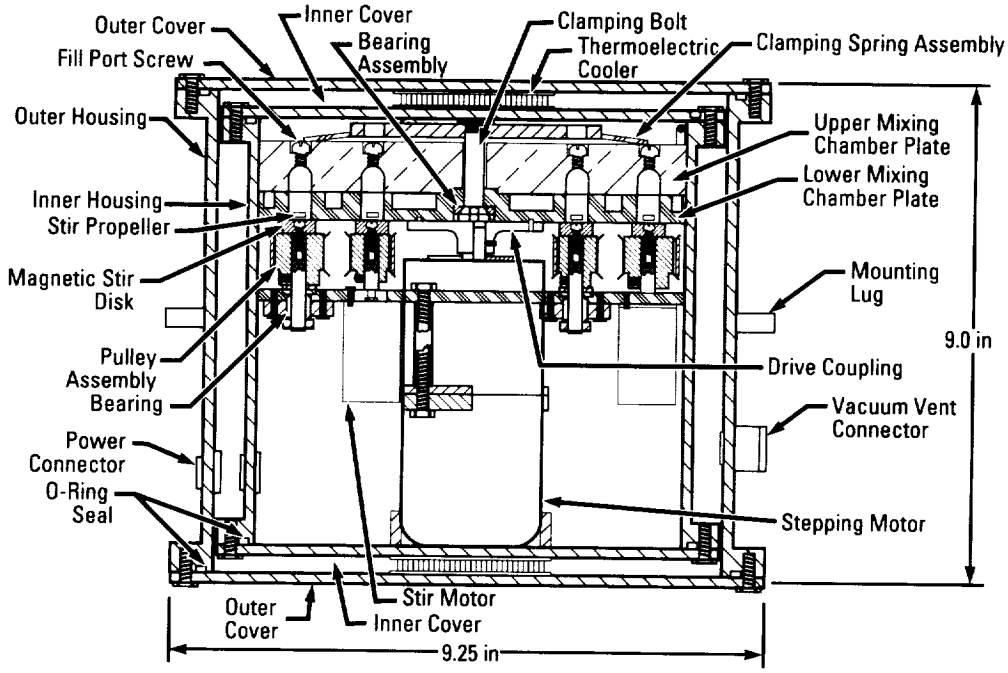

Sectional view of flight hardware concept, under development by SHOT, with a programmable, automated mixing and transfer system.

Pharmacological Assays

The aim of this investigation was to develop and evaluate new **bioassays** for chemical detection. The program entailed three tasks: (1) an understanding of the effects of **gravity** on biological cells; (2) an understanding of the effects of chemical addition on biological cells; and (3) the combined effects of **gravity** and chemicals on **pattern formation** in dense cultures of biological cells. Many cell types spontaneously form visible patterns when suspended in aqueous solutions. The causes and behavior of these pattern-forming cultures is a matter of great interest for designing biological detectors of toxicity.

The investigation first undertook ground-based experiments designed to test chemical effects on large cultures. Heavy metal pollutants (cadmium (Cd), nickel (Ni), copper (Cu)) served as test chemicals and yielded consistent and predictable changes in a culture's biological identity. Patent action was undertaken using the novel indicator of **pattern formation** as the endpoint of chemical testing.

Secondly, flight experiments were performed aboard NASA's KC–135 airplane. These studies sought to characterize the role of **gravity** in biological **pattern formation**. A unique aspect of the new experiment was the ability to track single-cell swimming direction and to follow changes in response to variable **gravity**. For single cells as well as highly concentrated cultures, **gravity** was found to strongly influence biological cell function.

The present work has led to two patents and numerous publications. Future work will continue these fruitful investigations of single-cell tracking with complimentary forces of electric fields and chemical gradients as competing effects with **gravity**.

Noever, D.A., "Fractal Dimension of Bioconvective Patterns," *J. Phys. Soc. Japan*, 59 (1990), p. 10.

Noever, D.A., "Fractal Dynamics of Bioconvective Patterns," *J. Phys. Soc. Japan*, 60 (1991), p. 10.

Noever, D.A., "Statistical Crystallography of Surface Micelle Spacing," *Langmuir*, 8 (1992), p. 1036.

H. Matsos/ES76
205–544–7814
Sponsor: Center Director's Discretionary Fund

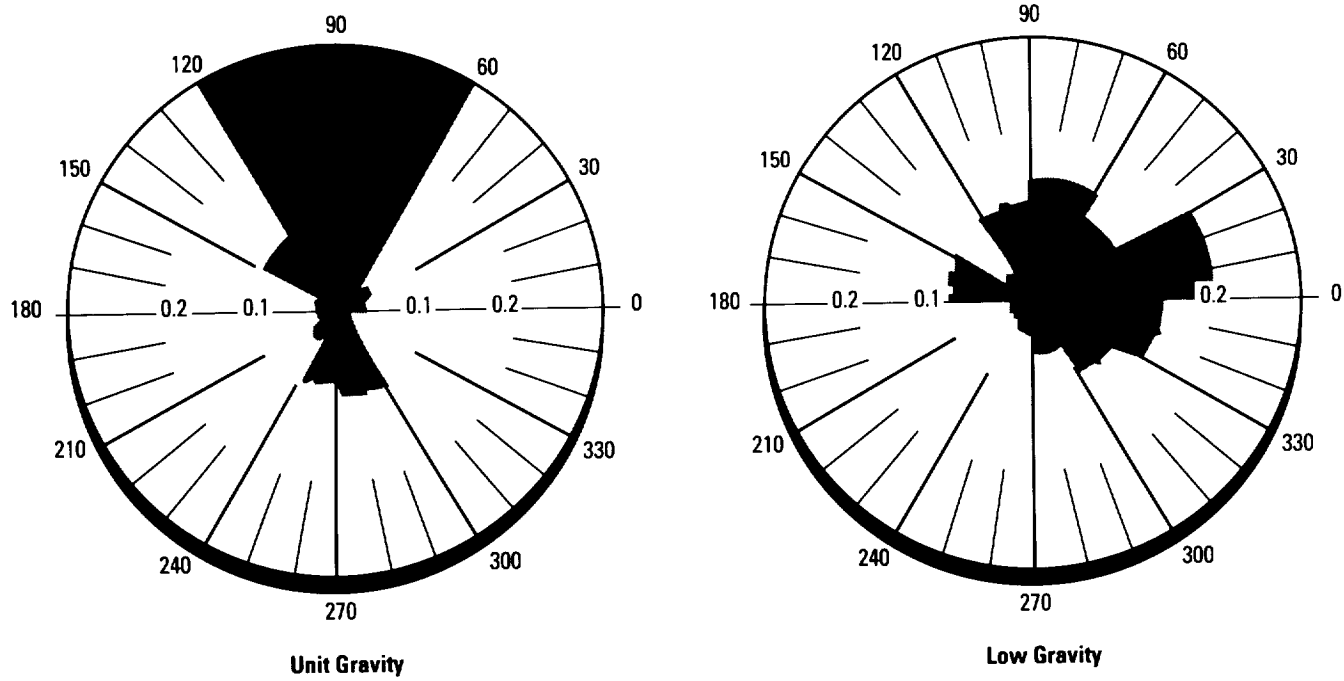

Effect of gravity on single-cell swimming direction. The left graph shows that cells swim predominantly upward in unit gravity, while the right graph shows a broad statistical spread in swimming direction during low-gravity flights.

Protein Crystal Growth

Protein crystallography is currently the most powerful method for determination of the three-dimensional (3–D) structure of **proteins** and other macromolecules. This method usually requires **crystals** that are relatively large (0.5 to 1.0 mm) and that possess a reasonably high degree of internal order. Consequently, **protein crystal growth** has become the subject of an increasing number of fundamental studies, including several ongoing microgravity experiments. The knowledge of the 3–D structure of macromolecules is of fundamental importance to the field of molecular biology, and it is presently receiving considerable attention from the biotechnology industry based on its promising potential for rational drug design and **protein** engineering.

A **protein** extensively studied at MSFC is human serum albumin (HSA). HSA is the most abundant **protein** of the circulatory system, contributing significantly to colloidal osmotic blood pressure. HSA is a large **protein** comprised of 585 amino acids. One of the outstanding properties of this molecule relates to the transport of many important biological and pharmaceutical molecules in the blood stream. As a class of **proteins**, the serum albumins are among the most studied and applied in biochemistry.

The resolution of the **crystal** structure of HSA has been extended to a resolution of 2.8 Å. The atomic coordinates of serum albumin, together with a series of drug/ligand binding studies, have revealed the basic underlying chemistry of this fascinating **protein**.

In addition to the determination of a series of serum albumin structures, this laboratory has also recently determined the first atomic structure of a major antibody to the acquired immune deficiency syndrome (AIDS) virus. This antibody is directed against the viral transmembrane **protein** gp41 and corresponds to the subclass IgG1. This structural work is part of a series that aims to elucidate the detailed nature of human monoclonal antibodies expressed against the AIDS virus together with their respective antigen complexes. Atomic

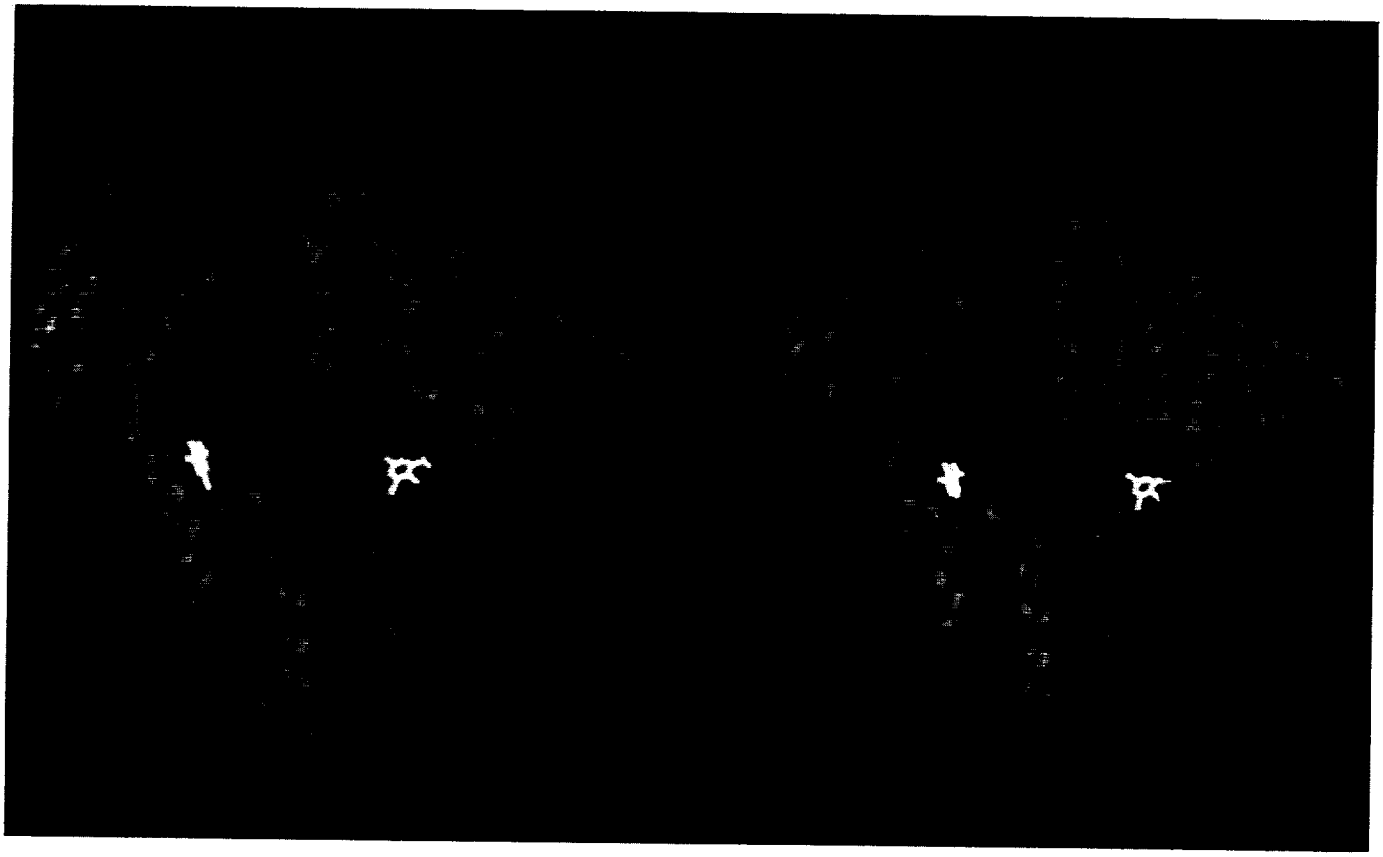

Stereo view illustrating the topology and secondary structure of HSA as determined at 2.8 Å. Bound ligands are shown in white.

Stereo view illustrating the topology and secondary structure of antibody 3D6 expressed against the AIDS virus.

coordinates produced from these studies should: (1) provide important information for future recombinant experiments with genetically engineered antibodies and smaller Fv **proteins**; (2) guide chemists in the selection of superior antigenic peptides for human immunodeficiency virus (HIV) detection; (3) yield further insight into the details of antibody-antigen recognition; and (4) aid in future **crystal** structures of human IgG antibodies of interest.

Recent **protein crystal growth** experiments performed aboard the First International Microgravity Laboratory (IML–1) produced significantly higher-quality **crystals** of HSA compared with ground-based controls. The success of the IML–1 results appears to be related to the longer **crystal growth** times. In this regard, the extended duration of the First U.S. Microgravity Laboratory (USML–1) should prove to be the most productive series of **protein crystal growth** experiments to date.

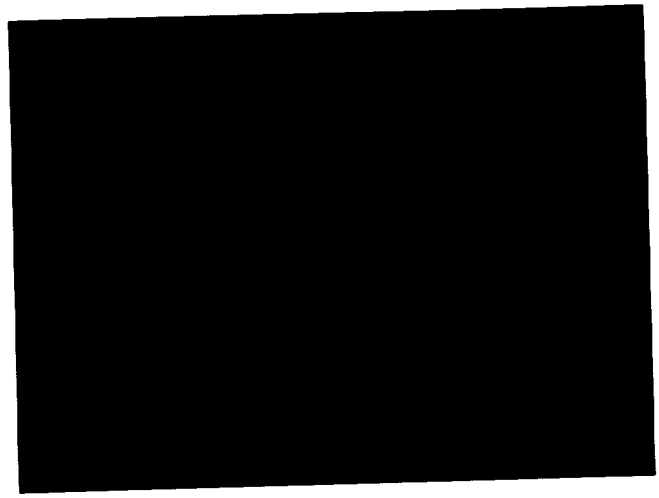

Crystals of antibody 3D6 complexed with a synthetic 35 amino acid fragment of gp41 of HIV–1.

He, X.M., and Carter, D.C., "Atomic Structure and Chemistry of Human Serum Albumin," *Nature*, Vol. 358, 1992, pp. 209–215.

He, X.M., Rüker, F., Casale, E., and Carter, D.C., "Structure of a Human Monoclonal Antibody Fab Fragment Against gp41 of the Human Immunodeficiency Virus Type I," Proceedings of the National Academy of Science, USA, in press, 1992.

Miller, T.Y., He, X.M., and Carter, D.C., "Comparison Between Protein Crystals Grown With Vapor Diffusion Methods in Microgravity and Protein Crystals Using a Gel Liquid-Liquid Diffusion Ground-Based Method," *J. Crystal Growth*, in press, 1992.

D. Carter/ES76
205–544–5492
Sponsor: Office of Space Science and Applications

Solution Crystal Growth

There is an extensive research program in **solution crystal growth**. This program includes both ground-based laboratory studies and flight experiments. It is directed toward increased understanding of the basic processes of crystal growth, **nucleation**, and growth techniques, and their applications and relations to a **microgravity** environment.

As part of MSFC's flight experiment program, investigations are being performed concerning problems associated with crystal **nucleation** from solutions in **microgravity**. A glovebox experiment entitled "**Nucleation** of **Crystals** From Solution" was flown onboard the 13-d Spacelab U.S. Microgravity Laboratory-1 (USML–1) mission, which was launched June 25, 1992. This experiment investigates **nucleation** using a new technique designed specifically for application in the **microgravity** environment. It involves localized injection of a heated, highly supersaturated solution into a host growth solution, and it is designed to control the onset, location, and character of **nucleation**. It also investigates the problems associated with heating and transport of solutions from reservoirs into growth cells where bubble generation can seriously inhibit the process. The apparatus for this experiment consists of a **nucleation** cell, a solution reservoir, and a fluid transfer unit. The material successfully nucleated on this flight is l–arginine phosphate (LAP), a crystal with interesting nonlinear optical properties. Analysis of the results of this experiment are about to begin and it is anticipated that it will lead to a deeper insight into the problems associated with **nucleation** in **microgravity** and also point the way to new solutions to these problems.

The above described experiment was carried out in the glovebox facility. This is a facility in which small experiments can be contained and isolated from the Spacelab crew environment and can be manipulated by the use of inserted gloves. The facility also provides each experiment with resources such as: electrical power, lighting, video, still photography, microscopy, and controlled air flow. This facility provided the essential isolation environment required to carry out MSFC's USML–1 experiment and will serve as an excellent facility for future flight experiments.

Besides providing support for flight experiments, MSFC's ground-based laboratory research serves as a source of independent research activities. It provides a sound foundation of information concerning crystal growth in a 1-g environment to serve as a reference of comparison for low-gravity data taken during flight experiments. Basic properties such as viscosity, density, thermal conductivity, and mass diffusivity are measured. Techniques have been developed for studying synthesis, purification, solubility, and **nucleation** of new materials for crystallization. The internal structure of solutions at or above supersaturation concentration is not well understood. An internal reflectance cell is being used to investigate the structure of such solutions using infrared (IR) spectroscopy.

A number of unique instruments has been designed and built to increase MSFC's laboratory capabilities. One such instrument, the rotating chamber crystallizer (RCC), is designed to simulate some of the **microgravity** crystal growth conditions. This is accomplished by growing a crystal in a rotating cylindrical solution chamber. In this apparatus, the concentration depletion region surrounding the growing crystal is not swept away by buoyancy, but is spiraled around the growing crystal, forming a depletion region similar in appearance to what occurs in a **microgravity** growth situation. This apparatus is also used to investigate injection **nucleation**. The rotation of the solution chamber keeps the injected fluid positioned along its axis and allows **nucleation** to occur in the interior of the chamber instead of at a wall, which would be the case if rotation was not maintained.

Optical techniques are widely used for enhanced visualization and for specific measurements. Schlieren and shadowgraph images are made of growing **crystals** to image their growth or dissolution plumes. Holograms and interferometric images are used for detailed measurements of growth rates, concentration depletion regions surrounding growing **crystals**, and density gradients due to temperature or concentration variations in a growth solution. A laser scattering microscope is used to map microscopic defects in **crystals**. Index of refraction measurements are made on solutions for direct concentration determination and for use in analysis of interferograms.

Ground-based research is also focusing on new candidate growth materials that have high-technology applications. Particular emphasis is being placed on nonlinear optical and IR detector materials.

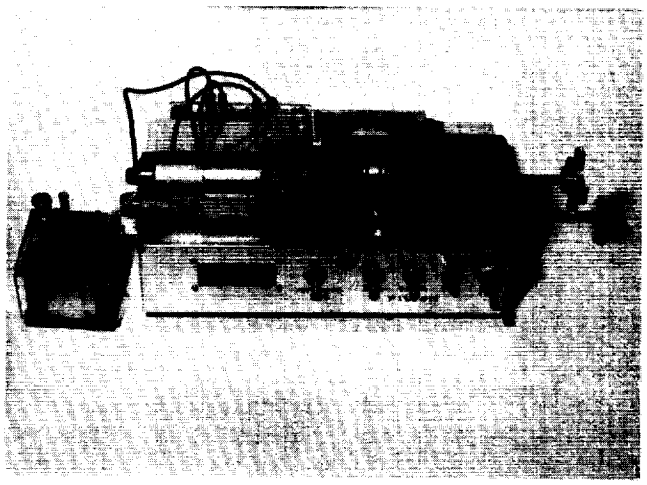

USM– 1 glovebox experiment.

Kroes, R.L., and Reiss, D.A., "Development of New Techniques for the Characterization of Crystals and Their Growth Solutions," NASA TM–100371, June 1989.

Kroes, R.L., Reiss, D.A., and Facemire, B., "Concepts for Microgravity Experiments Utilizing Gloveboxes," NASA TM–100378, September 1989.

Springer, J.M., Silbermann, E., Kroes, R.L., and Reiss, D., "Mapping Crystal Defects With a Digital Scanning Ultramicroscope," Society of Photo-Optical Instrumentation Engineers (SPIE), vol. 1557, 1991.

R.L. Kroes/ES74
205–544–7770
Sponsor: Office of Space Science and Applications

As our challenges grow, so does the necessity to develop innovative ways to overcome these challenges. We have learned to search for innovation not only in the more obvious areas of component, subsystem, and system development, but in the development processes themselves, which have served us so well. Timely and continuing attention to the processes that will help our productivity must be corollary necessities as we prepare for the future.

This section depicts representative selections describing innovative technology development in the areas of propulsion, materials and processes, avionics, automated systems, space systems, and structures and dynamics. Such reports give a clear statement of our belief that innovation is an extremely important factor for our future in space.

G.R. Wallace, Director
Research and Technology Office

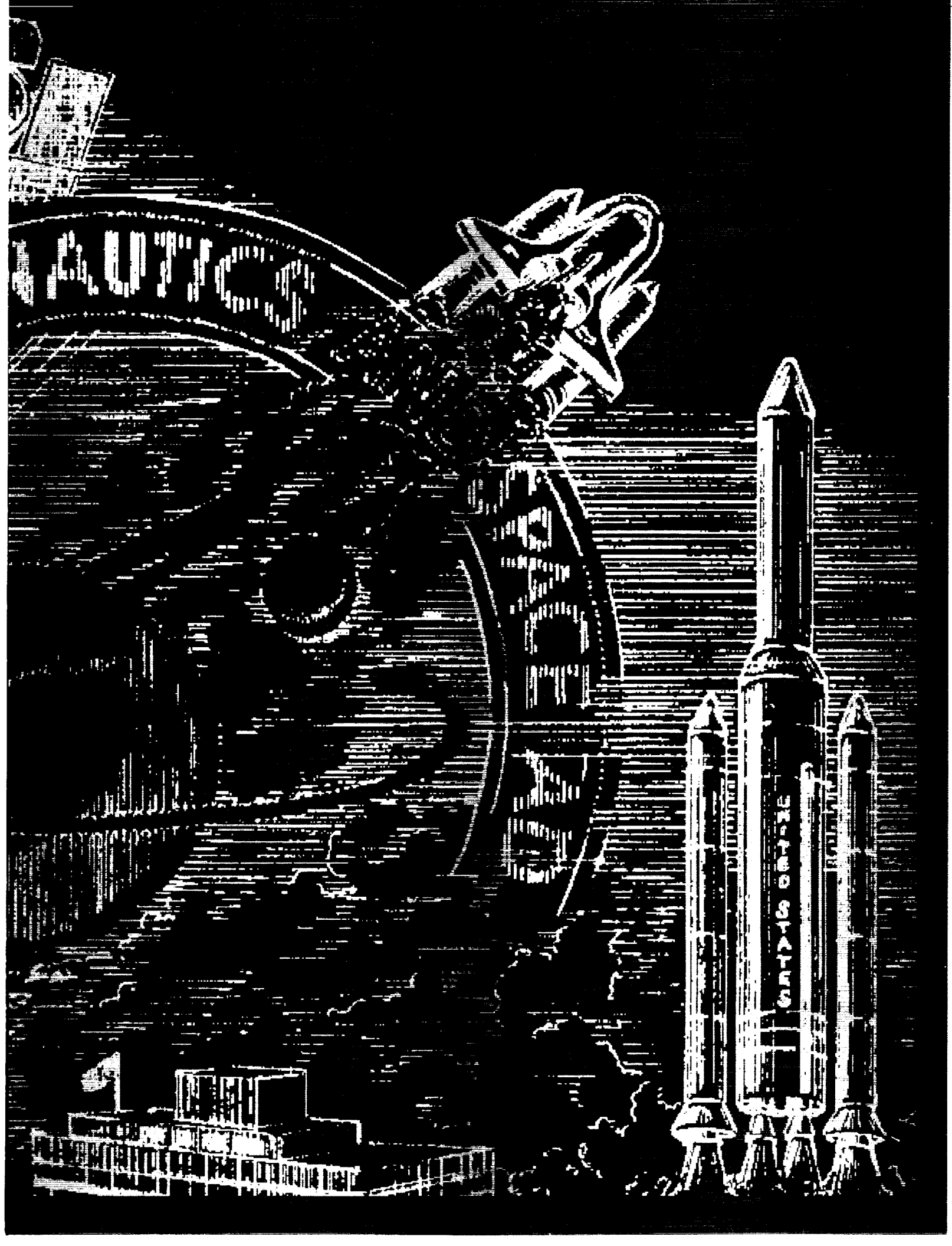
UNITED STATES

Diagnostic and Inspection System

A Cryogenic Pressure Sensor for Rocket Engine Applications

A four-channel **cryogenic silicon (Si) pressure sensor** unit is under development for measurement of fuel supply line **pressure** of space shuttle main engines (SSME's). The **pressure sensor** unit will consist of 4 **Si pressure sensor** dice mounted on 2 printed circuit boards (PCB's) in a **pressure** vessel, with 16 feedthroughs for electrical connections, and 4 separate amplifiers with their associated circuit components in a connector that mates to the **pressure** vessel. A **pressure sensor** unit of two-channel configuration has been selected as an intermediary developmental model that will be developed to a final version of a four-channel unit. This report is based on a two-channel developmental model of the **pressure sensor** units. The two-channel units have two **pressure sensor** dice and two amplifiers built into a **pressure** vessel; the entire unit is constructed to be exposed to a **cryogenic** environment.

The three most important areas of developing a **cryogenic** multichannel **pressure sensor** unit are: (1) **Si pressure sensor** dice, (2) **cryogenic**-compatible packaging of the **pressure** units, and (3) signal conditioning circuits that are integrated within the unit or attached next to the **pressure sensor** dice. **Si pressure sensor** dice require their diffused impurity density in the range of $5\times10_{10}$ to $2\times10_{20}$ atoms per cm^3 to avoid unpredictable variations of the **sensor's** offset voltage and sensitivity due to charge carrier freeze-out of the **sensors** at temperatures below –100 °C (–73 °F). Two remaining areas, namely, cryogenically compatible packaging and electronic circuits, were investigated with primary emphasis on packaging of a **cryogenic pressure sensor** unit.

Two channel **pressure sensor** units under development consist of (1) a **pressure sensor** card with two **Si pressure sensor** dice bonded on a PCB card, (2) an amplifier circuit card with two instrumentation amplifiers and resistors, and (3) a **pressure** vessel that houses the **pressure sensor** module and the amplifier circuit card.

Selected **Si pressure sensor** dice have their dopant density near $1\times10^{20}/cm^8$, and maximum **pressure** rating of the **pressure sensors** is 54 MPa (7,800 lb/in^2) absolute. For variations of offset voltages over a temperature range of –184 to 20 °C (–300 to 68 °F) for these **pressure sensors**, output temperature coefficients of these **sensors** are less than 0.0137 percent/degree Celsius (0.0076 percent/degree Fahrenheit) full scale. Profiles of temperature coefficient of offset voltages of **Si pressure sensors** both bonded to the PCB and free-standing show no determinable variations of thermally introduced stress on the **Si pressure sensors** over a temperature span of –184 to +50 °C (–300 to 122 °F). Bonding of the **Si pressure sensors** to the substrate was made with a **cryogenic** compatible adhesive, Crest–7450.

The **pressure sensor** board is a Teflon®-based PCB with copper (Cu) electrodes. The boards have been evaluated before and after a series of 10 thermal cycles from room temperature to liquid nitrogen (LN_2) bath. The boards show neither sign of degradation nor electrical discontinuity of electric leads at room and LN_2 temperatures. The amplifier circuit board consists of four instrumentation amplifiers (AD–524SD) and resistors. All of the electronic components were tested at a **cryogenic** environment before they were integrated onto the board. The **cryogenic** temperature responses of AD–524SD show that the output gain variations of these **sensors** were measured to be less than 0.0026 percent/degree Celsius (0.0014 percent/degree Fahrenheit) full scale.

Temperature coefficients of output offset voltage of these **sensors** are less than 0.01 percent/degree Celsius (0.0055 percent/degree Fahrenheit) full scale. Comparing the profiles of the **Si pressure sensor** offset voltages to those of the assembled unit, the effects of difference in temperature coefficients of the unit's components are minimal or negligible. Two consecutive **pressure** measurements were made with increasing **pressure** to 41.4 MPa (6,000 lb/in^2) and returning to 0 MPa (0 lb/in^2). Maximum static error and nonrepeatability are 0.45 percent and 0.41 percent of full-scale output, respectively. This level of error is a bit high for an accurate instrument; an improvement on accuracy is needed. The **pressure sensor** units have been tested on a shaker with a gravity-level at 80 g's with the shaker frequency sweeping from 25 to 2,000 Hz, and the units were also subjected to a sinusoidal shock level of 400 g's in an interval of 2.5 ms. The **pressure sensor** units neither showed any sign of damage nor exhibited detectable electrical output during these vibration and shock tests.

Cryogenic two-channel **pressure sensor** units for SSME's have been developed and tested over an extended temperature span from −184 to 50 °C (−300 to 122 °F) and a **pressure** range of 0 to 41.4 MPa (0 to 6,000 lb/in^2). The **pressure sensor** units have a typical sensitivity of 0.00116 mV/V/kPa (0.008 mV/V/lb/in^2) with maximum static error of 0.45 percent of full-scale output, based on best-fit straight-line method. Maximum nonrepeatability is measured at 0.41 percent of full-scale output (FSO). The **pressure sensor** units withstood repeated thermal shock tests over a temperature change of 200 °C/s (360 °F/s). The **pressure sensor** units are also immune to a sinusoidal shock up to 400 g's and vibration level of 80 g's from 25 to 2,000 Hz.

Temperature coefficients of output offset voltages are less than 0.0137 percent/degree Celsius (0.0076 percent/degree Fahrenheit) full scale over a temperature range of −184 to 50 °C (−300 to 122 °F). The instrument amplifiers show their temperature coefficients of output gain are less than 0.0026 percent/degree Celsius (0.0014 percent/degree Fahrenheit) full scale over the same temperature range.

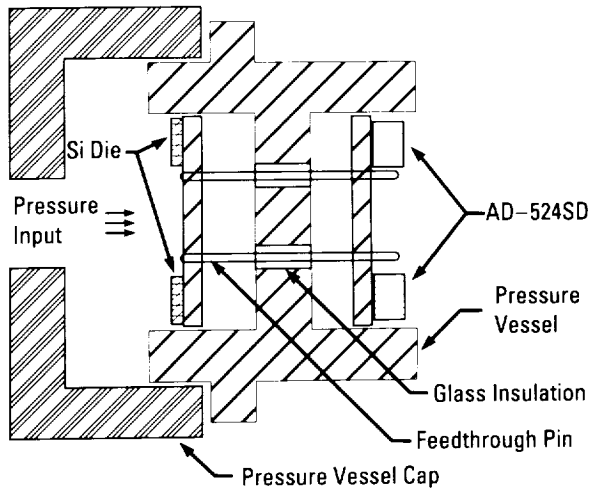

Cross section of a two-channel unit.

Kahng, S., Cruz, V.B., Langley Research Center, NASA, and Shams, Qamar, Analytical Services and Materials, Inc., "A Cryogenic Pressure Sensor for Rocket Engine Applications," 1992 Earth-to-Orbit (ETO) Technology Conference, MSFC, AL, May 1992.

W.T. Powers/EB22
205-544-3452
Sponsor: Office of Aeronautics, Exploration, and Technology

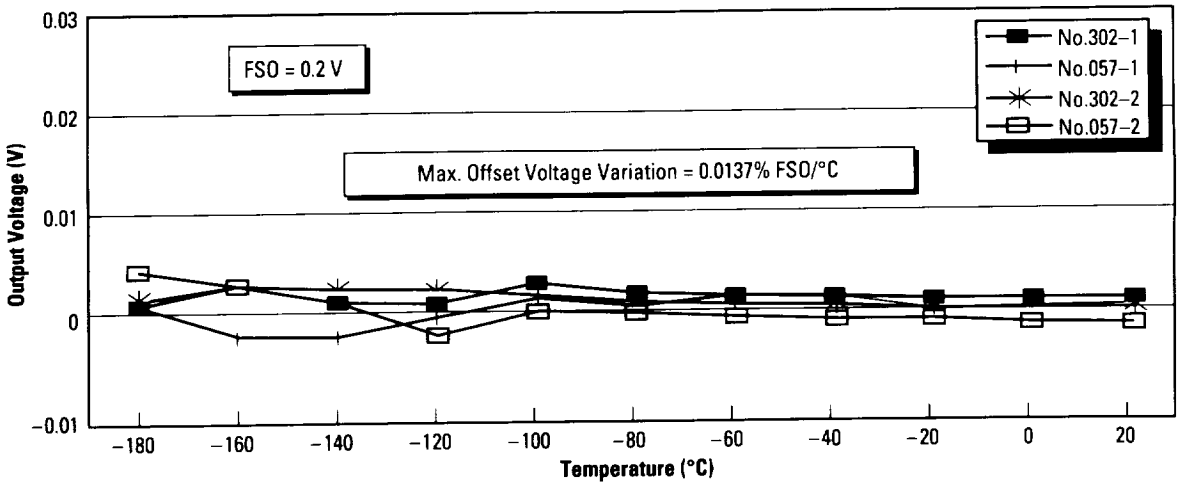

Offset voltage versus temperature.

Advanced Computed Tomography Inspection System

The advanced **computed tomography (CT) inspection** system (ACTIS) was developed to allow quantitative **inspection** of solid rocket motor (SRM) ablative materials and complex engine castings. The system is a large industrial **CT** scanner with variable geometry and x-ray beam energy. The flexibility of the system allows optimization for a wide variety of object sizes and densities.

A new off-line image analysis workstation was installed this year to improve system throughput by allowing off-line analysis of **CT** images. The workstation is an 80386-based Microsoft Disk Operating System (MS–DOS) platform that runs image analysis software written by Bio-Imaging Research (BIR), Inc. The workstation is connected to the main ACTIS console and can directly access the hard drive of the console to import images obtained with ACTIS. The workstation can perform all of the image analysis functions that are available on the console, so that image analysis can be performed off-line.

The workstation also features standard line, rectangle, and polyline regions of interest analysis to determine the **CT** numbers of individual points of interest on the image or the minimum, maximum, and mean **CT** numbers of regions of interest in specific images. The workstation software is capable of multiplanar reconstruction (MPR) analysis of up to 64 consecutive **CT** slices of a particular component that has been scanned. MPR allows the "stacking" of consecutive **CT** slices, resulting in the creation of a volume image, which can then be "sliced" by the software along planes transverse to that of the original **CT** slices. This technique allows the system operators to perform scans along the axis of symmetry of an object, or, if necessary, along the path of least x-ray resistance in order to obtain the necessary data in the most efficient manner, and then analyze the data with MPR to reveal structural detail and/or the nature of defects that span across several slices.

In addition to standard **CT** image analysis techniques, the workstation software is also capable of performing automated measurements of radii of parts with circular geometry at 45-degree increments, as well as edge, wall, and hole measurements. The system produces quality hardcopy of images on a continuous-tone thermal printer. The workstation is currently used on a daily basis in support of all major in-house flight and research programs. Goals for the coming year are to modify the system software to include more sophisticated image manipulation techniques such as on-screen **three-dimensional (3–D)** visualization of images and to provide enhanced automated measurement capabilities for complex part geometries.

MSFC also completed development of a separate low-cost **CT** system (ACTIS+) this year. The ACTIS+ system is an upgrade to an existing real-time radiography (RTR) system that provides the capability to rapidly perform high-resolution **CT inspection** of small components (up to 15.25-cm (6-in) maximum dimension in any direction). The system is based on an i860 processor running the UNIX operating system, and the system software is written in the XWindows user interface. The existing RTR system is equipped with a 160-kV microfocus x-ray tube, which has a minimum focal spot size of 5 μm (0.000254 in), and a 22.86-cm (9-in) diameter image intensifier. Video signals from the camera attached to the image intensifier are digitized by an image-handling board in the computer and are stored temporarily on the hard drive for reconstruction on a proprietary single-board **image processing** system capable of performing reconstruction tasks that are conventionally handled by large parallel-processed minicomputers. Image acquisition and reconstruction time are on the order of 60 s/slice. Maximum image resolution with the imaging equipment in the existing system is on the order of 10 line pairs per millimeter.

Planned activities for the coming year are development of standards and specifications for the system and acquisition of a discrete detector system to improve the image resolution to 20 line pairs per millimeter.

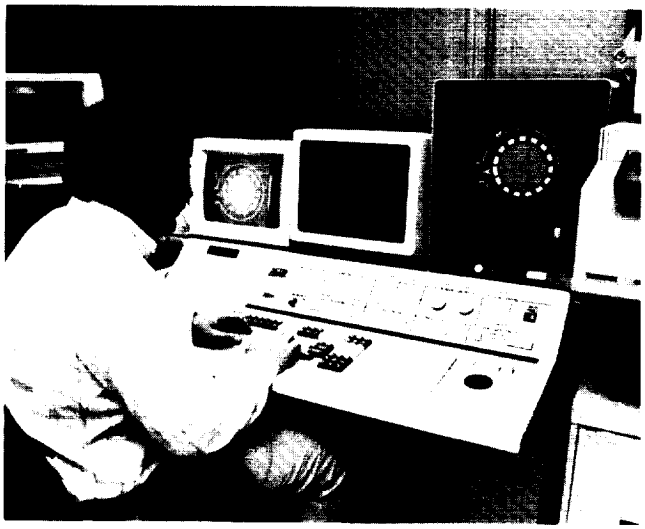

Technicians analyze images of an advanced liquid engine casting on the upgraded ACTIS.

L. Hediger/EH13
205–544–2544
Sponsor: Office of Space Flight

Automated Laser Dimensional Inspection System

An **automated** laser dimensional **inspection** system (ALDIS) has been developed at the Productivity Enhancement Complex at MSFC by NASA Materials and Processes Laboratory and Thiokol Corporation to enhance the integrity of the erosion data collected from solid rocket nonasbestos **insulation** tests. The previous manual methods have proven to be time-consuming, subject to human error, and require a course data grid. Erosion measurements were taken at specific points and the remaining surface was subjected to interpolation. In addition to these problems, the manual measurements also include touching the delicate char with a "depth micrometer," thus disturbing the test subject. ALDIS uses a **laser** beam and triangulation for precise depth measurements. Data taken before and after motor firing and again after char removal can be compared to determine erosion and the heat-affected zone of the test materials. In the past, the data were recorded by two engineers using a clipboard. The data were then transferred to a spreadsheet by entering data into a personal computer (PC) by hand. ALDIS will collect the data as read by the **laser**, plot the topography of the **insulation** on screen or plotter in real time, and record the values in a data base. The data may be retrieved at a later date for further analysis or plotted in a presentation format.

Specifically, the system utilizes an XR225 CIMCORP Gantry Robot with a Zyco **laser** probe and controller. The **laser** is mounted on a robotic end effector capable of six degrees-of-freedom (DOF). The **laser** probes the rocket motor insulated surface and records the topography of the **insulation** before and after the solid rocket motor (SRM) test. Each point is scanned 100 times and an average is computed and recorded for a higher level of accuracy. Realistic obtainable accuracy of the system is projected to be 0.00254 mm (0.001 in) for repeatability and reliability after all of the development work has been completed. The accuracy of the current manual measurements has not been fully determined; however, it is suspected to be in the order of ±1.524 mm (±0.060 in). The accuracy of the new system is established by comparing the analog signal of the **laser** to a linear variable deflection transducer (LVDT), which is accurate to 0.00254 mm (0.0001 in) on calibration blocks.

Integrated into this program was the concept of off-line programming to produce a model of any part to be inspected. The modeled geometric data are loaded into the robotic controller. This off-line programming system was completed in 1992 to align the component parts in the work cell. This system, which was developed by MSFC and Thiokol Corporation, consists of a Silicon Graphics 120 GTX workstation running a graphics software package known as the Interactive Graphics Robotic Instructional Program (IGRIP) from Deneb Robotics, Inc. The graphics system provides three-dimensional (3–D) solid representations of the cell and allows manipulation of the objects within the cell. The system will detect when the robot arm has reached its travel limits or when there is an impending collision between the robot and cell components. Alignment of component parts is optimized off-line on the workstation, translated into robot-compatible form, and downloaded to the robot.

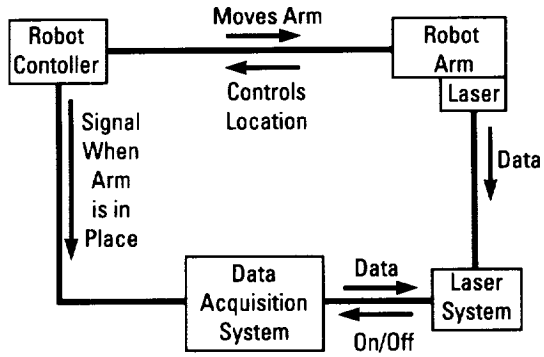

1. Verifies Turn-on Signal
2. Turn On Laser
3. Waits 2 s
4. Reads and Records Data at 20 samples/second for 5 s Averaged
5. Turns Off Laser
6. Waits For Next Turn-On Signal

ALDIS hardware system (current).

P. Gill/EH44
205–544–2557
Sponsor: Redesigned Solid Rocket Motor Program Office

Collisional Broadening Spectral Base Development

In order to support ground-level testing of the **space shuttle main engine** (**SSME**), the optical **plume** anomaly detector (OPAD) system is currently under development. Detection of engine failure is to be achieved through **spectral** resolution of **plume** emissions and subsequent identification of anomalous levels of elements that indicate engine erosion or component failure. To achieve this **spectral** resolution of the **plume**, the OPAD system employs two dispersing instruments, the OPAD spectrometer and the OPAD polychromator. The spectrometer allows for continuous **spectral** coverage from the near infrared (NIR) to near ultraviolet (NUV), while the polychromator monitors 16 specific wavelengths that correspond either to elements that signify possible component failure or to sources of background emission.

To date, the OPAD system has monitored 34 test firings of the **SSME** at the technology test-bed (TTB), which has generated an abundance of **spectral** data. Both the spectrometer and polychromator yield data that allow comparison of relative intensities of elements present in the plume. However, it is desirable to quantify this data so that absolute number densities of the elements of interests can be calculated. To achieve this, **spectral** line **broadening** mechanisms must be taken into account, since they affect the shape and shift of the **plume** signature. The two primary **broadening** mechanisms that will affect the **plume's spectral** data are Doppler **broadening** and collisional **broadening**. Doppler **broadening** of the **spectral** line is caused by the thermal motion of the species in emission, while collisional **broadening** of the **spectral** line is a result of the interactions of the emitting species and other perturbing particles in the **plume**, such as the by-products of the combustion process. Although Doppler **broadening** effects are relatively well defined and can be easily incorporated into a radiative transfer model, collisional **broadening** is more complex and will require further study to successfully interpret the existing **spectral** data.

At present, a theoretical study is being performed to establish a full quantum-mechanical treatment of the collisional **broadening** and shifting mechanisms that affect the **spectral** data from the OPAD system. Once established, these results will be compared to an existing data base of collisional **broadening** data and appropriate adjustments will be consolidated into a full radiative transfer model, which accounts for flow field properties, chemi-excitation rates, and known **broadening** mechanisms, to predict absolute number densities of elements present in the **plume** from their relative intensities obtained from the OPAD instrumentation.

W.T. Powers/EB22
205–544–3452
Sponsor: Office of Aeronautics, Exploration, and Technology

Fiber-Optic Pressure Sensor

Fiber-optic sensor systems, to be most useful, should have a digital transmission format so as to be independent of intensity variation. Thus, the number of light wave transmission parameters that can be utilized is limited (although these constraints do not limit the number of parameters that can be used for sensing). If single-mode fibers are used, then five characteristics of light can be applied to digital transmission: amplitude, intensity, wavelength, phase, and polarization.

However, multimode fibers, associated connectors, etc., are more readily available and have a superior reliability history compared to single-mode fibers. Multimode fibers restrict transmission schemes to digital intensity modulation (binary, pulse width, frequency, etc.), wavelength (or color) modulation, and color multiplexing. Transducers that produce digital signals directly are more desirable than those that require analog-to-digital (A/D) converters. Further, many systems require transducers that use only optical input power. With these criteria, a "digital-compatible" **sensor** can be any **sensor** that is not affected directly by amplitude variations (such as changes in fiber attenuation). The possibilities for **sensor** construction are as extensive as are the potential applications.

MSFC personnel have performed basic research on **Fabry-Perot** variable gap **pressure** and temperature **sensors** that involve a multiplicity of reflections such that interference and support of the components of a single light ray can occur many times. This multiple reflection phenomenon causes the **Fabry-Perot** gap to produce a unique reflective and transmissive spectral distribution characteristic (color). Such **sensors** have the desirable characteristic that the change in spectral output can be a very sharp function of the cavity width. The **Fabry-Perot** optical filter property involves the same effect as that which produces the multicolor reflections from the surface of an oil slick or soap bubble.

The **sensor** system consists of a broadband light source coupled into a fiber that transmits this broadband spectrum to the remote **sensor** element. The **sensor** element is a variable-gap **Fabry-Perot** cavity that modulates the reflected spectrum according to the gap dimension.

The reflected spectrum is fiber-transmitted back to a micro-optic demodulator that converts the spectrum to electrical signals. These signals are then interfaced with an IBM personal computer (PC) via the demodulation electronics. The microprocessor-based, data analysis, and signal-processing software further converts the signal to **Fabry-Perot** cavity spacing and **pressure**.

An important feature of this system is that it uses the power of a microprocessor to handle relatively complex control and analysis in a way that permits simplifying the mechanical design of the **sensor**. The increase in complexity to the processing causes a small or negligible increase in the processing cost, but the decrease in mechanical complexity realizes large savings in cost, as well as introducing the possibility of batch processing.

Preliminary results show the prototype system to be performing within predicted parameters.

James, K.A., Shrestha, N., Cal State University/Long Beach, and Quick, W.H. OPCOA, Inc., "Fiber-Optic Pressure Sensor for Combustion Chamber Monitoring," 1992 Earth-to-Orbit (ETO) Conference, MSFC, AL, May 1992.

W.T. Powers/EB22
205–544–3452
Sponsor: Office of Aeronautics, Exploration, and Technology

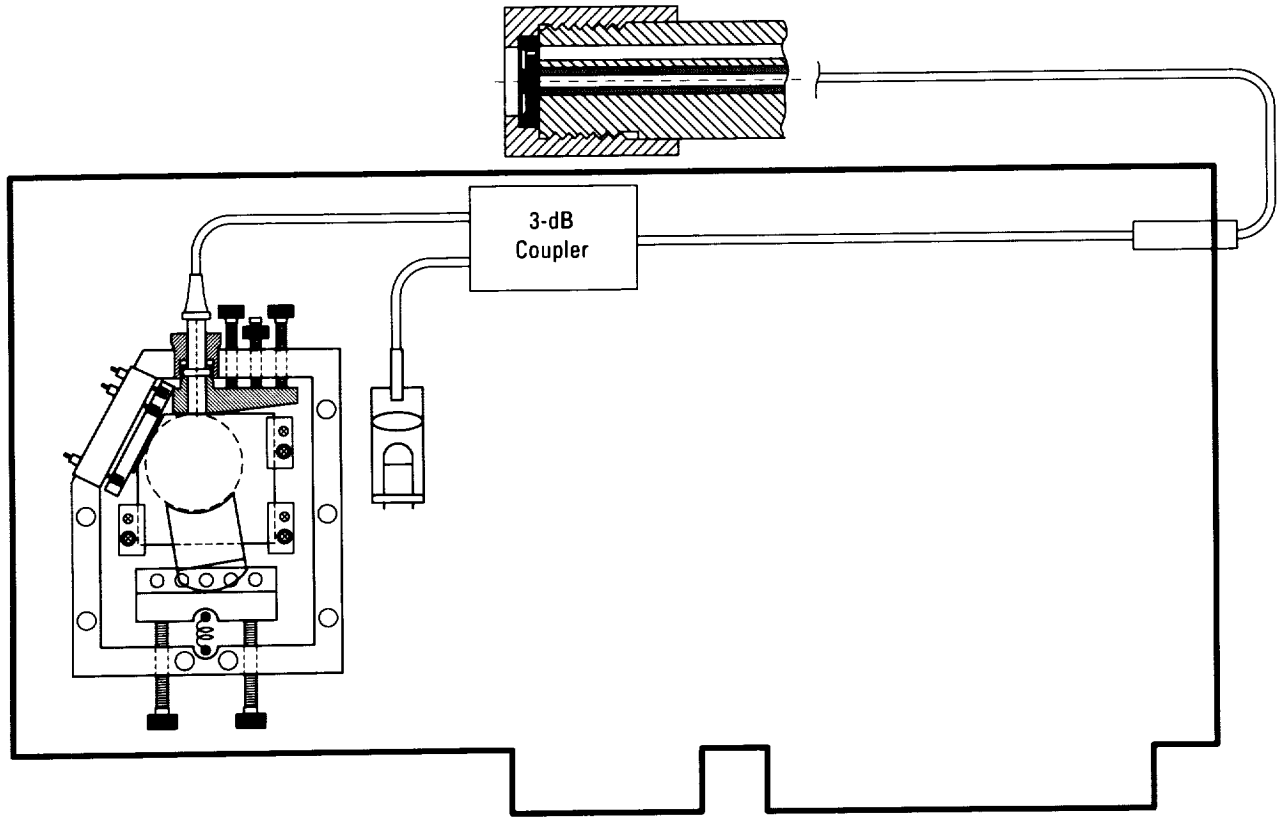

Fiber-optic Fabry-Perot pressure-sensing system.

Graphic Simulation of MNASA Motor Inspection System

A Silicon **Graphics** 120GTX workstation, in conjunction with the Deneb Robotics, Inc., Interactive Graphics Robotic Instructional Program (IGRIP) **graphics** software, is being used to support the development of an automated laser inspection system for MNASA **motor cases**. The system utilizes the CIMCORP XR225 cartesian **robot**. A laser proximity sensor is used at the end effector to map the inside diameter surface of the **motor case** and is later compared to the inside diameter of the same case to determine insulation erosion. Since the laser system measures displacement difference between prefire and postfire, **robot** arm repeatability and **motor case** reference position alignment are crucial to obtaining useful accuracies. A **model** of the CIMCORP **robot** in the Deneb library was downsized to dimensions of an existing **robot** and an MNASA **motor case** was added to create the current **model**. Utilizing this **model**, the end effector tool dimensions were designed and optimum tool length was established. **Robot** path programs of various component parts were completed and successfully transferred to the **robot** controller where the **robot** motions were verified.

An alignment procedure of the **robot** arm to the **motor case** has been established. Six position points (0, 90, and 270 degrees on front and back) located on the flanges of the MNASA aft center segment are defined by moving the **robot** to the six positions and recording the **robot** coordinates at those respective positions. These six points are uploaded to the graphic **model** on the Silicon **Graphics** workstation. After the alignment procedure is completed, the graphically generated mapping envelope for the **robot** arm is calibrated and ready to take measurements. The mapped surface consists of 15 circumferential paths located every 24 degrees and 18 points per path located every 5.08 cm (2 in) longitudinally. Plans are to measure an MNASA aft center segment with full-scale mapping consisting of 1,050 points. It is estimated that the full-scale mapping process will take approximately 4 h.

An estimated error tolerance as well as improvements for the alignment procedure shall be obtained. A program using the pristine data locations (alignment points) on the aft center segment as path points for the **robot** is used to take measurements. After the IGRIP software has aligned the part in the **graphics** work cell, the two sets of alignment points (before/after alignment) should match with a certain degree of accuracy. The downloaded alignment points are compared to the original points that were uploaded. Thus, an error tolerance for the alignment process is provided. Research is being conducted on the method of obtaining the uploaded alignment points in the production work cell.

Future work planned for this system includes the complete mapping of the topographical surface of insulation, standardization of all MNASA data measurements and nozzle erosion measurements, and the incorporation of a better laser to allow nozzle measurements. Other enhancements planned are the geometry inspection of machined parts, the incorporation of point inspection and Wavefront simulation, and the erosion measurement of sprayable ablatives in locations where conventional dimensional measuring devices would be impractical or unobtainable.

The automated laser dimensional inspection system results in cost savings to the Government in several ways. First, the human error factor is eliminated, and manhours on data reduction are saved. In addition, the process provides a more dense data grid, and a graphical representation of the automation is immediately available.

M. Day/EH43
205-544-1899
Sponsor: Office of Space Flight

Inspection and Performance Data Analysis

The integrated nondestructive data evaluation and reduction system (INDERS) is a software and procedures package that establishes a common format for several **nondestructive evaluation** (**NDE**) data sets to allow a direct comparison of images. INDERS also provides a method of relating mechanical and materials property data to **NDE** data to establish relationships between **NDE** measured anomalies and material performance. This year, INDERS has been upgraded to allow correlation of **NDE** defect data to part performance for subscale solid rocket nozzle materials. By comparing prefire and postfire computed tomography (CT) images, INDERS is able to automatically measure char and erosion in these materials. With operator direction, unusual char and erosion patterns are correlated with prefire defects in the materials. Until recently, these analyses were performed manually and required several man-weeks of effort. This upgrade has made it possible to perform a more reliable analysis in less then one-quarter of the time previously required. The system currently works in a hybrid personal computer (PC)/ Macintosh/VAX environment, but is being reworked for the UNIX/XWindows environment.

The image **data analysis** (IDA) workstation provides access to the information contained in inspection and manufacturing data as a practical resource for the solid rocket motor (SRM) manufacturing engineer. The objective of the workstation is to improve manufacturing reliability by providing the manufacturing engineer with the necessary tools to effectively trace defects to their root cause in the manufacturing process. This objective is being achieved by providing the manufacturing engineer with the following capabilities: (1) review defect and production data, (2) correlate defects/anomalies with specified and actual production parameters, (3) identify root causes of anomalies, and (4) determine effects of defects on part performance. A working prototype of the system was demonstrated this year. The user interface and materials traceability module software coding has been completed. The total coding effort is scheduled for completion by early 1993.

L. Hediger/EH13
205–544–2544
Sponsor: Office of Space Flight

Leak Detection From the Space Shuttle Main Engine Using Sequential Image Processing

The rapid detection of propellant leaks from the space shuttle main engine (SSME) during test firing is crucial to the prevention of catastrophic failures. Ruptures of high-pressure lines and internal components often result in failure modes with sufficiently long time constants for detection and safe shutdown. Recent advances in imaging and **image processing** technology provide the hardware necessary for visual and **infrared** (**IR**) observation of these phenomena and the computing capability required for processing the signals and detecting the occurrence of a leak within the field-of-view (FOV). Thus, a system capable of detecting leaks from images acquired sequentially during test firing in real time is of value to the development of the SSME and is realizable with current technology. This study investigated this approach and established its feasibility and applicability to the program.

To detect the occurrence of a leak, the temporal aspects of the process must be considered. Previous analysis by Shohadaee and Crawford showed that the occurrence of a leak results in a sudden change in intensity in a given region of an image. Furthermore, the change should be sustained for a typical leak. The time variation of the intensity at a point within the area of the leak is, therefore, similar to that of a step function, although other smaller intensity variations are also present due to normal operating conditions. The problem becomes that of detecting a step function in the presence of additive noise.

The **leak detection** system developed here was designed to quickly and automatically detect a step-like change in intensity in a sequence of images. Processing is carried out at each point in digitized **video** data. The system consists of a causal, recursive high-pass filter that removes slowly varying background intensities cascaded with a moving average filter that accumulates transmitted sustained changes. The absolute value of the output is averaged over the full-frame FOV to produce a time-varying mean value indicative of the level and spatial extent of a leak. It has been implemented on a standard digital image processor and applied to full-frame **video** data, with output data each frame.

Although it has not been implemented in real time as of this writing, execution times for the off-line processing carried out thus far indicate that such processing is achievable with present technology.

Laboratory experiments using **visible** wavelength **video** signals were conducted for an actual controlled gas leak with data processed off-line on a digital image processor. The gas leak was created using a thermos filled with liquid nitrogen (LN_2) and vented with tubing that directed the leak into the FOV. A **video** camera was used to acquire live images of the leak that was initiated by a solenoid valve placed on one end of the copper tubing. The leak was made **visible** by the forwardscattering of the light from the condensed water vapor droplets formed by the escaping cold nitrogen (N_2) gas.

For each experimental run, a brief (1 to 3 s) image sequence of this scene was acquired and stored on an optical disc **video** recorder/player. Several sets of data were acquired in this manner and were played back later for off-line causal processing. In a plot of the output mean value (average intensity of the output image) versus frame number for a selected experimental run (each frame corresponds to an elapsed time of 1/30 s), the increase in magnitude after initiation of the leak at frame 14 is evident.

The system has also been applied to **visible** wavelength image data acquired during an actual SSME test firing in which a premature shutdown occurred. Data supplied by NASA consisted of high-speed film images at approximately 64 frames/s transcribed into **video** format and replayed at 30 frames/s. Four image sequences of this test were processed, corresponding to four different views of the engine powerhead taken during the same test firing. (Data acquisition cameras were denoted numbers 1, 6, 7, and 8 by NASA.)

For these sequences, plots of the output mean value (average intensity of the output image) versus frame number were computed. The peaks detected during ignition were caused by lights being turned on and by the plume forming at the bottom of the nozzle as well as falling frost that had accumulated on various cold engine components. As the engine entered mainstage mode, the mean value output reduced to that caused by the noise. A leak near the low-pressure fuel turbopump (LPFTP) resulted in a large peak in the output mean value at approximately frame 400 (camera position 8), and smaller, but still noticeable, peaks at the same time in camera positions 1 and 6. The flash fire at frame 650 is evident in all the plots. It was detected by the monitoring systems presently in use and the shutdown sequence was initiated. The engine vibration and water spray associated with shutdown and post-test procedures also result in large peaks in the output mean value in all four plots.

If this system had been implemented for this engine test, the leak/no-leak decision would have probably been positive at approximately frame 400. This analysis of these four data sets thus demonstrates the potential value of this technique for monitoring SSME test firings.

The experimental studies demonstrate the ability of this system to detect leaks in a full-image frame using **image processing** hardware. The laboratory experiments show that the system is capable of correctly detecting leaks occurring within an FOV under controlled conditions. The analysis of the test-stand data indicates the applicability of this technique to actual SSME test firings and its ability to identify anomalous events.

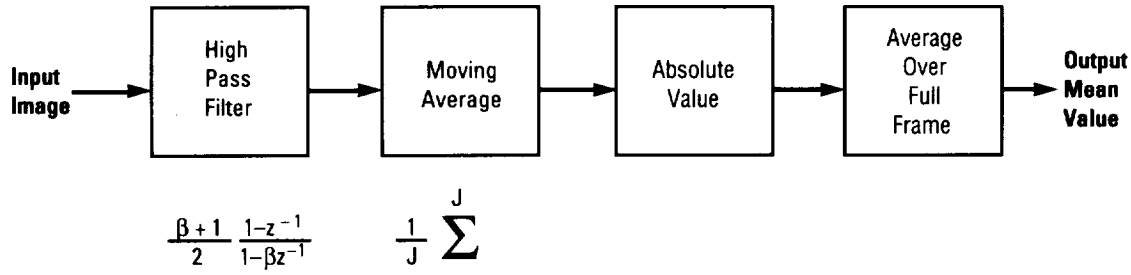

System flow diagram.

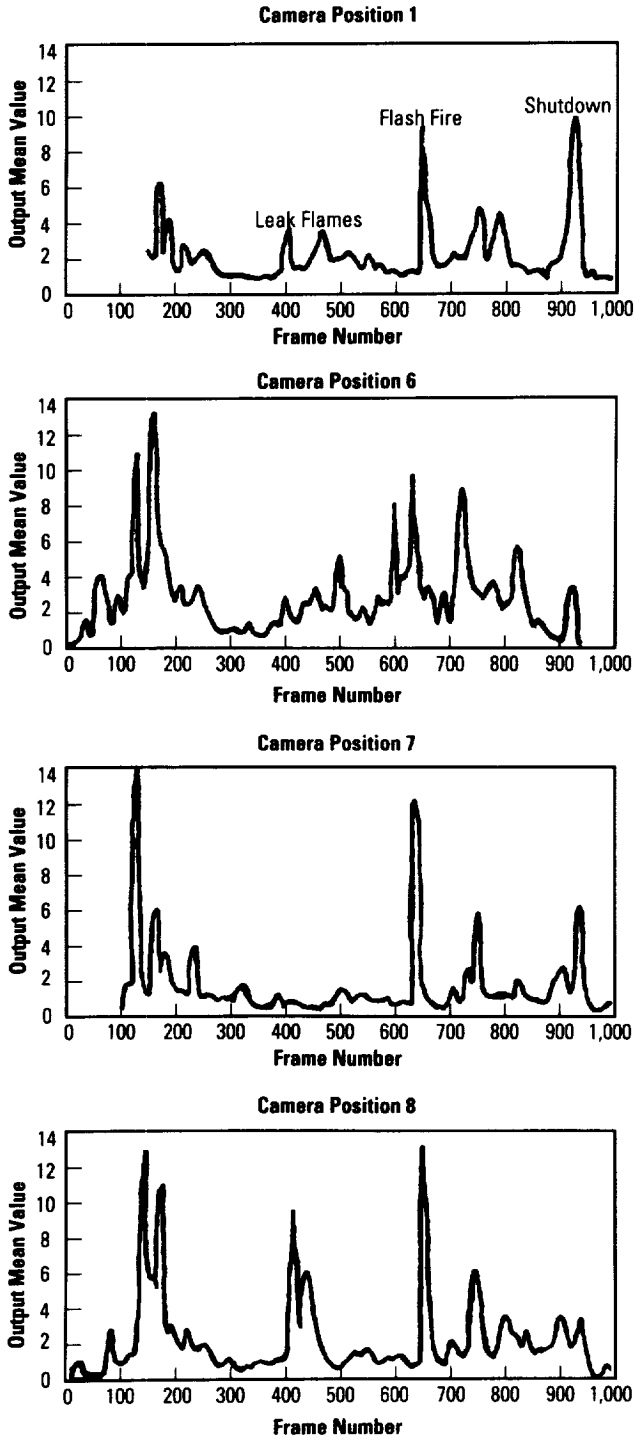

Plots of the output mean value versus frame number.

Malone, J.A., "A System for Leak Detection Using Sequential Image Processing," Master's thesis, Dept. of Elec. Engr., Univ. of Tennessee, Knoxville, TN, 1991.

Malone, J.A., and Smith, L.M., "A System for Sequential Step Detection With Application to Video Image Processing," to be published in *Institute of Electrical and Electronic Engineers (IEEE) Trans. on Industrial Electronics.*

Shohadaee, A.A., and Crawford, R.A., "SSME Leak Detection Feasibility Investigation by Utilization of Infrared Sensor Technology," Center for Advanced Space Propulsion Second Annual Technical Symposium Proceedings, Tullahoma, TN, Nov. 1990.

W.T. Powers/EB22
205–544–3452
Sponsor: Office of Aeronautics, Exploration, and Technology

Leak Imaging for Rocket Engine Systems

An optical leak imaging technology has been successfully demonstrated for liquid propellant rocket engine applications. The technology produces video images of the test object in which leaking **tracer gas** appears as a black cloud. It promises to significantly reduce the time required to perform engine leak testing and to greatly simplify the location of leaks. Successful preliminary tests have been performed with a space shuttle main engine (SSME) nozzle and an RS–27 nozzle used on the Delta rocket. Material-compatibility has recently been established between the leak **tracer gas** and all SSME fuel and oxidizer system materials.

Leak testing is performed for the SSME's twice before fueling, the first time with soap solution and the second with a helium (He) signature sniffer system. Two tests are required because soap solution is only applied to the engine joints, while the He signature test cannot locate the leak source. Soap solution can also miss large leaks.

The He signature test samples the air in the shuttle engine compartment, while the engines are pressurized with He. The He concentration detected can be used to determine the sum of the leakage from all sources on the engine. The soap solution test is performed by painting each of the engine joints manually one by one with soap solution, while the engine is pressurized. Bubble formation indicates a leak.

The new leak imaging technology promises to replace these two tests with one, while decreasing the required testing time and greatly simplifying the location of a leak. The technology employs one of several gases, such as nitrous oxide (N_2O) and sulfur hexafluoride (SF_6), that strongly absorbs **infrared (IR)** light at particular wavelengths. The area of interest is illuminated in the **IR** with a laser or a heat lamp. The scene is then imaged through a filter using an **IR** video camera. The filter is chosen to pass **IR** radiation only within the wavelength range absorbed strongly by the gas.

The video images display any leaking **tracer gas** as a black cloud. This provides the ability to detect a leak even if it is at the rear of a joint or in a piece of hardware obscured behind another. The ability to see the **tracer gas**, which can be well away from its source in many cases, eliminates the need to search around each joint using a mirror, as is presently necessary with soap

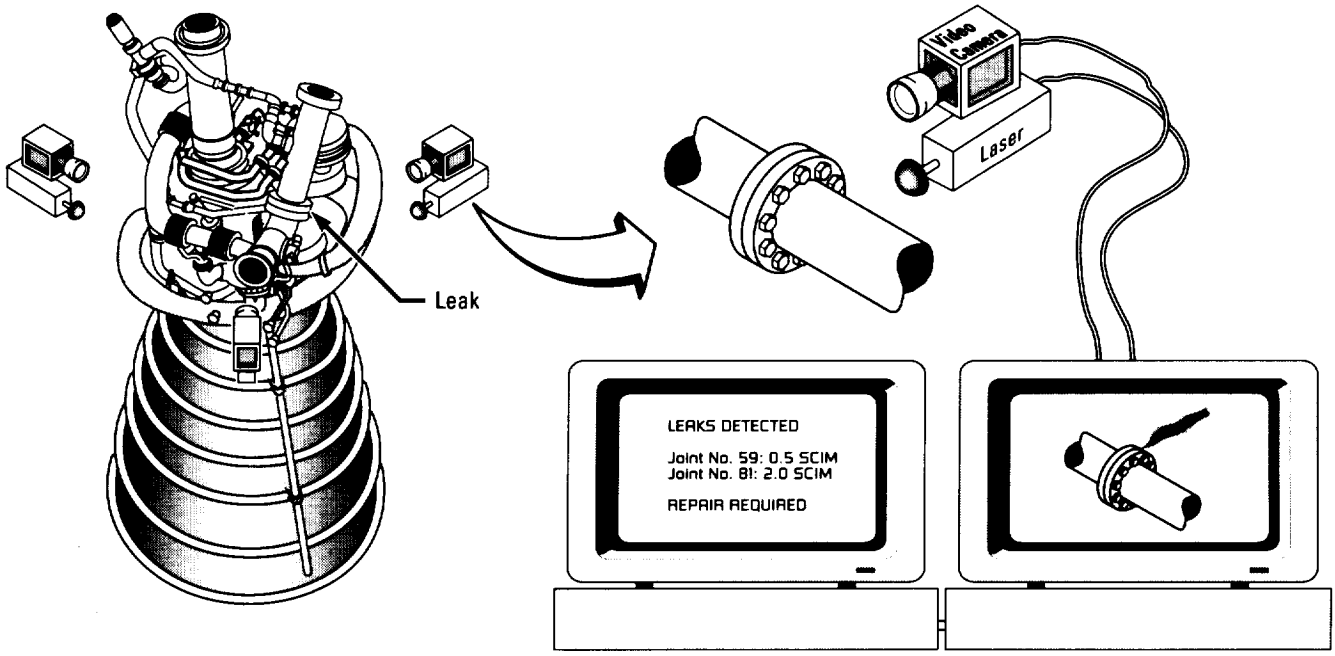

SCIM—Standard Cubic Inches/Minute

Optical absorption leak detection.

solution. The ease with which the gas can be seen also makes leak location rapid and simple and allows automatic electronic documentation by simply recording with a video tape recorder.

A breadboard leak imaging system has been tested to ensure the ability of the technology to meet SSME requirements. Leak rates of 0.07 cm^3/s (0.25 in^3/min), the maximum allowable leak rate for engine joints, have been imaged using both N_2O and SF_6 **tracer gases**. With N_2O, the gas cloud was seen extending approximately 23 cm (9 in) from its source, while the SF cloud could be seen over 1 m (3 ft) from its source.

The ability to quantify **tracer gas** leak rates has also been developed and demonstrated, using a personal computer (PC)-based video image processor. The measurement is made using a computer algorithm that calculates the amount of **tracer gas** in the image by comparing it with another image. The amount of gas in the image can be correlated to the leak rate. A similar algorithm can be used to enhance the sensitivity of the system.

A materials-compatibility study has established that N_2O is compatible with all materials in the fuel and oxidizer systems of the SSME. Safety and environmental assessments have also been made, in which N_2O was found to be acceptable.

Future plans are to construct a mobile **leak detection** system suitable for inspection of an SSME and to evaluate the system on test-bed engines. The system could then be qualified for flight engine use to replace the present soap solution and He signature **leak detection** methods for engine and vehicle ducts.

Delcher, R., Steffens, A., and Barkhoudarian, S., Rocketdyne Division/Rockwell, "Ground-Based Optical Leak Detection Technology," 1992 Earth-to-Orbit (ETO) Technology Conference, MSFC, AL, May 1992.

W.T. Powers/EB22
205–544–3452
Sponsor: Office of Aeronautics, Exploration, and Technology

Nonintrusive Diagnostics for Preburner Temperature Profiling

A **nonintrusive** optical means of measuring temperature profiles is needed to support liquid **rocket** combustor development and refinement. **Raman** scattering was selected to measure temperature profiles in the space shuttle main engine (SSME) fuel preburner. The combination of liquid access existing in the preburner, the lack of particles in the flow, and the low visible natural luminosity of the hydrogen/oxygen (H_2/O_2) flame favor **Raman** diagnostics in a backscattering configuration. The system permits profiling the preburner temperature distribution across a diameter from an existing transducer port on the SSME preburner.

The **fiber-optic Raman thermometer** (FORT) system consists of a continuous wave (CW) argon (Ar)-ion laser for excitation, an optical head attached to the preburner that focuses light into the combustor and collects backscattered light, a spectrograph and optical multichannel detector to disperse and rapidly detect the **Raman**-shifted radiation, and a computer system to acquire and analyze data. The most unique aspect of the instrument design is the use of multimode optical fibers to transmit laser radiation to the optical head and to conduct backscattered radiation from the head to the spectrograph. The use of small core optical fiber enables the transmission of light to and from the SSME in the presence of condensing vapors and vibration, and yet maintains the desired 1-cm (0.4-in) spatial resolution.

The **Raman** effect is an inelastic scattering process in which an electromagnetic light wave exchanges energy with the internal vibrational and rotational energy modes of molecules that are **Raman**-active. The scattered radiation depends on the degree of internal excitation of the gas and, therefore, the temperature. A **Raman** spectrum of H_2 measured for nominal preburner pressure and temperature conditions shows the structure of the Q-branch fundamental band. Transitions are labeled Q(j) according to the rotational quantum number. The temperature is determined from the Q-branch intensities because the rotational energies are Boltzmann-distributed when the degeneracy of the levels is taken into account.

A FORT diagnostic system was developed for measurements under the SSME alternate turbopump development (ATD) program. This system was used for testing the preburner before the turbomachinery was installed. Optical access to the preburner was provided by placing the optics behind a hemispherical, quartz dome at the position of one of the turbine bullets. In this location, a greater area in the combustor may be probed, as opposed to the sidewindow-mounted approach envisioned for SSME's. An optical design was chosen to enable temperature measurements to be made in a planar region downstream of the injector face. The optical system utilizes a pair of rotating prisms to point the optical axis within a conical region encompassing the full-diameter preburner.

Two test firings at 65-percent rated power level (rpl) were conducted with the **Raman** probe mounted in the checkout chamber. One test aborted after 4 s at full-scale pressure, 20.7 MPa (3,000 lb/in^2) absolute. The second test went to full duration, 30 s. Data were taken at 141 points within a measurement plane located 18 cm (7 in) from the apex of the dome; measurements were made at 13 different radii at equal intervals on each. The signal measured was essentially flat at approximately 2,000 counts for the 0.1-s collection time, with no discernible **Raman** signature. The signal was nearly constant as a function of wavelength, but varied significantly as a function of time. The probe in this case was making measurements in concentric circles in the combustor, so the variations seen in time could be spatial variations, such as streaks. However, no spatial correlation could be discerned in the data. Several sources of interference have been considered: overtone radiation from water vapor, H_2/O_2 continuum radiation, radiation from trace metallic species, and stray light in the spectrograph. Additional measurements with a wideband spectrometer will be necessary to identify the interfering radiation.

The envisioned FORT design for the test-bed facility eliminates many of the lenses and uses a dichroic mirror to separate the **Raman** signal path from the laser path to increase the optical efficiency. The laser is used at full aperture, and a series of lenses, arranged in a carousel, would be successively positioned in the optical path to move the probe volume across the combustor. This approach will be mechanically simpler and can be packaged in a smaller envelope, decreasing loads transmitted to the preburner hardware. The weight is estimated to be less than 4.54 kg (10 lb).

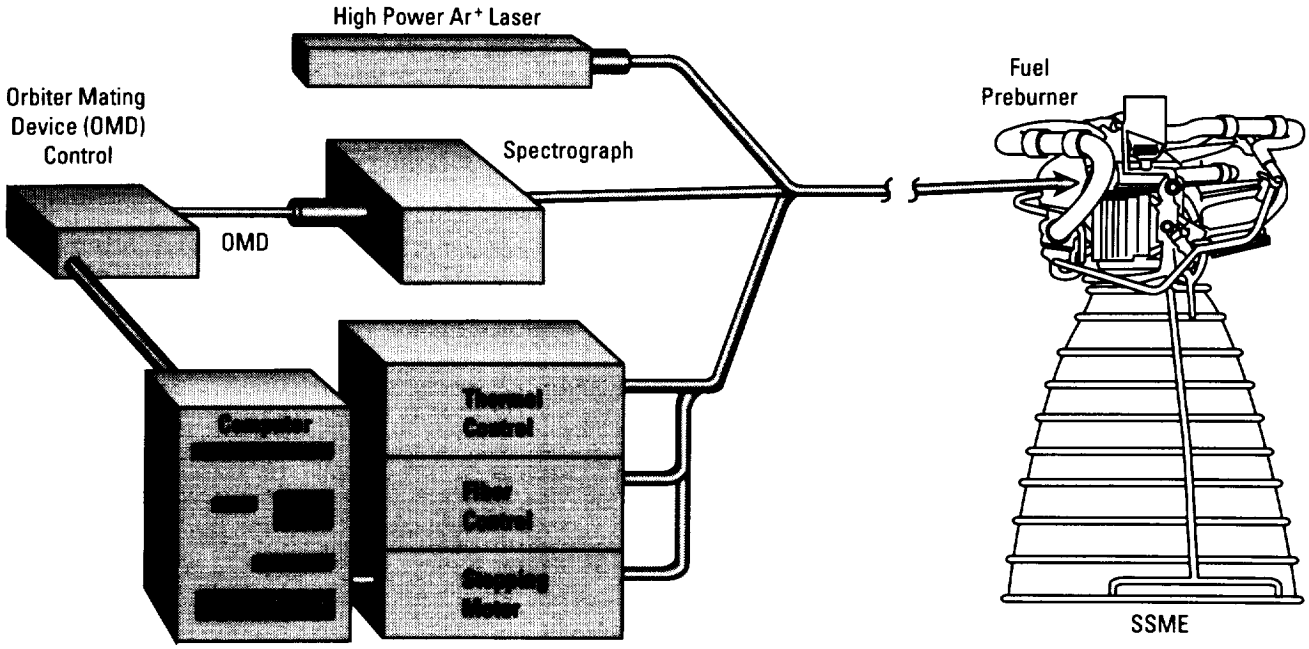

SSME FORT diagnostics.

Development and operation of the fiber **Raman** thermometry system will provide a unique capability for measuring gas temperatures nonintrusively within high-pressure **rocket** combustors, for which there is no existing technology.

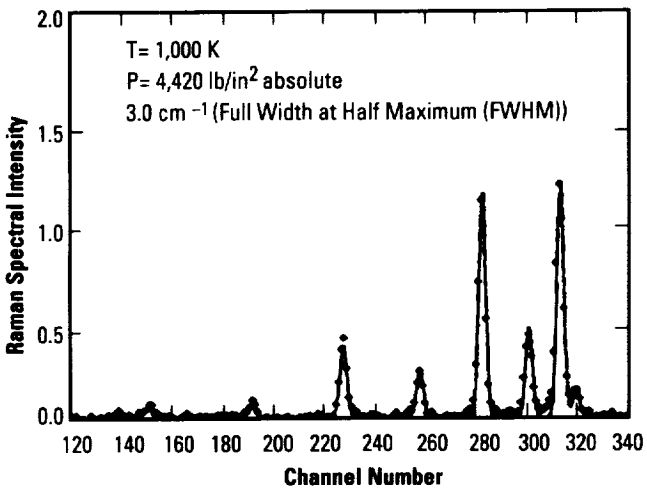

H_2 Q-branch Raman spectrum.

Shirley, J.A., United Technology Research Center (UTRC), "Progress in Laser Diagnostics for SSME Gas Phase Measurements," 1992 Earth-to-Orbit (ETO) Technology Conference, MSFC, AL, May 1992.

W.T. Powers/EB22
205–544–3452
Sponsor: Office of Aeronautics, Exploration, and Technology

Nonintrusive Hot-Gas Temperature Sensing for Advanced Rocket Engines

Existing **hot-gas temperature sensors** for the space shuttle main engine (SSME) are ruggedized resistance **temperature** devices that use a high-purity platinum wire resistive element as one arm of a Wheatstone bridge. This stable and highly accurate sensing element is inserted into the **hot gas** and is subjected to thermal shock and vibration from the high-velocity **hot-gas** flow. Failures have occurred in these **sensors** due to the opening of the resistive element, coaxial tube cracking, and charring of foam insulation within the **sensor** housing. Numerous improvements and modifications to the **sensors** and their manufacture have occurred over the years, including new annealing cycles and **temperatures**, brazes, protective coatings, lead wire terminations, and insulation material.

An ideal solution to providing accurate and reliable **temperature** sensing in this extreme environment is a **nonintrusive** optical approach. Such a **sensor** would stay outside of the high-**temperature**, high-flowrate environment and would not be subjected to the associated thermal extremes, thermal shocks, and high vibration rates for which previous **sensors** have been designed. An added benefit of this approach is the noninterference with the carefully designed and calculated gas flow geometries within the SSME **hot-gas** manifold (HGM).

The basis of the **nonintrusive hot-gas temperature** measurement is the sensing of the **infrared (IR)** emission in the 2.5- to 3.0-μm waveband from a **hot gas** containing water vapor. The **temperature** of a region of hot water vapor can be determined from the amount of light radiated in this waveband. The radiated energy increases with the concentration of gas in the path, becoming unity for a sufficient path length and pressure. Under these conditions, the gas radiates as a blackbody at that **temperature**, even though there can be little emission at other wavelengths. The change in detector output as a function of blackbody target **temperature** is obtained directly by integrating Planck's equation. Variations in emissivity are then readily transposed into

changes in indicated gas **temperature**. For mixture ratio and pressure variations (occurring simultaneously) of up to 25 percent, the calculated measurement error does not exceed 5 °C (9 °F) over the range 327 to 1,316 °C (620 to 2,400 °F).

Breadboard hardware was assembled to characterize the capabilities of this **sensor** approach. A miniature multijunction thermopile detector mounted behind a zinc-selenide (ZnSe) lens and a 3.03-μm center wavelength narrow bandpass filter viewed the flame from a precisely controlled flat flame burner. Independent **temperature** verification of the flame was provided by a type K shielded thermocouple probe mounted to the assembly to monitor the flame at the same time as the **sensor**. The optical uniformity of the **hot-gas** source was demonstrated with an Inframetrics 600 **IR** camera system used at the same 3.03-μm filter bandpass that the **sensor** used. The final analysis of **sensor** data taken under these conditions revealed excellent results. The **sensor**, when viewing the flame from a distance of 10 cm (4 in), provided output that tracked the camera/thermocouple data to within 0.2 percent over the 727- to 782 -°C (1,340- to 1,440-°F) **temperature** range.

Application of this **temperature** measurement approach to the SSME places specific constraints on the **sensor** design. The **sensor** tube will extend no further than the coolant liner wall and requires a diamond optical window and sapphire lenses for pressure isolation and thermal shock protection. Indium-arsenide (InAs) detectors, sensitive to 1.0- to 3.6-μm wavelength radiation, have inherently faster response times than that of the thermopile detectors or the resistance **temperature** device **hot-gas temperature sensor** presently in use in the SSME; these detectors will allow more accurate thermal tracking of transient conditions in the turbopump discharge ducts.

Two major tasks are currently being performed in the third phase of this effort. The prototype fabrication task is resolving the engineering design and fabrication concerns for prototype **sensors**. Upon receipt of the prototype **nonintrusive hot-gas temperature sensors**, the prototype testing task will be initiated. This will include environmental testing to the pressure and vibration requirements of the source control drawing specification and performance testing in both laboratory setups and in field settings on the representative HGM environment simulations.

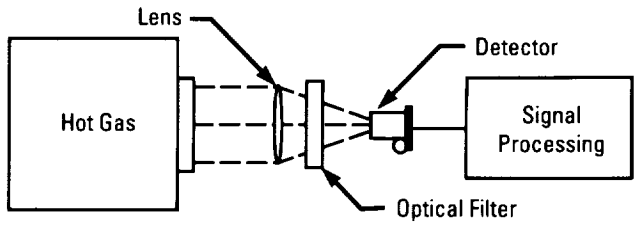

Basic sensor layout.

W.T. Powers/EB22
205–544–3452
Sponsor: Office of Aeronautics, Exploration, and Technology

Nonintrusive Speed Sensors for Rocket Engine Turbomachinery

Rotating shaft **speed** measurements provide information that is essential to the health and condition monitoring of liquid rocket engine turbomachinery components. While previous intrusive **speed sensors** have relied almost exclusively on a variable-reluctance technique to monitor shaft **speed**, a recent **nonintrusive speed sensor** (**NISS**) development task has reduced the risks associated with the use of such instrumentation in critical turbomachinery applications by eliminating the long cantilevered probe end. Many of the engineering challenges associated with liquid oxygen (lox) instrumentation design were mitigated by avoiding the severe lox environment found inside the space shuttle main engine (SSME) high-pressure oxidizer turbopump (HPOTP), with cryogenic flows in excess of 66 m/s (200 ft/s) and static pressures of more than 2.75 MPa (400 lb/in^2).

Of the many advanced instrumentation concepts examined as alternatives to the variable-reluctance technique for **speed** sensing, only the magnetic variable-source technique proved to be adaptable to existing SSME hardware design requirements. That four magnets could be safely embedded inside a piece of rotating turbomachinery and could be capable of providing a sufficiently high magnetic flux for **speed** sensing over a gap distance of 8.87 cm (3.5 in) was a technical milestone worth pursuing. The new **speed sensor** was to have been a direct replacement for the previous intrusive design, provided that the input signal characteristics of the SSME controller could be matched. With the development of high retained-magnetization materials, such as neodymium-boron-iron (Nd-B-Fe), magnetic shaft **speed** sensing over an 8.87-cm (3.5-in) gap became a real design goal, hence the **nonintrusive** nature of the **NISS** design.

The basic operating principle behind the **NISS** design is that a time-varying magnetic field is capable of producing an electric field, an electromotive force (emf), and an electric current in a loop of wire. A series of laboratory tests was used to evaluate **sensor** behavior under cryogenic conditions while steps were taken to optimize the magnetic circuit. This **sensor** optimization effort was aimed primarily at maximizing magnet volume within the **speed** nut housing against known slot wall thickness constraints to increase the **sensor** outpt signal. Magnetic field polarization axes were also studied to select the most favorable orientation among the tangential and radial options. All instrumentation design activities were aimed at improving **sensor** output signal characteristics while maintaining the **nonintrusive** aspects of the design.

From the experimental data, the amplitude dependence on shaft **speed** (frequency) is clearly seen for both cryogenic and ambient temperature conditions. By varying the number of turns associated with each **sensor** coil, the peak of the curve can be shifted to the left or to the right. Low-**speed** versus high-**speed sensor** performance rates were then used to determine the optimal number of coil windings required to achieve the design goal of 75-mV peak output over the design shaft **speed** range, 1,500 to 45,000 r/min. Data were gathered representing actual **sensor** output signals for a **NISS/speed** nut combination tested experimentally in Rocketdyne's spin pit as part of the **NISS** design optimization effort. These data show how, during cryogenic operation, the **sensor** output signal falls well below the design goal of 75 mV. Increased magnet size, as an enhancement to the magnetic field strength, use of a coils-in-series approach for winding the three output coils to minimize high-frequency capacitative couping losses, and the small gain in signal output due to the increased HPOTP operating temperatures (liquid nitrogen (LN_2) temperatures were at or below the curie temperature for K-Monel that added to the magnetic shielding effect responsible for some of the signal loss) were all used to boost the **NISS** signal.

Attentions aimed at isolating the magnet material within the **speed** nut housing were the design team's first priority, especially given the magnetic material's violent incompatibility with the HPOTP's lox environment. The method best suited to safely encapsulate the magnet material inside the modified turbine nut (**speed** nut) proved to be an electrodeposited-nickel (ED-Ni) process. The open area immediately above each of four slots was to be permanently capped by a 0.51- to 0.72-mm (0.020- to 0.028-in) thickness of ED Ni. The

addition of a conductive silver-filled epoxy to hold the magnets in place during nickel (Ni) plating was also specified to enhance bond strengths at the boundary between the epoxy and the ED Ni.

The hydrodynamic environment surrounding the HPOTP #3 bearing cartridge was also of particular concern to those who recognized that one of the **speed** nut's primary functions has been to flow lox past the #3 bearing as a coolant at nearly 2.3 kg/s (5 lbm/s), but not so vigorously as to produce a vortex shedding effect capable of degrading bearing cage performance. Borrowing from previous test experience with four-lobed and no-lobed turbine nut designs, a compromise was reached with the **speed** nut design where two notches were machined into the **speed** nut's outside diameter, first, to emulate the hydrodynamic environment of a two-lobed turbine nut and, second, to provide an appropriate surface for engaging an installation tool required to torque the **speed** nut in place on the shaft during HPOTP assembly.

Signal outputs from the triply redundant **sensor** coils were augmented by the selection of a highly permeable core material that was specially shaped to capture the magnetic lines of induction, even though such cores tended to contribute to high-frequency signal loss owing to its inductive properties. Improvements in low-frequency response were weighed against these high-frequency losses in selecting both an acceptable core material with an appropriate number of windings per coil. The possibility of retaining the existing electrical interface with the SSME controller was also given a high priority, given the expense associated with replacing its 12-kΩ input impedance network. **Sensor** outputs ranging from 10 mV to values approaching 200 mV were produced by the **NISS** when terminated into the 12-kΩ load under ambient temperature conditions, but were considerably less for the LN_2 condition. Under technology test-bed engine (TTBE) hot-fire conditions, the **sensor** output signal should be readily measured using facility instrumentation irrespective of the controller requirement.

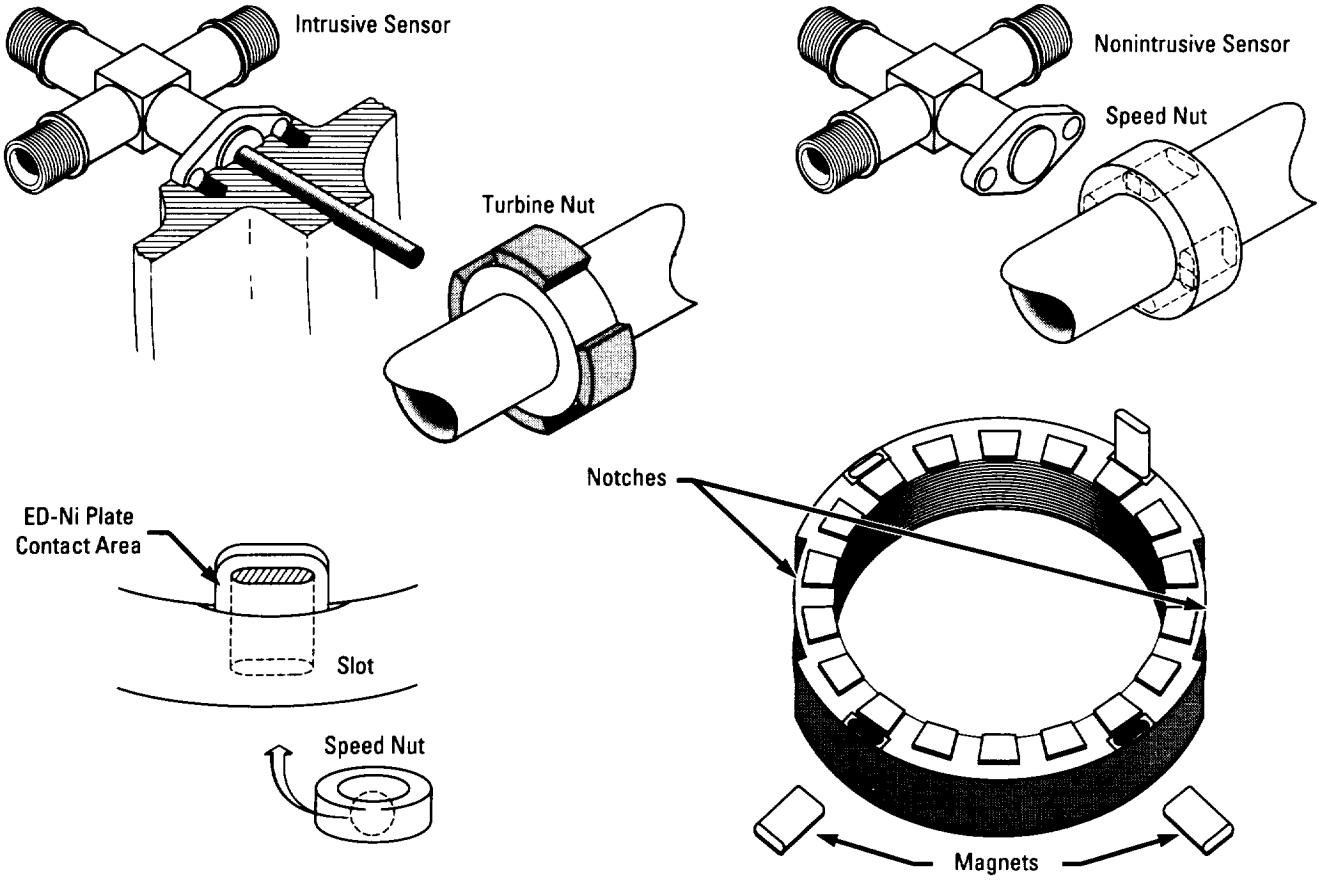

Speed sensor components.

Implementation of the **NISS** and **speed** nut designs on the TTBE has accelerated since the completion of critical development tasks, such as spin-pit testing the **NISS** components in Rocketdyne's Engineering Development Laboratory. Optimized **sensor** designs have been put forward to maximize **sensor** output signals while retaining every possible safety feature. Design reviews were readily able to resolve all of the design issues raised, leading one to the conclusion that NISS hardware is ready for hot-fire testing. The **NISS** technology is ready to support the SSME technology test-bed (TTB) and many of the other active rocket engine development programs such as the National Launch System (NLS) and national aerospace plane (NASP). Greater emphasis, however, must be placed on determining the utility of the design, with the results of imminent hot-fire tests tentatively planned for the TTBE later this fall (September 1992).

Reinert, J., Rocketdyne Division/Rockwell, "Implementation of the Nonintrusive Speed Sensor for the SSME High-Pressure Oxidizer Turbopump," 1992 Earth-to-Orbit (ETO) Technology Conference, MSFC, AL, May 1992.

W.T. Powers/EB22
205–544–3452
Sponsor: Office of Aeronautics, Exploration, and Technology

Optical Plume Anomaly Detector

The optical **plume** anomaly detection (OPAD) program is an experimental study to create a rocket **engine** health monitor based on detection of **anomalous** atomic and molecular species in the exhaust **plume** of a rocket **engine**. The OPAD program has been operating for several years. The original intention was to develop a failure detection device, but, in the process of pursuing the task, it was found that a proper phenomenological data base, with which the necessary computations could be supported, did not exist. Thus, one of the most important features of the program would be the creation of such a data base. That task necessitated acquiring data from such available sources as hydrogen/oxygen (H_2/O_2) rocket **engine** test stands, both large and small.

The basic method initially used for OPAD investigations is that of spectral emission, primarily from the shock structure in the **plume** referred to as the "mach disc." Because of the high temperatures in the disc, most metals radiate with sufficient intensity to allow detection of only a few parts-per-million or less. For altitude (diffuser) stands or for actual flight vehicles, since altitude stands have no mach disc and launched vehicles lose it with altitude, an absorption system is a likely choice and a program has been under way for sometime to investigate the ways of implementing flight measurements. However, converting data into information is currently the primary thrust of the OPAD program and a thorough understanding of the phenomenology involved is critical, whether it is obtained by emission or absorption techniques is not important.

While proper software development is expected to require several years, both qualitative and quantitative techniques are employed to interpret the monitored specie lines in post-test analysis. The quantitative techniques require the development of new codes, which, in turn, necessitate the generation of new or updated functions for high-temperature, high-pressure phenomena. To permit the possibility of near-real-time automated decision making, either for ground or flight operations, the application of artificial intelligence (AI) techniques to the problem of analyzing the data produced by and the information derived from the spectrometric system is anticipated.

To date, the OPAD program has acquired data on all 35 ground-level test firings of the **space shuttle main engine** (**SSME**) at the technology test-bed (TTB). While post-test analysis is now performed following each test to support Propulsion Laboratory reviews, an in-depth study (conducted in the past year) of data from several **SSME** tests indicated instances of **anomalous** metallic activity consistent with **engine** preburner faceplate **erosion**. At the request of the Propulsion Laboratory, OPAD spectrometer and polychromator data were examined to determine the time relative to **engine** startup and length of **erosion**. The study also provided relevant information necessary for system calibration and model validation. The current models include line-by-line radiative transfer calculations with options for self-absorption, iteration on species mole-fractions, and/or temperature, spectroscopic data from National Bureau of Standards (NBS)/National Institutes of Standards and Technology (NIST) tables of measured transition probabilities with over 5,000 transitions for selected atoms, pressure broadening and shifting rate data for various species and perturbers, additional options for convolving with arbitrary instrument functions, and application to either emission or absorption. When completed, the models will provide estimates of **erosion** rates and of material composition alloy(s) identification that may be compared to established redline levels to detect **engine** or component failure.

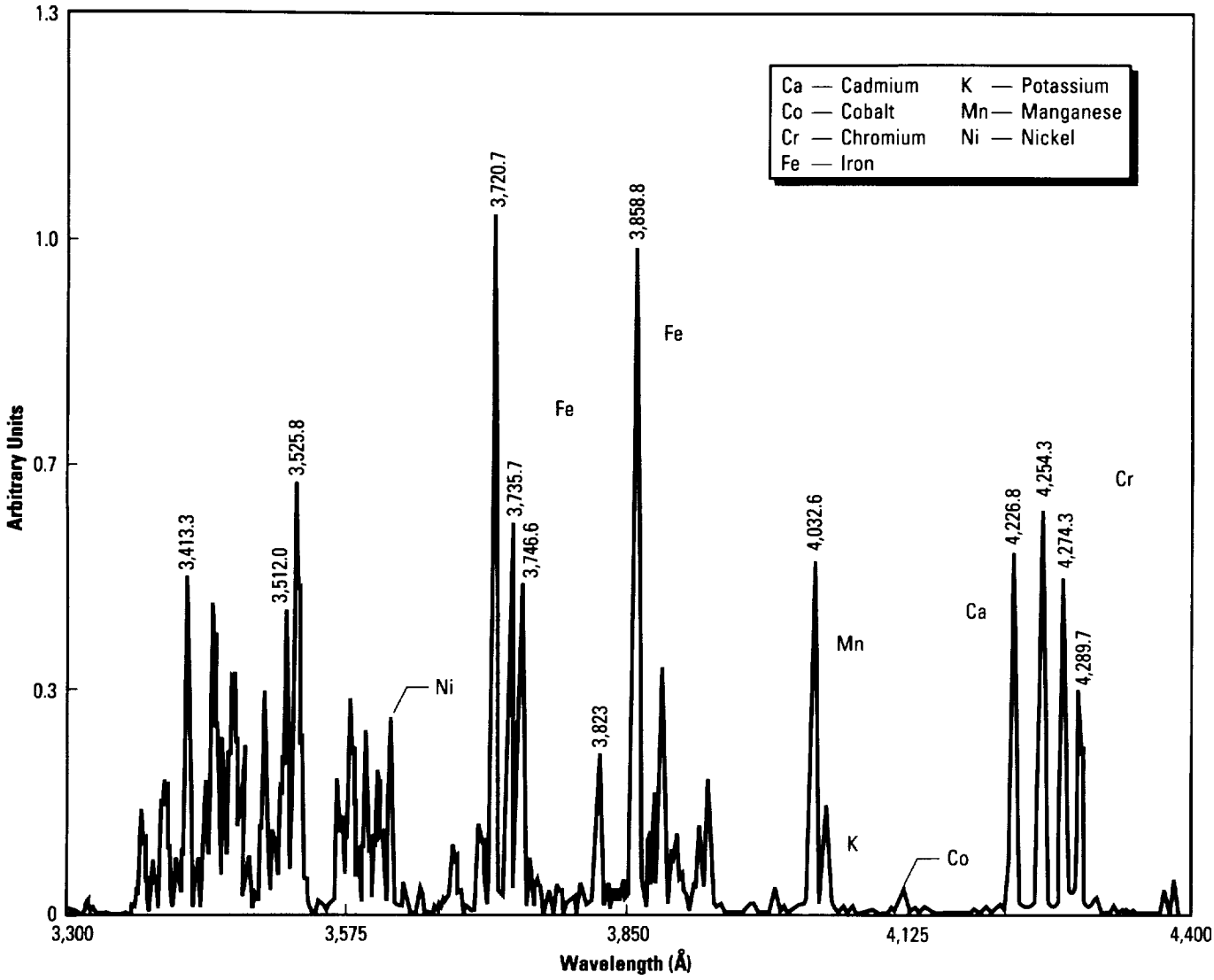

Theoretical spectrum convolved with instrument response; best fit to emission at t+4.5:TTB020.

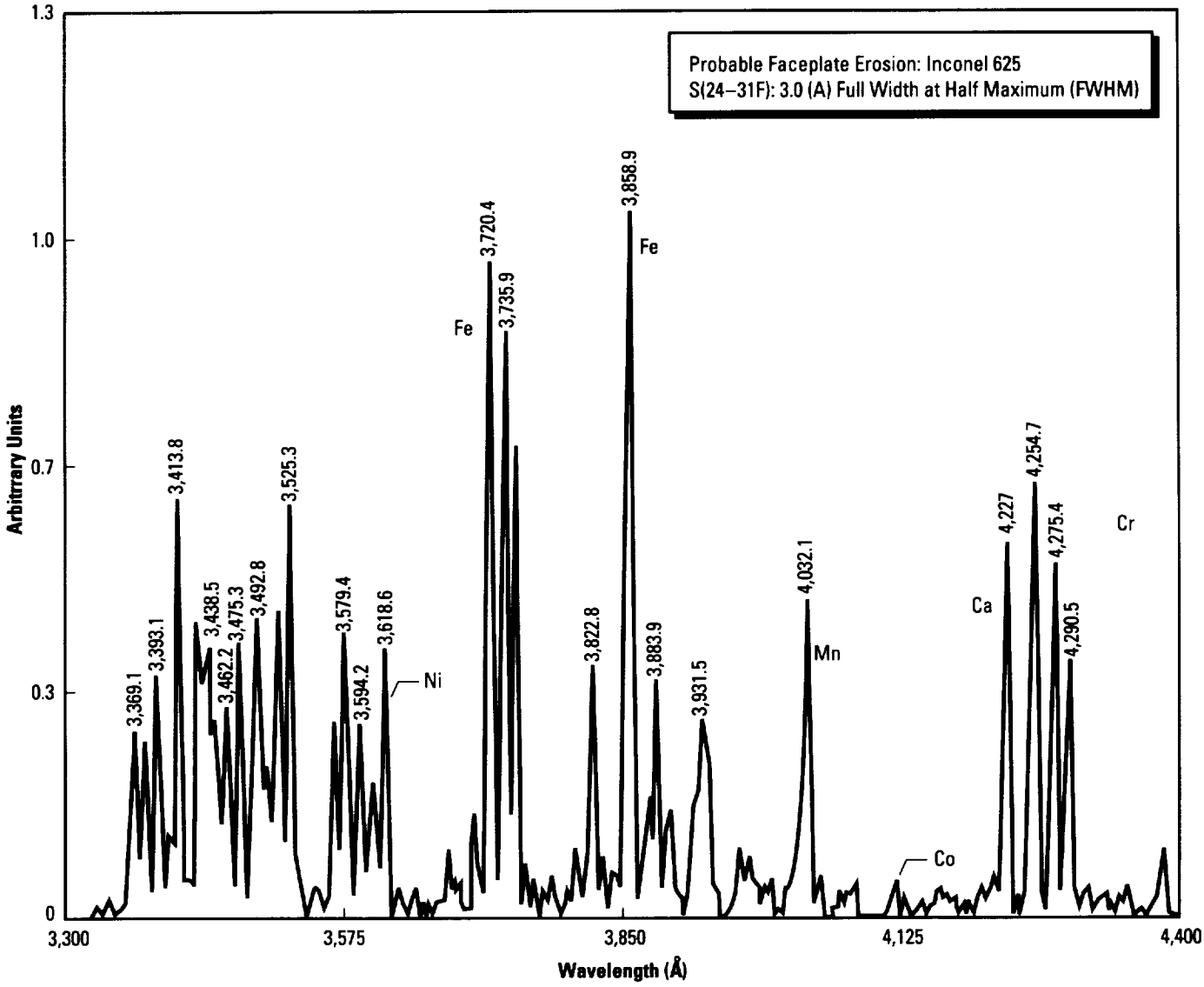

OPAD spectrometer: spectral emission of TTB020 at 4.5-s.

Powers, W.T., Cooper, A.E., and Wallace, T.L., "OPAD Through 1991—Status Report '2,'" Proceedings, Third Annual University of Cincinnati Health Monitoring Conference, Cincinnati, OH, November 1991.

Cooper, A.E., Powers, W.T., and Wallace, T.L., "OPAD Status Report: Investigation of SSME Component Emission," 1992 SAE Aerospace Atlantic, Dayton, OH, April 7–10, 1992.

W.T. Powers/EB22
205–544–3452

Sponsor: Office of Aeronautics, Exploration, and Technology

Propellant Leak Detection for Launch Vehicle Applications

Hydrogen (H_2) propellant **leak detection** for liquid rocket engines is a key technology that will reduce ground operations costs, improve flight readiness, and provide real-time engine health and safety monitoring. Presently, there are no flight H_2 **leak detection** systems and no localized **detection** systems in use during pre-launch operations. The objective of this project is to develop a flight **leak detection** system that can determine the location and magnitude of H_2 propellant **leaks** from a space shuttle main engine (SSME)- or space transportation main engine (STME)-type engine in real time and relay that information to the engine controller or operations personnel for appropriate action. Currently, a breadboard system is under development for testing in 1992, leading to a flight prototype system for the SSME in 1994.

The propellant **leak detection** system (PLDS) under development uses a distributed array of discrete point microsensors. The design incorporates both "site-specific" and "imaging" **sensors**. A typical system for a booster engine would use 100 to 200 of these **sensors** distributed throughout the engine. The **sensor** signals are multiplexed and processed using the knowledge-based software to interpret the data and to inform the engine controller or test personnel of **leak** conditions. The system software is currently being implemented on a microcomputer to support operations personnel and for validation testing.

The "site-specific" **leak sensors** are individual H_2 microsensors distributed within the engine compartment. These **sensors** are strategically located to detect **leaks** from a specific engine component such as a weld joint or flange and can be embedded in the insulation surrounding cryogenic propellant lines. High-probability **leak** sources are instrumented with the "site-specific" **sensors**. The proximity of these **sensors** to the **leak** source reduces the incidence of false alarms. The "imaging" **sensors** are distributed in different zones of the engine compartments to detect **leaks** from all possible sources. The "imaging" **sensors** also provide overall monitoring of potentially flammable conditions in the engine compartment, such as the space shuttle boattail. The location of **leak** sources is determined by triangulation from the response of several "site-specific" and "imaging" **sensors**. The magnitude of the **leak** is determined from the H_2 concentration at each of the **sensor** locations.

A prototype H_2 microsensor used in the PLDS is a solid-state metal insulated semiconductor (MIS) diode design that has been developed by NASA/Lewis Research Center (LeRC) and Sandia National Laboratories. The **sensor** consists of an n-type silicon (Si) wafer with a thin layer of oxide coated with an H_2-sensitive metal, typically a palladium (Pd)-based alloy. When the diode is reverse-biased and exposed to H_2, the reverse current generated is proportional to the H_2 concentration. The **sensors** are compact, lightweight, rugged, and have low power consumption. Characterization tests conducted in 1992 have demonstrated that the **sensors** effect a suitable response and recovery to H_2 exposure under rocket engine operating conditions.

Multiplexing of the **sensor** signals enables the large array of **sensors** to be distributed on the engine without excessive cabling requirements. Multiplexing of 16 **sensors** in the breadboard system requires only 8 total wires. The SSME prototype system under development for the testing at the technology test-bed engine (TTBE) uses 144 **sensors** and requires only 16 total wires. Signal conditioning is currently performed at a centralized processing unit. Advancements in on-chip signal processing technology may permit signal conditioning to be performed at each **sensor** in the future.

The system software performs data acquisition and interpretation functions. The software acquires and records data from each of the **sensors** and displays the H_2 concentration on a graphical user interface in real-time. The display includes a "plant diagram" of the engine showing H_2 concentration, alarm lights indicating threshold levels (i.e., flammability levels), and concentration versus time. The data interpretation function is performed using knowledge-based software to analyze the concentration-versus-time histories and to determine the location and rate of the **leak**. The software then produces a three-dimensional (3–D) iso-concentration image of the **leak** as visual feedback to

test personnel for evaluation. The data interpretation software is being developed using the CLIPS **expert system** shell and NETS **neural network** software tools developed by NASA/Johnson Space Center (JSC).

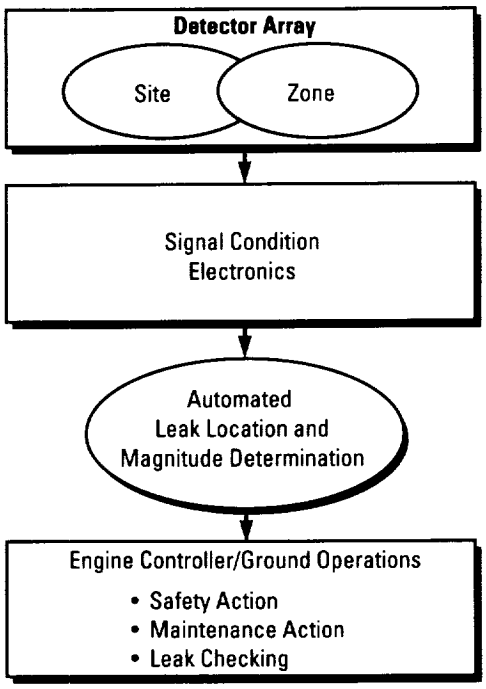

System organization.

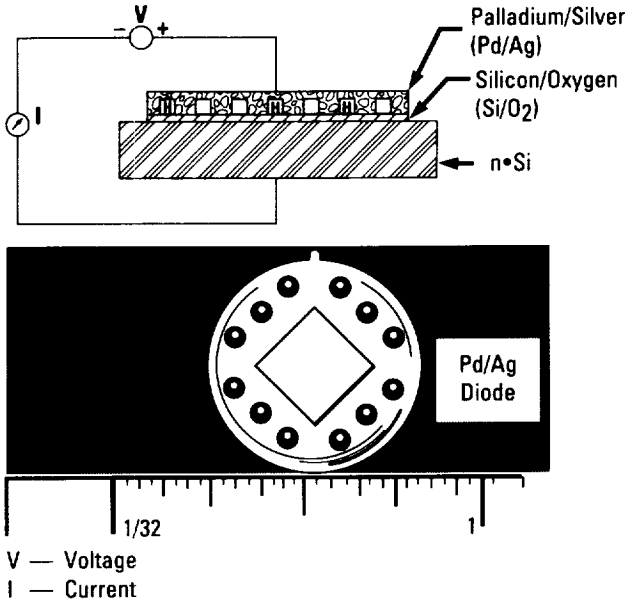

A prototype H_2 microsensor used in the PLDS.

W.T. Powers/EB22
205–544–3452
Sponsor: Office of Aeronautics, Exploration, and Technology

Robotic Eddy Current Inspection System

With the increased use of carbon-carbon and graphite epoxy materials in the aerospace industry also comes a demand for more sophisticated methods of **nondestructive evaluation** (**NDE**) of these types of materials. The integration of computers into **NDE** equipment, coupled with automated methods of scanning hardware, allows both inspection and interpretation of results to be performed on-line in real time. The development of these types of "smart" systems also results in shorter inspection times and a more accurate interpretation of results.

Under the direction of MSFC, The University of Alabama in Huntsville (UAH) has developed a "smart" system for **eddy current** inspection of both carbon-carbon and graphite-epoxy materials and hardware. The complete system consists of a robotic manipulator arm that holds an inspection probe, a turntable that allows automated rotation of cylindrical hardware, an **eddy current** instrument for test signal generation, and a visual interface to display results, all linked together by a supervisory computer that stores all of the test results. When this "smart" system is fully operational, the supervisory computer will also interpret the results in real time by identifying the type and location of any defects in the carbon-carbon and graphite-epoxy specimens, as well as be operator-friendly to some extent. Upon completion of the current contract, the system will be turned over to the **Nondestructive Evaluation** Branch at MSFC.

Preliminary laboratory tests have shown that digital **eddy current** testing may be a viable method for in-process monitoring of composite components. Once fully operational, the robotic **eddy current** inspection system will be used to perform analyses of graphite-epoxy and carbon-phenolic raw materials, in-process parts, and finished parts to identify general trends in processed materials, as well as localized changes in conductivity that might indicate changed mechanical or thermal properties. This information will be correlated with **NDE** data from other sources, such as computed tomography (CT) and ultrasonics through the integrated nondestructive data evaluation and reduction system (INDERS). A further contribution of digital **eddy current** testing is expected to be the extrapolation of ply-orientation from three-dimensional (3–D) readings of

directional conductivity. This technique provides critical orientation information in a quantitative format, which can then be used to support thermostructural analyses of as-built components. Preliminary testing with carbon-carbon specimens indicates this information is critical in predicting the failure load of composite rings and cylinders. Efforts to extract ply-orientation effects in wrinkled carbon-carbon cylinders have shown promise, but further development is required.

The information gained from this program will contribute to an increased understanding of the effects of processing on composite material properties and of the way composite materials fail.

C.C. Bryson/EH13
205–544–2553
Sponsor: Office of Space Flight

Small-Inertia, Clamp-On Cryogenic Flowmeter Transducer

Under contract NAS8–38429, a small **clamp-on** ultrasonic transducer has been developed by Panametrics of Waltham, MA, to measure flow in thin-wall ducts containing **cryogenic** liquids. The stainless steel (SS) (SS304)-housed transducer has a mass of 29 g (1 oz) and it fits within a 1-×2-×3-cm (0.4-×0.8-×1.2-in) envelope. It can be removably coupled at room temperature or at **cryogenic** temperature to ducts of wall thickness w≈2.5–3.5 mm (0.1–0.13 in), and of diameters less than 25 mm (1 in). The particular liquid or cryofluid, its sound speed, and location of the receiving transducer are relatively noncritical. For example, in a duct of inner diameter (ID) ≈ 100 mm (4 in), any single-axial spacing (S) between −100 and −150 mm (14 and 6 in) suffices whether the liquid is water or liquid nitrogen (LN_2), their sound speeds being approximately 1,500 m/s (4,600 ft/s) and 869 m/s (2,700 ft/s), respectively. Preliminary piggyback testing with LN_2 flowing in a 50.8-mm (2-in) tube (50.8-mm (2-in) outside diameter (OD) × 2.8-mm (0.11 in) wall) at MSFC Test Stand 115 showed that the new transducers, operated in conjunction with a commercial ultrasonic **flowmeter** (Panametrics' Model 6468), can measure flow up to at least 6 m/s (18 ft/s) as long as the cryofluid is single-phase.

Relatively large, commercially available **cryogenic** transducers are currently used on standard wall pipes, with the present MSFC-sponsored small design being used for 3-mm (0.12-in) thick pipe wall. Buffer rods isolate the piezoelement from direct exposure to the cryofluid and to its low temperature, but care must be exercised so that excessive heat does not enter the fluid through the rod in the attempt to prevent the piezoelement from getting too cold. Similar remarks apply to the "conventional" **clamp-on** for standard or thick wall pipe, but the **clamp-on** introduces two further complications. First, sound must be coupled reliably from wedge to pipe. Second, the receiving transducer must be positioned to receive sufficient energy despite a potentially large range in sound speeds in cases where not just one pure cryoliquid is involved. By way of background, the wetted buffers are currently used in a number of installations in Japan on 1-, 2-, 2.5-, and 3-in SS pipe having 3.5- to 5.5-mm (0.13- to 0.22-in) wall thicknesses. Accuracy of 1 percent relative to weighed liquid

was achieved but only after chilldown to single-phase liquid. (In an industrial plant, this can take 1 to 2 wk, or even longer, if the chillbox is defective).

Large ("conventional") **clamp-on** transducers are currently used in Korea to measure liquid natural gas (LNG) or methane (CH_4) and propane mixtures in 100-mm (4-in) schedule (sch) 40 SS pipe (100-mm (4-in) ID × 6-mm (0.25-in) wall). The couplant is one of several antigall, antiseize compounds normally used as a high-temperature lubricant. These **cryogenic** couplants were first demonstrated in Waltham with the small transducer.

A signal may be cleanly transmitted across LN_2 contained in a 100-mm (4-in) sch 10S pipe (wall thickness = 3 mm (0.12 in)). The relatively high signal-to-noise ratio (SNR) obtained in this LN_2 test at zero flow,

Transducers mounted on tubing.

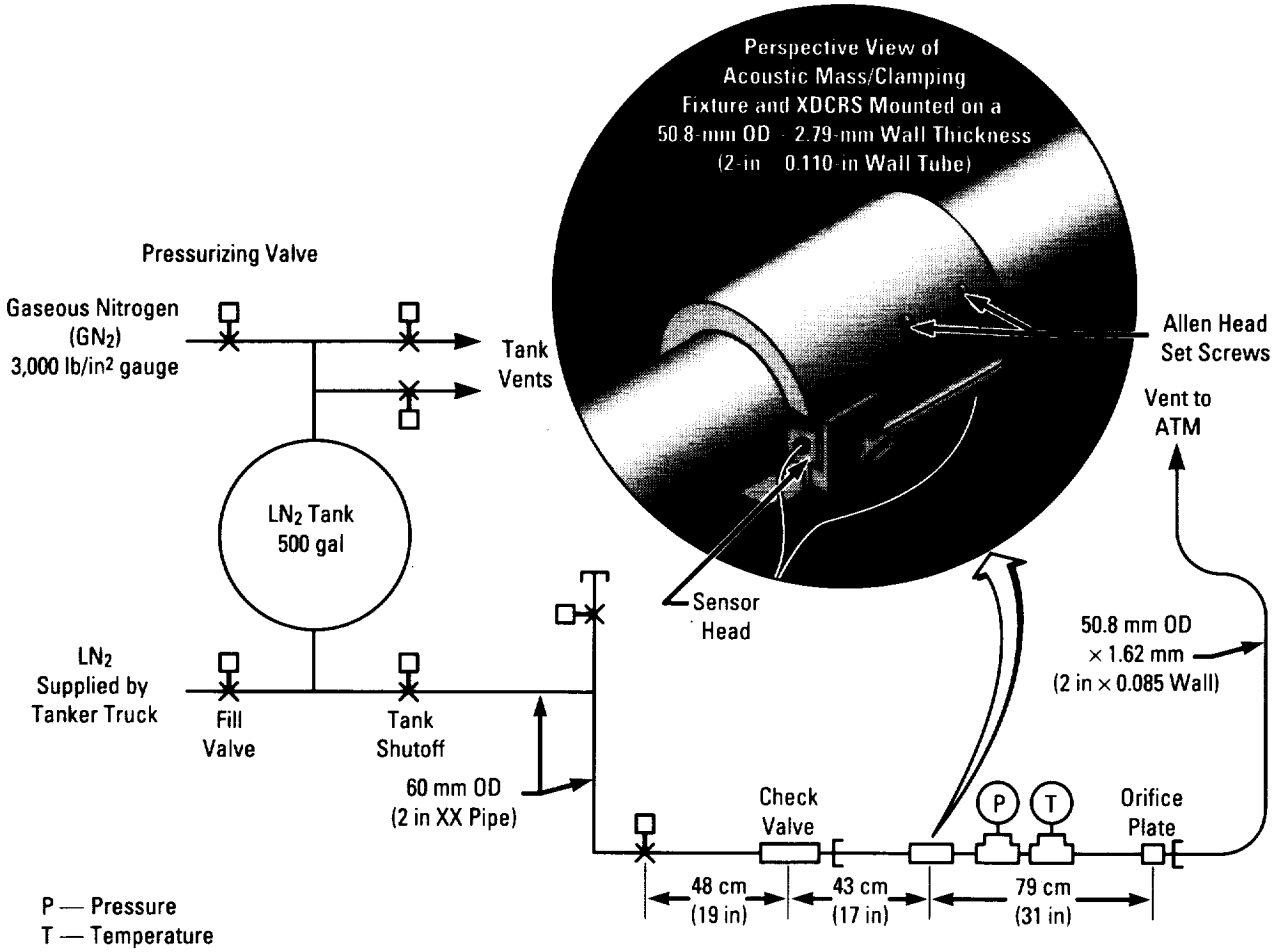

Schematic of cryogenic flow test at Test Stand 115 at the MSFC facility; test dates May 13–14, 1992.

together with the recently established feasibility of using the same transducers to measure LN_2 flows up to aproximately 6 m/s (18 ft/s), leads the investigators to conclude that the transducer developed in this contract has a good chance of **noninvasive** velocity measuring the flows of liquid cryogens in space shuttle main engine (SSME) applications. More testing is needed to establish this conclusion more firmly; to determine accuracy compared to a high-accuracy flow reference method (gravimetric, volumetric, or secondary standard); to work out attachment means for particular SSME (or other) ductwork; and to develop electronics fast enough to accurately sense flow transients.

Lynnworth, L., Matson, J., and Nguyen, T.H., Panametrics, Inc., "Small-Inertia Clamp-On Cryogenic Flowmeter Transducer," Earth-to-Orbit (ETO) Technology Conference, MSFC, AL, May 1992.

W.T. Powers/EB22
205–544–3452
Sponsor: Office of Aeronautics, Exploration, and Technology

Space Shuttle Main Engine Exit Laser Diagnostics

Maps of temperature, species concentration, and velocity, measured in a plane at the exit of the **space shuttle main engine** (**SSME**), would be valuable for anchoring engine performance codes and evaluating the performance of individual engines. Even if perturbations caused by physical probes were tolerable, it is not likely that probes could survive in the hot, high-velocity exhaust stream. **Nonintrusive, optical diagnostics** are being developed to measure gas-flow parameters at the exit of the **SSME**.

Raman scattering (RS) was selected for temperature and species concentration measurements because: (1) it has the ability to interrogate more than one species at a time; (2) it requires a single laser excitation source; and (3) the analysis of spectral data for species concentration and temperature is straightforward. However, RS is weak and requires relatively large collection optics near the **SSME** exit. To acquire measurements at the lower densities of the nozzle exit, a laser operating in the ultraviolet (UV) (e.g., krypton fluoride (KrF) excimer) must be employed to increase the small signal levels typical at visible wavelengths. A simple and efficient approach using filters to select portions of the hydrogen (H_2) Raman spectrum has been chosen for temperature measurements. Concentration measurements would use some of the same data channels as the temperature measurements.

A porous-plug burner operated premixed with a mixture of H_2, air, and nitrogen (N_2) has been studied. N_2 is added to the flow to maintain post-combustion gas at a temperature simulating conditions in the **SSME** exhaust. A composite spectrum spanning 35 nm (1.38 in) will show: H_2; water (H_2O) vapor and N_2 vibrational Raman bands; and H_2 rotational Raman bands and laser-induced fluorescence from hydroxyl radical in the premixed, N_2-cooled flame. The structure of the H_2 Q-branch is resolved except for the first rotational component, Q(O), at the band. The hot band is visible in the N_2 spectrum. The rotational Raman spectrum of H_2 is shown from S(1) to S(7). The series of spectral lines in the region 281 to 285 nm is due to laser-induced fluorescence from the molecular radical OH in the 1.0 band of the A–X transition. Comparison of the measured Raman Q-branch spectra of H_2 spectrum to

the calculated spectrum for a temperature of 1,200 K (1,700 °F), corresponding to a thermocouple measurement, shows good agreement.

The accuracy of relative concentrations determined from UV Raman has been checked by comparison to the known reactant flowrates in the premixed flame. The ratio of the H_2 concentration relative to the H_2O vapor concentration determined from the Raman measurements is 0.69/0.11 in the post-flame gas. This ratio implies a fuel equivalence ratio of 1.69/0.11, which agrees, within experimental error, with the equivalence ratio determined by the gas flowmeters, i.e., 1.60.

In the velocity measurement flow-tagging concept, a focused KrF excimer laser photodissociates H_2O by a two-photon absorption, resulting in the creation of a small zone in which the hydroxyl radical concentration is enhanced above the background level of OH resulting from combustion. Some of the OH generated in the photofragmentation process is electronically excited and fluoresces. In 1 or 2 μs, the enhanced OH zone would be convected several millimeters at **SSME** exhaust velocities. The distance the enhanced OH zone moves would be measured with the optical multichannel analyzer (OMA) by inducing OH fluorescence with a time-delayed, UV pulsed dye laser, tuned to an electronic resonance near 308 nm.

Experiments to evaluate the feasibility of enhanced OH flow tagging were undertaken to determine whether the enhanced OH lifetime under flame conditions is compatible with delays required for imaging. The decay rate of OH measured in the flame environment was compared with results of the CHEMKIN computer program calculations. The measured decay rate was found to be slower than the calculated rate. The CHEMKIN code does not include the effect of ions, which are believed to act as a reservoir that decreases the effective rate of decay. Additional measurements and theoretical modeling may be necessary to confirm that the decay rate in the **SSME** environment is compatible with the required

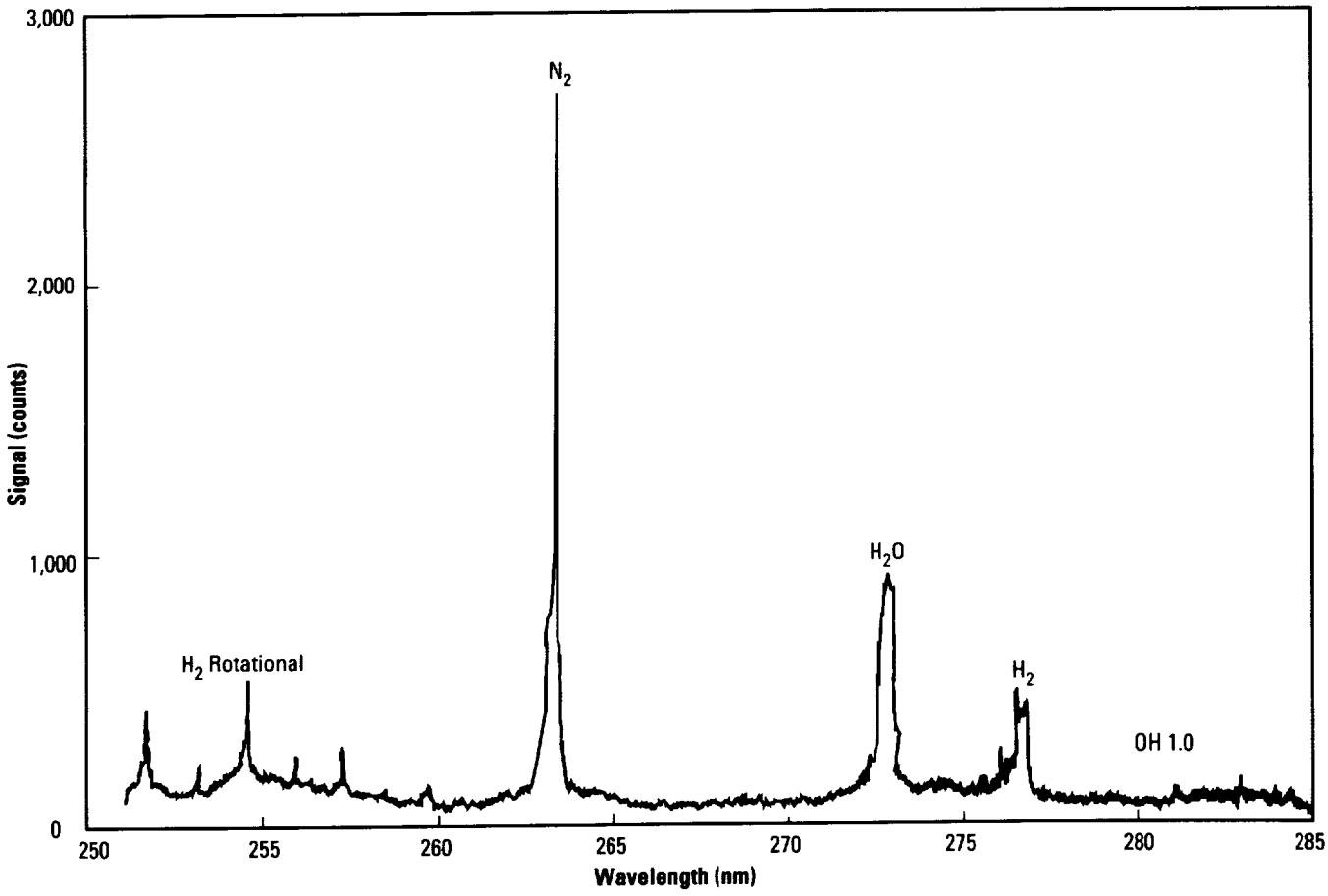

Spectrum of H_2-air-N_2 flame.

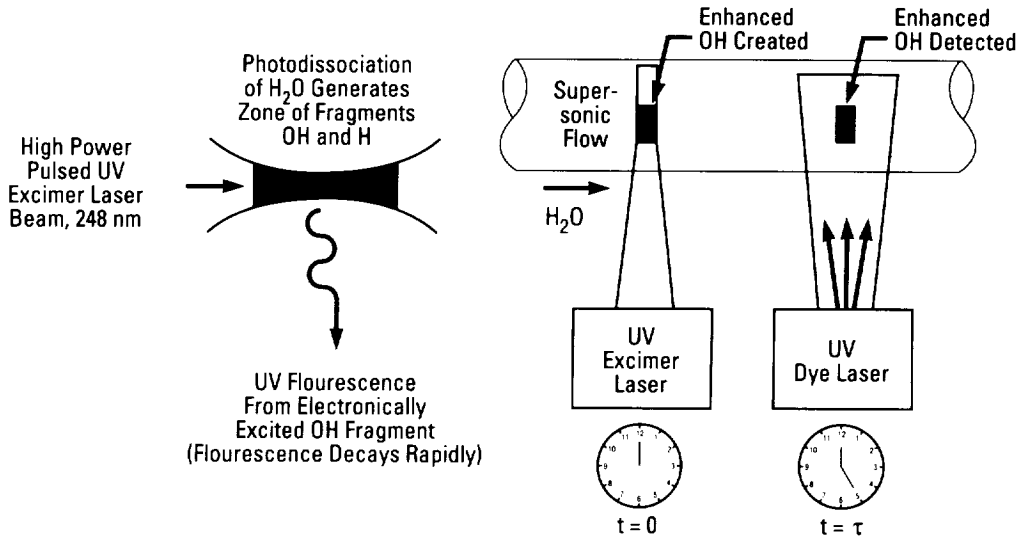

Flow testing for velocity determination.

laser pulse delay. Imaging using photodissociative flow tagging has also been demonstrated at the United Technology Research Center (UTRC), with velocity accuracy better than 2 percent demonstrated.

The design of optics to project and focus the laser beams at the **SSME** exit and to collect Raman-scattered light and OH flow-tagging images has been studied. It has been found that separate components are required. For focusing the lasers and collecting Raman signals, a Cassegrain telescope is desirable. For flow tagging, an imaging system with finite conjugates is required. A toroidal mirror system has been found to provide good optical performance.

Design and development of a laser-based diagnostic system to measure flow properties at the **SSME** will be an engineering challenge. Operation on the stand will be a significant advance in technology over that which now exists.

Shirley, J.A., UTRC, "Progress in Laser Diagnostics for SSME Gas Phase Measurements," 1992 Earth-to-Orbit (ETO) Technology Conference, MSFC, AL, May 1992.

W.T. Powers/EB22
205–544–3452
Sponsor: Office of Aeronautics, Exploration, and Technology

Technology Test-Bed Brushless Torquemeter Evaluation

To enhance bearing diagnostics and pump-design capabilities in rocket engine turbopumps (and in other rotating machinery) while using a minimum number of sensor ports, Rocketdyne has been developing a brushless **(noncontacting) torquemeter**. The brushless **torquemeter** already monitors shaft speed in addition to torque, and the combination of these two parameters gives shaft power. The development of the brushless **torquemeter** has been directed toward rocket engine turbopump applications, so it is ideal for applications in which access is extremely limited and the environment is severe.

The brushless **torquemeter** consists of one or more **magnetostrictive** deposits bonded to the rotating, load-bearing shaft and a sensor probe containing a pickup coil surrounded by a pair of permanent magnets with opposing magnetizations. When the deposit passes under the probe, it becomes magnetized by the first permanent magnet. As the deposit passes the pickup coil and approaches the second magnet, its magnetization undergoes a reversal, since the applied field seen by the deposit is changing in accordance with the opposed magnetization of the permanent magnets. By the time the deposit reaches the second permanent magnet, the magnetization of the deposit has rotated 180°. This switching of magnetization of the deposit induces a voltage pulse in the pickup coil.

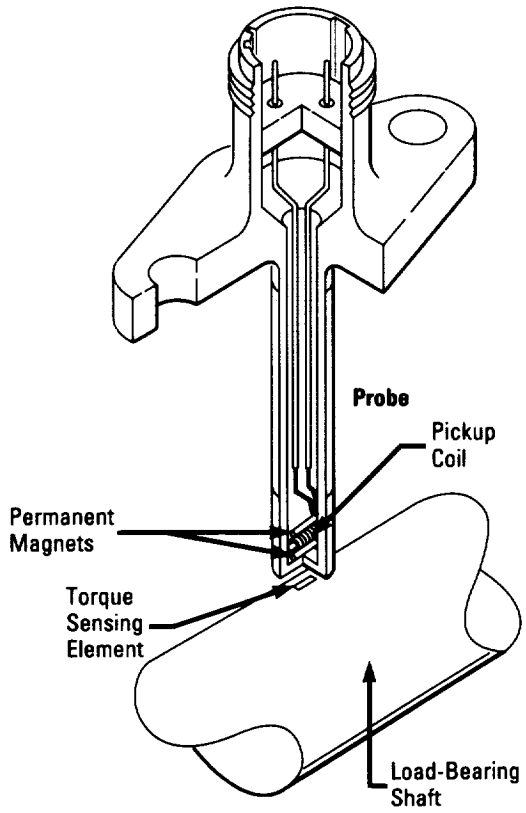

Torquemeter.

The magnetic switching characteristics of the deposit vary with strain, which is itself a function of shaft torque. A qualitative description of the magnetic interaction between the magnets in the sensor, the deposit, and the coil core provides an illustration of this phenomenon. The dependency of the magnetic switching characteristics of the deposit on the strain at the surface of the shaft manifests itself as a variation of peak-to-peak voltage with torque; this has been verified experimentally.

The pulse induced in the pickup coil occurs each time a given deposit passes under the sensor probe. Since the deposits are rigidly affixed to the shaft, the time between pulses is representative of shaft speed. Although the peak-to-peak voltage also varies with speed, compensation can be obtained because the period of the signal has been shown to vary with speed exclusively.

The feasibility demonstration of the brushless torquemeter employed an existing apparatus called the rotating demonstrator, which could present the **torquemeter** with varying shaft torque, speed, and position in three dimensions. This was achieved by forcibly applying a twist to a hollow tube, on which a torque-sensitive (**magnetostrictive**) film deposit is located, relative to a concentric solid shaft. The resulting torsional strain is adjustable and can be locked-in mechanically to provide a reproducible torque in the tube. The **torquemeter** probe is positioned with a three-dimensional (3–D) translation stage so the position of the probe relative to the shaft can be varied in precise increments. As the assembly rotates on bearings, the **torquemeter** views the tube as a vibrating, rotating

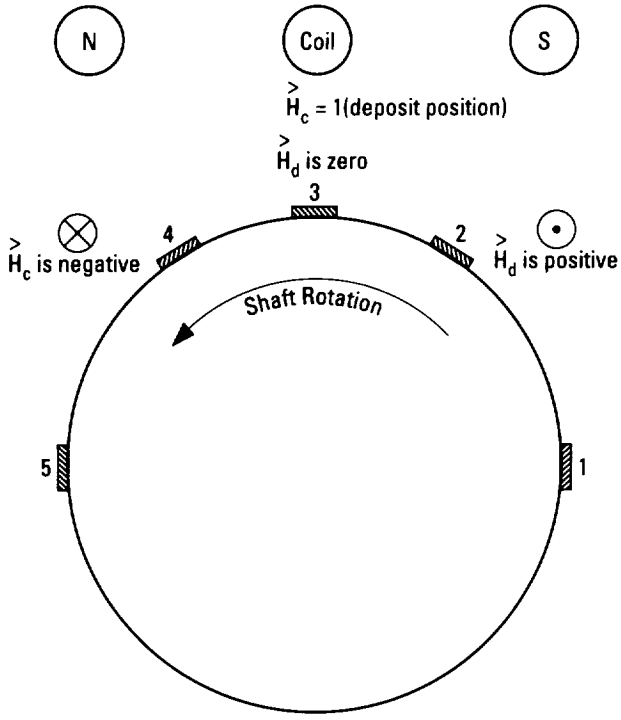

NOTE:—This drawing is not to scale.

Legend:

H_d is field applied to deposit.

H_c is field applied to coil.

1, 2, 3, 4, 5 are sequential positions taken by the deposit as the shaft rotates.

Assumptions:

Magnets have equal and opposite magnetic properties such that a plane of points equidistant from the magnets has H = 0.

Coil lies in the plane and has dimensions such that H_c due to magnets is zero.

Deposit has dimensions such that H_d due to magnets is zero when deposit is in plane of points equidistant from the magnets.

Position	Field Applied to Deposit, Coil
1, 5	$H_d = 0, H_c = 0$
2	H_d is positive, H_c is negative
3	$H_d = 0$, H_c is negative
4	H_d is negative, H_c is positive

Noncontacting torquemeter magnetic field diagram.

shaft under a dynamic torsional load. Turning the torque adjustment screw rotates the torque adjustment bar about the central axis relative to the threaded flange.

The side view illustrates the mechanical connections between the various parts of the rotating demonstrator. Since the flange is rigidly connected to the shaft, the bar is rigidly pinned to the tube, and the tube is rigidly pinned to the shaft at the left end, turning the adjustment screw results in a twisting of the tube relative to the shaft. A similar apparatus was employed in a low-temperature −196 °C (−320 °F), high-speed (45,000 r/min) feasibility demonstration.

The peak-to-peak voltage has been shown to vary with torsional strain as a peak-to-peak voltage versus torsion. The period (T1) of the signal varies with shaft speed. It must be noted that the peak-to-peak voltage, which is used to monitor torsion, also varies with speed, implying its proportionality to shaft revolutions per minute. However, this variation in the torque-sensitive, peak-to-peak voltage with speed can be compensated for by the fact that the variation of the period (T1) of the signal is a function of speed alone.

The TTB brushless **torquemeter** evaluation has thus far demonstrated the feasibility of monitoring shaft torque and speed using a single **noncontacting** sensor. The feasibility of the device has been demonstrated at ambient and cryogenic temperatures and at speeds up to 45,000 r/min. The design of the prototype sensor that will go into the TTB engine (TTBE) is complete. The design of the **torquemeter**-specific TTBE modification is complete. The hot-fire readiness demonstration of the brushless **torquemeter** is not presently funded but is anticipated to occur in fiscal year 1993–94 (FY93–94).

Schwartzbart, A., Rocketdyne Division/Rockwell, "Noncontacting Multiparametric Sensor for Shaft Speed, Torque, and Position," 1992 Earth-to-Orbit (ETO) Technology Conference, MSFC, AL, May 1992.

W.T. Powers/EB22
205–544–3452
Sponsor: Office of Aeronautics, Exploration, and Technology

Video Image Processing for Measurement of Strain and Displacement

The **digital image correlation** method determines the **strain** and **displacement** fields on the surface of a structure through image processing of digital video images of the surface. This process involves the comparison of a video image of the surface in an unstrained state to another video image of the same surface after a load has strained the structure. The **digital image correlation** method maps the image of a strained surface onto the image of the same surface in the unstrained state. This mapping generates a discrete representation of the **displacement** and the **strain** fields. The images are acquired by a solid-state video camera and a personal computer (PC)-based frame digitization board. The implementation of the correlation algorithm that computes the **strain** and the **displacement** fields is on the same PC as used for image acquisition. The surface of the structure being investigated must contain a random pattern so that each subset of the image appears different from any other region of the images. Typically, paint-over spray or a light dusting of powder is used as the random pattern.

Commercialization is possible as a substitute for **strain** gauges, moiré, and holography to determine the state of structures. When compared to the traditional approach of using many **strain** gauges, this method is attractive because the process is optically based, does not require contact sensors, and is full field. This method is much less sensitive to vibrations than moiré or holographic methods, thereby allowing use in a normal industrial environment. Only limited prior knowledge of the order of magnitude of the **strain** is required, allowing investigation of high **strain** materials or plastic deformation. Also, the generated **strain** information is organized in a matrix format representative of the specimen geometry allowing easy post-test processing. The acquired **strain** information can readily be processed by a failure criterion to estimate load-to-failure or Von Mises **strain**. Efforts are ongoing to develop this method for evaluation of advanced composite components by utilizing the measured **displacements** as boundary conditions in a finite-element model of the component.

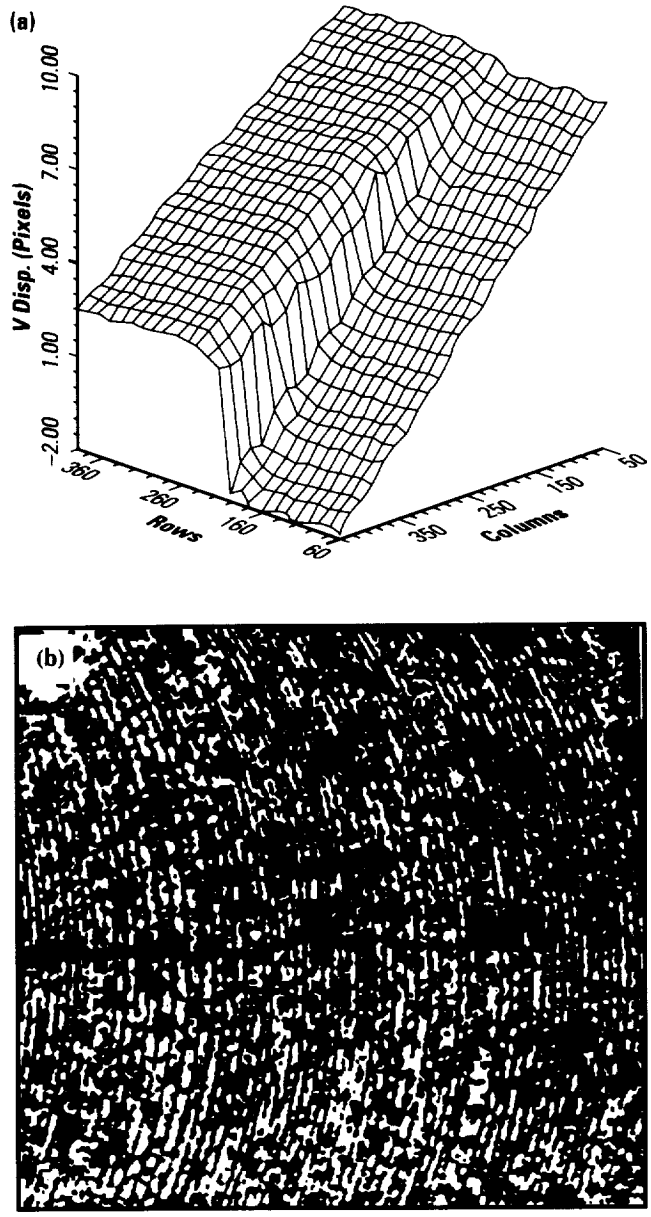

(a) In-plane displacement perpendicular to crack for 7075 – T73 A1 self-loading fracture specimen; (b) image of crack with powder speckle.

S.S. Russell/EH13
205–544–4411
Sponsor: Center Director's Discretionary Fund

Vortex-Shedding Flowmeter for the Space Shuttle Main Engine

Over the 1991–92 period, the **vortex-shedding flowmeter** work concentrated on four areas: (1) encapsulation of the vortex sensor, (2) design of the 2.8-cm (1.1-in) liquid oxygen (lox) **flowmeter**, (3) investigation of a new and possibly better vane design, and (4) finding a means of testing and calibrating the fuel **flowmeter** in hydrogen (H_2) gas.

The present meter design has the vortex sensor inside the envelope of the duct. Since insulating materials are generally organic, the lead zirconate titanate (PZT) vortex sensor and associated electrical leads need to be isolated from direct contact with lox. The sensor could be protected by the coating material often used for installation of instrumentation, but placing the sensor in a sealed metallic envelope is more desirable. A design has been completed for such an envelope consisting of a thin-walled, flat, rectangular tube with one end plugged and the other end inserted into a mounting flange. The PZT bimorph is potted into this tube with **cryogenic**-compatible epoxy resin to support the tube walls against the duct pressure. The free end of this tube is attached to the vane near the spring-mounted end. Bending this flat tube bends the PZT bimorph and produces the output signal.

The first 2.8-cm (1.1-in) duct **flowmeter** tested produced a signal that faded away completely for more than half the time. This fade is probably caused by a sequential rather than an instantaneous detachment of a vortex from the vane. This phenomenon gets worse as the W/D ratio decreases, where W is vane width and D the pipe diameter. The amount of fading also seems directly related to vane width (W) alone so that fading increases as pipe diameter (D) is decreased when W/D is held constant. It has been determined that, in the 2.8-cm (1.1-in) duct, a vane width of approximately 0.64 cm (0.25 in) eliminates the complete signal fade for vanes that either span or partially span the duct.

A vane design consisting of a circular cross section with a slot transverse to the flow and cut through parallel to and including the axis of the cylinder gives a better performance than the commercially designed triangular, trapezoidal, or rectangular cross-sectioned vanes. A circular cross-sectioned vane with two different slot widths in the 5.84-cm (2.3-in) diameter 7035 duct was tested. The tests showed that even the narrower of the two slots was apparently still too wide at the space shuttle main engine (SSME) duct flows because the spectrum lines narrowed with slot width but were still wider than obtained from the rectangular vanes. Narrower slots can be made using electrical discharge machining to cut them. The meter factors of the slotted vanes were not as constant with flow as found for the rectangular vanes. The small flow dependence of the meter factor observed for the slotted vanes can be corrected by calibration.

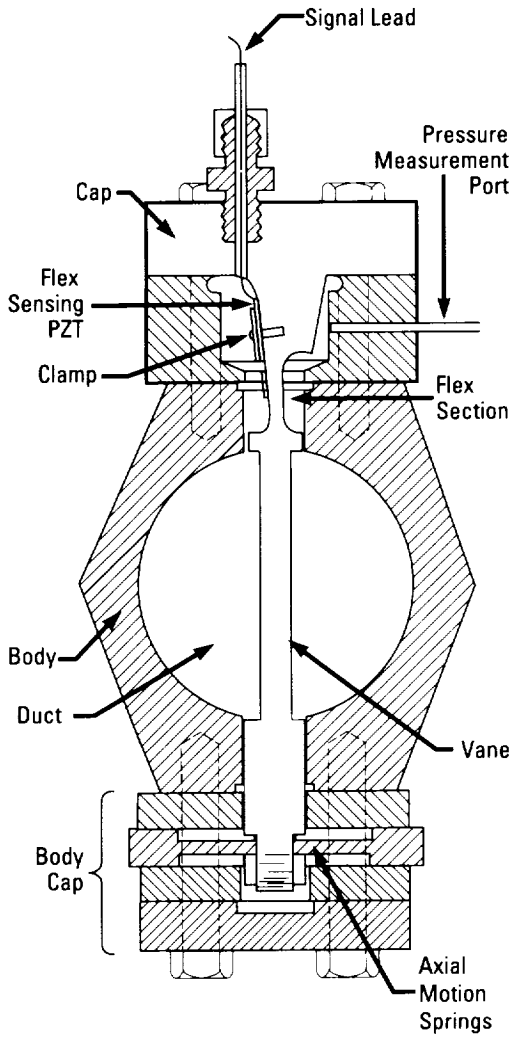

Cross-sectional view of a flowmeter of 51-mm (2-in) bore.

To date, the fuel meter testing has been performed using compressed air at ambient temperature and at a pressure that gives an air density the same as the H_2 density experienced in the ducts. Unfortunately, the **velocity** of sound in nitrogen (N_2) (or air) is less than one-fourth the **velocity** of sound in gaseous hydrogen (GH_2). In fact, the **velocity** of sound in air is so low that compressibility effects are encountered at approximately one-third the maximum flow at many of the meter sites in the SSME ducts. Air flow chokes at the meter at flow velocities of 131 to 164 m/s (400 to 500 ft/s). Three of the four SSME duct fuel **flowmeter** sites are subjected to velocities from 203 to 256 m/s (620 to 780 ft/s).

The fuel **flowmeter**, then, can only be tested and calibrated in GH_2 flow. The Component Test Facility (CTF) under construction at Stennis Space Center (SSC) is the only facility identified that has sufficient capacity to test fuel **flowmeters**. A test section using a choked nozzle for reference is used. Ambient-temperature GH_2 can be used for the initial testing of the **flowmeter**. The GH_2 could be supplied directly from the storage tanks. A 1-min test interval is satisfactory to achieve an equilibrium measurement.

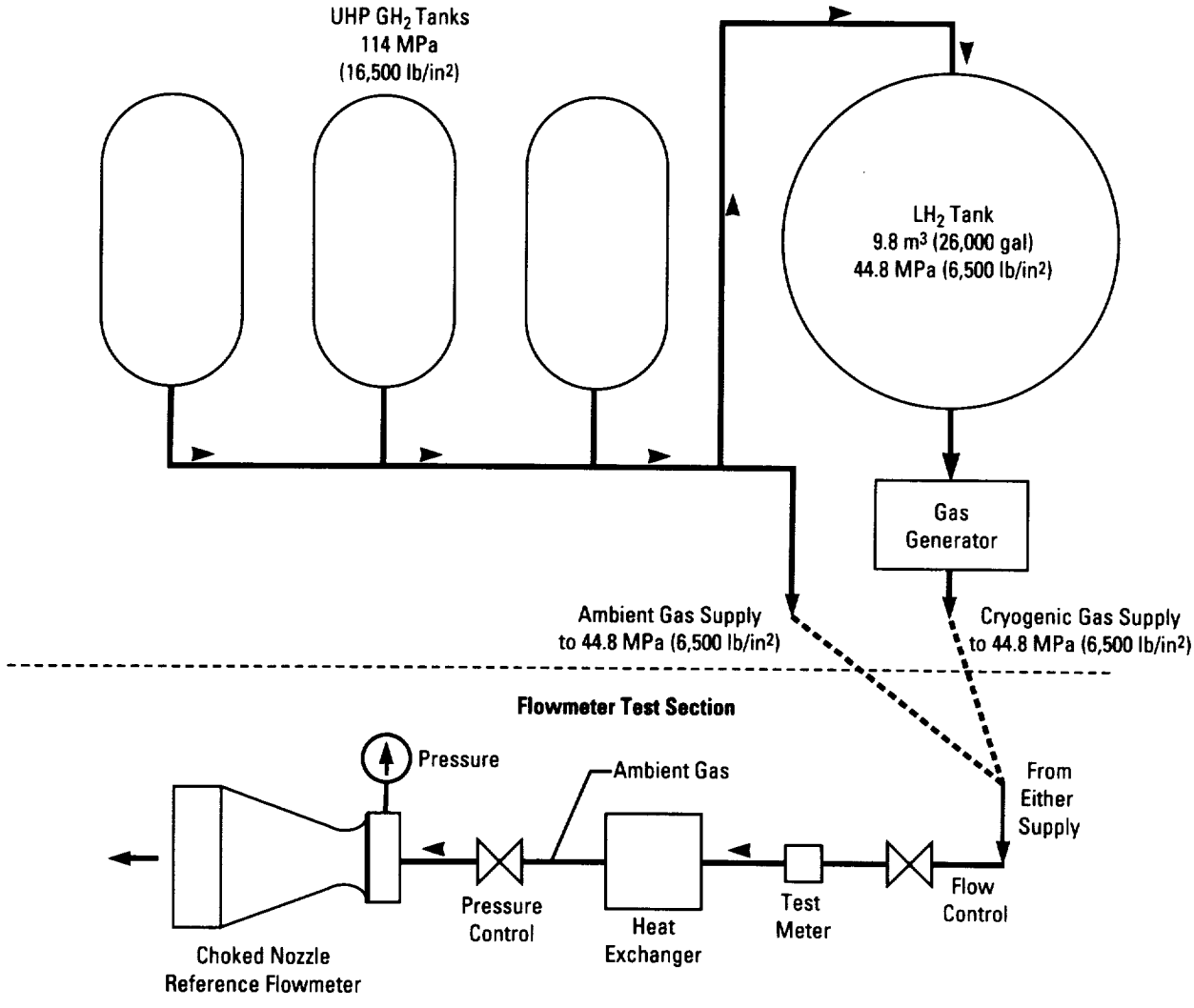

A fuel flowmeter test facility using GH_2 from the CTF.

For meter calibration, the GH_2 should be at the actual operating temperature. The test fluid would then be supplied from the pressurized liquid hydrogen (LH_2) tank, vaporized, and heated to the operating temperature. The mass of H_2 available in the liquid tank is less and the density at the **flowmeter** is higher. The test times at maximum flow are reduced as a result.

To achieve sufficient test times for two of these four meters, a larger source of high pressure LH_2 is needed. The proposed pumped LH_2 source, where liquid from an ambient pressure tank is pumped to the test pressure, is needed to calibrate the larger of these meters. The pump must deliver 56.8 kg/s (125 lb/s) at approximately 44.8 MPa (6,500 lb/in^2) to calibrate the **flowmeter** for the largest SSME fuel duct.

Maximum test run time for the fuel ducts using the CTF at the SSC

SSME Duct #	Ambient UHP Gas[1]	Cryogenic Gas[2]
RS007012	90 s	33.0 s
RS007034	94 s	56.0 s
RS009168	340 s	75.0 s
RS007030	34 s	12.5 s

1 Density of 28.25 kg/m^3 (1.76 lb/ft)
2 Tested at the temperature, pressure, and density of the operating conditions in the SSME ducts

Siegwarth, J.P. and Lewis, M.A., National Institute of Standards and Technology (NIST), "Vortex-Shedding Flowmeters for SSME Ducts," 1992 Earth-to-Orbit (ETO) Technology Conference, MSFC, AL, May 1992.

W.T. Powers/EB22
205-544-3452
Sponsors: Office of Aeronautics, Exploration, and Technology and Office of Space Transportation Systems

WELDSMART: A Vision-Based Weld Quality Assurance System

WELDSMART is a system being developed to apply computer analysis to images of welds for the purpose of evaluation. Certain types of faults can be classified, and an overall evaluation of success or failure of the weld can then be ascertained. Histograms are used in software analysis to preprocess the original images to aid in fault detection. The resultant images effectively highlight weld defects, such as cracks. Threshold imagery also highlights the edges of the weld and introduces some background noise in the form of randomly placed pixels. The isolational aspects of the noise and the smooth, rounded shape of the weld can be used to filter these pixels, resulting in a clearer image of the defect.

A number of basic image-processing routines has been coded and is currently running under the operating system (OS/2). A hierarchy of defects has been designed so that classification of observed defects can be implemented. Artificial intelligence (AI) mechanisms have been developed to take the information from the **image processing** modules and, ultimately, to assess the number, nature, and severity of the observed defects.

As this work is aimed at automating a very common task, i.e., visual inspection, its results are applicable to a wide variety of applications. Two likely areas to benefit from this work are quality inspection in space and commercial/industrial quality inspection. The space station has a need for periodic inspection and maintenance. A robotic manipulator could scan an electronic camera across the surface for this purpose. Previous scans could then be compared and possible defects brought to the attention of the appropriate personnel for further checking. Commercially, quality inspection is frequently needed in hostile environments such as nuclear plants and underwater construction or maintenance. Also, mass production applications using human inspection, which is expensive and prone to error, could benefit greatly from automated visual inspection.

The next step after the **image processing** routines is that of overall quality assessment. The questions of what constitutes an "acceptable" workpiece or specimen and to what extent defects may be tolerated must be evaluated. The C language integrated product system (CLIPS), which has been developed by NASA at the Johnson Space Center (JSC), was evaluated for the purpose of making pass/fail decisions. This system allowed the user to specify a collection of general "rules" and to define a collection of "facts" relating to the problem(s) at hand. The CLIPS "inference engine" iteratively compares the rules against the facts, derives sets of new facts, and continues until no further deductions can be made. A small expert system was constructed to examine the feasibility of determining which process faults contributed to the observed weld defects. This system performed acceptably.

Neural networks have been tested for specific tasks relating to welding quality control. NASA currently uses a weld profiling system to evaluate the weld bead surface. This operation is carried out in near-real time as a sensor examines the weld surface at a given location a few seconds after the weld solidifies at that location. A laser beam is scanned transversely across the weld bead, and the reflection is picked up by a video camera and analyzed in an **image processing** system. Alternatively, the digitized video weld profile image could be analyzed in a **neural network**, which would more effectively determine the location of the profile peak, or crown, its edges, and other relevant features of the weld.

One type of discontinuity that a quality inspector may be concerned with is that of undercuts, or indentations, along the weld edges. An off-centered welding torch (with respect to the material seam) would result in asymmetrical undercuts, i.e., the left undercut would be substantially deeper or shallower than the right undercut. The current NASA profiling system uses traditional algorithms in attempting to locate the weld crown, undercuts, and other features. These algorithms are not fully reliable, and thus, **neural networks** may be evaluated as alternatives in providing enhanced determinations of these conditions. Upon evaluation of the weld, the network might provide an alarm to the welding operator and indicate how the weld is of substandard quality. Further, the network might send a corrective control signal to the appropriate mechanism to rectify the problem. An off-centered torch, for example, could therefore be quickly driven back to the correct position during the welding process.

It has been found that visual analysis, using the image acquisition and evaluation concepts and methods applied to this project, may be used in certain applications to replace the more expensive and complex laser-based **weld inspection** system currently used by NASA.

W.L. Boglio/EB44
205–544–3806
Sponsor: Office of Commercial Programs,
Technology Utilization Office

Information, Electronic, and Optical Systems

Advanced X-Ray Astrophysics Facility Coating Investigation

Research and development efforts designed to identify the optimum coating materials and coating deposition techniques for use in the Advanced **X-Ray** Astrophysics Facility (AXAF) program expanded significantly during fiscal year 1992 (FY92). In early FY92, the AXAF Coating Working Group recommended that the Smithsonian Astrophysical Observatory (SAO) measure the **x-ray reflectivity** of nickel (Ni), **gold (Au)**, platinum (Pt), and **iridium (Ir) coatings** produced by both electron beam evaporation and direct-current-magnetron-sputtering (dc-magnetron-sputtering). The **coatings** were produced by MSFC and coating vendors under contract to the AXAF prime contractor. Highly polished Zerodur flats, ground and polished at MSFC, were used as substrates for the **coatings**. Results from the study have led the AXAF Coating Working Group to recommend that **Ir** be used for **coating** the AXAF mirror elements. In addition, the measurements indicate that sputter deposition is the optimum technique for obtaining the highest **x-ray reflectivity** when either Pt or **Ir coating** materials are utilized.

In the **reflectivity** data provided by SAO, it is evident that the **reflectivity** of the better dc-magnetron-sputtered **Ir** samples far exceeds that of the Pt and **Au** samples over a considerable range of **x-ray** grazing angles. The effect is very pronounced in a range of **x-ray** grazing angles between 32 and 38 arc min, or, in other words, near the critical grazing angle. In this case, a copper (Cu) anode with an Ni filter was utilized as the source of **x-rays** to obtain a predominately Cu K-line emission (approximately 8.05 keV photon energy). The **x-rays** reflected by the coated flats were collected within a limited angular region about the specular reflection angle. The most highly reflective Pt and **Ir coatings** measured in this phase of the study were produced via dc-magnetron-sputtering. In the case of the **Au coatings**, differences in sputter deposition and evaporative deposition did not appear to be significant. When compared with theoretical predictions, the **reflectivity** of the measured **coatings** appears to be somewhat less than what would be expected for 100-percent bulk-density **coatings**. At this time, it is believed that reduced density in the measured **coatings** is the primary cause of the difference in theoretical and experimental results.

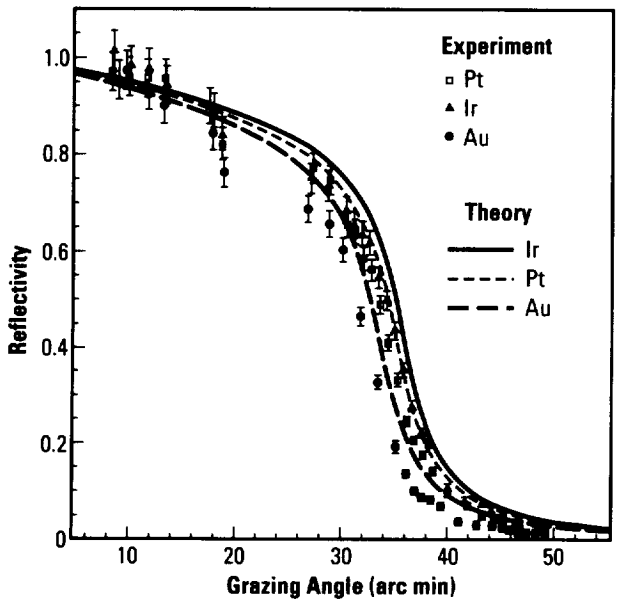

X-ray reflectivity of sputter-coated samples.

A.P. Shapiro/EB23
205–544–3488
Sponsors: Advanced X-Ray Astrophysics Facility Project Office and Office of Space Science and Applications

An Architecture for Functionally Redundant Intelligent Systems

This project is phase I of a Small Business Innovative Research (SBIR) contract that was awarded to Symbiotics, Inc. The three goals of the research are discussed below.

The first goal of this project is divided into two parts: (1) specify requirements and (2) design generalized models for different kinds of functional interactions among functionally **redundant** operations support applications. The investigation is focusing on four kinds of interaction: collation, synthesis, competition, and replication. One or two specific forms of synthetic interaction will be addressed.

The second goal of this project is to design a group-based control model for managing functionally **redundant** intelligent operations support applications. The model will include an organization of the set of functionally **redundant** applications into a discrete cluster, transparently mediate all interactions between outside systems and group members, and mediate all interactions between group members. This effort will exploit previous research on innovative **distributed computing** tools by Symbiotics, Inc., called SOCIAL, to develop a dedicated server-group agent.

The third goal is to develop a test scenario for demonstrating and validating the above design concepts that reflect actual autonomous coordination requirements in MSFC's space station module/power management and distribution (SSM/PMAD) system. This will include investigation of that system, and the design of a scenario that demonstrates interactions between autonomous systems for fault detection, isolation, and recovery (FDIR) and/or load balancing.

Work on the first goal to date has included a literature survey that reviewed the central design problems for **distributed computing** systems and popular strategies for addressing those problems. Major topics include distributed communication, client-server computing, and competing models for **distributed control**. This information is a major component of an article entitled "Design of Distributed Systems." In the context of architectures for **distributed control**, the article discusses process groups, SOCIAL, and strategies for achieving fault tolerance. The piece was commissioned by John L. Wiley and Sons for their Encyclopedia of Software Engineering, which will be published within the next 8 to 12 mo.

The approach to the second goal of this phase I SBIR work plan is to develop generalized group-based models for cooperative distributed problem-solving (CDPS) by building on existing capabilities and agent types within SOCIAL. Design efforts have focused on two basic directions:

- Formulating two group-based models (one largely centralized, the other more distributed) that could be implemented using SOCIAL in its current form
- Formulating more elegant and efficient designs that would require extending the basic architecture of SOCIAL's underlying communication layer to two new primitive structures.

Requirements for generalized group-based model CDPS include:

- Naming services (for managing logical group names and membership)
- Capabilities to model agents as well as to remotely access such models
- Support for distributed, intelligent coordination models (problem decomposition, task allocation, collecting/processing task results)
- Capabilities to monitor the availability of agents
- Capabilities to dynamically alter behavior and/or organizational structure
- Supporting or enabling message-passing services (point-to-point, multicast).

Once the new design is in place, a demonstration prototype distributed system will be developed to illustrate

and validate the proposed SOCIAL group-based agents. This effort will be based on a review of literature describing **intelligent systems** under development at MSFC and Lewis Research Center (LeRC) for power management on Space Station *Freedom* (S.S. *Freedom*). Implementation of the SOCIAL design extensions described in this progress report and applying the resulting agents to construct the demonstration prototype will constitute the core of any phase II SBIR follow-on effort.

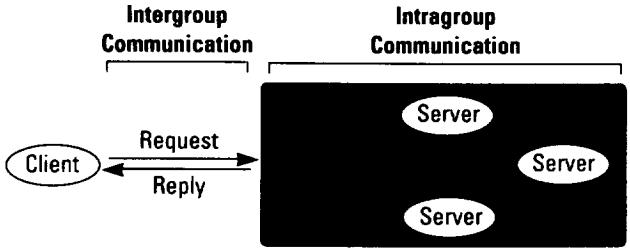

Group-based client-server computing.

B. Walls/EB12
205–544–3311
Sponsor: Office of Commercial Programs,
Small Business Innovative Research Program

Coherent Doppler Lidar Research and Development

A number of studies dating back as early as the late 1960's have documented the potential of **light detection and ranging** (**lidar**) as an enabling technology for automated space vehicle **rendezvous** and **capture**. Few of these studies considered the use of **coherent lidar**. **Coherent lidars** incorporate lasers with line widths narrow enough to permit direct measurement of velocity via Doppler shift. Although **coherent lidar** has been used for atmospheric velocity measurements for over 20 yr, the technology involved carbon dioxide (CO_2) gas lasers, which, because of problems with packaging and consumables, were not well suited to space-based applications. Recent advances in both eye-safe, short-wavelength, solid-state lasers, and CO_2 laser technology offer real potential for the development of compact, reliable, lightweight, and efficient **coherent lidar** for space applications.

MSFC has been active in the area of Doppler **lidar** for atmospheric velocity measurement for a number of years. The Optical Systems Branch of the Information and Electronics Systems Laboratory is currently applying this experience to the evaluation of Doppler **lidar** technology for the **rendezvous** and **capture** problem.

A Center Director's Discretionary Fund (CDDF) effort to demonstrate the feasibility of Doppler **lidar** for **rendezvous** and **capture** is in its second year. A survey of lasers, detectors, and other components required to construct **lidar** breadboards for evaluation has been completed, and key breadboard components are being purchased. **Lidar** breadboards will be constructed and used to evaluate key components such as lasers and detectors. Algorithms for extracting target information will be tested, using digitized **lidar** return signals.

A Small Business Innovative Research (SBIR) contract was awarded to study the use of the high-resolution **lidar** data for automatic target recognition and determination of target orientation. The study combines optical correlation with a syntactical pattern classification system based on fuzzy logic set theory to discriminate among objects. The use of fuzzy set methods permits nonexact or ambiguous information to be included in the classification of objects and allows the decision itself to be fuzzy, thereby allowing qualitative decision-making similar to human experts. The first phase of this study will be completed this fiscal year.

A paper detailing a first-cut analysis of the performance of **coherent lidar** was presented to the NASA Automated **Rendezvous** and **Capture** Review held in Williamsburg, VA, in November 1991. This paper analyzed a class of **lidars** that use **coherent** detection coupled with an imaging-type array detector to provide not only the target range and angle information capability of a noncoherent **lidar**, but also to provide information about target attitude and rotation. Because of the sensitivity of **coherent** detection, these **lidars** can operate without the retroreflectors, which are required by noncoherent **lidar**.

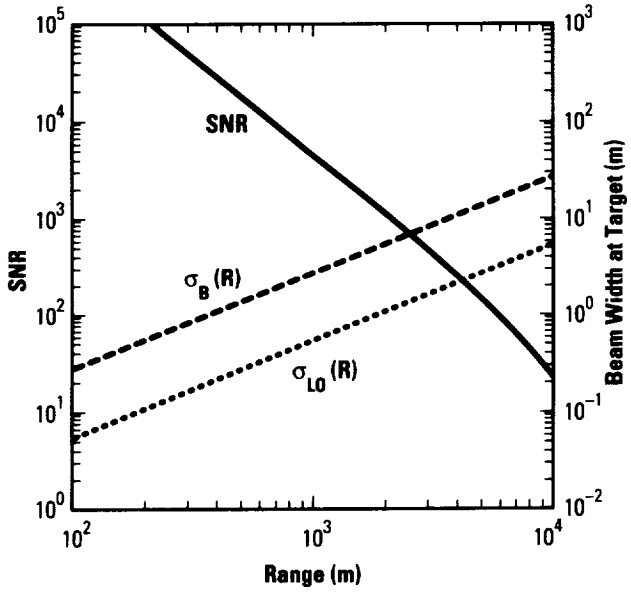

Lidar performance in detection mode; signal-to-noise ratio (SNR), transmitter beam size $s_B(R)$, and pixel resolution size $s_{LO}(R)$ versus range (R).

Frehlich, R., Bilbro, J., Dunkin, J., "Coherent Doppler Lidar for Automated Space Vehicle Rendezvous, Station-Keeping, and Capture," NASA Automated Rendezvous and Capture Review, Williamsburg, VA, November 19–21, 1991.

J.A. Dunkin/EB23
205–544–3690
Sponsors: Center Director's Discretionary Fund and Office of Commercial Programs, Small Business Innovative Research Program

Color Television Camera Breadboard Development

The objective of this effort is to develop a breadboard standard scan, solid-state, three-chip, **charge coupled device (CCD)**, color television (TV) **camera** using lower class parts that have equivalent grade-1 replacements. Currently, there are no fully **space-qualified CCD cameras** available for space applications. Furthermore, it is impossible to upgrade a commercial **camera** with grade-1 parts without extensive redesign of the **camera**.

This **camera** breadboard development effort started in November 1991. The image sensors being used in the **camera** are manufactured by Texas Instruments and have a pixel count of 786×488. The **camera** is being designed to be split apart into two components comprised of a head assembly and a **camera** electronics unit. This will allow the small **camera** head to fit into areas where space is a limiting factor. The head assembly will contain the prism block assembly and the **CCD** driver electronics. The **CCD** driver electronics boards have been designed and fabricated and are in the process of being built and tested. The prism block has been purchased and the block assembly is in the process of being designed and built. The **camera** electronics unit will contain the remaining boards that are required for the **camera**. The **camera** power supply board has been designed and fabricated and is being built and tested. The **camera** driver board, which contains the **CCD** timing generator and supporting electronics, has been designed and fabricated and is also in the process of being built and tested. The **camera** encoder board, which contains some of the **camera** color processing, has been designed and is currently being fabricated. Efforts are currently focusing on the design of the **camera** color processing and genlock circuitry.

In the remaining period of 1992, efforts will concentrate on completing the **camera** breadboard design and fabrication. Performance testing will be performed on each electronics board as it is completed and as an integrated **camera** breadboard upon completion of the electronics boards. After the **camera** breadboard is completely built and tested to meet in-house performance requirements, the **camera** will be evaluated as a candidate to be upgraded for space applications.

E.L. Corder/EB23
205–544–3473
Sponsor: Center Director's Discretionary Fund

Control Electronics for Multihorsepower Electromechanical Actuators

Thrust vector control (TVC) actuators and propellant flow control actuators for large space boosters, such as the shuttle vehicle, have historically been powered by hydraulic systems. While these actuators have performed well, the problems associated with maintaining reusable high-pressure hydraulic lines and assemblies incur high operating costs. New launch vehicles, such as the National Launch System (NLS), have been baselined to use electrically driven actuators for both TVC and propellant flow control. This report discusses the development of the electronic controller for the TVC actuator. Propellant flow actuators, though similar, require significantly less power.

The power requirements for the NLS TVC actuators are in the range of 22,500 W (30 hp), representing a force of 177,929 N (40,000 lb) at 0.127 m/s (5 in/s). The actuator is comprised of a small high-speed, electric motor driven through appropriate spur gearing to a roller screw-type of gear for converting torque to linear forces. Losses in the power source, motor, electronic controller, and gears result in a typical overall **efficiency** of 60 percent, raising the input power required to the 40,000-W (53.6-hp) range. The baseline system, which calls for this power to be shared among three motors/controllers operating in parallel, will provide fail/operate redundancy.

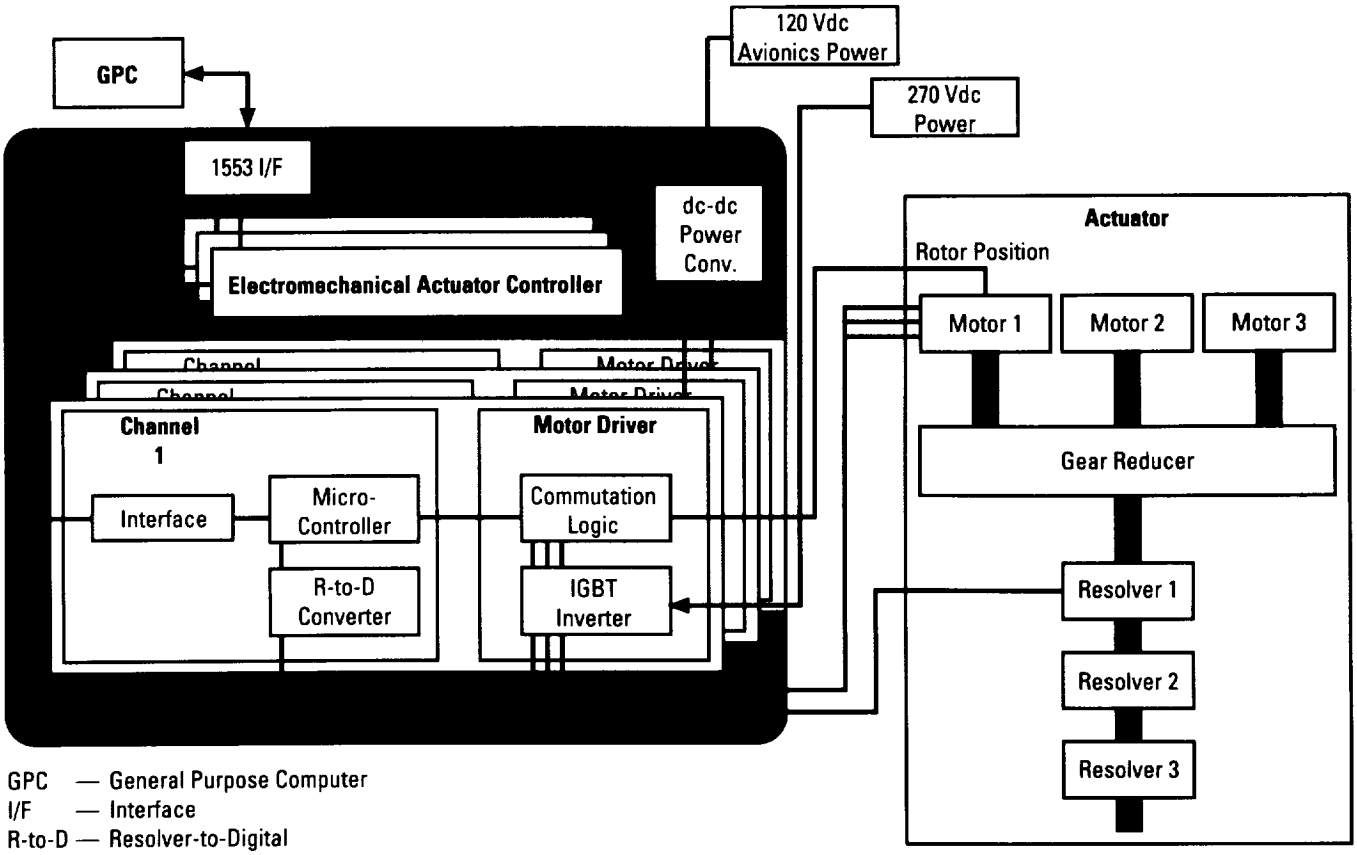

NLS–TVC controller.

Each channel of controller electronics is comprised of high-voltage, high-current, motor-driven electronics; low-power, motor-control electronics; a health monitoring and redundancy management computer; and a 1553 data bus.

At the center of this research is the use of **insulated gate bipolar transistors (IGBT's)** configured to provide six-step commutation to a three-phase, permanent magnet, brushless direct current (dc) motor. The **IGBT's** were selected for their ability to handle high currents (400 A maximum) at high voltages (600 Vdc), with switching times of less than 1 μs. This power inverter interfaces with the motor windings, motor rotor position sensors, and, through optoelectronic couplers, receives motor current commands from the motor control electronics module. Power to this inverter is provided by the 270-Vdc battery pack.

The motor control electronics module consists of a resolver to digital converter and analog circuitry that implements the actuator position loop control law. This module interfaces with the position resolver, motor-driven electronics, and redundancy management computer.

Each controller is a full **four-quadrant** controller (±acceleration, ±braking) and manages the motor-braking energy under full control. This braking energy is dumped into a passive load.

The controller **efficiency** has been measured on the lab bench to be better than 95 percent at 100 A. The controller features adjustable current limit and is rated at 100 A, with a peak current of 150 A for a voltage level of 240 Vdc minimum. Preliminary tests of linearity, step, and frequency response have been performed with good results. Additional testing is under way.

J. Montenegro/EB24
205–544–3514
Sponsor: National Launch System (NLS)

Correlation of Hydrogen and Air Flow in Critical Flow Nozzles

Operation of the space shuttle main engine (SSME) test-bed requires accurate measurement of high flowrates of gaseous **hydrogen** (GH_2). A critical **flow** venturi (CFV) is proposed to provide this measurement. **Calibration** of the CFV in a primary facility is costly; however, the cost can be reduced significantly if the meter is calibrated in **air** rather than in GH_2. The goal of this project is to determine correlating parameters that enable the nozzle to be calibrated in **air** and then used to measure the **flow** conditions expected in the SSME test-bed.

When a compressible fluid **flows** through a converging/diverging channel, the velocity reaches a maximum at the point of minimum area (the throat). The throat velocity increases as the inlet pressure increases. The limiting value of the velocity at the throat is the speed of sound. Further increases in inlet pressure will not result in an increase in throat velocity; this is termed critical **flow** or choked **flow**.

The CFV is a converging/diverging channel configured as a **flow** measurement device. With critical **flow**, the volumetric flowrate is dependent only on the gas temperature, the throat cross-section area, and a **calibration** constant. The mass flowrate is dependent only on the throat area, fluid density, and the **calibration** constant. While increasing the upstream pressure will not increase the volumetric flowrate, the mass flowrate will increase in proportion to the density of the fluid in the throat. A CFV can be used to accurately measure mass flowrate with appropriate pressure and temperature measurements.

The CFV is widely used as a transfer standard because the behavior is well predicted by theory. Additionally, it has no moving parts, is not susceptible to physical damage, and does not require a differential pressure measurement. It is, therefore, well suited to provide a **hydrogen** (H_2) **flow** measurement for the SSME test-bed.

The uncalibrated accuracy of a CFV is inadequate for the requirements of the SSME test-bed. **Calibration** to determine actual values for the discharge coefficient is required. Complete **calibration** with H_2 is very costly. The cost can be reduced significantly if the meter is calibrated in **air** with these results being used to predict H_2 performance. The objective of this project is to provide a **correlation** between **air** and H_2 performance based on **calibration** data.

With a primary **calibration**, the flowrate is determined from primary measurements of mass, length, and time. The operation of a primary **calibration** facility is conceptually quite simple. A pressure vessel is used to provide fluid **flow** through a test section. The mass of fluid within the pressure vessel is determined before and after a timed test period. The average mass flowrate is the change in fluid mass divided by the test period time interval.

Primary **calibrations** are further classified as gravimetric or volumetric. With a gravimetric system, the mass flowrate is defined by the change in mass of the fluid within a closed tank divided by the change in time. With a volumetric system, the mass flowrate is defined by the change in density of the fluid within a fixed volume tank divided by the change in time. The system described here is a volumetric system. It is also called a "PVTt" system because measurements of pressure, volume, temperature, and time are combined to provide a measure of mass flowrate.

With a primary **calibration** system, two **flow** paths are provided to supply a test section. The **calibration** tank is the source of **flow** during the test period. The startup tank supplies startup **flow** that allows the meter being tested to achieve stability. Once stability has been achieved, the test section **flow** is diverted from the startup tank to the **calibration** tank. This is accomplished by means of a diverter valve system. The **flow** diversion begins and ends the test period. Signals from optical sensors that detect the position of the diverter valves are used to measure the duration of the test period. The initial and final mass of the fluid within the **calibration** tank are calculated from pressure and temperature measurements.

The tank volume provides a significant contribution to the system uncertainty. An accurate measurement of the **calibration** tank volume is, therefore, critical. **Calibration** tank volume was determined by adding a known mass of **air** and recording the resulting change in density. The tank volume is the change in added mass divided by the resulting change in density. A total of 22 data points was recorded in the process of tank volume measurement. The volume was determined to be 1.8494 m^3 (65.3085 ft^3). The standard deviation was 0.000204 m^3 (0.00719 ft^3).

This system diverts the test section **flow** between startup tank and **calibration** tank sources. The **flow** diversion is accomplished by a pair of ball valves mounted on a single actuator. They are mounted such that one valve is fully open while the other is fully closed. The double-acting actuator rotates the valve stems 90° upon the application of a compressed gas. The two valves are either fully open or fully closed except during actuation. The timing system consists of an electronic timer and a pair of optical switches mounted on the valve actuator. The optical switches detect the start and end of the diversion cycle.

Ideally, the **flow** diversion occurs instantaneously, and the start and end of the test period can be readily detected. In reality, diversion takes a finite amount of time, and defining the test period is more complex. The relationship between diverted flowrate and time is called the valve law. With a knowledge of the valve law, the starting and ending times for the test period can be accurately defined. A theoretically based estimate has been made of the valve law for this diverter system. Bench tests of the diverter system yielded a switching time of 108 ms. The variation from test to test was observed to be less than 100 μs.

Following are some general considerations regarding pressure control within the system.

- The **calibration** tank final pressure must be greater than the test section pressure.
- The difference must be high enough to maintain the mass flowrate.
- The startup tank final pressure must be greater than **calibration** tank initial pressure.
- At the switch from startup to primary, the pressure in the diverter valve section must exactly match the startup pressure.

With a primary **calibration**, it is assumed that all the mass that exits the **calibration** tank will **flow** through the test meter. The exception to this assumption is called a "trapped volume," which is any volume within the system where the final pressure and/or temperature is different at the beginning of a test than at the end of a test. The difference in fluid mass is accounted for when the mass flowrate is calculated.

The total uncertainty (with a 95-percent confidence level) in mass flowrate for the system has been estimated to be 0.08 percent.

Kegel, T.M., Colorado Engineering Experiment Station, Inc. (CEESI), "Correlation of Hydrogen and Air Flow in Critical Flow Nozzles," 1992 Earth-to-Orbit (ETO) Technology Conference, MSFC, AL, May 1992.

W.T. Powers/EB22
205–544–3452
Sponsor: Office of Aeronautics, Exploration, and Technology

Design of an Intelligent Load Controller

A Small Business Innovative Research (SBIR) contract has been established to investigate intelligent protection for **space power** applications. This work is focused on the use of distributed intelligence in the space station module/power management and distribution system (SSM/PMAD) at the lowest levels of operation, including the generic controller (GC) and the **remote power controller** (**RPC**). The goal of this work is to design an **intelligent load controller** (**ILC**) to replace the GC and **RPC** that will provide enhanced protection capability, lower power consumption, less weight, and smaller size. These features will provide a more efficient power system for space station use.

The research is divided into two major areas of work. The first deals with the characterization of arcing on direct current (dc) power systems. This research examines the conditions that allow undesirable arcing to occur and potentially remain for substantial periods of time. Laboratory experiments have been setup to simulate fault situations that could occur within the power distribution system. Data have been collected characterizing the electrical phenomena that accompanies arcing conditions. These data have been plotted and studied for use in determining possible detection algorithms that could be incorporated into an **ILC**.

The second area of research work involves the design of an **ILC**. This device will use state-of-the-art metal oxide semiconductor field effect transistors (MOSFET's) to provide current limiting and load protection. It will replace the functionality of the GC and the **RPC**. The **ILC** will offer lower power consumption, less weight, and smaller size as advantages over the present power-hungry design. In addition, it will offer fewer components and fewer interconnections, as well as reducing the total number of devices system-wide, thus improving the reliability of the power management system. Further, the **ILC** will have enhanced protection features, e.g., **arc detection**. The **ILC** has had the requirements defined and the system specifications are now in place. Design and implementation will take place next, such that the **ILC** may be installed in the PMAD test facility located at MSFC.

It has been determined that conditions exist that would allow arcing to go undetected by conventional protection techniques. A loose power connector or a break in the power conductor has been shown to produce arcing that can last for several seconds in a condition that could go undetected by standard overcurrent or undervoltage protection devices. Such arcing can cause reductions in load voltage of only 20 V and can show a decrease in current. These conditions could produce situations of severe shock hazards and potential for fire aboard a space vessel.

The data are now under study to determine potential algorithms for **arc detection** on dc power distribution systems. It is not clear at this time that such detection can be done reliably.

Further work is needed in determining potential methods for detecting undesirable arcing conditions. Such methods would enhance the safety of crew and equipment aboard the space station. The **ILC** will be completed and installed in the test facility for space station power distribution studies. It will perform conventional protection methods and incorporate appropriate methods for **arc detection**.

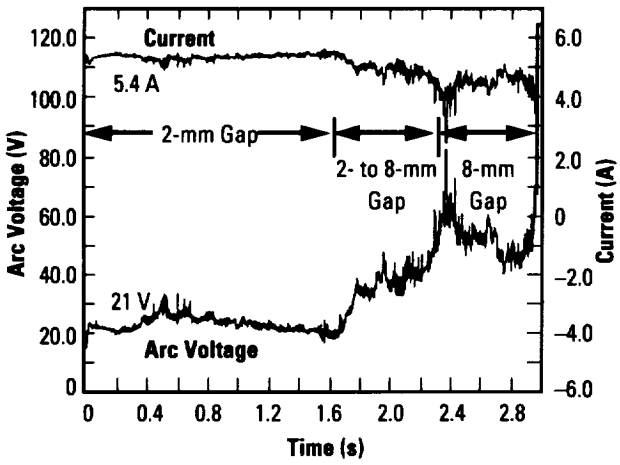

Current and voltage of a 120-Vdc power system arc gap.

N.R. Dugal-Whitehead/EB12
205–544–3304
Sponsor: Office of Commercial Programs,
Small Business Innovative Research Program

Development and Implementation of an Ion Figuring System for Optical Components

A new **precision optical fabrication** facility is currently being implemented at NASA's MSFC. One of the technologies being evaluated to complement the standard fabrication techniques is **ion figuring**. This process involves a kinetic energy transfer from inert gas molecules that results in molecular-level sputtering of the substrate material. A specific profile of neutralized gas ions is generated to act as the material removal tool. This "beam" is then directed toward the optical component and performs deterministic material removal to create the desired surface contours. **Ion figuring** of optical components is a relatively new technology that can alleviate some of the problems associated with traditional contact polishing. Because the technique is noncontacting, edge distortions and rib structure print-through are not a problem.

Ion figuring can be utilized in final figure correction or implemented as the primary figuring process. In both situations, the material removal depth is limited to the micrometer scale due to the relatively low-sputter yields of the substrate materials. The process under development is primarily aimed at producing a large radius of curvature mirror segments from polished flats of single crystal silicon (Si) or chemical vapor deposited (CVD) **silicon carbide** (**SiC**). These segments have a hexagonal shape and will be used to form the primary of a 12-m (40-ft) class beam expander to direct laser energy through the atmosphere. The adaptive system will be used to compensate for the phase perturbations caused by atmospheric turbulence.

This facility is being constructed around a surplus sputtering chamber obtained for this program. This chamber is being retrofitted with a 3-cm (1.2-in), filament-type ion source. This source is driven by a programmable power supply that can provide current densities to 10 mA/cm^2 (64 mA/in^2). The mirror substrates will be attached to a two-axis translation stage with a rotary table. The stage has X–Y ranges to 100 mm (4 in) and 360° rotation at speeds up to 15 r/min. The motion of the system, as well as the ion source, will be controlled by an 80486-based personal computer (PC).

In this procedure, the Gaussian ion distribution is transformed into a spherical material removal function by the translation and rotation of the sample. In alternate methods, a masking procedure is used to create the required spherical distribution.

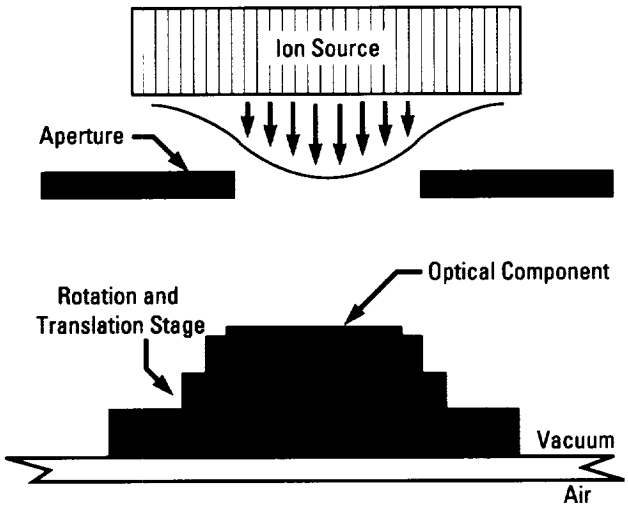

Ion figuring process schematic.

A phase I Small Business Innovative Research (SBIR) program on **ion figuring** of optical components has recently been successfully completed under the sponsorship of the Optical Systems Branch at MSFC. A phase II program is in place to continue this effort. The information gained from these projects will significantly benefit the development of the experimental **ion figuring** program for the mirror segments. Preliminary investigations are aimed at determining the basic parameters involved with using **ion figuring** to produce finished optical components. The primary areas of consideration are the material removal rates and the resulting surface finishes. Multiple CVD **SiC** samples that have been polished or ductile-ground to angstrom-level surfaces are being characterized to determine the optical and topographic surface information. The surface evaluation consists of bidirectional reflection distribution function (BRDF), profilometry, interferometry, and scanning electron microscopy. These surfaces are then ion-machined at specific material removal rates. The finished surfaces are characterized to evaluate the effects of the ion **machining** process with respect to the material removal rate and the previous processing techniques. This study will provide some of the information required to effectively utilize ion **machining** as a primary figuring procedure for optical components.

There are many benefits to using the **ion figuring** process. The process is relatively deterministic and should lend itself to automated manufacturing. Since the technique is noncontact, the edge distortion and support structure print-through problems associated with traditional contact polishing are eliminated. The process can also enhance the application, adhesion, and durability of the optical coatings if they are applied prior to breaking vacuum. This could potentially lead to a complete fabrication procedure where the segment mirrors are lithographically patterned and etched with edge sensors and controllers, figured with the desired mirror surface, and, finally, coated with the high-energy laser coating while in the vacuum environment. The current investigations at MSFC will be evaluating the **ion figuring** potential of various substrate materials for the mirror segments. Future investigations will evaluate lithographically patterned sensors and controls as well as the application of wavelength specific laser coatings.

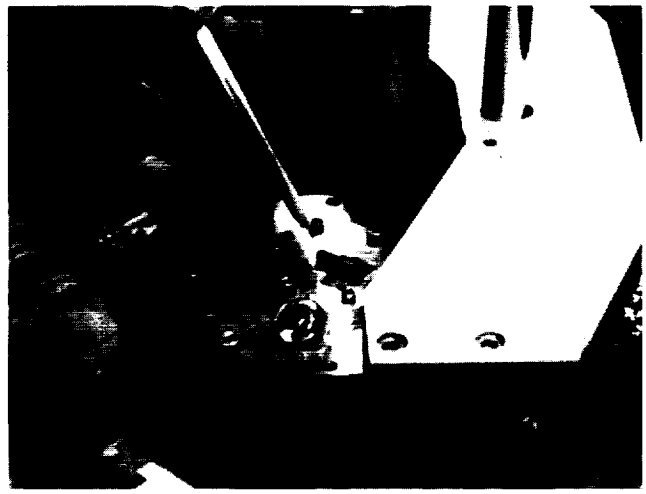

Ion figuring apparatus.

S.C. Fawcett/EB23
205–544–6931
Sponsors: Office of Aeronautics, Exploration, and Technology and Office of Commercial Programs, Small Business Innovative Research Program

Development of Active and Adaptive Optical Systems

Active segmented **optics** are now being developed at MSFC. These **optics** will be implemented in the form of 3- to 6-cm (1- to 2.5-in) hexagonal mirror segments, incorporating precision **actuators** and **sensors** to align adjacent segments. This allows an array of segments to simulate a continuous mirror surface. Feedback from a wavefront error sensor drives the segmented mirror array to a shape, or figure, that corrects for atmospheric turbulence and other errors, thus providing a perfectly corrected optical system. The present work is in support of the Space **Laser** Energy (SELENE) Program, which envisions **laser** power transmission to a lunar base and other space uses of power generated on Earth. SELENE envisions a high-power, near-infrared (NIR) **laser** on Earth and a cooperative receiver with a **laser** beacon on the target. The technologies developed will have direct application to other systems, such as large, high-performance telescopes.

Work at MSFC is being directed at developing technologies for the three components of the active segment concept. Mirror segments will be generated by processes adapted to large quantity, low-cost production. Final polishing and figuring to the desired surface curvature will be accomplished by deterministic processes, i.e., an automated process that starts with a mirror blank and delivers a finished product with little or no intermediate testing or handling. The techniques presently under consideration involve precision molding of glass mirror materials, plasma-assisted chemical etching (PACE) of chemically reactive mirror materials, and ion figuring of all types of mirror materials. The selection of mirror segment material requires tradeoff of many requirements, including cost, availability, processing technology, and physical properties relating to stiffness, mass, transmissivity, and thermal effects. The materials being studied in the present work are fused silica (SiO_2), silicon (Si), and silicon carbide (SiC). Specimens of each are being processed by traditional optical shop method, ion figuring, and PACE.

The second component of the segmented active optical system is the edge sensor technology. Edges of the hexagonal mirror segments must be matched to a precision of approximately 10 nm (4×10^{-7} in) to simulate a continuous surface and to avoid reflected wavefront distortion. When wavefront correction requires a segment to tilt, the six adjacent segments must also move, in both tilt and piston (normal to the simulated mirror surface) to emulate a continuous mirror. Existing concepts using inductive bridge techniques are presently being used and refined. In addition, MSFC is working in-house and through university and Small Business Innovative Research (SBIR) contracts to develop other technologies promising improved performance, lower cost, and automated fabrication. This work is also being assisted via an interagency agreement with the Lawrence Livermore National Laboratories, in order to use their unique capabilities to identify and locate existing and potential technology for both **sensors** and **actuators**. The third component of a segmented mirror assembly is the actuator. This provides the rapid, precise movement of the mirror segment in response to the error correction signal.

Each segment incorporates three symmetrically spaced **actuators** that can provide movement of approximately 10 μm (4×10^{-4} in) about a zero position at a bandwidth of a few kilohertz. Requirements for the SELENE program are still under study, but appear to be around the ±25-μm (±0.001-in) range and 1 to 10 kHz; the SELENE mission requirements are very stringent due to operational considerations. **Actuators** presently in use are based on electromagnetic devices and piezoelectrics. MSFC is working both in-house and through industry. The in-house work is directed toward innovative techniques to obtain actuator stroke, bandwidth, and low cost while eliminating operational problems observed with present technology. A study is being performed on innovative techniques of incorporating wavefront error sensing into the active segment, thus incorporating all elements of an active **optic** into one assembly. MSFC is fabricating in-house small, solid Cassegrain telescopes that will be mounted on the back of transparent mirror segments. The segment will use a narrow-band-pass filter on the front surface to pass a **laser** reference signal while reflecting NIR light used to transmit power. The integral wavefront sensor telescope can see both the **laser** and the leakage of the power beam through the filter. By focusing both beams on a detector, wavefront error signals are generated and utilized in a closed-loop feedback system. Integrating the wavefront sensor and control into the active segment provides localized control and actuation to provide improved performance.

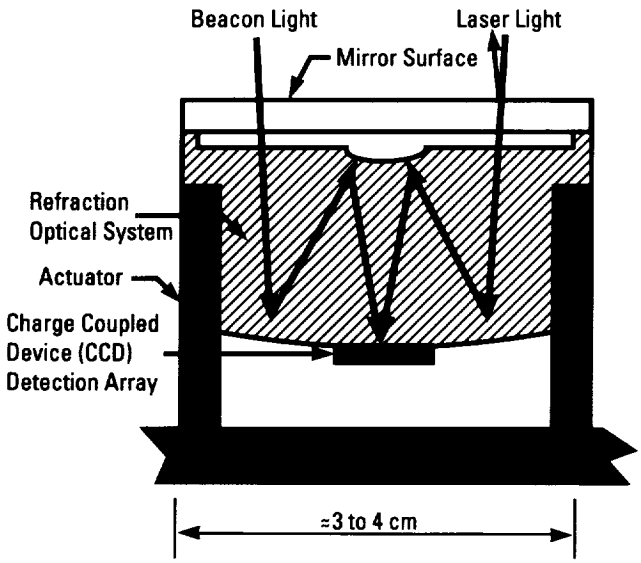

Integrated, wavefront-sensing, adaptive optics system.

R.W. Rood/EB23
205–544–3483
Sponsor: Office of Aeronautics, Exploration, and Technology

Electrical Power System Fault Study

Over the last 3 yr, a study into the most common **electrical power system (EPS) faults** was conducted. The overwhelming response to the most common **EPS** fault was that the fault is in the terminal end-user load. There are, of course, other faults that occur in an **EPS**.

In the past year, the first phase of the test facility was completed and some of the initial faults were injected into the **EPS** breadboard. So far, direct shorts to ground (DSTG), some low-resistance faults to ground, and some transient faults have been injected into the breadboard with some interesting results. There have also been other faults that occurred on their own and have also been observed for data. Some of the latter include: switches failing shorted (always closed), loads failing, switch-shorting a part and tripping off, battery cell capacity decreasing, bus shorts, and solar array simulator (SAS) isolation diode shorted.

The Large Autonomous Spacecraft **EPS** (LASEPS) is a facility that has been created by integrating two power system breadboards: the **autonomously managed power system (AMPS)** breadboard and the space station module power management and distribution (SSM/PMAD) breadboard. The SSM/PMAD breadboard is an advanced development test-bed for power system automation.[1] The **AMPS** breadboard was the result of a much earlier study of power system automation and distributed control of the **EPS**.[2] As a result of the systems in which the faults have been placed, the hardware and software responses to these faults are being evaluated.

The results of the testing are being reported in two papers written for the Intersociety Energy Conversion Engineering Conference (IECEC) in August 1992. The papers are entitled "Results of an **Electrical Power System Fault** Study" and "Large Autonomous Spacecraft **Electrical Power System** (LASEPS)."

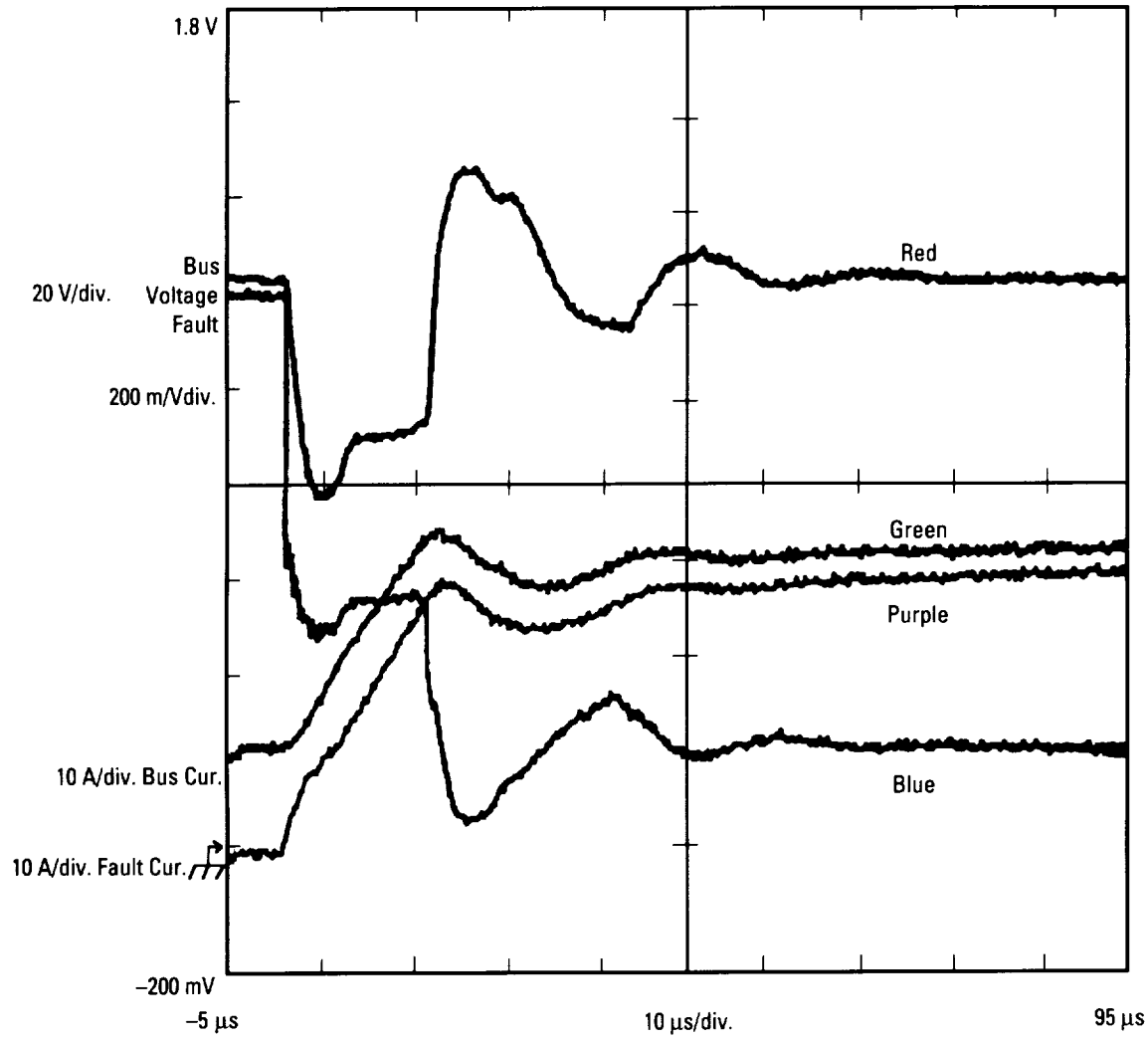

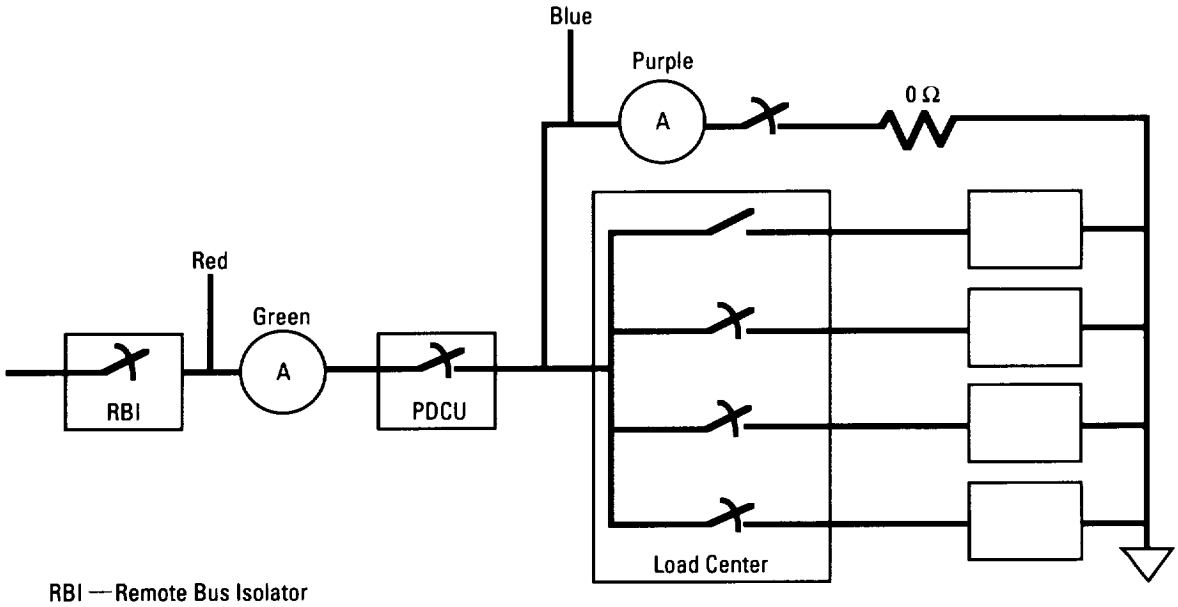

DSTG of a power distribution control unit (PDCU) switch.

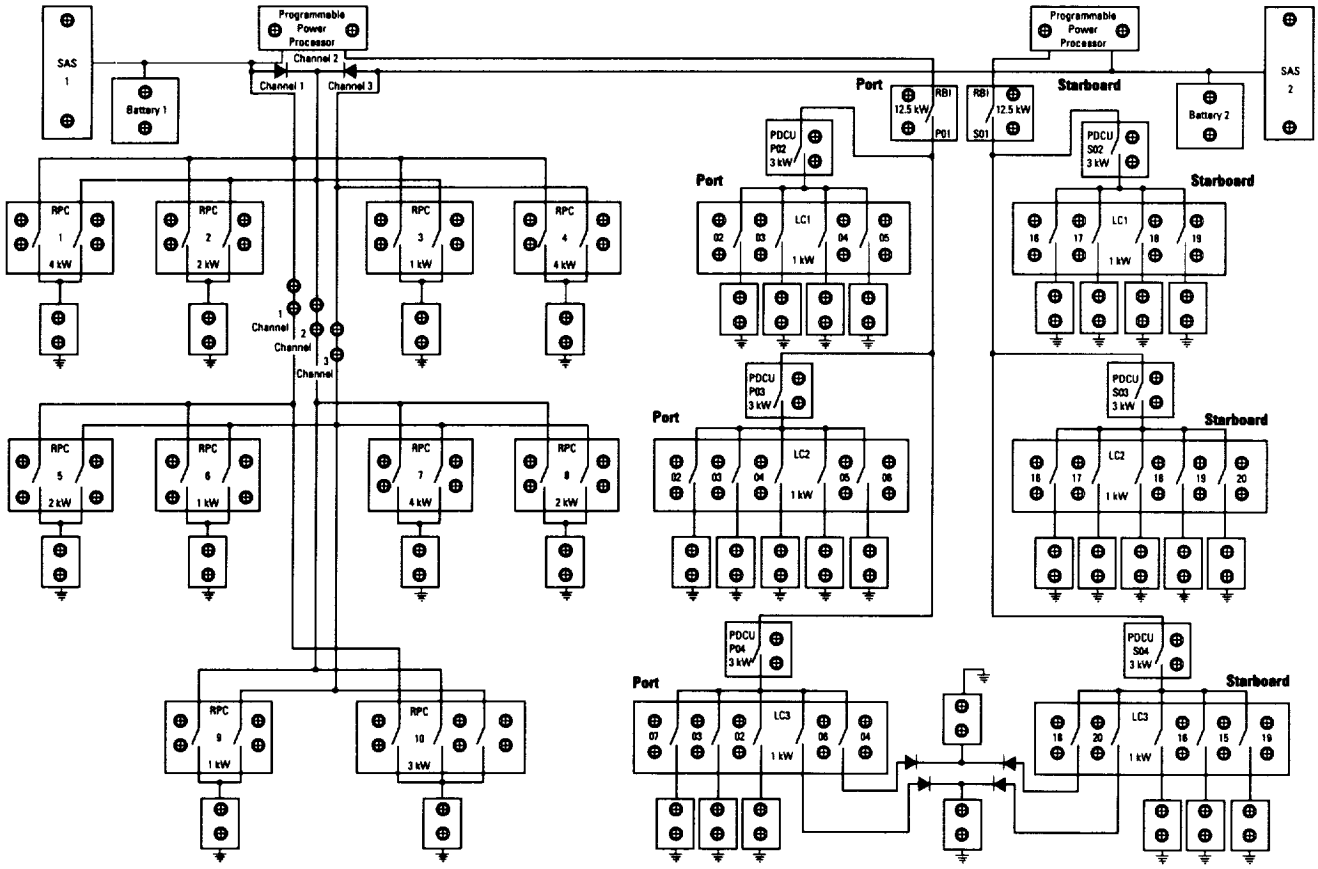

LC—Load Center
RPC—Remote Power Controller

LASEPS annunciator panel.

[1]Lollar, L.F., "Automating a Spacecraft Electrical Power System Using Expert Systems," NASA Technical Paper 316, October 1991.

[2]TRW Defense & Space System Group, "Space Power Distribution System Technology Final Report," TRW Report Number 39243-6001-UT-00, Contract NAS8-34539, NAS8-236484, March 1987.

N.R. Dugal-Whitehead/EB12
205-544-3304
Sponsor: Center Director's Discretionary Fund

Engine Control and Health Monitoring System

The objective of this task is to design, fabricate, test, and deliver to the Government two engine control and **health monitoring** systems (EC&HMS's) that use innovative design approaches to achieve a modular, reconfigurable, flexible, fail-operate/fail-safe design. The design shall easily accommodate the insertion of new electronics technology as it evolves.

Existing design **space shuttle main engine (SSME)** controllers are specific-purpose digital computers, designed to utilize presently identified **SSME** components and interfaces. As engine components change and engine design evolves over the next couple of decades, it will be impractical, from a cost standpoint, to modify the existing controllers to accommodate these changes. A modular, flexible-designed controller is required to enable insertion of new engine technology into the MSFC technology test-bed (TTB), as well as insertion of new electronic technology into the controller. Once proven as a brassboard design in these facilities, the design will offer a starting point (or possibly a complete design) for a next-generation SSME controller. The architectural approach may also be applicable to other engine control applications.

A contract was signed with Allied Signal Aerospace Company, Bendix Guidance Systems Division, in November 1990 to accomplish this task. The contract is 5 yr in duration and will culminate in the delivery of two brassboard units and electrical ground support equipment (EGSE). One unit will be utilized in a laboratory environment to generate and verify engine test software or to perform **health monitoring** algorithms; the other unit will be available to actually control an **SSME** test firing.

In preparation for the architectural definition phase, the contractor performed assessment studies in the area of sensors, effectors, control technology, **health monitoring**, and fault tolerant methods. By folding present **SSME** requirements into predicted future requirements, an EC&HMS requirements document was generated. Various architectural schemes were identified that would satisfy the contract requirements of modularity, flexibility, etc., as well as meet the existing engine control requirements. A multicomputer architecture for fault tolerance (MAFT) architecture was selected as the best-suited candidate to design the EC&HMS. The MAFT design is fault-tolerant, Byzantine-resilient, processor-independent, and runs loosely synchronized. In very general terms, an operations controller (OC) provides for interlane communications between processors, synchonization, voting, scheduling, and failure detection. This relieves the application processor (AP) of management responsibilities and allows it to run the appplication software unencumbered.

The preliminary design activity for this task began in early 1992 and will culminate in a preliminary design review (PDR) at the end of the calendar year. The program will then enter into a 1-yr detailed design period. Delivery of the brassboard units is scheduled for mid-1995.

R.M. Mattox/EB32
205–544–3571
Sponsor: Office of Aeronautics, Exploration, and Technology

Hermetically Sealed Aluminum Electrolytic Capacitor

NASA awarded a phase I Small Business Innovative Research (SBIR) contract to Boundary Technologies, Inc., in January 1991. The phase I research was considered successfully completed, with warrantable phase II research. The phase II contract has been awarded with work to begin as soon as all official paperwork is processed. The following text gives a summary of the phase I initiative.

The purpose of this research is to develop a **hermetically sealed aluminum electrolytic capacitor (ALEC)**, suitable for use in space power systems, that can replace the large and heavy tantalum **capacitors** presently used. In phase I, a prototype low-gassing **capacitor** electrolyte was developed for use at 250 V and at temperatures from –55 to 105 °C (67 to 221 °F). The relationship between gas generation rate and **capacitor** leakage current was determined for different electrolyte compositions and operating conditions. The feasibility of maintaining low pressure in **capacitors** with this electrolyte was demonstrated in **capacitor** tests.

The test **capacitors** are of a special type with which it is possible to monitor the internal pressure during the test, and the seal design minimizes vapor loss. Life tests are being run at 250 V and 105 °C (221 °F), and results through 600 h are available at the end of phase I. At 160 h, **capacitors** containing the recommended electrolyte have a pressure increase of 3.447×10^3 N/m^2 (0.5 lb/in^2), compared with an 82.728×10^3-N/m^2 (12-lb/in^2) increase in **capacitors** made with a conventional wide-temperature range electrolyte used for military applications. The pressure increase with the proposed electrolyte is linear with time (or charge), and, after 600 h, the pressure is 13.788×10^3 N/m^2 (2 lb/in^2). With conventional electrolyte, the pressure is 151.668×10^3 N/m^2 (22 lb/in^2) at 600 h, and it is estimated that with a hermetic seal it would have been 310.23×10^3 N/m^2 (45 lb/in^2).

It is calculated that **hermetically sealed capacitors** rated at 250 working voltage at 105 °C (221 °F) would have internal pressure of 20.682×10^3 N/m^2 (3 lb/in^2) after operating at nominal conditions of 200 V and 65 °C (149 °F) for 20 yr. Such a low pressure is well within the capability of hermetic seals. The seal will be designed in phase II.

Other applications for **ALEC**'s are found in commercial satellites and in medical electronic implants. When used in conventional **capacitors**, the new electrolyte will provide higher reliability at high temperatures and will be particularly beneficial for power electronics applications such as inverter circuits.

P.P. Edwards/EB13
205–544–3373
Sponsor: Office of Commercial Programs,
Small Business Innovative Research Program

Integrated Power and Attitude Control System for Space Station and Other Applications

The SatCon Technology Corporation of Cambridge, MA, is currently developing an **inertial energy storage** system under a Small Business Innovative Research (SBIR) contract to MSFC. The storage of electrical energy onboard spacecraft for use during eclipse periods is a function that can strongly impact the vehicle's performance. This function is almost exclusively performed by batteries at this time. Traditional nickel-cadmium (NiCd) batteries have a specific energy of less than 10 Wh/kg (4.5 Wh/lb), while nickel-hydrogen (NiH_2) batteries of the type used on the Hubble Space Telescope (HST) are in the 15-Wh/kg (6.8-Wh/lb) range. Clearly, the weight of the **energy storage** subsystem is a major portion of the total weight of a typical spacecraft.

One alternative technology for **energy storage** is rotating **flywheels**. Tests at Oak Ridge National Laboratory have demonstrated wheel-only specific energies of as much as 240 Wh/kg (109 Wh/lb) before burst using composite materials. Although the specific energy of a complete energy subsystem would be less, there is obviously a potential for significant spacecraft weight savings with a **flywheel inertial energy storage** system. Further, **flywheels** designed to store the energy required for typical missions by default have stored more than enough momentum to perform **attitude control** functions as well. As a result, there exists an opportunity to save additional weight by integrating the **attitude control** and **energy storage** functions in a single **inertial** system.

SatCon Technology Corporation is presently involved in a phase II SBIR effort to develop an integrated power and **attitude control** system (IPACS) to demonstrate the combined **energy storage/attitude control** capabilities of a **flywheel**. The wheel is made of composite material with an integrated motor/generator and mounted with magnetic bearings. Demonstration goals include:

- Specific energy capability of 40 Wh/kg (18 Wh/lb)
- Round-trip efficiency of 86 percent
- Low power requirements for torquing the wheel for **attitude control** applications
- Control techniques that reduce synchronous vibrations resulting from mass unbalance.

At present, all major system components have been designed and a **flywheel** has been delivered to SatCon Technology Corporation. This wheel will be subjected to evaluation testing before being integrated with the motor/generator, bearings, and other system elements. System-level testing is scheduled to begin in the fall of 1992. Test conditions will be speeds up to 40,000 r/min and depths of discharge up to 75 percent (1/2 speed). At these conditions, the wheel will store a maximum of approximately 1,800 Wh, with 1,300 Wh (less losses) available for use by the spacecraft. This would provide capability of as much as 2 kW for a typical low Earth orbit (LEO) profile.

Oglevie, R.E., and Eisenhaure, D.B., "Advanced Integrated Power and Attitude Control System (IPACS) Study," NASA Contractor Report 3912, November 1985.

Olszewski, M., and O'Kain, D.U., "Advances in Flywheel Technology for Space Applications," Proceedings 21st Intersociety Energy Conversion Engineering Conference, San Diego, CA, August 25–29, 1986.

R.T. Bechtel/EB12
205–544–3294
Sponsor: Office of Commercial Programs,
Small Business Innovative Research Program

K6 Mass Data Storage Unit

The objective of the **solid-state recorder** (**SSR**) project is to advance flight data storage technology to improve the capability of monitoring launch vehicle engine performance. The evaluation of the postflight health and status of a complex system, such as a **space shuttle main engine** (**SSME**), requires acquisition and postflight analysis of much sensor data; however, current technology (tape recorders) does not support the data storage requirements of future **engine health monitoring** systems and does not support operation in a high-vibration environment near the **SSME's**. Unlike a magnetic tape recorder, an **SSR** is ideal for space flight applications because it incorporates no moving parts. MSFC and Fairchild Space Company of Germantown, MD, will research, design, and develop advanced technology in the area of digital **mass data storage** for critical rocket engine data.

A solid-state technology study report has been delivered to MSFC and a preliminary design review of the project was successfully completed in April 1992. The **SSR** project is divided into two phases: phase I involves a study of available solid-state memory technologies and will result in a limited capacity prototype to demonstrate and test the concept; phase II of the contract will culminate in a space-qualified recorder with potential applications with the space shuttle or Space Station *Freedom* (S.S. *Freedom*).

The **SSR** will be an all-digital unit to obtain the flexibility needed to interface effectively with the various components of the engine data acquisition system (DAS). Fairchild has begun hardware design of the microprocessor board and the built-in test (BIT) functions. A widely used military standard bus (MIL–STD–1553B) has been incorporated into the design to control the recorder, and an additional 1553B bus in the **SSR** will accommodate data from an **engine health monitoring** system or another source. The **SSR** will have the capability to record up to eight serial digital data streams having a maximum combined data rate of 20 Mb/s. Fairchild Space Company has proposed using an advanced multichip module (MCM) approach for electronic packaging of widely available memory devices to ensure the MSFC goal of a 10-Gb capacity. Design of the memory controller and the input/output (I/O) interface circuit boards has been completed and testing of the prototype engineering model **SSR** is scheduled for October 1992.

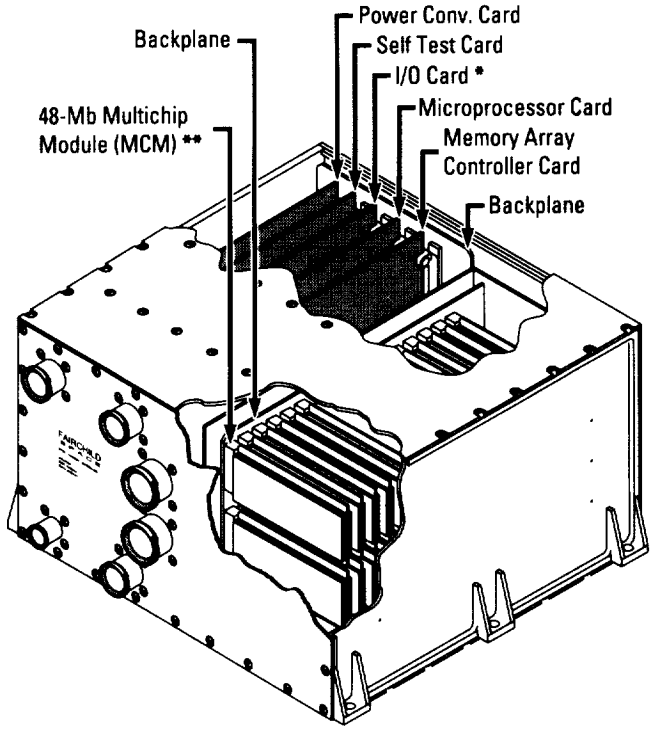

NOTE. — * The backplane will accomodate up to five I/O Cards. The number will be based on the mission I/O requirements.

** The number of MCM's could be augmented to accomodate up to 16.4-Gb memory.

Earth-to-orbit (ETO) SSR (conceptual design).

S.L. Bridge/EB33
205–544–8572
Sponsor: Office of Aeronautics and Space Technology

Light Treatment for USML–1 Payload Operations Control Center Shift Workers

Within the field of **circadian physiology**, experiments during the past decade have shown that bright light can have a significant effect in regulative the circadian system. The circadian system controls daily rhythms such as sleep/wake (S/W) cycles, body temperature, hormone secretion, and other physiological parameters including cognitive functions.

Working when the body is normally asleep generally produces decreased production, performance, and alertness and increased fatigue-related accidents and health problems including higher risk of cardiovascular disease, gastrointestinal illness, cognitive and emotional disorders, and sleep disorders. The *New England Journal of Medicine*[1] reports a study under laboratory conditions concluding the following:

> "Maladaptation of the human circadian system to night work, with its associated decline in alertness, performance, and quality of the daytime sleep, can be treated effectively with scheduled exposure to bright light at night and darkness during the day."

Experimental Gerontology[2] reports that, on one occasion, an Apollo command module pilot fell asleep while on duty and resorted to using amphetamines to stay awake. A survey in this article reported that shuttle crew members suffered sleep disruption and slept less in flight than on the ground. Many had to use sleeping pills during their mission. Analysis of their S/W schedules revealed misalignment of **circadian rhythms** and that the misalignment might play an important role in these disturbances. An Office of Technology assessment report submitted to Congress in September 1991 addresses shiftwork problems and current methods to ameliorate those conditions, including the use of bright light.[3]

Bright light treatment has been used on flight crews beginning with STS–35 (Astronomy Payload–1 (Astro–1)). By subjective report, the crews were unanimous in that they were able to sleep more soundly during the day and remain much more alert during the night by using the bright light.

A number of ground support personnel are also subjected to the pressures and disadvantages of shiftwork. This study will focus on a sample of Payload Operations Control Center (POCC) Cadre members supporting the first U.S. Microgravity Laboratory (USML–1) launch in June 1992. Cadre members currently have no shifting procedures and often use sick leave or annual leave when resynchronizing either post-mission or due to launch slips. In a survey conducted among past and current Cadre members, 54 percent of the respondents felt their performance was degraded, 65 percent felt their quality of sleep was degraded, and 32 percent experienced illnesses they believed to be related to shiftwork.

This study investigated the effects of using portable bright light units augmented with a light delivery system to improve performance and alertness, reduce shift-related illnesses, and expedite reversion to a normal schedule during launch delays and/or post-mission for non-first-shift POCC Cadre members. For USML–1, volunteers from both the Blue Team (on the 4-p.m. to 1-a.m. (approximately) shift) and the White Team (on the midnight to 9-a.m. (approximately) shift) were divided into Blue and White Experimental and Control groups. Baseline data, including normal sleep patterns, were collected. **Bright light treatment** began aproximately 3 to 5 d before launch; maintenance doses of light were administered during the mission. The subjects were thoroughly briefed on equipment usage and will administer the bright light themselves in their homes. Subjects rated the treatment protocols as highly effective for promoting adjustments to their shifted work schedules and indicated their interest in using light treatment for future missions. This study demonstrates that light treatment is both feasible and useful for NASA personnel who must work on shifted schedules.

Further, this research provides preliminary data, justification, and guidelines for operationally implementing this procedure as standard protocol for future space flight missions requiring cadre and other ground personnel to work third-shift schedules.

[1]Czeisler, C., "Strategies for Resetting the Human Circadian Clock," *New England Journal of Medicine*, May 3, 1990, p. 1306.

[2]Czeisler, C., "Research on Sleep, Circadian Rhythms, and Aging: Applications to Manned Spaceflight," *Experimental Gerontology*, vol. 26, 1991, p. 217.

[3]Office of Technology Assessment (OTA), "Biological Rhythm Implications for the Worker," OTA-BA-463, September 1991.

B.C. Hayes/EO23
205–544–9276
Sponsor: Spacelab Payload Projects Office

Miniature Dexterous Hand

This is a phase II Small Business Innovative Research (SBIR) contract with Bonneville Scientific, a firm based in Salt Lake City, UT. This contract will produce a **miniature dexterous** hand utilizing tactile sensing. Some of the many applications of this design include automated manufacturing and autonomous robotic systems for space applications. Eventually, two hands will be constructed and tested in this phase II effort. The most innovative aspect of this contract is the small **piezoelectric** motor utilized within the **dexterous** hand. A patent has been filed for the **piezoelectric** motor developed in this SBIR contract.

The **miniature** dexterous hand will have low mass and will be energy-efficient to provide low power usage and less heat-rejection problems. The primary motor will be very simply constructed to be both reliable and inexpensive. The actuators utilized will be self-contained to provide easy change-out. Adequate space will be reserved within the fingers to accommodate leads, sensors, and electronics. When the hands sustain a power loss, the fingers go limp so they will not damage their surroundings. One of the most important features is the tactile sensing capability to allow **dexterous** manipulation of desired objects.

Bonneville Scientific, Inc., phase II SBIR proposal, Salt Lake City, UT.

P. Nelson/EB24
205–544–3645
Sponsor: Office of Commercial Programs,
Small Business Innovative Research Program

Monitoring and Diagnosing the Environmental Control and Life Support System

The **environmental control and life support system** (**ECLSS**) advanced automation project (AAP) is in its fourth year of developing an intelligent system to monitor and diagnose Space Station *Freedom's* (S.S. *Freedom's*) **ECLSS**. **Model-based diagnosis** is the technology chosen to provide **fault detection and diagnosis** of the **ECLSS**. The model-based reasoning algorithm requires a model of the system. It then analyzes this model and automatically detects and diagnoses faults. For monitoring the system, a graphical user interface is provided that consists of a schematic of the system and critical sensor information.

Currently, a model of the **ECLSS** carbon dioxide removal assembly (CDRA) has been developed for monitoring and diagnosing purposes. This model consists of complex structural and behavioral relationships of the subsystem's components. Faults are detected by noting discrepancies between subsystem and model sensor values. A fault candidate list is generated by fault diagnosis procedures, which list the parent components of the faulty values. Various operations are performed on the fault candidate list, including model inversion, to remove suspected components from the candidate list. A candidate list of one component is declared to be the faulty component.

The monitoring and diagnosis software forms the basis of a ground support fault detection and isolation system. The **ECLSS** AAP is targeting the technology toward test-bed and flight support applications. The software is currently being integrated into the predevelopment operational system test (POST), which tests integrated **ECLSS** components. Participation in the POST allows the **ECLSS** AAP to fine-tune the CDRA model using data from the test-bed and also to prove the technology to the test-bed engineers. The goal for this project is to incorporate the monitoring and diagnosis technology into an S.S. *Freedom* ground support facility, such as the Space Station Control Center.

A.N. Cardno/EB42
205–544–3039
Sponsor: Office of Space Flight, Space Station *Freedom* Engineering Prototype Development

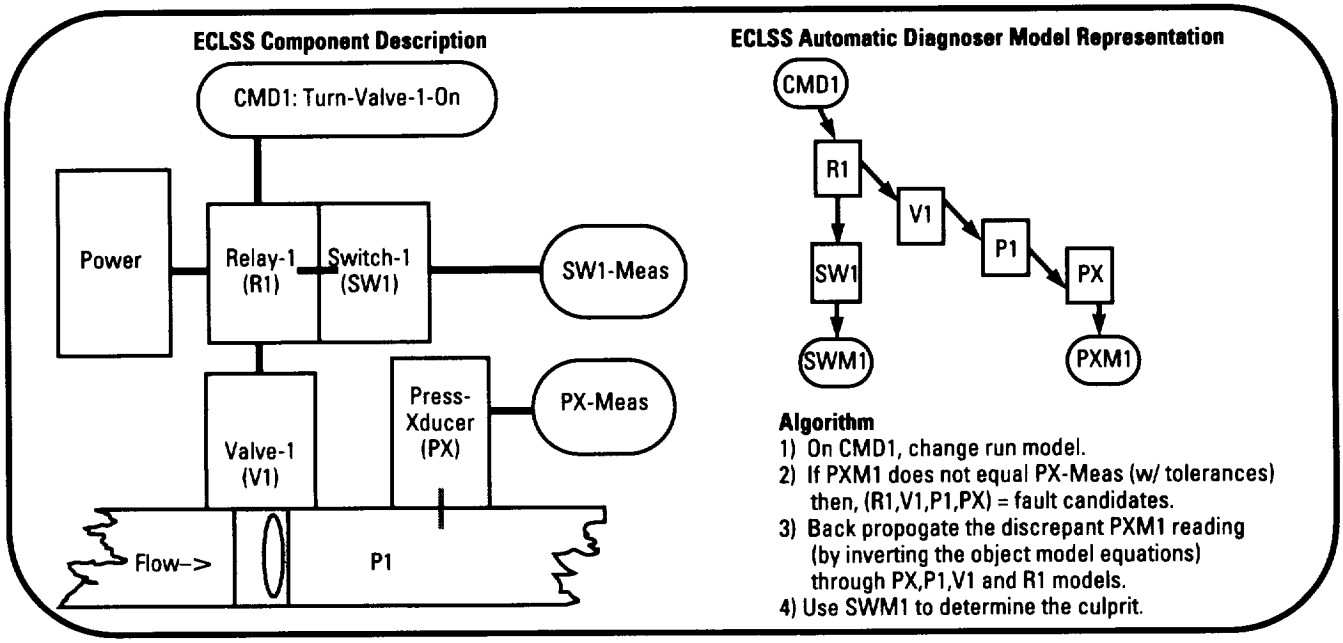

The ECLSS advanced automation project: model-based diagnosis.

ROBOSIM: A Robotic Simulator

ROBOSIM is a NASA-developed, graphics-based **robotics simulation** software package for support of both industrial and aerospace design applications. During previous years, a number of achievements have been made by the research contractor working in this area, including the development of a **simulation** library, a graphical editor, and the porting of ROBOSIM into the Intergraph Corporation's **computer-aided design/**computer-aided manufacturing (**CAD/**CAM) environment being used at MSFC.

ROBOSIM was used to develop industrial robotic applications for a variety of shuttle systems, control algorithms for optimal control of robotic welding systems, and modeling of robotic systems control concepts for use on **Space Station** *Freedom* (S.S. *Freedom*). The objective of this project is the further development and transfer of ROBOSIM technology for distribution within NASA, as well as among other government, industry, and academic centers.

Porting ROBOSIM to an Intergraph workstation consisted basically of two tasks: (1) porting of the basic ROBOSIM kernel and (2) porting of the **simulation** library. The basic ROBOSIM kernel port consisted of converting the X-Windows graphic-display software as used with the contractor's Hewlett-Packard HP350SRX workstation to the Environ V windowing environment used with an Intergraph workstation. This consisted primarily of translating between the Move and Draw commands of the two windowing environments. The **simulation** library port primarily involved code changes to take advantage of the specific three-dimensional (3–D) drawing routines and the input/output (I/O) devices available on the Intergraph platform. This software conversion/translation has resulted in the availability of the ROBOSIM program and its **simulation** library on the Intergraph platform/environment used at MSFC.

During the past year, the research contractor delivered to the MSFC Data Management Branch updated versions of ROBOSIM for the Intergraph Unix workstation and disk operating system (DOS) 386 personal computer (PC) environments; these updates enable the user to more efficiently command the software operation to simulate the activity of a robot. Simplification was achieved by being able to load up ("string") several commands together into a single command file to simulate a sequence of robot movements.

At the request of the MSFC Technology Utilization Office, a 30-s videotape feature of ROBOSIM operation was produced at MSFC for use at the Tech 2002 Conference in December 1992. The video included two Data Management Branch engineers and a local television personality, Bob Baron, describing and demonstrating the use of ROBOSIM in the Intergraph/Unix robotic **simulation** environment.

M.K. Smith/EB44
205–544–3813
Sponsor: Office of Commercial Programs,
Technology Utilization Office

Solid Rocket Booster Implementation and Use of a Still Video System

Photography plays a key role in the processes of safety, reliability, quality control, and mission assurance of flight hardware. Photographs often serve as backup material to the official documentation for visually describing a structure. These photos are helpful in that they functionally and literally represent a "picture worth a thousand words" when a requirement exists to provide a description of the appearance of a piece of flight hardware, especially if the hardware is reused, such as the solid rocket boosters (SRB's) of the integrated space shuttle. **Still video cameras** recently replaced 35-mm **cameras** previously used in closeout **photography** activities performed as a part of daily operations. The **still video cameras**, though similar in appearance to the standard 35-mm **cameras**, are slightly bulkier, are made by Sony Corporation, and record images on a 2-in square floppy disk. Up to 50 images can be recorded on a disk, played back on a video screen, and printed out in seconds with approximate quality and resolution obtained from a regular 35-mm film negative. The **still video camera** has zoom-lens capability with microfocusing to within a few inches of the object of interest. The **camera's** recording disk is 12 times faster than a "normal" computer disk and records the photo using 500 lines of resolution per inch. Each disk can be erased and used over numerous times. Sony, the manufacturer, guarantees that double exposures are not possible with the system. Users of the system benefit from the reduced time delay to get "hard" prints into the hands of analysts and engineers.

The advantages to the **still video** system are: (1) user-friendliness; (2) ease and speed of color photo transmission by electronic transfer along communication lines; (3) film processing costs and delays being eliminated; (4) closed-out areas not having to be reopened; (5) the ability to view disks on the monitor, thereby reducing the need for film prints; (6) quality control viewing disks immediately and making retakes/adjustments as necessary; (7) reducing storage requirements; and, best of all, (8) projected collateral cost savings of approximately $730,000 through the life of the SRB contract with its prime contractor, United Technologies/United Space Boosters, Inc. (USBI).

L. Dinges/SA45
205–544–6647
Sponsor: Office of Space Transportation Systems

Space Shuttle Wind Profiler

Measurement of winds is required to safely launch and land the space **shuttle**. Balloons are currently used in both instances to produce the necessary wind profiles. The balloons require an hour to rise through the altitude range, sometimes drifting far from the area where the wind measurement is desired. As a result, the correlation between the winds encountered by the vehicle and those measured is reduced. MSFC and other NASA Centers are investigating the potential of alternate wind sensors to produce more local wind measurement in less time to increase this correlation.

Laser-radar (lidar) and **radar wind profilers** are currently being evaluated through a series of demonstrations coincident with **shuttle** launches and landings. Profiles to 20 km (65,617 ft) are required for launches and to 10 km (32,808 ft) for landings. The **lidars** transmit a narrow, collimated laser beam and profile winds by measuring the Doppler-shifted laser signal return from entrained aerosols in the atmosphere. The **radars** transmit a narrow, conical, radio frequency beam and profile winds by measuring the Doppler-shifted signal return from atmospheric refractive index variations. The **lidar** signals are blocked by clouds but can provide wind measurements in cloud-free regions where desired, including along the **shuttle** flight path. The **radars** are less affected by the weather, but lack the high spatial resolution of the **lidars** and require 0.5- to 1-h integration times. The **lidar** and **radar** performances are compared with the existing wind-profiling instrumentation and the actual **shuttle** flight performance. Velocity accuracy, altitude resolution, maximum range, update rate, and performance in adverse environments are among the factors being compared.

Two demonstrations, one involving a carbon dioxide (CO_2) **lidar** and another involving a neodymium:yttrium aluminum garnet (Nd:YAG) **lidar**, occurred during 1991 at Kennedy Space Center (KSC) coincident with **shuttle** launches. The **lidars** were selected due to their availability and because they represented the two leading **lidar** technologies. The CO_2 **lidar** was eyesafe, operating at a wavelength of 10.6 μm (417.323 μin). The Nd:YAG **lidar** was noneyesafe, with a wavelength of 1.06 μm (41.732 μin). Both **lidars** emitted approximately 1 J/pulse. The CO_2 **lidar** demonstration occurred prior to the eruption of Mt. Pinotubo, operating in a very clean atmosphere. The Nd:YAG **lidar** demonstration took place after the eruption. As a result, the altitude performance of the Nd:YAG **lidar** exceeded 20 km (65,617 ft) while the altitude performance of the CO_2 **lidar** was approximately 6 to 10 km (19,685 to 32,808 ft). In subsequent testing, the CO_2 **lidar** performance has also exceeded 20 km (65,617 ft) using the same pulse energy.

A demonstration of two **lidars** and a boundary layer **radar** is scheduled for winter 1993 at Kennedy Space Center (KSC), coincident with a **shuttle** landing. **Lidar** capabilities are closely matched to the landing application since both the **lidars** and the **shuttle** require clear air. The **lidars** involved are the CO_2 **lidar** tested during 1991 and a holmium (Ho), thulium (Tm):YAG **lidar**, operating at a 2.1-μm (82.677-μin) wavelength and a pulse energy of 50 mJ. The **lidars** are both eyesafe. Testing of the two **lidars** is intended to resolve issues relevant to the selection of the appropriate **lidar** wavelength for the landing application. The **radar** is capable of continuous, autonomous operation with an altitude range spanning the gap between 120 m (394 ft) and the minimum altitude of the large KSC **radar wind profiler**. The test program will conclude with analysis of the landing wind profiling demonstration results.

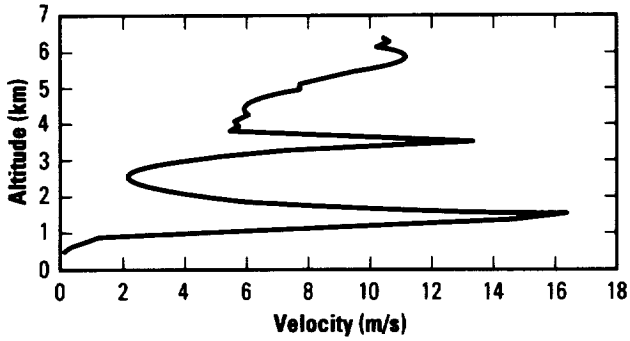

CO_2 lidar wind velocity profile.

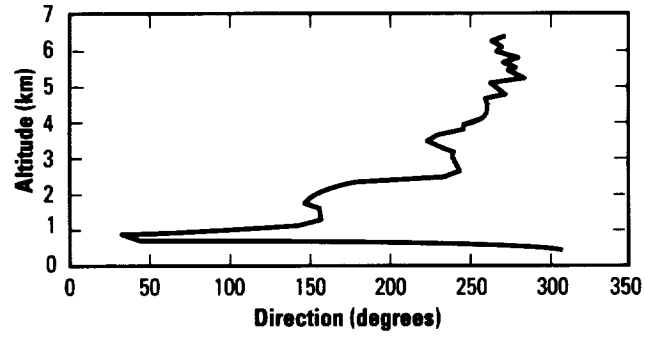

CO_2 lidar wind direction profile.

S. Johnson/EB23
205–544–3478
Sponsor: Office of Space Flight

The Space Station Module/Power Management and Distribution Automated Subsystem

The space station module/**power management and distribution** (SSM/**PMAD**) automated subsystem project was begun to investigate **automation** techniques appropriate to a large secondary **PMAD** system, such as the one that will exist within a Space Station *Freedom* (S.S. *Freedom*) habitation or laboratory module. With the support of Martin Marietta Space Systems Group, a high-fidelity SSM/**PMAD** test-bed was developed. The test-bed hardware has two power distribution control units (PDCU's) and three load centers rated at 18 kW. Further, the test-bed includes remote bus isolators (RBI's) and remote power controllers (RPC's) rated at 3 kW and 1 kW. Lastly, a lowest level processor (LLP) is included in each PDCU and load center. In the software area of the test-bed, autonomy is pushed down to the lowest levels, specifically, to the LLP's and through the switch interface processors to the "smart" switchgear. Three **expert/knowledge-based** (**E/KB**) **systems**—the fault recovery and management expert system (FRAMES), the load priority list management system (LPLMS), and the master of automated expert scheduling through resource orchestration (MAESTRO)—reside above and communicate with the other processors through the communications and user interface (CUI) software. In order to efficiently operate these three **E/KB systems** together, a simultaneous multiagent knowledge manager function called the knowledge management and design (KNOMAD) system was designed and built. KNOMAD utilizes a distributed data base management function to provide a modified blackboard management capability.

The three **E/KB systems** interact such that, when a hard fault occurs, the **PMAD** is immediately safed by smart switchgear in a few milliseconds. FRAMES recognizes the new configuration and decides if any other actions need to take place. FRAMES diagnoses the fault, recommends corrective action, and, where appropriate, autonomously implements the corrective action. If the system determines that the current loads schedule has been perturbed by the anomaly, MAESTRO is directed to reschedule the loads for the remainder of the crew period. The LPLMS then generates a new global load shedding list, which is downloaded to the LLP's. A similar sequence autonomously occurs in the event of a soft fault (except the switchgear does not trip) or when new directions or power allocation levels are sent to the **electrical power system** (**EPS**) (through the operator interface). Thus, intermediate levels of manual control are available, and the operator is made aware of the consequences of actions he/she proposes to take.

The system can now detect and diagnose any of hundreds of combinations of faults, safing the system and notifying the operator of what has occurred. The schedule is automatically adjusted and the changed schedule is implemented. The operator can test out of service hardware and can return hardware to service, or the operator can choose to manually control parts or all of the EPS and release manual control when desired. These capabilities are all presented to the operator through a high-quality user interface to make for a very powerful EPS control system.

Several efforts are under way to make the breadboard more robust and to integrate this technology into operating S.S. *Freedom*. The initial tasks for providing intermediate levels of autonomy (ILA) have been developed. This development includes a planning system, the knowledge augmentation and negotiation tool (KANT), to perform power system negotiations between the system and the operator. The ILA tasks allow an override capability without the operator taking complete control of the breadboard.

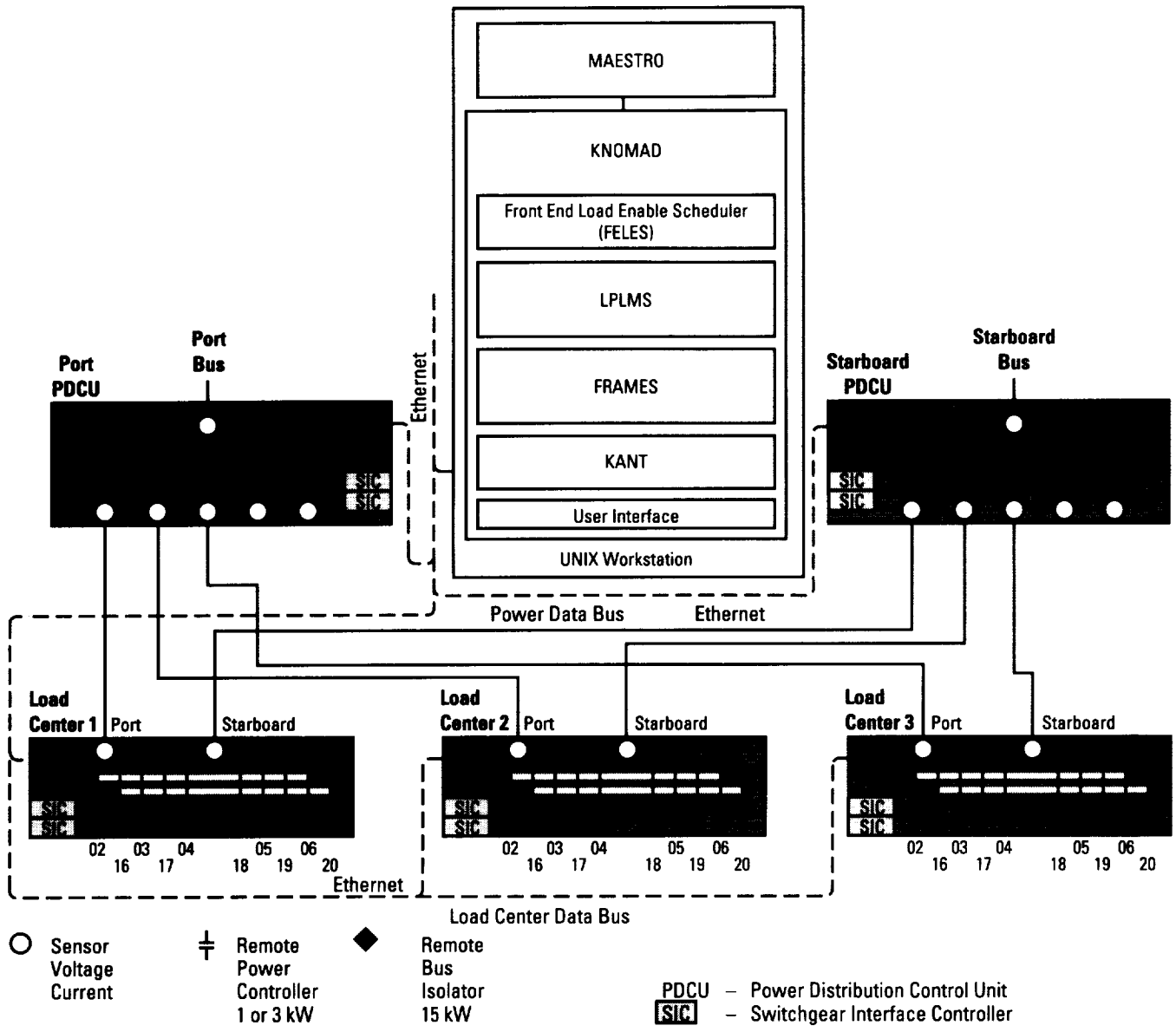

SSM/PMAD system schematic.

Lollar, L.F., "Automating a Spacecraft Electrical Power System Using Expert Systems," NASA Technical Paper 3161, October 1991.

Lollar, L.F., "Knowledge-Based Systems for Power Management," American Institute of Aeronautics and Astronautics (AIAA) Space Programs and Technologies Conference, March 1992.

B. Walls/EB12
205–544–3311

Sponsors: Office of Space Systems Development, Space Station *Freedom* Program, and Office of Aeronautics and Space Technology

Virtual Reality Applications Program

A **virtual reality (VR) applications** program has been under development at MSFC since 1989. Other NASA Centers, most notably Ames Research Center (ARC), have contributed to the development of the **VR**-enabling technologies and **VR** systems. This **VR** technology development has now reached a level of maturity where specific applications of **VR** as a tool can be considered.

The objective of the MSFC **VR applications** program is to develop, assess, validate, and apply **VR** as a **human factors** design and operations analysis tool and to assess and evaluate **VR** as a tool in other applications (e.g., training, operations development, mission support, teleoperations planning, etc.). The long-term goal of this technology program is to enable specialized **human factors** analyses earlier in the hardware and operations development process and to develop more-effective training and mission support systems.

The approach of the **VR applications** program is to develop and validate appropriate **virtual environments** and associated object behavior and dynamics attributes for specific classes of applications. These application-specific environments and associated simulations will be validated, where possible, through empirical comparisons with existing, accepted tools and methodologies. These validated **VR** analytical tools will then be available for use in the design and development of space systems and operations and in training and mission support systems.

Before **VR** can be used with confidence in a particular application, **VR** must be validated for that class of applications. The validation approach is to compare the results from the **VR** analyses or application with a specific past or present analysis, design, and/or actual flight experience.

Phase I applications, utilizing the **VR** system currently in place at MSFC, fall primarily into viewing analyses (including visualization of spatial layouts) and reach envelope analyses. Three studies are planned to begin validating **VR** for these classes of applications. Subsequent phases progress towards "real world" applications. These later phases still contain a real-world counterpart to enable some level of validation.

The first study will use the Spacelab Payload Operations Control Center (POCC) and a Virtual POCC (VPOCC). Test scenarios will be performed in both and their results will be compared to ascertain what, if any, distortions arise in a virtual world (VW). The test scenarios will focus on what one can see from a variety of eye reference points and on what one can touch from a variety of shoulder reference points. The latter will include a range of real and virtual anthropometric sizes.

A second phase I **VR** validation study involves a proposed redesign of the crew interface coordinator (CIC) console. In this study, viewing and reach envelope analyses will be conducted on both a Fomecor and virtual operational mock-up of the CIC console. Results of these analyses will then be compared to determine the relative merits of **VR** vis-á-vis, an existing, "standard" human factor tool.

A third study will revisit a **human factors** concern identified with the Electromagnetic Containerless Processing Facility (TEMPUS), an experiment to fly on the Second International Microgravity Laboratory (IML-2) Spacelab mission. IML-2 is currently scheduled to fly in June 1994.

The issue was whether a crewmember could adequately control the position of the sample in the facility with controls located in the right half of rack 10 while monitoring the results of a cathode ray tube (CRT) in the right half of rack 8. A full-scale part-task Fomecor mock-up of both racks was fabricated to determine the crewmembers' abilities to view the CRT while touching the controls. A virtual mock-up of racks 8 and 10 will be developed and placed inside of a virtual Spacelab module. Viewing and reach envelope analyses will then be conducted and the results will be compared to the previously conducted Fomecor study.

Future studies and applications being proposed include applications related to initial Spacelab crew and POCC cadre training, late Spacelab stowage configuration training, and Space Station *Freedom* (S.S. *Freedom*) Payload Operations Integration Center (POIC) design.

J.P. Hale II/EO23
205-544-2193
Sponsors: Space Station *Freedom* Program,
Center Director's Discretionary Fund,
Summer Faculty Fellowship Program, and
Engineering Technical Base (Institutional)

Materials and Manufacturing Processes

Advanced Sprayable Ablator for Solid Rocket Booster Nonmotor Segments

The evolution of the ideal material for insulating broad metallic acreages of the space shuttle's solid rocket boosters (SRB's) is advancing through an ambitious program to develop the third generation in the family of formulations called the Marshall sprayable **ablator** (MSA). In response to the approaching phaseout by the **Environmental Protection Agency (EPA)** of **ozone**-depleting solvents and carcinogenic **chlorinated hydrocarbons**, United Space Boosters, Inc. (USBI), materials engineers associated with the MSFC Materials and Processes Laboratory are pursuing an innovative **water-based formulation**. The development of water-based MSA–3 will resolve current dependency on MSA–2, which uses the **chlorinated solvents** methylene chloride and perchloroethylene.

With a base of water-dispersible resin, surfactant, defoamer, and fillers, such as particulated cork and glass, MSA–3 represents a decided shift in technical emphasis. Like its MSA predecessors, MSA–3 incorporates diverse solids, adhesives, and an emulsifying liquid into a slurry that can be air-atomized onto a painted aluminum surface. After cure and weatherizing, the **ablator** must retain sufficient physical and ablative properties throughout low atmospheric launch. The critical challenge in converting the **ablator** from a chlorinated solvent to a water medium lies in stabilization of the emulsion, adhesive wetting of the interfacing application surfaces, and removal of the water following application to gain cure strength.

An early formula demonstrated that water could indeed function as the solids emulsifier and carrier solution and that bond strengths similar to MSA–2 were possible, but at 3 to 4 mm (nominal 1/8-in) sprayed thickness would be limited to low-heat regions of the booster. The subsequent design phase located the water-dispersible glass fibers that add material strength (and increased thickness); fibers of the same dimensions as those in MSA–2 were obtained for performance similarity. Lab comparisons then isolated an epoxy resin with adhesive strength higher than that used in MSA–2, an asset for material bond and char integrity.

Averaging three sprays each week in the sprayable **ablator** research cell at the Marshall Productivity Enhancement Complex, 1992 work on formula design is optimizing the baseline to produce the 6- to 13-mm (1/4-in to 1/2-in) layers needed for booster protection. A recent variation has already produced a sprayed MSA–3 layer 360 mils thick (9.1 mm (slightly above 1/3 in)) that exhibited physical properties comparable to the MSA–2 being flown. Preliminary thermal verification, which subjects a candidate to simulated booster environments, is planned in the last quarter of 1992, when laboratory qualification begins for the emergent formulation. Physical and mechanical qualification testing will include a process sensitivity study to establish the production tolerances for mixing, applying, curing, and repairing the optimum material on an actual flight structure. After final verification at Marshall simulation facilities, MSA–3 will be poised for certification and transition into the assembly and refurbishment spray cells, where production validation will occur.

Although MSA–3 is an innovation in material design, it will function very much like the highly successful MSA–2. The economical and time-saving advantages of a sprayable **ablator** transformed the concept of booster **insulation** by displacing the tedious and costly handfitting of bondable sheet cork throughout the curved acreage surfaces.

In bringing along MSA–3, the Productivity Enhancement Complex at MSFC is fulfilling its mission as one of the Nation's preeminent research centers. Considering the tightening regulations against **ozone**-depleting and carcinogenic solvents, the succession of MSA–3 into the space shuttle arena will be timely. As an environmentally compliant aerospace material, water-based MSA–3 will be available for other launch programs and, for the Nation at large, will affirm the industrial feasibility of relinquishing the solvenated technology that continues to pose an environmental hazard.

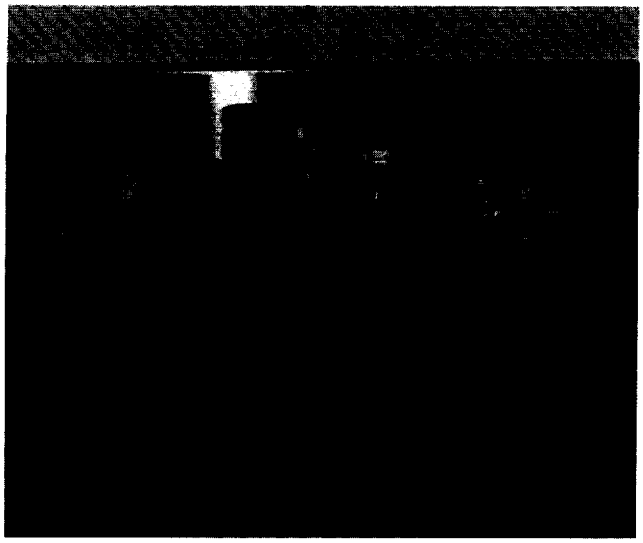

The evolution of MSA to an environmentally compliant formulation.

C.N. Lester/EH43
205–544–4804
Sponsor: Solid Rocket Booster Project Office

An Enhanced Whipple Bumper System

Manned spacecraft missions that require extended lifetimes in low Earth orbit (LEO), such as Space Station *Freedom* (S.S. *Freedom*), are more susceptible to major damage from collisions with **orbital debris**. The present baseline design of the S.S. *Freedom* module meteoroid/debris (M/D) shield system can prevent penetration of aluminum debris on the order of 0.64 cm (0.24 in) in diameter and smaller, dependent upon collision velocities and angles. To improve protection for **orbital debris** greater than 0.6 cm, tests were initiated to evaluate materials that could enhance or augment the existing M/D shield design. The **augmented material** test program was undertaken in five phases with phase I having been conducted this past year.

All phase I tests were performed at the Space Debris Impact Facility utilizing a two-stage light gas gun (LGG) firing spherical aluminum projectiles. All tests were performed with a 0.92-cm (0.375-in) diameter projectile impacting the target at 6.2 km/s (20,341 ft/s). The target configuration consisted of a 0.16-cm (0.063-in) thick 6061–T6 aluminum shield placed 10.16 cm (4 in) ahead of a 0.3175-cm (0.125-in) thick rear wall panel. The materials being tested were placed halfway between the shield and the rear wall. For comparison, all test samples were of areal densities equivalent to either a 0.16-cm (0.063-in) or a 0.3175-cm (0.125-in) thick aluminum panel.

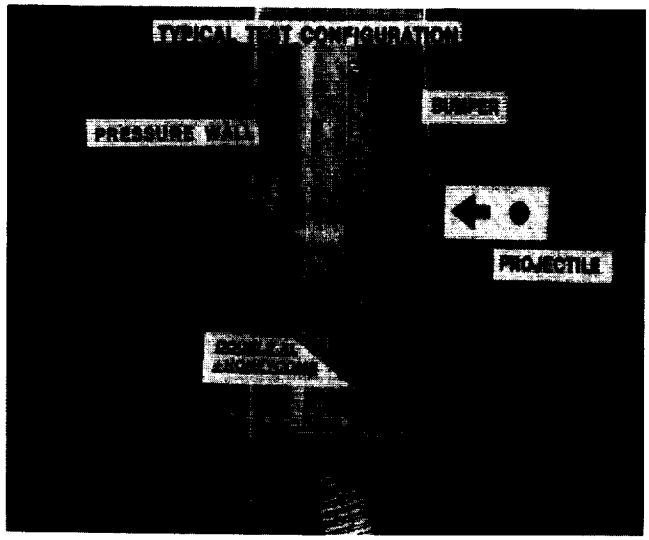

M/D augmented bumper material study typical test configuration.

In a typical test configuration, the projectile impacts the shield and is broken up. The resulting **debris cloud** then impacts the test sample located halfway between the shield and the rear wall. The **debris cloud** continues on and impacts the rear wall. Since the **debris cloud** encounters the test sample prior to the rear wall, the pressure exerted on the rear wall should be reduced. Should there be a penetration of the rear wall, there are witness plates behind it to provide a rough indication of the magnitude of penetration. After each test, the rear wall was examined to see if penetration occurred. If penetration of the rear wall did not occur, a depth profile in the x and y direction was taken of the rear wall panel. The materials that performed best under these impact conditions were the Spectra-Krayton honeycomb composites for a 0.3175-cm (0.125-in) equivalent density and the Kevlar cloth blanket for a 0.16-cm (0.063-in) equivalent areal density.

The most promising materials from phase I testing will be further evaluated in subsequent phases. Future plans will be at lower velocities, with larger projectiles, and at various impact angles.

A. Nolen/EH15
205–544–9245
Sponsor: Space Station *Freedom* Project Office

Test materials and results

Material	Configuration	Max. Depth 0.16-cm Equivalent	Max. Depth 0.3175-cm Equivalent
6061 aluminum	Single-sheet	PEN *	PEN
	Double-sheet	PEN	13.9 cm
6061 aluminum/Nomex honeycomb composite	Al-Nomex-Al	12.5 cm	PEN
Composite sandwich structure with Nomex phenolic core	Face Sheets:		
	Kevlar epoxy	PEN	9.05 cm
	Spectra epoxy	PEN	Not tested
	Spectra Krayton	12.76 cm	6.65 cm
	Spectra/Kevlar	PEN	9.53 cm
Fiber blankets	Kevlar	10.16 cm	7.12 cm
	Nextel	PEN	7.79 cm

*PEN refers to cases where penetration of the rear wall occurred.

Carbon Phenolic Constituent Test Methodology and Specifications

Foreign competition in the aerospace industry and a continual need to improve reliability is forcing American industry to rethink the traditionally closed private industry competitive process. Private industry competition has promoted lower proposal costs; but the domestic aerospace industry has also been slow to incorporate new technology. NASA/MSFC has exhibited the leadership necessary to provide private industry with a forum to address **test methodology** and specification issues on a noncompetitive basis. A particular problem is that the cost of developing new analytical tests for the aerospace industry can far exceed most corporate budgets. By working with private industry, NASA/MSFC has exposed major suppliers to new technology while receiving valuable responses.

To improve the reproducibility, reliability, and uniformity of solid rocket motor (SRM) **nozzles**, a NASA-sponsored solid propulsion integrity program (SPIP) has established an industry **advisory committee** to improve **test methodology** on carbon phenolic **constituent materials**, prepreg, and cured materials. The industry **advisory committee** is a voluntary group that is represented by domestic aerospace material suppliers, fabricators, and designing organizations. The committee has met biannually since 1988 to improve the performance of American-manufactured SRM **nozzles**.

The ninth committee meeting was recently held on May 14 and 15, 1992, in New Orleans, LA, with a record 51 participants.

The eighth and ninth meetings were preceeded by a joint SPIP/advanced SRM (ASRM) conference to address common specification and **test methodology** issues. The ASRM program has followed the work of the industry **advisory committee** and is currently using many of the test method recommendations.

An example of the committee activity relevancy was the adoption of a new test method to assess the oxidation sensitivity of candidate carbon fiber for the ASRM improved ablatives program. Lot 01551 carbon yarn was manufactured for the ASRM program and was certified acceptable by all conventional test methods. The final acceptance test performed was for oxidation sensitivity, using the committee-developed SPIP–3 procedure. This technique uses a conventional Perkin Elmer thermal gravimetric analysis (TGA) apparatus to measure isothermal thermal mass loss rates in air at five temperatures. The rates are subsequently semi-log cross-plotted against 1/T (where T = temperature) to assess compliance to the Arrhenius equation.

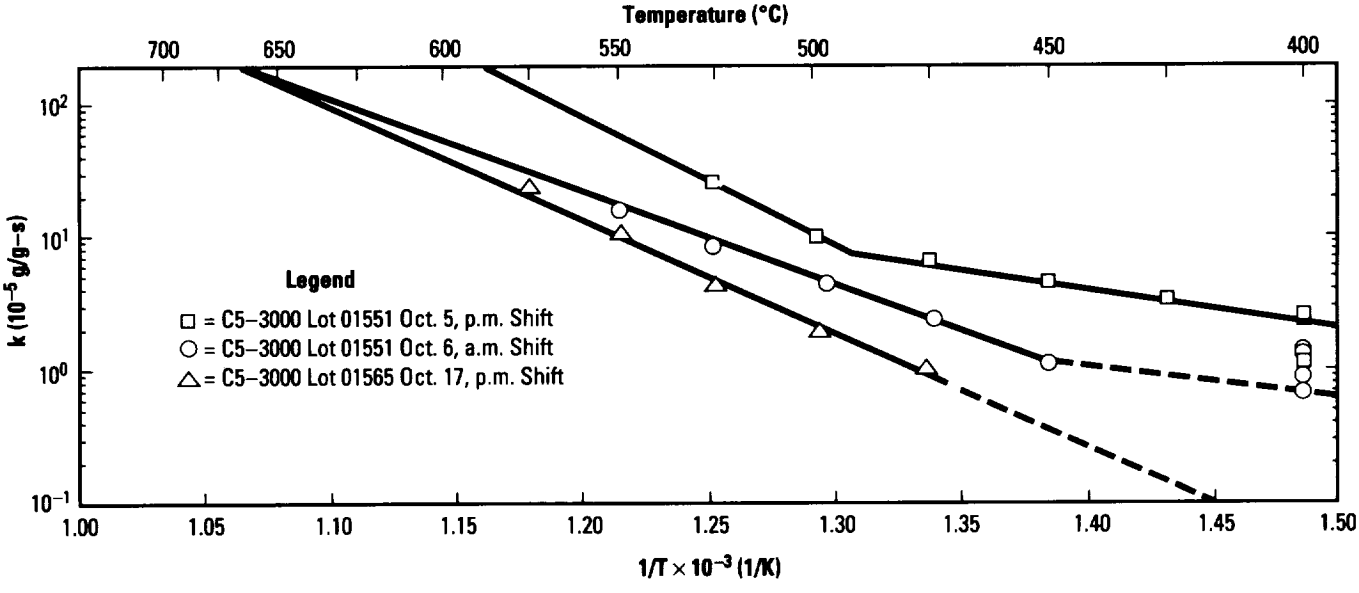

ASRM improved ablative material program.

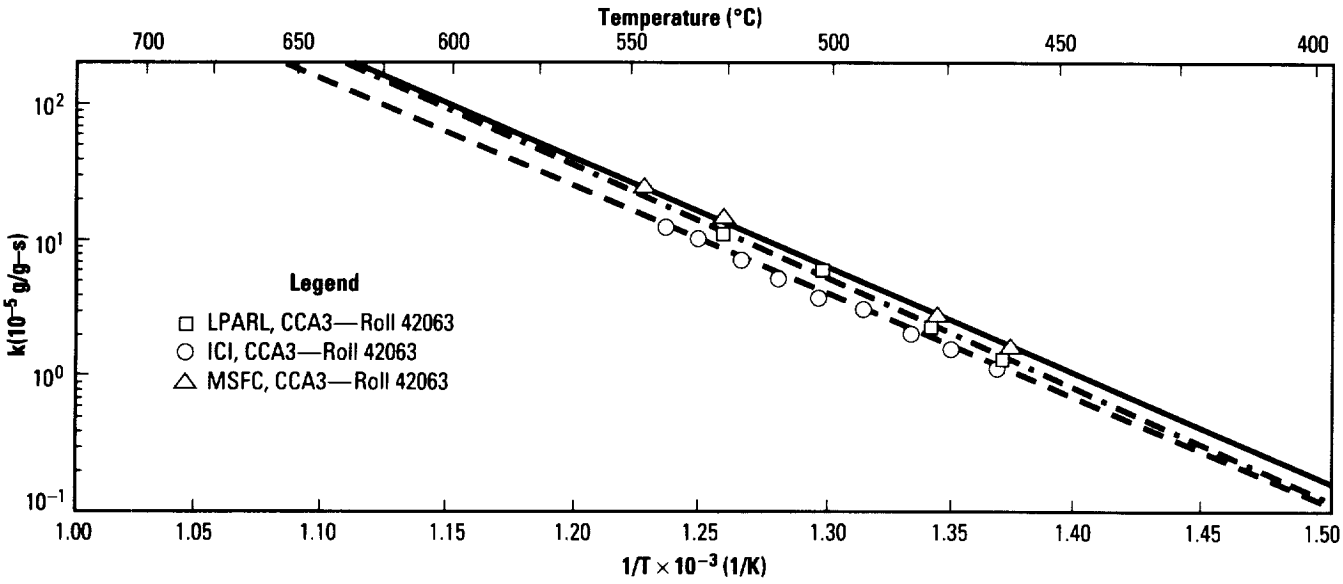

Testing carbon fabric for oxidation mass loss.

Lot 01565, manufactured October 17, 1991, in the evening shift, is included to demonstrate the desired oxidation rate versus temperature sensitivity. The initial lot 01551 yarn, produced October 5, 1991, shows a definite "knee" in the relationship at approximately 500 °C (932 °F). At the end of the production run October 6, 1991, the "knee" had shifted to approximately 450 °C (842 °F). The end of the run sample also exhibited a significantly higher oxidation resistance. Using these two indications of unacceptable oxidation resistance, further samples of yarn were run at 400 °C (752 °F) only. The industry **advisory committee** had previously demonstrated that catalytic action by sodium (Na) contamination would induce a "knee" in the relationship. Subsequent testing for residual Na confirmed the presence of excess Na. The vendor subsequently confirmed the presence of excess Na and identified improper process controls, which caused the problem. Corrective action was taken by the vendor and the poor quality yarn did not impact the program objectives.

With NASA leadership, the industry **advisory committee** is committed to the advancement of American-manufactured SRM **nozzles** through improved **test methodology** and specifications.

Testing carbon fabric for oxidation mass loss

Effect of Na on Oxidation Rate of Exp. 108 Fabric		
Temperature (°C)	A.R.* Air Oxidation Rate (g/g–s)	Influence of Na (% Rate Increase)
500	24.4×10^{-5}	102
475	16.5×10^{-5}	194
450	9.09×10^{-5}	258
425	5.61×10^{-5}	415
400	3.40×10^{-5}	681

*As received

C. Upton/EH34
205–544–5755
Sponsor: Office of Space Flight

Castable Aluminum and Magnesium Matrix Composites for Space Structural Application

Graphite-magnesium and **graphite-aluminum** are valuable **metal matrix composite** (**MMC**) materials for space structural components such as mechanical joints and connecting mechanisms. These typical **MMC** materials provide very high specific strength and stiffness properties with a near-zero coefficient of thermal expansion. They also have excellent resistance to long-term exposure effects in a space environment. Despite the many technological breakthroughs during the last 2 decades, such **MMC** products are still prohibitively expensive for most applications. This problem has recently driven the **MMC** component development toward various inexpensive casting processes when compared with **MMC** components produced by traditional methods such as powder metallurgy, thermal arc plasma spray, and diffusion bonding. This research effort aims to develop innovations directed toward castable aluminum and magnesium composite methods in which typical defect-free **MMC** components can be cast with near-net-shape dimensional tolerance and to provide high production rate capabilities at low cost and with less labor. Castable **MMC** methods must be able to produce very complex-shaped structural components.

In January 1992, Foster-Miller, Inc., was awarded a 6-mo phase I Small Business Innovative Research (SBIR) contract with MSFC through the Materials and Processes Laboratory to perform this research effort (contract NAS8–39319). Phase I of this contract is under way to demonstrate the feasibility of producing a typical space joint component. A complex-shaped joint component will be selected, fabricated, and evaluated during this phase. Several candidate components were considered in the trade-off analysis task and a typical clevis tube end-fitting joint component design was selected to be cast. This joint component will also incorporate strategically placed metallic inserts that will enable efficient load transfer across the joint component. The casting process will be optimized to demonstrate repeatability in component mechanical properties during the follow-on SBIR phase II effort.

Rohatgi, P., "Advances in Cast MMC's," *Advanced Materials and Processes*, February 1990, p. 39.

Hammond, D., "Castable Composites Target New Applications," *Modern Casting*, September 1990, p. 27.

J.A. Lee/EH23
205–544–9290
Sponsor: Office of Commercial Programs,
Small Business Innovative Research Program

Composite Materials Research Using Design of Experiments

The Materials and Processes Laboratory at MFSC has been heavily involved in research of **damage tolerance** of **composite materials**. The typical test matrix has consisted of holding all but one independent variable (e.g., impact energy) constant and determining the dependent variable (usually compression-after-impact (CAI) strength) as a function of only the one changing independent variable. The examination of multiple independent variables on a dependent variable became costly and time-consuming since many tests had to be performed. In addition, if two of the independent variables had an interaction effect on the dependent variable, this would go unnoticed and would probably be interpreted as "experimental scatter." For example, if the specimen thickness was the independent variable, the size of the impactor (as well as all other controllable variables) would be held constant while only the specimen thickness was varied, but it may be possible that thin samples are much more susceptible to damage when hit with a small impactor than with a larger one. Unless various-size impactors were also changed along with the specimen thickness, this interaction effect would go unnoticed.

Using advanced experimental design or **design of experiments (DOE's)** techniques, less testing needs to be performed to gather important information about the effect of selected variables, and interactions of these variables, on a dependent variable. The most often used technique for **damage tolerance** research is the Box-Behnken[1] three-level design. This design allows three independent variables to be tested at three levels or settings (referred to as low, medium, and high settings). All combinations of variables need not be tested when utilizing this technique. Only 13 tests are run. Two further duplicates of the test during which all variables are at the medium setting are performed to test for repeatability in the dependent variable.

The levels used for the three variables are –1, which represents the low setting; 0, which indicates the medium setting; and +1, which represents the high setting. An example of actual values used in an impact **damage tolerance** screening of candidate toughened carbon/epoxy systems identified for possible use on Space Station *Freedom* is impact energy, where –1=4 J, 0=8 J, and +1=12 J. CAI strength is the dependent variable in these tests.

Box-Behnken three-level design

Test Number	Variable X_1	Variable X_2	Variable X_3
1	+1	+1	0
2	+1	–1	0
3	–1	+1	0
4	–1	–1	0
5	+1	0	+1
6	+1	0	–1
7	–1	0	+1
8	–1	0	–1
9	0	+1	+1
10	0	+1	–1
11	0	–1	+1
12	0	–1	–1
13	0	0	0
14	0	0	0
15	0	0	0

The value of the predicted dependent variable or response can be represented by the following equation:

$$Y = \text{Const.} + AX_1 + BX_2 + CX_3 + A_S X_1^2 + B_S X_2^2 + C_S X_3^2 + A_{ab} X_1 X_2 + B_{ac} X_1 X_3 + C_{bc} X_2 X_3$$

where Y is the dependent variable; A, B, and C are regression coefficients for the linear terms of each X; A_S, B_S, and C_S are coefficients for the quadratic terms of each X; and A_{ab}, B_{ac}, and C_{bc} are coefficients for the corresponding linear interaction terms between the associated X's. The constant appearing in the equation represents the CAI strength when the three independent variables are all set at the medium level. The coefficients help identify the most important variables and interactions. In the example data presented here, the

Actual values used in damage tolerance testing of IM7/977–2 carbon/epoxy

Test Number	Impact Energy (J)	Tup Diameter (mm)	Number of Plies	CAI Strength (MPa)	Predicted CAI Strength (MPa)	Difference (MPa)
1	12	19.0	16	304	292	12
2	12	6.4	16	287	311	–24
3	4	19.0	16	410	386	24
4	4	6.4	16	380	392	–12
5	12	12.7	24	327	328	–1
6	12	12.7	8	276	263	13
7	4	12.7	24	407	420	–13
8	4	12.7	8	349	348	1
9	8	19.0	24	313	324	–11
10	8	19.0	8	212	237	–25
11	8	6.4	24	344	319	25
12	8	6.4	8	278	267	11
13	8	12.7	16	319	317	2
14	8	12.7	16	306	317	–11
15	8	12.7	16	325	317	8

coefficients are: A=–44; B=–6.25; C=34.5; A_S=40.8; B_S=–12.2; C_S=–17.7; A_{ab}=–3.25; B_{ac}=–1.75; C_{bc}=8.75. These numbers show that the impact energy and specimen thickness are the dominant variables, with the response decreasing as impact energy increases, and the response increases for increasing specimen thickness. The interaction terms are relatively small with the top diameter/specimen thickness interaction being the most important for this material system.

Using this advanced experimental design technique, comparisons between various material systems can be made with the relative importance of each independent variable being identified with as little as 15 specimens per material system.

[1]Box, G.E.P., and Behnken, D.W., "Some New Three-Level Designs for the Study of Quantitative Variables," *Technometrics*, 2 (1960), pp. 445–475.

A.T. Nettles/EH33
205–544–2677
Sponsor: Space Station *Freedom* Project Office

Debris Cloud Momentum Distribution During Hypervelocity Impact

The long-term operation of Space Station *Freedom* (S.S. *Freedom*) requires a scheme to protect it from **hypervelocity** impacts by both manmade particles and micrometeoroids. One such scheme is the use of metal plates to serve as shields against such orbital debris. These "bumper" plates, as they are referred to, serve to break up any incident particle and redistribute its momentum over a larger area, thus reducing the penetrating power. Up to the present time, several attempts have been made to measure the momentum of the **debris cloud** by using a ballistic pendulum. Such systems are designed to measure the total momentum produced by the **debris cloud** by catching all the ejecta simultaneously. In an MSFC-funded research study at Auburn University, a system was developed that is capable of measuring the momentum of the **debris cloud** at discrete locations within it. This resulted in the ability to characterize the momentum more thoroughly than previously possible. In addition to providing a method for obtaining **momentum distributions**, the data obtained from the **momentum monitoring system** will measure the total system momentum during **hypervelocity** impact. This is necessary in determining the role played by the bumper in providing protection for space vehicles.

The **momentum monitoring system** consists of a total of six pendulums employed at intervals of 10 degrees beginning with 10 degrees from normal incidence toward one side and ending at 30 degrees and beginning with 15 degrees from normal incidence and ending at 35 degrees on the other side. The pendulum assemblies consisted of an aluminum pendulum bar, impact block, and timing blade. The velocity of each pendulum was determined by movement of its timing blade past an infrared (IR) photo-interrupter diode. The device was tested in the Space Debris Impact Facility utilizing the two-stage light gas gun (LGG). All tests were with 0.635-cm (0.25-in) diameter projectives impacting 6061–T6 aluminum bumper panels that were 0.1016 cm (0.040 in) and 0.2032 cm (0.080 in) thick. The velocities of these initial tests were 6.0 and 7.2 km/s (19,685 and 23,622 ft/s). Four different impact conditions were analyzed with at least two tests at each condition having been made to ensure reproducibility. It is evident from these test calculations that the shield impact process results in a multiplication of the momentum by a factor of approximately 2.3 to 3. This momentum gain does not violate the conservation of momentum since the primary impact also generates backscattered debris, which is not measured in this study. Future work will be done using different projectile materials and sizes and impact velocities to determine the possible effects of material properties and other variables on **momentum distribution**.

LeMaster, P., Mount, A., and Zee, R.H., "Momentum Distribution in Debris Cloud During Hypervelocity Impact," American Institute of Aeronautics and Astronautics (AIAA) Space Programs and Technologies Conference, March 1992.

A. Nolen/EH15
205–544–9245
Sponsor: Space Station *Freedom* Project Office

Development of Low Thermal Conductivity PAN-Based Fibers for SRM Nozzle Applications

The Materials and Processes Laboratory initiated an effort to evaluate low thermal conductivity (LTC) **polyacrylonitrile** (**PAN**)-based **carbon fibers** as potential replacements for the rayon-based **carbon fibers** traditionally used as reinforcement in carbon phenolic **ablative nozzle** material applications. The need for a rayon replacement is driven primarily by supplier instability. Historically, five companies have supplied aerospace-grade carbonizable rayon since 1964. Each has been sole-source, forcing the industry through several expensive requalification programs, including the "restart" of the Avtex facility. Rayon-based carbon phenolics have also exhibited undesirable failure modes including pocketing, ply lift, and wedge-out, which depend on component design. Further, more recent composite materials constructed from Avtex restart and North American Rayon Corporation yarns have exhibited permeability values several orders of magnitude lower than "historical" materials. A **PAN** fiber replacement offers supplier stability, multiple domestic sources, and a greater resistance to the characteristic rayon-based carbon phenolic pore pressure-driven failure modes, based on limited laboratory results and subscale solid rocket motor (SRM) tests. The disadvantages of **PAN**, including high thermal conductivity, increased weight, and lower resistance to delamination (reduced across-ply tensile strength), are being addressed in the subject program and the Solid Propulsion Integrity Program (SPIP) effort on "standard" **PAN**-based **ablatives**.

Results from the first phase of the LTC **PAN** fiber development have been reported elsewhere.[1,2] In summary, the materials demonstrated comparable erosion, lower char depth, and comparable heat-affected depth versus graphite cloth phenolic materials in forty pound charge (FPC) subscale SRM tests. Based on results from phase I, the MSFC nozzle insulation test motor (NITM–2) subscale SRM tests, and results from the SPIP industry workshop on the **PAN** efforts, a second series of FPC motor tests was defined. This test series also includes the modification of the FPC motor **nozzle** for evaluation of exit cone materials. It is emphasized that this second phase marks the unification of the LTC **PAN** and SPIP **PAN** development efforts. New materials have been added to this test plan to provide data necessary to address industry needs. Specific test plan changes and approach drivers are summarized in the following sentences. Textron Specialty Materials produced spun versions of both candidate fibers, Avcarb B–2 and G, for evaluation. BASF revised its processing parameters to meet electrical resistivity goals, which resulted in a viable candidate. Amoco–25 and Hercules LFP–1 candidates have been dropped. There is increased emphasis on LTC materials (based on phase I results and industry response), P–39 phenolic resin performance (based on NITM–2 results), and "off-the-shelf" standard **PAN** fibers, such as Amoco T–300 and Hercules AS–4 (based on industry response).

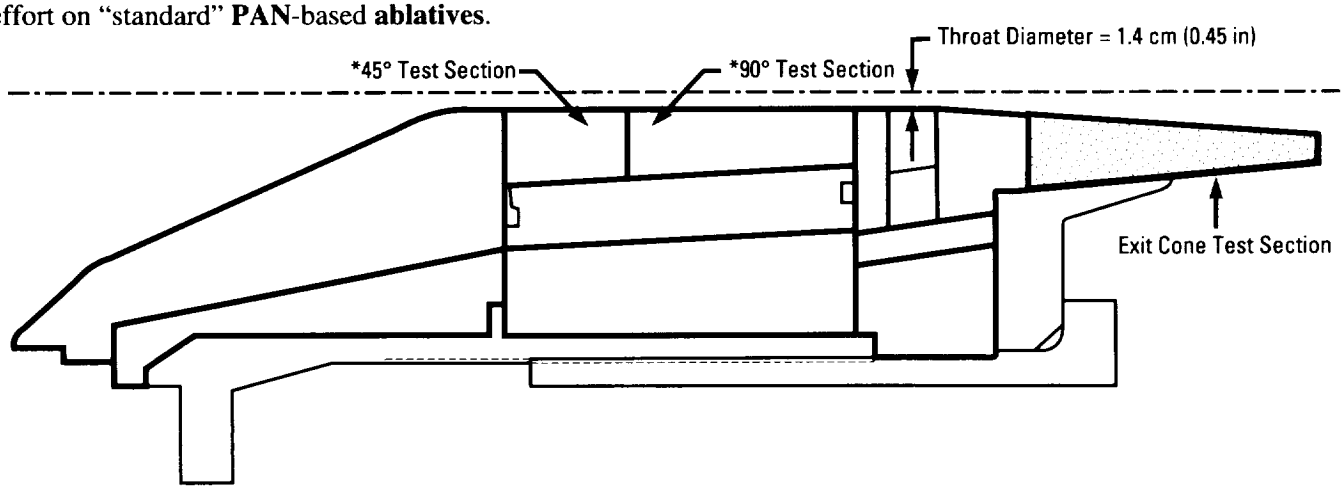

*Indicates Ply Angle to Centerline

FPC motor nozzle cross section with exit cone modification.

Materials for phase II FPC motor tests

LTC PAN's (< 1,000 °C)		
Product Code	Fiber/Fabric	Resin
FM5936	AMOCO–23	91LD
New Product*	Hercules LFP–2	91LD
New Product*	BASF	91LD
New Product*	AVCARB G	91LD
New Product*	AVCARB G Spun	91LD
New Product*	AVCARB B–2	91LD
New Product*	AVCARB B–2 Spun	91LD
New Product*	AMOCO–23	p39
New Product*	LFP–2	p39
New Product*	AMOCO–23	GRF–D1216
Higher Fired "Standard" PAN's		
Product Code	Fiber/Fabric	Resin
FM5928	HITEX 6K (1,650 °C)	p39
MX4904	AVCARB Spun (1,650 °C)	SC1008
New Product*	AS4 6K (1,250 °C)	p39
New Product*	T300 (1,300–1,500 °C)	91LD
FM5796	T300 (1,300–1,500 °C)	p39
New Product*	VCX–15 (1,650 °C)	p39
New Product*	VCX–15 (1,650 °C)	91LD
MX4933**	T300 (2,300 °C)	SC1008 (Modified)
MX4934**	T300 (2,300 °C)	GRF–D1216
MX4952	T350/35XLD Spun (1,650 °C+)	SC1008
MX4963	T350/35XLD Spun (1,650 °C+)	FF26
New Product*	VCX–14 (1,650 °C+)	p39
MX4972	VCX–14 (1,650 °C+)	SC1008

* Product code is not available.
** Materials were combined in a single nozzle test.

To date, 14 FPC motor tests have been conducted, providing data for the evaluation of 15 materials; one **nozzle** had two materials. The propellant formulation for all motors is 88/20 hydroxyl terminated polybutadiene (HTPB), with a typical burn time of 30 s. Results to date indicate that of the previously listed **PAN** disadvantages; high thermal conductivity and delamination sensitivity[3] can be reduced to a level comparable with rayon-based composites. Although some promise has been demonstrated in weight reduction, especially projected at the system level, significant improvements are beyond program scope. Complete phase II results, including mechanical and thermal properties and performance data, will be reported in 1993.

[1]Clinton, R.G., Jr., "Development of Low Thermal Conductivity PAN-Based Fibers for SRM Nozzle Application," *Research and Technology 1991, Annual Report of the Marshall Space Flight Center*, NASA/MSFC, AL.

[2]Clinton, R.G., Jr., Pinoli, P.C., and Canfield, A.R., "Development of Low Thermal Conductivity PAN-Based Fibers for Solid Rocket Nozzle Application," Joint Army, Navy, NASA, and Air Force (JANNAF) Rocket Nozzle Technology Subcommittee (RNTS), Pasadena, CA, October 1990.

[3]Hoover, C.B., Dunkin, M.B., Poteat, R.M., and Koenig, J.R., "Screening Characterization of Two Amoco Low-Fired PAN Carbon Phenolics and UGT Post-Test of Low-Fired PAN, NARC, and Avtex Rayon-Based Carbon Phenolics," BMO–TR–91–22, Headquarters Ballistic Missile Organization, Norton Air Force Base (AFB), CA, January 1992.

R.G. Clinton, Jr./EH34
205–544–2682
Sponsor: Office of Space Systems Development

Enhanced Aerospace Insulation Systems

A laboratory dedicated to the development of aerospace-specific **insulation** materials was activated in late 1991 that will enable NASA to reduce its reliance on low-volume commercial **insulations** that are being phased out of production. It will also provide more timely response to regulatory and market impacts.

The initial efforts of this laboratory were directed at the development of foam **insulation** materials for the space shuttle external tank (ET) with enhanced properties over currently used **insulation**. Four such candidates were successfully developed:

- 1RP185, thermally stable, reaction injection moldable formulation
- 1HP184, hand-pourable **cryogenic** and high-heat closeout formulation
- 2HP168, high-temperature composite tooling formulation
- 1SPI16, high-temperature sprayable **insulation**.

These candidate systems provide alternate/backup material candidates to reduce the ET's reliance on sole-source commercial materials that are being phased out of production and are currently under review for potential flight qualification and commercial applications.

Current efforts of this laboratory are in the development of **cryogenic insulation** systems for the space shuttle ET that incorporate low- to zero-**ozone** depletion potential (ODP) **blowing agents**. All of the currently used ET **cryogenic insulations** use **chlorofluorocarbon** 11 (CFC 11) as a **blowing agent**. **Chlorofluorocarbons** have been implicated as a major contributor to stratospheric **ozone** depletion and are being phased out by all major industrialized nations. For this reason, research efforts are now directed toward the development of low ODP, second-generation **blowing agents** as a short-term solution, and zero ODP, third-generation **blowing agents** as the ultimate solution. The low ODP **blowing agent** hydrochlorofluorocarbon 141b (HCFC 141b) has been identified as the optimum interim **blowing agent** for ET **insulations**. This material will be used in these **insulations**, beginning in 1995, until zero ODP **blowing agents** can be sufficiently developed. Work is continuing on the development of zero ODP, third-generation **blowing agents**. Current efforts are investigating hydrocarbons, fluorinated hydrocarbons, fluorinated ethers, carbon dioxide (CO_2) (produced from water-isocyanate reaction), and gas injection as possible candidates.

E.A. Weaver/EH43
205–544–3466
Sponsor: Office of Space Flight

External Tank Process Development Advisor: Information Management for Process Development and Control

The process development advisor (PDA) tool for the spray-on foam insulation (SOFI) is being developed to work in **real time**. Several software components are being developed on MicroVax computers using G2 software from the Gensym Corporation. The PDA software incorporates the **real-time expert system**, the monitor control, and the occurrence of variable speed pumping system ratio control.

Three major modules of the software component have been completed. First, the design of the schematics of the isocyanate and polyol circulation system, the hydraulic system, the heat exchanger system, and the spray head assembly have been modeled. These schematics enable the operator or programmer to monitor flows, valves, and an overall operation of the pumping system during a simulated test or production run. The bridge code interface sends and receives data across the Allen Bradley data highway that communicate with the Allen Bradley programmable logical control (PLC). The PLC controls the spray head and the variable-speed pumping system, which monitors the density of the two SOFI compounds—isocyanate and polyol.

Second, the objects, rules, procedures, displays, and simulation rules have been reorganized. The programmer has the ability to document and make changes to the knowledge base much easier and faster. The following eight pump attributes are monitored: (1) tank pressures, (2) filter inlet, (3) filter outlet, (4) pump suction input, (5) pump suction output, (6) system outlet, (7) system flow output, and (8) system flow output ratio. The PDA operator interface provides an intelligent control panel for the operator, schematic and graphic displays of the process operation, and mechanisms for textual and graphic interaction in the event of faults.

Third, the G2 diagnostic assistant (GDA) software from Gensym Corporation has been implemented. The GDA software supports the development of diagnostic applications that provide the **real-time** monitoring, information, root cause analysis, and intervention that minimize malfunctions. The GDA software also permits statistical process control that is used to detect trends such as a shift in the mean, a change in the variance, or both, which can be used to detect and diagnose process faults before becoming critical.

The PDA combines **symbolic computing** with **numerical computing** to control the isocyanate and polyol circulation systems. **Numerical computing** consists of demonstrate process and reduction, simulations and quantitative models, statistics and probability, and numerical algorithms; its application covers algorithmically tractable problems. **Symbolic computing** consists of data interpretation, nondeterministic and qualitative models, search and heuristic, and robust solution strategies; its applications cover algorithmically intractable problems. These computing concepts provide both **numerical computing** and **symbolic computing** in coupled systems.

M. Day/EH43
205-544-1899
Sponsor: Office of Space Flight

External Tank Spray-On Foam Insulation Kinematic Simulation System

The external tank (ET) **spray-on foam** insulation (SOFI) research cell in the Productivity Enhancement Complex is utilized to support development and qualification of environmentally compliant SOFI materials and the application process.

A three-dimensional (3–D) **graphic simulation** of the ET aft dome work cell was created using a software package called the **Interactive Graphics Robotic Instructional Program (IGRIP)** by Deneb Robotics, Inc. The **IGRIP** software runs on a multiprocessor Silicon Graphics 4D–240GTX workstation with a 1,280×1,024 pixels per inch high-resolution color monitor. The NASA/Martin Marietta-designed simulation contains solid models of the new General Motors/Fanuc (GMF) S–420 articulated **robot** manipulating a variable output spray head and an aft dome cap mounted on a new vertical turntable.

The models were manipulated within the work cell and tested against the **robot's** work envelope to determine the optimum placement of the SOFI equipment within the work cell. This eliminated the need to reposition the heavy equipment once it had been placed in the SOFI work cell because the first position was not satisfactory. The data were given to SOFI personnel who began preparing the work cell for operation, uninterrupted by the **robot** programming being generated **off-line** with the **IGRIP** software. The simulation that graphically represents the motions of the **robot** was used to check for **robot** joint overtravels and collisions with other devices within the work cell.

The finished **robot** program was **downloaded** to the GMF KAREL controller via an RS–232 fiber-optic link. The file was translated at the controller into a **robot** machine code file, tested, and put into operation.

The simulation and the state-of-the-art Silicon Graphics equipment are used to increase the productivity and efficiency of the SOFI work cell. Material waste and downtime are reduced due to reduced errors and increased safety. This results in a cost savings to the work cell and NASA.

M. Day/EH43
205–544–1899
Sponsor: Office of Space Flight

Facility for Investigating Combined Space Environmental Effects

Development of an improved facility to simulate combined **space environmental effects** has long been a goal for MSFC's Materials and Processes Laboratory. The **Space Environmental Effects** Facility (SEEF) has been developed to fulfill this goal. The SEEF houses several systems dedicated to simulation of the space environment. Samples can be exposed to energetic **protons, electrons, ultraviolet (UV) radiation,** thermal cycling, and high vacuum. The SEEF offers the unique capability to perform simultaneous exposures to many of these effects as well as in-situ analysis.

The combined environmental effects test cell 2 (CEETC2) system provides energetic **protons** over the range from 0.5 to 2.5 MeV and **electrons** from 0.1 to 0.4 MeV. This system operates at a base pressure of 5×10^{-6} torr. Beam currents are measured by a series of in-line Faraday cups and beam shape is determined by beam profile monitors (BPM's). Present in-situ analysis capabilities include proton-induced x-ray emission (PIXE) and Rutherford backscattering spectrometry (RBS).

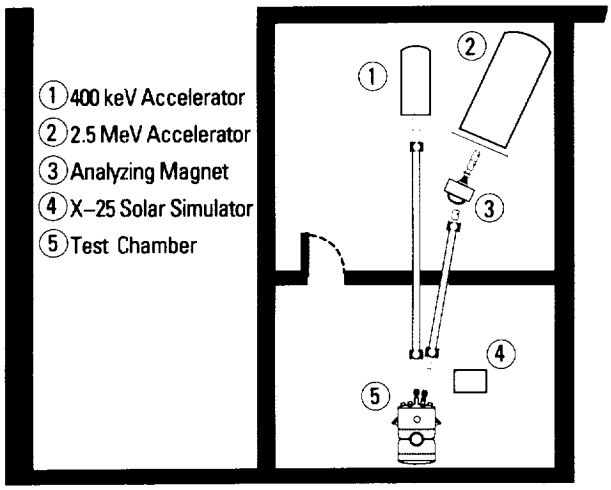

Combined environmental effects test cell 2 (CEETC2).

The combined environmental effects test cell 3 (CEETC3) system generates energetic **protons** over the range from 0.1 to 0.8 MeV and **electrons** from 0.5 to 2.5 MeV. Similar to the CEETC2 system, the beam currents are measured using Faraday cups and the beam size is measured using BPM's. The test chamber will include the capability to perform in-situ optical **reflectance** over the range of 250 nm (9.7×10^{-6} in) to 2,500 nm (9.7×10^{-5} in). Both of these systems have the capability to expose samples to **UV radiation** from 200 nm (7.8×10^{-6} in) to 1,800 nm (7×10^{-5} in) and thermal cycling over a range of temperatures.

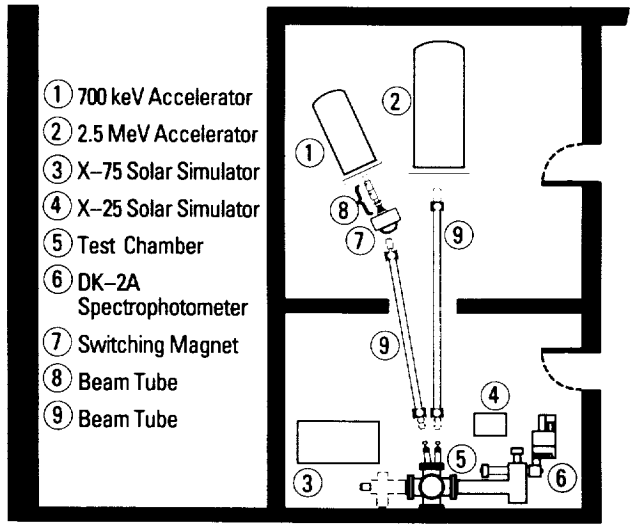

Combined environmental effects test cell 3 (CEETC3).

D.L. Edwards/EH15
205-544-4081
Sponsor: Space Station *Freedom* Project Office

Fiber Placement: New Technology for Automated Composite Manufacturing

Automated fiber placement is a **manufacturing process** used for producing complex **composite** structures. It represents a significant advancement in the state-of-the-art for automated **composite manufacturing**. Fiber placement capability was established at MSFC's Productivity Enhancement Complex in 1992, in collaboration with Thiokol Corporation.

Fiber placement was developed as a distinct solution to problems inherent to other automated **composite manufacturing** systems. This equipment provides unique capabilities to build **composite** parts in complex three-dimensional (3–D) shapes with concave and other asymmetrical configurations. Components with complex geometries and localized reinforcements usually require expensive manual effort; the fiber placement system has the features necessary to overcome these conditions. The mechanical systems of the equipment have the motion characteristics of a filament winder and the fiber layup attributes of a tape-laying machine, with the additional capabilities of different tow payout speeds, compaction, and cut-restart to selectively place the correct number of fibers where the design dictates.

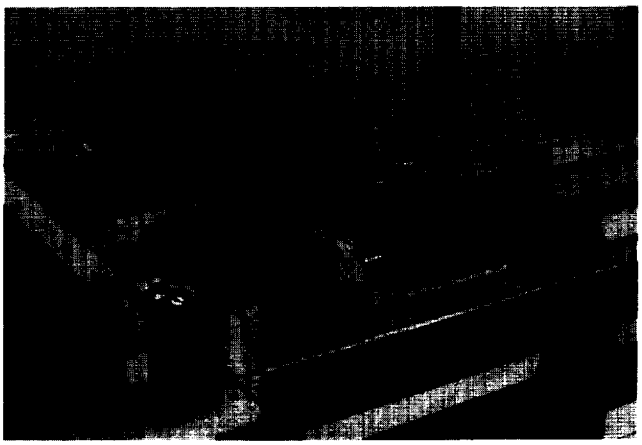

Equipment used in the automated composite manufacturing process.

J.H. Vickers/EH44
205–544–3581
Sponsor: Office of Space Transportation Systems

Foam Applications Development

The development and testing of the **variable output** pumping system (VOPS) and a multinozzle turret spray head for the **spray-on foam insulation (SOFI)** used on the external tank (ET) have been completed. This development was part of the advanced technologies effort for **urethane** processing in ET **SOFI** applications. This spray system was specifically designed to address the processing and reliability problems of current **SOFI** applications. The capabilities of the system for automatic volumetric calibration, diagnostic, flow, and function testing specifically address abort and reliability issues of the current proportioning system used in ET production operations.

A **variable output SOFI** process was developed and tested during fiscal year 1991 (FY91) using the VOPS/multinozzle spray system to provide real-time precision ratio and **variable output** control of specific **SOFI** components. A **variable output** spray process was designed to improve the thickness and density control of specific **SOFI** applications on the shaped surfaces of the ET aft dome and forward ogive. The **variable output** spray process tests were conducted over a wide range of application rates and rate changes that demonstrated significant improvements for surface finish, density, and thickness control on liquid hydrogen (LH_2) tank barrel simulations and liquid oxygen (lox) forward ogive simulations. Process variability was significantly reduced over fixed output spray methods currently used in ET production operations. Frequently occurring **SOFI** manufacturing problems, such as low-density material, rollover, and waviness, were shown to be totally avoided by the **variable output** process enhancements tested.

The **variable output** processes and equipment are now being implemented in ET production operations.

E.A. Weaver/EH43
205–544–3466
Sponsor: Office of Space Flight

Fully Automated Variable Polarity Plasma Arc Welding

Computer-controlled variable polarity plasma arc (VPPA) **welding** has been used in the production of the space shuttle external tank (ET) since 1983. This **welding** system provides control of the critical **welding** parameters in addition to providing historical documentation of programmed and actual **welding** parameters for all welds. The **welding** operator, however, is still responsible for providing real-time adjustment to weld current, seamtracking, wire feed entry, and plasma jet orientation. Therefore, the quality and repeatability of VPPA welds are still dependent on human judgement and skill.

MSFC has undertaken the design and development of the Marshall **automated** weld system (MAWS) to eliminate the possibility of weld defects caused by human error. The system integrates multiple **sensors** (providing real-time information on weld bead geometry, weld joint location, and wire feed entry) with a weld model (describing weld geometry in relation to critical parameters) and computer-controlled VPPA equipment. This system will provide real-time, closed-loop control of the weld as it is being made. A secondary benefit of this system is the potential of **automated** weld inspection, either during or after **welding**, of weld width, peaking, and mismatch for quality assurance.

Presently, design and development of each individual component of the overall system are in progress. The **welding** control computer has been defined to a "real-time" UNIX-based **controller** able to integrate processing many sensors and axes of coordinated motion. Second- and third-generation **sensors** based on stereo imaging and multiple light sources are being developed for seamtracking. The second-generation seamtracker is an industrially packaged, scaled-down version with improved lighting over the previous design, and it has been trial-tested on the shuttle ET weld tool fixtures.

NASA's checkout and testing of the second-generation **sensors** identified the need for computer-controllable apertures in the seamtracker's charge coupled device (CCD) cameras and confirmed the need for the **sensors** to take images at the weld pool. The third-generation seamtracker, which is being developed under a research contract, processes information taken directly from the weld pool. Prototype **sensors** and a special VME computer board set to directly interface with the UNIX-based **controller** have been completed; delivery and NASA checkout are forthcoming this year. A second-generation optical laser sensor has been fabricated for weld bead profiling and torch rotation. This smaller packaged sensor will eliminate some of the time delays

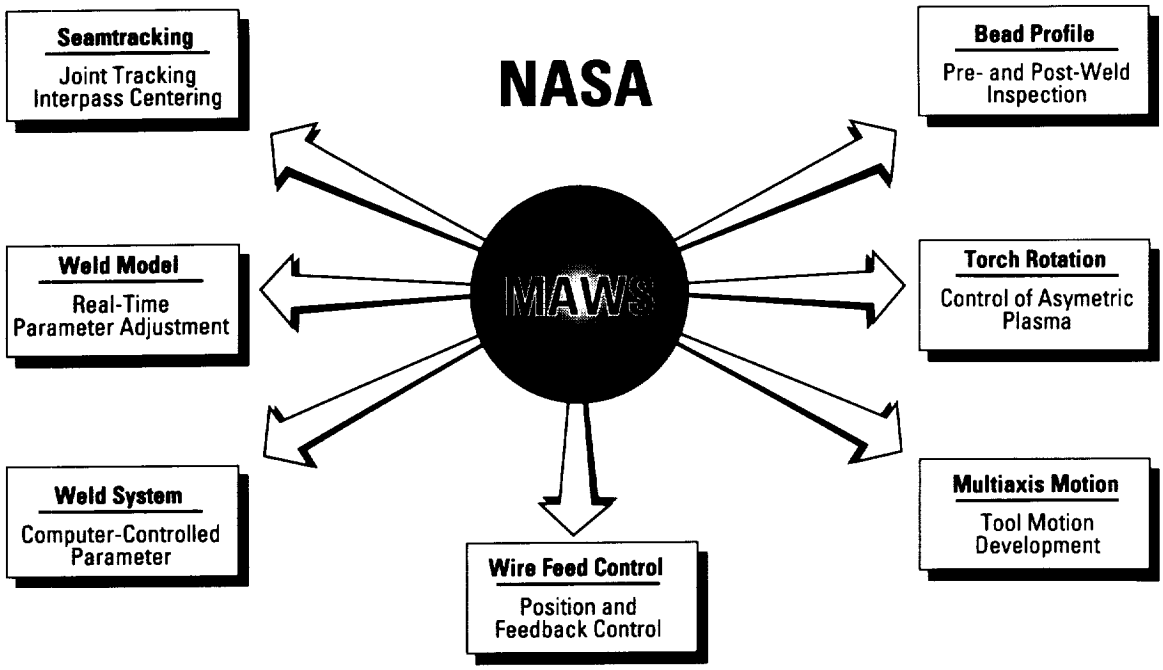

Automatic weld system.

in VPPA torch rotation by taking vision data closer to the arc. A three-axis automated wire feed control system has been successfully demonstrated. The system utilizes multiple **sensors** to feed the wire at a precise location in the weld and with desired pressure on the base plate. The system also uses a sensor to monitor the quantity of wire remaining. The weld model theoretical relations have been identified and a computer simulation of the VPPA process is nearing completion. Evaluation of the weld model utilizing statistical methods is also nearing completion.

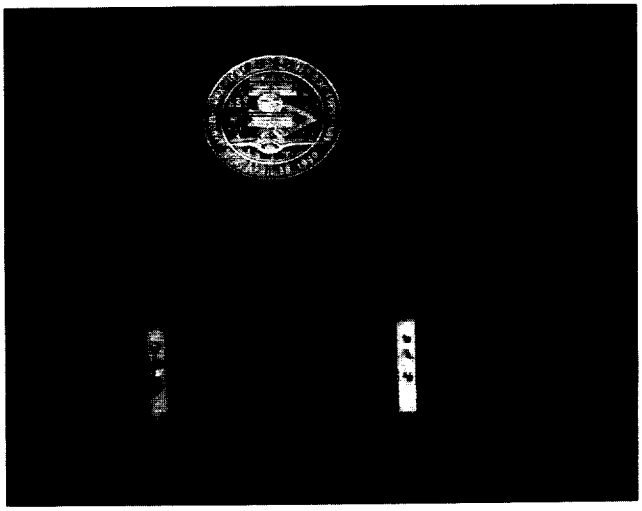

Seamtracker.

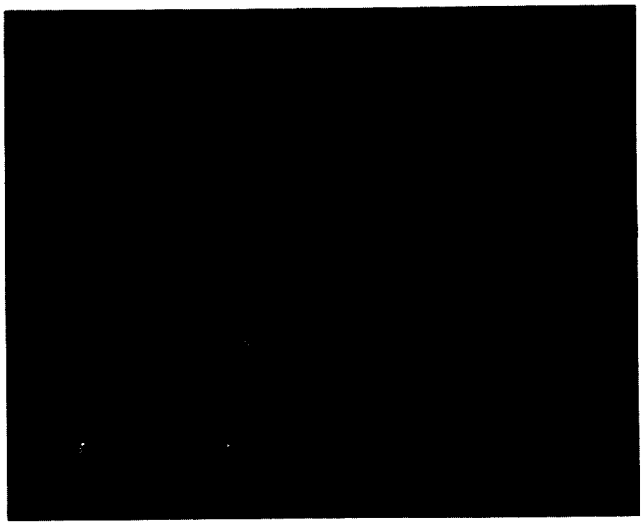

Bead profiler/torch rotation sensor.

K. Lawless/EH42
205–544–2821
Sponsor: Office of Space Flight

Long Duration Exposure Facility Experiments

Selection of materials for construction of long-duration mission spacecraft has presented many challenges to the aerospace design community. After nearly 6 yr in low Earth orbit (LEO), NASA's **Long Duration Exposure Facility** (**LDEF**), retrieved in January 1990, has provided valuable information on both the nature of the space environment as well as its effects on potential spacecraft materials.

MSFC's Materials and Processes Laboratory continues to investigate and work three **LDEF** experiments including: A0171—solar array materials passive **LDEF** experiment; A0034—**atomic oxygen** (**AO**) stimulated outgassing; and S0069—thermal control surfaces experiment (TCSE). All three experiments have been subjected to **AO** impingement, micrometeoroid/space debris, **ultraviolet** (**UV**) radiation, hard vacuum, and thermal cycling.

LDEF experiment A0171 consisted of a wide variety of materials, including solar cells, composites, thin films, organic and inorganic protective coatings, reflectors, metals, and polymers. Much of the work this year has been centered on the evaluation of metal and polymeric specimens. Based on sample mass gain analysis and electron spectroscopy for chemical analysis (ESCA), many of the metals flown showed evidence of surface **contamination** and oxidation. Optical properties, including **reflectance**, solar absorptivity, and solar emissivity, showed evidence of degradation due to space exposure when compared to corresponding protected metal surfaces. Reactivity and accommodation numbers have been calculated for most of the pure metals. More work is required to conclusively identify the formed oxides on the alloy specimens before reactivity and accommodation calculations can be made. Like the metal specimens, the polymeric materials, including Halar, Peek, and RTV 511, were also affected by the space exposure. The most prominent observation noted was the profound yellow-brown color induced in Halar and RTV 511 specimens, which are characteristically colorless and white, respectively. Severe outgassed **contamination** from RTV 511 (room temperature vulcanized) deposited on neighboring samples and appeared to drift slightly across the experiment plate.

Changes in optical and mechanical properties due to **contamination**, radiation, and **AO** were generally confined to the polymer surface or near surface.

LDEF experiment A0034 consisted of dual passive exposure modules mounted on the **LDEF** leading and trailing edges for comparison of environmentally induced effects on selected thermal control coatings. Optical mirrors were included adjacent to the thermal coatings for deposition of outgassing products. For each of the experiment modules, an array of 25 compartmentalized coatings and mirrors were exposed through open apertures, **UV** grade windows, and metal covers for evaluation of the effects of individual environmental parameters. Evaluation of contaminant collector mirrors indicated that **AO** redirected from adjacent thermal control coatings significantly influenced the amount of residual **contamination**, particularly for the polyurethane coatings, and, for selected mirrors, changed the basic nature of the mirror coatings. Fluorescence studies of the thermal control coatings indicated both stimulated and quenched emission as a result of exposure to **AO** and solar **UV** radiation.

TCSE was the most complex experiment flown on **LDEF**. TCSE was a microcosm of complex electro-optical payloads required to perform in-space measurements of total hemispherical **reflectance** over the wavelength range from 250 to 2,500 nm. This was a unique instrument that, for the first time, provided the capability to directly measure in-flight optical **reflectance** of exposed surfaces. During the **LDEF** mission, measurements were performed and recorded for 25 samples mounted on a rotating carousel. Data were

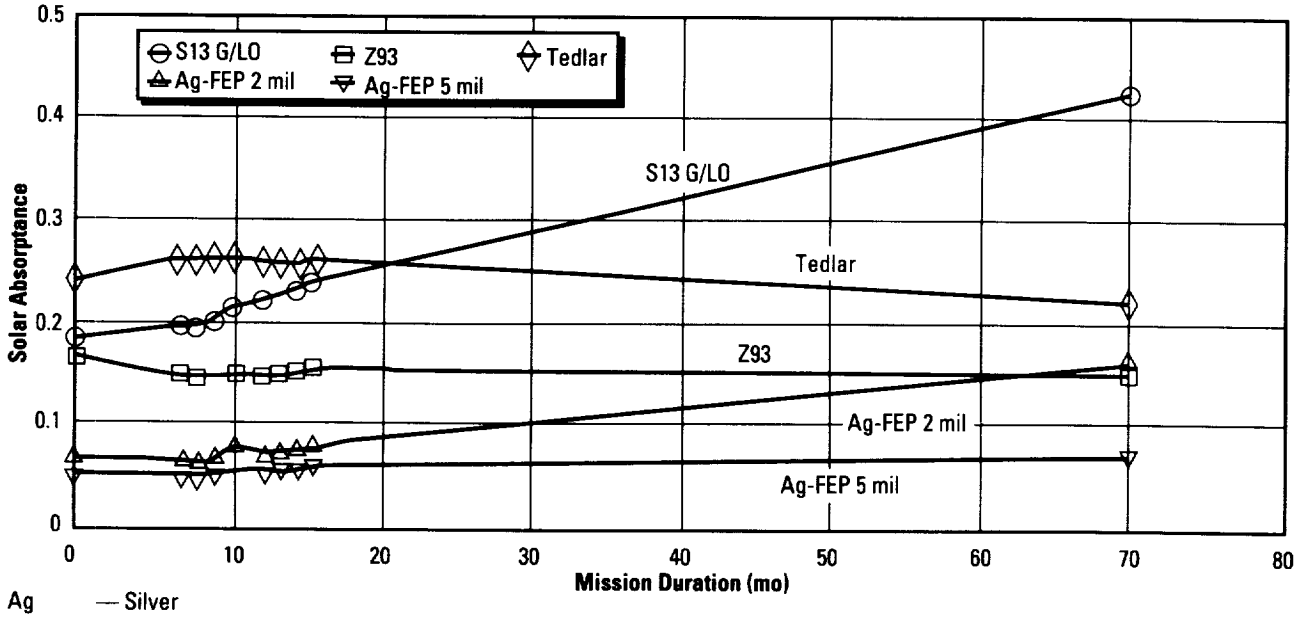

Ag — Silver
FEP — Fluorinated Ethylene Propylene (Teflon)
S13 G/LO — Zinc Oxide Paint
Tedlar — Polyvinyl Fluoride Film

TCSE flight data.

AO effects and mechanical property data for A0171 polymers

Property	Halar	Peek	RTV 511	TFE* Teflon®
AO Reactivity ($10^{-24}cm^3$/atom)	2.1	2.3	**	0.20
Solar Absorptivity				
Flight	0.71	0.76	0.31	—
Control	0.65	0.63	0.22	—
Solar Emissivity				
Flight	0.95	0.95	0.92	—
Control	0.92	0.89	0.91	—
Shore Hardness				
Flight	72 – 76D	83 – 87D	44 – 46A	—
Control	74 – 76D	83 – 87D	38 – 42A	—
Elongation (%)				
Flight	72 – 87	17 – 22	120 – 136	—
Control	63 – 77	27 – 47	—	—
Yield Strength (ksi)				
Flight	5.2 – 5.3	13.5 – 13.6	0.14 – 0.26	—
Control	5.1 – 5.2	13.0 – 14.2	—	—
Young's Modulus (10^5 lb/in^2)				
Flight	2.1–3.2	3.8–5.7	—	—
Control	2.2–3.1	3.4–4.0	—	—

* TFE—Tetrafluoroethylene
** Mass loss is essentially attributed to outgassing rather than to an AO attack.

stored on a four-track tape recorder during the first 18 mo of the **LDEF** mission. These **reflectance** data were combined with the solar flux absorbed by these coatings (solar absorptance). A plot of these reduced data demonstrates that some coatings degraded during space environmental exposure, while others, such as the white Z93 (zinc orthotitanate) paint, appeared almost unchanged.

Whitaker, A.F., and Young, L.E., "An Overview of the First Results on the Solar Array Passive LDEF Experiment (SAMPLE)," A0171, Proceedings of the First Post-Retrieval LDEF Conference, Orlando, FL, June 1991.

A.F. Whitaker/EH11
205–544–2510
Sponsor: Office of Aeronautics, Exploration, and Technology

Manufacturing With Aluminum-Lithium Alloys

Over the past decade, development of a new **aluminum-lithium (Al-Li)** family of alloys has resulted in a system designated weldalite 049 that shows great potential for cryogenic tank applications. One particular alloy, 2195 with 4-percent copper (Cu) and 1-percent lithium (Li), not only has the material properties needed at cryogenic temperatures, but is also readily weldable and formable. To demonstrate this material for future launch vehicles, MSFC has proposed to undertake a tank fabrication program to demonstrate the manufacturability and design properties of this new alloy.

The **variable polarity plasma arc (VPPA)** welding process is used to weld this new alloy. Unlike traditional 2219-alloy Al, root-side shielding is needed to control the oxidation of the molten metal. Several techniques and shielding gas combinations have been investigated to assure that this additional welding requirement will not be a detriment to large-scale tank fabrication. Development efforts have also revealed the necessity to remove approximately 2.54 mm (0.10 in) from the surfaces of plate material to be joined due to an oxidized layer that can contribute to porosity in the welds.

The ductility of 2195 also makes it a good candidate for new forming operations developed in recent years. **Extruding** barrel panels with integral stiffeners has been successfully demonstrated. **Spin-forming** domes and dome caps has also been accomplished with the tank diameter as the limiting factor for this technology. **Super-plastic-forming** and age-forming are also being demonstrated on 2195 for dome gore panel applications.

To evaluate these new manufacturing techniques and the material properties of 2195, MSFC is considering the fabrication of a subscale 8.38-m (27.5-ft) diameter cryo tank for testing. This tank would provide valuable information on the manufacturability of this alloy on a scale applicable to both the shuttle external tank (ET) program and the National Launch System (NLS) program. It will provide design data needed to baseline this material for NLS and retrofit of the ET. The tank is tentatively scheduled for completion in 1997. Current efforts are concentrating on testing material properties in plate and extruded forms, weld development using design of experiments (DOE's) techniques, and preliminary design of the test cryo tank.

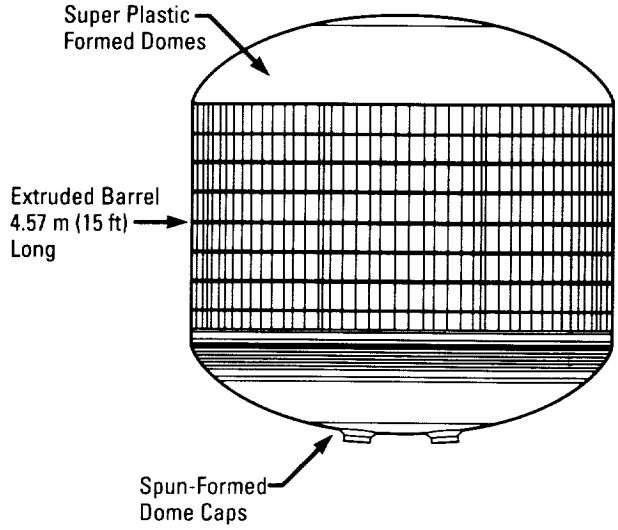

Al-Li test article.

C. Russell/EH42
205–544–2705
Sponsors: Office of Space Flight and Office of Space Systems Development

Microbial Ecology of Closed Recirculating Water Systems

Microorganisms will, without question, be part of the environment of any space capsule inhabited by humans. NASA's Space Station *Freedom* may be viewed as a volume partially closed to the exchange of **materials** for a number of years, consisting of living organisms and nonliving substances interacting to produce an exchange of **materials** between the living and nonliving parts (**ecosystem**). The assemblage of organisms colonizing the space station, determined predominantly by human activity, is expected to adapt to the environment in ways not entirely predictable from the information derived from human habitations on Earth. Increased surface-to-volume ratio, vastly decreased dilution by air and water, and reduced diversity of living organisms are among the factors that can potentially lead to unique relationships among **microorganisms** and between **microorganisms** and the **materials** and subsystems they colonize.

A primary concern in creating a water reclamation system for long-duration, manned space flight is the control of microbial contamination, which can jeopardize water quality, compromise human health, and degrade constituent **materials** of the system. Because microbial processes occur primarily on surfaces, experiments are being conducted to investigate the dynamics of microbial **biofilm** formation. The interaction of bacterial species in the development of **biofilm**, their response to the introduction of additional species or disinfectants, and their interactions with underlying **materials** are being studied.

The factors of **biofilm** age, species composition, and sequence of introduction of bacterial types to a **biofilm** are being investigated for their significance in terms of response of a **biofilm** to **disinfection** and the addition of new organisms. In static experiments, varied sequence and timing of species introduction in binary bacterial **biofilms** on 316L stainless steel elucidate the mechanisms involved in **biofilm** formation. In a second type of static experiment, **biofilms** constructed of one to seven species are challenged by the introduction of an additional organism or by disinfectants to examine the relationship between community structure and **biofilm** response to these challenges.

In bench-scale, closed-loop recycling water systems, the response of **biofilms** to iodine **disinfection** is investigated. Studies have shown 1 to 2 mg/L of iodine (I_2) to be ineffective against some planktonic bacteria and mixed population microbial **biofilms**. Much higher I_2 concentration (15 to 20 mg/L of I_2), tested in the bench-scale system, has been shown to be necessary to completely disinfect a stable **biofilm**. *Staphylococcus aureus* and *Escherichia coli* introduced to this system, which contained natural mixed population **biofilms**, resulted in their colonization in the **biofilms**, and increased their survival time from 3 to 5 d, as unattached cells, to over 60 d when protected in the **biofilms**. I_2 concentrations of 0.5 to 9.0 mg/L eliminated these organisms from the bulk water, while over 4.0 mg/L were necessary to completely eliminate them from the **biofilm**.

Methods for rapid monitoring of **microorganisms** in flowing water systems are being developed. Video image analysis and the detection of the adherence of very small mass (a few bacterial cells) by means of a quartz crystal microbalance are two current areas of research.

In studying the influence of microbial growth on metallic and nonmetallic **materials** that are candidates for use in space capsules, analytical techniques have emerged that could become standard NASA methods for **materials** selection. Image analysis and electrochemical impedance spectroscopy yield reliable information on the susceptibility of **materials** to microbially influenced degradation.

Small, materially closed **ecosystems** are being studied to generate information about: (1) how closed systems function in general; (2) the characteristics of surviving organisms; (3) how energy and **materials** are cycled through a biological system; (4) whether and how soon stability is reached; etc. Such information will be useful for a space station or lunar or Mars habitat in predicting the numbers and kinds of organisms that are likely to become established and in learning how to control them through knowledge of their requirements for energy and **materials**.

Rodgers, E.B., Obenhuber, D.C., and Huff, T.L., "Microbial Biofilm Studies of the Environmental Control and Life Support System Water Recovery Test for Space Station *Freedom*," NASA Technical Memorandum, TM-103579, 1992.

Smithers, G.A., Rodgers, E.B., Obenhuber, D.C., and Huff, T.L., "Aquatic Biofilms and Their Response to Disinfection and Invading Species," 22nd International Conference on Environmental Systems, Seattle, WA, 1992.

E.B. Rodgers/EH32
205-544-2647
Sponsor: Space Station *Freedom* Program

Mobile Robotic Hydroblast System

The first mobile robotic hydroblast system (MRHS) has been certified for use at Kennedy Space Center (KSC), following development by NASA and United Space Boosters, Inc. (USBI), at the Productivity Enhancement Complex at MSFC. The qualification/certification program was an MSFC/KSC cooperative venture that changed the untried prototype into a refined veteran system that has radically improved the postflight **stripping** of the space shuttle solid rocket boosters (SRB's).

When recovered from splashdown, the boosters present a massive unassembled structure of two forward segments, four solid rocket motor (SRM) segments (SRM mid-body), and an aft skirt around the protruding SRM nozzle. Before flight, all thermally sensitive surfaces, exterior components, and cable tunnels on each booster are insulated with an assortment of tenacious materials. After flight, this expended **insulation** must be removed to permit disassembly of the flight unit into individual structures for checkout and **refurbishment**. The MRHS, essentially a portable high-pressure **waterblasting** system, was designed to mechanize the manual water **stripping** that has heretofore pitted bunnysuited technicians against an onslaught of water, debris, extreme noise, and the 34-kg (75-lb) backthrust of a handheld **stripping** wand. As a new form of **automation**, the "**robot** waterblaster" brings a new dimension of **safety**, precision, repeatability, and speed to the boosters' West Wash Disassembly Facility, with minimal intrusion to the normal operating flow.

The MRHS consists of a six-axis GMF S–420 **robot**, waterproofed and mounted on a vehicular (wheeled) carrydeck. From a waterproofed, soundproofed, air-cooled cab, an operator and assistant drive the carrydeck to a given **stripping** station along the horizontal flight unit; once secured, the deck can be elevated and leveled as high as 83.8 cm (33 in) by its four hydraulic cylinders, which are essential for hard-to-reach areas imposed by the sheer size of the hardware. Inside the Plexiglas cab, the MRHS operator mans the control center consisting of **robot** controller and remote valves that divert the water (brought by umbilical from the facility's pump station) into a selected **stripping** nozzle on the **robot** arm from which it exits at 103,425 kPa (15,000 lb/in^2). On the forward deck, the GMF **robot** sports a robust end effector designed to shift between a customized single-orifice nozzle or a commercial dual-orifice rotating nozzle. During the **high-pressure stripping** process, any out-of-range parameter forces a shutdown that safeguards both personnel and hardware. In practice, the system has operated steadily under very harsh conditions.

The first use of MRHS on flight hardware occurred on STS–37, April 8, 1991. This event began the 12-mo certification characterized by continuous **stripping** runs at the West Wash interspersed with off-line software refinements at the MSFC complex, 1,126 km (700 mi) north.

Consecutive validation runs were completed on space transportation system (STS) flights 39, 40, 43, 48, 44, 42, and 45. USBI engineers were on-site for each run, training personnel and identifying modifications to the **stripping** programs, which grew into a 48-cycle library. After final enhancements, the MSFC software was released to KSC in April 1992. Technical input was also provided to the systems requirements and specifications document and the user's guide that paralleled the on-site engineering work. The first MRHS solo operation by West Wash technicians took place in May 1992 on STS–49.

Throughout design and development of the hydroblaster, an essential tool has been the high-powered **graphic simulation** computer at the MSFC complex, loaded with kinematic models capable of designing and preverifying the system and definitive **stripping** paths without benefit of physical mockup. This three-dimensional (3–D) simulation has proved indispensable from selection of the **robot** and integration of deck components to the orientation of tag point coordinates for robotic maneuvers, verification of **robot** reachability, and detection of collision paths.

Until the 1991–92 transfer of the traveling waterblast system, the West Wash remained a fully manual, high-risk operation. With the MRHS on-site, serial time for flight **refurbishment** has decreased by 20 h (40 percent).

The MRHS is already drawing attention as a high-powered cleaner/stripper for work pieces as diverse as rocket motors, aircraft skins, and ship hulls. For the Nation at large, it holds promise as an ideal alternative to the use of passive chemical strippers that will soon be outlawed from the American scene.

Removal of thermal protection system from the SRB system tunnel.

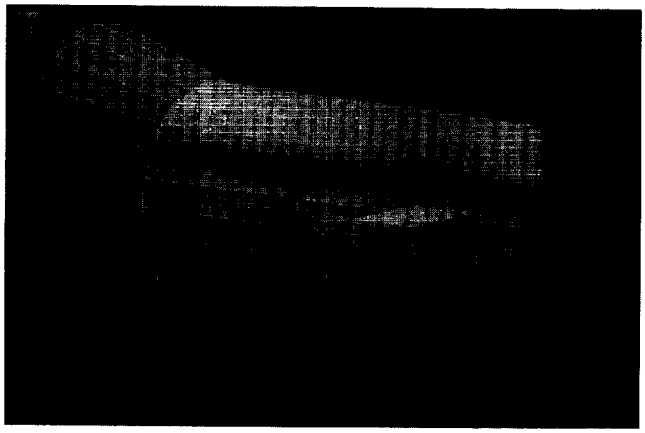

Offline programming through graphic simulation.

Removal of thermal protection system from the SRB field joint.

M.K. Babai/EH44
205-544-2795
Sponsor: Office of Space Flight

New Direction in Phthalocyanine Pigments

Phthalocyanines have been used as pigments in coatings and related applications for many years. These **pigments** are some of the most stable organic **pigments** known. The phthalo blue and green **pigments** have been shown to be ultraviolet (UV) stable and thermally stable to over 400 °C (752 °F). These **phthalocyanines** are both a semiconductor and photoconductor, exhibiting catalytic activity and photostabilization capability of polymers. Many metal-free and metallic **phthalocyanine** derivatives have been prepared. Development of the new classes of **phthalocyanine** pigment could be used as coatings on NASA spacecraft material such as glass to decrease the optical degradation from UV light and as a coating on solar cells to increase lifetime and efficiency.

The **synthesis** of the single-ringed **phthalocyanine** based on 1,2-didodecyloxy-4,5-dicyanobenzene has been completed and the compound has been purified. The **characterization** of this single-ring compound by UV/visible, Fourier transform infrared (FTIR), nuclear magnetic resonance (NMR), x-ray diffraction, and mass spectroscopy is well under way.

Although the process for **synthesis** of bisphthalocyanine has been attempted several times, it has not been successful. It is felt that the reason for this unsuccessful **synthesis** is due to the stability of the intermediate structures. The cyclic intermediate compounds (substituted naphthalene imide bisimines) will be evaluated using the AMPAC program for heat of formation and bond strength stability of the tautomer. A substituted naphthalene system may be used to destabilize the tautomer relative to the parent bisimine. If the theory is correct, the new naphthalene system should form the **phthalocyanine** of choice. The AMPAC calculations are producing some very interesting results as far as determining the appropriate substitution leaving group on the **phthalocyanine** precursor. The process of synthesizing the naphthalene intermediate from the bisnitrile is under way.

The evaluation of **phthalocyanines** for protecting plastics (in this case, mylar) from UV damage has been conducted. Samples of mylar with no inhibitor, 3-percent phthalo blue (commercial) and 3-percent phthalo green (commercial), respectively, were prepared. These will serve as standards for comparison

with the newly synthesized **pigments**. The sample and reference material have been tested for tensile strength, gloss, color, and changes within the infrared (IR) spectra after exposure to UV light. The degradation of the pigmented mylar was greatly reduced after exposure to 100 h of UV light (1.5 Sun level) under vacuum and at ambient temperature. Further degradation studies are planned incorporating longer UV exposure times and increased Sun levels.

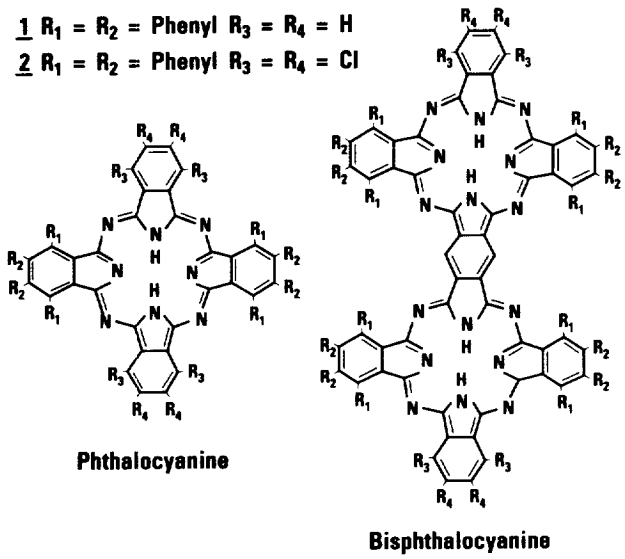

Phthalocyanine and bisphthalocyanine.

D.V. Trinh/EH32
205-544-6797
Sponsor: Center Director's Discretionary Fund

Plasma Arc Welding Repair of Space Flight Hardware

Repair or refurbishment of flight and test hardware can extend the useful life of very expensive components. A technique to **repair** space shuttle main engine (SSME) main combustion chambers (MCC's) has been developed at the MSFC Productivity Enhancement Complex. The technique involves the use of the **plasma** arc **welding** (PAW) process and active cooling to **repair** cracks and pinholes in the hot-gas wall of an MCC liner.

The hot-gas wall of the SSME MCC liner is made of a copper (Cu) alloy known as **NARloy-Z**. The wall is approximately 1 mm (0.04 in) thick and separates the combustion chamber from the many cooling channels that run axially around the circumference of the liner. These channels are sealed opposite the hot-gas wall with an electrodeposited (ED) layer of Cu and nickel (Ni), respectively. With successive hot firings of the SSME, the MCC hot-gas wall will develop cracks and pinholes extending through to the cooling channels.

The only way to efficiently **repair** these defects is to add metal and fuse the material surrounding the defect. This must be accomplished without effecting the geometry of the cooling channels and the strength of the surrounding material. These necessities levy stringent requirements on the **welding** process.

The **welding** technique developed utilizes computer-controlled PAW with the **welding** torch mounted on a **robotic** arm. The weld controller provides precise control over all critical **welding** parameters such as current, voltage, travel speed, wire feed rate, and **plasma** gas flow. This, in turn, allows control over the amount of **welding** heat being transferred to the liner. This is critical since the weld must not penetrate into the liner cooling channels, thus altering coolant flow. The PAW process also provides a restricted arc that helps confine heating to a small area. To prevent oxidation of the weld penetration, the coolant channels are purged with argon (Ar) gas during **welding**.

Equally important to the success of this **welding repair** is the use of cooling methods that quickly and efficiently remove heat from the surrounding material. Active cooling is a term used to describe methods used to cool the work piece while a weld is being performed. Two techniques are being utilized to cool the MCC liner during **welding**.

The first technique is to introduce flowing water on the ED-Ni side of the liner. An assembled MCC includes an Inconel 718 structural jacket that shrouds the outside of the liner, thus providing a gap in which water can be introduced. The water is continually circulated in this vacant area via two small ports already located through the structural jacket. This method cools the ED Ni layer, preventing it from being weakened due to heat effects.

On the front side of the weld, water-cooled Cu chill bars rest on the **NARloy-Z** surface. This represents the second cooling technique. The chill bars are closely located within 5 mm (0.2 in) on each side of the weld. They act to quickly conduct heat away from the area of the weld. Water is continuously circulated through each chill bar for additional cooling.

The precisely controlled PAW process, combined with the active cooling methods, has allowed defects to be successfully repaired in a lab environment. Both cracks and pinhole-type defects have been repaired on portions of scrapped MCC liners. Weld penetration has been kept to a minimum and no indication of detrimental heat effect on the surrounding structure has been found.

An ongoing effort will focus on making the **welding** process more robust and enhancing the active cooling techniques. In addition, the PAW **repair** process has the flexibility to be adapted to a stand-alone system that could be used to perform field **repairs**. Future work will also include the development of such a system.

D.S. Hoffman/EH42
205–544–2713
Sponsor: Office of Space Flight

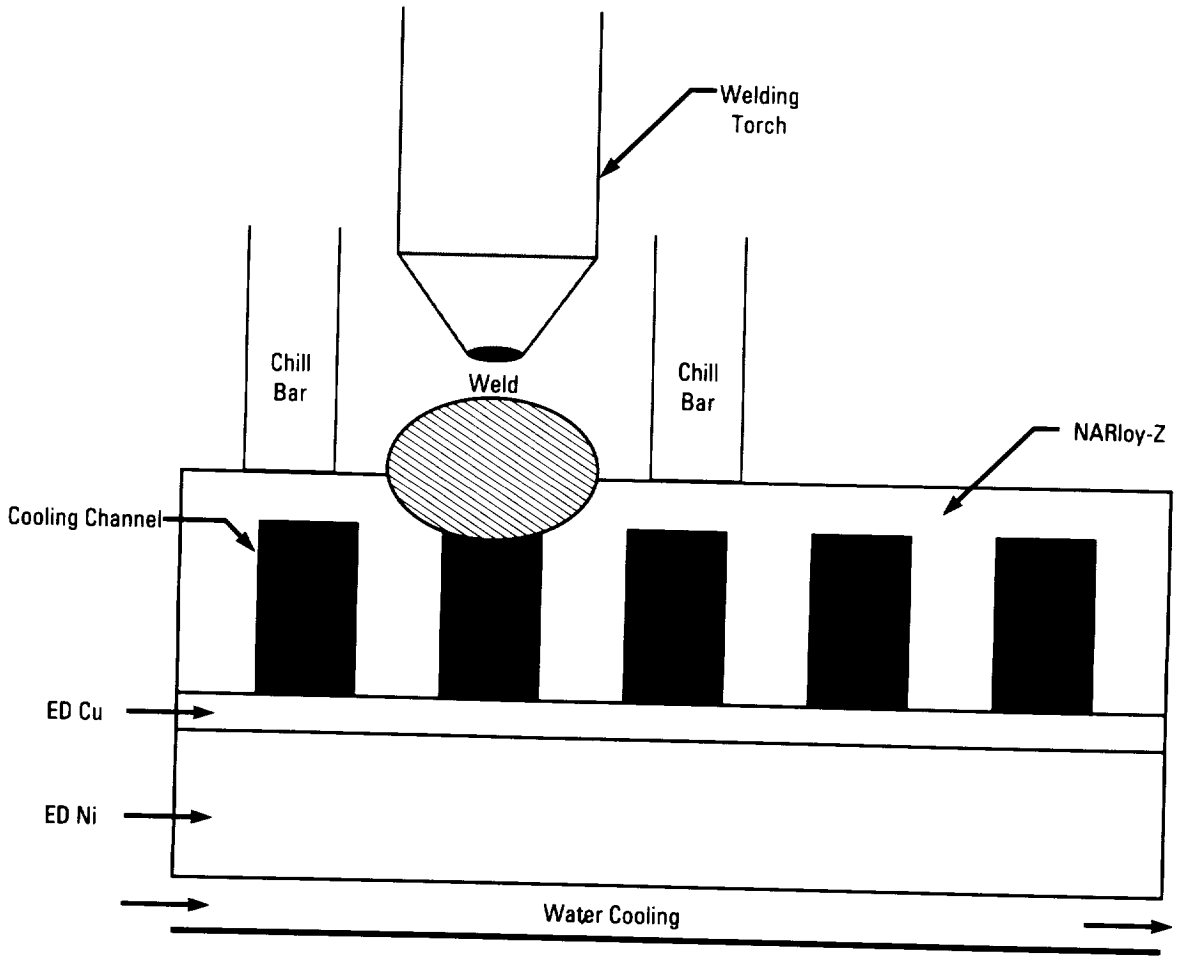

Plasma arc weld repair of MCC liner.

Production of Oxy-Acetelyne Torch Diamond Films

Continuous films of **diamond** offer a number of outstanding material properties with practical application in aerospace systems. **Diamond** boasts the highest hardness and the highest room-temperature thermal conductivity of any known material. **Diamond** also possesses a small coefficient of thermal expansion and a low coefficient of friction. **Diamond** films have applications in areas such as impact-resistant surfaces, turbine blade edge coatings, cooling-tube surface coatings, and combustion chamber linings.

The objectives of the project are to understand the processes underlying the nucleation and growth of oxy-acetylene **torch**-produced **diamond** films and to use the results to produce large area continuous films. In the first year of the project, using a preliminary setup comprised of simply the mass flow controllers and a thermocouple, some of the early **torch** work reported in the literature[1] was reproduced. The final success with that system was the production of small islands of pure **diamond** crystals.

In the second year of the program, the system was reconfigured. A pyrolaser was incorporated into the system to provide reliable temperature and emissivity measurement and the system was automated using the Labview software platform. The system software integrates temperature and emissivity readings from the pyrolaser, flow measurement and control of mass flow controllers, and motion control of the substrate holder. The system software also incorporates a high degree of modularity, which has allowed convenient evolution of the software as the knowledge base has increased.

In the most recent year, the cooling system has been redesigned to provide efficient thermal transfer from the substrate and to provide the ability to overcool the surface. **Process control** algorithms have been added, as well as sine wave control of the flow gas levels. The initial **process control** work was presented at this year's modeling and simulation conference in Pittsburgh, PA.[2] Raman spectroscopy was used to investigate the composition of recent **diamond** growth on silicon (Si) wafer

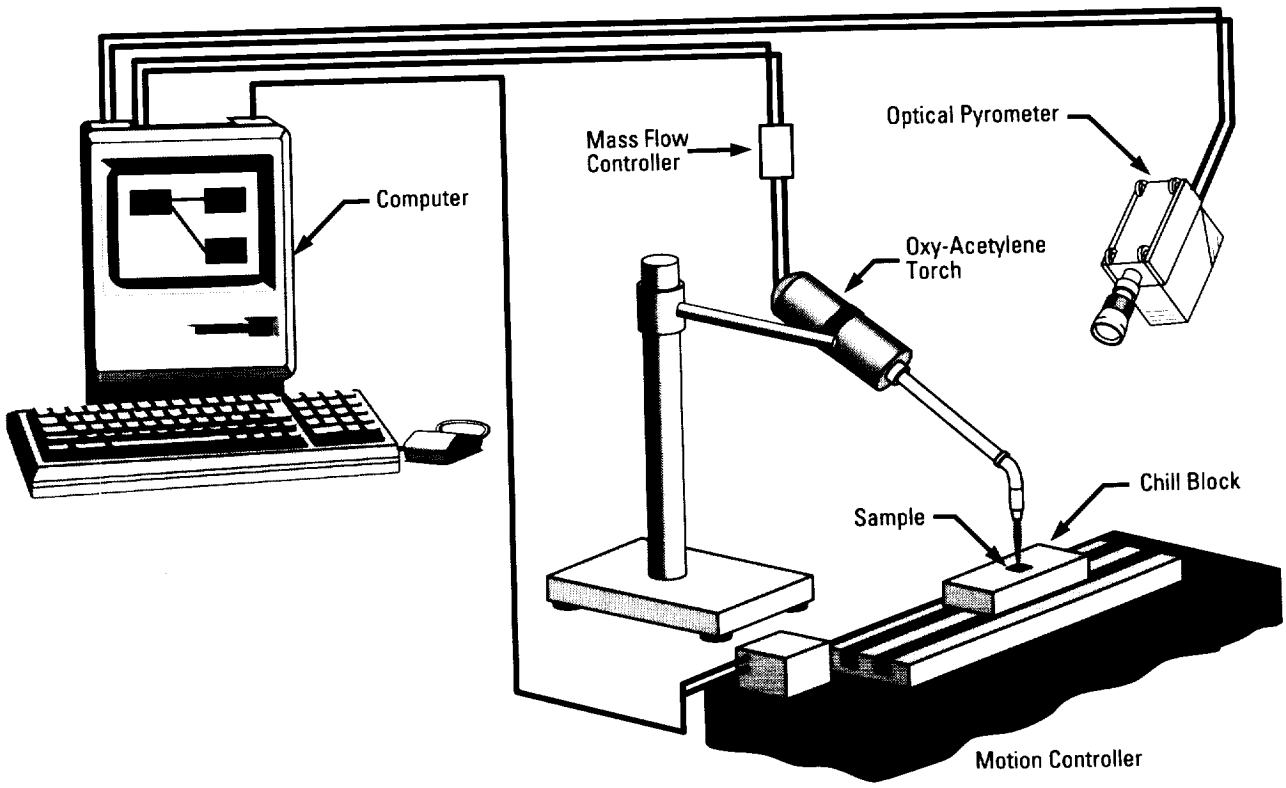

Continuous diamond film production schematic.

a-3

substrates. The spectrographic data clearly identified the presence of high-quality **diamond**. The samples also showed a characteristic sharp faceted structure under an optical microscope.

This year has seen significant progress in the **deposition** of **diamond** on alternate substrates. **Diamond** films have been deposited on substrates such as copper (Cu), Si, and molybdenum (Mo). The literature results for the **deposition** of **diamond** on Si and Mo have been duplicated. Additionally, the laboratory here at MSFC is the first laboratory to produce **diamond** on Cu substrates using the flame production process.

Success has been achieved in the production of high-quality films of continuous "white" **diamond**. The high-quality films were produced using novel process developments not heretofore reported in the literature. Current work is focused on a series of designed experiments to fine-tune some of the developments of the past year. Process optimization is the primary goal of the next project phase.

The technology developed in this program is already being used in other programs at MSFC. The Space Station *Freedom* (S.S. *Freedom*) group is using software developed in the MSFC **diamond** lab to test components of the carbon dioxide (CO_2) environmental air recycling system test loop. The software has been transferred and has undergone only cosmetic changes before being used in the S.S. *Freedom* CO_2 recycling component test setup.

Freestanding diamond film grown on Mo.

[1]Carrington, W.A., Hanssen, L.M., Smail K.A., Oakes, D.B., and Butler, J.E., "Diamond Growth in O_2+C_2H_4 Flames," *Metallurgical Transactions*, vol. 20, July 1989, pg. 1282.

[2]Roberts, F.E. III, "Control System Application of a Diamond Nucleation and Growth Model to Diamond Torch Film Deposition," Presented at the 23rd Annual Conference for Modeling and Simulation, Pittsburgh, PA, 1992.

F.E. Roberts III/EH34
205–544–1967
Sponsors: Office of Space Flight and
Center Director's Discretionary Fund

Proton Irradiation of Zerodur

The effects of high-energy **protons** on **Zerodur** are currently being investigated in the **Space Environmental Effects** Facility (SEEF). **Zerodur**, a glass ceramic, is baselined for use on the Advanced X-Ray Astrophysics Facility (AXAF) mirror system. Previous work exposing **Zerodur** to ionizing radiation indicates that **Zerodur** exhibits a compaction that is directly related to fluence. This investigation shows that measurable compaction begins at a fluence of 1.6×10^{13} **protons**/cm^2 (1.03×10^{14} **protons**/in^2).

The **Zerodur** samples used in this investigation were 7.62-cm (3-in) diameter disks. The samples were placed in a holder that exposed half of the surface to the radiation. This provided a definite interface between the exposed and unexposed regions. The samples were exposed to a 2.0 MeV **proton** flux that was generated by a Van De Graaff **accelerator**. Studies were performed to examine the effects of increasing fluence while maintaining a constant flux, then increasing the flux while maintaining a constant fluence. Compaction measurements were taken at the interface of the exposed and unexposed regions using a noncontact interferometry technique.

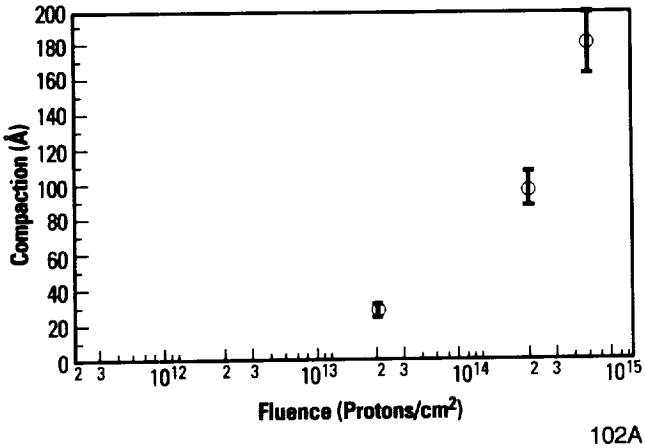

Zerodur compaction as a function of increasing proton fluence (constant flux: 5×10^{10} protons/cm^2/s (3.23×10^{11} protons/in^2/s)).

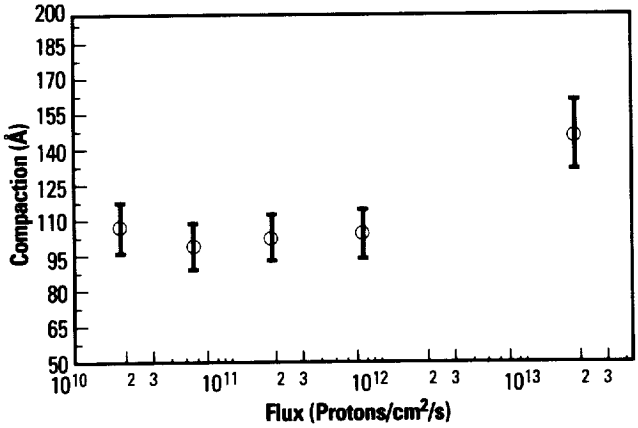

Zerodur compaction as a function of increasing proton flux (constant fluence: 2×10^{14} protons/cm^2 (1.3×10^{15} protons/in^2)).

A **thermography** system, which detects infrared (IR) emission, was utilized to measure the temperature increase of the sample while irradiated by the **proton** beam. Results from this test indicate the sample surface increased by 22.2 °C (40 °F). This temperature increase does not exceed the operational parameters of the material. The next step in this investigation will examine the effects of various **proton** energies on the compaction of **Zerodur**.

Higby, P.L., Friebele, E.J., Shaw, C.M., Rajaram, M., Graham, E.K., Kinser, D.L., and Wolf, E.G., "Radiation Effects on the Physical Properties of Low-Expansion-Coefficient Glasses and Ceramics," *J. Am. Ceram. Soc.*, vol. 71, No. 9, 1988, pp. 796–802.

D.L. Edwards/EH15
205–544–4081

Sponsors: Space Station *Freedom* Project Office and Advanced X-Ray Astrophysics Facility Project Office

Robotic Assembly of Welded Truss Structures in Space

The focal problem considered in this investigation is the joining of a tubular truss strut between two nodes using a special **welding end-effector** mounted on a **robot**. It is part of a **space construction** research program for construction of a large-diameter (37-m (120-ft)) **aerobrake** structure. A vehicle of this size is clearly too large to be preassembled on Earth, so it is stimulating development of in-space assembly and construction techniques.

A welded or brazed metal joint has a unique combination of properties including light weight, high strength, and essentially no maintenance requirements. Such characteristics make these permanent metal joints ideal for systems requiring a hermetic seal in combination with a high strength-to-weight ratio. Applications would include the assembly of metal structures where high strength and light weight are critical, and fluid piping systems where sealing of joints under high vibration or stress conditions and low maintenance requirements are the important considerations. Mechanically preloaded joints of this type are less suitable for applications such as the **aerobrake** where predictable strength and stiffness are required over a greater fraction of the load-bearing capacity of component parts. Welded joints maintain a linear and symmetric stiffness up to the failure of component materials. They are simple and more efficient than preloaded alternatives. The joints are permanent and do not shake loose when subjected to vibration.

A butt weld with a "**slip joint**" is used to facilitate assembly and align the joint for **welding**. A **slip joint** has been devised that will perform the functions of a "double-action" mechanism to compensate for misalignment where the space between nodes to which struts will connect is either more or less than anticipated. This eliminates the need for creating an **end-effector** with built-in jacking mechanisms and variable length.

Components for the assembly include: a graphite/epoxy tubular strut (60 to 150 mm (2.5 to 6 in) in diameter), a metallic connector (ferrule) attached to the graphite/epoxy tube, a metallic receptacle that receives the connector and provides attachment to a "node (scar)," and a node that connects the truss members together at their intersection.

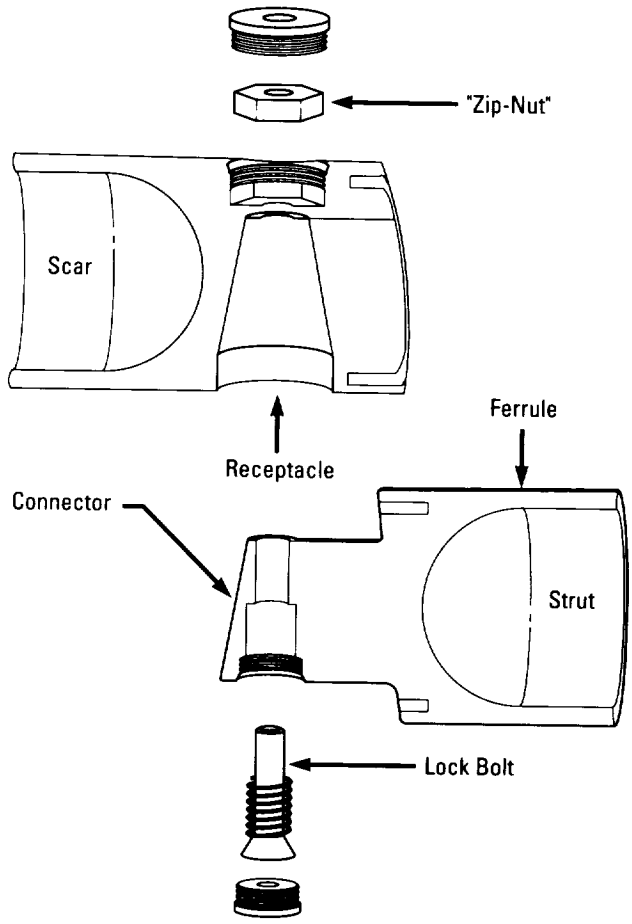

Cross-sectional, exploded view of a "slip-joint" connector.

An **end-effector** to assemble and weld the **slip joint** performs location and retrieval of the struts to be assembled by use of a special stud inserted into "**Zip-nuts**" located on the strut. After the connector on the strut-end has been mated with a receptacle on the node, acquisition is completed by inserting a hexagonal "ball-tipped" Allen wrench in the head of the lock-bolt housed in the **slip joint** alignment cone and turning. Verification requires visual indication in addition to a specified lock-bolt torque. The connector and receptacle should now be aligned and ready to weld.

The **welding** torch in the current scenario is an electric **arc** device that heats the metal by means of a transferred plasma **arc** between the tungsten-alloy electrode and the parts being joined. The torch is mounted rigidly to a shield or hood and faces radially inward toward the strut axis. Torch motions are those of the shield.

The **end-effector** proposed is relatively less complex and massive because a simple mechanical joint was employed to align the weld interface. It can accommodate struts of varying diameter and length. It will be possible to repair and replace failed members. High-density launch packaging of strut components is facilitated through a "hexagonal close pack" arrangement.

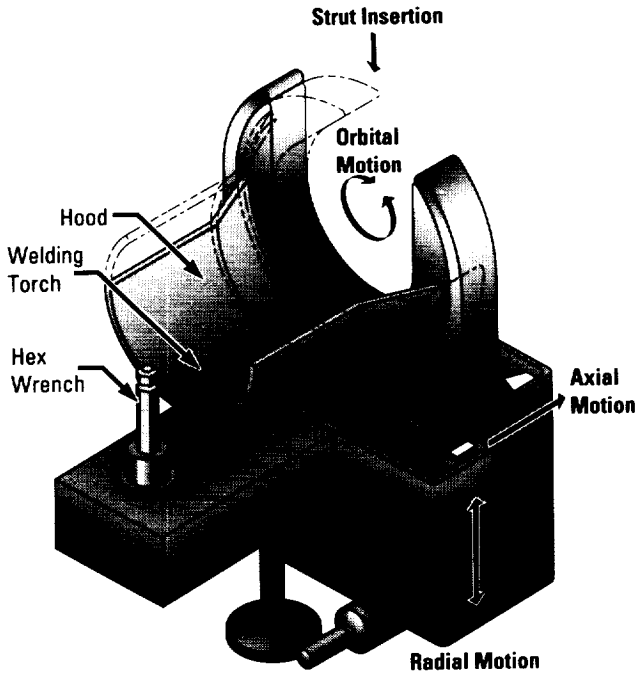

Welding end-effector diagram.

C.S. Jones/EH42
205–544–2701
Sponsor: Office of Aeronautics, Exploration, and Technology

Solid Rocket Booster Coatings Technology

National health, safety, and environmental interests have compelled three **coatings** replacement programs that have reached advanced qualification in a joint endeavor by United Space Boosters, Inc. (USBI), and the MSFC Materials and Processes Laboratory. In compliance with rising **Environmental Protection Agency** (**EPA**) standards, alternatives coming on-line will replace the anticorrosion **coating** for the **shuttle booster** aluminum (Al) substrate, the weatherized **coating** for the exterior insulation materials (the thermal protection system (TPS)), and the **polysulfide** sealant that prevents water intrusion into fastener holes, faying areas (where two metal surfaces meet), and other locations where salt water can collect and cause **corrosion**.

One of these programs will replace PR–1422 with a sealant that raises the service limit beyond 135 °C (275 °F) and exhibits greater physical/mechanical durability. Increased durability will be advantageous in retaining undamaged recyclable sealant during the high-pressure waterblast process that removes abutting TPS materials. The oncoming PR–1770 also lacks the hazardous chromium (Cr) of the current material.

Current chemical deficiencies in the **primer/paint** system that provides **corrosion** protection for the solid rocket **booster** (SRB) Al surface drive solvents from the carrier that cause unacceptable levels of **volatile organic compounds** (**VOC's**) and include a lead (Pb) additive in the **primer**. After TPS materials are applied, a rubber-based topcoat **paint** protects the relatively porous layer from the damaging effects of the Florida environment. Studies will provide a water-based **topcoat** for the TPS and a low-**VOC**, high-solids **paint** system for the underlying substrate. The 1991 **paint** candidacy culminated with a hardware configuration test on a full-scale SRB nose cap that was sprayed with MSA–2, one of the major insulation materials, to prove compatibility in the current production environment. Ease of **paint** application was also proven on actual SRB hardware. Prime **topcoat** candidate Urethabond 3015 Mod #3 was tested at the MSFC's improved Hot Gas Facility, successfully withstanding 170 kW/m^2 (15 Btu/ft^2–s) in a simulation of the frictional loading of an accelerating SRB. The TPS **topcoat** must burn, or char, while resisting liquefaction and disintegration.

In 1992, the **primer/paint** and TPS **topcoat** candidates are being eased into the production flow at several subcontractor locations. First, components for the new **primer/paint** are the aft skirt's thrust vector reservoir and the **booster** separation motors (BSM's). Initial components for the TPS **topcoat** are the aft and forward BSM's.

All three qualification programs include a broad-spectrum properties verification series with separate qualification tests to confirm each candidate's adhesion to adjacent materials, **corrosion**-inhibiting capability, ease of application, curing characteristics, durability during normal handling, and resistance to the cycle of beach exposure, flight, and ocean submersion.

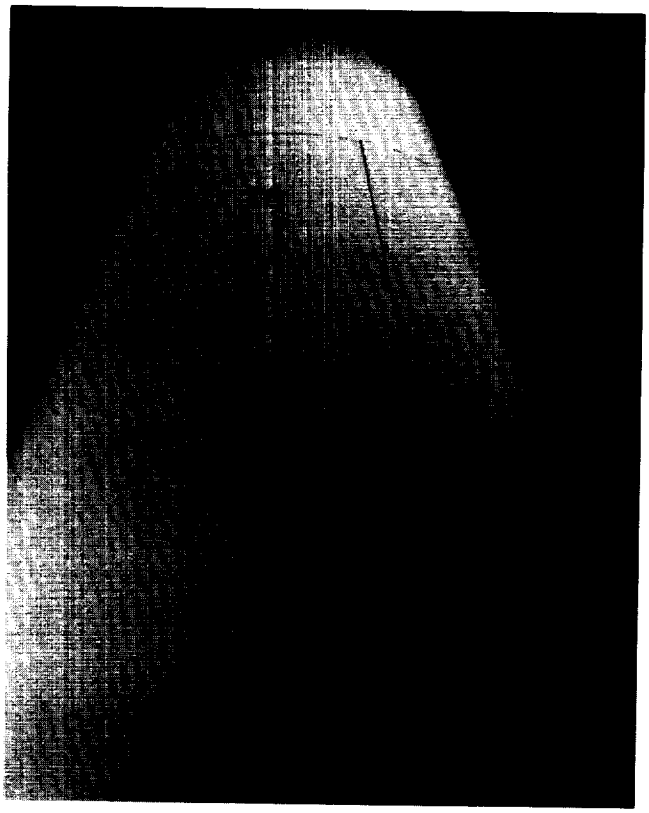

Paint application test on a booster nose cap, comparing a candidate polyurethane system (left segment) with a candidate epoxy system (right segment).

C.N. Lester/EH43
205–544–4804
Sponsor: Solid Rocket Booster Project Office

Solid Rocket Motor Nozzles: Tape Wrap Machine Kinematic Simulation

A **tape wrap** machine, located in MSFC's Productivity Enhancement Facility, is utilized in research to produce high-quality **solid rocket motor (SRM) nozzle** components. The **tape wrap** machine is currently connected to an IBM XT. The XT mimics an Alan Bradley Data Highway system. This system is also used to control the machine off-line. The XT deciphers part programs and downloads the program in the machine's language format. The machine uses a language called GNL 409 that is accessed through the XT. Although the XT provides an off-line programming technique, this technique does not allow for off-line verification of input coordinates. A simulation developed by MSFC and Thiokol Corporation consists of a Silicon Graphics IRIS model 120 GTX workstation running a graphics software package known as the Interactive Graphics Robotic Instructional Program (IGRIP) from Deneb Robotics, Inc. The IGRIP software provides three-dimensional (3–D) solid representations of the cell and allows real-time manipulation of these objects. The robot coordinates are displayed and updated emulating the XT controller. This system will detect and alert the operator when the machine has reached a travel limit, allowing the operator to graphically visualize how the machine will perform without turning on the machine.

A video tape of the **tape wrap** process was produced with Wavefront Technologies Animation software to enhance the analysis data taken from a **nozzle** as it was wrapped with the **tape wrap** machine. This animation depicts carbon-phenolic tape being wrapped on a mandrel and thermal gradient analysis data as the tape is being wrapped. This video assists in clarifying what the analysis data represent and provides an excellent demonstration aid.

M. Day/EH43
205–544–1899
Sponsor: Office of Space Flight

Trowelable Ablator Processing for Booster Structures

The year 1991 was a watershed for the final production engineering of a safe, ablative material for closing out the insulated metal substrate of the space shuttle solid rocket **boosters** (SRB's). As part of the **thermal protection** layer for launch and reentry, the **booster** trowelable **ablator** (BTA) makes its maiden flight on the aft skirt of STS–52, scheduled for launch in late 1992. Thereafter, BTA is expected to incrementally displace two current troweled **ablators** on the aft and forward assemblies: Marshall trowelable **ablator**-2 (MTA–2), with a curing catalyst whose carcinogenicity marks it for extinction, and K5NA, a commercial product containing a human mutagen, making reduced usage both ergonomically and economically desirable.

With the 1990 closure of the material qualification program, patented BTA moved into the process engineering phase under the auspices of United Space Boosters, Inc. (USBI), developers and the Process Engineering Division of Marshall's Materials and Processes Laboratory. In 1991, the originating engineers extrapolated the mixing parameters from the 7.6–L (2-gal) MSFC development mixer to the 37.9–L (10-gal) mixing system at the NASA/USBI production facility at Kennedy Space Center (KSC).

After verifying fully automated BTA batch production, BTA was signed off at level III NASA reviews, and developers returned in April 1992 to apply BTA for

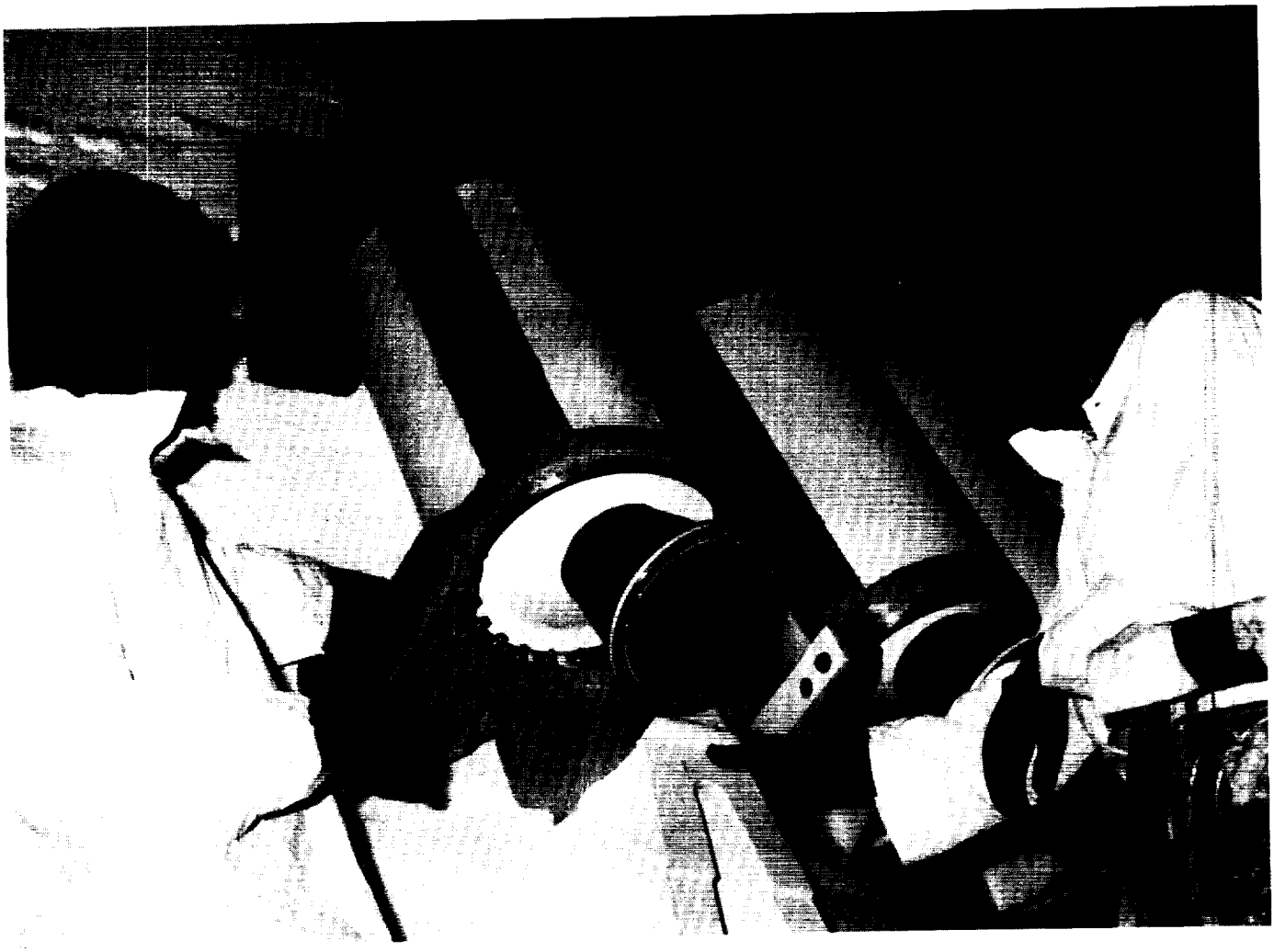

BTA maiden flight on STS–52 as closeout for booster separation motors.

flight. The STS–52 aft skirt (right-hand) will be flying BTA as a closeout between cork sheets on a **booster** separation **motor** and as a 10.2-cm (4-in) coating on the **motor's** support structure. Forming a stable single layer at 10.2 cm (4 in) with no slumping in the overhead position, BTA has also been demonstrated at a double-layer 15.2 cm (6 in) and a multilayered 30.5 cm (12 in) and above. It cures to a low-density, very durable material that adheres well to acreage regions under stress. STS–52 layups averaged 4.48×10^6-N/m^2 (650-lb/in^2) flatwise tensile strength.

In other NASA programs, BTA continues as the standard insulator for assorted developmental **motors** and a test stand for hot fires. It is also being considered for use in the space shuttle redesigned and advanced solid rocket motor programs. The material can also be cured into a presculpted **mold** for a contoured piece part.

BTA is a safe, inert, three-component formulation whose ablative properties are enhanced by mixing under vacuum. It applies more easily than K5NA and MTA–2 and cures at ambient conditions. Thermal tests confirm low-conductivity, slow recession rate, and a char integrity that will yield stability during flight. The advent of BTA sets the stage for a family of specialized trowelable-moldable **ablators** that are inherently well-suited to an improved aerospace industry.

C.N. Lester/EH43
205–544–4804
Sponsor: Solid Rocket Booster Project Office

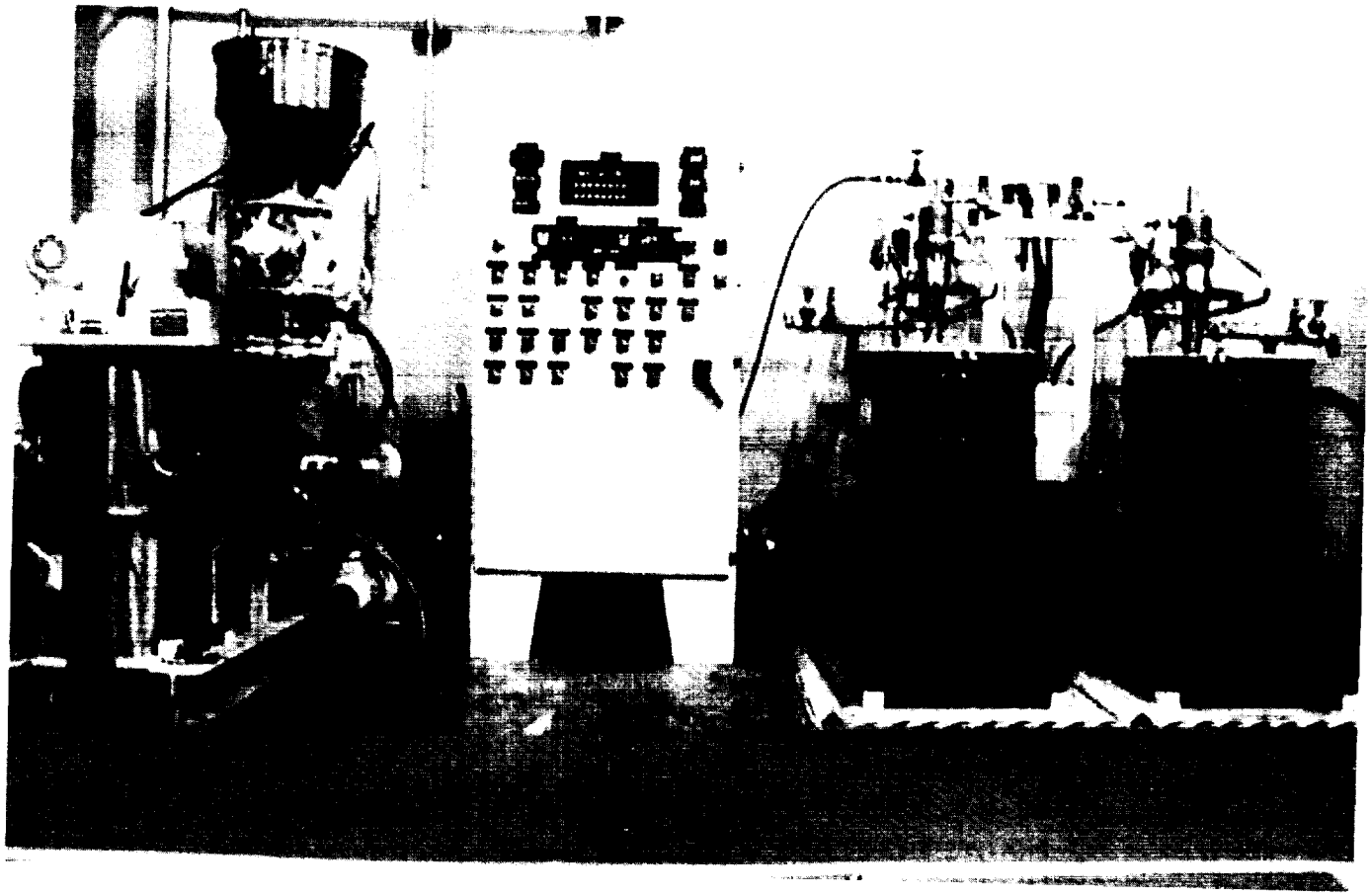

BTA automated mixer with liquids transfer station (right), mixer with solids transfer hopper (left), and integrated control system (center) (produced from a video still).

Vacuum Plasma Spray Deposition of SSME MFVH Copper Tie-In Bands

A **vacuum plasma spray** (**VPS**) process to apply the copper (Cu) insulation tie-in bands to the surface of the space shuttle main engine (SSME) titanium (Ti) **main fuel valve housing** (**MFVH**) has been developed. Due to the extremely low temperature of liquid hydrogen (LH_2) (–253 °C (–423 °F)), the **MFVH** must be insulated. The polyurethane foam insulation is protected by an electrodeposited (ED) nickel (Ni) coating that is anchored to the flanges of Ti housings. However, ED Ni will not adhere to Ti. This difficulty is overcome by depositing Cu tie-down bands, to which the ED Ni will adhere, on the flanges. These Cu bands were previously applied by air plasma spray. Oxidation of the Cu and the Ti surface during air plasma spray often resulted in brittle coatings, which failed to adhere well to the Ti. On the average, three applications were required to achieve one good coating. This problem was regarded as one of the top 10 problems in the manufacture of the SSME. Unlike the air plasma spray process, the **VPS** process consistently achieves a tenacious coating that does not peel away from the Ti.

The **VPS** process is conducted in a low-pressure, inert atmosphere inside a vacuum chamber. The plasma is generated by passing a mixture of inert gases (80-percent argon (Ar) and 20-percent helium (He)) through a direct current (dc) arc. The resulting high-temperature plasma exits a supersonic nozzle into a low-pressure (nominally 6.6 kPa (50 torr)) environment, achieving velocities greater than Mach 3. The **MFVH** is heated with the plasma torch to 454 °C (850 °F) in the low-pressure inert atmosphere. Oxides on the Ti surface are then removed by reverse-polarity transferred arc cleaning. High- purity Cu powder is then injected into the plasma plume, which melts the Cu particles and accelerates them toward the target. The length of the plasma plume is adjusted by varying the vacuum so that the particles remain in the plume long enough to become thoroughly softened, but not so liquid that they splatter on impact. The velocity of the particles before impact is estimated to be approximately half that of the plasma velocity.

An engineering change proposal (ECP) has been approved, making the MSFC-developed VPS coating the standard procedure for application of Cu to the **MFVH** flanges. Five **MFVH's** were **VPS** Cu-coated in mid-1992. All future **MFVH Cu coatings** will be applied using **VPS** by a qualified contractor.

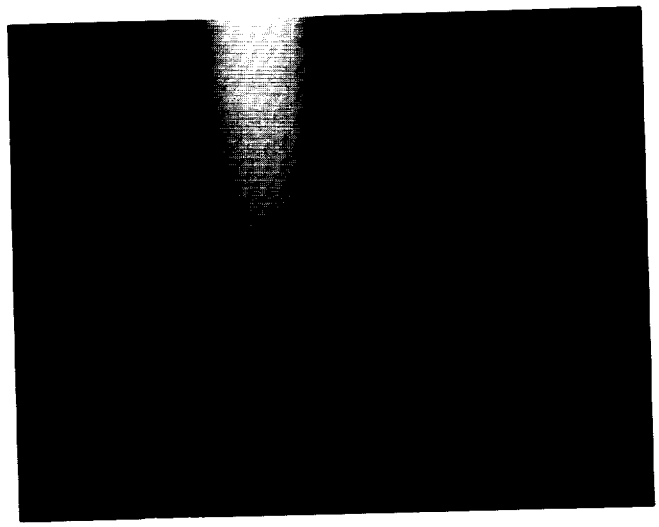

Preheat of MFVH prior to VPS deposition of Cu tie-in bands. (Note that all areas except the band to be coated are masked to prevent Cu deposition.)

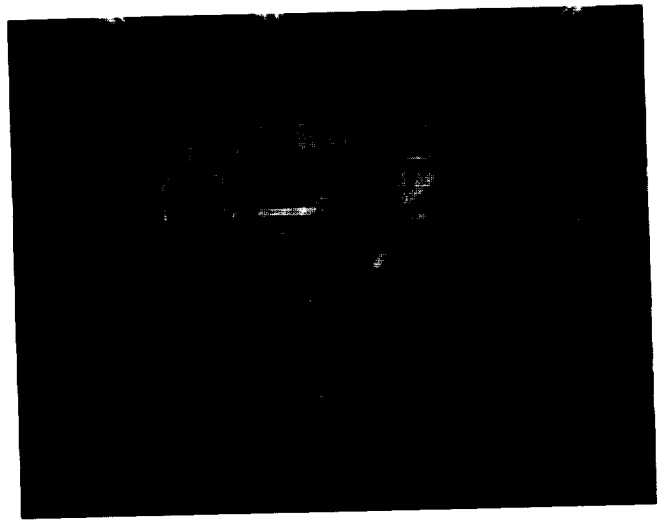

MSFC vacuum plasma spray cell.

F.R. Zimmerman/EH42
205–544–4958
Sponsors: Office of Space Flight and
Office of Aeronautics, Exploration, and Technology

Vacuum Plasma Spray Forming of Main Combustion Chamber Liners

The MSFC **vacuum plasma spray** (**VPS**) cell is supporting the development of innovative processes for the fabrication of aerospace hardware, such as **main combustion chambers** (**MCC's**). The **VPS** process is conducted in a low-pressure, inert atmosphere inside a vacuum chamber. The plasma is generated by passing a mixture of inert gases (argon (Ar) plus small percentages of helium (He) or hydrogen (H_2)) through a direct current (dc) arc. The resulting high-temperature plasma exits a supersonic nozzle into a low-pressure chamber (6.6 kPa (50 torr)) achieving velocities greater than Mach 3. The target is heated with the plasma torch to a predetermined temperature before any material is deposited. Then, nonconducting materials (e.g., oxides or organic materials) are removed by reverse-polarity transferred arc cleaning. High-purity metal powder is then injected into the plasma plume, which melts the particles and accelerates them toward the target. The length of the plasma plume is adjusted by varying the vacuum so that the particles remain in the plume long enough to become thoroughly softened, but not so liquid that they splatter on impact. The velocity obtained by the particles before impact onto the target is estimated at Mach 1.5 (approximately one-half the plasma velocity). Properties of metals deposited by **VPS** often approach those of the wrought form of the alloy.

Early work in **VPS** forming at MSFC produced a subscale test combustion chamber by **VPS**-forming the **NARloy-Z** liner and the Inconel 718 structural jacket. This unit was hot-fire tested with excellent results.

For a number of technical and economic reasons, the method of choice to fabricate a full-size **MCC** requires that the liner be **VPS**-deposited on the inside of a cast jacket. Results of recent mechanical testing show inside-diameter (ID) sprayed **NARloy-Z** has a fully dense, recrystalized microstructure similar to the wrought form of this alloy. Work continues in optimizing the ID **VPS** parameters to produce mechanical properties comparable to those of the wrought form. The project goal is fabrication of a prototype **MCC**, which will be hot-fire tested on MSFC's technology test-bed (TTB) before the end of 1994.

Fabrication of an **MCC** by this method will eliminate most of the welds (many of which are not fully inspectable) along with the costly and troublesome electrodeposited (ED) nickel (Ni) process used in the current space shuttle main engine (SSME) **MCC** channel closeout.

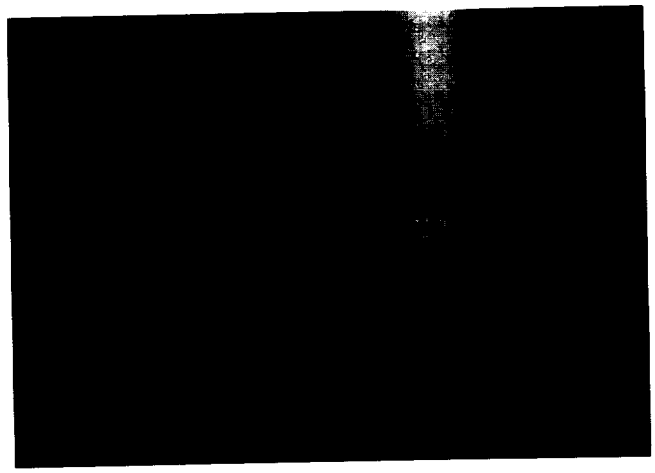

A subscale motor fabricated by the VPS ("inside-out" technique).

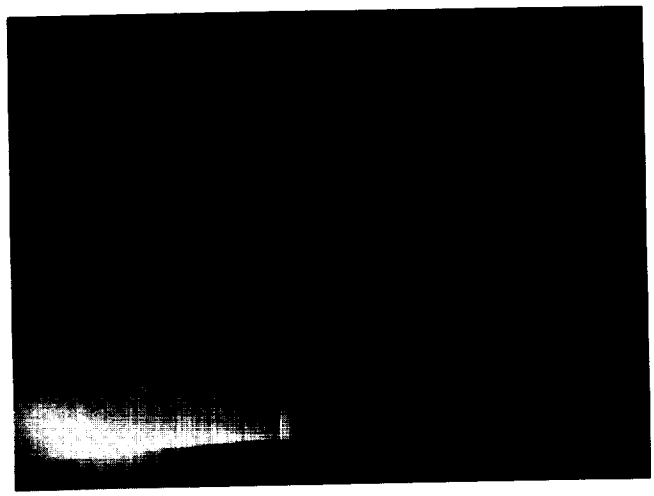

VPS of NARloy-Z into the inner surface ("inside-out" technique) of a 10-in diameter MCC throat section simulator.

F.R. Zimmerman/EH42
205–544–4958
Sponsors: Office of Space Flight and
Office of Aeronautics, Exploration, and Technology

Weld Process Modeling

Mathematical **modeling** of the variable polarity **plasma arc** (VPPA) **welding** process has been undertaken as part of a current project to develop a multivariate control for a **welding** system playing a major role in the fabrication of the space shuttle external tank (ET). The development has taken place through progressive elaboration of a series of complete models rather than completion of a single elaborate model. The most elaborate model to date now incorporates the effects of shield and **plasma** gas flowrate variations on weld bead geometry (keyhole mode). Experimental studies of heat sink and weld speed effects on penetration have revealed unanticipated power losses from the weld metal (presumed due to radiation and/or convection), which are being analyzed. Other experimental studies have detailed voltage changes due to alterations in the relative amount of reverse-polarity cleaning incorporated in the **welding** cycle; these changes are currently thought to be an effect of surface structure and temperature on electron emission at the electrode in straight polarity and at the work piece in reverse polarity. A preliminary version of a model-based control system has been discussed and is in preparation. It is anticipated that this version will use one of the simpler weld system models, that it will control error gains rather than absolute system parameters, and that it will estimate probable errors for outputs not measurable by available sensors.

Insight obtained from **modeling** studies is being applied to investigate the cause of weld strength variations on the order of 5 percent (aluminum (Al)) or greater that occasionally occur among tensile test coupons cut from the identical weld bead. Power source variations (ΔP) at low weld speeds (V) can be roughly estimated from variations (Δw) in mean weld width as in the following equation:

$$\frac{\Delta P}{P} = \left(\ln \frac{4.492\alpha}{wV} \right)^{-1} \frac{\Delta w}{w}$$

where P = power delivered to weld, V = weld speed, α = thermal diffusivity of the weld metal, and w = weld width.

To complete this picture, a relationship between weld geometry variations and weld strength variations is needed. Precise studies comparing Al butt weld strength variations to predictions of a prior weld bead geometry effect model indicate a need to allow strain and hardness to vary over the cross section of the theoretical weld bead. This modification to the weld strength model is almost completed.

Spectroscopic studies indicate that not only can **arc** contamination be detected from the **arc** emission **spectrum**, but, since hydrogen (H_2) content appears to rise noticeably if the weld keyhole closes and the **plasma** jet no longer passes through the work piece, it would seem that weld penetration can be monitored from **arc** (crown-side) spectral measurements without the need to have access to the weld root-side.

Torres, M.R., McClure, J.C., Nunes, A.C., and Gurevitch, A.C., "Gas Contamination Effects in Variable Polarity Plasma Arc Welded Aluminum," *Welding Journal*, vol. 71, No. 4, April 1992, pp. 123-s to 131-s.

Martinez, L.F., Marques, R.E., McClure, J.C., and Nunes, A.C., Jr., "Front-Side Keyhole Detection in Aluminum Alloys," *Welding Journal*, vol. 71, No. 5, May 1992, pp. 49–52.

Bastias, P.C., Hahn, G.T., Nunes, A.C., Kim, K.Y., and Rubin, C.A., "Contributions of Weld Geometry to the Strength of Aluminum Alloy Butt Welds," Poster Presentations, Third International Conference on Trends in Welding Research, Gatlinburg, TN, June 1–5, 1992.

A.C. Nunes/EH42
205–544–2699
Sponsor: Office of Space Flight

Propulsion

A Computer Model for Liquid Jet Atomization in Rocket Thrust Chambers

The process of **atomization** has been used as an efficient means of burning liquid fuels in rocket engines, gas turbine engines, internal combustion engines, and industrial furnaces. Despite its widespread application, this complex hydrodynamic phenomenon has not been well understood, and predictive models for this process are still in their infancy. The difficulty in simulating the **atomization** process arises from the relatively large number of parameters that influence it, including the details of the injector geometry, liquid and gas turbulence, and the operating conditions.

The main objective of this research has been the development of numerical models for various physical processes encountered in rocket thrust chambers such as primary **atomization**, secondary **atomization**, **atomization** of swirling jets, and the **atomization** of **impinging** jets. Models were developed from first principles to quantify the effects of various parameters influencing **atomization**. Computer codes were developed for each of these **atomization** processes. The results obtained from these models were validated with existing experimental data.

An important outcome of this research is the development of a novel method for coupling a **coaxial** injector **atomization** model with a **computational fluid dynamics** (**CFD**) code. This method is based on the jet-embedding technique in which the equations governing the liquid jet core are solved separately using a space marching technique. The equations governing the gas phase are solved separately by the **CFD** code. The liquid- and gas-phase solutions, however, are coupled through the initial and boundary conditions at the interface between them. The coupled solutions are obtained by an iterative procedure. Preliminary results of this model were reported in the 1991 Research and Technology issue. Since then, several improvements have been made, including a log-normal distribution of **drop sizes**, an improved evaporation model, and improved algorithms to make the coupling procedure more robust. This method is shown to be computationally more efficient than the volume-of-fluid method, yet it captures all the details of this complex flow field.

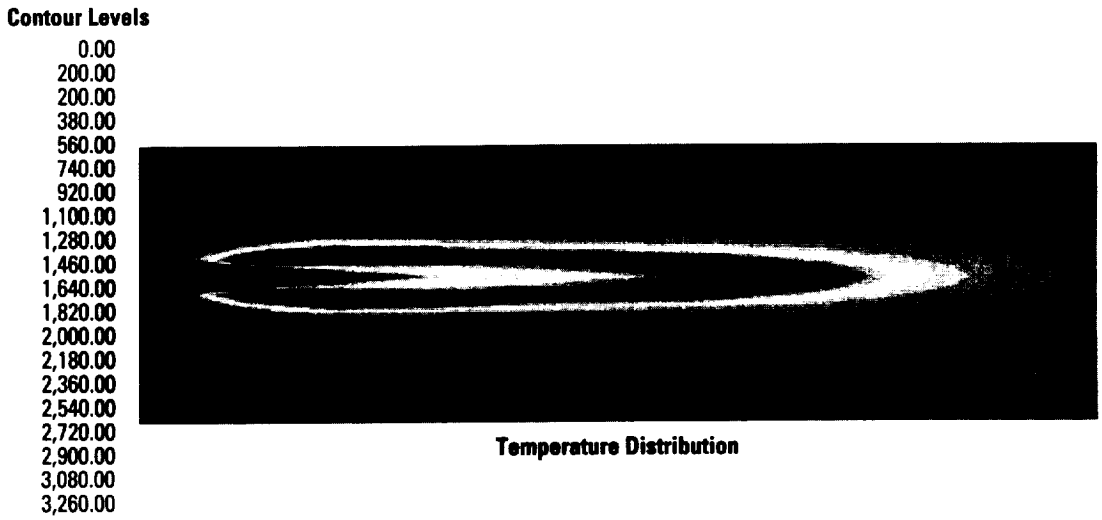

Temperature contours in SSME preburner diffusion flame.

The models developed during this study provide a sound foundation for further research and development (R&D) as well as for many commercial applications. Some applications of this research, including the study of **atomization** in gas turbine and diesel injectors, are currently under way.

This Small Business Innovative Research (SBIR) phase II effort has been completed by the **CFD** Research Corporation in Huntsville, AL, under contract NAS8–38425, with Dr. A. Przekwas as the principal investigator. The final report[1] is available with limited distribution. The associated **atomization** model has been programmed into the **reactive flow equation solver (REFLEQS)**, and the program is operational on MSFC's mainframe computer.

[1]Giridharan, M.G., Lee, J.G., Krishnan, A., Yang, H.Q., Ibrahim, E., Chuech, S., and Przekwas, A.J., "A Computer Model for Liquid Jet Atomization in Rocket Thrust Chambers," CFDRC Report 4041/1; Contract NAS8–38425, CFD Research Corporation, Huntsville, AL, December 31, 1991.

K.W. Gross/EP55
205–544–2262
Sponsors: Office of Aeronautics, Exploration, and Technology and Office of Commercial Programs, Small Business Innovative Research Program

A Model of Critical and Supercritical Evaporation of Drops in Clusters

Rocket engine combustion processes always occur in a high-pressure environment well above the critical pressure. For example, the space shuttle main engine (SSME) operates anywhere from 340 atm in the preburner to 200 atm and 153 atm in the main engine. Drops of liquid oxygen (lox) and liquid hydrogen (LH_2), which are at temperatures below their critical temperature, are injected into a high-temperature environment where they evaporate and burn; the flame temperature is in excess of 3,600 K (6,480 R).

Considering the fact that **supercritical** liquid combustion is used in the SSME, the space transportation main engine (STME), the space transportation booster engine (STBE), and the variable thrust engine (VTE), there is a surprising lack of understanding of the physical phenomena controlling **supercritical** liquid spray combustion. This lack of understanding translates into inability to control combustion chamber operation. Another issue related to combustion control is that of safety and reliability. In the absence of understanding of **supercritical** combustion, it is never certain that a plausible combustion regime, found through trial-and-error tests, is not liable to destructive combustion instabilities in the case of small perturbations.

Since improvement of the combustion processes cannot be achieved effectively by trial-and-error testing alone, due to both difficulty and the cost of such tests, there is a definite need to develop a body of understanding regarding **supercritical** liquid spray combustion. Selected tests can contribute to this understanding and can define desirable ranges of operation with more precision.

The short-range objective of this effort is the development of a unified model describing the succession of **subcritical**, critical, and **supercritical** evaporation of collections of single-component fuel drops in an initially **supercritical** gaseous environment. Because LH_2 evaporates much faster than lox, this physical picture is an excellent approximation of the bipropellant system.

The main building block for the **cluster model** is the model depicting the evaporation of one drop in a **supercritical** environment. At critical and **supercritical** conditions, the majority of the traditional assumptions made in modeling usual combustion phenomena are no longer valid. New effects that have been considered in this new model are:

- Both liquid and gas phase must be described by transient equations
- Solubility of the gaseous ambient inside the liquid drop could be important
- Nonideal behavior of the gas phase; real gas effects must be included through a realistic equation of state which is also computationally efficient
- The composition of the real gas mixture at the drop surface must be calculated using the concept of fugacity
- The concept of latent heat of evaporation no longer holds; instead, one must calculate the energy required for phase change
- The transport coefficients must now be calculated using procedures based on nonequilibrium gas dynamics.

All these effects are tightly coupled through the full transient equations that have been developed in phase I for a drop evaporating in an infinite, quiescent, **supercritical** environment. Once these equations have been derived, the emphasis is placed on deriving a consistent set of assumptions, while retaining the main physics. This will make the solution of this massive set of equations economical and easier for programming (phase II).

Since this phase of the work is considered crucial for the overall success of the effort, particular attention is being devoted to it. Several approximations tried so far were either inconsistent with the other parts of the model or did not retain the **supercritical** aspects. Work in progress considers yet another set of approximations.

The work is done at the Jet Propulsion Laboratory (JPL) in Pasadena, CA, by Dr. J. Bellan and Dr. K. Harstad.

K.W. Gross/EP55
205–544–2262
Sponsor: Office of Aeronautics, Exploration, and Technology

Combustion of Liquid Oxygen With Gaseous Hydrogen Under Subcritical, Critical, and Supercritical Conditions

Significant progress has been made in the experimental and theoretical investigation of **combustion** processes of liquid **oxygen** (lox) and gaseous **hydrogen** (GH_2) under **subcritical** and **supercritical** conditions. During the gasification and burning processes of lox droplets inside a liquid rocket engine at near-critical and **supercritical** conditions, the effects of solubility of ambient gases in the liquid phase and variations of thermodynamic and transport properties are important. These effects can influence both **evaporation** and **combustion** characteristics of the droplet. Therefore, prior to the development of a complete **combustion** model, it is useful to examine the above effects under nonreacting situations. One of the major obstacles involved in the study of single droplets is that lox droplets are usually too small to allow detailed measurements of flow properties in its neighborhood. To overcome this problem, a liquid strand test setup has been employed to maintain the top surface of the lox at a fixed location. For safety considerations, helium (He) is employed to pressurize the system instead of **hydrogen** (H_2). The other reason for using He is due to its very similar solubility features as compared with H_2.

A comprehensive theoretical model, consisting of the conservation equations of mass, momentum, energy, and species concentrations for a multicomponent system, has been formulated and is being solved numerically with the consideration of the solubility of ambient gases as well as variable thermophysical properties. In addition, a fugacity-based, multicomponent, thermodynamic, phase equilibrium analysis with quantum-gas mixing rules has been modeled and solved numerically to treat the ambient gases solubility at the interface of a lox/He system. The results of the high-pressure vapor-liquid equilibrium for the **oxygen** (O_2)/He system at three different pressure levels show very good agreement with the experimental data of Herring and Barrick (1965). It is observed that the mole fraction of He in the lox (1-mol fraction of lox) increases with the pressure for a fixed temperature. This tendency clearly indicates that the effect of the ambient gases solubility in the liquid phase becomes more important at high pressures.

Experimentally, **evaporation** rate and surface temperature were determined for lox liquid strand vaporizing in He environments at pressures ranging from 5 to 68 atm. The data points reported were obtained from four tests at different pressures while maintaining a purge gas flow velocity at 0.2 cm/s (0.08 in/s) and temperature at 291 K (524 R). In general, the **evaporation** rate increases with increasing pressure. The liquid surface temperature is slightly lower than the corresponding boiling temperature of pure O_2 at **subcritical** pressures. In **supercritical** regime, the liquid surface temperature is very close to the lox/He critical mixing temperature. To understand the high-pressure transport behavior associated with the **evaporation** process, the species concentration distributions are being measured using gas chromatography. These data can be used to validate the theoretical model under cold-flow conditions. Prior to the use of the H_2/lox system for **combustion** studies, the ignition of methane (CH_4)/O_2 gaseous diffusion flame in the test chamber has been achieved by using a spiral nichrome-wire igniter. Meanwhile, to explore the overall diffusion flame structures, Schlieren flow visualization methods will be employed in the near future to observe the density gradient change across the flame

zone. The high water-vapor concentration region, which indicates the active reaction zone of O_2 with H_2, will be inspected through the use of a laser-sheet technique. In addition, hydroxyl-radical distributions will be measured with a planar laser-induced fluorescence (PLIF) system. The burning-rate characteristics of lox/GH_2 will also be determined under various operating conditions. Results generated from diffusion flame studies will not only be useful in verifying submodels of various chemical and physical processes involved in the **combustion** of lox with GH_2 but also to enhance an understanding of the effects of differential diffusion coefficients, reaction-zone broadening, and the existence of nonequilibrium species.

This effort is being conducted under grant NAG8–174, Task 1, by the Pennsylvania State University in University Park, PA, with principal investigators being Professor K.K. Kuo and Dr. W.H. Hsieh.

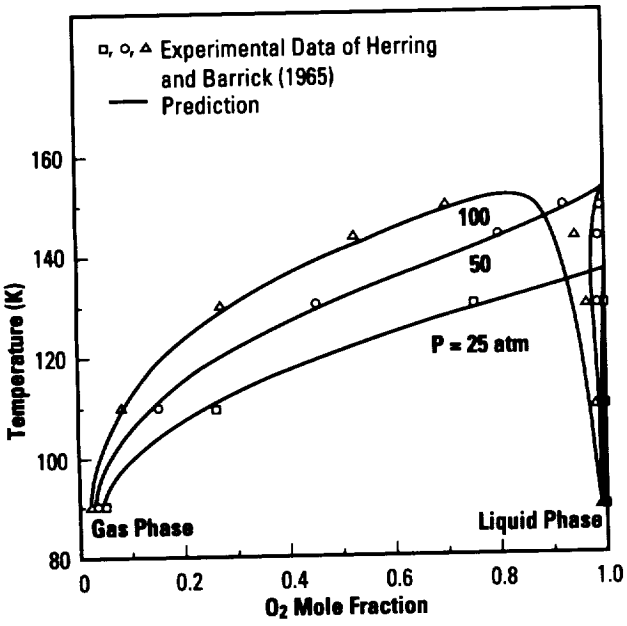

Comparison of calculated and experimental results for high-pressure phase equilibrium in the O_2/He system.

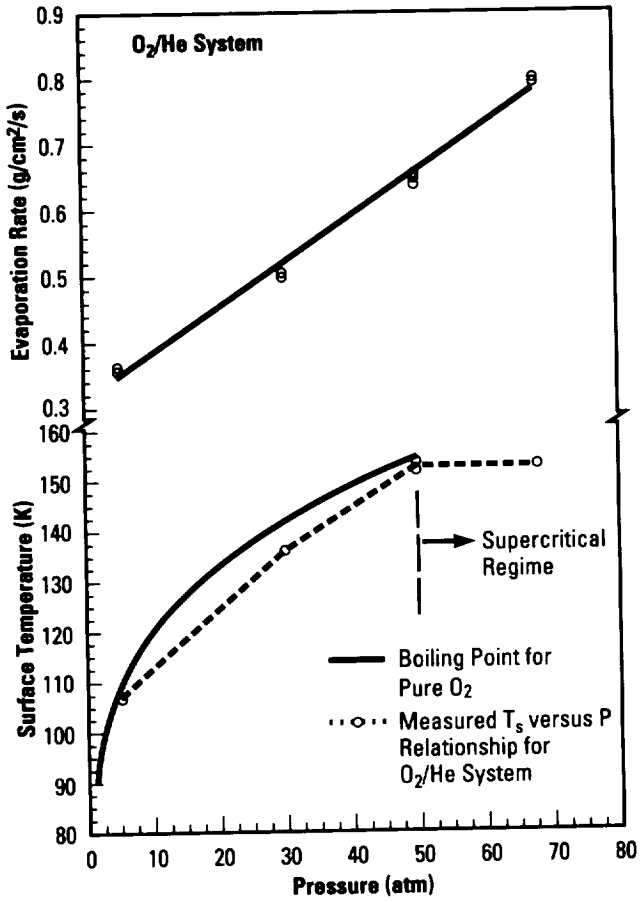

Measured evaporation rate and surface temperature versus pressure for lox liquid strand vaporizing in He environments (purge flow: velocity = 0.2 cm/s (0.08 in/s), temperature = 291 K (524 R)).

Herring, R.N., and Barrick, P.L., "Gas-Liquid Equilibrium Solubilities for the Helium-Oxygen System," *Advances in Cryogenic Engineering*, vol. 10, pp. 151–159, 1965.

K.W. Gross/EP55
205–544–2262
Sponsor: Office of Aeronautics, Exploration, and Technology

Droplet-Turbulence Interactions in Vaporizing Sprays Injected Into Supercritical Environments

The objective of this research is to characterize the behavior of liquid **droplets** in highly convective flows typical of those encountered in coaxial and impinging-type liquid rocket sprays. Of particular interest are **droplet** dispersion, drag, heating rate, and **vaporization** rate. Experiments are conducted in specially designed flow systems that are capable of operation at pressures up to 150 atm and temperatures of up to 600 K (1,080 R). Single **droplets**, well-defined sprays of liquid nitrogen (LN_2), or hydrocarbons (HC's) are injected into a subcritical or **supercritical** environment, and measurements are made of the **droplet** trajectory, velocity, size, and temperature.

During the past year, the following tasks have been completed.

- An LN_2 **droplet** generator for injection into high-pressure environments has been designed, constructed, and made operational.
- A two-dimensional (2–D) Raman imaging system for characterizing **supercritical droplets** has been acquired and set up, and the feasibility of making such measurements has been demonstrated.
- **Droplet** drag measurements have been made under nonvaporizing, laminar flow conditions.
- **Droplet** dispersion measurements have been made under nonvaporizing, turbulent flow conditions.

This experimental work is conducted by Professor D. Santavicca of the Pennsylvania State University in University Park, PA, under grant NAG8–160.

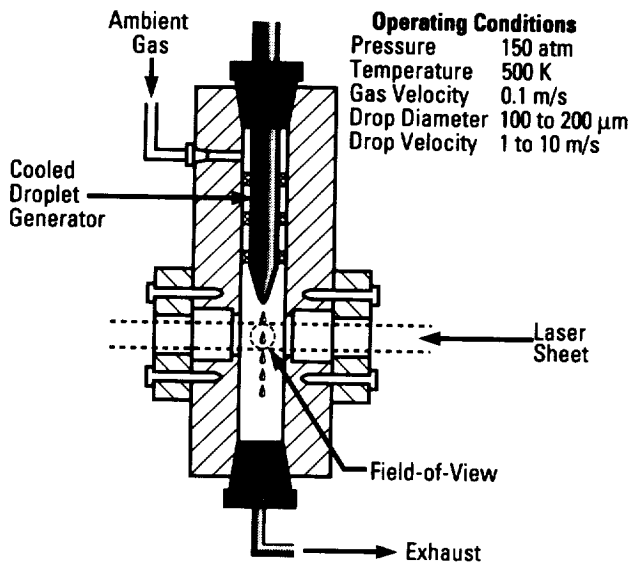

High-pressure droplet chamber.

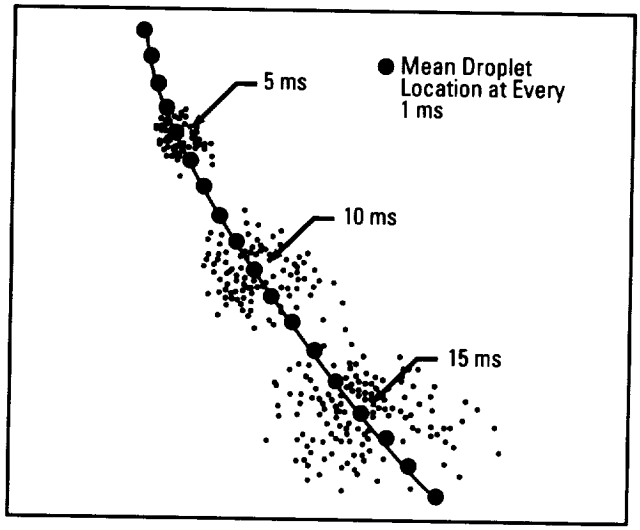

Dispersion of droplets transversely injected into a turbulent flow.

K.W. Gross/EP55
205– 544–2262
Sponsor: Office of Aeronautics, Exploration, and Technology

Experimental Observation of Dense Spray and Mixing of Liquid Jets Emanating From Doublet Injectors

The work described here is part of a continuing research effort in the area of liquid jet breakup and **dense sprays**. One of the most important issues in the development of advanced liquid rocket engines for space propulsion is how to control the **mixing** of liquid propellants and alleviate the problem of combustion instability due to inadequate sprays in thrust chambers. Owing to the experimental difficulties in observing **dense spray** behavior, most of the spray combustion studies performed in the past have focused on the dilute spray region. Very little work has been conducted to explore the characteristics of the **dense spray**. In view of this, an experimental project has been carried out to investigate the dynamic interaction between two **impinging jets** in the near-injector region using advanced diagnostic techniques. The objective is to visualize the inner jet breakup and **mixing** processes as well as the outer spray boundary configuration to obtain a clear understanding of the physical phenomena controlling spray development from doublet injectors with impingement angles of 15, 30, 45, 60, and 75 degrees.

Observation of jets at similar Reynolds numbers with increasing impingement angles (15, 30, and 60 degrees) shows that, as the impingement angle increases, the spray fan broadens due to directional changes in jet momentum. At larger impingement angles, the wave structure is less pronounced due to turbulence caused by a sharper turning angle at the injector inlets. The Ohnesorge number (defined as $\mu/(\rho\sigma d)^{1/2}$) for the series of tests considered was 2.63×10^{-3}, and the Reynolds numbers based on jet exit diameter ranged from 2.9×10^{3} to 1.0×10^{5}. The entrance angle of the orifice (the acute angle between the axis of the orifice and the entrance plane of the orifice) at the inner surface of the injector apparently has an important effect on the jet spreading rate at the injector exit. The smaller the entrance angle, the more the jet spreads before impingement; this is due to flow separation inside the injector. Higher flow-turning angles at the orifice entrance exhibit larger separation zones. The separation zone then causes a local pressure drop within the orifice, allowing cavitation to occur. The turbulence level of the flow thereby increases due to cavitation, which is believed to be responsible for transitioning the jet into the **atomization** regime.

Based on the data obtained in this effort, there are five spray regimes (i.e., closed-rim, periodic-drop, open-rim, fully developed, and **atomization**/cavitation regimes). These regimes are represented in terms of pressure drop and mass flowrate versus impingement angle. Within the Reynolds number range tested, the 15- and 30-degree injectors did not exhibit the final regime of flow. On the surface, the impingement angle has strong effects on the transition to the **atomization**/cavitation regime. However, the transition is not governed by the angle of jet impingement but essentially by the internal flow characteristics, specifically the size of the separation zone within the injector. Also, the boundary of the transition to the **atomization**/cavitation regime may not correspond to the initiation of the separation and/or cavitation. The onset of cavitation was observed to occur at a lower pressure drop through the use of a transparent injector assembly.

This effort is being conducted under grant NAG8–174, Task 2, by the Pennsylvania State University in University Park, PA, with principal investigators being Professor K.K. Kuo and Dr. F.B. Cheung.

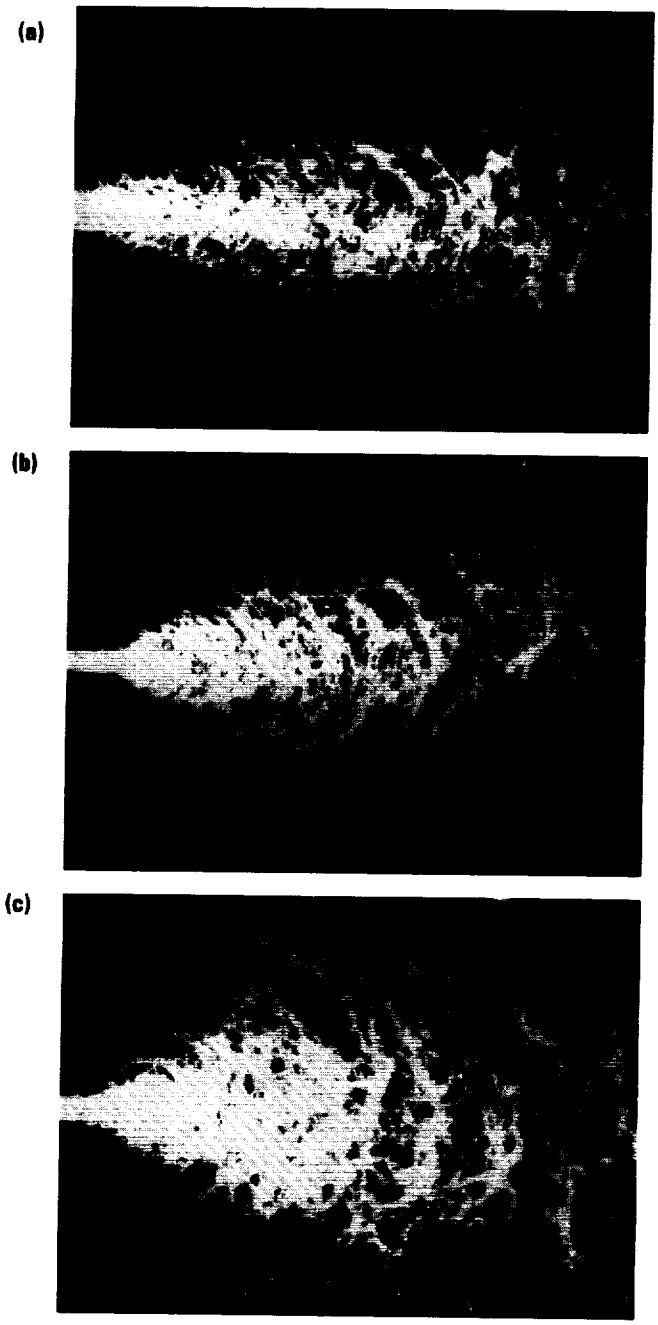

Instantaneous photographs of the spray with increasing impingement angles: (a) 15 degrees, $Re_d \approx 3.53\times10^4$; (b) 30 degrees, $Re_d \approx 3.56\times10^4$; (c) 60 degrees, $Re_d \approx 3.26\times10^4$.

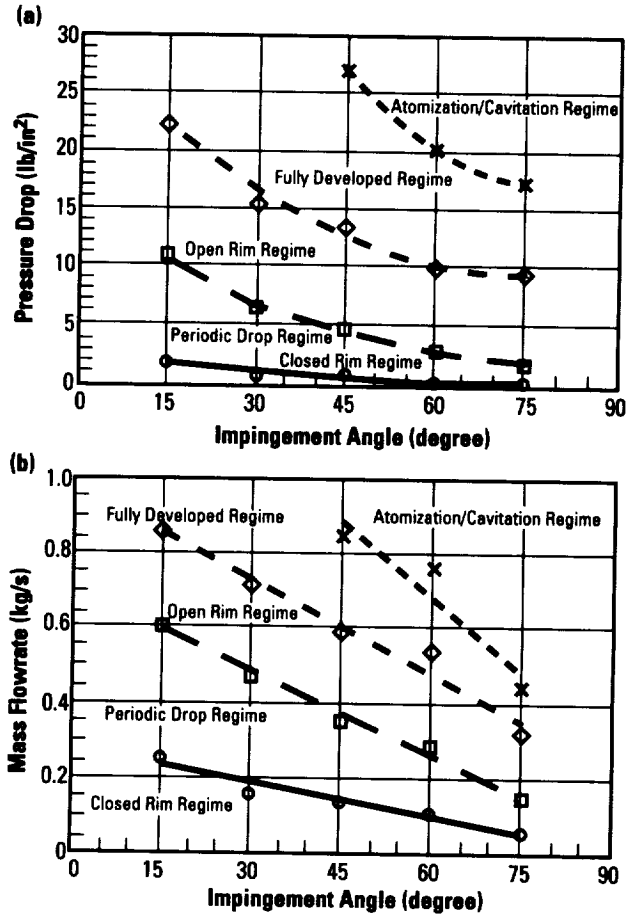

Regime definition by observation: (a) pressure drop versus impingement angle; (b) mass flowrate versus impingement angle.

K.W. Gross/EP55
205–544–2262
Sponsor: Office of Aeronautics, Exploration, and Technology

Formed Platelet Combustor Liner Construction Feasibility

Rocket engine combustion chambers must be cooled to withstand the severe high-temperature environment that they contain. The construction of the **cooling liners** for the combustors is a time-consuming, intricate, and costly operation. Current practice employs the use of copper (Cu) alloy liners with hundreds of axial grooves machined in the outer surface. These slots are "closed out" by an electroforming process, usually using nickel (Ni), to form the cooling passages. Machining tolerance capability currently limits the minimum hot-gas wall thickness to approximately 63.5 mm (0.025 in) where wall temperatures are in the 732 °C (1,350 °F) range.

An alternate **cooling liner fabrication** approach is being investigated that has the potential for reducing liner fabrication time by an initial estimate of 50 percent and of improving the liner's cooling capability by lowering wall temperatures to 177 °C (350 °F). This alternate approach is based on the use of diffusion-bonded stacks of Cu alloy material sheets called **platelets**, which are 20-mm (0.008-in) thick or greater and which have been photoetched to form cooling passages. The **platelet** stacks are formed into contoured sections by a stamping process and are joined to form the desired **combustion chamber liner**.

A nozzle assembly containing a zirconium-Cu (Zr-Cu) **formed platelet cooling liner** and sized to fit a 178-kN (40,000-lb) thrust combustor has been hot-tested to verify the design and fabrication approach. Testing will continue to verify the thermal life cycle capability of the design. The **cooling liner** has been designed to operate at 20.7 MN/m^2 (3,000 lb/in^2) chamber pressure using hydrogen (H_2) as the coolant. The predicted hot wall temperature is 371 °C (700 °F), with a predicted thermal life cycle capability of greater than 100 cycles. The validation process for application to large-scale size has been started, with design work begun for an H_2-cooled **formed platelet** liner sized for a space shuttle main engine main (SSME) combustion chamber.

F. Braam/EP52
205–544–7055
Sponsors: Office of Aeronautics, Exploration, and Technology and Space Transportation
Main Engine (National Launch System)

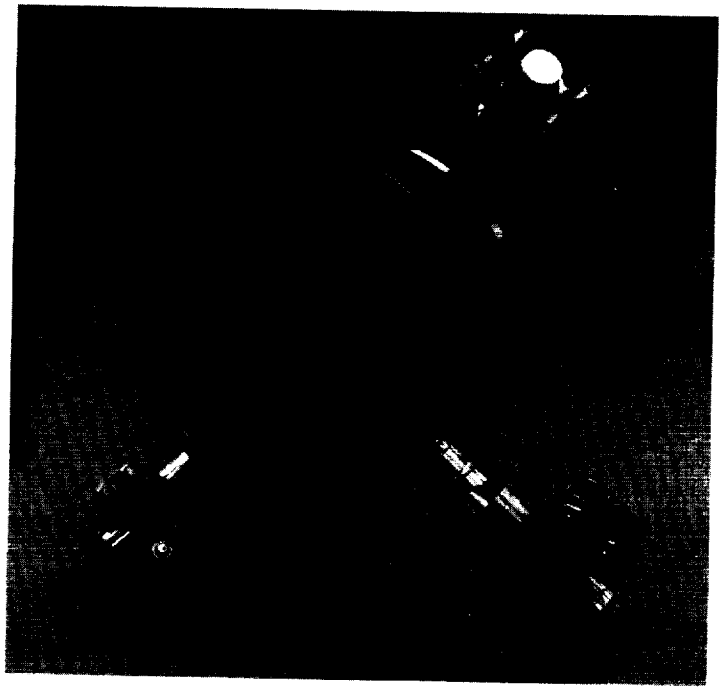

40k combustor with formed platelet liner.

Liquid Thrust Chamber Performance

Modeling of liquid rocket combustion is complicated by the presence of several physical processes, each with different time and length scales, all strongly coupled. Understanding the phenomena, such as **atomization, droplet interaction** and dispersion, group effects of droplets, evaporation, and combustion, provides the necessary knowledge for a better design of combustors. The **liquid thrust chamber performance (LTCP)** program under development now is such an advanced tool for the performance predictions. This code features the solution of axisymmetric/two-dimensional (2–D), time-dependent Navier-Stokes equations for **two-phase** flow with equilibrium chemistry as well as multistep finite rate reactions, including third-body efficiencies. The program treats dense sprays by using an Eulerian-Eulerian approach. The discretization scheme is fully implicit and based on the Lax-Friedrichs total variation diminishing (TVD) scheme for the gas phase and the Steger-Warming TVD scheme for the droplet phase. The code simulates the history of bipropellant fuel/oxidizer droplets. There are three group combustion model options available in the program. They are:

- Modified Twardus-Brzustowski model
- Chiu's model
- Bellan-Harstad model.

The **LTCP** code offers two turbulence models, the Cebeci-Smith algebraic model and a fully coupled Chien's low Reynolds number kinetic energy (k)-dissipation rate (ε) (k-ε) model, where the turbulent production and dissipation equations are fully coupled to the flowfield and chemistry. These characteristics are especially important for stability in the solution process.

For nozzles with actively cooled walls by transpiration flow or tangential slot injection, **LTCP** provides a feature that can be used efficiently. There are also three **atomization** models structured into the code representing single circular injectors, coaxial injectors, and impinging jets.

The **LTCP** code is based on primitive variable linearization using partial pressure, velocity, and temperature for faster convergence at low-speed flows and particularly for fine-mesh grids. The code features an interactive front-end technique for user-friendliness, which contains a built-in grid generator for nozzle flow, including the film cooling by tangential slot injection. This code uses some methods from previously developed programs, such as two-dimensional kinetics (TDK) and viscous interaction performance evaluation routine (VIPER), for rocket engine performance predictions, due to their verified effectiveness with which the propulsion community is familiar. Adopting, for instance, the wall geometry definition, the equilibrium chemistry package, and the finite reaction rate processor from the previously mentioned existing codes with the same input variables will minimize the learning process undoubtedly.

To demonstrate the present analytical capability and to check out the computer program, a test case for a **two-phase** injection process in a combustion chamber was executed. The solution clearly exhibits the temperature variation when uniformly distributed gas, consisting of oxygen/hydrogen (O_2/H_2) reaction products for a mixture ratio equal to one, and embedded O_2 droplets of 25 μm (1×10^{-3} in) with an initial axial velocity of 30 m/s (98.4 ft/s) undergo an evaporation, mixing, and multistep finite **rate chemistry** process.

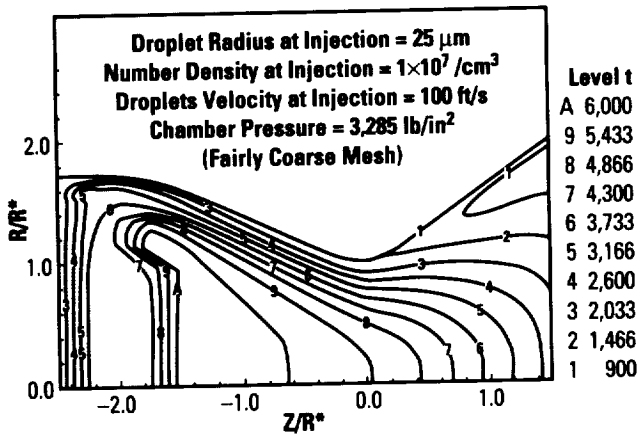

Temperature contours for premixed G(H_2+O_2) at O/F=1, and lox injection temperatures = 1,500 °R for the G(H_2+O_2) = 300 °R for lox.

From a thermodynamic aspect, the increase in temperature from the injection condition, the location of the flame at the highest temperature level, followed by the temperature decrease in the expansion process, is notable. The associated fluid dynamic development of the flowfield is evident from the Mach number contours.

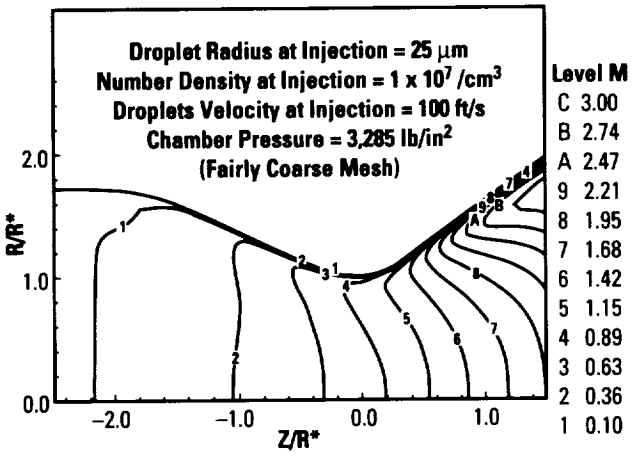

Mach number contours for premixed $G(H_2+O_2)$ at O/F = 1, and lox injection temperatures = 1,500 °R for the $G(H_2+O_2)$ = 300 °R for lox.

This effort is being conducted under contract NAS8–38798 by Physical Research, Inc., in Irvine, CA, with principal investigators being Dr. A. Dang and Dr. H. Navaz.

K.W. Gross/EP55
205–544–2262
Sponsor: Office of Aeronautics, Exploration, and Technology

Orbital Maneuvering Vehicle Thrust Chamber Performance

The **variable thrust engine** (**VTE**) has been intended to meet the operational requirements of orbit maneuvering vehicles (OMV's). The optimum **performance** and reliability of this engine requires a thorough understanding of the complex internal reactive flow field. The design and development of this engine, however, has been based on test programs that focus only on the overall operation and the **performance** characteristics. The objective of this project is to develop a mathematical analysis tool to aid design modifications and **performance** evaluation of the **VTE**. To accomplish this task, the existing **reactive flow equation solver** (**REFLEQS**) code is being modified.

A number of simulations was performed to assess the effects of various parameters on the mixing characteristics and **performance** in terms of specific impulse (ISP). The parametric study of droplet initial velocities indicates that the mixing and reaction process in the combustor is sensitive to droplet initial conditions. Higher droplet velocities lead to smaller residence times and hence insufficient mixing is achieved, whereas lower droplet velocities give rise to better mixing characteristics. The parametric study of droplet initial sizes suggests that the smaller size droplets provide better mixing patterns than do the bigger droplets.

An analysis was also performed to estimate the effects of the heat shield on the flow field in terms of entrainment and heat transfer from the combustor walls.The computational grid for this analysis is extended beyond the nozzle exit to resolve the expansion of the exiting flow into the vacuum environment. An instantaneous reaction model was used to simulate the **hypergolic** chemistry. It was found that the expansion of the combustion products at the nozzle exit causes fluid to be entrained into the shield region. The amount of combustion products circulating into the heat shield domain is estimated to be approximately 0.05 percent of the total mass flowrate through the nozzle. The circulating fluid has an extremely low density (due to low pressures on

the order of 1.0E–06 Pa (1.45E–10 lb/in^2)); therefore, its influence on the flow dynamics and the heat transfer process inside the thruster are judged to be negligible. However, the heat shield is expected to play a prominent role in influencing radiative heat transfer and cooling of the nozzle.

To study the radiative heat transfer in the heat shield, a radiation model is currently being developed. There are many radiative transfer methods available, each having its own advantages and disadvantages. Among these methods, the discrete ordinate method is found to be very amenable to coupling with a **computational fluid dynamics (CFD)** code. In the discrete ordinate method, the radiative heat transfer equation is integrated over a finite control volume for a given set of discrete ordinate directions. This method has several advantages. First, this method is relatively simple to implement for polar and boundary fitted coordinate (BFC) geometries. Secondly, the evaluation of in-scattering term is relatively simple. This method has already been coded into the **CFD** code and is now being tested with several benchmark cases. This method will be used to analyze the radiative heat transfer processes in the OMV thrust chamber.

This work, conducted by **CFD** Research Corporation in Huntsville, AL, under contract NAS8–37196, is nearing completion, with Dr. A. Przekwas as the project manager.

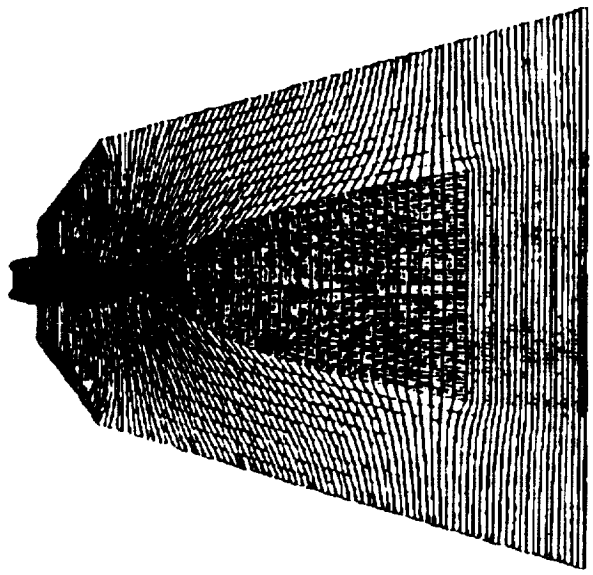

Computational grid for the heat shield analysis.

K.W. Gross/EP55
205–544–2262
Sponsor: Office of Aeronautics, Exploration, and Technology

Temp.	Contours
FMIN	2.944E+02
FMAX	4.494E+03
Contour	**Levels**
1	2.944E+02
2	4.392E+02
3	5.840E+02
4	7.288E+02
5	8.736E+02
6	1.018E+03
7	1.163E+03
8	1.308E+03
9	1.453E+03
10	1.598E+03
11	1.742E+03
12	1.887E+03
13	2.032E+03
14	2.177E+03
15	2.322E+03
30	4.494E+03

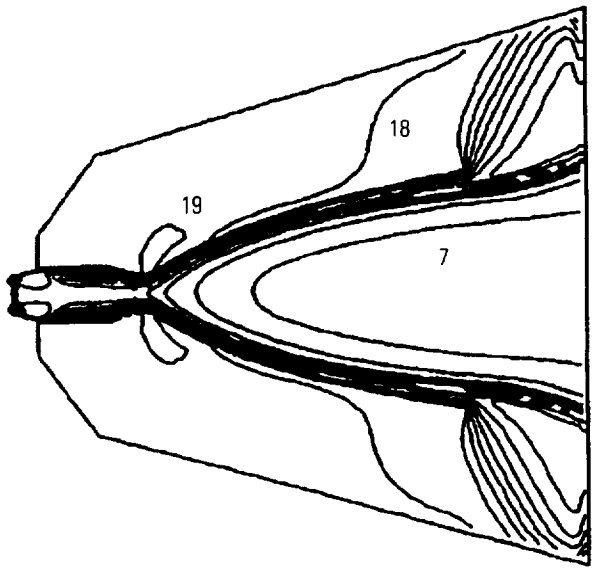

Temperature distribution in the chamber and heat shield.

Physical Processes of Injection and Atomization of Liquid Fuels

Under grant NAG8–126 with Carnegie Mellon University in Pittsburgh, PA, with Professor N. Chigier as the principal investigator, the fundamental physical processes of injection and **atomization** of liquid propellants for rocket engines were investigated experimentally. **Coaxial** airblast atomizers were used in this investigation. Microphotography was used to obtain details of wave disturbances on liquid surfaces. Direct **measurements** were made of wavelength and amplitude growth rate on liquid surfaces. Wave frequencies were measured using a laser beam attenuation technique. Wavelength and amplitude were found to increase along the length of the liquid surface while frequency remained constant.

Detailed **measurements** have been made in the sprays using the phase Doppler particle analyzer (PDPA). **Measurements** of drop size, velocity, and number density are related to the disintegration process. Initiation of disturbances occurs in the injector or by interaction with the surrounding gas stream. The gas stream drives the waves and accelerates the liquid surface.

The principal findings of this research are summarized below.

- **Coaxial** injector elements do not provide high-quality **atomization** compared to gas turbine liquid fuel injectors.

- During startup and shutdown, low liquid momentum jets can generate hook shapes, caused by large eddy structures from the coflowing gas stream. Large drops are formed under these conditions.

- Classical liquid jet breakup classifications have been revised for **coaxial** coflowing liquid-gas atomizers.

- Waves developed on liquid sheets and jets generate clusters of droplets with the same pulsation frequency as the wave frequency. These pulsations may trigger combustion instabilities. Measured surface wave frequencies were in the same acoustic range as combustion instabilities encountered in rocket engines.

- Liquid surface wave growth was found to be nonlinear. Relative velocity between gas and liquid flow has a major influence on **atomization**.

- Changes in liquid viscosity and surface tension were of secondary importance for **atomization**, as compared to relative velocity.

- The dynamic behavior of liquid sheets was found to be very similar to that of hard spring systems. The analogy can be used for theoretical analyses and interpretation of results.

- Turbulence intensity and large-scale eddy size in the coflowing gas stream were found to have an important influence on **atomization**. Significant reductions in liquid breakup length and drop sizes were achieved by increasing turbulence intensity in the gas stream to 25 percent.

- Increasing turbulence intensity and scale in the liquid jet resulted in distortion and eruption of the liquid surface. Liquid spray angle is increased and breakup lengths are reduced.

The entire effort is complete and has been documented in a final report.

K.W. Gross/EP55
205–544–2262
Sponsor: Office of Aeronautics, Exploration, and Technology

Pressure-Velocity Algorithm for Multiphase Chemical Reacting Flows

For the last decade, most pressure-based methods have employed iterative techniques applied mostly to low-speed subsonic flows. These methods are inefficient in handling multiphase **reacting flows** due to the iterative procedures required. In this study, a new **pressure-velocity algorithm**, suitable for fluid flows at all speeds, has been extended to couple with a Lagrangian particle tracking scheme and an efficient stiff ordinary differential equation solver for multiphase chemical **reacting flow** calculations.

The current method is based on the **operator-splitter technique** and allows a differential operation on different flow variables as well as fluid-particle interaction terms, thus establishing physically correct pressure correction equations including extra second-phase effects. The final pressure-velocity forms are time-accurate and general and can be integrated in finite-volume, finite-difference, or finite-element methods (FEM's). The present algorithm has been implemented in the **multiple all-speed transient** (**MAST**) computer code. Very efficient solutions have been obtained for: transient single-orifice liquid jet, solid and hollow cone spray, kerosene spray combustion burner, and supersonic hydrogen/oxygen (H_2/O_2) diffusion flame calculations. This method has also been applied to examination of the space transportation main engine (STME) subscale nozzle cooling problems and spray combustion calculations with swirling injection elements.

Several papers on this subject have been presented at conferences. Articles for publication in technical journals, as well as a final report, are in preparation. This analytical effort is conducted under grant NAG8–128 at The University of Alabama in Huntsville, with Professors S.T. Wu and C.P. Chen as principal investigators. An up-to-date version of the **MAST** computer program is operational on MSFC's mainframe computer.

K.W. Gross/EP55
205–544–2262
Sponsor: Office of Aeronautics, Exploration, and Technology

The Chemical Kinetics of Liquid Oxygen/ Hydrocarbon Combustion

A Small Business Innovative Research (SBIR) contract, NAS8–38486, with Software and Engineering Associates, Inc., Carson City, NV, with Mr. G. Nickerson as principal investigator, is addressing combustion processes occurring in rocket engines fueled with liquid oxygen (lox)/**hydrocarbon** (**HC**) propellants. As a result of the contract, which ends in mid-1992, a computer code has been developed and verified that can predict kinetically controlled combustion processes that occur in lox/**HC** propellant rocket engines of current and projected interest to NASA. For example, when these devices are operated fuel-rich, extensive **sooting** is often observed. However, if the mixture ratio is less than a certain threshold value, then little or no **sooting** is observed. This effect is found to be the result of finite **rate chemical** kinetics, i.e., below a certain temperature, the reaction process is stopped. The availability of oxidizer and fuel to the gas phase chemical reaction process is governed by propellant "**vaporization**" and mixing. Thus, the model incorporates **vaporization**, mixing, and chemical kinetics.

An extension of the Priem[1] model is used to calculate bipropellant spray **vaporization**. Mixing is treated by an adaptation of an empirical method developed by Nurick.[2] Chemical kinetics are treated using unidirectional cracking reactions,[3] followed by finite **rate** elementary reactions that lead to acetylene, which is regarded as a precursor to soot. **Sooting** is treated by using a scheme developed by Frenklach and others. In this scheme, the path to soot is controlled by the formation of successive polycyclic aromatic rings. When a sufficiently large ring is formed, it is assumed to go directly to soot.

The above mentioned finite **rate** combustion models have been verified with existing engine data for the areas identified as critical as a result of a phase I study. Results obtained from the computer analysis have been compared to liquid rocket engine gas generator experiments using lox/rocket propellant-1 (RP–1), lox/propane, and lox/methane (CH_4) propellants. Predictions for exhaust species concentrations, **sooting** onset, and relative **sooting** amounts compare very well to the experiments.

One such set of experiments is those obtained from the high-pressure preburner tests conducted for NASA by the Aerojet-General Corporation (AGC). A comparison of predicted versus measured characteristic velocity (C*) values has been observed. These results show that high C* efficiencies cannot be achieved in this type of device because of the kinetically controlled values of the combustion process.

A final product of the study is a computer code with predictive capability for nonequilibrium combustion processes, including **sooting**. The code is suitable for conducting rocket engine thrust chamber design studies and is capable of accurate prediction of rocket engine thrust chamber performance. The computer code, containing the analytical features, and the final report will be available contingent on the SBIR distribution rules.

[1]Priem, R.J., and Heidman, M.F., "Propellant Vaporization as a Design Criterion for Rocket-Engine Combustion Chambers," NASA Technical Report R–67, 1960.

[2]Nurick, W.H., "DROPMIX—A PC-Based Program for Rocket Engine Injector Design," 27th Joint Army, Navy, NASA, and Air Force (JANNAF) Combustion Meeting, Cheyenne, WY, November 1990, vol. II, pp. 435–468.

[3]Murata, M., Saito, S., Amano, A., and Malda, S., "Prediction of Initial Product Distributions From Pyrolysis of Normal Parrafinic Hydrocarbons," *J. Chem. Eng. Japan*, 6 (1973), pp. 252–258.

K.W. Gross/EP55
205–544–2262

Sponsors: Office of Aeronautics, Exploration, and Technology and Office of Commercial Programs, Small Business Innovative Research Program

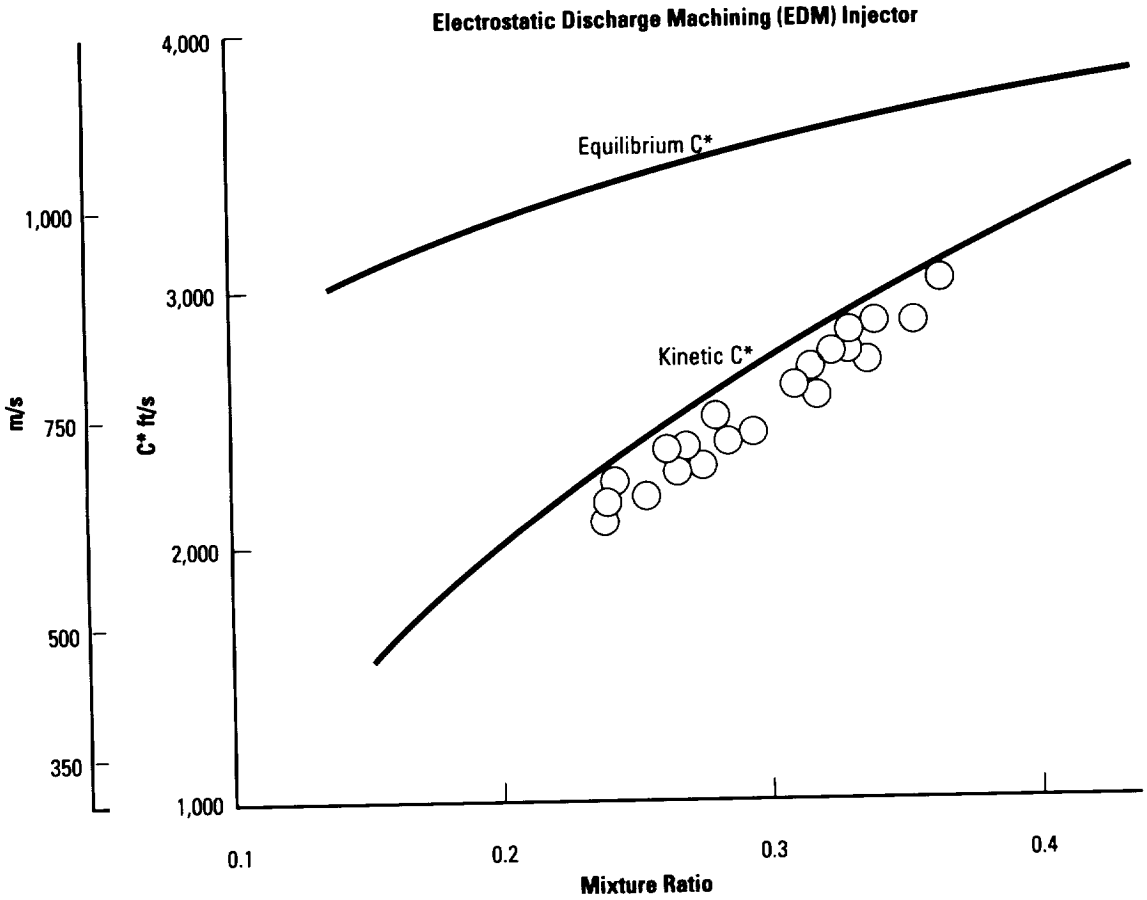

Predicted versus measured values of C* for a fuel-rich, high-pressure lox/RP–1 preburner.

Turbulence Modeling for Liquid Rocket Thrust Chambers

In response to a workshop reviewing various **turbulence models** used in existing liquid thrust chamber performance simulation, it is recommended that a useful turbulence model must be capable of treating inhomogeneous and anisotropic flow characteristics, which are present during the operation of a rocket motor. Such a quality is apparent in the second-moment **Reynolds stress model (RSM)**, which has been chosen as the baseline model for simulating turbulent flows in a rocket thrust chamber.

In this study, the RSM has been developed with options, such as the **algebraic Reynolds stress model (ARSM)** combined with several **kinetic energy (k)-dissipation rate** (ε) (**k-ε**) models, to account for current computer limitations. The **ARSM** contains all essential elements of the **RSM** and accounts for some complex effects such as curvature, rotational swirl, and gravitational body forces. The key elements of modeling anisotropic effects, embedded in the pressure-strain tensor of the **RSM** (or **ARSM**), are based on the linear return to isotropy model of Rotta and an isotropization production (IP) model. The nonhomogeneous effects are achieved, using Rodi's hypothesis by approximating the convective and diffusive parts of the Reynolds stress transport equation in terms of the turbulent kinetic energy transport.

The current model has been implemented in a general **computational fluid dynamics (CFD)** code called the **multiple all-speed transient (MAST)** computer code for a sequence of verification tests, including flat plate compressible turbulent flow with cold and hot walls, recirculating flows, curved flows, swirling flows, as well as space shuttle main engine (SSME) nozzle flows. Technical publications, as well as a final report, are in preparation. This analytical effort is still in progress under contract NAS8–36955 DO 122 at The University of Alabama in Huntsville, with Professor C.P. Chen as the principal investigator. An up-to-date version of the **MAST** computer program, carrying the described **turbulence models**, is operational on MSFC's mainframe computer. Also, a short outline for the computer program operation has been prepared.

K.W. Gross/EP55
205–544–2262
Sponsor: Office of Aeronautics, Exploration, and Technology

Two-Dimensional Kinetics/ Boundary Layer Module/ Mass Addition Boundary Layer Technical Support

The **two-dimensional kinetics (TDK)** computer program, coupled directly with the **boundary layer module (BLM)** and the **mass addition boundary layer (MABL)** programs, is a large software package that is used to predict the **performance** of liquid rocket **thrust chambers**. Many options are available for a variety of problems, and several **boundary layer** analysis modules are coupled with the code. Recently, substantial modifications have been made to the program, and rigorous documentation has been prepared so that the code's analytical capability can be used for the development of projected future engine designs.

Software and Engineering Associates, Inc., located in Carson City, NV, has been awarded a contract (NAS8–39048) that will support the application of the **TDK** code to the space transportation main engine (STME) development program. This work will address the interaction of the **TDK performance** prediction analysis with the **power cycle** and energy release computer programs. At present, only the **thrust chamber performance** is determined with the **TDK** code, based on the provided interface conditions. However, engine component optimization depends strongly on flow distribution, especially for the gas generator cycle to be used in the STME. To accomplish this goal, the interaction with **power cycle** and energy release codes must be coordinated. Losses from the injection element operation and from the **boundary layer** interaction with flow injection are of special interest.

```
**********************************************************************************************************************
                                    TWO DIMENSIONAL KINETIC PROGRAM (TDK): NOVEMBER 1991

                                    SOFTWARE AND ENGINEERING ASSOCIATES, INC.
                                    1000 E. WILLIAM STREET, SUITE 200, CARSON CITY NEVADA 89701
                                    (702) 882-1966
                                    EMAIL: UUNETISEASERVISTU
**********************************************************************************************************************
 TITLE F/S NLS 650K ENGINE: GG SUBSONIC AND SUPERSONIC INJECTION . . . 2 ZONE
 DATA
   $DATA
   ODE = 1, ODK = 1, TDK = 1, MABL = 1, IMABL = 3, MABLE = T,
   ECRAT=2.682, ASUB=2.682, NASUB=1,
   ASUP = 7.,43.097, NASUP = 2,
   RSI = 6.90, RWTU = .494, RWTD = .20, THETAI = 25.420, RI = 1.598,
   THETA = 29.228, ITYPE = 1,
   IWALL = 4, NWS = 18,
   RS = 0.0,1.252232,1.541037,1.888917,2.267946,2.661167,3.058127,3.452169,
   3.838668,4.214417,4.576776,4.924005,5.254459,5.567102,5.860643,
   6.134528,6.388157,6.564863,
   ZS = 0.0,0.498084,0.973261,1.54774,2.203318,2.935726,3.742109,4.62085,5.571712,
   6.592352,7.683121,8.841478,10.067299,11.358459,12.715493,14.135952,15.618718,
   16.777452,
   THE = 8.312, EPS = 43.097,
   XIC = 5.36, NXIC = 1,
   XWGG=2.836,3.267,NWGG=2,AFWGG=2*1.0,EQLGG=T,
   NZONES = 2, XM = .930,.070,
   TRI=T, OFCORE=.878656,.83333, FFCORE=.121344,.16867, GFCORE=2*0.0,
          OFGG = .47617, FFGG = 0.0, GFGG = .52383,
   RS = 0.0,1.267731,1.578379,1.815589,2.123255,2.41037,2.632024,3.097544,
   3.931336,4.372876,4.830611,5.349851,5.879168,6.251605,6.564847,
   ZS = 0.0,.506004,.9981,1.384943,1.905862,2.425128,2.848849,3.801114,
   5.794617,7.047505,8.521854,10.46309,12.83014,14.81643,16.77742,
   NWS = 15, THE = 8.397, THETA = 29.073,
   $END
 REACTANTS
 O 2.                    100.      -2899. L  100.33O   1.149
 H 2.                    100.      -1963. L   40.33F   .0709
 H 2.                    100.      -1963. L   40.33G   .0709

 NAMELISTS
   $ODE
   RKT = T,
   P = 2250, XP = 2*1.0, PSIA = T,
   POGG = 77.0,204.0, TOGG = 2*1184.0, DELH = 2*52.2,
   $END

 REACTIONS
 H + H = H2          ,M1, A  =  6.4E17,  N =  1.0,  B =   0.0,  (AR)  BAULCH 72 (A) 3OU
 H + OH = H2O        ,M2, A  =  8.4E21,  N =  2.0,  B =   0.0,  (AR)  BAULCH 72 (A) 1OU
 O + O = O2          ,M3, A  =  1.9E13,  N =  0.0,  B = -1.79,  (AR)  BAULCH 76 (A) 1OU
 O + H = OH          ,M7, A  =  3.62E18, N =  1.0,  B =   0.0,  (AR)  JENSON 78 (B) 3OU
 END TBR REAX
 O2 + H = O + OH       , A  =  2.2E14,  N =  0.0,  B =  16.8         BAULCH 72 (A) 1.5U
 H2 + O = H + OH       , A  =  1.8E10,  N = -1.0,  B =  8.9,         BAULCH 72 (A) 1.5U
 H2 + OH = H2O + H     , A  =  2.2E13,  N =  0.0,  B =  5.15,        BAULCH 72 (A) 2U
 OH + OH = H2O + O     , A  =  6.3E12,  N =  0.0,  B =  1.09,        BAULCH 72 (A) 3U
 LAST REAX
 INERTS H2O2, HO2,END
 THIRD BODY REAX RATE RATIOS
 M1 = 25*H, 4*H2,10*H2O,25*O,25*OH,1.5*O2
 M2 = 12.5*H,5*H2,17*H2O,12.5*O,12.5*OH,6*O2,
 M3 = 12.5*H,5*H2,5*H2O,12.5*O,12.5*OH,11*O2,
 M7 = 12.5*H,5*H2,5*H2O,12.5*O,12.5*OH,5*O2,
 LAST CARD
   $ODK
   JPRNT=-2, EP = 43.097,
   $END
   $TRANS
   MP = 225, DRMIN = 0.00050,
   $END
   $MOC
   EXITPL=F,
   NC = 0,
   $END
   $MABL
    DXI=2,0E-4, NDXI=50, NYI=115,
    DXLIM = 0.0020,0.020, LDXLIM=2, XLIM=5.,10.,
    FXMGG=.004718,.023792,
    ADBATC =0,
    OFC=2, DISTRB=0,
    XCO=-2.58986,
    XCE=2.836,
    ETAC=1,
    NTQW=25,
    XTQW=-1000.,-2.67,-1.8,-1.4,-1.1,-0.6,-0.2,-0.1,0.05,0.23,0.85,1.3,2.,2.3,
    2.75,3.24,4.35,5.84,7.33,8.82,10.31,11.79,13.28,14.77,15.98,
    TQW =2*1100.,1350.,1300.,1325.,1250.,1350.,1300.,950.,850.,850.,800.,850.,
    600.,1200.,1215.,1197.,1523.,1684.,1759.,1793.,1806.,1811.,1803.,1744.,
   $END
```

TDK program.

TDK PERFORMANCE SUMMARY : F/S NLS 650K ENGINE; GG SUBSONIC AND SUPERSONIC INJECTION . . . 2 ZONE
********** FIRST TDK SOLUTION : WITH BOUNDARY LAYER **********
POTENTIAL WALL CONTOUR 2 ZONES

FIRST
TDK/MABL SOLUTION

THRUST CHAMBER OPERATING CONDITIONS

CHAMBER PRESS	[PSIA]	2250.000
CHAMBER TEMP	[R]	6663.754
MIXTURE RATIO	[–]	7.031046
H (OXID)	[CAL/MOLE]	–2899.000
H (FUEL)	[CAL/MOLE]	–1963.000
HCHAM (ODE)	[BTU/LB]	–308.8130
DELH (AVERAGE)	[BTU/LB]	52.20000
DELH1 (AVE)	[BTU/LB]	0.0000000 E+00

THRUST CHAMBER GEOMETRY

ECRAT	[–]	2.682000
RI	[–]	1.598000
THETAI	[DEGREES]	25.42000
RWTU	[–]	0.4940000
RSI	[INCHES]	6.900000
RWTD	[–]	0.2000000
NIT	[–]	221.0000
THE	[DEGREES]	8.397000
THETA	[DEGREES]	29.07300
EP (NOZZLE)	[–]	43.09700

EXIT FLOW PROPERTIES

P (AXIS,EXIT)	[PSIA]	0.0000000E+00
P (WALL,EXIT)	[PSIA]	7.244118
T (WALL,EXIT)	[R]	2289.546
V (WALL,EXIT)	[FT/SEC]	13809.66
MA (WALL,EXIT)	[–]	4.002679

ONE-DIMENSIONAL FLOW PERFORMANCE

ISP (ODE)	[SECONDS]	449.7332
ISP (ODK)	[SECONDS]	449.2070
ISP (ODF)	[SECONDS]	422.8336
CSTAR (ODE)	[FT/SEC]	7383.0
CSTAR (ODK)	[FT/SEC]	7385.7
CSTAR (ODF)	[FT/SEC]	7250.3

TWO-DIMENSIONAL FLOW PERFORMANCE

CD	[–]	0.9831281
CF (TDK)	[–]	1.912063
CSTAR (TDK)	[FT/SEC]	7514.012
THRUST (TDK)	[POUNDS]	643476.8
WDOT (TKD)	[LB/SEC]	1440.999
ISP (TDK)	[SECONDS]	446.5490

BOUNDARY LAYER PARAMETERS

DFPOT (MABL)	[POUNDS]	–3667.025
DF (MABL)	[POUNDS]	–5712.191
DISP (MABL)	[SECONDS]	–3.851033
THETA (EXIT)	[INCH]	0.3463149
DEL* (EXIT)	[INCH]	0.5676326
DEL* (THROAT)	[INCH]	–0.5946785E–02

EP (REGEN)	[–]	6.892843
SQDOT (REGEN)	[BTU/SEC]	75219.13
SQDOT (LOSS)	[BTU/SEC]	15472.30
SUM QDOT	[BTU/SEC]	90691.43
DH (SUM QQDDOT)	[BTU/LBM]	61.14216

B/L PARAMETERS WITH MASS ADDITION

DEL* BODY	[INCH]	1.002842
DF THETA	[POUNDS]	14286.05
DF DEL* BODY	[POUNDS]	–2045.167
DF MDOT	[POUNDS]	–17953.07

THRUST CHAMBER PERFORMANCE

THRUST (TC)	[POUNDS]	649188.9
CF (TC)	[–]	1.877274
WDOT (TC)	[LB/SEC]	1483.288
ISP (TC)	[SECONDS]	437.6689

TDK performance summary.

K.W. Gross/EP55
205–544–2262
Sponsor: Office of Aeronautics, Exploration, and Technology

Structures and Dynamics

A Comparison of Single-Cycle Versus Multiple-Cycle Proof-Testing Strategies

Multiple-cycle proof testing (**MCPT**) is used as a supplement to conventional nondestructive evaluation (NDE) methods on a number of space shuttle main engine (SSME) components as a means of screening-out gross manufacturing or material deficiencies to provide additional quality assurance for delivered hardware. The current **MCPT** protocol, which specifies five cycles at a proof factor of 1.2, is based primarily on engineering experience. This combined analytical and experimental research program is designed to develop a fundamental understanding of flaw growth during **MCPT** and, ultimately, to provide a rigorous basis to optimize **MCPT** procedures.

Surveys of defective hardware found that semicircular surface cracks were characteristic of many actual flaws. The experimentally measured growth of such cracks in laboratory specimens under single applications of large loads has been measured. The resistance of surface flaws to ductile crack growth is known to be substantially greater than the resistance of through-cracks from conventional compact tension specimens. This indicates that specimen and crack geometry, by influencing near-tip constraint, play a key role in determining effective material toughness.

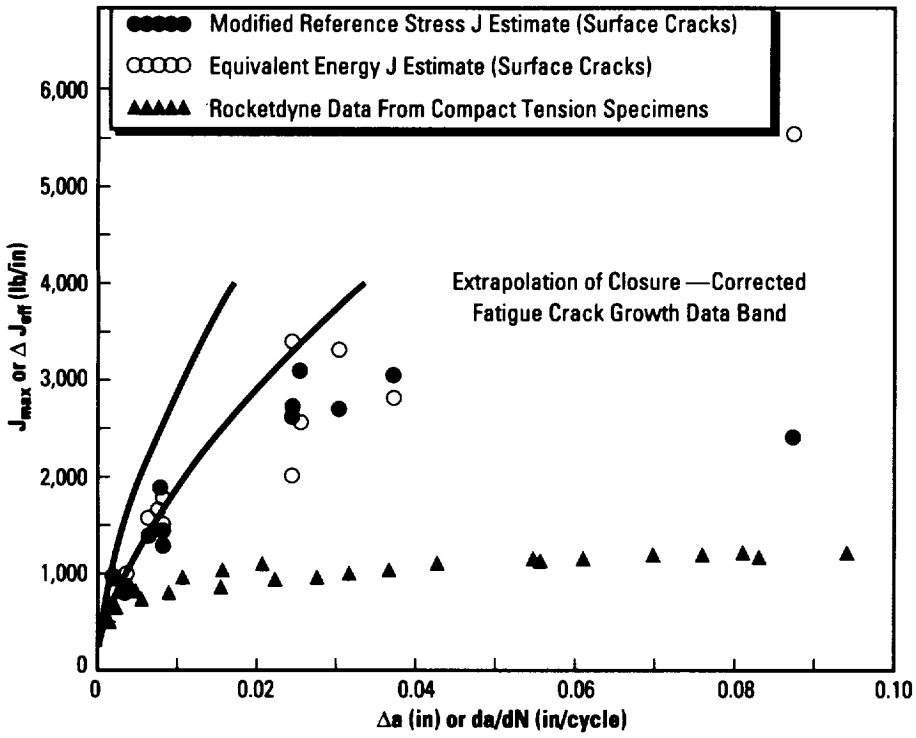

Resistance curve data for Inconel 718 with superimposed fatigue crack growth curve.

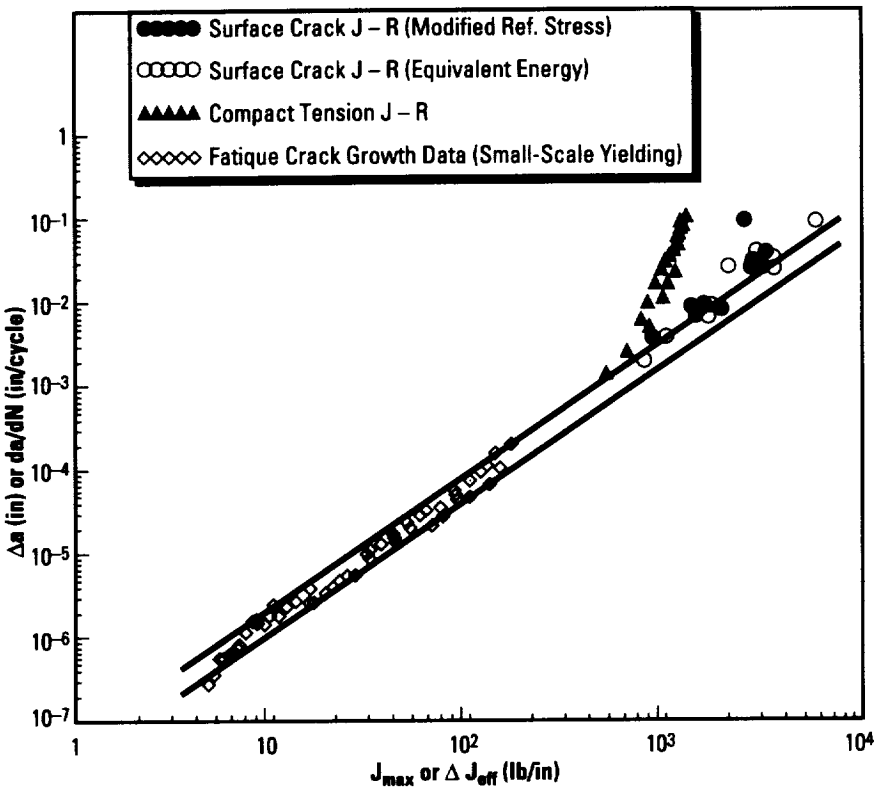

Fatigue crack growth data for Inconel 718 with superimposed resistance curve data.

Also studied is the coincidence between the initial "blunting line" portions of the resistance curves and the scatterbands associated with conventional fatigue crack growth rate testing when fatigue crack closure is properly taken into account. Apparently, the basic mechanisms of crack advance in **low-cycle fatigue** (**LCF**) crack growth are essentially the same as in the initial blunting portions of a ductile tearing event. This same coincidence has been observed from a different perspective by superimposing the resistance curve data on the traditional fatigue crack growth plot.

This relationship between "fatigue" and "fracture" events provides support for a combined resistance curve-**LCF** crack growth approach to the analysis of **MCPT**. A limited number of simulated **MCPT** experiments have been conducted. The nature of the control mode (zero-max load cycling versus zero-max displacement cycling) was found to have a significant impact on crack growth during subsequent cycles, due to the loss of constraint on the first cycle. An **LCF** approach to crack growth that incorporated crack closure successfully correlated all data. These results again confirm the importance of constraint and control mode on flaw growth during **MCPT** and indicate that optimum **MCPT** strategies are likely to vary from component to component.

McClung, R.C., and Hudak, S., "Surface Crack Behavior in Inconel 718 During Elastic Plastic Cycling," Southwest Research Institute, 1992 American Society for Testing Materials (ASTM) 24th Natioinal Symposium on Fracture Mechanics.

H.M. Lee/ED25
205–544–7245
Sponsor: Office of Aeronautics and Space Technology

Advanced Telerobotic Control Using Neural Networks

An effort is currently under way to develop an improved control system for remote manipulators utilizing **neural networks**. Existing systems, such as the shuttle's remote manipulator system (RMS), often have difficulty providing either the accuracy in end-effector placement or the smoothness of operation required by demanding tasks such as satellite servicing or in-space structural assembly. These deficiencies exist primarily as a result of compromises made in solving the complex nonlinear equations of motion governing the **manipulator dynamics** during real-time operation. These equations in their natural form would overtask the capabilities of even the most powerful modern microcomputers; therefore, a need exists for a more enlightened approach. One such concept is **neural networks**, which offer the advantages of adaptivity, speed, and compactness, in addition to the ability to control many **nonlinear systems**.

Accurate Automation Corporation (ACC) of Chattanooga, TN, is currently developing a complete neural-net-based **teleoperator** control system offering the flexibility needed to support both space- and ground-based manipulators. Under phase I of their Small Business Innovative Research (SBIR) contract (NAS8–38443), AAC demonstrated the feasibility of this approach utilizing a two degree-of-freedom (DOF) **manipulator dynamic** simulation operating in a vertical plane. The control algorithms were able to successfully adapt to changes in end-effector mass in both 1- and 0-g environments, while still providing smooth and accurate operation.

Currently, under SBIR contract phase II (NAS8–38967), the simulation is incrementally being expanded to six DOF's in anticipation of testing the algorithms with a shuttle RMS model. Under this same contract, AAC will deliver a hardware implementation of the controller and interface it with an existing manipulator in MSFC's **robotics** laboratory for further refinement. It is expected that this technology will find applications both within NASA and commercial enterprises, owing to its adaptive architecture.

R. Dabney/ED13
205–544–1473
Sponsor: Office of Commercial Programs,
Small Business Innovative Research Program

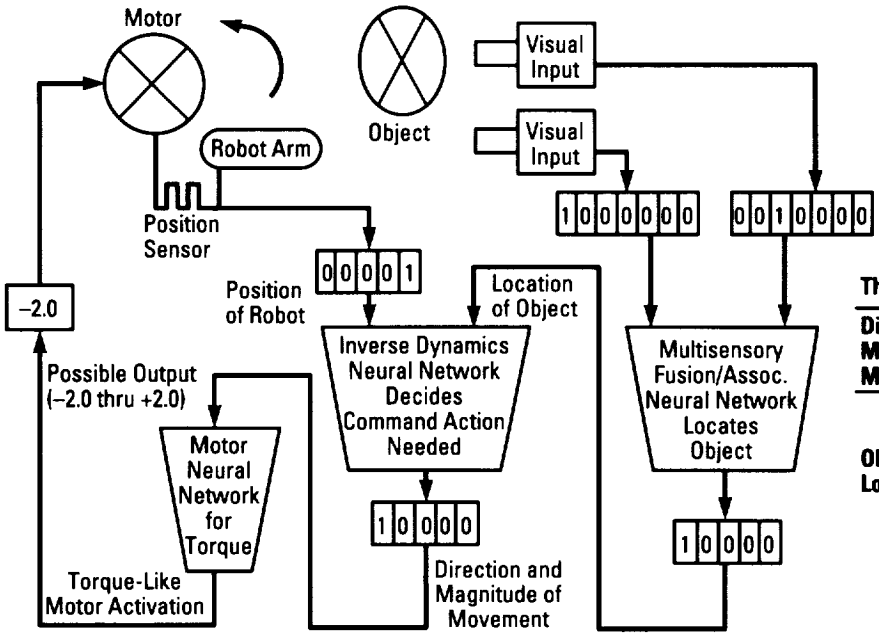

The Command:

Direction and Magnitude of Movement	Robot's Position				
	10000	01000	00100	00010	00001
00001	00001	*	00001	*	00100
00010	*	*	*	*	*
00100	00001	*	00100	*	10000
01000	*	*	*	*	*
10000	00100	01000	10000	10000	10000

Object Location

* Untrained Situations

Block diagram of the robotic neural network system.

Analysis of Static and Dynamic Nonlinear Viscoelastic Response

By performing **biaxial propellant testing**, the **Jet Propulsion Laboratory** (**JPL**) has provided NASA with a more accurate understanding of space shuttle solid rocket booster (SRB) propellant behavior. This type of testing will build a more complete data base for structural integrity analyses of current and next-generation booster rockets.

JPL is currently involved in three primary areas of propellant biaxial testing: (1) cutting/machining test specimens to carry out multiaxial, **nonlinear (large deformation) viscoelastic response** of polybutadiene acrylonitrile (PBAN) propellant; (2) refurbishing test equipment, including data collection software and test hardware; and (3) labor required for testing, data reduction, and documentation of results.

The following is a summary of the biaxial structural testing series that has been achieved at **JPL** as of March 1, 1992:

- Biaxial multistep stress relaxation testing—four temperatures and four biaxial angles
- Uniaxial multistep stress relaxation testing—room temperature
- Biaxial multistep constant strain rate testing—four temperatures and four biaxial angles
- Fabrication of a new biaxial tester frame and load cell system.

Further work to be completed by **JPL** includes the following:

- Biaxial creep tests (multiple steps at different temperatures)
- Cyclic biaxial tests
- Completion of the installation of a new biaxial tester
- Initiation of theoretical and experimental work to develop three-dimensional (3–D) failure surface of solid propellants/fracture mechanics
- Development of nonlinear, time-dependent viscoelasticity theory of solid propellants based on the theories of continuous mechanics and irreversible thermodynamics.

Landel, Robert F., "Analysis of Static and Dynamic Nonlinear Viscoelastic Response," quarterly status report, November 1991.

Landel, Robert F., "Analysis of Static and Dynamic Nonlinear Viscoelastic Response," quarterly status report, March 1992.

F. Ledbetter/EH33
205–544–2673
Sponsor: Solid Propulsion Integrity Program

Analytical Modeling of Nonorthogonal Three-Dimensional Carbon-Carbon Composites

Three-dimensional (3–D) **carbon-carbon** materials have been used primarily as throat rings in tactical solid rocket motors (SRM's). Their extensive use in other motor types has been limited due to a number of reasons. One reason is the material complexity and the inability to analytically predict stresses, strains, and composite damage in these materials under in-service conditions. Adding to the complexity is the fact that some 3–D **carbon-carbon** materials are woven in a nonorthogonal arrangement. Nonorthogonal **carbon-carbon** is anisotropic, and, therefore, orthotropic **minimechanics** models are not applicable.

Material Sciences Corporation (MSC), of Blue Bell, PA, under a Small Business Innovative Research (SBIR) contract, is presently developing a method to predict the composite thermoelastic properties for nonorthogonally woven, 3–D **carbon-carbon** materials. Their approach is to apply elasticity considerations at the fiber and **fiber bundle** levels, thereby developing an analytical prediction of the composite elastic moduli and thermal expansion coefficients from the fiber and matrix properties. For a given **fiber bundle** arrangement and bundle orientation, the method predicts the composite properties at each point in the material.

MSC is also developing a **numerical scheme** for predicting failure in these materials that incorporates their analytical method for determining the composite properties from the constituent properties. This **numerical scheme** not only incorporates this method, but is only made possible by its development. The **numerical procedure** is described as follows. The composite properties at each location are determined from the constituent properties and by knowing the **fiber bundle** orientation. The loading is applied to the composite material and the fiber and matrix stresses and strains are determined from the composite stresses. A

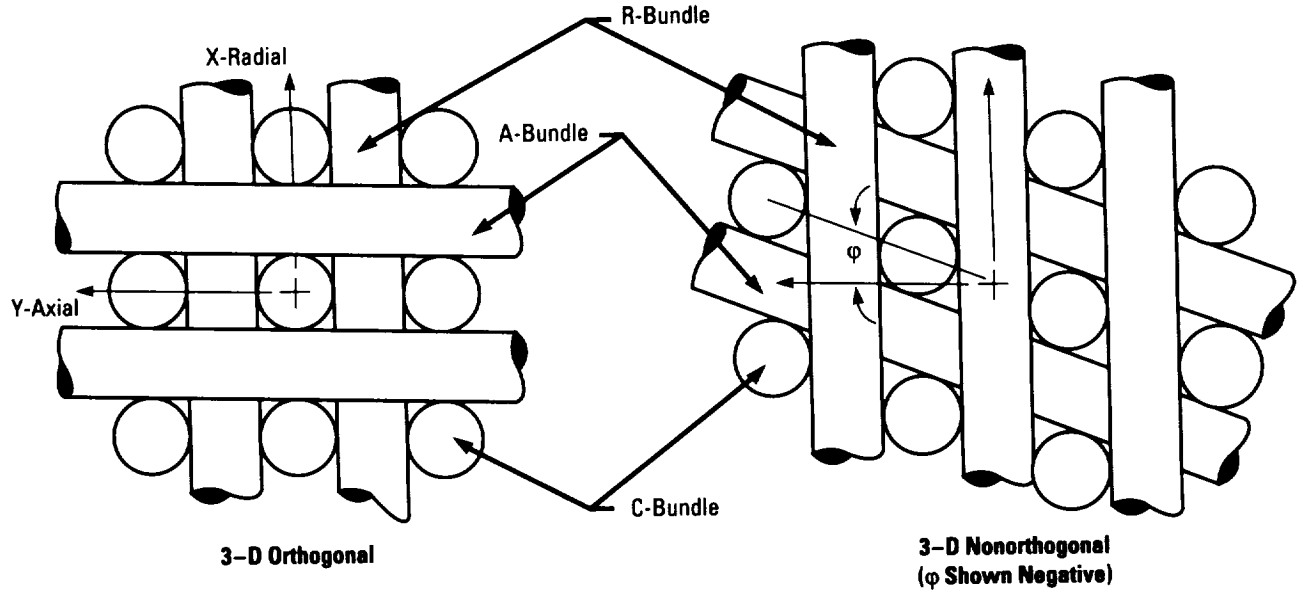

Sketch showing the fiber bundle orientation for orthogonal and nonorthogonal weaves.

judgement is made as to whether localized failure has occurred at the fiber or matrix level. If localized failure has occurred, the constituent properties are then degraded accordingly, the composite properties are determined with the degraded constituent properties, and the load is reapplied. This series of procedures is repeated until catastrophic failure of the composite or the end of the **numerical simulation**.

Future efforts involve verification of these analytical and **numerical techniques** by performing a correlative experimental investigation. The experimental investigation will be performed by Southern Research Institute, of Birmingham, AL. PDA Engineering, of Costa Mesa, CA, will also assist in this investigation by reviewing the test plans, aiding in developing the material modeling, and performing the thermostructural analysis.

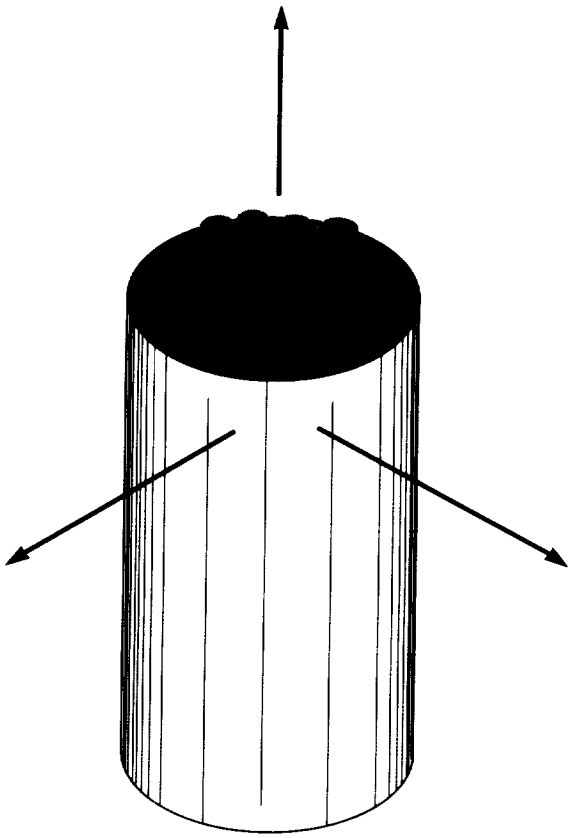

Fiber-Matrix Bundle

Sketch showing the fibers and fiber arrangement in the fiber bundle.

R.M. Sullivan/ED24
205–544–7240
Sponsor: Office of Commercial Programs,
Small Business Innovative Research

Buckling of Composite Beams

Open-section beams offer many advantages over their closed-section counterparts, among them being stackability, reduced weight, and the ability to serve as easily accessible conduits as well as primary structural members. A major problem in using open-section structural elements, however, is the inherent bending/torsion coupling that occurs when they are loaded. This research effort involves an investigation into the effect that **laminate layup** has on the load-carrying capability of **open-section composite beams**, as well as the layup's effect on this coupling. Composite beam manufacturing methods and nondestructive evaluation (NDE) techniques will also be examined.

The study has been divided into two phases. Phase I, which is now complete, involves material selection and the manufacturing and testing of flat beams. This was done to evaluate both the manufacturing and testing procedures to ensure repeatability for the beams to be made in phase II. In phase I, the flat beams were subjected to bending loads only, while, in phase II, the beams will face bending, axial, and combined axial/bending loads. Pre- and post-test NDE, though not performed on the flat beams, will be done on the open-section beams in phase II. For each of the segments of the study, the layup of the plies will be unsymmetric. This method of ply layup control (i.e., orientation, angle of the plies, and number of plies) will give the open-section beam the ability to carry greater loads than metallic structures, maintaining torsional rigidity, even when the load is applied at the geometric center rather than the shear center.

In phase I, two flat beams comprised of 24 plies of graphite epoxy material were manufactured. The beams had a thickness of 0.3175 cm (0.125 in) and measured 38.1 cm (15.0 in) long.

The open-section beams for phase II are currently undergoing fabrication, with NDE, testing, and analysis slated for the summer of 1992. Both Structures and Dynamics Laboratory personnel and Albert Zvarick, a Vanderbilt University graduate student (funded through the Graduate Student Researchers Program), are involved in the analysis of the test data.

These researchers are working toward putting together a procedure or computer code that uses **interlaminar shear stresses**, normal shear stresses, and in-plane stresses to predict failure in open-section beams. This procedure will also provide for the sizing of composite structural members and selection of an optimum ply layup angle for a given load condition.

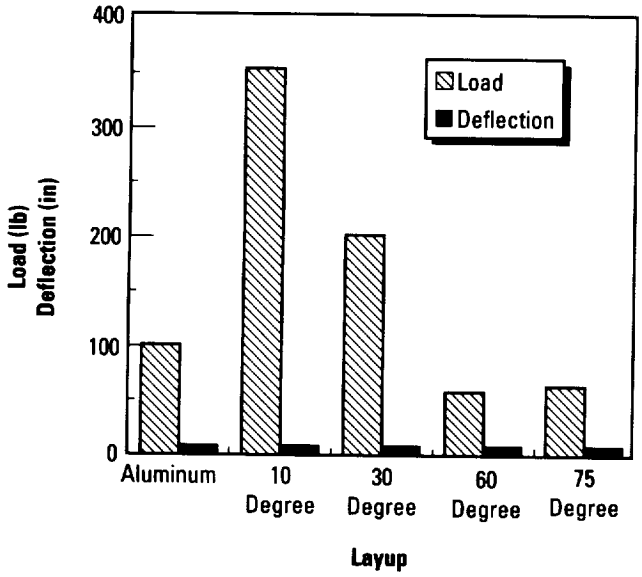

Composite versus aluminum deflections.

Ply angles, maximum deflection, and applied loads for the phase I flat beams

Ply Layup (deg)	Maximum Deflection (cm (in))	Applied Load (kg (lb))
10	17.15 (6.75)	154.2 (340)
30	17.15 (6.75)	90.7 (200)
60	15.88 (6.25)	29.2 (60)
75	17.78 (7.00)	21.8 (48)

P. Thompson/ED52
205–544–7017
Sponsor: Center Director's Discretionary Fund

Characterizing Structural Design Uncertainties Using Probabilistic Analysis Methods

Uncertainties in the definition of loads and environments, material properties, geometric variables, manufacturing processes, engineering models, analysis tools, and all types of testing, including verification and certification, lead to uncertainties in space vehicle and structure design, and, ultimately, in safety. Clearly, quantifying and understanding "problem uncertainties" and their influence on design variables develops a better-engineered, better-designed, and safer structure. Two formats are available for characterizing design uncertainties: (1) deterministic/**safety factor** and (2) **probabilistic/reliability**. The classical deterministic analysis approach accounts for design uncertainties in "lump sum" fashion by multiplying the maximum expected applied stress (a single value) by a factor of safety. In contrast, the **probabilistic** format attempts to map each individual parameter uncertainty into a probability density function. Transformation equations are then used to combine the density functions into a cumulative distribution function of the design variable, e.g., applied stress.

The main purpose of this research work is to examine the merits of two **probabilistic** analysis tools that have been under NASA development and project control since 1985. These two analysis tools are: (1) the Jet Propulsion Laboratory (JPL) **probabilistic** failure analysis (PFA) methods and (2) the **Numerical Evaluation of Stochastic Structures Under Stress (NESSUS)** code, a **probabilistic** finite element software code developed by Southwest Research Institute. Basic to the JPL methods are simulation analysis and response surface techniques.[1] The **NESSUS** code uses fast probability integration (FPI) routines known as the first-order reliability method (FORM) and the second-order reliability method (SORM), along with a relatively new method known as the advanced mean value (AMV), published in 1989 by Justin Wu.[2]

The research program is structured into three phases: (1) analyzing simple example problems using the various **probabilistic** analysis tools and methods; (2) educating engineers in the fundamental engineering and mathematical principles involved in **probabilistic**

analysis, along with special training in software codes, such as **NESSUS**; and (3) using the **probabilistic** analysis techniques with a number of specific work examples to show applicability. Also, a fourth phase is being planned that will define a testing program for **probabilistic** technology demonstration purposes. The ultimate goal of these research efforts is to develop expertise within MSFC for the application of **probabilistic** structural design and analysis techniques in current and future programs.

The project has been under way since fiscal year 1991 (FY91). Several findings are now evident. First, it will be very difficult to develop a design code that is based solely on the **probabilistic** format. True **reliability** must be demonstrated, not simply estimated, from an analysis. "Demonstrated **reliability**" is virtually nonachievable due to the small number of structures that NASA builds. However, it may be possible to develop a more-consistent design code that uses the **probabilistic** format in combination with the accepted **safety factor** approach to design. The civil engineering profession has successfully used a combined format in the development of the **load and resistance factor design** (**LRFD**) code for steel structures.[3] Developing this concept for application within NASA offers a natural extension to the current work tasks and provides a practical area for future research. New techniques for identifying the sensitivities of design variables and their uncertainties, analysis tools for determining response surfaces of problem drivers, and simulation analysis tools that are applicable to a broad range of engineering problems are some of the benefits that have resulted from this research project.

[1]Moore, N.R., Ebbeler, D.H., Newlin, L.E., Sutharshana, S., and Creager, M., "An Improved Approach for Flight Readiness Certification—Methodology for Failure Risk Assessment and Application Examples," JPL Report under NASA Research and Technology Objectives and Plans (RTOP) 553–02–01, May 1992.

[2]Wu, Y.T., and Wirsching, P.H., "Advanced Reliability Methods for Probabilistic Structural Analysis," *Structural Safety and Reliability*, American Society of Civil Engineers (ASCE), 1989.

[3]Eight LRFD papers in *The Journal of the Structural Division*, vol. 104, No. ST 9, September 1978.

J.S. Townsend/ED22
205–544–1499
Sponsor: Office of Safety and Mission Quality

Cold Air Flow Turbine Testing of the Oxidizer Technology Turbine Rig

To advance the state-of-the-art in **turbine** design, an oxidizer technology **turbine** rig (OTTR) is being designed for testing in the MSFC **turbine** test equipment (TTE). The OTTR uses high turning blades and represents the type of oxidizer **turbine** proposed for use in the space transportation main engine (STME) program. Testing will evaluate **turbine** aerodynamic **performance** and will be used to validate various computational fluid dynamic (CFD) codes used during the design phase. The results of the rig testing will be incorporated with advanced CFD studies to define an advanced oxidizer **turbine**.

The MSFC TTE is a blowdown facility that operates by expanding high-pressure air from 2,756-kPa (400-lb/in^2 gauge) storage to atmospheric conditions. Power absorption is provided by a 447-kW (600-hp) drive train consisting of a torquemeter, gear box, and dynamometer. **Turbines** are tested at scaled shaft speeds, mass flows, pressures, and temperatures. The ability to test up to full-scale turbopump **turbines** and to accurately control the pressure, temperature, shaft speed, and pressure ratio make the facility unique among government and industry facilities.

The OTTR is a single-stage, 50-percent scale air flow model with **volutes** at the **turbine** inlet and exit. Extremely high turning blades are being used to meet the power requirements with a single **turbine** stage. The blade turning angle is 157°, compared with a 113° turning angle for the space shuttle main engine (SSME) alternate turbopump development (ATD) high-pressure fuel **turbine** (HPFT) blade. The ATD HPFT blade is typical of **turbine** blades currently being used in liquid rocket engine **turbines**. Both the **volutes** and the **turbine** will be highly instrumented with detailed pressure, temperature, and flow angle measurements to accurately define the operating environment and **performance**. Unsteady pressures will be measured on the rotor blade surfaces, and extensive laser Doppler velocimeter (LDV) measurements will be taken in the inlet and exit **volutes**. The capability to vary the axial gap spacing, the tip clearance, and the blade number will be

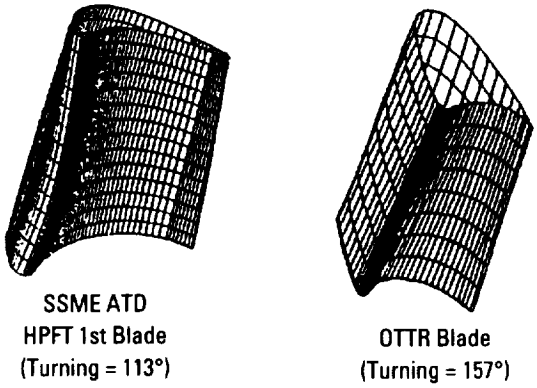

Blade contour comparison.

built into the OTTR. The rig can also be tested with both capped and uncapped blade tips. The rig requirements have been defined, and the OTTR is currently being designed and fabricated. The **turbine** will be tested in mid-1993.

S.T. Hudson/ED35
205–544–1582
Sponsor: Office of Aeronautics and Space Technology

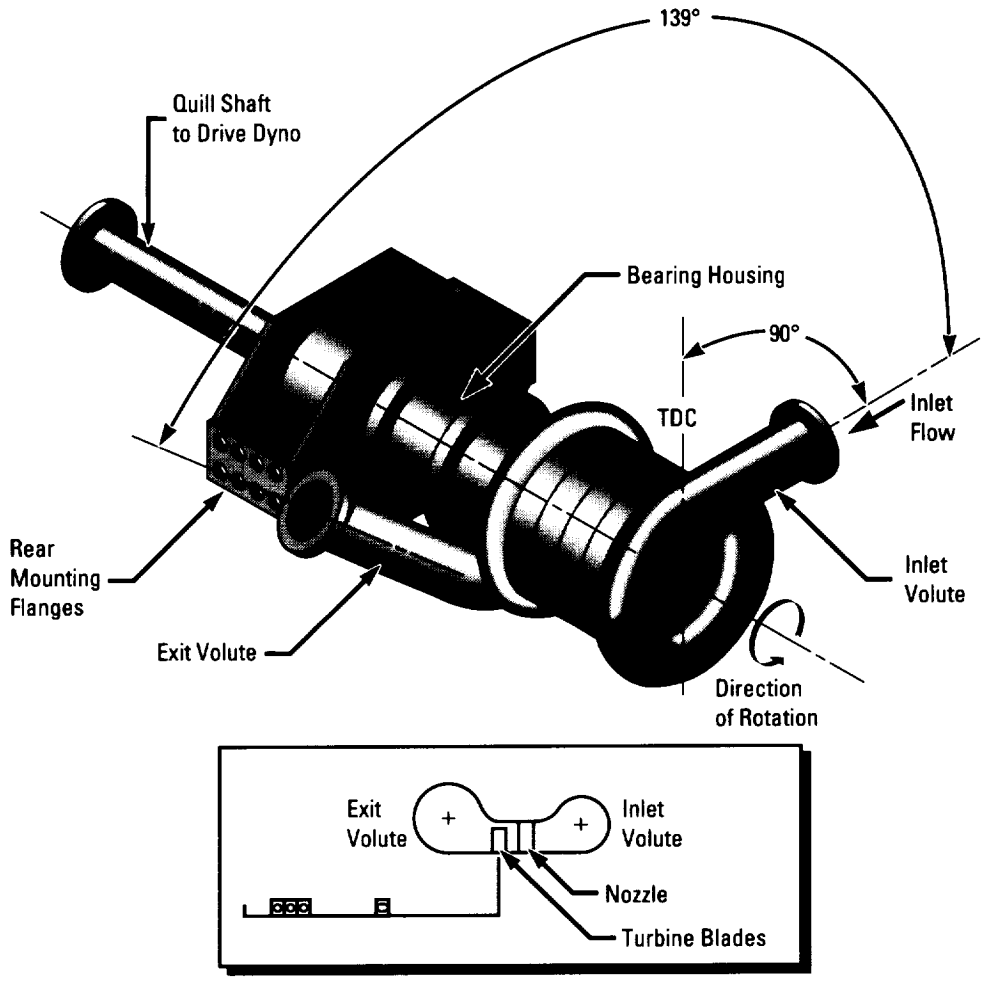

TDC—Top Dead Center

OTTR schematic.

Computational Fluid Dynamics Combustion Analysis Evaluation

Several numerical and physical models have been evaluated and tested for a **computational fluid dynamics** (**CFD**) code for the improved analysis of **burning sprays** in **liquid rocket engine combustors**. The implementation of a dispersion width transport model has demonstrated its capability of representing dispersion in nearly homogeneous and inhomogeneous turbulent flows with improved efficiency over the delta function stochastic separated flow model. This model, in conjunction with an existing droplet collision and coalescence model and a Taylor analogy breakup model, was incorporated into a state-of-the-art **multiphase** all-speed transient flow solution procedure.

A sequence of validation cases involving nonevaporating, evaporating, burning, dilute, and dense spray has been tested. The predictions show a reasonable good agreement with experimental data in terms of spray penetration, drop sizes, and overall configuration of a burning spray flame. The computed configuration of this burning spray flame has the overall agreement with the measured ones. The current model is ready for some future extensions such as the development of strong interphase coupling between the multiple-pressure correction procedure and volume of fluid method and the implementation of equilibrium and finite-rate chemistry packages for efficient transient reacting flow calculations in **liquid rocket engine combustors**.

This work is progressing under contract NAS8–36955 at the Consortium for **CFD** Research Institute, The University of Alabama in Huntsville, AL.

T.S. Wang/ED32
205–544–0503
Sponsor: Office of Aeronautics, Exploration, and Technology

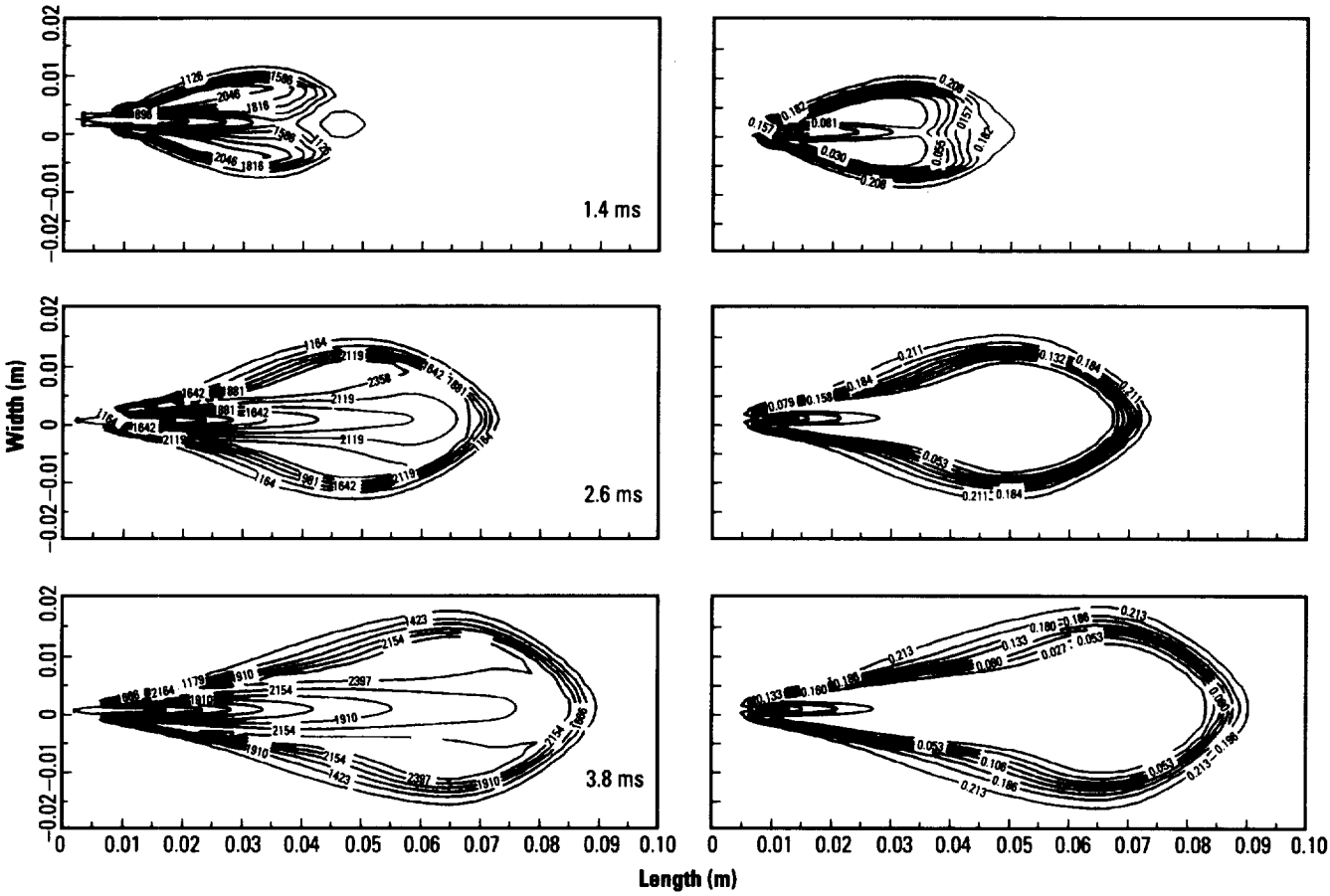

Contours of temperature and oxygen (O_2) mass fraction in a burning spray.

Damping Seals for Turbomachinery

The interactions and phase relations between a rotor system's elastic and inertial forces are apt to give rise to subsynchronous whirl, a type of self-excited vibration at frequencies near the lowest critical frequency of the rotor. This potentially destructive phenomenon imposes limits on the performance of the engine. **Damping seals** have been shown to inhibit subsynchronous whirl by providing more damping than whirl forces.

Damping seals were substituted for conventional labyrinth seals in the high-pressure oxidizer turbopump (HPOTP) of the **space shuttle main engine** (**SSME**). The additional support stiffness and damping provided by the **damping seal** increased the second critical speed and improved rotor **stability**. **Damping seals** were also substituted for the smooth interstage seals in the high-pressure fuel turbopump (HPFTP) of the **SSME**. The additional damping from the **damping seal** has eliminated the 50-percent subsynchronous vibration from the fuel pump.

SSME testing has resulted in six cases where the HPOTP bearing lost axial preload because of excessive wear. In each instance, the **damping seal** proved itself as a reliable bearing. The ball bearings were worn out, and the **damping seal** held the rotor for many starts and stops without visible wear on the knurled silver sleeve, i.e., the stator. Because of this experience, an HPOTP was built with the pump end ball bearings replaced by a **damping seal/bearing**. This HPOTP has been successfully tested at the engine level on Marshall's technology test-bed.

Damping seals have been shown to provide additional damping to improve rotor **stability** and sufficient stiffness to support the rotor as a bearing. However, experimental data that relates these desirable characteristics to such parameters as pocket depth, preswirl, and rotating speed are limited. To obtain the desired data, NASA commissioned Wyle Laboratories to design, build, and operate a test rig in which **damping seals** are evaluated. This test rig utilizes water pressured to 1.379×10^7 N/m^2 (2,000 lb/in^2) and obtains speeds of 21,000 r/min. Data from this test rig are used to verify computer codes that analytically predict **damping seal** performance. Further experimental work coupled with analysis will provide insight into how **damping seal** technology can be used to improve engine performance and reliability.

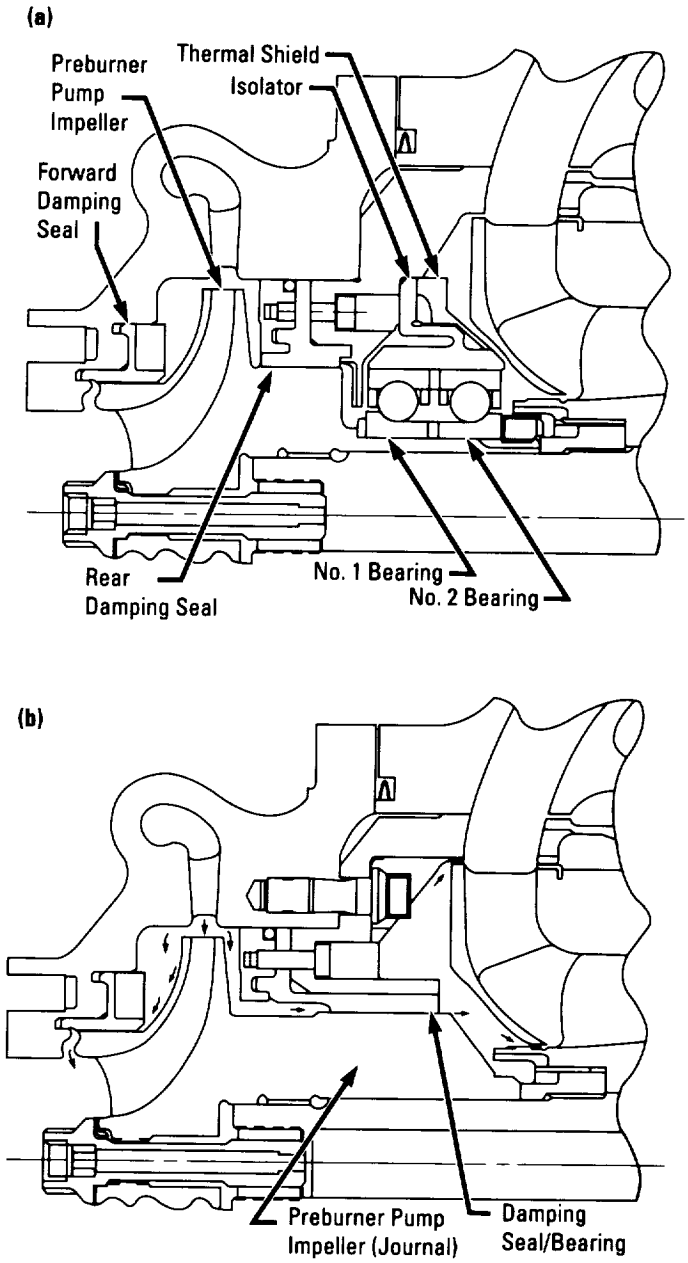

(a) Flight configuration of the HPOTP, phase II; (b) HPOTP damping seal/bearing.

E. Earhart/ED14
205–544–2417
Sponsor: Office of Aeronautics, Exploration, and Technology

Fracture Control/Damage Tolerance Methods for Composite/Anisotropic Materials

Composite/anisotropic materials are increasingly being considered for structural use in space systems. These materials are capable of providing many benefits to structural systems due to their strength capabilities, thermal properties, reduced weight, etc. However, there is an increased need to accurately establish their **damage tolerance** capabilities. **Damage tolerance** is the ability of a structure to sustain loads after crack initiation. Large amounts of research on the **damage tolerance** of **composite/anisotropic materials** have been carried out over the past 20 yr. However, there remains a need to compile and consolidate the various aspects of the research that have been carried out in this area. **Damage tolerance** consists mainly of three aspects: (1) residual strength provides the maximum damage the structure can resist under fail-safe loads; (2) crack propagation defines the time period in which a crack grows from a defined detectable length to the allowable length determined by the residual strength requirements; and (3) damage detection specifies inspection methods and intervals needed to identify flaws. The work in this task involves the residual strength and crack propagation aspects of **damage tolerance** of **composite/anisotropic materials**.

The objectives of this research task are to develop a guidelines handbook for damage-tolerance testing of **composite/anisotropic materials** and to test verified algorithms for calculating **flaw growth** in these materials. These algorithms are to be in a format that can readily be inserted into existing computer codes.

A review of current state-of-the-art testing methods for **flaw growth** and **fracture toughness** will be conducted on **composite/anisotropic materials**. Materials to be considered will include fibrous, laminated and particulate **composite**, and **anisotropic materials**, with specific emphasis on those with load-carrying capabilities. A wide range of parameters will be considered including geometric, loading, and testing environment features. Also, special attention will be given to assess state-of-the-art methods for monitoring damage growth. In addition, a thorough review of crack growth theories for **composite/anisotropic materials** will be conducted.

Engineering algorithms for calculating fatigue crack growth life for **composite/anisotropic materials** will be developed. A wide range of crack type, geometry, and loading cases will be considered. When available, laboratory test data will be used to verify the accuracy of the developed algorithms.

R. Ortega/ED25
205–544–5448
Sponsor: Office of Aeronautics, Exploration, and Technology

Fracture Mechanics Life Analytical Methods—NASCRAC™ Verification

NASA Crack Analysis Code–Version 2.0 (**NASCRAC™**) is a second-generation fracture analysis code developed for NASA/MSFC. The code uses a weight function approach to solve traditional fracture problems such as K_I and life calculation due to fatigue. **NASCRAC™** also contains capabilities for advanced fracture analysis, e.g., **crack** retardation, life calculation due to creep, and elastic/plastic stress redistribution near the **crack** tip. Since **NASCRAC™** includes the computationally efficient weight function approach and a broad spectrum of advanced capabilities, NASA/MSFC expects to use the code as an integral component of the NASA Fracture Control Program. This critical role of **NASCRAC™** in future NASA analyses dictates both a complete and objective independent **verification** and validation of the code.

The **NASCRAC™ verification** and validation plan is a three-tract comparative approach: (1) documented solutions from the literature, including closed form and graphical solutions; (2) finite element solutions; and (3) testing. **NASCRAC™** capabilities were categorized into basic information, synthesized results, and advanced capabilities. The basic information category included **crack** length versus elastic stress intensity factor (a vs. K_I), **crack** length versus nonlinear elastic stress intensity factor (a vs. J), and a **crack** opening area. Similarly, the synthesized results category included life calculations due to fatigue and creep, tolerable **crack** size, proof-test logic, and tearing instability. The advanced capabilities category included elastic/plastic stress redistribution and **crack** transitioning. Basic information **verifications**/validations are expected to be completed using literature solutions and finite element methods (FEM's). Synthesized results and advanced capabilities **verifications** and validations will require a combination of analysis and testing.

Verification of synthesized results solutions will be accomplished with combinations of literature surveys, alternative numerical solutions, and experimental tests. Prostochastic test methodologies that separate randomness and experimental error from the assessment of **NASCRAC™'s** intrinsic accuracy will be used. Test materials will be single lot 2119–T851 with well-defined material properties and known grain structures and roll patterns. **Verification** of synthesized results solutions will be performed using a three-step **verification**/validation: (1) check coding and logic of implementation, (2) check against existing experimental results, and (3) check against new experimental results. To check for coding and logic errors in synthesized results solutions, closed form solutions, alternative codes, or FEM's will be applied if possible.

Integration of weight functions using numerical recipes

Configuration	Geometry (in)	Stress Distribution	NASCRAC™ Result ($lb/in^2\ in^{0.5}$)	Direct Integration ($lb/in^2\ in^{0.5}$)
201	a = 0.1	$1{,}000 + 200x + 10x^2$	567	566
203	a = 0.1 w = 10	$4{,}000 - 800x + 40x^2$	2,513	2,524
204	a = 0.1 w = 10	Linearly increasing 500 Æ 1,500	319	316
204	a = 0.1 w = 10	$4{,}000 - 800x + 40x^2$	2,509	2,483

a – Crack length
w – Specimen width

Independent integration of three **NASCRAC™** weight function solutions using the subroutine QROMD (an algorithm that permits singularities at the integration limits)[1] has been completed. The three geometries were: (1) a **crack** in an infinite plate, (2) an edge **crack** in a plate, and (3) double edge **cracks** in a plate. In the three cases observed, good agreement between **NASCRAC™** and QROMD was obtained even though significant differences in the numerical integration scheme existed. (**NASCRAC™** actually integrates from 0 to 1 a normalized quotient with the weight function in the numerator and $\sqrt{1-x}$ in the denominator.)

Results of testing will be used to verify and validate the **NASCRAC™** code. The end result of the **verification** and validation program will be to provide the user a specified confidence level for each solution in **NASCRAC™**. The **verification** and validation program will conclude in fiscal year 1994 (FY94), with a final report to be provided to users on validity and error bounds of the **NASCRAC™** code.

(NASCRAC™ is a registered trademark of Failure Analysis Associates, Inc.)

[1]Ingraffi, T. (Cornell University), Favensi, J., Lambert, J. (Nichols Research), Stallworth, R., Wilson, C. (MSFC), "NASCRAC™ Fracture Mechanics Code Verification," 1992 Earth-to-Orbit (ETO) Propulsion Technology Conference.

R. Stallworth/ED25
205–544–7189
Sponsor: Office of Aeronautics and Space Technology

Ground Test Facility Development

The objective of this program is to develop a **ground test facility (GTF)** in which large structures characteristic of future space platforms can be analyzed and controllers can be designed and tested. Key **control** structure interaction (CSI) methodologies will be demonstrated in the CSI **GTF**. The current configuration of the CSI **GTF** is that of the proposed **control** and structures experiment in space (CASES). CASES is a proposed shuttle-based or free-flying flight experiment in which a 32-m (105-ft) boom supports an occulting plate that points toward a star, the Sun, or the galactic center to perform an x-ray experiment. The **control** objective is to maintain alignment of the occulting plate at the tip with the detector at the boom base on the shuttle. **Control** authority is provided by two-axis thrusters at the boom tip, a two-axis set of angular momentum exchange devices (AMED's) at a midpoint on the boom, and a three-axis set of AMED's at the boom tip. Primary objectives of both the ground and proposed flight experiment are to investigate CSI in a **flexible space structure (FSS)**, perform guest investigator (GI) programs to test and evaluate **FSS control** and **system identification (ID)** techniques, and to enable comparisons between ground predictions and flight results.

The CASES configuration is the baseline **GTF** configuration. The primary focus of the activity associated with the CSI **GTF** development over the last year has been the integration of the various structural components comprising the facility and subsystem testing. End-to-end system testing, **system ID**, and **closed-loop control** implementation is expected to occur by the end of the fiscal year. The major facility modifications are complete. The main platform (6.7×7.62 m (22×25 ft)) at the 40.23-m (132-ft) level of the southwest tower leg in the load test annex (LTA) of Building 4619 supports the entire system (e.g., disturbance system (DS) and experiment). Eight access platforms (2.44×2.74 m (8×9 ft)) with stairs and ladders provide access to the upper portion of the boom. An enclosure of the test area consisting of a hard wall up to the 10-m (32.8-ft) level with curtains extending from the top of the LTA down to that level has been constructed to provide a degree of

environmental **control**. The test article is the 32-m (105-ft) solar array flight experiment-I (SAFE–I) boom, which was modified in 1990 for the **GTF**. Modal and dynamic deployment tests of the test configuration have been completed. The data are being used to refine the **GTF** computer models.

The boom is attached to a simulated mission peculiar experiment support structure (MPESS). The MPESS/ boom configuration is attached to a tripod that floats on an air bearing system which consists of an epoxy-filled ring and three air bearings mounted to the tripod. The tripod supports the experiment through the simulated

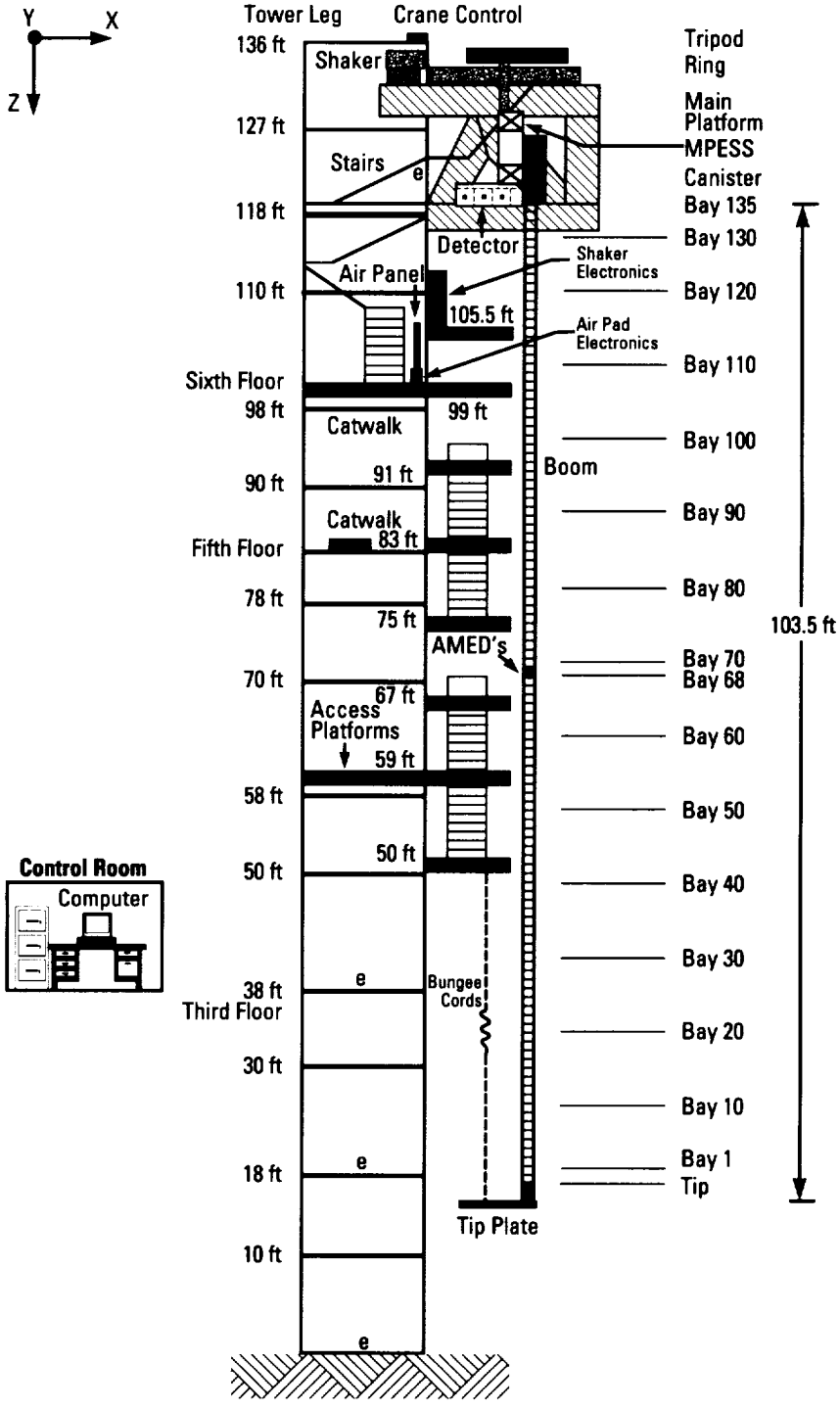

CSI GTF schematic.

MPESS and the ring provides a flat surface on which the air bearings float. Disturbances are provided via two electromechanical shakers that move the tripod. A custom-designed mechanical interface system to connect the shakers to the tripod has been implemented. The signals output from disturbance system/subsystem testing come from the string potentiometers, which output the position of the tripod.

Two orthogonal thrusters are used primarily for pointing the boom in the flight experiment; they are also used for vibration suppression in the ground experiment. The AMED's are used for vibration suppression at a midpoint and at the tip of the boom. The midlength AMED package consists of two motors attached to reaction wheels and two two-axis gyros. The tip AMED package has three motors with reaction wheels and two two-axis gyros. The AMED's are installed and are undergoing subsystem testing.

The custom-designed real-time computer system has been integrated in the facility and the special-purpose **control** software has been developed. A number of custom electronic circuits, including multiplexers, demultiplexers, filters, signal conditioning circuits, AMED electronics, and the power supply system, have been designed, fabricated, and integrated. An autonomous safety monitoring system has been developed and will be integrated in the facility by the end of July 1992. A video monitoring system has also been obtained and is being integrated in the facility. The latter two systems will provide the means to electronically and visually monitor system conditions during experiments.

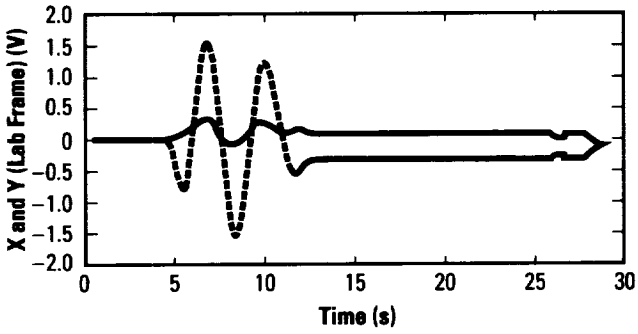

DS test: manual Y motion.

A.P. Bukley/ED12
205–544–0054
Sponsor: Office of Aeronautics, Exploration, and Technology

Highly Accurate Adaptive Techniques for Damage Modeling and Life Prediction of Aerospace Structures

In the design of components of aerospace structures, such as the space shuttle main engine (SSME), reliability considerations and **life prediction** are of extreme importance. There exist several damage and fatigue theories designed to estimate reliability and life of aerospace materials. These theories can be combined with advanced computational methods to create a reliable and computationally efficient tool for the design and analysis of aerospace structures under severe cyclic thermomechanical loading environments.

A phase I Small Business Innovative Research (SBIR) activity is under way in which the coupling of advanced solution-adaptive techniques with **continuum damage theories** and nonlinear **constitutive material models** is being investigated. Adaptive finite element methods, based on rigorous error estimates, automatically adjust the structure of the computational mesh to provide the best solution at minimum computational cost.

The focus of this project is to couple adaptive methodologies with **continuum damage theories** and nonlinear **constitutive material models** in a three-dimensional (3–D) finite element code for predicting microcrack nucleation, growth, and ultimate life expectancy for geometrically complex bodies subjected to complex time-dependent loads.

The phase I technical objectives include:

- Determining the feasibility of developing a 3–D **solution-adaptive finite element code** for modeling the nonlinear behavior of metallic structures undergoing cyclic loading with continuum damage
- Identifying appropriate damage models for modeling continuum and cyclic damage of metallic structures under severe cyclic thermomechanical loadings
- Determining if these damage models can be efficiently implemented within the context of a **solution-adaptive finite element code**

- Determining if standard interpolation and/or residual error estimation techniques used in the analysis of linear and nonlinear problems are appropriate for estimating errors in the numerical solutions of problems with continuum damage

- Determining the level of reliability that can be expected from continuum damage models in terms of damage accumulation and life expectancy.

J.B. Min/ED25
205–544–1564
Sponsor: Office of Commercial Programs,
Small Business Innovative Research Program

Integrated Smart Data Base

There have been over 1,600 tests of the space shuttle main engine (SSME). The data from these tests represent a valuable resource to the rocket engine community. As new analysis tools become available to the engineer, often times that further analysis of the historic data can provide new insights into present failures and point toward new avenues of engine development. The integrated **smart data base** will provide a solution to keeping this historic data in a form that will be **permanent** and easily accessible to the analyst.

The present archiving system does not interact with the user to search the data for generic or relational types of data that might have a bearing on the analysis to be performed. Presently, there is a long lead-time for retrieving data, which becomes even longer if the user is not clear on the relevant items that describe the exact data needed. This usually requires an overkill on the amount of data requested and the user winds up with an enormous number of tapes that have to be shipped and then converted and analyzed to determine if the desired data are included. This effectively rules out any short turnaround of analysis.

The integrated **smart data base** system will consist of three components, each contributing a necessary function to the data base. These components are a data acquisition component, a smart component, and an archiving component. The data acquisition part of this system will acquire as much data from the Stennis Space Center (SSC) as can be salvaged as well as acquiring data from recent engine tests. These data will be sampled and ultimately stored in digitized form on an **optical** medium that should last for up to 100 yr. At first, the data will reside on the magnetic disc section of the archiving system for some period of time where it will be accessible to the users at a fast turnaround time for either analysis or correction. When a large portion of this disc area is used, the data with low recall or usage will be stored on the long-term **optical** media. The smart component will interface between the user and these two storage media to retrieve the user-requested data in an **interactive** and intelligent manner. This will allow a user search of stored data for test segments, groups of tests, or unique tests that contain certain conditions or exhibit certain characteristics or relations. The data that the user obtains from this search will be sent to a user-designated site for further processing.

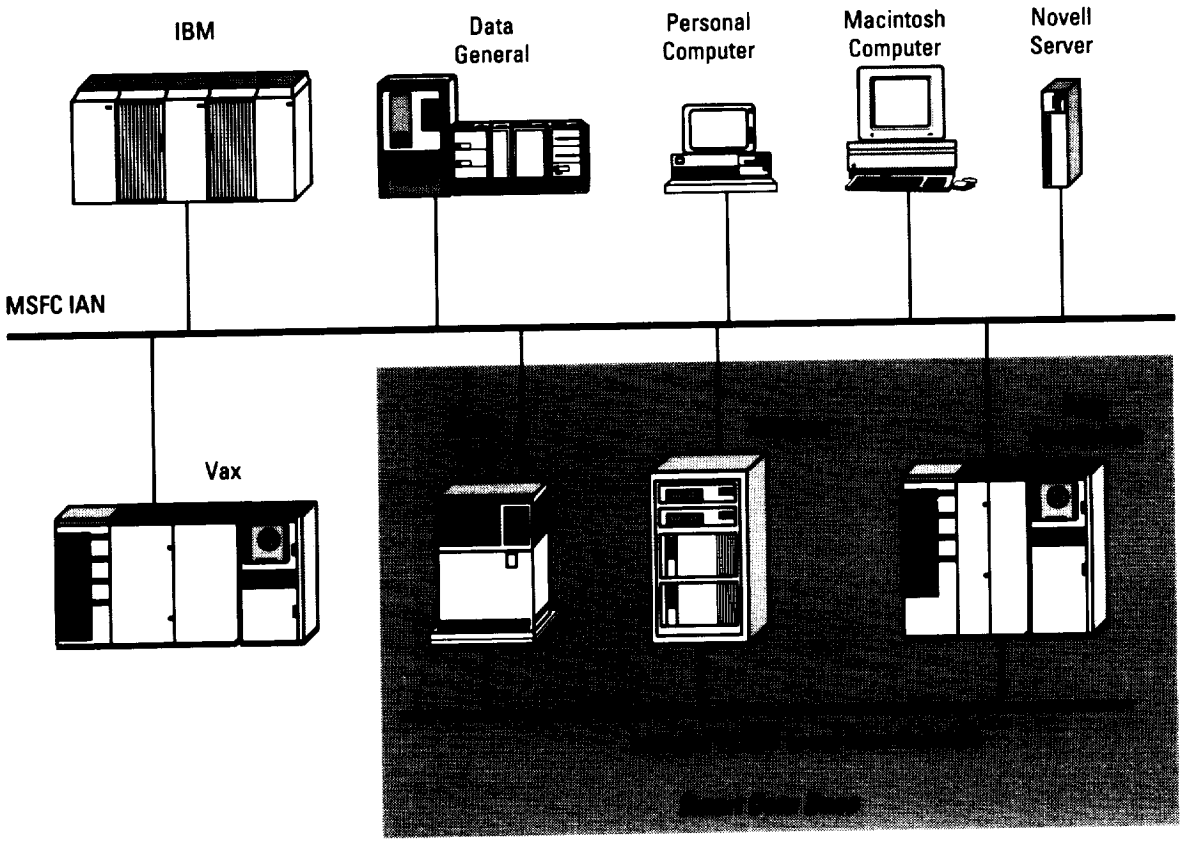

IAN – Institutional Area Network
TCP/IP – Transmission Control Protocol/Internet Protocol

The components of the integrated smart data base system.

T. Fox/ED14
205–544–1462
Sponsor: Office of Aeronautics and Space Technology

Joint NASA/MSFC-Sandia National Laboratories Hypervelocity Impact Testing

Due to the continuously growing and increasingly dangerous orbital environment, one of the primary design considerations for space structures is **shielding systems** to protect against micrometeoroid and **orbital debris** (M/OD). The most recent M/OD environment model defines the average impact velocity of **orbital debris** as 10.3 km/s (23,000 mi/h) and that of micrometeoroids as 19 km/s (42,500 mi/h). As a result of this and preceding environment definitions, there has been great interest in evaluating shielding concepts at these velocities; however, these impact velocities are not obtainable through conventional light gas gun technology.

Sandia National Laboratories (SNL) has recently improved the **hypervelocity** launch technique of their modified two-stage light gas gun and has achieved impact velocities of 12 km/s (26,800 mi/h) with half-gram flat plate projectiles. As a result of this demonstrated capability, NASA's MSFC and SNL have extended the joint effort between the two facilities to exploit this capability in an effort to evaluate the performance of thin aluminum Whipple shields at impact velocities from 8 to 12 km/s (17,900 to 26,800 mi/h). The information from these tests can be used to verify the results of theoretical models used to predict Space Station *Freedom* shield performance in the high-velocity regime.

The test program conducted under the joint effort consisted of impacting nine thin aluminum Whipple shields with an aluminum flat plate traveling between 8 and 12 km/s (17,900 to 26,800 mi/h), with impact obliquities varying between 0 and 60 deg. Upon impact of the flat plate on the Whipple shield, a photographic and flash x-ray record will be created of the debris cloud formation, propagation across the standoff distance, and impact on the back wall structure. A photographic record will also be created of the rear face of the back wall structure for evidence of perforation.

The Whipple shield concepts to be tested under the joint effort consist of a 0.127-cm (0.050-in) 6061–T6 aluminum bumper with a 0.3175-cm (0.125-in) 2219–T87 aluminum back wall separated by a 10.16-cm (4.0-in) standoff.

The test program will identify the **ballistic limit** (e.g., the point identified by a combination of diameter and velocity of projectile that will just penetrate the back wall structure) for this **shielding system** concept at 8, 10, and 12 km/s (17,900, 22,400, and 26,800 mi/h) for flat plate projectiles. Traditionally, the **ballistic limit** curves have been defined for spherical projectiles; therefore, further analysis is required to convert the "critical" flat plate into an equivalent "critical" sphere.

S.A. Hill/ED52
205–544–4106
Sponsor: Space Station *Freedom* Project Office

Lightweight Composite Heat Pipes

Weight reduction of **radiator** systems is essential for future space missions. Lightweight systems cannot only enhance payload capabilities but can also offer improved heat rejection with minor weight impacts. **Heat pipes** are often integral components of these designs and can comprise significant portions of overall weight.

Heat pipe exteriors are typically constructed from aluminum tube and/or extruded aluminum shapes. Replacing these elements with **composite** materials in combination with aluminum powder wicks can result in weight savings. Under this NASA Small Business Innovative Research program, a prototype **composite heat pipe** was developed. The prototype consisted of a 25-mm (1-in) diameter tube, 610 mm (24 in) in length, constructed from carbon fiber/epoxy **composite**. The capillary wick was a polymer-bonded aluminum powder. Ammonia was selected as the working fluid for the prototype development.

Composite resin and working fluid compatibility was a major concern for this development. Testing on various resin samples indicated none were totally immune to the effects of anhydrous ammonia. To minimize working fluid contact with the resin, an aluminum foil liner was bonded to the **composite** tube's interior between the tube and the capillary wick. The foil lining also ensures the tube's vacuum capability and serves as a noncondensable gas barrier.

Testing on this design has shown that even minute exposure of the ammonia, e.g., the bond line contact of the foil liner, was unacceptable. To negate this effect, a welded foil liner has been incorporated into the design with the **composite** layup being added to the liner rather than the foil being bonded into the tube after tube assembly. This process continues to be refined, but, at present, the welded foil liner represents a major advance in this development.

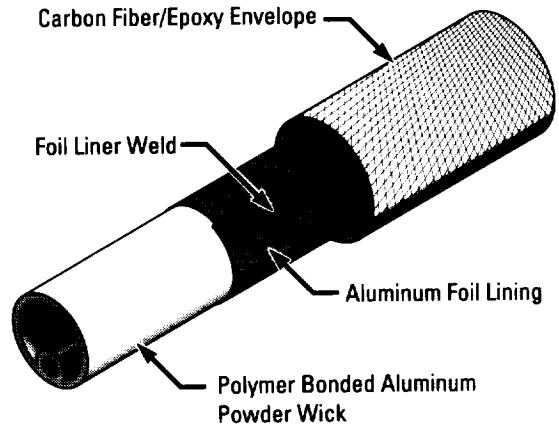

Composite heat pipe construction.

W.A. Till/ED63
205–544–7205
Sponsor: Office of Commercial Programs,
Small Business Innovative Research Program

Main Injector Assembly Computational Fluid Dynamics Analysis Code

Fluid flow and heat transfer in the **main injector assembly** of the powerhead in **liquid rocket engine**s are complex phenomena. The basic understanding of these phenomena is essential to achieve optimum performance during normal operating conditions and maintaining structure integrity during off-design operations. The mixture ratio and mass flowrate distributions of the **main injector assembly** will greatly affect the engine performance and the heat loads of the combustion chamber; the latter effect is especially directly linked to the durability of the engine. This project, therefore, focuses on the development of an analysis tool capable of accurately predicting the flow, heat transfer, and mixing characteristics of hot-gas flow around the **main injector assembly** and the local mixture ratio distribution of the flow entering the main combustion chamber.

The latest **computational fluid dynamics** (**CFD**) techniques are used, including multizone, nonstaggered grid, conservative formulation in curvilinear coordinates, high-order spatial and temporal discretization, and advanced multiple-pressure correction algorithms. The concept of **porosity** is employed to describe the blockage and drag force due to the presence of the liquid oxidizer-posts within the assembly. A nonisotropic **porosity** model is incorporated, and volume and surface **porosity** parameters, which are based on the configurations of local liquid oxidizer-post clustering and flow shield design, are introduced into the governing equations.

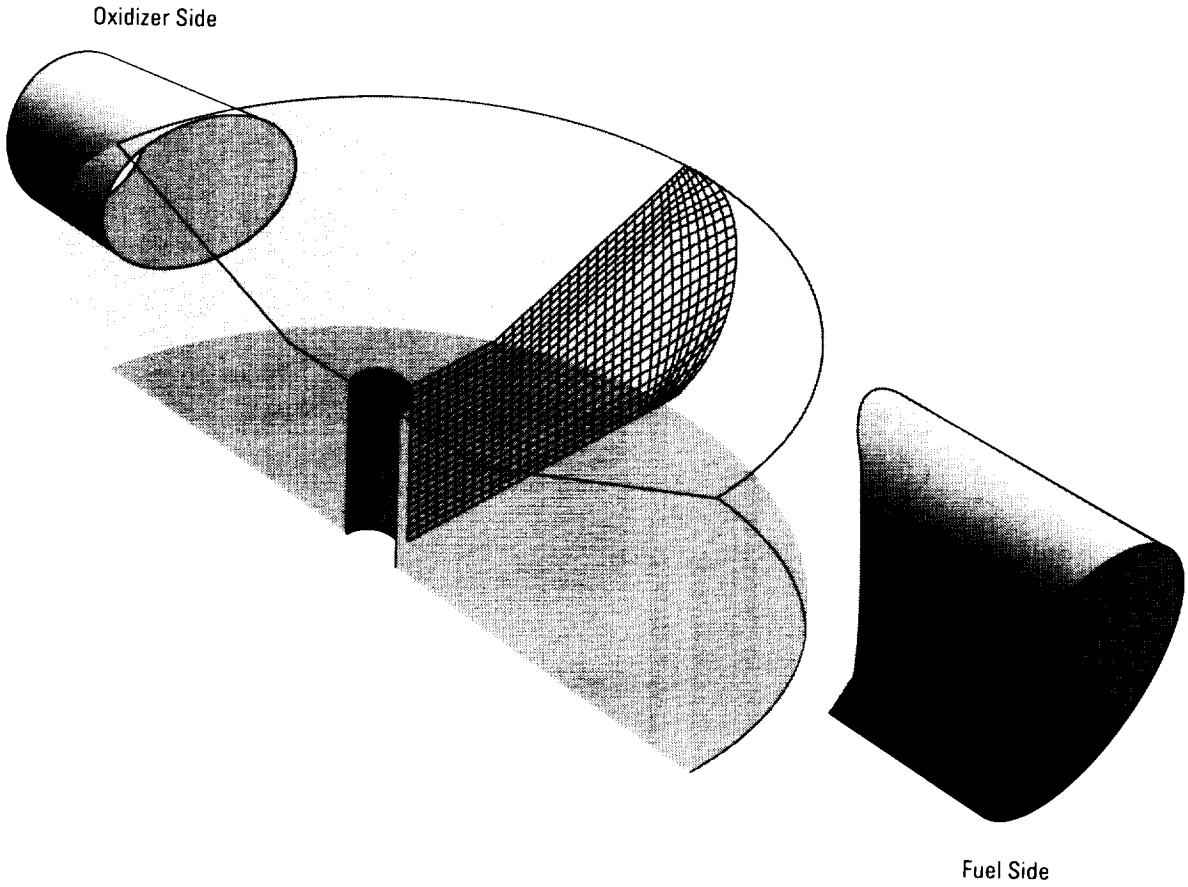

The geometry and grid system of the hot-gas injector assembly.

Numerical studies have been conducted to identify the drag coefficients of the flows both through tube banks and around the shielded posts over a wide range of Reynolds numbers. Empirical, analytical expressions of the drag coefficient as a function of local flow Reynolds number were then reduced. The three-dimensional (3–D) **CFD** analysis is divided into three parts: liquid oxidizer dome, hot-gas injector assembly, and hydrogen (H_2) cavity.

The analysis reveals that the mass flowrate at the injector face is relatively uniform. The predicted mixture ratio is close to stoichiometric around baffle elements at the 104-percent power level; this might cause hot spots around baffle elements. However, due to the assumptions made in the **porosity** model and the use of a relatively coarse grid system, the numerical results can only provide a qualitative trend. The proposed model should be further tested and refined in the future. This effort is being conducted by SECA, Inc., in Huntsville, AL, under contract NAS8–38871.

T.S. Wang/ED32
205–544–0503
Sponsor: Office of Aeronautics, Exploration, and Technology

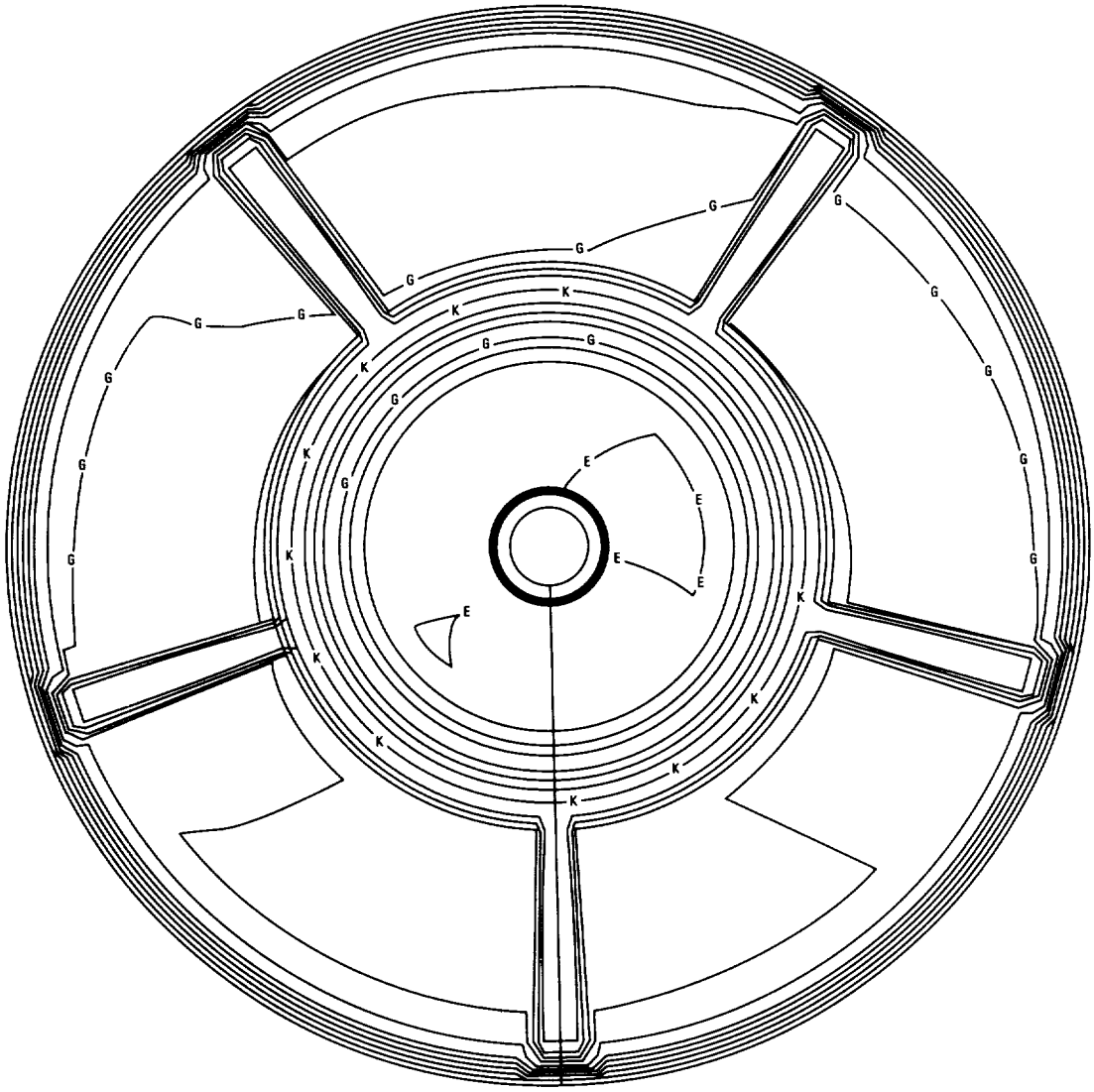

The oxidizer/fuel (O/F) ratio contours of the SSME main injector assembly at the 104-percent power level.

Microstructural Propellant Constitutive Theory

For nearly three decades, various constitutive theories have been proposed for the description of the mechanical behavior of **solid propellants.** These theories have ranged from the relatively simple linear elastic and linear viscoelastic theories applied in the 1950's to the more mathematically sophisticated theories of the 1970's and 1980's. Many theories have been offshoots of techniques used in the rubber industry.

Two problems have plagued **solid propellant** constitutive theories: (1) they were too simple to predict the complex behavior of propellants or (2) they relied too heavily on curvefitting without physical rationale. Some predictive ability was noted for simple loading situations in simple geometries after simple environmental histories; but, outside of the parametric region in which the curvefitting was performed, theoretical predictions generally strayed from experiment. Effort was expended on defining correction factors and functionals to bring the predictions into line with experimental phenomena (**phenomenological theory**). Since the correction factors are experimentally determined, the **phenomenological theory** cannot demonstrate validity outside of the range of experimental parameters to which it was curvefitted.

Under the auspices of NASA Headquarters, MSFC is sponsoring work that will provide a correct physical description of the microstructure which will generate a predictive ability of sufficient generality to apply outside of the curvefitted region. The more nearly correct the **microstructural description** is, the further outside the curvefitted region one will be able to make accurate predictions.

Since **solid propellant** consists of two primary components, the solids and the binder, it seems logical to concentrate the efforts for a **microstructural description** on three phases: the binder, the solids dispersion, and the binder/solids interface. Once each of these three phases is successfully described, a fourth phase is needed to consolidate the three phases into an operating description capable of predicting macroscopic propellant behavior. The current research will concentrate on:

- The binder description
- The solids dispersion description
- The dewetting stress measurements
- The consolidation technique.

It is hoped that the **microstructural description** theories will start replacing **phenomenological theories** in the thinking of researchers working in this area. Eventually, the material nonlinear microstructural constitutive law will be incorporated into a large deformation (geometric nonlinear) finite element code.

Carter, R.G., "Polymeric Response Based on Molecular Structure: Obtaining Individual Chain Force Laws," 1989 Joint Computational Mechanics Committee/Structures and Mechanical Behavior Subcommittee (CMC/S&MBS) Subcommittee Meeting, Pasadena, CA, November 6–9, 1989.

T. Kovacevich/ED24
205–544–4813
Sponsor: Solid Propulsion Integrity Program

Modeling Debris Cloud Formation and Stagnation With Strength, Fracture, and Smooth Particle Hydrodynamics

This Small Business Innovative Research (SBIR) project involves developing smooth particle **hydrodynamics** (SPH) into an effective technique to numerically evaluate **hypervelocity impact phenomena**. Phase I of the effort, which is currently under way, involves the addition of a strength model, a failure/fracture model, and a more robust equation of state library to an existing SPH code. After implementing these models, several experimental case studies will be modeled and the results will be compared to existing test and hydrocode simulation data. Development of this code will provide a powerful tool for predicting damage to space structures that are shielded by complex meteoroid and **orbital debris** protection systems that could cause traditional Eulerian and LaGrangian hydrocodes to generate erroneous results.

S.A. Hill/ED52
205–544–4106
Sponsor: Office of Commercial Programs,
Small Business Innovative Research Program

Multibody Modeling, Verification, and Controls

The primary focus of the 5-yr **multibody modeling**, verification, and controls (MMVC) program, initiated in November 1990, is the verification of the Tree Topologies (TREETOPS) analysis code via experimental data to be obtained in the MMVC laboratory under development at MSFC. TREETOPS is a menu-driven program used to model and analyze flexible multibody structures exhibiting either open or closed tree topologies. The menu program also provides the means to implement gains for a standard proportional, integral, differential (PID) controller or to include a user-defined controller. The verification process is a key step in advancing toward the computational controls activity, also conducted under this research and technology (R&T) project. This activity will enhance the TREETOPS suite of routines to include various model reduction techniques, improved computational efficiency, thermal effects, optical path analysis, and expanded controller design capability to include inverse dynamics and model reference **adaptive control**.

TREETOPS embodies many complex modeling features that must be validated for various multibody configurations. Some of the features to be examined are body flexibility, including large motions with small and large deformation; interface degree-of-freedom, including point and line interfaces undergoing translation and rotation; geometric stiffness, including gravity and foreshortening; and constraints, including prescribed motions and closed-tree topologies. The top-level design of a basic set of experiments that emphasize critical modeling features presently included in TREETOPS has been completed. Beginning with a simple single-beam experiment and expanding to multiple beams, joints, and various topologies, the experiments will grow in complexity as each modeling feature is examined. The final experiment will feature a test article traceable to an Advanced X-Ray Astrophysics Facility (AXAF)-type flight vehicle. Experiment hardware has been fabricated, and individual components are being tested. Detailed procedures for system-level experiments are being developed.

Critical to the experiments is the design and development of a test facility. A facility design was chosen such that the exiting platform, located on the west side of the control room between the high bays in Building 4619, will be modified to accommodate the MMVC experiments. Additional structure will be added to the platform to provide a support for the test articles. The facility design has been finalized, and fabrication should be completed next year.

A real-time **closed-loop** system (RTCLS) will be an integral part of the laboratory. Its function will be to process the sensor inputs, implement the controller, and provide the real-time output signals to the actuators. The system has been delivered, and acceptance testing was successfully completed. MSFC personnel are currently familiarizing themselves with the system and assessing its capability.

A.P. Bukley/ED12
205–544–0054
Sponsor: Office of Aeronautics, Exploration, and Technology

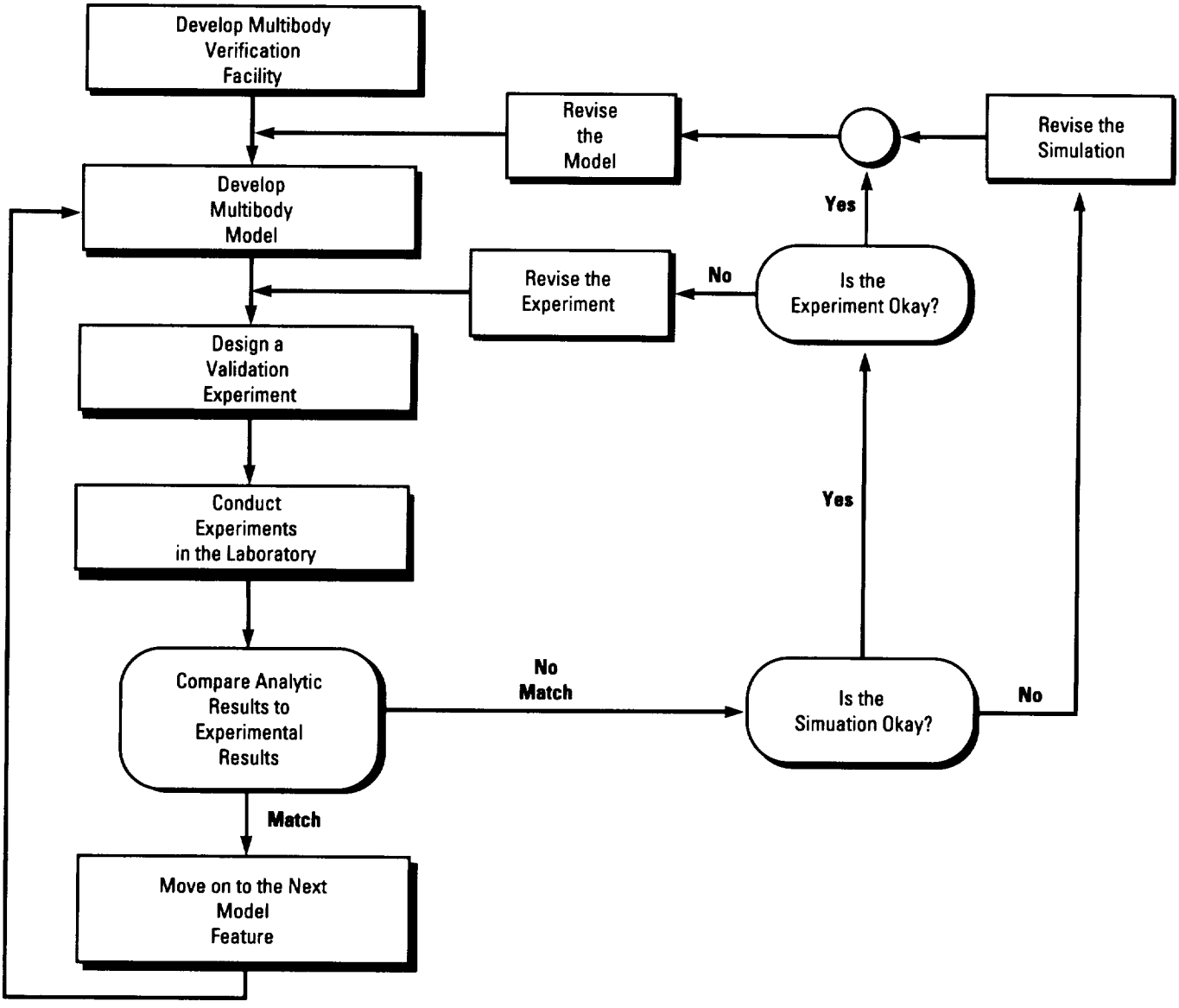

MMVC methodology.

Nonazeotropic Mixtures for Spacecraft Heat Transport

Rejecting waste heat is an important problem faced by spacecraft designers. Heat rejection is normally accomplished by means of radiators outside the spacecraft body. The heat is transported to the radiators by many different means, depending on the size of the spacecraft, the amount of heat to be rejected, and the types of heat loads inside the spacecraft.

Low-power spacecraft, such as satellites, utilize passive conduction and heat pipes to transport heat to the radiator surface. At increased power levels, as are found on the space transportation system (STS), mechanically pumped, single-phase liquid loops are employed to transport the waste heat from various sources throughout the spacecraft to the radiator surface. Future projects, such as the space station, will have much higher power levels and will have multiyear mission duration. Thermal management will be even more important on these missions, due to the long duration, the large amount of waste heat to be rejected, the long physical distance to transport the heat, and the wide variety of payloads and missions to be accommodated.

The objective of the phase II project described herein, sponsored by the NASA Small Business Innovative Research (SBIR) program, is to develop a system utilizing a **nonazeotropic** binary mixture that will provide a means of efficient heat transfer from the heat sources to the radiator surface for large spacecraft with high power levels.

Heat transport for large spacecraft with large and varied thermal loads will be split into a three-part utility system consisting of the following: (1) heat acquisition from the various sources; (2) **heat transport** from the acquisition sites to the heat rejection site; and (3) heat rejection through radiator systems. The concept can be implemented by using two loops, an internal loop that collects waste heat from the various sources and an external loop that rejects heat via the radiator systems. Either one (or both) of the loops, along with an interloop heat exchanger, serves the purpose of transporting the heat from the acquisition site to the heat rejection site. Generally, low-toxicity, single-phase fluids, such as water, are the choice of the working fluid for the internal loop. In the system being developed for the phase II SBIR program described herein, the external loop will use a **nonazeotropic** binary refrigerant mixture as the working fluid. **Nonazeotropic** mixtures offer the advantages of both single-phase and **two-phase** fluids by undergoing a **nonisothermal** phase change. The temperature gradient inherent to single-phase fluids is advantageous because it can be controlled to match the temperature gradient of the internal loop single-phase fluid, therefore allowing for more efficient heat transfer in the interloop heat exchanger. In addition, the average heat rejection temperature in the radiator is higher, resulting in a weight savings due to radiator area reduction. **Two-phase** fluids offer high heat of vaporization as an efficient means of heat transfer, allowing the mass flow to be decreased. This results in pumping power savings and reduced line sizes. Normal **two-phase** evaporation and condensation processes occur isothermally, and, therefore, require a saturation temperature below the minimum temperature of the internal loop. This decreases the heat-rejection temperature in the radiator, thus requiring more radiator area and more weight.

The term "**nonazeotropic** binary mixture" refers to two working fluids of different volatility that change composition as they evaporate or condense. As mentioned above, the unique and useful characteristic of the **nonazeotropic** mixture is that the phase change during constant-pressure evaporation and condensation occurs over a temperature range. The magnitude of this temperature range depends on the properties of the particular refrigerant pair as well as the mixture composition. The temperature gradient that occurs during the **nonisothermal** phase change can be matched to the temperature gradient of the internal loop single-phase fluid by selection of the mixture constituents and composition. Therefore, irreversibilities in the interloop heat exchanger can be reduced while receiving the increased heat transfer associated with a phase change.

The four main components in the system developed under this phase II SBIR program are:

- A positive displacement gear pump, which is designed to pump liquid, but can accommodate vapor during transients, such as startup or load shift
- An interloop heat exchanger downstream of the pump to absorb waste heat rejected by the internal single-phase loop; the liquid nonazeotropic refrigerant evaporates and increases in temperature as it absorbs the waste heat
- A set of radiator panels that rejects the heat of the (now vapor) nonazeotropic refrigerant to space, causing it to undergo **nonisothermal** condensation; the liquid exiting the radiator panels enters the pump
- A bypass line between the inlet of the radiator panels and the inlet of the pump for system control.

Specific objectives of this project are to:

- Select the **nonazeotropic** binary refrigerant mixture constituents and composition
- Measure heat transfer coefficients and pressure drop characteristics for **nonazeotropic** binary refrigerant mixtures and match the measurements to an analytical model developed to predict these data
- Design and build a **nonazeotropic** binary refrigerant mixture **heat transport** loop
- Optimize the control system for the **heat transport** loop.

D.G. Westra/ED63
205–544–3120
Sponsor: Office of Commercial Programs,
Small Business Innovative Research
Program

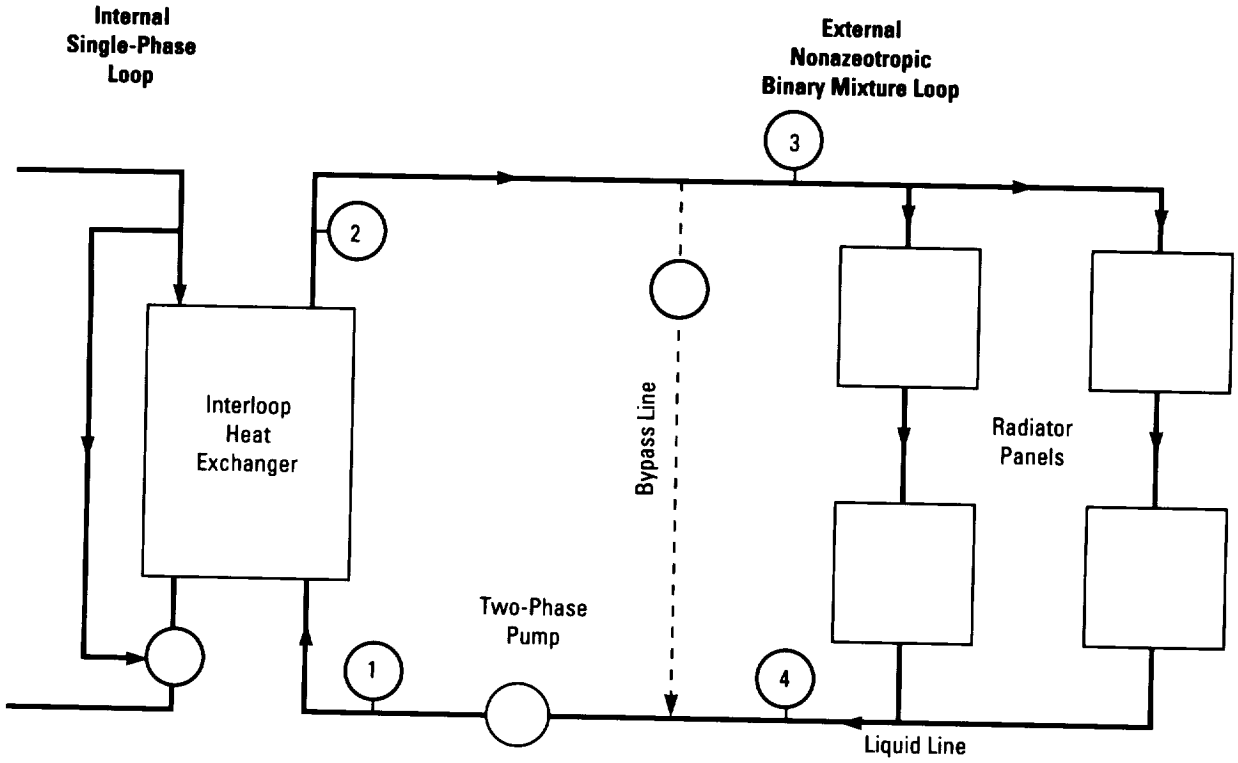

Nonazeotropic binary refrigerant mixture heat transport loop.

Rocket Engine Transient Simulation

Analysis of the mechanical and control systems of the **space shuttle main engine** (**SSME**) has required models that describe their operation. The models describe a pump-fed liquid propellant rocket engine and the **controller** necessary for the **SSME** steady-state/transient operation. There are several different models that are used to (1) perform engineering analysis for stability, parameter sensitivity, control gains, and failure determinations; (2) provide definitions for future research; (3) predict engine behavior; and (4) provide other system parameters.

Each of these models have their own strengths and weaknesses. The **digital transient model** (**DTM**) is a fine-grain model that incorporates some **SSME** dynamics. This model is used to perform time-domain analysis. It is slower than some of the other models and lacks true high-frequency dynamics description. It also has very poor documentation. It is the finest grain model for moderate **SSME** dynamics. The **power balance model** has no dynamics at all but it does contain many nonlinear equational descriptions. It is used to determine gains and coefficients for **SSME** adaptation data. There are several slightly different models which have simplified equational descriptions that have the worst of the nonlinearities omitted; these models are lumped together as the analog versions. They have use in time modeling of the **SSME** behavior and for control analysis. They run quickly, but are not fine-grained descriptions.

As hardware changes are made to the **SSME**, they must be reflected in the mathematical description of the model. This requires that model documentation be good and that a recompilation of the program take place with each change, which must then be tested to see if the model behaves as expected (i.e., determine mistakes in programming, modeling, or both). The **rocket engine transient simulation** (**ROCETS**) program is designed to replace all of these models. **ROCETS** will allow a structured modeling that removes many of the former objections. It contains improved engine dynamics and engine component descriptions at various levels of fidelity. This means the user has the advantage of model components that can be compiled, checked, and analyzed separately from the engine model. These free-standing components can be aggregated together on an as-needed basis for a particular engine description. The models also have full documentation, which includes derivations and historical evolution.

W. Adams/ED14
205–544–1425
Sponsor: Office of Aeronautics and Space Technology

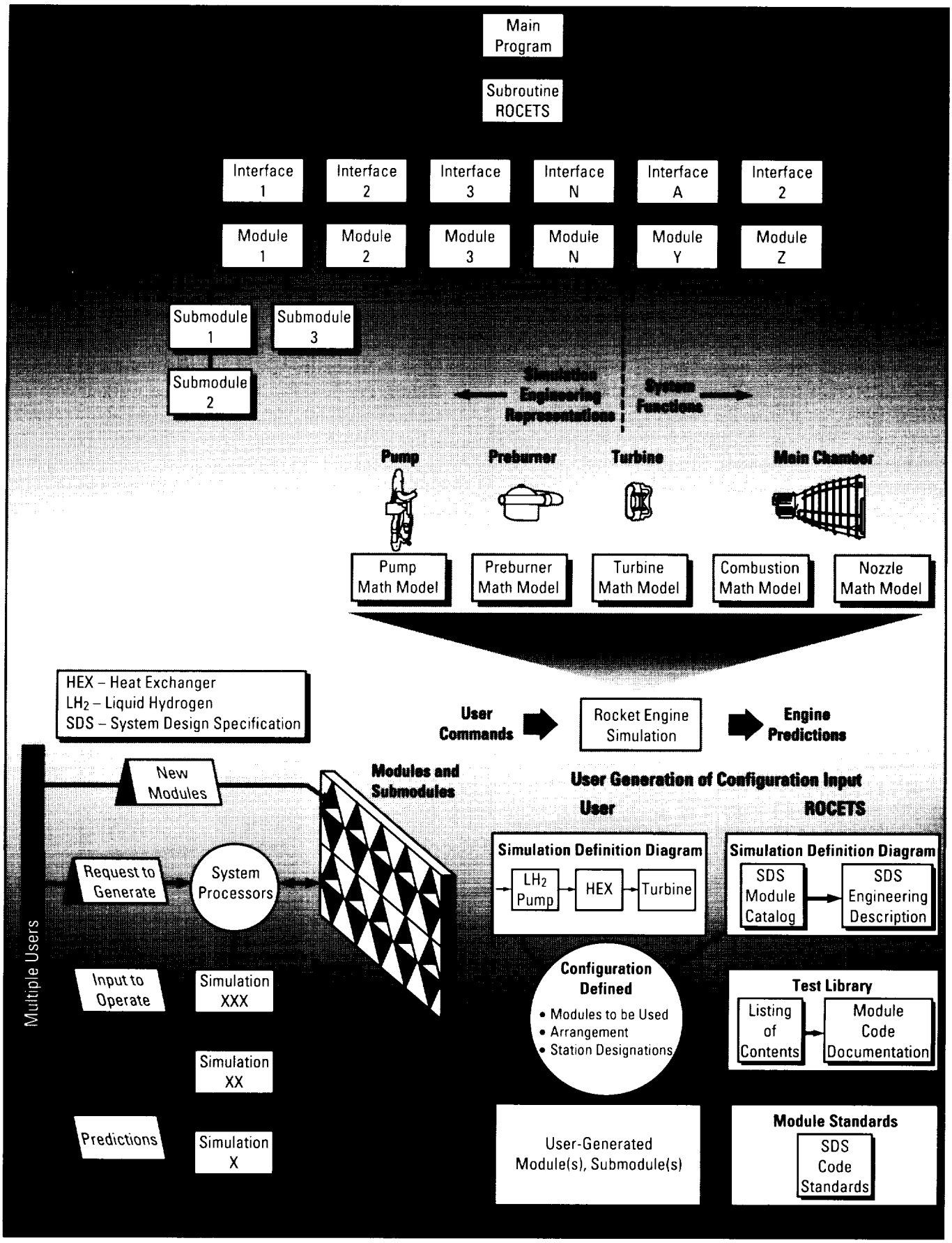

ROCETS architecture.

Shuttle Payload Modal Testing Techniques

Development of verified structural dynamic models of shuttle payloads generally requires modal survey testing of the flight hardware and subsequent model updating using measured data. Historically, fixed-base testing has been used in this model verification process. Unfortunately, there is a number of problems associated with fixed-base testing, such as contamination of data due to fixture/article coupling, difficulty in accurately simulating flight boundary conditions, and cost of construction and checkout of the fixture. For these reasons, free-free **modal testing** augmented by **residual flexibility** measurements has been studied and, to a very limited degree, applied in the model updating process. The purpose of the current research effort is to investigate the use of the **residual flexibility** approach for deriving constrained modes of shuttle payloads and to implement the test/analysis procedure in-house. The approach would then be available as an alternative procedure when fixed-base testing proves undesirable; it is applicable to all future shuttle payloads.

Modal test procedures for the **residual flexibility** approach involve the measurement of free-free modes as well as the residual functions for the payload interfaces. The residual flexibilities approximate the higher-order modes that are not measured in the free-free test. Shuttle-constrained modes of the payload are calculated using the measured free-free modes and residuals.

Implementation of the **residual flexibility** technique at MSFC requires the test and model correlation technologies discussed below.

The ability to calculate shuttle-constrained modes using measured free-free modes and **residual flexibility** is required. Also required is a technique for determining the accuracy of these calculated constrained modes and the ability to determine the number of free modes required and to assess which residual terms are needed.

Another requirement is the ability to perform **residual flexibility** measurements in the MSFC Dynamics Test Laboratory, assess quality of the measurements, and provide data in a form directly usable in model updating. This will require modification of existing modal analysis software.

Use of free-free modes and residual measurements to improve payload models is required. Residual flexibilities must be used to determine model deficiencies in the interface regions and to assess effects of updates.

The first capability listed was developed in the initial phase of the research effort (summarized in Admire et al., pp. 1614–1622) in which the technique was applied to a space station module prototype and the Material Science Laboratory (MSL). Results of phase I showed that the **residual flexibility** method worked very well for both payloads, yielding accurate constrained modes with reasonably small sets of free-free modes. The second phase of the study will address the other required technologies. The main activities in the second phase will be to design a simple test article, develop techniques for measurement of the residual functions, and use the residuals for updating the model of the simple article.

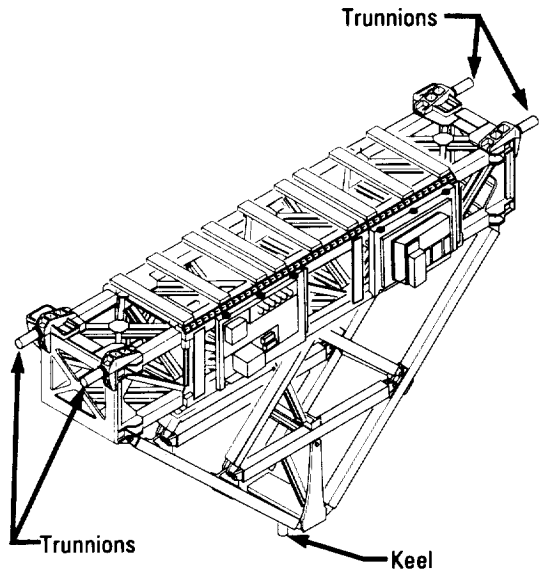

Shuttle payload with orbiter connections.

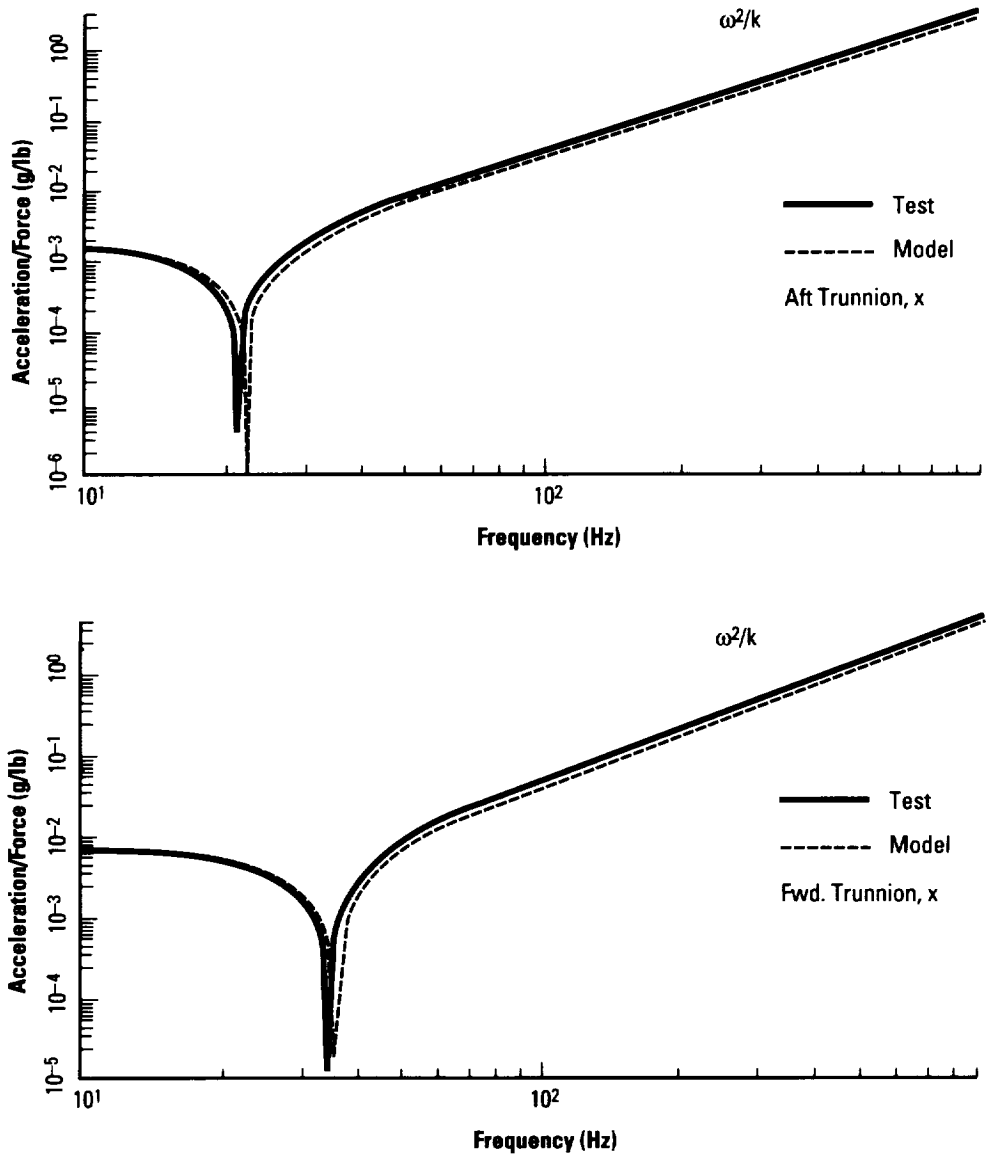

Typical comparisons of residual functions from test and updated models.

Admire, J.R., Tinker, M.L., and Ivey, E.W., "Residual Flexibility Test Method for Verification of Constrained Structural Models," Proceedings of 33rd Structures, Structural Dynamics and Materials Conference, April 13–15, 1992, Dallas, TX, pp. 1614–1622.

Blair, M.A., "Interface Characterization Modal Test Techniques," Engineering Memorandum (EM) Alternate Test Techniques for Interface Characterization (ATTIC) (EM ATTIC) 002, Lockheed Missiles and Space Company, Sunnyvale, CA, June 1991.

Rubin, S., "Improved Component Mode Representation for Structural Dynamic Analysis," *American Institute of Aeronautics and Astronautics (AIAA) Journal*, vol. 13, 1975, pp. 995–1006.

M.L. Tinker/ED22
205–544–4973
Sponsor: Space Station *Freedom* Project Office

Small Expendable Deployer System

The small expendable deployer system (SEDS) is a lightweight, spinning-reel type system designed to deploy a payload attached to the end of a 20-km (12-mi) long **tether**, which is cut and discarded after use. The key objectives are to validate the design concept and to study the **dynamics of tether deployment**. SEDS weighs approximately 39 km (85 lb), including the **tether** weight of 7 km (15 lb). The **tether** is made from a high-strength, low-density, polyethylene fiber called SPECTRA. SEDS will fly on a Delta II launch vehicle in mid-1993. Hardware development was completed in 1989 on the mechanical systems and in 1992 on the electrical systems. Both will be tested in late 1992. Analysis and planning leading up to the physical integration of SEDS into the Delta II began in 1991 and will continue until the launch.

During flight, the payload, weighing 23 km (50 lb), will be deployed toward Earth. Payload instruments are an accelerometer, a tensiometer, and a magnetometer (for orientation information). The experiment will last approximately 2 h, ending when the **tether** is fully deployed and has swung to a near-vertical position, pointing toward Earth. The **tether** is then cut, allowing it and the payload to reenter the Earth's atmosphere.

Numerous future applications of SEDS are being considered. One is the routine deorbiting of Space Station *Freedom* (S.S. *Freedom*) waste materials, packaged in small, lightweight containers that can be folded for easy storage during shuttle trips to the station. Another is the boosting of small payloads like The University of Alabama in Huntsville student-built satellite called SEDSAT (which stands for Students for the Exploration and Development of Space and Satellites) to higher orbits—from 185×740 to 680×792 km (115×460 to 423×492 mi). The most obvious use of SEDS will be to place instruments in the 90- to 120-km (56- to 75-mi) altitude region for upper atmospheric research.

J.K. Harrison/FA34
205–544–0629
Sponsor: Office of Space Flight

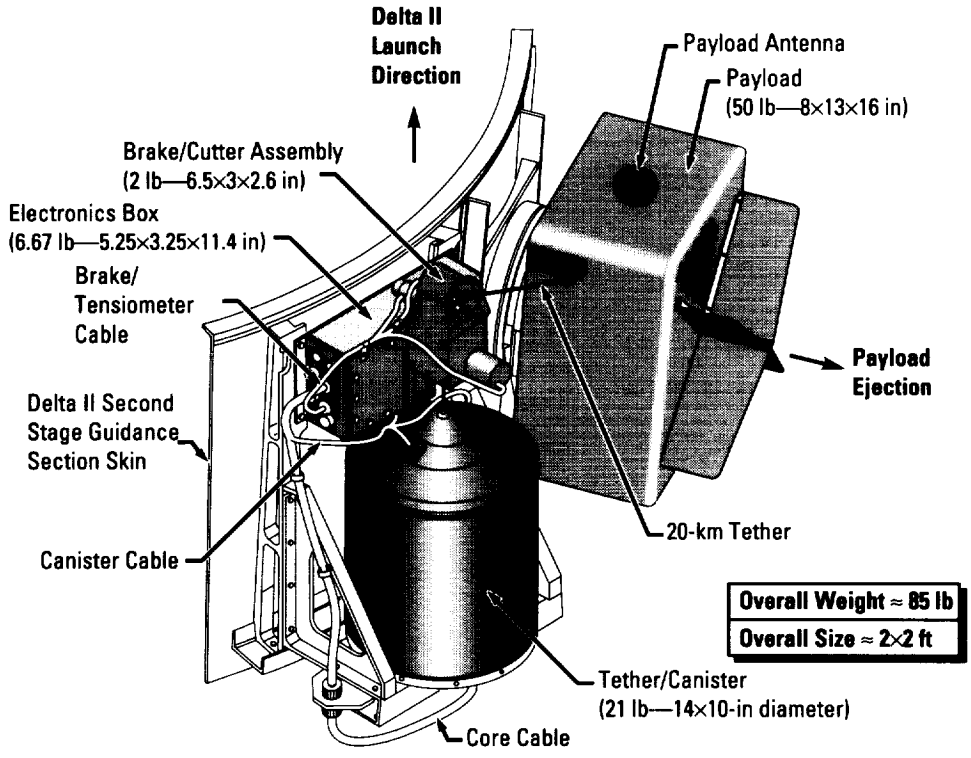

SEDS on Delta II.

Solid Rocket Motor Propellant and Polymer Materials Structural Test Program

Current structural analysis of **solid propellant grains** employ linear viscoelastic theory. It has been assumed in the past that linear analysis was adequate to predict the response of the propellant grain, since most strains induced in a solid rocket motor (SRM) during storage and operation were less than 20 percent. Nonlinear analysis codes have been developed, but material property measurement techniques that provide input to the codes have been slow in developing. Recently, questions have arisen as to the validity of the assumption of linearity of propellants below 20 percent strain. A small body of evidence indicates that **nonlinear behavior** in propellants may begin as early as 1 to 2 percent strain. If so, the **Boltzmann superposition principle** employed throughout the propellant industry to characterize propellant behavior may be in error. It is the goal of this 3-yr study to determine the validity of the **Boltzmann superposition principle** and to establish as complete a characterization of the current and advanced SRM (ASRM) propellant as possible to facilitate structural analyses and determinations of factors of safety for the system.

The **Propulsion Directorate of the U.S. Army Missile Command (MICOM)** is currently designing, developing, analyzing, and testing specimens and constituent materials to support analyses and investigations of the space shuttle SRM and components.

The following is a summary of the structural testing series that has been achieved at the Propulsion Directorate/**MICOM** as of March 1, 1992:

- Uniaxial tensile characterizations
  - Post-cure testing
  - Aging testing
- Uniaxial stress relaxation characterization
  - Incremental strain testing
  - Aging testing
- Linear coefficient of thermal expansion
- Crosslink density determination
- Cyclic thermomechanical testing
- Set strain experiment.

Further work to be completed by the MICOM Propulsion Laboratory includes the following:

- MICOM personnel will continue to attempt to determine the history and pedigree of the shuttle segment from which the aged propellant samples were taken
- Creep compliance determination at 125 °F (1-wk duration)
- Continued efforts on the damage investigation will focus on analytical studies of uniaxial tests and possible methods to predict simple stress histories.

Little, Robert R., "NASA Solid Propulsion Integrity Program (SPIP) Program Quarterly Status Report, 4th quarter, FY91," Letter Report RD–PR–91–54, November 20, 1991.

Little, Robert R., "NASA SPIP Program Quarterly Status Report, 2nd quarter, FY92," Letter Report RD–PR–92–24, March 11, 1992.

F. Ledbetter/EH33
205–544–2673
Sponsor: Solid Propulsion Integrity Program

System for Anomaly and Failure Detection

Since ground testing of the **space shuttle main engine (SSME)** began in 1975, there have been 28 major incidents. These failures occurred despite an extensive internal system of self-checking and redlines that were designed to safeguard the **SSME**. This small number of failures has occurred generally during **SSME** design changes and almost seems insignificant when compared to over 1,500 tests without major incidents. However, these failures have costs associated with them that belie their small numbers. These include costs from engine and stand damage, analysis costs, engine component loss, loss of failure evidence, and schedule impacts.

The analysis of these failures showed that most of them could have been detected earlier than the redline method with an improved **health monitoring system (HMS)**. A program was started to catalog all the **SSME** failures and which engine sensor(s) indicated engine deterioration and incipient engine failure. This effort showed that almost all of the engines involved in these failures could have been shutdown earlier than the redline-initiated shutdowns. The study defined a small list of generic failure types and determined the necessary instrumentation to provide engine observability. A development program was initiated for a detection algorithm based on these results. Development was also started on a ground-based computer system to contain the **real-time failure control (RTFC)** algorithm. This algorithm has been run with seven hot-fire tests that contained failures, three digital transient simulations of failures from tests, and two hypothetical engine failures. In all cases, the **RTFC** algorithm showed an improvement over redline methodology. All past engine failures should be detected early by the algorithm, barring catastrophic failures, due to the instrument selection process. The algorithm has also been tested against runs without failures to demonstrate no issuance of inadvertent shutdowns.

The previous studies have culminated in a stand-based computer system for the early detection of incipient engine failure called the **system for anomaly and failure detection (SAFD)**. The computer and operating system have been designed to operate with other improved health-monitoring algorithms as well as the **RTFC** algorithm. The algorithm can be run in a stand-alone mode or in conjunction with other active algorithms. The **SAFD** system and **RTFC** algorithm are presently in the early stages of testing and are performing in a satisfactory manner.

S. Douglas/ED14
205–544–4513
Sponsor: Office of Aeronautics, Exploration, and Technology

SSME simulated actual and hypothetical failures

Test No.	Failure	Redline Cutoff (C/O) (s)	SAFD C/O (s)
901–136	Bearing	300.20	300.12 *
901–173	Liquid oxygen (lox) post fracture	201.16	188.88
901–225	Main oxidizer valve (MOV)	255.63	255.61 **
901–284	Lee jet failed	9.88	7.14
901–340	Turnaround duct crack	405.50	295.42
901–364	Hot-gas intrusion to rotor coolant	392.15	290.19 *
902–249	Turbine blade	450.58	440.54
902–428	Oxidizer preburner (OPB) injector	204.12	204.04 *
902–471	Fuel duct	147.68	146.76 **
750–285	Feedline	223.50	212.48
Hypothetical	Preburner (PB) pump discharge duct	N/A	C/O
Hypothetical	High-pressure fuel turbopump (HPFTP) discharge flow block	N/A	C/O

* Algorithm was hampered by tank venting. It has been improved since this simulation and it is felt that this failure would be caught earlier.
** Minimal damage reduction.
NOTE.— A simulation of engine 0215 in test 901–666 showed that a shutdown command issued only 0.38 s earlier than the redline shutdown would have avoided significant engine damage.

Tailored Composite Bumpers for Protection Against Orbital Debris

With the recent increases in orbital debris and the high cost per pound to launch hardware, it has become increasingly important to design **orbital debris shielding** for orbiting vehicles as efficient as possible. Lower-weight shielding may be tailored to increase the shield performance by varying materials and combinations of materials. Novel **composites**, both homogeneous and sandwiched plates, are being developed and tested to determine their efficiency, as compared to traditional aluminum shields. Innovative methods of **damage evaluation** are also being investigated for more objective measurements of shield effectiveness. Computer scans of the damage on the structure protected by the shield can provide graphical categorization of damage, which can then be numerically analyzed. This research contract is expected to produce valuable information in the development of efficient shielding from **meteoroids** and orbital debris for both government and industry space applications.

J.H. Robinson/ED52
205–544–7013
Sponsor: Office of Commercial Programs,
Small Business Innovative Research Program

Thermomechanical Bearing Analysis Program for Use on a Personal Computer

Cryogenic liquid propulsion systems for manned spacecraft use high-performance turbopumps with rolling element **bearings** supporting the turbine and pump shaft. These **bearings** operate at high speed in the cryogen being pumped and are highly loaded and poorly lubricated. These conditions produce extreme sensitivity to thermomechanical interactions that cause rapid loss of **bearing** operating clearance, increases in heat generation and component temperatures, and rapid rise of contact stresses that can lead to premature **bearing** deterioration or failure. This research, performed by SRS Technologies, defined and developed a modeling technique to simulate the thermomechanical characteristics of turbopump **bearing** systems operating in cryogenics. Developing and installing the **simulation** on a personal computer (PC) was also shown to be feasible.

The program was developed by modifying the **systems improved numerical differencing analyzer (SINDA) thermal** analysis code and using a modified **shaft bearing thermal (SHABERTH) bearing** mechanical code as a subroutine to **SINDA**. The code can accommodate a system of up to five **bearings** mounted on a shaft. This analysis capability allows the rapid determination of the **thermal** and mechanical interactions in a **bearing** or a system of **bearings** for a given set of operating parameters. Use of **SINDA** for **thermal** analysis allows more detailed modeling of the large temperature gradients that exist in cryogenic **bearings** at these high speeds. In many cases, surface temperatures exceed the saturation temperature of the coolant, and two-phase fluid conditions exist at the solid-fluid interface. The difference in surface and saturation temperature has a strong influence on the thermodynamic state of the fluid at the interface and consequently the magnitude of the fluid heat transfer coefficient. It is, therefore, important to have a detailed representation of the surface temperature to appropriately determine the boundary fluid heat transfer coefficient. The code determines a local heat transfer coefficient for each fluid boundary node, considering local vapor quality and relative velocities of fluid and solid. The program executes rapidly, allowing the determination of both steady-state and transient solutions. Converged solutions have high resolution and have correlated well with test data.

The thermomechanical **bearing** program was tested and verified by simulating two **bearing** applications. The **bearing** and seal materials tester (BSMT) at MSFC and the Pratt and Whitney (P&W) advanced high-pressure oxidizer turbopump (HPOTP) test rig were used as test cases because of the extensive **bearing** test data for these applications. The results of the **simulations** showed very good predictions for **bearing** outer race temperature measurements and the exit coolant temperature measurements.

Results of this effort proved that the **SHABERTH bearing** code could be used as a subroutine to the **SINDA thermal** analysis program to develop a thermomechanical **bearing** program that can determine steady-state and/or transient **bearing** temperatures, heat generation, contact stresses, and clearance changes. Also, using **SINDA** as the basis of the program permits users experienced with **SINDA** to quickly learn to perform **bearing** thermomechanical analysis. However, experience with the **SHABERTH** code is recommended. The code is a useful design tool for parametric evaluation and optimization of **bearing** configurations for specific applications. For example, ball **bearing** race curvatures and internal clearances can be varied to optimize operating characteristics, such as Hertz contact stresses, contact heat generation, ball excursions, and component temperatures. The availability of the code on a PC allows convenient and cost-effective evaluation of a broad range of **bearing** features, providing the designer with a powerful analysis tool for **bearing** shaft system evaluation. This program can be used for **simulation** and analysis of a wide assortment of high-speed **bearing** applications, not only for spacecraft but also commercial applications such as superchargers, turbochargers, and jet turbines.

The thermomechanical analysis software and models were developed to run on a PC or a workstation. The code was successfully installed and executed on a Northgate 486–33 Elegance PC. The results of the test cases modeled were verified with the mainframe version. It was determined that running the models on the PC was not only a viable option but a desirable alternative to running on the mainframe. Turnaround times for the analysis are faster and running the code is less complicated on the PC. The transient program is able to run very quickly on the IBM 3084 mainframe (300 **SINDA/SHABERTH** iterations in 30 control processing unit (CPU) minutes). On a 486–33 PC, the transient program takes 50 CPU minutes to do 300 iterations. However, the wall clock time on the PC is much faster than the mainframe (200 to 300 percent faster) because the PC can be dedicated to one job. The minimum hardware requirements needed to practicably utilize the thermomechanical software are as follows: a PC with speed equivalent to or greater than a 16-MHz 80386 IBM compatible PC, a math co-processor, a minimum of 25 Mb free-disk space, 6 Mb of random access memory (RAM) or a virtual memory manager, and a full-feature FORTRAN 77 compiler.

The **SINDA/SHABERTH** thermomechanical **bearing** analysis program has been used by MSFC personnel to perform steady-state analysis of both the pump-end and turbine-end **bearings** of the Rocketdyne (RKD) HPOTP and to make pretest predictions of **bearing** operation in the BSMT to support redline determination. P&W has also used the programs in analysis of **bearing** operation in their space shuttle main engine (SSME) alternate turbopump designs, and they are currently using the code to assist in the design of the **bearing** for the liquid oxygen (lox) turbopump of the space transportation main engine (STME) for the National Launch System (NLS).

H. Gibson/EH14
205–544–2513
Sponsor: Office of Aeronautics and Space Technology

Index of Contacts

☆ U.S. Government Printing Office: 1993—734-785